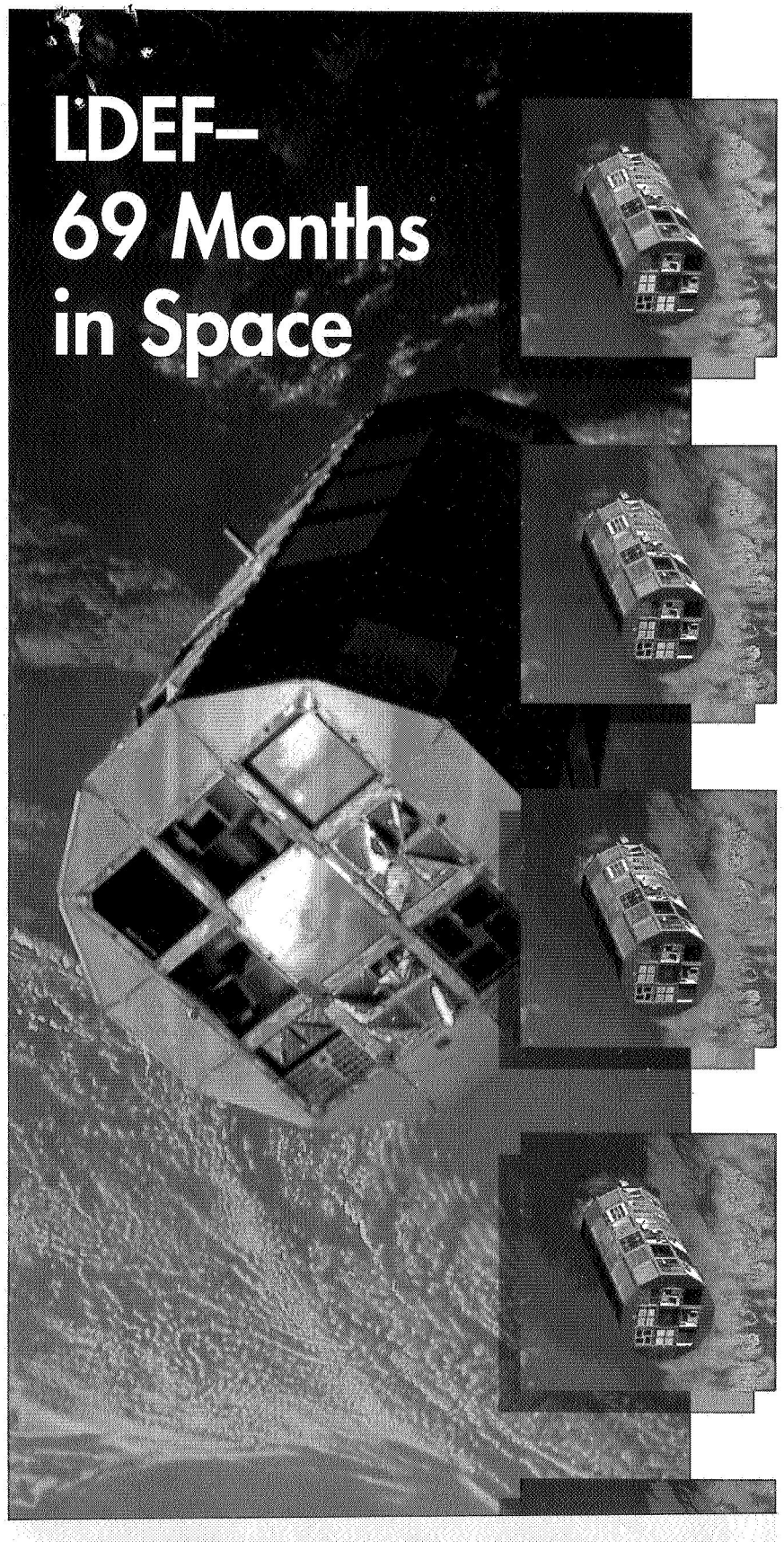

LDEF– 69 Months in Space

Second Post - Retrieval Symposium

June 1-5, 1992
San Diego, California

Sponsors:

LDEF Science Office
NASA Langley Research Center

American Institute of
Aeronautics and Astronautics

NASA Conference Publication 3194
Part 4

ORIGINAL PAGE
BLACK AND WHITE PHOTOGRAPH

National Aeronautics and
Space Administration

(NASA-CP-3194-Pt-4) LDEF: 69 MONTHS IN SPACE. PART 4: SECOND POST-RETRIEVAL SYMPOSIUM (NASA) 309 p

N93-29682
--THRU--
N93-29708
Unclas

H1/99 0164920

American Institute of Aeronautics and Astronautics

LDEF–
69 Months
in Space

NASA Conference Publication 3194
Part 4

Second Post - Retrieval Symposium

Edited by
Arlene S. Levine
NASA Langley Research Center
Hampton, Virginia

Proceedings of a symposium sponsored by the National Aeronautics and Space Administration, Washington, D.C., and the American Institute of Aeronautics and Astronautics, Washington, D.C., and held in San Diego, California
June 1-5, 1992

National Aeronautics and
Space Administration

Office of Management

Scientific and Technical
Information Program

1993

FOREWORD

Nineteen hundred ninety-two, designated The International Space Year (ISY), coincided with the 35th anniversary of the International Geophysical Year (IGY). The International Space Year honored space exploration and the planet Earth and also marked the 500th Anniversary of Christopher Columbus's discovery of the New World. Langley Research Center, the home of the Long Duration Exposure Facility (LDEF), celebrated its 75th anniversary. In addition, 1992 marked the second anniversary of the LDEF retrieval. Since publication of the First LDEF Post-Retrieval Symposium Conference Publication in January 1992, the LDEF principal investigators, co-investigators, and collaborating investigators have had an additional 12 months to analyze and interpret the data from LDEF's 57 onboard experiments and to reach a better understanding of the space environment (ionizing radiation, meteoroids, space debris, and atomic oxygen in the upper atmosphere) and the effects that prolonged exposure in this environment will have on future spacecraft such as large low-Earth orbit (LEO) platforms, Earth-orbiting spacecraft, and on future manned and unmanned spacecraft to the Moon and to other planets.

Results of the second year LDEF studies were presented at the Second LDEF Post-Retrieval Symposium, held at the Town and Country Hotel, San Diego, California, June 1 to 5, 1992. This symposium was co-sponsored by NASA Langley Research Center and the American Institute of Aeronautics and Astronautics. This document contains the full-length papers presented at the second symposium. The collection includes invited review papers on ionizing radiation, meteoroids and debris, environmental effects on materials, environmental effects on systems, and archiving of the LDEF data. Contributed papers on ionizing radiation, meteoroids and debris, space effects on materials and systems, the LDEF mission and induced environments, microgravity, and life science are also included. The document organization is very similar to that of the symposium.

LDEF Mission and Induced Environments
Space Environments - Ionizing Radiation
Space Environments - Meteoroid and Debris
Space Environments - Microgravity
Space Environmental Effects - Materials
Space Environmental Effects - Systems
Space Environmental Effects - Biology
The Future

During the symposium William H. Kinard chaired the first half of the general session containing the invited review papers, and Bland A. Stein chaired the second half of the general session containing the invited review papers, plus the Mission and Induced Environments papers, and a Microgravity paper. Thomas Parnell chaired the Ionizing Radiation sessions; J.A.M. McDonnell, Jean-Claude Mandeville, Dale R. Atkinson, Michael Zolensky, and Donald Humes chaired Meteoroid and Debris sessions; Joan Funk and John Davis chaired the Data basing session; Ann Whitaker and Bruce Banks chaired the Coating session; Philip Young chaired the Polymer session, and R.C. Tennyson chaired the Polymer Matrix Composites session. Roger Linton chaired the Metals and Metal Matrix Composites session. Gale Harvey and Bland Stein chaired the Contamination session. James Mason, Joel Edelman, and Harry Dursch chaired the Systems sessions. William H. Kinard chaired the closing general session containing papers on biology and future activities.

I wish to thank the contributing authors whose research greatly enhanced the knowledge of space environments and their effects on materials, systems, and biology. The papers contained in this volume underwent a technical review by peer reviewers and an editorial review. I also wish to thank the technical reviewers for their time and effort in making this collection as current and accurate as it is. I would like to thank Maureen Sgambelluri, who assisted with the symposium logistics, and who cheerfully reformatted some of the papers contained in this publication. I would like to gratefully acknowledge Susan Hurd, Mary Edwards, Lisa Levine, Alisa Hollins, and Jeanne Gordon, for their support in editing this document.

This conference publication is the second in a series of three LDEF Post-Retrieval documents. In June 1991, over 400 LDEF investigators and data users convened in Kissimmee, Florida for the First LDEF Post-Retrieval Symposium. The results of the symposium (130 papers) are printed in a three-part NASA Conference Publication, ***LDEF-69 Months in Space: First LDEF Post-Retrieval Symposium,*** January 1992, (NASA CP-3134.) The LDEF Science Office plans to hold a third symposium in November 1993, in Williamsburg, Virginia. Published abstracts for the third symposium will be available at the meeting. Additional information on these symposia may be obtained by contacting:

Arlene S. Levine
LDEF Science Office M/S 404
NASA Langley Research Center
Hampton, Virginia 23681-0001
Telephone: 804 864-3318
Fax: 804 864-8094

The use of trade names or manufacturers in this publication does not constitute an official endorsement of such products or manufacturers, either expressed or implied, by the National Aeronautics and Space Administration.

CONTENTS

---

* Part 1 is presented under separate cover.

Part 2*

Space Environments - Meteoroid and Debris

---

* Part 2 is presented under separate cover.

Space Environments - Microgravity

Part 3*

Space Environmental Effects - Materials

---

* Part 3 is presented under separate cover.

Part 4

Space Environmental Effects - Systems

Space Environmental Effects - Biology

The Future

*Poster Presentation
† Oral and Poster Presentation

PART 4

SPACE ENVIRONMENTAL EFFECTS

SYSTEMS

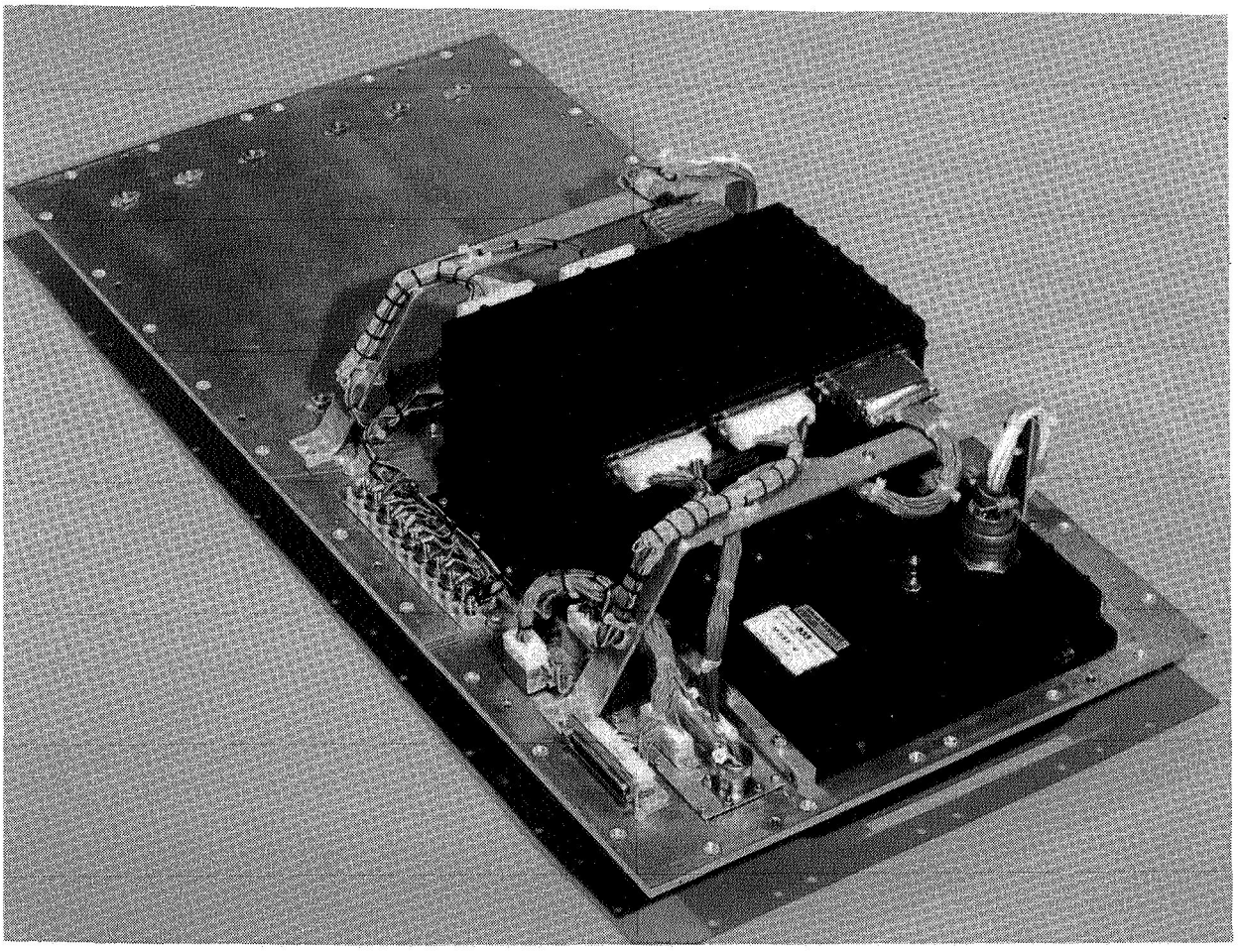

ORIGINAL PAGE
BLACK AND WHITE PHOTOGRAPH

ORIGINAL PAGE
BLACK AND WHITE PHOTO

L-78-5005

N93-29683

OVERVIEW OF THE SYSTEMS SPECIAL INVESTIGATION GROUP INVESTIGATION

50163
Pg 12

James B. Mason
NASA Goddard Space Flight Center
Greenbelt, Maryland 20770

Harry Dursch
Boeing Defense & Space Group
Seattle, Washington, 98124

Joel Edelman
LDEF Corporation
Silver Spring, Maryland 20905

SUMMARY

The Long Duration Exposure Facility (LDEF) carried a remarkable variety of electrical, mechanical, thermal, and optical systems, subsystems, and components. Nineteen of the fifty-seven experiments flown on LDEF contained functional systems that were active on-orbit. Almost all of the other experiments possessed at least a few specific components of interest to the Systems Special Investigation Group (Systems SIG), such as adhesives, seals, fasteners, optical components, and thermal blankets.

Almost all top level functional testing of the active LDEF and experiment systems has been completed. Failure analysis of both LDEF hardware and individual experiments that failed to perform as designed has also been completed. Testing of system components and experimenter hardware of interest to the Systems SIG is ongoing. All available testing and analysis results have been collected and integrated by the Systems SIG. This paper provides an overview of our findings. An LDEF Optical Experiment Database containing information for all 29 optical related experiments is also discussed.

INTRODUCTION

The Systems SIG, formed by the LDEF Project Office to perform post flight analysis of systems hardware, was chartered to investigate the effects of the extended LDEF mission on both satellite and experiment systems and to coordinate and integrate all systems analyses performed during post flight investigations.

PRECEDING PAGE BLANK NOT FILMED

The approach to the testing of hardware by the System SIG has always emphasized the testing of each system at its highest practicable level of assembly. The results at this level provided the direction for further testing in the form of either nominal or anomalous behavior. The Systems SIG divided the investigations into four major engineering disciplines represented by the LDEF hardware: electrical, mechanical, thermal, and optical systems. Almost all functional testing of the active experiments has been completed while system component hardware is still being evaluated. This paper discusses the results from System SIG investigations and those generated outside of the Systems SIG, e.g. by other SIGs or experimenters.

To disseminate LDEF information to the spacecraft community, the Systems SIG has completed the following activities: (1) distribution of a semi-quarterly newsletter containing updates on current results from all aspects of the various ongoing LDEF evaluations. Because of the newsletter's popularity (currently at 2400 copies), the LDEF Project Office has assumed responsibility of this activity; (2) development and release of standardized test plans for systems-related hardware, (3) release of the Systems SIG Interim Report in January, 1991; and (4) release of the Systems SIG Report in June, 1992.

For additional information regarding information presented in this paper, the reader is referred to the June, 1992 Systems SIG Report.

FINDINGS

General Observations

LDEF results demonstrate that shielding from the effects of atomic oxygen, micrometeoroids, space debris, and ultraviolet radiation must be considered for extended mission lifetimes in LEO.

There were several major system anomalies. However, the analysis to date has indicated that none of these can be solely attributed to the long-term exposure to LEO. Design, workmanship, and lack of pre-flight testing have been identified as the primary causes of all system failures. Degradations in system or component level performances due to the long-term exposure to the LEO environment were noted. The combination of any of the individual low Earth orbit environmental factors such as UV, atomic oxygen, particulate radiation, thermal cycling, meteoroid and/or debris impacts and contamination can produce synergistic conditions that may accelerate the onset and rate of degradation of space exposed systems and materials.

The most detrimental contamination process observed during LDEF's mission was the outgassing and redeposition of molecular contaminants which resulted in a brown film on the surfaces of LDEF. This brown film was widely dispersed over the trailing rows and both the Earth and space ends. Thermal control surfaces, optics hardware and solar cells were most susceptible to this

contamination. Ram facing surfaces appeared "clean" due to atomic oxygen attack (i.e., cleaning) of the brown film.

Mechanical

The LDEF deintegration team and several experimenters noted severe fastener and hardware removal difficulties during post-flight activities. The Systems SIG has investigated all reported instances, and in all cases the difficulties were attributed to galling during installation or post-flight removal. To date, no evidence of coldwelding has been found. Correct selection of materials and lubricants as well as proper mechanical procedures are essential to ensure successful on-orbit or post-flight installation and removal of hardware.

The finding of no coldwelding indicated a need to review previous on-orbit coldwelding experiments and on-orbit spacecraft anomalies to determine whether the absence of coldwelding on LDEF was to be expected. The results of this investigation showed that there have been no documented cases of a significant on-orbit coldwelding event occurring on U.S. spacecraft. There have been a few documented cases of seizure occurring during on-orbit coldwelding experiments. However, the seized materials had been selected for the experiment because of their susceptibility to coldweld during vacuum testing on Earth. This susceptibility was enhanced by effective pre-flight cleanliness procedures.

All seals and the majority of lubricants used on LDEF were designed as functioning components of experiments and were, therefore, both shielded and hermetically sealed from exposure to the LEO environment. Post-flight testing has shown nominal behavior for these materials. However, several lubricants were exposed to the LEO environment as experiment specimens. Post-flight analysis showed a range of results for these specimens ranging from nominal behavior to complete loss of lubricant, depending on the particular lubricant and its location on LDEF. For example, Figure 1 shows Everlube 620, a MoS_2 lubricant within a modified phenolic binder, before and after the 69 months in LEO. Several specimens of this material, deposited on to a stainless steel substrate, were flown on the trailing edge as part of Boeing's materials experiment. Post-flight inspection of the specimens showed that none of the Everlube 620 remained. The binder apparently decomposed due to UV exposure and then outgassed (evaporated). This led to the MoS_2 becoming separated from the substrate. This is an example of failure of the lubricant system, not the lubricant.

With few exceptions, adhesives performed as expected. Several experimenters noted that the adhesives had darkened in areas that were exposed to UV. One of the most obvious adhesive failures was the loss of four solar cells. Two of the four solar cells were on the leading edge and the other two were mounted on a trailing edge using an epoxy adhesive. Upon retrieval of LDEF, it was noted that all four cells were missing. No adhesive remained on the two leading edge mounting plates but some remained on the trailing edge plate. This indicated that the bond failed at the cell/adhesive interface and then

the exposed adhesive was attacked by atomic oxygen. Possible causes of failure include poor surface preparation and/or thermal expansion mismatch between the solar cell substrate and the aluminum mounting plate.

An additional adhesive failure involved polymeric lap shear specimens that used RTV 560 (+12% graphite) silicone adhesive. Four specimens were flown on the leading edge and four flown on the trailing edge. All eight specimens failed during the mission. Another finding involved composite lap shear specimens that used three different epoxy adhesive systems and were flown on the leading and trailing edges. Results ranged from post-flight increases in lap shear values (when compared to pre-flight values) for two of the three systems, to a decrease in shear strength for the third system.

One of the most notable observations made during the on-orbit photo survey was the loose silverized Teflon thermal blankets located on a space end experiment (Figure 2). 3M's Y966 tape was used to hold the edges of the thermal blankets to the experiment tray frame. The blankets apparently shrunk in flight causing the tape to fail. Portions of the tape were attached to both the blanket and frame, indicating that the tape had failed in tension. Post-flight adhesion testing showed that the tape retained adequate adhesive properties.

The viscous damper, used to provide stabilization of LDEF from deployment caused oscillations, performed as designed and exhibited no signs of degradation. The damper has undergone extensive post-flight testing and has been returned to NASA LaRC in a flight ready condition.

Both the rigidize-sensing grapple, used by the RMS to activate the active experiments prior to deployment, and the flight-releasable grapple, used by the RMS to deploy and retrieve LDEF, worked as designed. The grapples are currently awaiting functional testing to determine their post-flight condition.

The most significant finding for the fiber-reinforced organic composites was the atomic oxygen erosion of leading edge specimens. While the measured erosion was not unexpected, the detailed comparison of ground based predictions vs actual recession rates has not been completed. Thin protective coatings of nickel/SiO_2 and polyurethane based paints were used on leading edge specimens to successfully prevent this erosion.

Electrical

Electrical/mechanical relays continue to be a design concern. Two of the most significant LDEF active system failures involved relay failures. The Interstellar Gas Experiment was one of the more complex experiments on LDEF, with seven "cameras" located on four trays. Each camera contained five copper-beryllium foil plattens, which were to sequentially rotate out of their exposed position at pre-determined intervals. This experiment was never initiated due to a failure of the experiment's master initiate relay. The Thermal Control Surfaces Experiment recorded on-orbit optical properties of various thermal control coatings using a four-track Magnetic Tape Module. The latching

relay which switched track sets failed to operate when switching from track 3 to track 4. Consequently, portions of the early flight data on track 1 were overwritten and lost.

The Experiment Initiate System (EIS) provided the initiate signal to the active experiments which directed them to turn on their power and begin their operational programs. Post-flight inspection and testing, using the original ground support equipment, showed the condition of the EIS to be nominal.

NASA supplied seven Experiment Power and Data Systems (EPDS) to record on-orbit generated data. All EPDS units were similar, consisting of a Data Processor and Control Assembly (DPCA), a tape recorder (the Magnetic Tape Module), and two $LiSO_2$ batteries, all of which were attached to a mounting plate designed to fit into the backside of the experiment tray. The EPDS components were not directly exposed to the exterior environment, being protected by their mounting plate and by external thermal shields. Although simple compared with today's data systems, the EPDS contained many elements common to most such systems, including various control and "handshake" lines, programmable data formats and timing, and a data storage system. EPDS electronic components were procured to MIL-SPEC-883, Class B standards, and were not rescreened prior to installation. Data analysis and post-flight functional testing showed that all EPDS functioned normally during and after the LDEF flight.

Three different types of batteries were used on LDEF: lithium-sulfur-dioxide ($LiSO_2$), lithium carbon monofluoride (LiCF), and nickel-cadmium (NiCd) batteries. NASA provided a total of 92 $LiSO_2$ batteries that were used to power all but three of the active experiments flown on LDEF. Ten LiCF batteries were used by the two active NASA MSFC experiments. One NiCd battery, continuously charged by a four-array panel of solar cells, was used to power an active experiment from NASA GSFC. A loss of overcharge protection resulted in the development of internal pressures which caused bulging of the NiCd cell cases. However, post-flight testing showed that the battery still has the capability to provide output current in excess of the cell manufacturer's rated capacity of 12.0 ampere-hours. All the LiCF and $LiSO_2$ batteries met or exceeded expected lifetimes.

LDEF provided valuable knowledge concerning the viability of using various solar cells and solar cell encapsulants (adhesives and coverglass materials). Coverglass materials such as ceria doped microsheet and fused silica withstood this particular environment. Measurable degradation of some widely used antireflection coatings was observed. Results from some low cost materials such as silicone, Teflon, and polyimide indicated that these materials will require additional research before full-scale replacement of the conventional encapsulants (fused silica coverglass and DC 93500 adhesive) is justified. Micrometeoroid and debris impacts will continue to be a significant solar cell performance degradation mechanism. Solar cell performance degradation due to the deposition of contamination on the surfaces was also

well documented. However, the majority of electrical characterization and analysis of on-orbit data remains to be completed.

Pyrotechnic devices, flown on Experiment A0038, were successfully fired during post-retrieval ground testing.

Thermal

The change in performance of a wide variety of thermal control coatings and surfaces was moderate, with a few exceptions. A significant amount of these changes has been attributed to contamination effects. Certain metals (esp. chromic acid anodize aluminum), ceramics, coatings (YB-71, Z-93, PCB-Z), aluminum coated stainless steel reflectors, composites with inorganic coatings (Ni/SiO_2), and siloxane-containing polymers exhibited spaceflight environment resistance that is promising for longer missions. Other thermal control and silicone based conformal coatings, uncoated polymers and polymer matrix composites, metals (Ag, Cu) and silver Teflon thermal control blankets and second surface mirrors displayed significant environmental degradation. In addition, post-flight measurements may be optimistic because of bleaching effects from the ambient environment.

The results of thermal measurements on different samples of the same materials made at different laboratories have proven to be remarkably consistent and in agreement, lending additional credibility to the results. Confidence in designers' thermal margins for longer flight missions has been increased.

Initial functional tests were performed for each of the three heat pipe experiments flown on the LDEF, and the heat pipe systems were found to be intact and fully operational. No heat pipe penetration occurred due to micrometeoroid or debris impact.

Actual measured temperatures within the interior of the LDEF ranged from a low of 39°F to a maximum of 134°F and were well within design specifications. External thermal profiles varied greatly, depending on orientation, absorptance/emittance, and material mounting and shielding. The thermal stability of the LDEF adds to the accuracy of existing thermal models and enhances our ability to model the LDEF thermal history, as well as other spacecraft.

The loss of specularity of silver Teflon thermal blankets, one of the earliest observations noted at the time of retrieval, had no significant effect on the thermal performance of those materials. This loss of specularity is the result of first surface erosion and roughening by atomic oxygen.

The thermal performance (absorptance/emittance) of many surfaces was degraded by both line-of-sight and secondary contamination. The specific contamination morphology in various locations was affected by ultraviolet radiation and atomic oxygen impingement. Overall, the macroscopic changes

in thermal performance from contamination appear to be moderate at worst. Limited measurements on surfaces from which the contamination was removed post flight suggest that the surfaces beneath the contamination layers have undergone minimal thermal degradation.

Over 50% of all LDEF's exterior surfaces were chromic acid anodized (CAA) aluminum. Extensive optical testing of LDEF's CAA aluminum tray clamps was performed because of their wide distribution around the LDEF and representation of a complete spectrum of spaceflight environmental exposures. The tray clamps provided a complete picture of the spaceflight environmental effects on this surface treatment. Comparison of front-side (exposed), backside (shielded) and control clamps showed slight changes in the optical properties. However, the variations in absorptance and emittance have been attributed to the inherent variability in anodizing, to variations in measurements, and to the effects of on-orbit contamination deposited on tray clamp surfaces.

Betacloth which was exposed to the atomic oxygen flux was seen to have been cleansed of the many minute fibers that normally adorn its surface. This has been observed to have no measurable effect on the thermal performance of the betacloth, although some associated contamination issues are raised.

Optical

Contaminant films and residue were widespread in their migration over LDEF and onto optical experiment surfaces, especially due to the decomposition and outgassing of several materials, at least two possible sources being identified as those from the vehicle itself, as well as those materials used in some of the experiments.

Four experiments flew fiber optics and a fifth experiment evaluated fiber optic connectors. Four of these five experiments recorded on-orbit data using the NASA provided EPDS. Overall the fiber optics performed well on-orbit, with little or no degradation to optical performance. Most environmental effects were confined to the protective sheathing. However, one fiber optic bundle was struck by a meteoroid or debris particle causing discontinuity in the optical fiber. Preliminary data has indicated the need for additional study of the temperature effects on fiber optical performance. Post-flight testing performed on fiber optics flown on the Fiber Optic Exposure Experiment showed an increase in loss with decreasing temperature, becoming much steeper near the lower end of their temperature range.

Four LDEF experiments contained a variety of detectors. Most detectors were not degraded by the space exposure, with one notable exception. The triglycine sulfide had a 100% detectivity failure rate on both the control and flight samples.

Several types of optical sources were flown on LDEF including solid and gas lasers, flashlamps, standard lamps, and LEDs. To date, the results indicate that most optical sources operated nominally except for two gas lasers (HeNe

and CO_2) which would not fire during post-flight testing and a flickering deuterium lamp arc. During post-flight testing of the two gas lasers, no laser action could be obtained from the tubes. The characteristics of the tubes suggested that the mixture of fill gas had changed during the period between pre-flight and post flight tests. This result is consistent with changes expected due to gas diffusion through the glass tube. The tubes were in good physical condition, and survived the launch and recovery phases without apparent degradation.

Micrometeoroid and debris impacts on optical surfaces caused localized pitting, punctures, cracking, crazing, and delaminations. Examples of the effect of impacts are shown in Figure 3.

Spectral radiation from both solar and earth albedo sources was indicated both in the modifications of surface coating materials (chemical decomposition caused by ultraviolet radiation). This was particularly noticeable on an experiment located on the trailing edge where the holographic gratings had a 30% to 40% degradation of reflectivity from exposure to solar radiation and cosmic dust. Experimenters also noted that changes to coating interfaces as a result of infrared absorption may have contributed to mechanical stresses and failures from thermal cycling.

Atomic oxygen had a major effect in the oxidation of many physically "soft" materials, including optical coatings and thin films, as well as oxidation of uncoated, metallic reflective coatings (copper and silver). In general, "hard" uncoated optical materials were found to be resistant to the LEO environment.

Synergistic conditions of degradation resulted from the multiple and combined effects of environmental factors; for instance, UV and atomic oxygen attacked, changed, or even eroded away some of the overlaying contamination, modifying the broadband and spectral content of optical inputs to the sample beneath .

An LDEF Optical Experiment Database was created (using Filemaker Pro database software) that provides for quick and easy access to available experimenter's optic's related findings. The database contains a file for each of the LDEF experiments that possessed optical hardware (database currently contains 29 files). Each file contains various fields that identify the optical hardware flown, describe the environment seen by that hardware, summarizes experimenter findings and list references for additional information. A copy of this database is available upon request.

LDEF NEWSLETTER

The LDEF *Newsletter*, now in its third year, continues to see its distribution expand to increasing numbers of universities, corporations, government agencies, and countries. From its initial distribution of under three

hundred names, the distribution (Figure 4) has reached a level of more than 2400; which includes pickup stacks at several NASA field center libraries and internal distribution in some corporations. This continuing circulation growth has been by word of mouth; there has never been any solicitation for increased distribution of the *Newsletter.*

The *Newsletter* has expanded from its initial eight-page issue to 24 pages or more as the LDEF investigation has begun to produce more results. The nominal length has hovered around an average of 16 pages which is near the limit for a one man level-of-effort but, more important, keeps the document at an easily readable and digestible length. The balance of size and frequency has appeared to be satisfactory for its specific purposes and there are no plans to deviate significantly in the foreseeable future.

The *Newsletter* has been serving as a useful interface between the engineering research and engineering applications communities (Figure 5), although with most of the information flow being LDEF research results transmitted to aerospace industry projects. There is some consideration being given to the notion of providing reverse information flow, since this communication "link" is well established, and using the *Newsletter* to transfer project information such as materials or design needs to the research community.

Several potential articles in this vein have been identified and are targeted for issues in the near future. However, as LDEF results continue to pour in, it will be a challenge to find time and space to present increased coverage within our current scope. At this time, significant LDEF activities have been slotted for each of the next four or five issues of the *Newsletter*, and in keeping with our charter, these will be receiving more attention and higher priority.

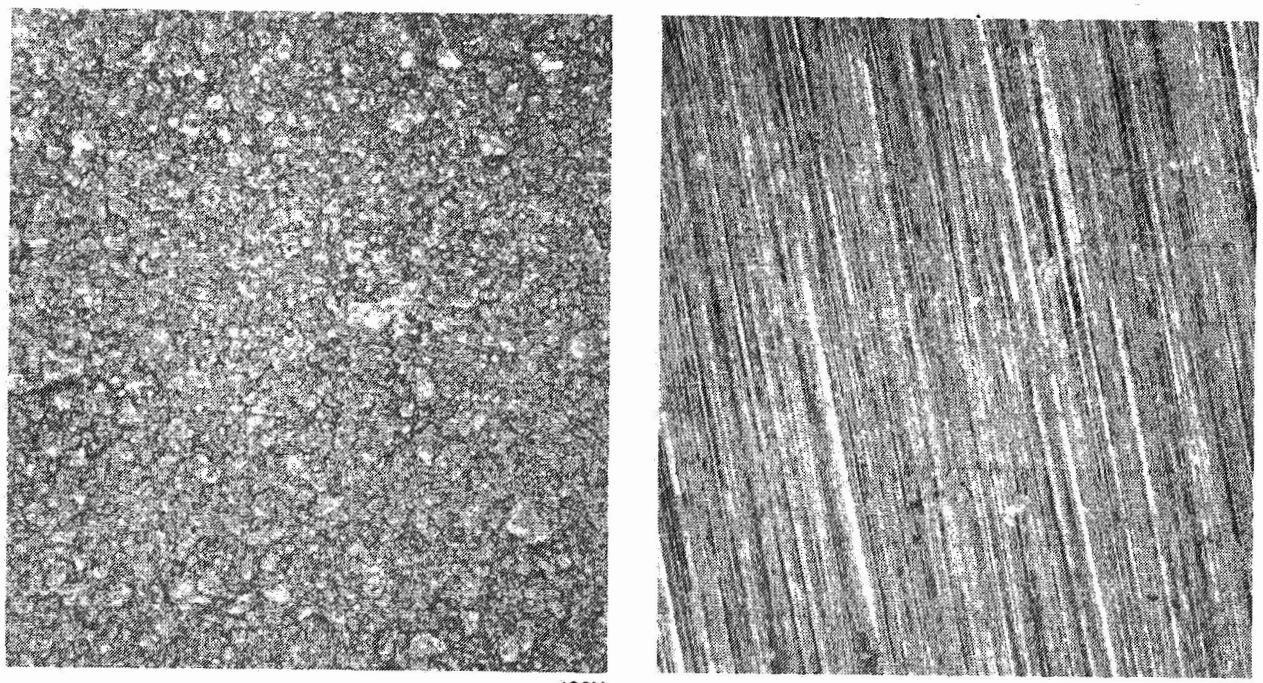

Non-flight Specimen 100X

LDEF Specimen 100X

Figure 1. Everlube 620C Lubricant

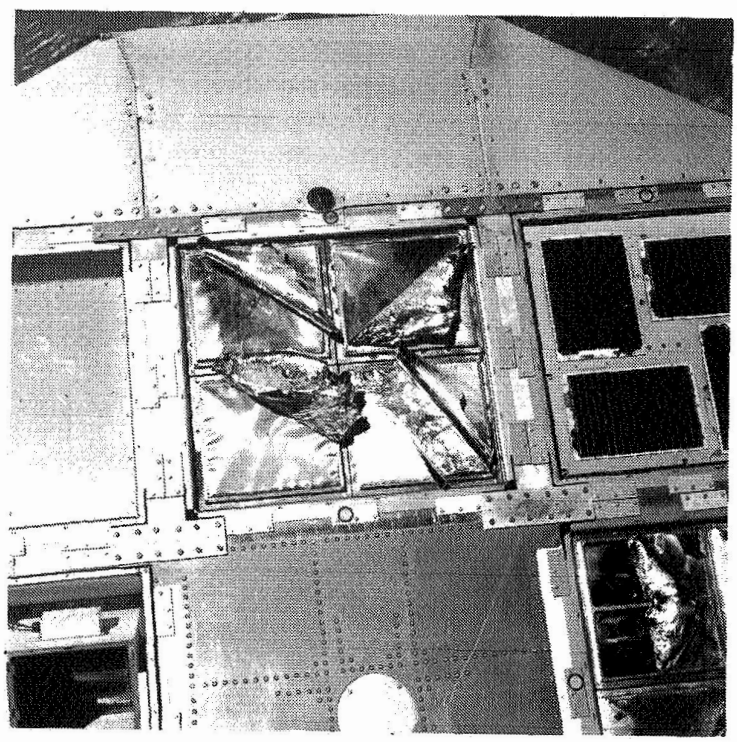

Figure 2. Loose Silverized Teflon Thermal Blankets

ORIGINAL PAGE
BLACK AND WHITE PHOTOGRAPH

ORIGINAL PAGE
BLACK AND WHITE PHOTOGRAPH

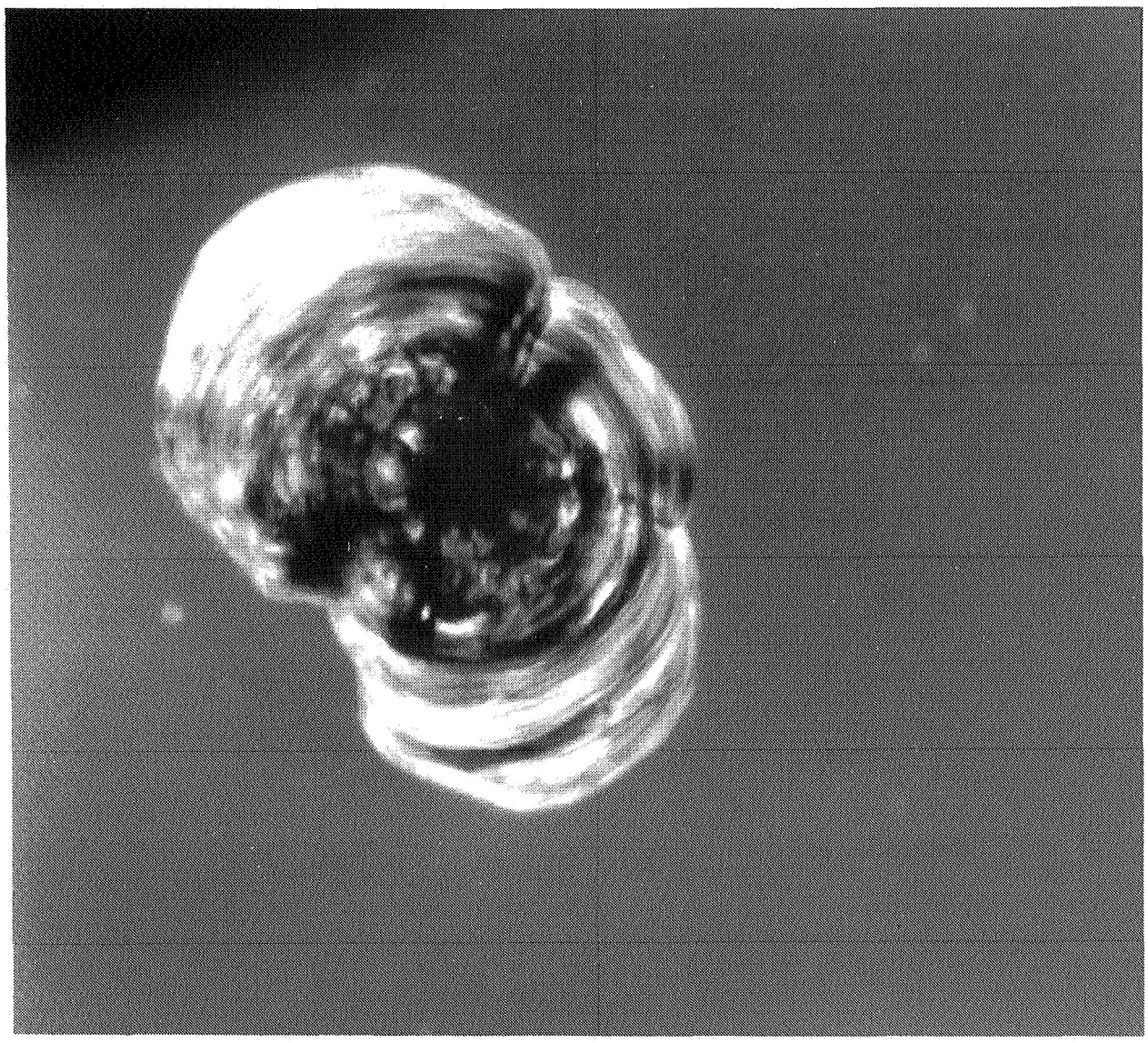

Figure 3. Effect of a Micrometeoroid on Debris Impact on a Quartz-Silver Second Surface Mirror

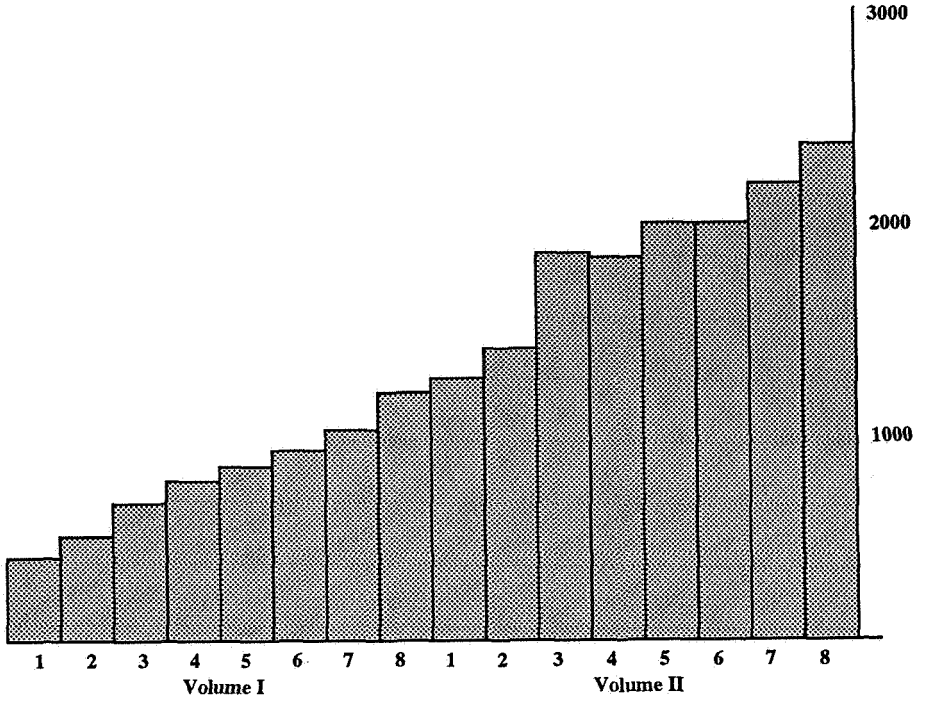

Figure 4
The chart above shows the continuing increase in the distribution of the LDEF Newsletter.

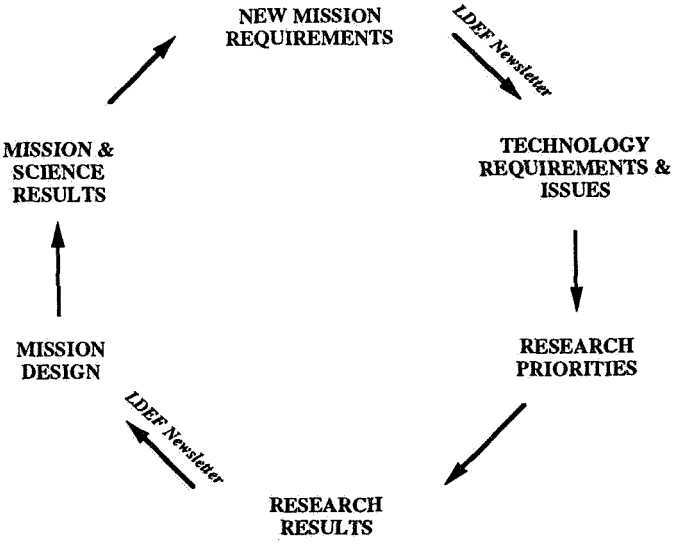

Figure 5
The chart above illustrates the dual role of the LDEF Newsletter in a simplified schematic of the relationship between the research and engineering communities.

N93-29684

501707
p.16

POST-FLIGHT ANALYSES OF THE CRYSTALS FROM THE M0003-14 QUARTZ CRYSTAL MICROBALANCE EXPERIMENT

W.K.Stuckey and G. Radhakrishnan
The Aerospace Corporation
2350 East El Segundo Blvd.
El Segundo, CA 90245
Phone: 310/336-7389, FAX: 310/336-5846

D. Wallace
QCM Research
PO Box 277
Laguna Beach, CA 92652
Phone: 714/497-5748, FAX 714/497-7331

SUMMARY

Quartz Crystal Microbalances constructed by QCM Research were flown on the leading and trailing edges of LDEF as one of the sub-experiments of M0003. Response of the crystals coated with 150 Å of In_2O_3 was recorded during the first 424 days of the mission. A second QCM with crystals coated with 150 Å of ZnS was also flown but not monitored. After the flight, the QCMs were disassembled and analyzed in The Aerospace Corporation laboratories. The samples included the crystals from the leading and trailing edge samples of both types of coatings along with the reference crystals, which were inside the QCM housing. Analyses were performed by scanning electron microscopy, energy dispersive X-ray analyses, X-ray photoelectron spectroscopy, ion microprobe mass analysis, and reflectance spectroscopy in the infrared and UV/visible regions. The crystals are contaminated predominantly with silicone compounds. The contamination is higher on the leading edge than on the trailing edge and higher on the exposed crystals than on the reference crystals.

I. INTRODUCTION

Quartz crystal microbalances (QCMs) were flown on the Long Duration Exposure Facility (LDEF M0003-14) by QCM Research, Laguna Beach, California, as contamination monitors. This sub-experiment was one of 19 sub-experiments that comprised the M0003 experiment assembled by The Aerospace Corporation. The QCMs used 10-MHz quartz crystals with two types of coatings. One set of leading and trailing edge QCMs consisted of crystals with 9000Å of aluminum and aluminum oxide (Al + Al_2O_3), and a top layer of 150 Å of indium oxide (In_2O_3). The second set of crystals on the leading and trailing edges consisted of 9000 Å (Al + Al_2O_3) and a top layer of 150 Å zinc sulfide (ZnS). Each of the QCMs consists of a pair of crystals, one exposed to the environment and termed the "sense" crystal, and one that remained unexposed and, hence, termed the "reference" crystal. The beat frequency monitored between the "sense" and "reference" crystals represents the change in mass of the "sense" crystal as a result of exposure, relative to the unexposed "reference" crystal.

The QCM response was recorded for about 14 months, the lifetime of the data acquisition batteries. The crystals continued to be exposed to the Low Earth Orbit Environment on Row 9 on the leading edge of LDEF and Row 3 on the trailing edge for the entire LDEF mission, even though the response was no longer recorded. An analysis of the crystals was performed at The Aerospace Corporation after retrieval to deter-

mine the accumulated contamination deposition and the effects of exposure of the crystals to the space environment.

II. QUARTZ CRYSTAL MICROBALANCE DATA

On-orbit information was recorded by the Experiment Power and Data System (ref. 1) from various sensors located throughout the four experiment trays constituting the M0003 experiment. Special circuits were included to measure QCM frequency, which allowed monitoring the frequency of one set of the crystals during the data acquisition part of the mission. The crystals with the In_2O_3 coating were selected for the on-orbit data acquisition. Data were recorded in bursts lasting a period of 111.7 min (about one LDEF orbit). During this 111.7-min period, each data channel was scanned 32 times, producing a profile for the entire orbit. After the burst period, the data system rested for 93.16 h before the start of the next burst period. Data were taken in this manner until the end of the recording media was reached, 424 days after launch. The maxima and minima frequencies recorded for the leading and trailing edge QCMs during each period are shown in Fig. 1. The variation is due to the temperature response of the QCMs during each orbit. The variations in the maxima response curves are consistent with the temperature response variations due to the solar exposures. Note that the trailing edge QCM indicates a slight increase in weight during the 424-day data acquisition period while the leading edge shows an apparent weight loss.

III. ANALYSES OF QCM CRYSTALS

Post-flight analysis of the separate quartz crystals (QCs) constituting the QCMs has been performed at The Aerospace Corporation in an effort to determine the effects of the 69-month-long exposure on the surface composition of the crystals. The frequency and temperature response curves of the QCMs were measured by QCM Research, following which they were disassembled and then cleaned with acetone and hexane. The individual crystals were then brought to The Aerospace Corporation for analysis. The QCs are numbered 1-8 in the following sections, in correspondence with the numbering sequence in Table 1.

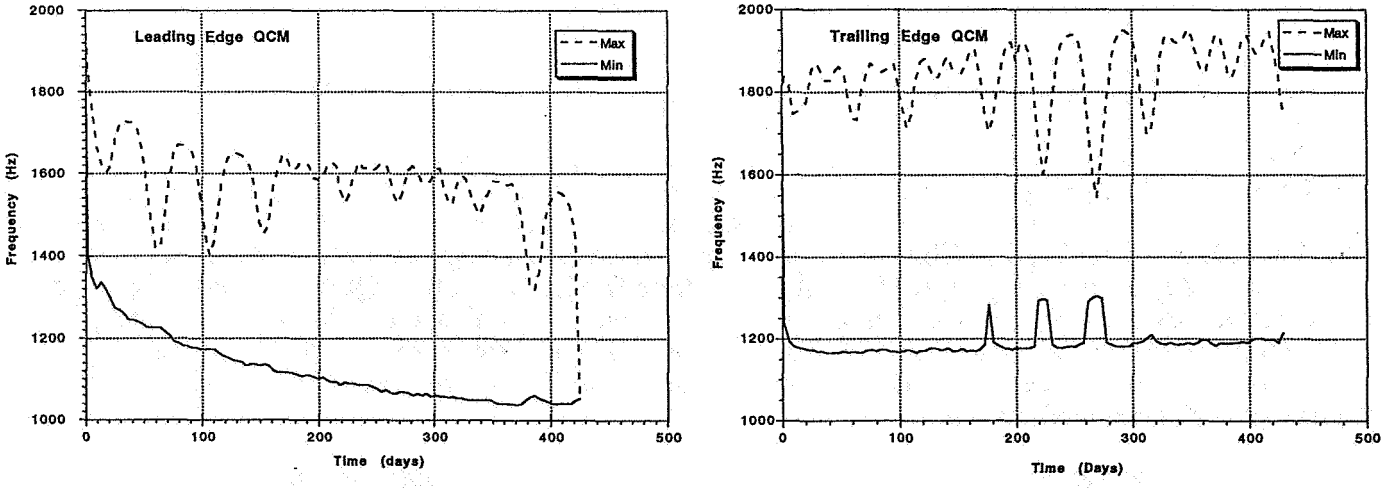

Figure 1. Quartz crystal microbalance data recorded on LDEF.

Table 1. Quartz Crystal Identification.

QC#	QCM Location	QCM#	Composition	LDEF Position
1	Sense	TP329	Al + Al_2O_3 (9000 Å) / In_2O_3 (150 Å)	Leading Edge, Active
2	Reference	TP329	Al + Al_2O_3 (9000 Å) / In_2O_3 (150 Å)	Leading Edge, Active
3	Sense	TP330	Al + Al_2O_3 (9000 Å) / ZnS (150 Å)	Leading Edge, Passive
4	Reference	TP330	Al + Al_2O_3 (9000 Å) / ZnS (150 Å)	Leading Edge, Passive
5	Sense	TP318	Al + Al_2O_3 (9000 Å) / In_2O_3 (150 Å)	Trailing Edge, Active
6	Reference	TP318	Al + Al_2O_3 (9000 Å) / In_2O_3 (150 Å)	Trailing Edge, Active
7	Sense	TP353	Al + Al_2O_3 (9000 Å) / ZnS (150 Å)	Trailing Edge, Passive
8	Reference	TP353	Al + Al_2O_3 (9000 Å) / ZnS (150 Å)	Trailing Edge, Passive

Table 2. Large Area EDAX Analyses at 5 kV with Sample Surface at Normal Incidence (4 mm x 5 mm), and with Sample Surface Inclined 60° (2 mm x 5 mm).

Sample	QC	Sample Orientation	Atomic %				
			In	Zn	Si	Al	S
In_2O_3 Leading Edge	Sense #1	0°	19	n.d.	2.9	79	n.d.
		60° tilt	22	n.d.	7.8	70	n.d.
	Ref. #2	0°	19	n.d.	n.d.	81	n.d.
		60° tilt	21	n.d.	7.9	71	n.d.
ZnS Leading Edge	Sense #3	0°	n.d.	2.2	2.6	94	1.3
		60° tilt	n.d.	2.9	5.5	87	4.2
	Ref.#4	0°	n.d.	4.2	5.0	83	7.5
		60°tilt	n.d.	5.6	5.2	75	14
In_2O_3 Trailing Edge	Sense #5	0°	21	n.d.	2.0	77	n.d.
		60° tilt	24	n.d.	1.3	75	n.d.
	Ref. #6	0°	20	n.d.	0.7	80	n.d.
		60° tilt	21	n.d.	4.0	75	n.d.
ZnS Trailing Edge	Sense #7	0°	n.d.	6.0	0.8	85	8.0
		60° tilt	n.d.	8.5	4.5	72	15
	Ref. #8	0°	n.d.	5.4	n.d.	86	8.4
		60° tilt	n.d.	7.4	7.9	69	16

A. SEM / EDAX Measurements

SEM photographs of all the crystals were obtained at magnifications of X10, X50, X1000, and X5000. More revealing are the large area EDAX measurements (spanning an area of 10 to 20 mm^2) shown in Table 2. Elements not detected are marked n.d. The detection of silicon (Si) with the probe beam at normal incidence to the sample at 5 kV suggests the presence of Si primarily as a contaminant on the surface of these crystals and to a lesser extent coming from the underlying quartz. To further enhance contributions of elements present on the surface and better identify contaminants on the surface of the crystals, data were taken with the sample tilted 60° with respect to the probe beam. As seen in Table 2, the 5-kV measurements performed with tilted samples confirm the presence of Si primarily as a contaminant on the surface. For the In_2O_3-coated crystals, on the leading edge, in both the sense and reference crystals 1 and 2, a significantly

higher concentration of Si (factor of 3 or more) is detected on the tilted sample relative to the untilted sample. It should also be pointed out that in both crystals, the levels of In detected in the tilted samples are just slightly higher than the corresponding untilted samples, while the levels of Al are lower on the tilted samples, suggesting that Al is a bulk component. The concentrations of In, Si, and Al are observed to be nearly equal on the sense and reference crystals on the leading edge. On the trailing edge samples 5 and 6, while the behavior of In and Al are quite similar to the leading edge counterparts 1 and 2, it can be seen that the detected levels of Si on the trailing edge are (i) not as high as on the leading edge and (ii) higher on the reference crystal 6 than on the sense crystal 5. This suggests that on the In_2O_3 samples, there is (i) higher surface contamination by Si on the leading edge crystals than on the trailing edge crystals, and (ii) on the trailing edge, a slightly higher contamination on the reference crystal than on the corresponding sense crystal. A comparison of Figs. 2 and 3 clearly shows the higher Si levels on the leading edge In_2O_3 crystals.

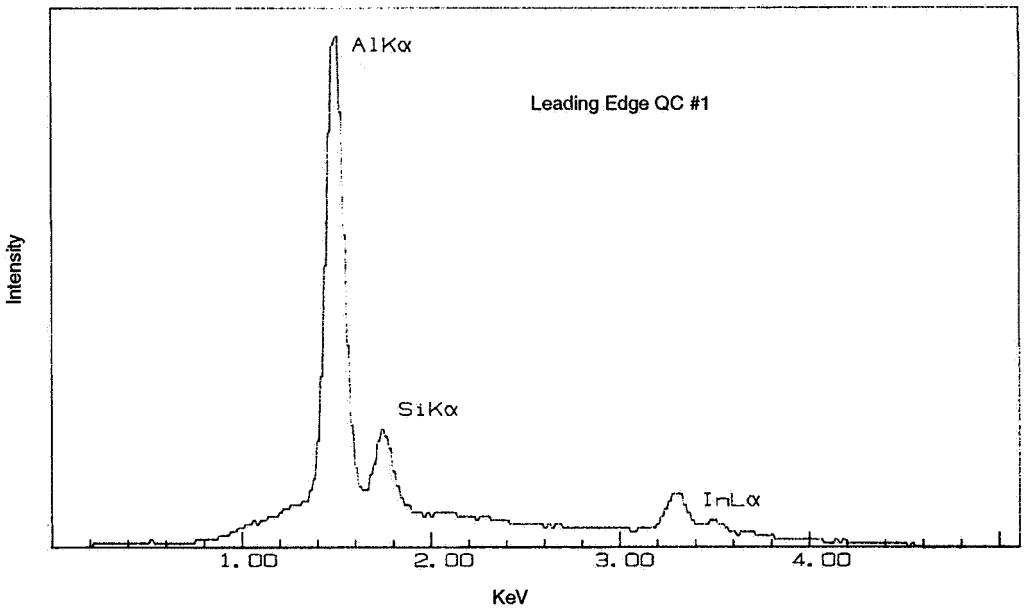

Figure 2. EDX Spectrum of Leading Edge In_2O_3 Crystal (QC #1)

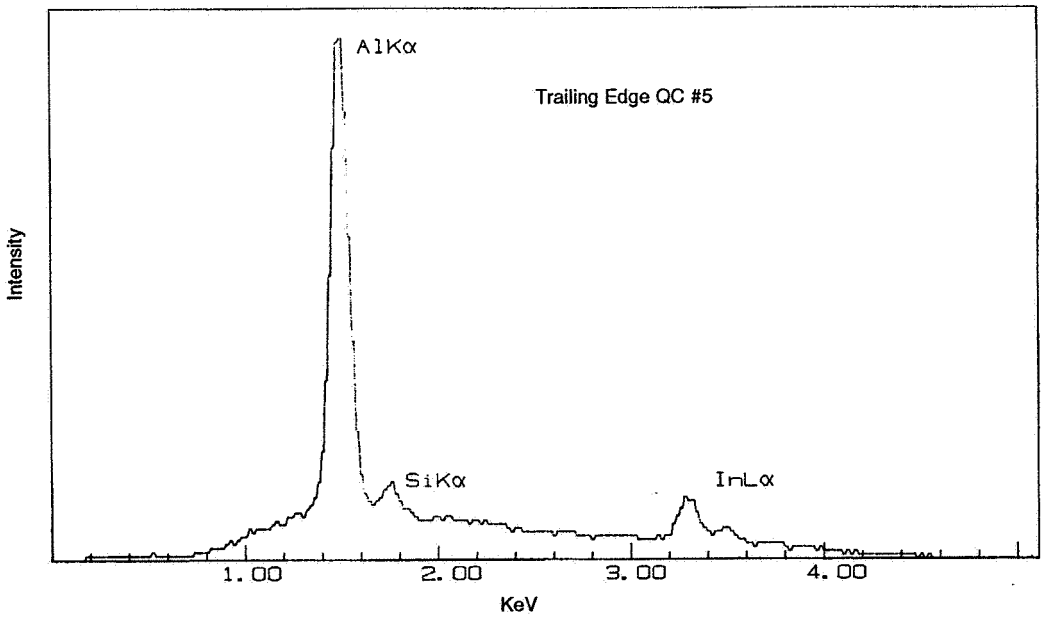

Figure 3. EDX Spectrum of Trailing Edge In_2O_3 Crystal (QC #5)

With the ZnS coated crystals, it is observed that on the leading edge, while the sense crystal 3 shows a factor of 3 higher Si when tilted, the reference crystal 4 shows no measurable difference in Si levels with tilt. On the trailing edge crystals 7 and 8, however, there appears to be significantly higher levels of Si on tilting the crystals. All four crystals show an increase in concentration of both Zn and S when tilted. While the increase in Zn is nearly the same in all four samples (~ 1.3), the concentration of S increases by a factor of ~3 in QC 3 and ~2 in QCs 4, 7, and 8. The results can be summarized as (i) higher Si contamination on the sense crystal on the leading edge than on the sense crystal on the trailing edge, but a higher Si contamination on the reference crystal on the trailing edge than on the leading edge, (ii) comparing sense crystal 3 with reference crystal 4 on the leading edge and with crystals 7 and 8 on the trailing edge, it is observed that although the increase in the Zn and S concentrations on tilting are comparable, the ZnS coating appears to have thinned in sense crystal 3, as indicated by considerably lower percentages of both Zn and S in QC 3 relative to QCs 4, 7, and 8. While these measurements were not performed before flight, all samples were deposited such that the coatings should have been identical.

B. XPS Analyses

The instrument used for analysis was a VG ESCALAB MK II. A Mg Kα X-ray source (hν = 1253.6 eV) was chosen for irradiation. Base pressure during analysis was approximately 5 x 10^{-} torr. Secondary electron imaging was used to align each crystal for XPS analysis to ensure that edge effects were minimized. The analysis on these crystals was performed as received, and the analysis area was approximately 4 mm x 5 mm. XPS analyses were conducted on all of the above crystals. XPS is a very surface sensitive technique, probing only about 100 Å of the outermost surface.

A comparison of leading edge crystals (1, 2, 3, and 4) vs trailing edge crystals (5, 6, 7, and 8) indicates that there is a higher percentage Si coverage on the leading edge. In addition, a comparison of the sense crystals vs the reference crystals indicates a higher percentage Si coverage on the sense crystals. The results are tabulated in Table 3 . A comparison of the XPS data and the 5-kV EDAX data reveals several interesting features. These are discussed below, taking pairs of sense and reference crystals one at a time on the leading and trailing edges.

Table 3. XPS analyses of QC surfaces (n.d. = not detected and tr = trace)

		Surface Mole % (Normalized)													
Sample	QC	C	O	Si	In	Sn	Zn	S	Pb	K	Na	N	Cl	Al	Ag
In_2O_3 Leading Edge	Sense #1	17	58	23	0.7	0.2	n.d.	0.1	n.d.	tr	0.3	0.8	tr	n.d.	n.d.
	Ref. #2	53	31	1.9	6.4	1.0	0.1	0.1	0.5	0.1	1.0	4.5	0.2	n.d.	n.d.
ZnS Leading Edge	Sense #3	48	35	10	n.d.	0.2	0.9	0.5	0.1	tr	0.4	3.5	0.1	1.4	n.d.
	Ref.#4	61	23	1.0	n.d.	0.2	2.0	5.5	0.3	tr	0.7	4.7	0.4	n.d.	1.2
In_2O_3 Trailing Edge	Sense #5	68	25	1.5	n.d.	0.3	n.d.	0.1	0.3	n.d.	0.1	4.7	0.2	0.4	n.d.
	Ref. #6	65	24	0.2	2.3	0.7	0.1	0.2	0.4	n.d.	0.1	6.3	0.1	n.d.	n.d.
ZnS Trailing Edge	Sense #7	67	25	2.3	n.d.	0.4	0.1	0.1	0.4	n.d.	0.1	4.5	0.3	n.d.	n.d.
	Ref. #8	68	20	n.d.	n.d.	0.3	1.4	3.9	0.3	tr	0.3	4.1	0.3	n.d.	0.6

QC 1 (Sense) and QC 2 (Reference): 150 Å In_2O_3 Coating; Leading Edge

In crystals 1 and 2, while EDAX measured nearly equal percentages of In (19% or ~22% when tilted), XPS analyses indicated nearly an order of magnitude lower value of In in the sense crystal 1 (0.7) compared to the reference crystal 2 (6.4). XPS also indicated a much higher Si coverage on the sense crystal (23) than on the reference crystal (1.9), also illustrated in Figs. 4 and 5. The data suggest that in crystal 1, surface

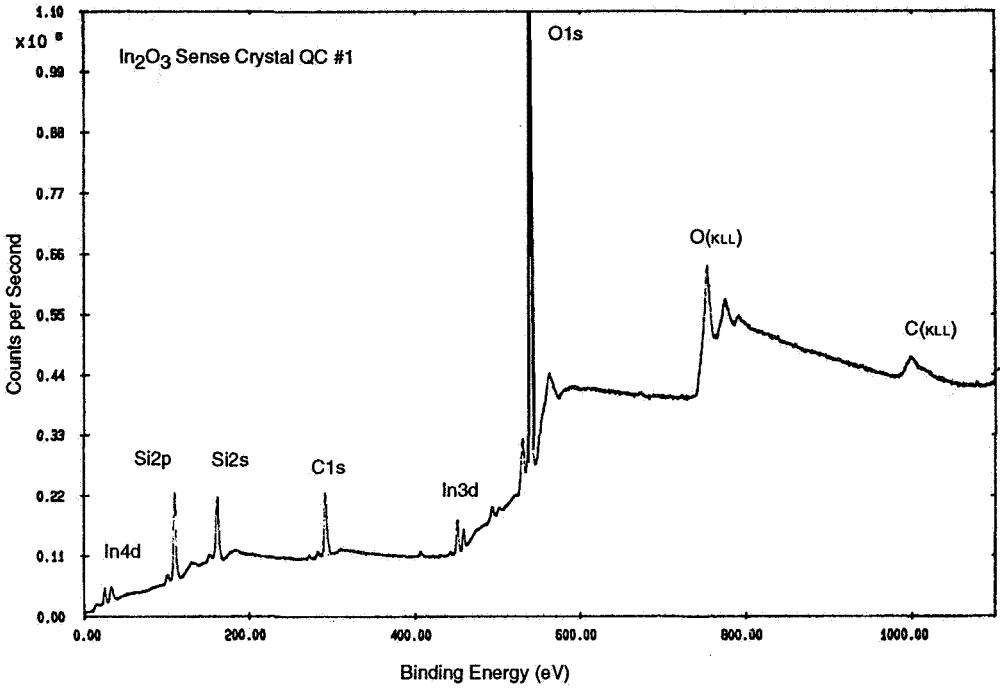

Figure 4. XPS Spectrum of Leading Edge In_2O_3 Sense Crystal (QC #1)

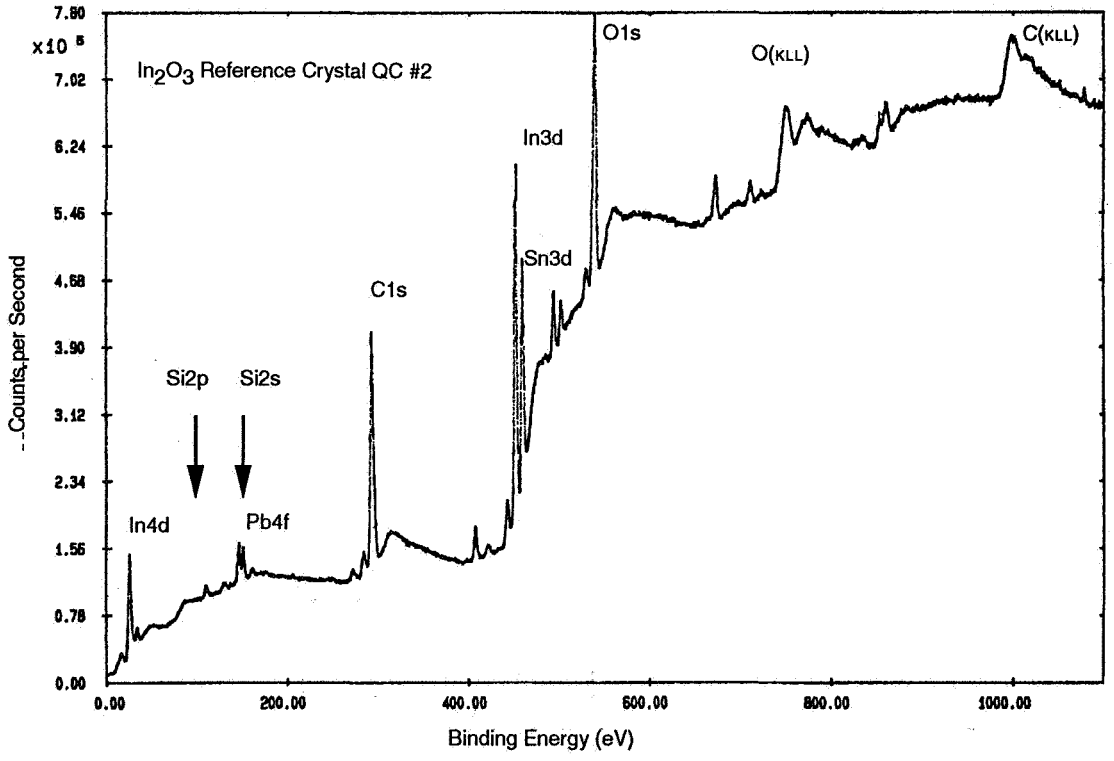

Figure 5. XPS Spectrum of Leading Edge In_2O_3 Reference Crystal (QC #2)

contamination and coverage of the In_2O_3 layer by Si could most likely be the cause of the lower In content as detected by XPS. While these results are in qualitative agreement with the normal incidence EDAX data, the tilted EDAX data do not indicate a difference in Si between QC 1 and QC 2.

QC 5 (Sense) and QC 6 (Reference) : 150 Å In_2O_3 Coating; Trailing Edge

Similar to the leading edge pair 1 and 2, EDAX measurements indicate nearly equal percentages of In in the sense and reference pairs 5 and 6 on the trailing edges (~21% and an average of ~22 % when tilted). In is not detected on the sense crystal 5 by XPS analysis, while it is detected in the reference crystal 6 (2.3). This appears to be consistent with the fact that a factor of 7 higher Si concentration is measured on the sense crystal 5 by XPS, in comparison to the reference 6. Again, the normal incidence EDAX results are in qualitative agreement with the XPS results, indicating a factor of 3 higher Si concentration on the sense crystal 5 relative to reference 6. However, the tilted EDAX measurements show a reverse trend.

QC 3 (Sense) and QC 4 (Reference) : 150 Å ZnS Coating; Leading Edge

In this pair of crystals, both XPS and EDAX measurements are in agreement with respect to the nearly 50% lower Zn concentration on the sense crystal 3 compared to the reference crystal 4. While XPS measures a much lower S concentration on QC 5 than on QC 6 (factor of 11), EDAX results show a smaller difference (~factor of 5). There is a discrepancy in the amounts of Si detected by these two methods, whereby XPS indicates a 10-to-1 ratio of Si between the sense and reference, while normal incidence EDAX indicates a reverse trend with a 50% higher Si concentration in the reference sample, and tilted EDAX shows no measurable difference.

QC 7 (Sense) and QC 8 (Reference) : 150 Å ZnS Coating; Trailing Edge

In this case, EDAX measures nearly equal concentrations of Zn (~6% and ~8% when tilted) as well as of S (~8% and ~16% when tilted) on the sense and reference crystals. XPS measures significantly lower concentrations of both Zn and S in the sense crystal (Zn: 0.1, S: 0.1) than in the reference crystal (Zn: 1.4, S: 3.9). With both XPS and normal incidence EDAX, Si is only detected on the sense crystal, not on the reference crystal. However, with tilted samples, a reverse trend is observed, and more Si is detected on the reference crystal than on the sense crystal. The XPS data are once again suggestive of Si coverage on the sense crystal, which will attenuate the amount of Zn detected.

C. SIMS Analyses and Depth Profiling

To gather more information on the Si contamination and coverage issues, depth profiles using the secondary ion mass spectrometry (SIMS) technique were made on each of the QCM samples. A thin film of carbon was first deposited on the surface of all the samples to minimize charging, and the analyses were performed by sputter etching through the carbon film. This technique worked well on the In_2O_3-coated crystals. It did not work as well on the ZnS-coated crystals.

Depth profiles and elemental analyses were made with an Applied Research Laboratories (ARL) ion microprobe mass analyzer (IMMA) using a 1 nA primary beam of oxygen ($^{18}O_2^+$) ions accelerated to 4.5 kV and focused to approximately 15 μm in diameter. The primary beam was rastered over an area measuring 100 μm x 80 μm, and data was collected from the center utilizing an electronic aperture to minimize

contribution from the crater edges. The IMMA detects secondary ions emitted from the surface in the area probed by the primary ion beam. The depth profiles were made following elements of each of (a) the contaminants (Si, K, Mg), (b) the coating (In, Zn), and (c) the substrate (Al).

Silicon, presumably from silicone, was detected on the surfaces of QCs 1, 3, 5, and 7. In addition to the elements given in Table 4, a significant Pb peak (Pb/Zn = 0.381) was detected on reference QC 8. The K appears to have been deposited with the Si, and its origin is unknown at this time. The source of the Mg detected is also unknown. Table 4 gives the ratio of the major ions of these elements detected at the surface of the coatings with respect to an element of the coating. The ratios are the peak level of a contaminant element ion vs the peak level of a coating element ion. A survey of the table shows that the Si+ intensity (a) is approximately 1 to 2 orders of magnitude higher on the sense crystals compared to the reference crystals, and (b) appears to be approximately an order of magnitude higher on the leading edge sense crystals compared to the trailing edge sense crystals.

Table 4. Ratios of Elements at QC Surfaces detected by SIMS Analysis

		Ion Ratios		
Sample	QC	Mg^+/In^+	Si^+/In^+	K^+/In^+
In_2O_3 Leading Edge	Sense #1	0.058	0.27	0.094
	Ref. #2	0.00060	0.0010	0.019
In_2O_3 Trailing Edge	Sense #5	0.0067	0.036	0.31
	Ref.#6	0.0012	0.0015	0.014
		Mg^+/Zn^+	Si^+/Zn^+	K^+/Zn^+
ZnS Leading Edge	Sense #3	0.43	63	60
	Ref. #4	0.13	0.41	5.1
ZnS Trailing Edge	Sense #7	0.17	6.8	25
	Ref. #8	0.35	0.41	18

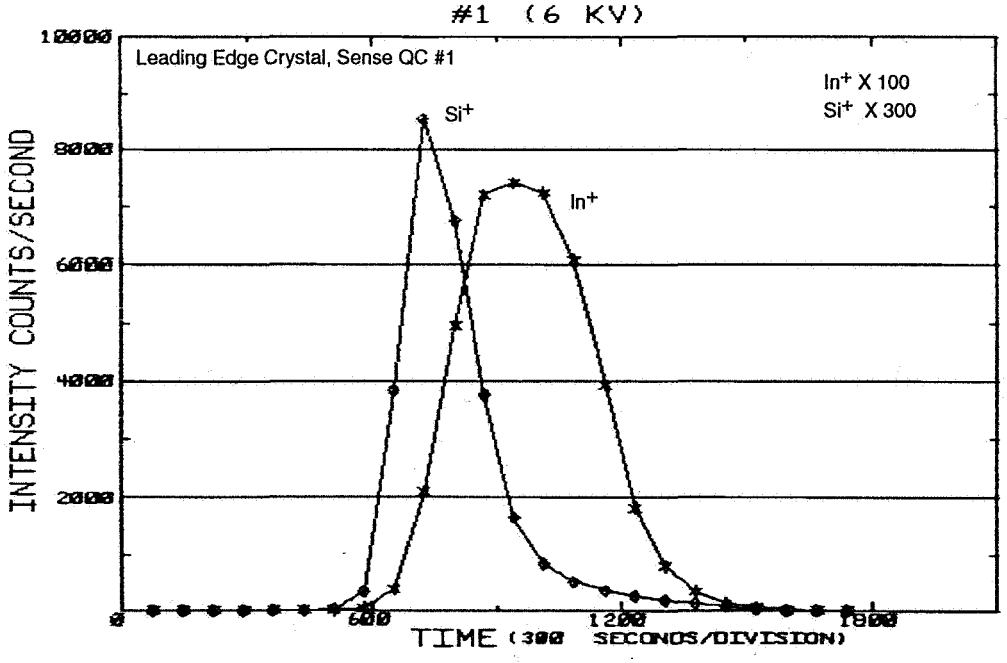

Figure 6. SIMS depth profiles on Si^+ and In^+ (leading edge, sense crystal, #1).

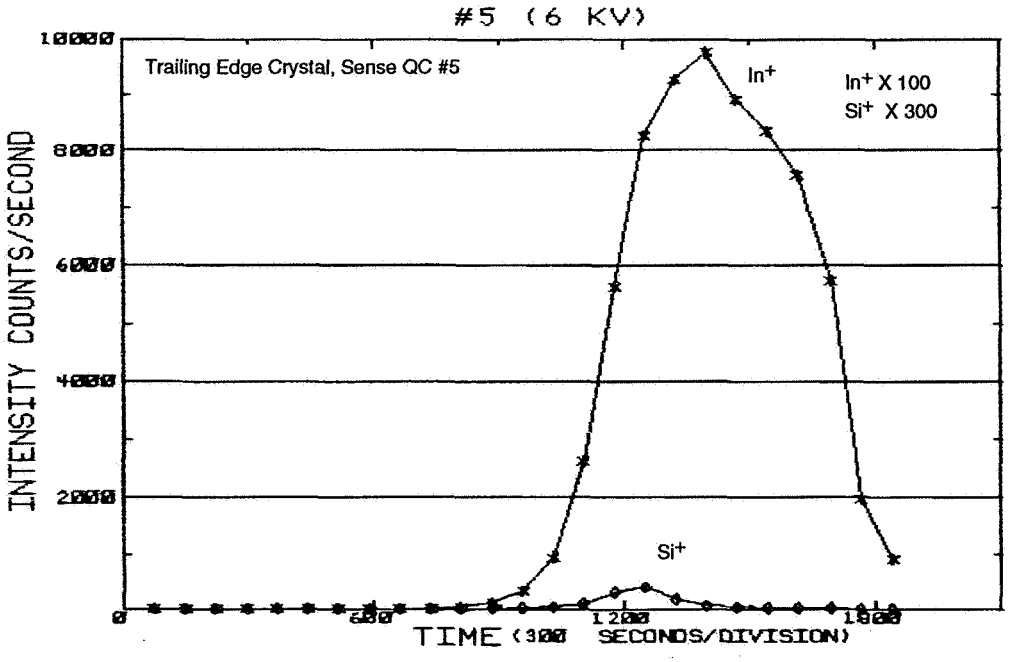

Figure 7. SIMS depth profiles on Si^+ and In^+ (trailing edge, sense crystal, #5).

deposited on the surface prior to analysis. On the sense crystal 1, a layer of Si occurs above the In_2O_3 layer. On the reference crystal 2, there is no distinct indication of Si coverage of the In_2O_3 layer. The presence of a significantly smaller Si layer above the In_2O_3 layer is detected on the sense crystal 5 in Figure 7, while on the reference crystal 6, Si is not present on the surface. Similar results are obtained from the ZnS-coated crystals although interpretation is hindered by charging of the sample upon reaching the ZnS layer.

D. FTIR Measurements

Infrared spectrometric analysis was performed with a Nicolet MX-1 Fourier Transform Infrared (FTIR) spectrometer, using the specular reflectance technique. Infrared radiation in the region 4000 to 400 cm^{-1} was obtained from a Globular Source. The beam was 5 mm in diameter at the sample. One hundred and twenty eight scans were taken for each sample at 3 to 4 seconds per scan with a resolution of 2 cm-1. Infrared spectroscopy is a surface-sensitive technique with a probing depth of < 0.5 μm. The FTIR spectra of the leading and trailing edge crystals are shown in Figs. 8 and 9. Important qualitative information may be derived from these measurements, and the results are summarized below.

An absorption characteristic of the Si-O stretching vibration (refs. 2 and 3) is observed on the leading edge sense crystals 1 and 3 at 1061 cm^{-1}. The most noticeable observation about these spectra is the absence of absorption at 1061 cm^{-1} on the leading edge reference crystals 2 and 4, as well as on all the trailing edge crystals 5 through 8. Since we know from the other measurements that Si is indeed present on the surface of the sense crystals on both the leading and trailing edges, results from the FTIR spectra must be interpreted as a measure of the relative concentrations of Si on the leading vs the trailing edges, as well as sense vs reference crystals, scaled by the sensitivity of this measurement.

Other absorptions due to C-H, C=O, and C=C stretching vibrations and C-H deformations were observed in both the leading and trailing edge crystals at approximately the same frequencies. All the crystals indicate the presence of C-H vibrations (refs. 2 through 4) in the range 2900 to 2500 cm^{-1}. In QC 3, there is

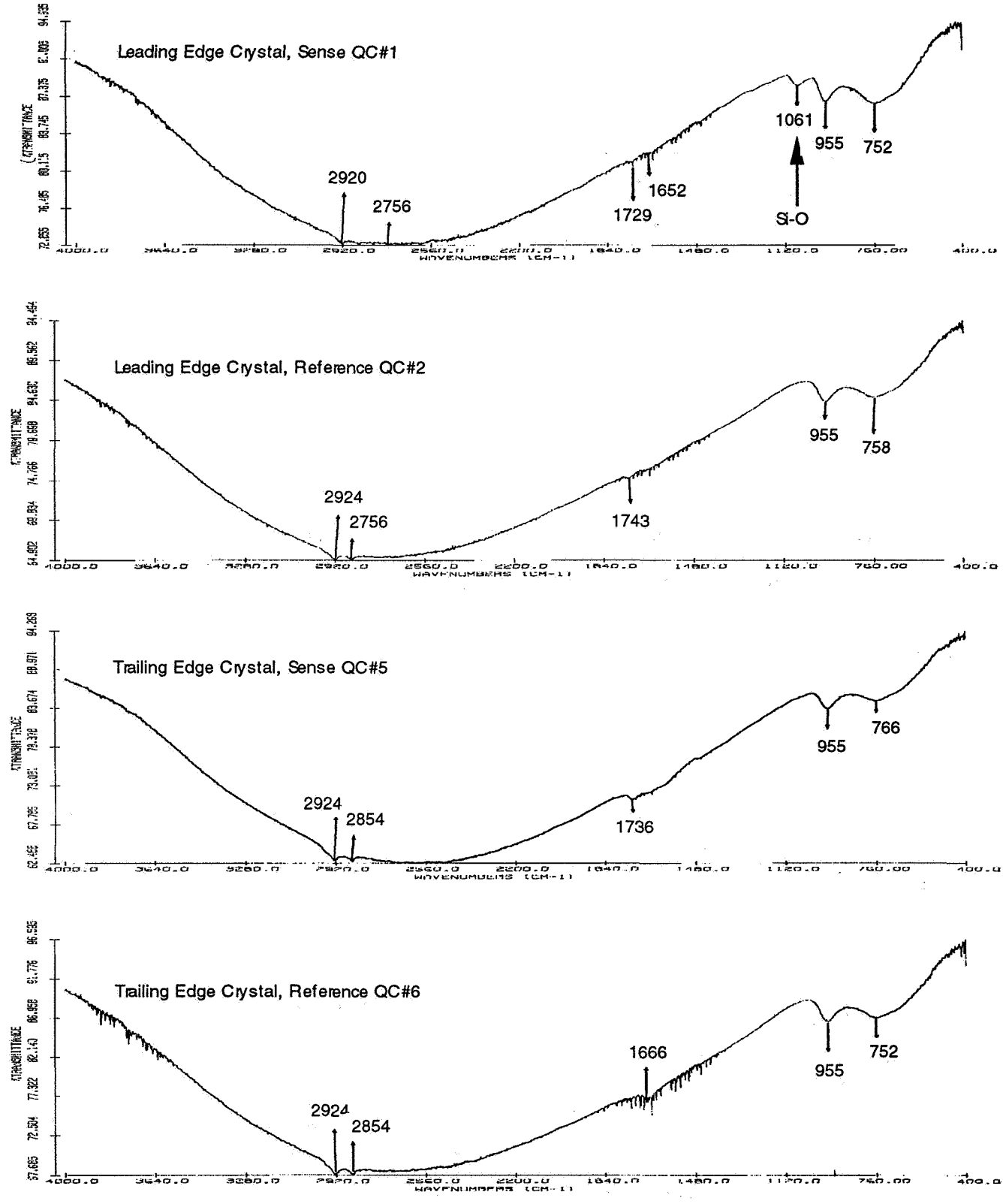

Figure 8. FTIR spectra of In_2O_3 crystals.

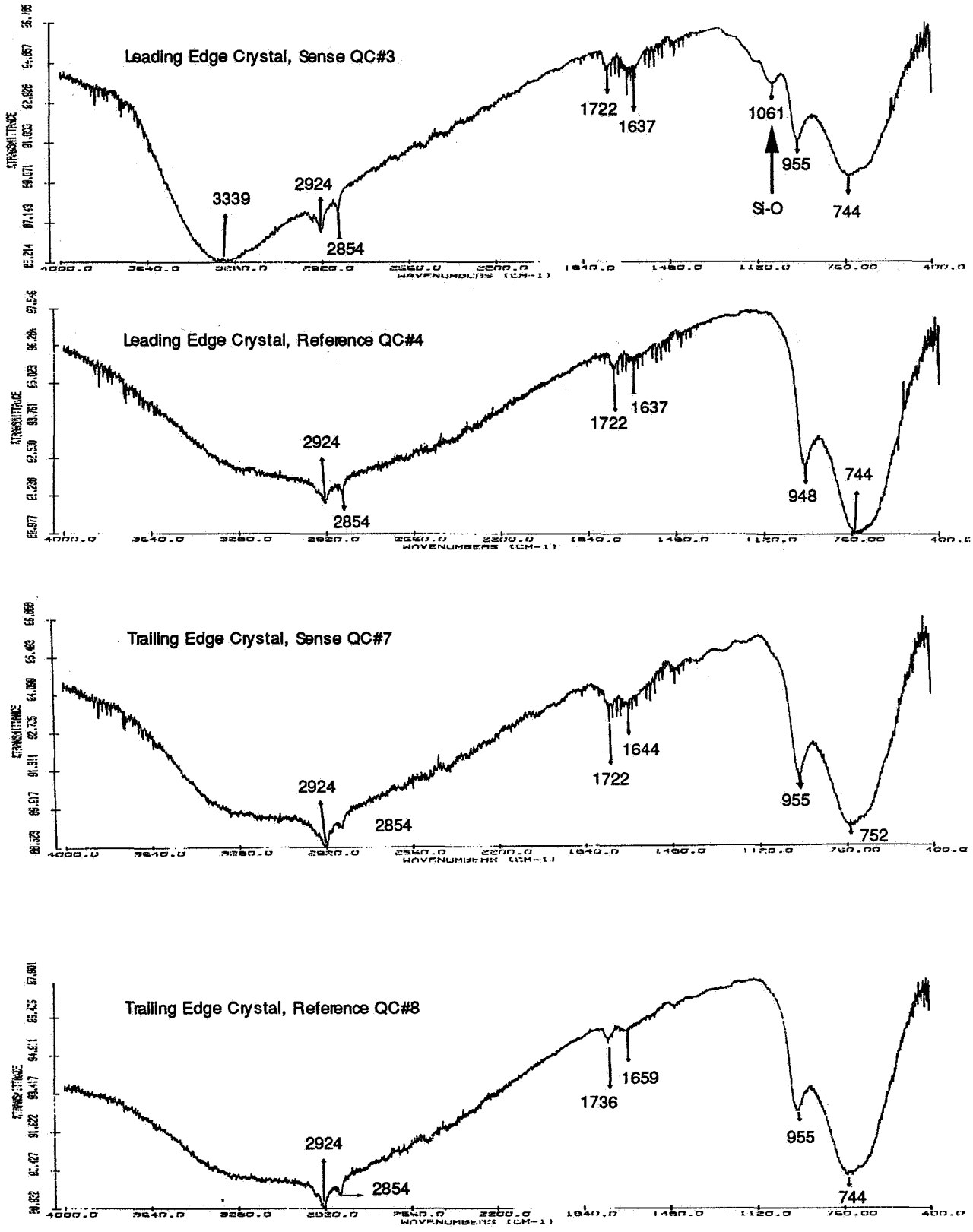

Figure 9. FTIR spectra of ZnS crystals.

strong absorption at 3339 cm^{-1}, which is due to the O-H stretch from water or alcohols on the surface.(ref. 4) A weak absorption at ~1740 cm^{-1}, seen in crystals 3, 4, 5,7, and 8 with varying intensities, is due to a carbonyl C=O group on the surface (ref. 4), while the most likely assignment of another weak absorption at ~ 1640 cm^{-1} seen in crystals 3, 4, 6, 7, and 8 is the C=C stretch from unsaturated hydrocarbons (ref. 4). An absorption at 955 cm^{-1} appears fairly consistently at the same position in all crystals with the exception of sample 4 where this peak is shifted to 948 cm^{-1}. Although the assignment of the absorption at 955 cm^{-1} remains ambiguous at the present time, it is most likely due to C-H deformations from alkenes (ref. 4). Other likely causes for this absorption could be the symmetric and asymmetric bends from SiH_3 or an Si-O-R (aromatic) stretching vibration. Shifts in the Si-O stretching vibrations, which generally occur in the range 1110 to 1000 cm^{-1}, from either Si-O-R (aliphatic) or Si-O-Si, may be alternative explanations (refs. 2 through 4). An absorption that generally appears in the range 760 to 740 cm^{-1} in both the leading and trailing edge crystals is found to be always shifted to higher frequencies in the sense crystals compared to the corresponding reference crystals. The most likely assignment of this absorption is the Al-O stretch (ref. 3) from the aluminum oxide layer present in all the crystals. C-H deformations due to alkanes (ref. 4) could also contribute to absorption at this frequency. Changes in local environment, especially on the sense crystals, could account for the shifts in the position of this peak.

E. Reflectance Measurements

Uncorrected diffuse reflectance was measured as a function of wavelength for each pair of sense-reference crystals on the leading and trailing edges. A Perkin Elmer Lambda-9 spectrophotometer was used for measuring the reflectance of the crystals. The light source was a deuterium lamp for the spectral range 319 nm to 250 nm. A halogen lamp was used for visible and infrared wavelengths longer than 300 nm. The reflected beam was collected by a lead sulfide detector for the infrared and a photomultiplier tube for the visible range. The data are given in Figs. 10 through 13. It should be pointed out that due to

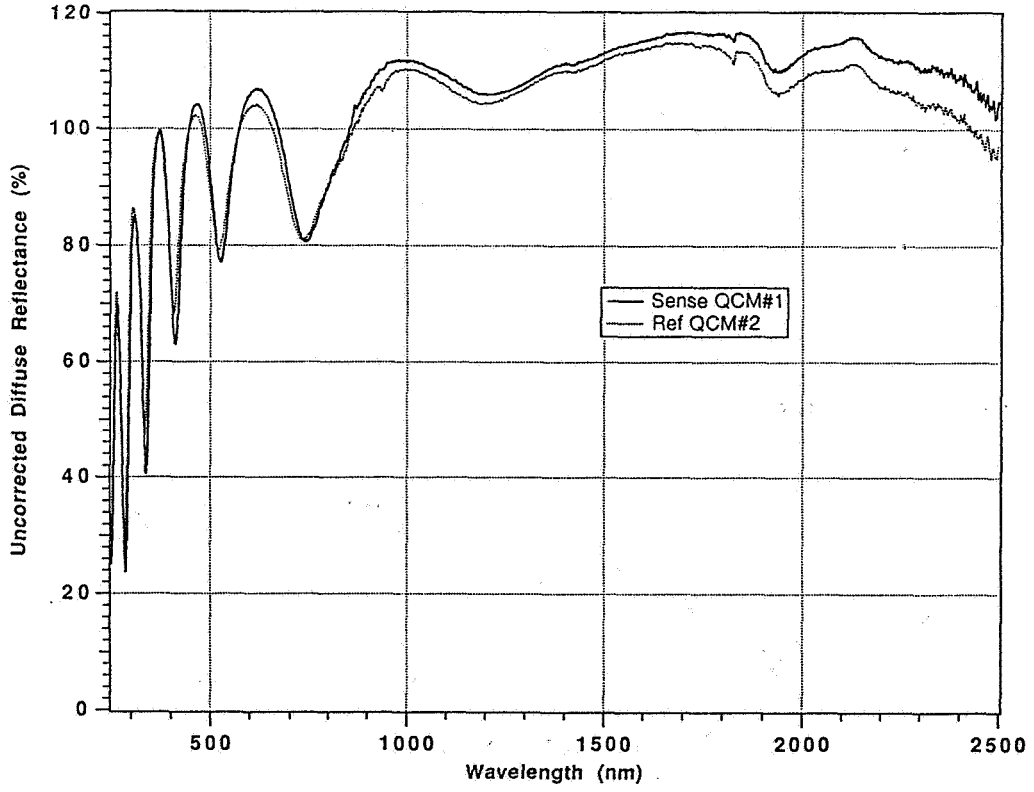

Figure 10. Diffuse reflectance spectra of leading edge crystals 1 and 2.

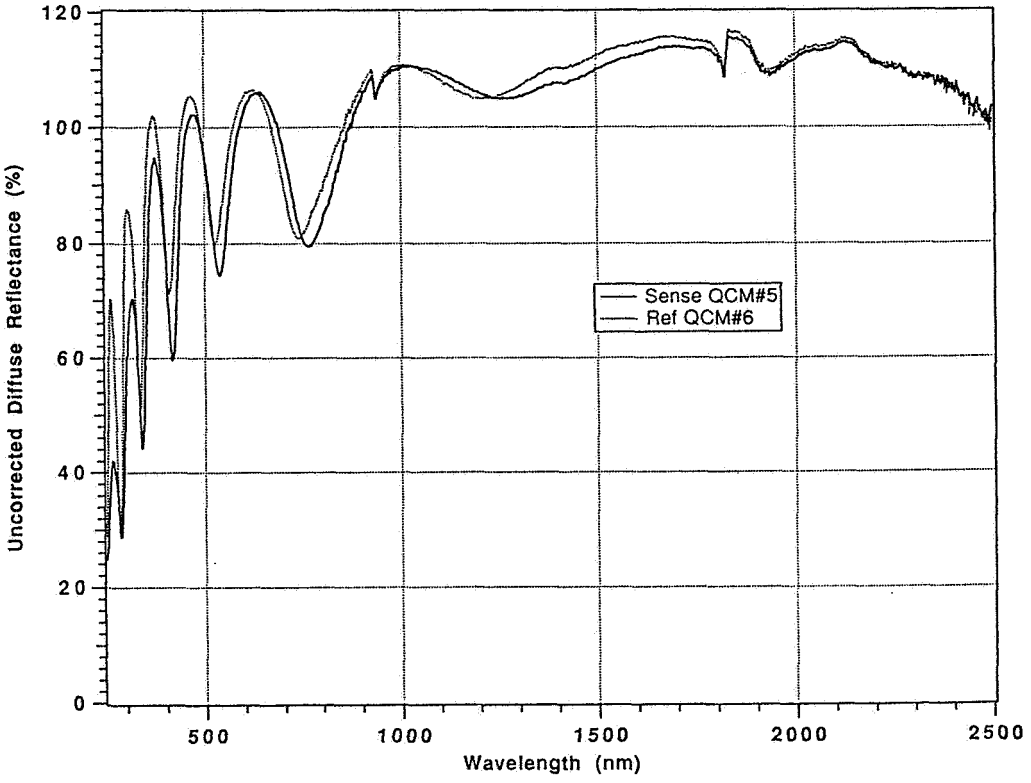

Figure 11. Diffuse reflectance spectra of leading edge crystals 3 and 4.

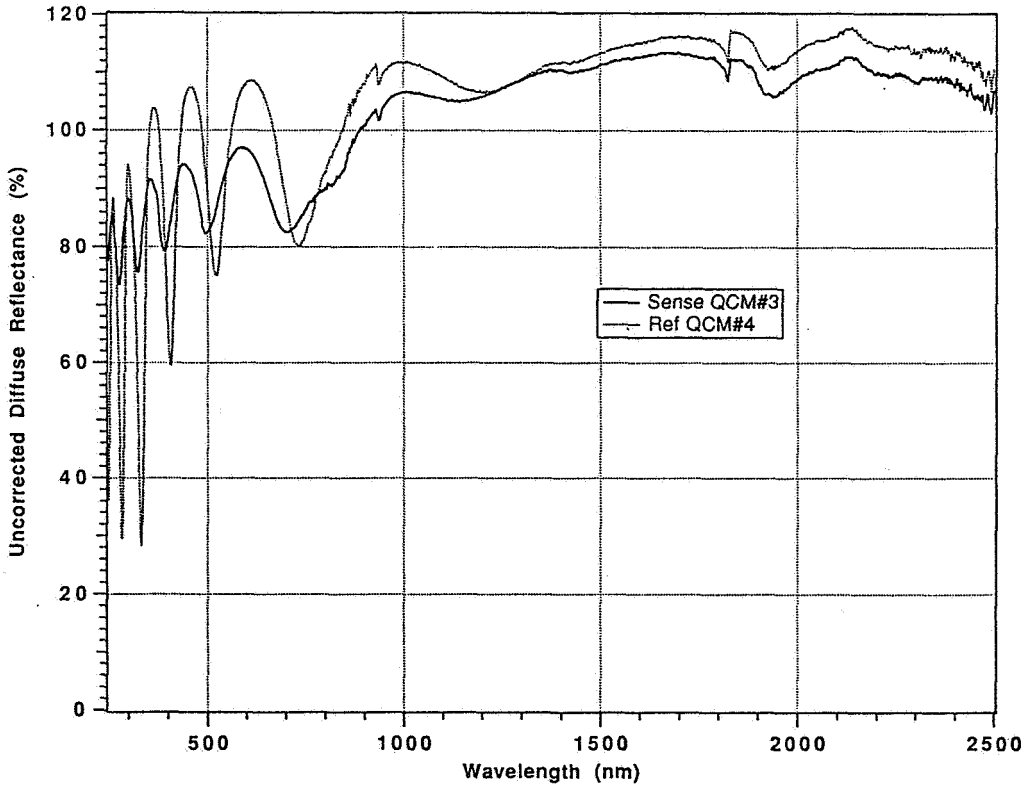

Figure 12. Diffuse reflectance spectra of trailing edge crystals 5 and 6.

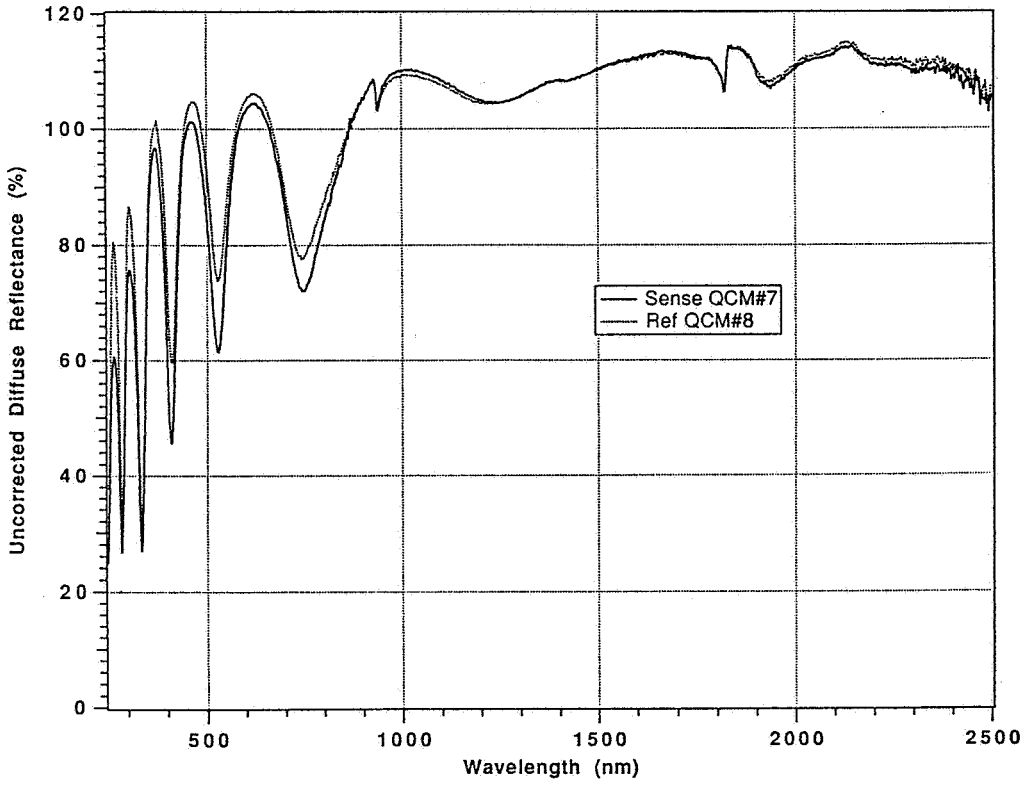

Figure 13. Diffuse reflectance spectra of trailing edge crystals 7 and 8.

a specially constructed experimental arrangement used to mount the crystals in the spectrophotometer, the reflectance data could not be normalized. Hence, they are plotted as uncorrected diffuse reflectance in arbitrary units, and it is only meaningful to compare relative values within each pair of crystals rather than the absolute values.

For all the crystals, it can be seen that with increasing wavelength, there is an increase in the corresponding average reflectance. In addition, it is seen that all the crystals also display thickness interference patterns in their reflectances. While the modulation amplitudes in crystals 1 and 2 are nearly identical, differences in modulation between QCs 5 and 6, and QCs 7 and 8 fall within a wide range of 2 to 20% in the wavelength range 2000 to 5000 Å. The most striking differences are observed with the pair 3, 4, where it is seen that the modulation amplitude in crystal 3 is significantly lower (by 10 to 50%) over the entire wavelength range (2000 to 10000 Å) than that of the reference crystal 4. On observing the positions of the wavelength maxima and minima in the interference patterns in each of the sense-reference crystal pairs, we see they appear to be negligibly shifted with respect to each other as well as with respect to the other crystal pairs, and are not large enough to result in significantly different values for the product (n x d), where n is the refractive index of the film, and d is the film thicknesses. In addition, the range of wavelengths at which these interferences are observed (2000 to 12000 Å) is so large that a 150 Å top layer either of In_2O_3 or ZnS cannot be responsible for the interferences, which are more likely due to the underlying Al/Al_2O_3 layer. A likely explanation for the observed behavior is that surface roughness can cause an increased scattering, which, in turn, can dampen the modulated amplitude of the reflected wave. In particular, EDAX analyses of the tilted samples reveal that QC 3 shows an overall thinning of the top ZnS layer, and particularly shows a reduction in the concentration of zinc present on the surface. This could result in scattering by sulfur particles or other contaminants on the surface and an overall damping of the modulated amplitude.

V. CONCLUSIONS

Silicon is the key contaminant identified on the surface of all the crystals. This conclusion is common to each of the analytical techniques employed, namely EDAX, XPS, SIMS, and FTIR. A second general conclusion supported by all these techniques is that the level of Si contamination is found to be higher on the leading edge than on the trailing edge, by about an order of magnitude. In addition, contaminants such as Mg, Ca, K, Na, Ag, Cl, Sn, and Pb have been detected on several of the crystals.

FTIR measurements detect a characteristic Si-O stretching vibration at approximately 1060 cm^{-1} only on the leading edge sense crystals, QC 1 and QC 3, which is consistent with the higher Si coverages observed on these crystals by XPS and SIMS. Reflectance measurements display modulations due to thickness interferences, with a significant damping on QC 3, which could be strongly related to the rather significant reduction of ZnS on the surface of this crystal and scattering caused by particulates or other contaminants on the surface. There were no surface compositional characteristics, which might explain the differences in frequency vs temperature curves observed on the trailing-edge QCMs after the LDEF flight.

Although all of the analytical techniques described above agree that Si, presumably from silicone, is the major contaminant on the QCs, the sources of silicone have not been unequivocally identified. There are, however, several likely candidates. Among these are the Z306 black paint in the interior of the spacecraft, silicone contaminant films on the surface of some trays prior to launch, silicone RTVs that were used to stabilize some components with respect to launch vibration, and tray cover gaskets. The relative contribution of all these sources has not been determined. In addition, while both ultraviolet radiation and atomic oxygen have been considered key factors responsible for the contamination, their relative roles, as well as the exact mechanism of contaminant production and deposition, are yet to be resolved.

ACKNOWLEDGEMENTS

The experimental contributions and useful discussions with John Coggi, Carol Hemminger, Nicholas Marquez, Mike Meshishnek, Nathan Presser, Barry Sinsheimer, Dave Sutton, Gloria To, and Joe Uht are gratefully acknowledged.

REFERENCES

1. "Long Duration Exposure Facility Experiment M0003 Deintegration/ Findings and Impacts" M.J. Meshishnek, S.R. Gyetvay, and C.H. Jaggers, Ist LDEF Post Retrieval Symposium, NASA CP-**3134**, Part 2, p. 1073–1107, Jan. 1992.
2. *Spectrometric Identification of Organic Compounds*, R.M. Silverstein, G.C. Bassler, and T.R. Morrill, John Wiley NY (1974).
3. *Infrared Spectra of Organic Compounds*, R.A. Nyquist and R.O. Kagel, Academic Press NY (1971).
4. *Introduction to Practical Infrared Spectroscopy*, A.D. Cross, Butterworths Publications, London (1960).

N93-29685

50713
pg 6

RADIATION SENSITIVITY OF QUARTZ CRYSTAL OSCILLATORS EXPERIMENT FOR THE LONG DURATION EXPOSURE FACILITY (LDEF)--PART II

J.S. Ahearn and J.D. Venables*
Martin Marietta Laboratories
1450 S. Rolling Rd.
Baltimore, MD 21227
Phone: 410/247-0700, Fax: 410/247-4939

ABSTRACT

The stability of high precision quartz crystal oscillators exposed to the radiation environment of NASA's Long Duration Exposure Facility (LDEF) has been studied. Comparisons between pre-flight and post-flight frequency drift rates indicate that oscillators made from swept premium Q quartz exhibited a significantly greater post-flight drift rate than before exposure, but that the effect annealed after five months aging at 75°C (the operating temperature). The result that six years worth of radiation damage annealed out in less than six months suggests that if the oscillators had been powered during the LDEF mission, no net change in drift rate beyond their normal baseline value would have occurred.

INTRODUCTION

In a prior paper,[1] we compared the stability in an LDEF environment of quartz crystal oscillators made from (1) synthetic swept premium Q quartz and (2) Brazilian natural quartz. These two particular grades of quartz were chosen because they exhibited large differences in radiation sensitivity when examined in the transmission electron microscope (TEM). Specifically, it was observed that under the influence of the electron beam (even for incident electron energies as low as 20 keV) defect clusters formed in both materials with the premium Q quartz exhibiting a more rapid development of the clusters and a larger cluster size (albeit at a lower volume density) for a given electron dose. We speculate that the clusters most probably formed from displaced atoms which condense at impurity sites, and that the clusters induce large strains in the lattice as evidenced by their black-dot contrast. The LDEF experiment, then, was an attempt to determine if there is a correlation between the damage produced in the electron microscope for different grades of quartz and oscillator drift rates which would be expected to be influenced by strain fields in the lattice.

PRIOR RESULTS

In Part I of this paper we reported on pre- and post-flight frequency drift rates for a total of 16 resonators, all of which were 5MHz fifth overtone AT-cut made for us by Bliley Electric. Eight of these were fabricated from synthetic swept premium Q material obtained from Sawyer Research Co. and the others from Brazilian natural quartz. Four resonators (two from each grade of quartz) were used as controls in the LDEF tray by shielding them from radiation with tantalum covers. Ten other resonators (five from each grade) were exposed to the space radiation environment and the two remaining (one from each grade) were kept in the laboratory as additional controls. For all oscillators, the drift rates were measured over two periods of approximately five months each prior

* Retired

PRECEDING PAGE BLANK NOT FILMED

to the LDEF flight to establish a "natural" drift rate, and then for five months after retrieval (post-flight) to determine the effect of the LDEF environment.

The results of our pre-flight and first post-flight aging studies (which were all done at 75°C) are summarized in the first two columns of Table I. It is evident that the radiation (estimated to total about 1×10^3 rads) has had little effect on the drift rates of the natural quartz resonators which, within experimental error, are the same before and after the flight. The swept premium Q resonators, however, exhibited a significantly greater drift rate in the post-flight studies that is positive in sign, i.e., the frequency increased with aging time. Since it is generally observed that radiation induced drift rates are negative when measurements are made during exposure (except at extremely high dose rates),[2] our result suggests an annealing effect in which the damage created during the LDEF flight is being healed during the 75°C aging studies. To test this hypothesis and an alternate possibility that the drift rate had been permanently altered in the swept premium Q resonators by the LDEF environment, we have performed a second series of post-flight aging studies.

SECOND POST-FLIGHT FREQUENCY DRIFT MEASUREMENTS

A second post-flight aging study was done in the same manner as the first by Bliley Electric with the resonators held at 75°C throughout the test. The data, which are summarized in the third column of Table I, indicate that the drift rates of the natural quartz resonators were again the same (within experimental error) as they were in the pre-flight and the first post-flight studies; no effect of the radiation environment was observed. The swept premium Q resonators that had been exposed to the LDEF radiation, and which had exhibited a relatively large positive post-flight drift, now show second post-flight drift rates approximately the same as the pre-flight value. This effect is further highlighted in Fig. 1 which compares the aging characteristics of a typical irradiated swept premium Q resonator during the first post-flight aging study (labelled 1990) and during the second one (labelled 1992). Evidently, the drift rate, which was initially high during the first post-flight study, has reverted back to its pre-flight value. We interpret this behavior as being due to an accumulation of radiation damage during the passive LDEF mission that anneals out during the 75°C aging tests, effectively recovering to the original condition (labelled 1982 in Fig. 1) during the first post-flight five-month aging period. By contrast, other premium Q resonators that had been shielded from radiation exhibited essentially no difference between pre-flight, first post-flight and second post-flight drift rates as shown in Fig. 2.

DISCUSSION

The data presented in Part I and Part II of this paper suggest some very important conclusions with regard to the stability of high precision quartz crystal oscillators in a space radiation environment as follows:

1. High precision quartz resonators made from swept premium Q quartz accumulated radiation damage during the LDEF mission that is evidenced by a marked increase in the initial post-flight frequency drift rates relative to the pre-flight values.

2. The effect slowly anneals out during the post-flight aging studies and after approximately six months in the aging environment (75°C) the drift rates return to their pre-flight values within experimental error. We attribute this annealing effect to the higher temperature seen in the aging studies than during flight when the mean tray temperature was estimated to be no higher than 30°C.

3. No effects of the LDEF mission environment were observed for resonators made from natural quartz.

4. The observation that nearly six years worth of radiation damage anneals out in less than six months at the normal operating temperature of quartz crystal resonators suggests that if the resonators had been powered during the LDEF mission, no net change in drift rate beyond their normal baseline value would have occurred. This observation has important implications for the use of quartz oscillators made from swept premium Q material, which has distinct advantages over natural quartz in some applications. For example, resonators made from swept premium Q material have been shown to be much more resistant to the effects of very high intensity, pulsed radiation than those made from natural quartz.[3]

5. Finally, it is worth noting that the LDEF mission has provided a unique opportunity to study the behavior in a true space environment of an important component of space communications and navigation, namely the high precision quartz crystal oscillator. It is true that many ground-based studies have been made in the past of radiation effects in quartz resonators, but to our knowledge never before have such studies been done at the extremely low dose rates characteristic of the levels incurred in this flight. For example, the lowest dose rate reported in the literature that we are aware of for ground-based studies was 1.4×10^{-2} rads(Si)/min. used recently by Norton.[4] By way of comparison, the rate of exposure seen in the present study on LDEF was approximately 3×10^{-4} rads(Si)/min. The significance of this is that even these very low dose rates can effect the drift rates of high precision oscillators. The good news, however, is that the effect apparently can be annealed out as fast as it is generated if the units are continuously powered.

REFERENCES

1. Ahearn, J.S. and Venables, J.D.: Radiation Sensitivity of Quartz Crystal Oscillators Experiment for the Long Duration Exposure Facility (LDEF). Proc. of First LDEF Post-Retrieval Symposium, NASA CP-3134, Part 3, Jan. 1992, pp. 1523-1531.

2. Suter, J.S.: IEEE Trans. Nuclear Scit. 37 (1990), pp. 524-528.

3. Euler, F., Lipson, H.G., and Ligor, P.A.: Proceedings of the 34th Frequency Control Symposium (1980), pp. 72-80.

4. Norton, J.R.: BVA-Type Quartz Crystal Oscillators for Spacecraft. Proceedings of the 45th Annual Symposium on Frequency Control, Feb., 1991, pp.426-430.

Table I. Mean Drift in Resonant Frequency after 5 Months Aging (ΔF IN p X 10^{-10})

Type of Quartz	Pre-Flight	First Post-Flight Aging (irradiated only) 1990	Second Post-Flight Aging (irradiated only) 1992
Swept Premium Q	53 ± 53	217 ± 69	34 ± 24
Natural	40 ± 34	61 ± 47	60 ± 33

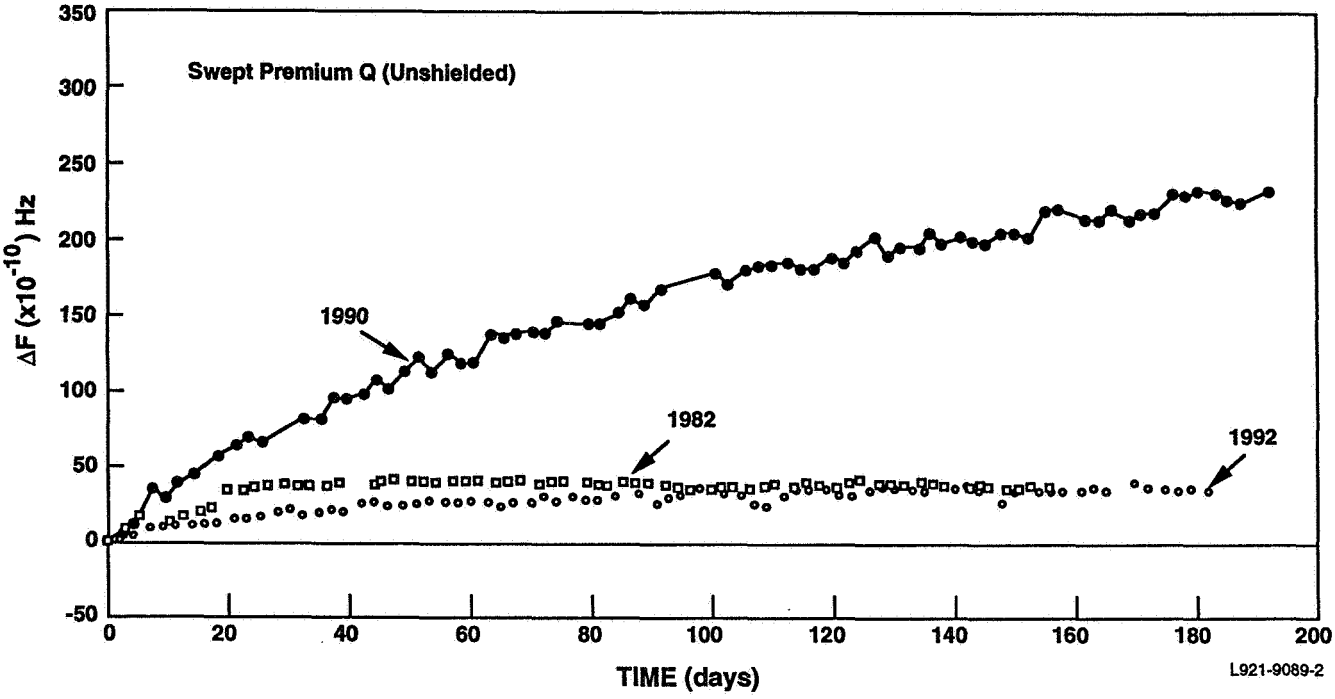

1. Aging results of unshielded resonator showing the change in resonant frequency as a function of time for Bliley Type BG61AH-5S resonators fabricated from Saywer Swept Premium Q material. Aging temperature 75°C.

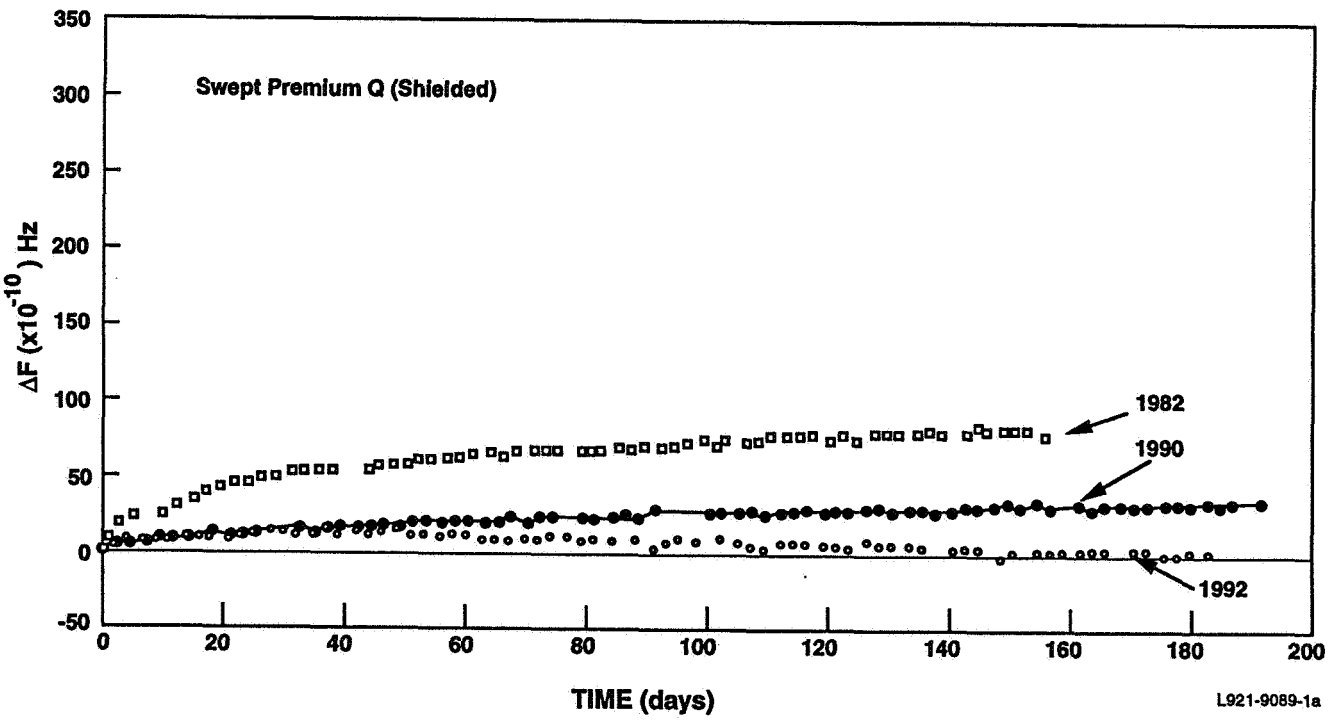

2. Aging results of shielded resonator showing the change in resonant frequency as a function of time for Bliley Type BG61AH-5S resonators fabricated from Saywer Swept Premium Q material. Aging temperature 75°C.

N93-29686

THE EFFECT OF THE LOW EARTH ORBIT ENVIRONMENT ON SPACE SOLAR CELLS: RESULTS OF THE ADVANCED PHOTOVOLTAIC EXPERIMENT (S0014)

501715
P35 12

David J. Brinker
NASA Lewis Research Center
Cleveland, OH 44135
Phone: 216/433-2236, Fax: 216/433-6106

John R. Hickey
The Eppley Laboratory, Inc.
Newport, RI 02840

David A. Scheiman
Sverdrup Technology, Inc.
Brook Park, Ohio 44142

SUMMARY

The results of post-flight performance testing of the solar cells flown on the Advanced Photovoltaic Experiment are reported. Comparison of post-flight current-voltage characteristics with similar pre-flight data revealed little or no change in solar cell conversion efficiency, confirming the reliability and endurance of space photovoltaic cells. This finding is in agreement with the lack of significant physical changes in the solar cells despite nearly six years in the low Earth orbit environment.

INTRODUCTION

The Advanced Photovoltaic Experiment (APEX) is an LDEF science experiment designed to provide reference cell standards for laboratory photovoltaic performance measurements as well as to investigate the solar spectrum and the durability of space solar cells in the low Earth orbit environment. APEX, one of the first group of experiments accepted for inclusion on LDEF, was designated experiment S0014 and occupied position E9 on the leading edge of the satellite.

The accurate evaluation of the on-orbit performance of a solar cell intended for use in space power generation is crucial to ensuring sufficient electrical power over the lifetime of the satellite. If the conversion efficiency of a solar cell is overrated, as determined by laboratory-based measurements, adequate power will not be available to meet satellite mission objectives. If underrated, more cells than necessary will be used, increasing both cost and the amount of heat which must be dissipated by the spacecraft thermal management system. An accurate determination of the space, or Air Mass Zero (AM0), performance of a solar cell is complicated by the circumstance that the efficiency of a cell for collecting a photon is a function of the wavelength of the photon. This wavelength dependent efficiency is known as the spectral response and depends on the choice of the semiconductor used for the cell, the design of the electrical junction in the cell and its anti-reflection layer. Because neither a laboratory solar simulator nor terrestrial sunlight exactly matches the spectral content of extraterrestrial sunlight, reference cells with the same spectral response of the cells under test must be calibrated in true

PRECEDING PAGE BLANK NOT FILMED

AM0 sunlight to enable accurate measurements. This restriction creates the requirement for large numbers of reference cells, one for each unique cell design.

Over the last 35 years, the era of space photovoltaic power generation, a number of ground-based AM0 calibration techniques have been developed. These, including sounding rockets, high altitude balloons and aircraft, and mountain-top measurements, had to suffice because of limited access to space. The Long Duration Exposure Facility represented the first opportunity to expose a large number of solar cells directly to AM0 sunlight, record the pertinent data and safely return the cells for use in the laboratory. Thus the principle objective of APEX was to calibrate reference standards. The timely return of the cells and flight data would enable their use as reference standards.

A second objective was to determine the endurance of these advanced cell designs in the low Earth orbit environment. This was to be accomplished by the acquisition and recording of cell performance data during the planned eleven month flight from the 120 calibration standards, as well as another 16 cells for which the entire current-voltage characteristic was measured. The measurement of the energy distribution of the extraterrestrial solar spectrum was the third objective. Three instruments designed to measure both broadband and spectral irradiance were included: an absolute cavity radiometer, sixteen narrow bandpass filters coupled with silicon solar cell detectors, and a dichroic mirror which divided the solar spectrum into two parts. However, the unexpected increase in flight time from eleven to sixty-nine months resulted in the inability to meet some of these original objectives.

Details of the design of APEX, as well as the preliminary results, were presented at the First LDEF Post-Retrieval Symposium (Refs. 1, 2). In this paper, more detailed results concerning the endurance of the space cells included in the experiment will be discussed. Further results concerning the performance and durability of the optical components of APEX have been published elsewhere in these proceedings (Ref. 3). Data concerning some of the micrometeoroid/debris impacts and resulting features from the front plates of APEX has also been reported here (Ref. 4).

SOLAR CELL FLIGHT SAMPLES

When the announcement of opportunity for LDEF experiments was released in 1976, a launch of about 1980 was envisioned. As a result, the solar cell samples prepared for APEX represented the state-of-the-art in space cell technology as of 1979, as well as samples of cells in use on a variety of satellites. Flight samples were solicited from the principal industrial and governmental groups who either manufactured or conducted research and development on space photovoltaic devices. These APEX solar cell investigators and the number of cells each supplied are:

A.F. Wright Aeronautical Laboratory	8
Applied Solar Energy Corporation	14
COMSAT Laboratories	7
European Space Agency	9
Jet Propulsion Laboratory	34
NASA Lewis Research Center	56 (Includes 19 sensor cells)
NASA Marshall Space Flight Center	11
Solarex Corporation	7
Spectrolab, Inc.	9

Each group provided cells representative of technologies which were either in development

or production. The experiment was designed to accommodate a total of 155 such cells, including the silicon cells which were employed as sensors for the spectral radiometer portion of the experiment. All cells were permanently mounted on aluminum plates with a thermistor in contact with the rear of the cell. Because the short-circuit current (Isc) of a solar cell is directly proportional to the intensity of the incident light and is strongly dependent upon the spectral content of that incident light, it was therefore the principal parameter of interest. 139 cells were designated as Isc cells, 120 to be calibrated as reference standards and returned to the investigators, eighteen for use as spectral radiometer sensors and one as a night sensor to signal the data acquisition system that conditions were correct for the requisite periodic calibration of the cavity radiometer. For these cells, the short-circuit current was converted to a voltage through the use of a precision load resistor. In most cases a 0.1 Ω value was used. The remaining sixteen cells were designated IV cells, that is the entire current (I) - voltage (V) characteristic curve was measured through the loading of the cell by a series of appropriately sized resistors.

The delay in the launch of LDEF by several years provided both the opportunity and necessity for updating the sample set, to one including the most recent advances. The cell investigators were invited in mid-1982 to submit new cells. Of the 136 calibration cells (120 Isc and 16 IV cells), 69 were replaced. Many of those which were not replaced were either standards previously calibrated by other techniques or representative of cells in use on a variety of satellites.

At that time, cells made of silicon were the only type in production, with the development of gallium arsenide in its early stages and years from production and utilization in space. This is reflected in the distribution of these semiconductor types in the APEX complement, which is summarized by cell type and size below:

Silicon:		Gallium Arsenide:	
105	2 x 2 cm	10	2 x 2 cm
21	2 x 4 cm	1	1.3 x 1.6 cm
2	5 x 5 cm	11	
15	5.9 x 5.9 cm		
1	6 x 6 cm (module)		
144			

The cells were mounted on 127 aluminum plates of twelve different sizes and configurations. 28 of the mounts each held two 2 x 2 cm cells. Each mount was equipped with a Yellow Springs Instruments Type 16429 thermistor (10,000 Ω @ 25 °C). An additional thermistor monitored the Eppley absolute cavity radiometer.

POST-FLIGHT CELL EXAMINATIONS

After deintegration of the Advance Photovoltaic Experiment from LDEF it was returned to the Lewis Research Center and the flight Magnetic Tape Memory was removed for processing. Functional testing of the data acquisition system was conducted prior to removal of the various sensors for post-flight testing and recalibration. The results of these tests have been previously reported (Refs. 1,2). The solar cells were then removed from APEX. The leads from the data acquisition system to both the thermistor and cells contacts were cut near their attachment points at the back side of the mounting plate feedthrough. The leads were cut rather than unsoldered to avoid any possible contaminating fumes from molten solder. All cells were then visually inspected and individually photographed.

The overall condition of the cell sample set was excellent. The contaminating film seen over much of LDEF was present to a varying degree on APEX, the thickness of the layer

dependent upon location. No loss of cell coverglass nor significant changes in color or appearance was observed. Several of the cells were cratered from micrometeoroid and/or debris impacts, with the range of damage spanning from microscopic craters in the coverglass surface to penetration of the coverglass and cell and cratering of the underlying aluminum mounting plate. However, even the few cells in which the cratering extended into the solar cell itself, or caused a crack in the coverglass and cell, electrical continuity was maintained. Loss in current proportional to the damage area and increase in fill factor due to cell cracking was observed. The electrical leads from the mounting plate feedthrough to the cell front and rear contacts were found to open in six cells. A silver ribbon of about 3 mil thickness was used for these cells. Where the flat portion of the ribbon faced the ram direction, the ribbon was severely eroded, creating an open circuit. In most cases the ribbon twisted through 90° at the feedthrough so that the narrow (3 mil) edge faced the ram direction; here the silver ribbon remained intact. Examination of the flight data indicates that the erosion did not occur to any extent that would affect cell performance during the data recording portion of the flight, the first eleven months. Post-flight performance testing of these cells was accomplished by direct probing of the cell contacts, no significant change from pre-flight performance was seen.

The first post-flight electrical test performed was measurement of the short-circuit current utilizing the precision load resistor mounted on each cell for the flight. The resistors were soldered to the cell mounting plate electrical feedthroughs on the underside of the cell mounting plates. These measurements, as well as subsequent current-voltage (I-V) tests, were carried out in the Solar Cell Evaluation Laboratory at Lewis Research Center using a Spectrolab X-25L solar simulator. This simulator employs a short-arc xenon lamp as the light source and provides uniform, collimated illumination. The intensity of the simulator was set using an aircraft calibrated silicon standard which is identical to the standard used at Eppley Laboratory for pre-flight testing, where a xenon arc lamp simulator was also utilized. Cell temperature was monitored using the flight thermistors. One thermistor was found to be open. An examination of the flight data showed abnormal readings from it, indicating that the failure occurred before launch. With this sole exception, all of the thermistors functioned properly, providing values in close agreement with a temperature sensor used in controlling the laboratory test fixture. The short-circuit current values obtained in these tests are useful in comparison with both pre-flight performance and flight data. The values obtained were in most cases in excellent agreement with pre-flight values, with the exception of those cells without coverglass.

Upon completion of the measurement of the short-circuit current, the load resistor was removed from the circuit by cutting one of its two leads. If LDEF had been retrieved on schedule and the value of the cells as calibration standards was retained, the load resistors could not have been removed. However, the absence of data from the last five years on-orbit negates their usefulness as standards. The complete I-V characteristic of all cells were then measured at 25 °C and recorded. A representative sampling of the silicon cells flown on APEX is shown in Table 1. All of these cells are n-p type, as were most of the silicon cells flown, the standard configuration for silicon space cells due to its superior radiation tolerance. The post-flight illuminated current-voltage characteristic of each of the six cells of Table 1 is shown in Figures 1 through 6. Also included for comparison in the figures are the pre-flight values (measured at Eppley Laboratory) of short-circuit current (Isc), open circuit voltage (Voc) and fill factor (F.F.).

Cell IV#7 (Mount B-1L) was manufactured by Spectrolab for the Solar Maximum Mission satellite. The base resistivity of the cell was 10 Ω-cm with an anti-reflection coating of Ta_2O_5. A similar cell, but 2 x 4 cm in size, was also flown as sample ISC#32. As can be seen in Figure 1, little change in cell performance due to time on-orbit has occurred. The small differences in Isc and Voc are within experimental accuracy. The results from ISC#32 are nearly identical to that of IV#7.

The cell of Figure 2, ISC#95, is a large area (5.9 x 5.9 cm) cell in which the front contact wraps around the edge of the cell enabling all leads to be attached from the rear. This cell is the predecessor to the Space Station Freedom cell. Seven such cells were flown. Little change in Isc or Voc was noticed, however the drop in fill factor of about 2 percentage points was typical of this set of cells. A set of four cells with the same design but with conventional top/bottom contacts also showed little change in Isc or Voc. The drop in fill factor was larger, ranging from 6 to 18 percentage points.

Cell ISC#112 (Figure 3) has a base resistivity of 1 Ω-cm and an anti-reflection coating of Ta_2O_5. Its 30 mil coverglass is the thickest on APEX and the only grooved design. The grooves are situated above the cell collection fingers and serve to reflect light to those areas where it can be collected. No decrease in performance was seen with an identical cell, IV#9, having similar results.

The cell of Figure 4, ISC#114, and a companion cell, IV#11, employed a texturized surface to optimize photon absorption and thus increase short-circuit current. The cells have a base resistivity of 10 Ω-cm and also use a Ta_2O_5 anti-reflection coating. The post-flight currents of the cells, in excess of 189 ma, are the largest current densities of the APEX cell complement.

The last two cells of Table 1 were two of fifteen silicon cells which did not have coverglasses. The purpose of a coverglass is to prevent energetic protons from damaging the semiconductor material and degrading its electronic transport properties, which, in turn, reduces cell conversion efficiency. The choice of coverglass material and its thickness are determined by the energy and flux of the protons, which varies with orbital inclination and altitude. Proton damage is evidenced by the drop in Isc as well as the substantial loss of Voc. Similar drops in performance were seen in the entire set of unglassed cells. Cell ISC#83 has a base resistivity of 10 Ω-cm and is consequently more radiation tolerant than the 1 Ω-cm material of cell ISC#63. This is confirmed by the data of Figures 5 and 6.

Table 2 is a summary of the gallium arsenide solar cells contained in the APEX sample set. Ten of the eleven cells were fabricated by Hughes Research Laboratory using the liquid phase epitaxy techniques. Post-flight simulator calibration for the gallium arsenide cells was accomplished using a gallium arsenide aircraft standard of the same design and vintage of these Hughes cells. The remaining cell, ISC#111 (Figure 7), is a metal-oxide-semiconductor structure made at JPL and primarily of interest as a terrestrial cell. The cell is covered with a coverglass of unknown material. At this time the source of the increase in current from pre-flight to post-flight is not known. A change in the junction structure (formed by the metal and oxide layers) is unlikely as the open-circuit voltage is unchanged. The contaminating film covering the cell may have served to improve the anti-reflection properties of the front surface of the coverglass.

The remaining three cells of Table 2 (Figures 8 through 10) are similar in design with the exception of the junction depth (Dj). Each cell, ISC#71, ISC#76 and ISC#77, represents a set of three flown on APEX. The effect of the fused silica coverglass on ISC#71 is most apparent in the open-circuit voltage, with that of the uncovered cells sustaining significant losses. As in the case of the silicon cells, this is due to the energetic protons found in LEO. The decrease in Voc and Isc of cell ISC#77 is greater than that of ISC#76 due to the shallower depth of its junction (0.35 μm versus 0.50 μm).

CONCLUSIONS

Post-flight examination and performance testing of the complete cell complement of APEX has been conducted. The overall condition of the sample set is excellent with no loss of coverglasses nor significant changes in color or appearance. Several of the cells sustained micrometeoroid/debris impacts with varying degrees of subsequent damage. However, in no case was the electrical functioning of the cells totally impaired. With the exception of one pre-flight failure, all 128 thermistors functioned perfectly in post-flight testing, as did the cell load resistors. Very little degradation in cell conversion efficiency was demonstrated by post-flight performance measurements. The open-circuit voltage and short-circuit current of those cells that did not have a coverglass did decrease, as expected.

REFERENCES

1. Brinker, D.J., Hickey, J.R. and Scheiman, D.A.: Advanced Photovoltaic Experiment, S0014: Preliminary Flight Results and Post-Flight Findings. Proc. First LDEF Post-Retrieval Symposium, p. 1395, NASA CP-3134, 1991.

2. Hickey, J.R.: Passive Exposure of Earth Radiation Budget Experiment Components LDEF Experiment AO147: Post-Flight Examinations and Tests. Proc. First LDEF Post-Retrieval Symposium, p. 13493, NASA CP-3134, 1991.

3. Hickey, J.R., Brinker, D.J. and Jenkins, P.P.: Studies of Effects on Optical Components and Sensors: LDEF Experiments AO-147 (ERB Components) and S-0014 (APEX). Proc. Second LDEF Post-Retrieval Symposium, 1992.

4. Coombs, C.R., Atkinson, D.R., Allbrooks, M. and Wagner, J.D.: Damage Areas Due to Craters on LDEF Aluminum Panels. Proc. Second LDEF Post-Retrieval Symposium, 1992.

Table 1 - SILICON CELLS

Cell Number		Description	Coverglass	Remarks
IV#7	B-1L	Spectrolab, Solar Maximum Mission	12 mil Crng. 7940	Little pre- to post-flight change
ISC#95	M-5	ASEC, Large Area, Wrap Around Contact	6 mil Fused Silica	SSF predecessor
ISC#112	B-2R	COMSAT Very High Blue Sensitivity	30 mil 7070	V-grooved cover
ISC#114	B-4R	COMSAT Non-Reflecting	12 mil Fused Silica	Textured surface High current
ISC#63	NA-10	Solarex, Back Surface Field/Reflector	No cover	ΔVoc = 65 mV ΔIsc = 13.1 mA
ISC#83	B-21R	LeRC A/C Standard	No cover	ΔVoc = 46 mV ΔIsc = 4.7 mA

Table 2 - GALLIUM ARSENIDE CELLS

Cell Number		Description	Coverglass	Remarks
ISC#111	A-2	JPL, AMOS	Unknown material	Only heterostructure cell on APEX
ISC#71	NB-15L	Hughes, Dj = 0.5 μm	12 mil F.S.	ΔVoc = -10 mV ΔIsc = 14.5 mA
ISC#76	NB-29R	Hughes, Dj = 0.5 μm	No Cover	ΔVoc = 65 mV ΔIsc = 21.7 mA
ISC#77	NB-29L	Hughes, Dj = 0.35 μm	No Cover	ΔVoc = 85 mV ΔIsc = 23.7 mA

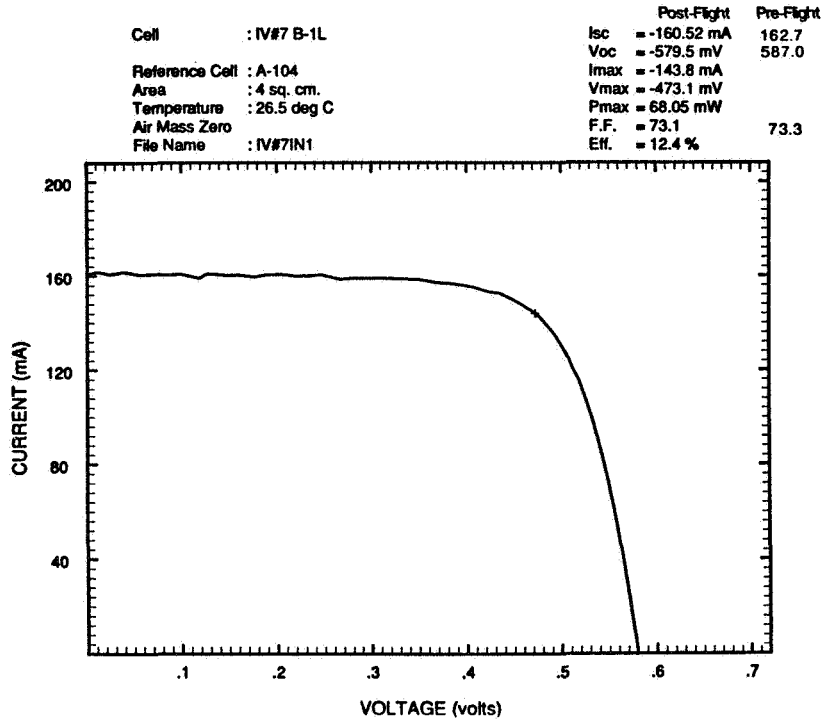

Figure 1 - Illuminated Performance of Silicon Cell IV#7, B-1L

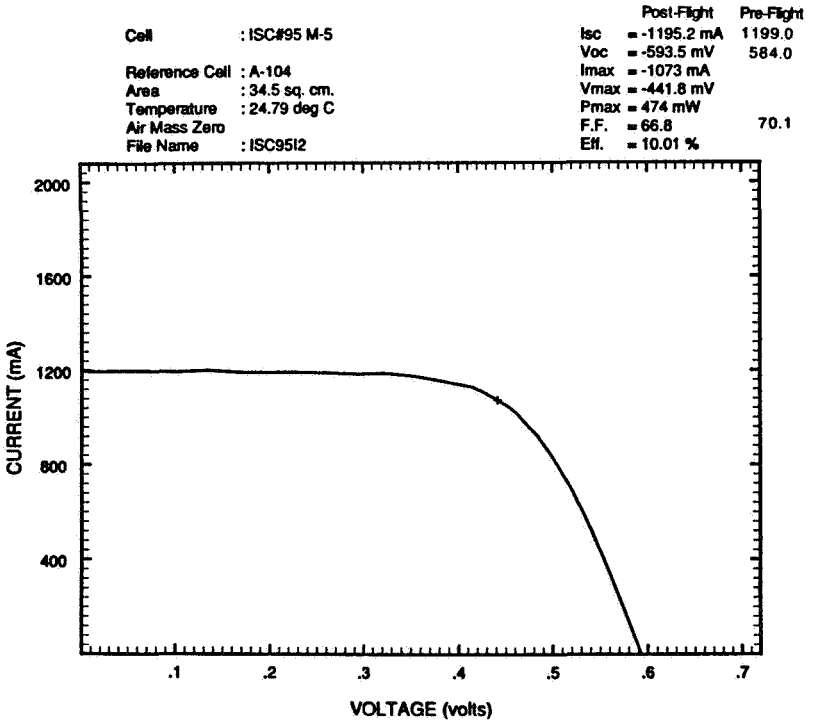

Figure 2 - Illuminated Performance of Silicon Cell ISC#95, M-5

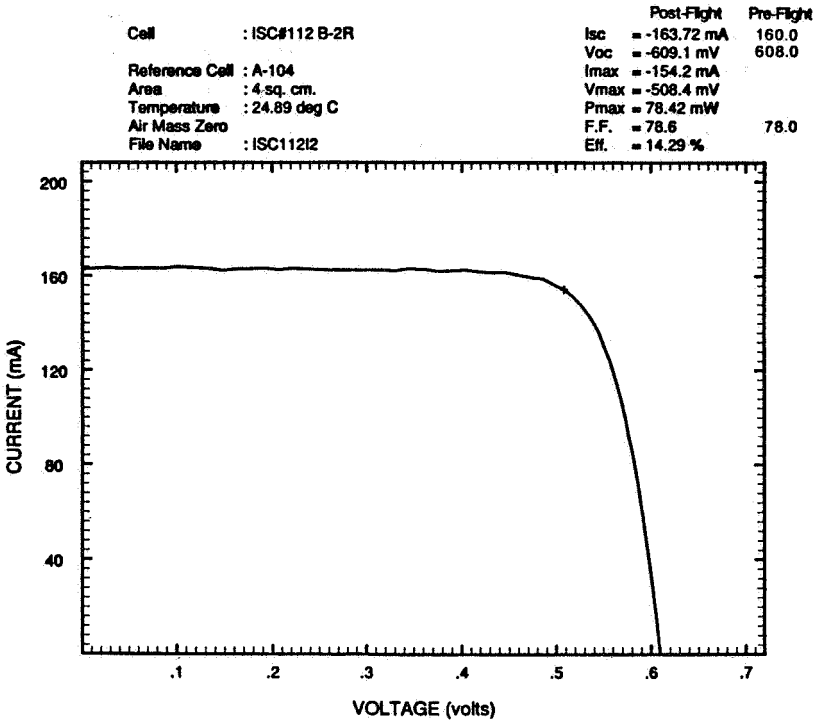

Figure 3 - Illuminated Performance of Silicon Cell ISC#112, B-2R

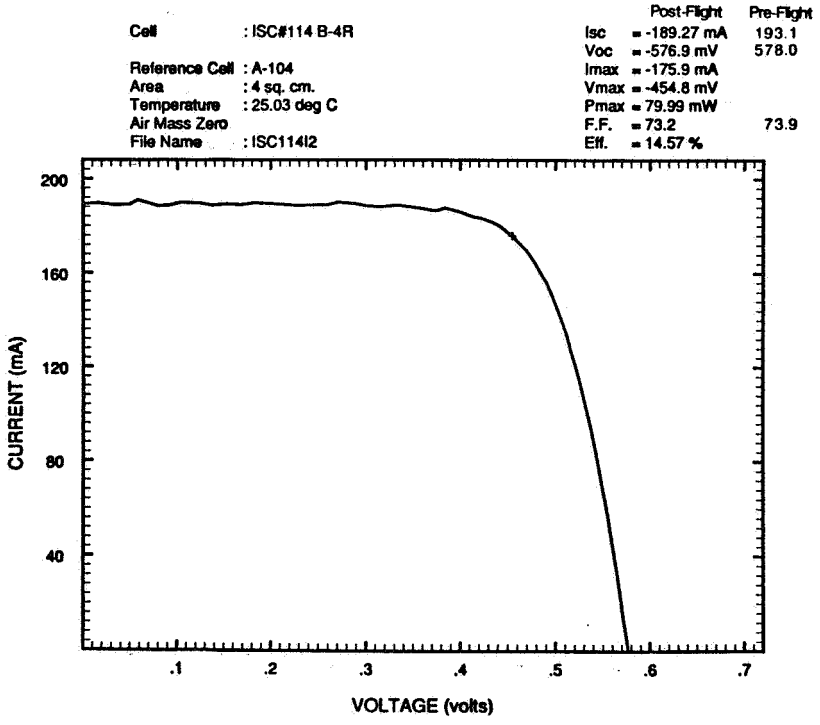

Figure 4 - Illuminated Performance of Silicon Cell ISC#114, B-4R

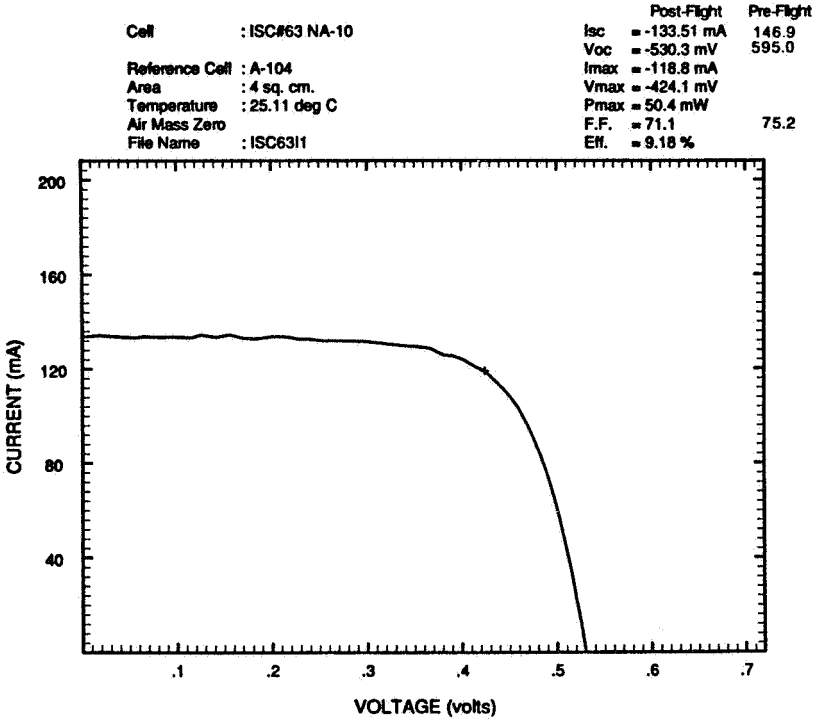

Figure 5 - Illuminated Performance of Silicon Cell ISC#63, NA-10

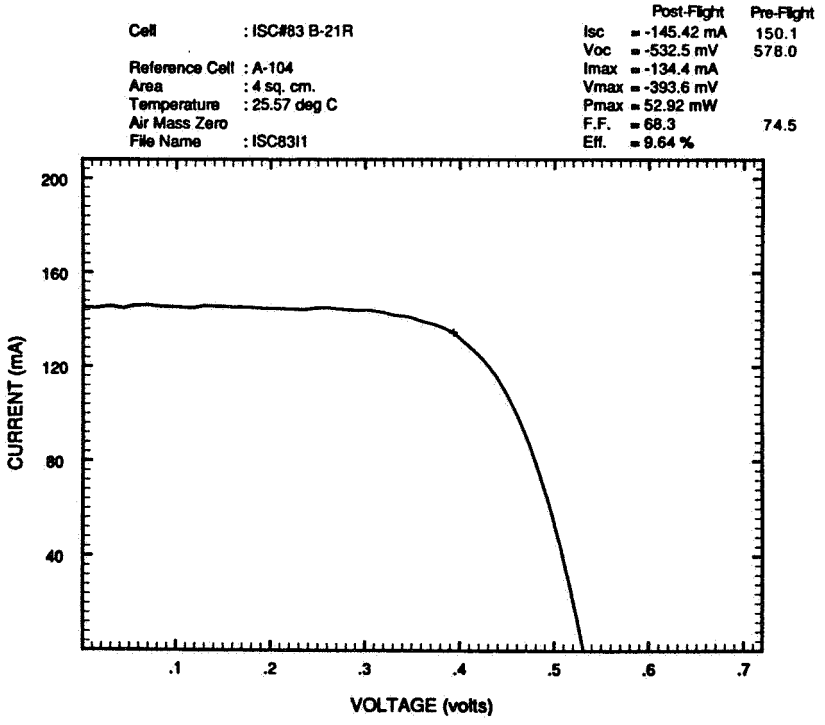

Figure 6 - Illuminated Performance of Silicon Cell ISC#83, B-21R

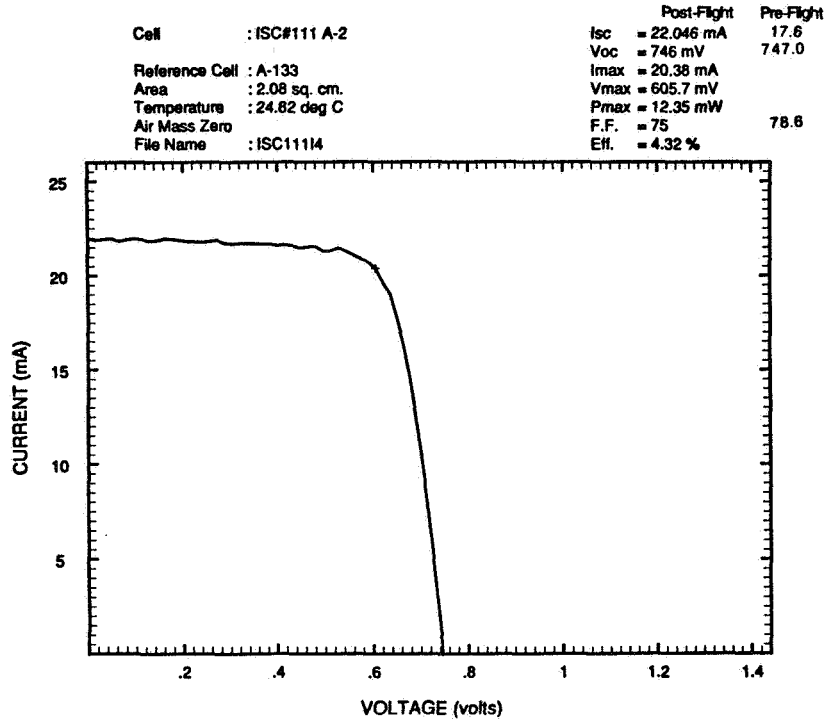

Figure 7 - Illuminated Performance of Gallium Arsenide Cell ISC#111, A-2

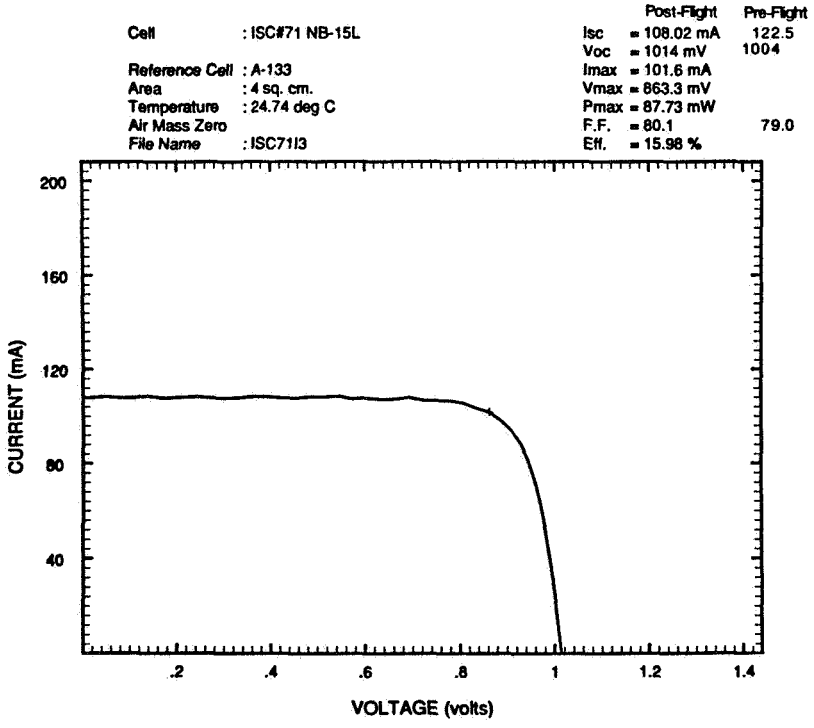

Figure 8 - Illuminated Performance of Gallium Arsenide Cell ISC#71, NB-15L

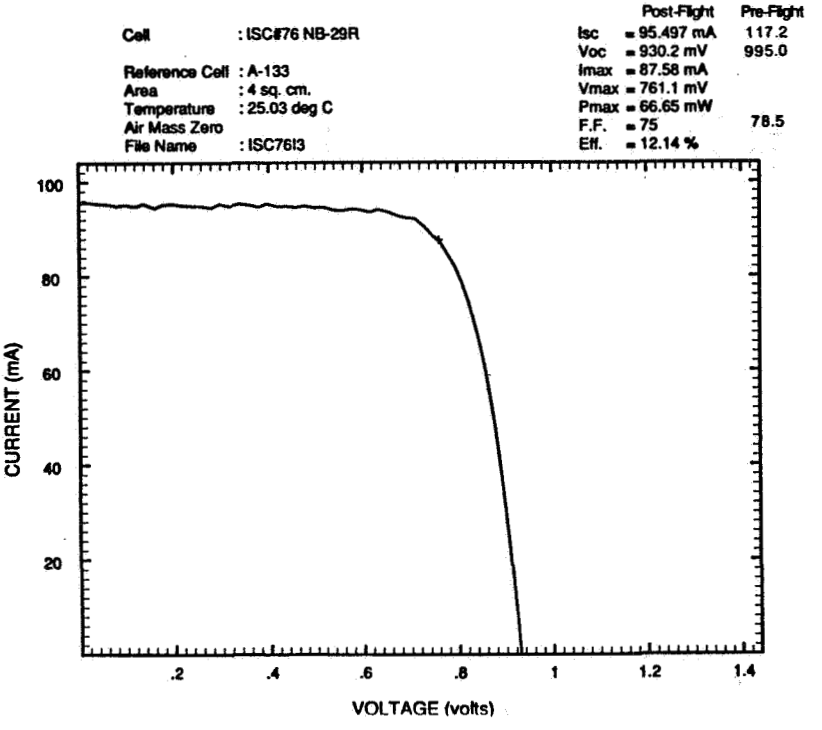

Figure 9 - Illuminated Performance of Gallium Arsenide Cell ISC#76, NB-29R

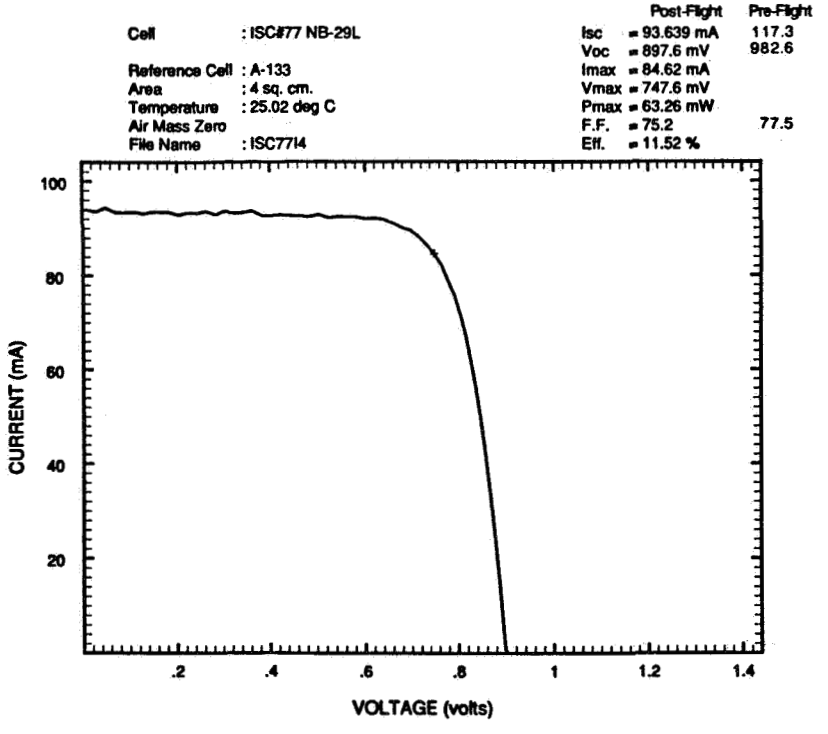

Figure 10 - Illuminated Performance of Gallium Arsenide Cell ISC#77, NB-29L

N93-29687

LEO EFFECTS ON CANDIDATE SOLAR CELL COVER MATERIALS

501719
P5-12

Paul M. Stella
Jet Propulsion Laboratory
California Institute of Technology
Pasadena, CA 91109

SUMMARY

In 1984, the LDEF (Long Duration Exposure Facility) was placed in LEO (Low Earth Orbit) for a mission planned to last approximately one year. Due to a number of factors, retrieval was delayed until 1990. An experiment, prepared under the direction of JPL, consisted of a test plate with thirty (30) individual thin silicon solar cell/cover samples. The covers consisted of conventional cerium doped microsheet platelets and potential candidate materials, such as FEP Teflon, silicone RTVs, glass resins, polyimides, and a silicone-polyimide copolymer encapsulant. This paper discusses the effects of the LDEF mission environment (micrometeorite/debris impacts, atomic oxygen, UV and particulate radiation) on the samples.

INTRODUCTION

The JPL experiment was part of SAMPLE (Solar-Array-Materials Passive LDEF Experiment), experiment number A0171, which included contributions from NASA-MSFC, NASA-LeRC and NASA-GSFC. SAMPLE was located at A08, a near ram position.

The JPL subplate consisted of an 11" x 16.3" (28 cm x 41.4 cm) aluminum plate with thirty (30) cell/cover samples. The cells were 50 micron thick 2x2 cm^2 silicon devices fabricated by Solarex Corporation. Silver-plated Invar tabs were welded to each cell to facilitate pre and post flight electrical performance measurements. Each cell and tab assembly was bonded to a slightly oversize sheet of 25 micron thick Kapton insulation bonded to the aluminum plate. The bonding materials were standard space-type silicone RTVs. Protective covers were attached to the front surface of the cell. These covers consisted of a variety of materials, including cerium doped microsheet, teflon film and various encapsulants.

The G.E. Company prepared the samples and assembled the experiment. The LDEF flight test was part of an evaluation to develop a protective cover alternative to the conventional fused silica or microsheet platelet covers. Although the conventional covers are not expensive (compared to the cell), the process of covering the cell is time-consuming and expensive. Ideally, a spray-on or roll-on coating would significantly reduce the cost and assembly time for array fabrication. It is important that such a cover not only protect the cell from radiation and enhance the cell emissivity, but that it not be degraded. The LDEF flight provided a means to directly evaluate the behavior of the cover materials in the space environment, including their ability to protect the cells. The post flight experiment review consisted of visual examination, cell electrical performance measurements and data analysis. The results are discussed below.

VISUAL OBSERVATIONS

Observation of the recovered test plate revealed a number of changes (Figure 1). All exposed (uncovered by adhesive or encapsulant) tab surfaces darkened from the original shiny silver

appearance as the result of atomic oxygen interactions. In many cases, the darkened silver tab surfaces showed signs of stress by the formation of platelets. The dark surface material was readily removed by gentle mechanical abrasion revealing a shiny, albeit rough, surface underneath. In some areas, it appeared that the original surface had flaked off during the mission. The resultant surface region was slightly lower than the surrounding regions and the color was less dark -- more gray than blue/black -- suggesting less exposure time to the pertinent environment. Although initially it appeared that the damage to the silver plating did not extend to the Invar, recent efforts to rub off additional blackened regions showed that this was not completely correct. There were a few small areas on the tabs where removal of the darkened surface revealed the Invar surface, suggesting that a minimum thickness of unreacted silver remains on the exposed interconnector. The initial silver thickness was not noted (the problem of atomic oxygen not anticipated at the time of experiment assembly), but typically ranged from four to six microns.

The initial view of the test plate quickly revealed many changes had occurred. Although no major damage was noted, the test plate and samples looked contaminated, with brownish-orange stains particularly apparent around the test samples. This was apparently the residue of silicone adhesives and/or encapsulants that had reacted with the LDEF space environment. The samples with Teflon covers appeared "charred" with the Teflon surface appearing brownish-gray. The cell gridlines were visible as yellow brown lines. Various samples with encapsulants were distinct in the lack of the normal dark blue cell appearance. Instead, colors varied from medium to very light blue (almost green), with clear indication of encapsulant crazing, peeling and flaking. Some cells with silicone encapsulants had exposed areas free of coating where the cell surface was clearly visible (with AR coating intact), although exposed silver grid lines were now blackened. Beyond these rather large scale changes, some of the larger impact craters were evident, such as an impact with a cell covered by Teflon (Figure 2). On a smaller scale, some light-colored, hazy areas evident along the sides of the test samples were most likely attributable to outgassing of cell to Kapton or Kapton to substrate silicone adhesives.

Upon completion of the initial visual examination, photographs were made to record the appearance, especially since it was possible that ambient reactions might be further altering the materials' conditions. (However, no significant changes have been noted during the two years following the initial observations.) Following this, a microscope-aided inspection of impact craters was performed followed by a measurement of test cell electrical performance. These are discussed in the following sections.

As might be expected, the cover system appearing the least changed was that of the conventional microsheet platelet. These samples generally appeared as if newly assembled.

DEBRIS/MICROMETEORITE IMPACTS

Inspection of the plate revealed a large number of impact craters, predominantly in the aluminum plate, ranging in size from 1 mm (Figure 3) to 0.05 mm in diameter. Most impacts appear to be normal to the plate (circular crater). The physical appearance of these impacts is discussed for various impact surfaces in the following sections.

Cratering in the Aluminum Plate

Since the majority of the test plate area consisted of the uncovered aluminum mounting plate, the majority of impacts were located in the plate. These were generally similar in appearance, and typified by the example in Figure 3. The impact formed a circular crater with a surrounding ridge ejected out from and over the plate surface. The crater bottom was crystalline in appearance, unlike

the scratched and machined plate surface, showing evidence of melting and resolidification. This crater pattern was observed for all sizes from 1 mm diameter on down. Of the 157 impacts observed (over the entire test plate/sample surface), seven were 0.5mm or larger. Depth measurement of the seven indicated a crater depth (measured from crater bottom to top of surrounding ridge) ranging from one-half to one-third the crater diameter. Only a few craters were noted with an elliptical shape that might be attributable to an impact with a particle with a large non-normal velocity component.

Invar Interconnector Impacts

Although the total area occupied by the silver-plated Invar tabs was small, tab impacts did occur. The results of the impacts were visually surprising, but offer clear indication of the high particle impact velocities and corresponding impact energies. Figure 4 is a typical example of one such impact. It is observed that the tab has been completely penetrated. The region of Invar immediately surrounding the 0.5mm diameter penetration hole shows clear indication of melting and resolidifying. In addition, the impact generated gases have peeled the top silver plating away from the Invar and blown those layers out from the impact area. The silver/Invar separation is well-identified by the lack of any atomic oxygen darkened residual silver. Indeed, the inner surface of the peeled back silver plating has now darkened from atomic oxygen interaction. The remainder of the silver plated Invar tab away from the impact still appears shiny due to a thin layer of silicone adhesive which has provided protection during the mission.

Impacts with Polymer Cell Covers

The appearance of impacts with a relatively thick polymer cell cover, such as Teflon FEP, shown in Figure 5, is remarkably similar to the above-described silver-plated Invar tab. For Teflon, the incident particle readily penetrated and impacted the silicon cell below. The impact with the silicon has generated gases which, in turn, lifted the Teflon away from the cell and blew out the central area. The flexible Teflon, unlike the rigid silver metallization, has settled back somewhat onto the cell surface. A light-colored ring can be observed around the blowout region, corresponding to an area of Teflon/silicon delamination, where physical contact, if not adherence, has been recovered. It is clear that the Teflon provides negligible protection against the high energy impacts. However, it was noted that the electrical performance of this cell was not noticeably different from other similarly covered cells, indicating minimal effects from the impact.

Impacts to Silicon and Microsheet

The silicon and microsheet impacts are discussed together because of the many similarities. Both materials are brittle and tend to shatter under severe loading. Figure 6 is a photograph of an impact in silicon (through a few micron thick polymer cover) and Figure 7 is a view of an impact into a 100 micron thick microsheet coverslide. Both impact areas are comparable in size (~0.1mm central "hole"), the difference in the photographs being due to different magnification levels. In view of the limited number of such impacts, it is not clear if these are truly typical. However, both materials have a well-defined crater with any ejected material blown completely away. Both crater perimeters appear nearly rectangular. For the silicon, this reflects the crystalline nature of the material, although this would not be expected for the microsheet. Of interest, the silicon cell was completely penetrated, with the formation of a near hexagonal-shaped through hole. The microsheet impact is limited in area, and radiating cracks were not visible. In the case of the microsheet impact, it was not possible to determine with certainty that damage was limited to just the

microsheet and immediately underlying silicone adhesive. However, it is believed that the impact was spent in the microsheet and that the adhesive was able to absorb any residual gas/debris, without a significant silicon interaction. No degradation was noted in the electrical performance of the covered solar cell.

ELECTRICAL PERFORMANCE

As mentioned earlier, the experiment consisted of thirty (30) solar cells. Six (6) had 100 micron thick microsheet covers, using five (5) different cell/cover silicone adhesives, including the widely used DC 93500. Ten (10) cells had 50 micron thick FEP Teflon covers, bonded with five (5) different silicone adhesives. Ten (10) cells were covered with six (6) different silicone encapsulants. Of the ten, six employed soft coatings, such as DC93500, and the other four had hard coat silicone encapsulants. Two cells were covered with GE X-76 polyimide, and the remaining two (2) cells with Bergstron and Associates/GE BE-225HUP silicone-polyimide copolymer. The encapsulant thicknesses ranged from a low of approximately 12 microns to a high of 75 microns. The large number of sample variations and relatively small number of samples meant that in a few cases only one sample of a particular combination was tested. In general, however, at least two of each combination were tested.

Rather than present the results of the electrical performance measurements on each cell, the cells have been grouped by cover/encapsulant type. There are obviously some variations in performance due to actual material differences and the significant variations will be noted. Table 1 lists the categories and changes in Isc (short circuit current). Little change was noted in Voc, other than that due to the decreased currents.

An additional source of measurement error was attributable to the extreme length of time over which this experiment was conducted, i.e., more than ten years from experiment assembly to final tests. As a result, the original simulator and standard cell were not available for the post flight tests. Fortunately, JPL possesses balloon calibrated solar cells from the same production run as the test cells and one was selected as a new standard. A Spectrolab pulsed xenon simulator was used for these tests. The electrical tests were performed by Spectrolab, Inc. with JPL assistance.

The smallest percentage loss measured was for the cerium doped microsheet samples and the BE-225HUP copolymer samples. The latter, however, had very low initial output current and the post flight samples had cell areas clearly free of encapsulant. The next lowest losses were measured on the polyimide encapsulant, soft silicone encapsulants and the hard coat silicone encapsulants. For the X-76 polyimide, the cell was extensively denuded of encapsulant, so the current shown is in some part that of a bare cell (Figure 8). The hard coat silicones also exhibited some coating loss and crazing (Figure 9). In general, minimal cell exposure was noted for the various soft silicone encapsulants and only at the cell corners. Thickness measurements of the encapsulants were not taken post flight due to the lack of sufficiently accurate pre-flight data, so that the only assessment of coating removal was based on noting any visible exposure of the underlying solar cell.

The largest current loss was exhibited by the Teflon covered samples, although the variation was extremely high, ranging from a loss of 10 percent to a loss of 43 percent. In one case the Teflon cover was missing with only a layer of RTV remaining on the cell. Whether this occurred during flight or during retrieval is not known. The cell current with only an RTV layer left showed an Isc loss of 10 percent equal to the best of the remaining Teflon covers. The variation in losses for the Teflon covers is not understood. However, UV reaction with Teflon has been well-documented and the top surface of the Teflon covers exhibited considerable damage as defined earlier. In review, the surface appearance varied from a hazy white to a brownish discoloration. The later samples showed the greatest Isc loss. In addition, the surface was soft and somewhat tacky (Figure 10). In terms of electrical performance then, no encapsulant or Teflon cover system provided output at the

end of the mission comparable to the microsheet covered system. All of the non-microsheet cover systems exhibited visible erosion or reaction with the space environment.

CONCLUSION

The LDEF experiment provided a unique opportunity to view and evaluate the effects of a wide variety of environmental interactions. These included micrometeorite/space debris impacts, UV and particulate radiation and atomic oxygen. The relative importance of these interactions is highly dependent on orbital altitude. In addition, the LDEF experiment did not remain at a fixed altitude throughout the mission. Consequently, the extrapolation of these results to other orbits must be made with care. At present, numerous investigators are reviewing a wide variety of experiments in order to approach a comprehensive understanding of the LDEF results. Recent data indicates that the total fluence of atomic oxygen in the vicinity of this experiment was on the order of 6×10^{21} atoms/cm^2(1).

For the JPL experiment, a relatively high fluence of debris/micrometeorite impacts ($\sim$ 1300 impacts/m^2) of size $\geq$ 0.05 mm diameter was observed over the mission duration. These were typically of small size and of high energy, as evidenced by penetrations of materials such as Invar tabs and thin silicon solar cells. There is no indication that the impacts with the test samples (including solar cells) caused any electrical degradation. Evidence from a number of LDEF experiments suggests that the majority of the impacts observed on this experiment were of space debris, rather than micrometeorite origin (2).

Although the concept of polymer-type cell covers may look attractive for low cost cell protection, all tested samples exhibited losses in performance. In many cases, coating erosion was sufficient to remove most of the polymer material, allowing damage to occur to the cell grid metallization by atomic oxygen. The most durable polymer material was FEP Teflon, which continued to provide protection against atomic oxygen to the cell below. However, the Teflon material was not free of damage and exhibited visible surface darkening and softening, with some material loss. The best Teflon systems, i.e., those bonded to the cells with high quality silicone adhesives, displayed approximately eight percent greater cell current loss than the samples employing conventional cover glass material. For the latter, material integrity after nearly six years' space exposure was outstanding. Overall cell current losses were typically on the order of three percent, within the range expected from UV darkening. Clearly, the optical qualities of the conventional platelets remain unmatched by the other materials. In addition, only the relatively hard conventional covers appear to provide any protection against incident micrometeorite or debris. For orbits containing similar types of environmental threats, conventional coverglass materials are preferred, and a quality polymer replacement has yet to be demonstrated.

Acknowledgment

The work reported herein was performed by the Jet Propulsion Laboratory, California Institute of Technology, under contract to the National Aeronautics and Space Administration.

References

1. Bourassa, Roger J. and James R. Gillis, "Atomic Oxygen Fluence for Each LDEF Tray", LDEF Spaceflight Environmental Effects Newsletter, Vol. 111, No. 1, March 30, 1992.

2. Ellis, David, "Micrometeoroid and Debris SIG is Focus for Many Issues", LDEF Spaceflight Environmental Effects Newsletter, Vol. 1, No. 8, January 23, 1991.

Cover/Encapsulant	Isc (mA)		Δ(%)	Comments Cover/Encapsulant
	Preflight	Postflight		
Microsheet (Ceria)	136.5	132.4	-3	
FEP Teflon	136.8	106	-22	Darkened top surface loss varies from -10% to -43%
Silicone (soft)	132	115	-13	Crazing, some loss near cell edges
Silicone (hard coat)	135	112	-17	Crazing, flaking, close to complete removal
BE-225 HUP Polyimide-silicone Copolymer	125	121	-3	Partially removed - Voids
GE X-76 Polyimide	129.5	119	-8	Encapsulant significantly removed

Table 1. Solar Cell Assembly Electrical Performance

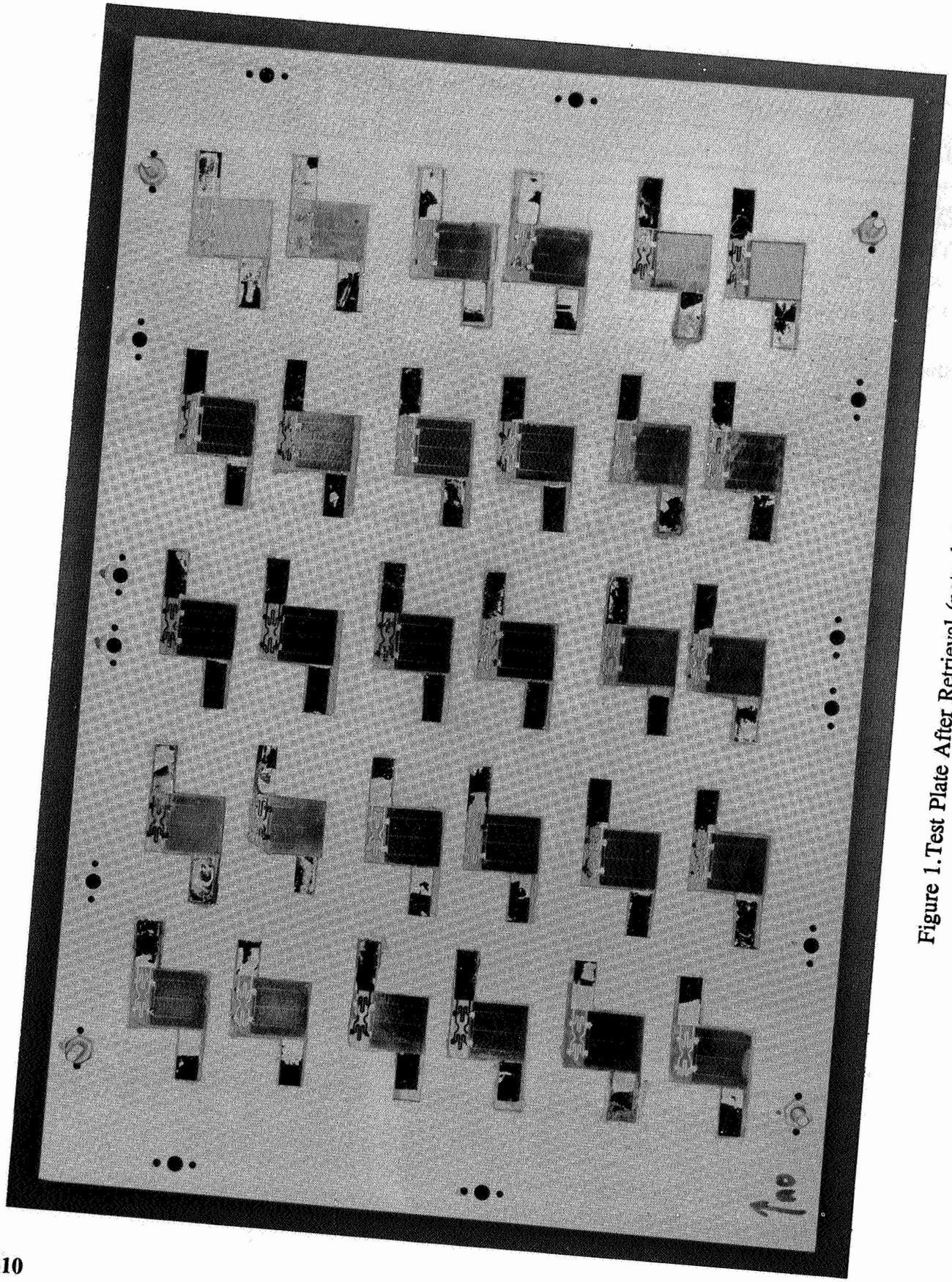

Figure 1. Test Plate After Retrieval (note darkened tabs)

ORIGINAL PAGE
BLACK AND WHITE PHOTOGRAPH

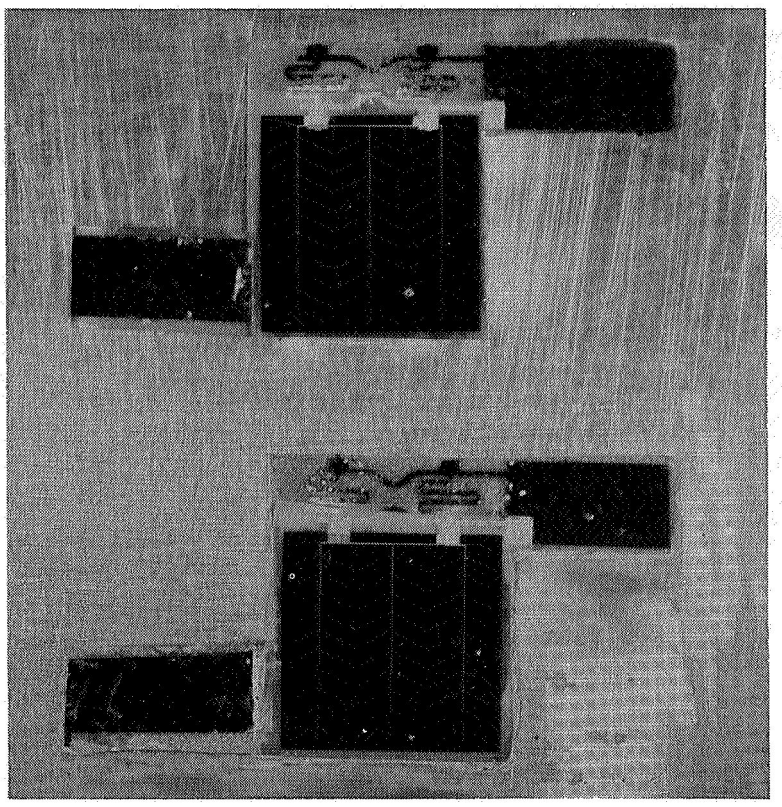

Figure 2.Impact with Teflon Cover (Lower Part of Upper Cell)

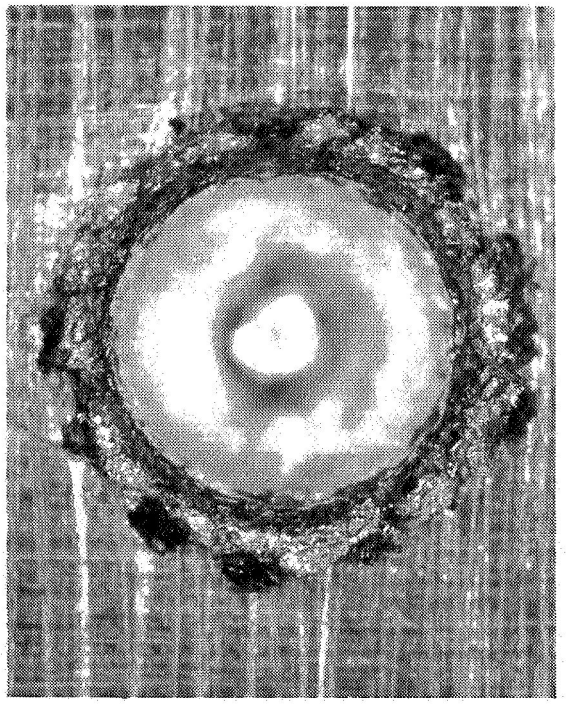

Figure 3.Largest Impact Crater (~1 mm diameter)

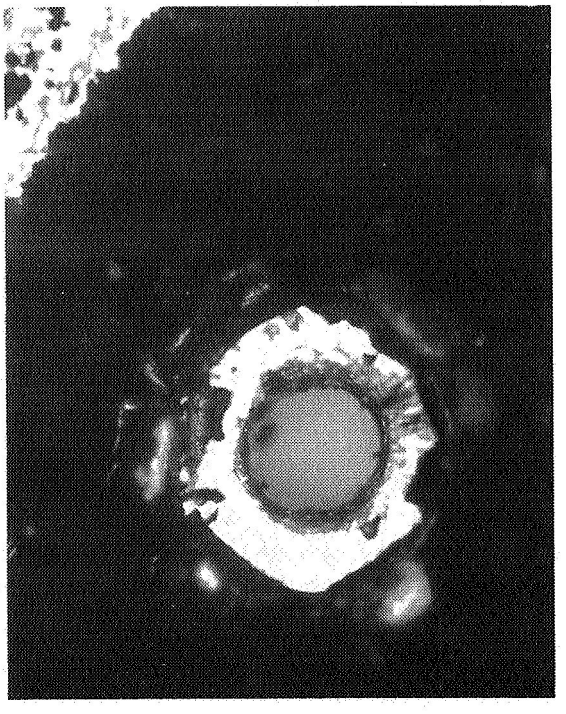

Figure 4.Ag Plated Invar Impact

ORIGINAL PAGE
BLACK AND WHITE PHOTOGRAPH

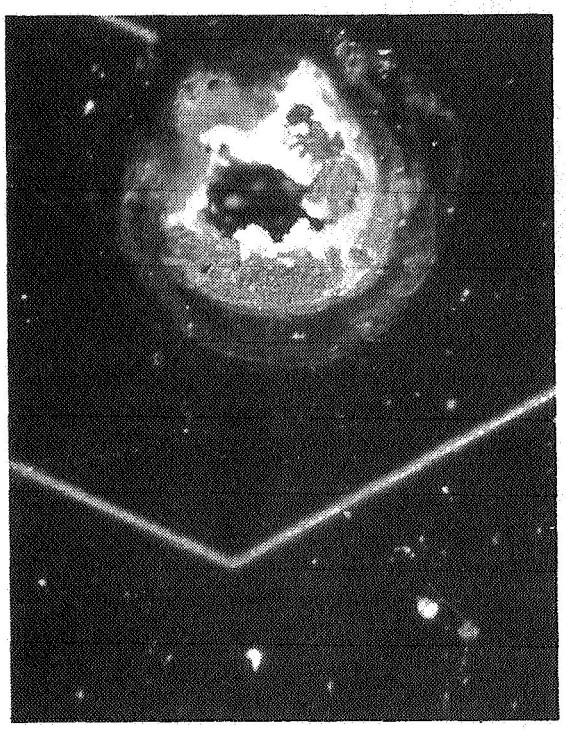

Figure 5.Teflon Cover Impact

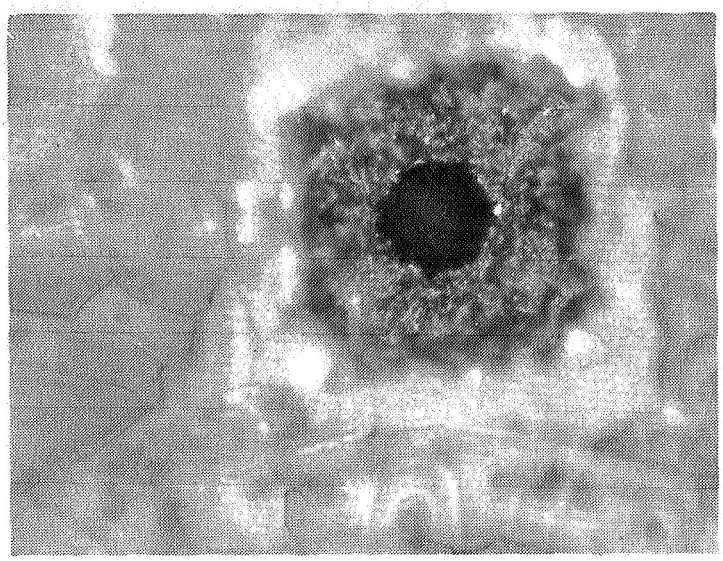

Figure 6.Silicon Impact (200X)

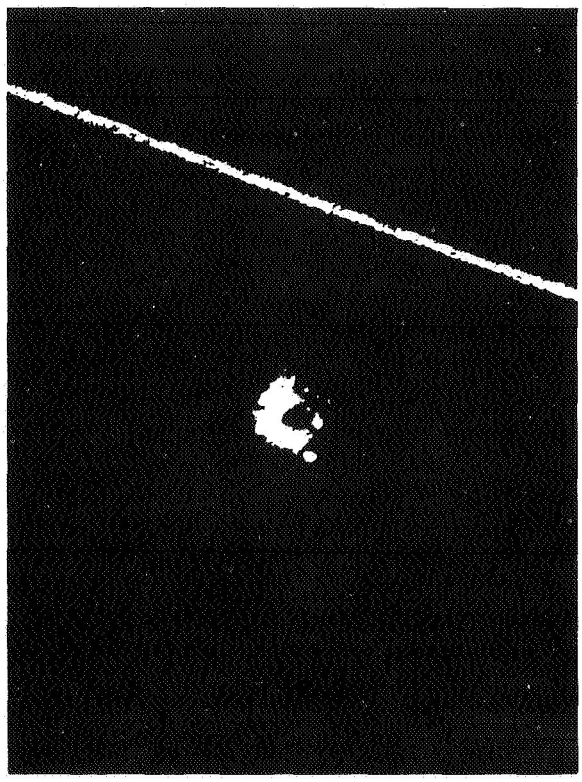

Figure 7.Microsheet Cover Impact (7X)

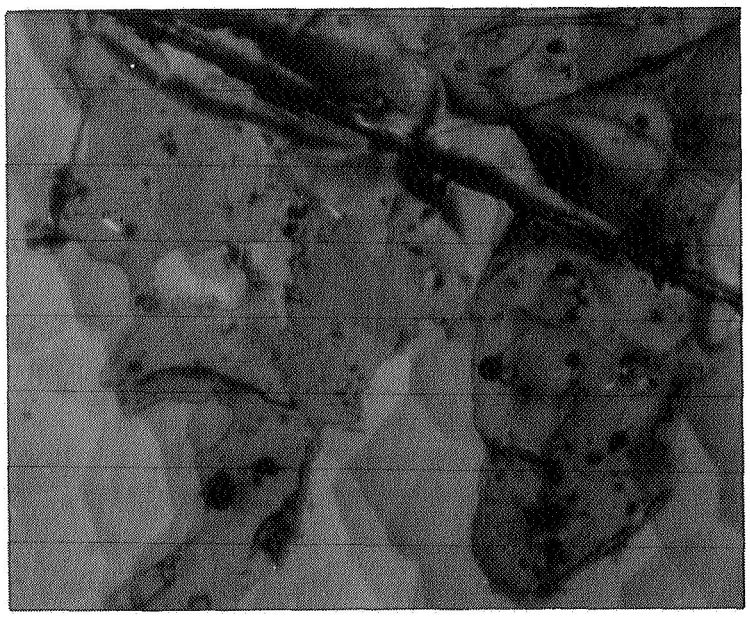

Figure 8.Polyimide Encapsulant Degradation

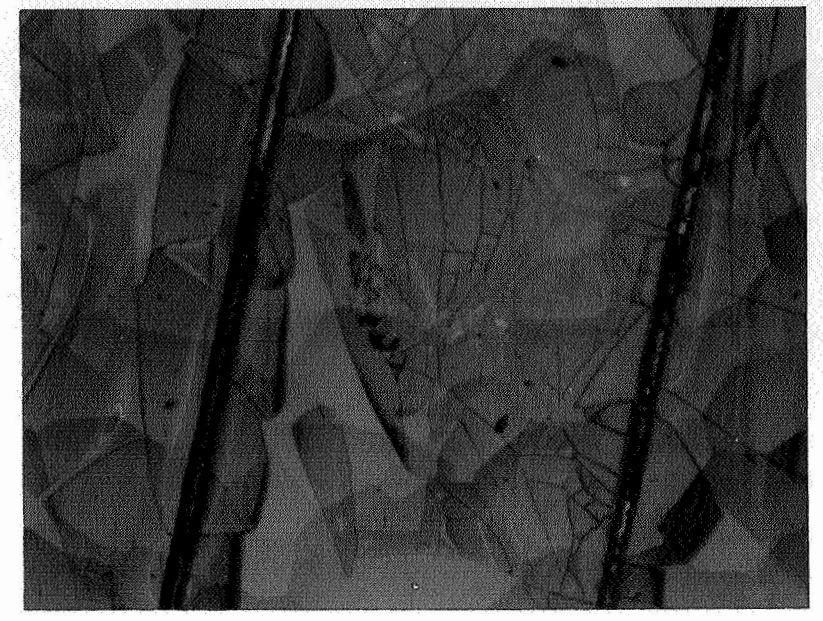

Figure 9.Hard Coat Silicone Degradation

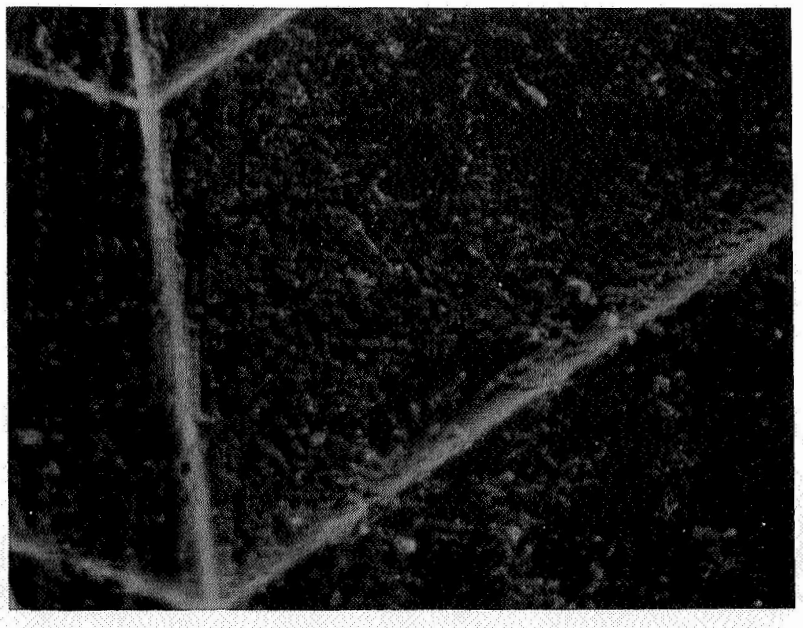

Figure 10.Softened Teflon Cover

ORIGINAL PAGE
BLACK AND WHITE PHOTOGRAPH

N93-29688

501720
p 5 B

NEW RESULTS FROM FRECOPA ANALYSIS

Christian Durin
CNES RA-DP EQ/QM
18, av E. Belin Toulouse FRANCE
Phone (33) 61 28 14 39, Fax (33) 61 27 47 32

SUMMARY

This paper discusses new results from the ongoing analysis of the FRECOPA's (FREnch COoperative PAssive payload) system hardware. FRECOPA (AO138) was one of the 57 experiments flown on the LDEF satellite. The experiment was loacted on the trailing edge (Tray B3) and was exposed to UV radiation (11,100 equivalent sun hours), ≈ 34,000 thermal cycles, higher vacuum levels than the leading edge, a low atomic oxygen flux and minor doses of protons and electrons. Due to LDEF's extended mission (5.8 years), CNES decided to set up a team to analyse the FRECOPA system. Initial results were presented at the First Post-Retrieval Conference, June, 1991. This paper summarizes the results obtained since then.

INTRODUCTION

The first subject of our analysis is the study of the kinematic system. We observed damage on the DELRIN gears and lubricant ageing. The results are based on comparative appraisals between components after flight and those stored on ground in laboratory conditions. We also observed the aluminum surface treatment in the exposed areas and measured the thermo-optical properties changes. We also examined the welds on the FRECOPA structure.
The second point is the analyses of shadows observed on the tray including one inside (canister shadow) and three on the back side of the tray (bolt, rivets and wire shadows). We used surface analysis techniques such as X ray, Rutherford Back Scattering (R.B.S.) and Electron Spectroscopy for Chemical Analysis (E.S.C.A.) to determine the origin of contaminations. We worked with the same techniques on the teflon glass fabric and painted areas used on the back side where we observed color changes.
Now with all the results stored, we try to give an appraisal on the use of FRECOPA materials in LEO space environment.

PRECEDING PAGE BLANK NOT FILMED

OPENING/CLOSING MECHANISM

It is composed of a stepping motor driving two screw nuts via a double 6-stage reduction set-up. The raising or lowering of the nuts, fixed to the canister, allows the canister to be opened or closed. The figure 1. illustrates a reduction set-up. Note that we alternated gears made of DELRIN and gears made of steel to avoid the risk of micro-welding and to ensure lubrication.
Between metal parts (nut, screw), powdered MoS_2 was used as a lubricant.The whole opening mechanism operated correctly before and after the flight. The resistance couple was found to have increased by 50 % but there was still a safety margin of 22.

The motors

Appraisal of the motors (2 flight models and 1 ground model), carried out by the manufacturer, SAGEM, showed slight ageing of the materials - especially the paintwork - and oxidation on the stator of one of the motors. On dismantling, friction corrosion was also observed on the ball bearings.
The inside of the motors appeared to be rather dirty but no free particles were found on the flight models.

The general behavior of the motors after use in space was very satisfactory.

The gears, screws and nuts

On all the mechanical parts, steel gears, bronze /Be screws and the steel nuts, no mechanical alterations were noted. On the exposed surface of the nuts, organic contamination had caused yellowing.
On the DELRIN gears, however, all the parts exposed to UV radiation were discolored.
Electron microscopy (as seen in fig. 2) showed extensive ageing of the material. The matrix was cracked and slight erosion was seen in this zone. Similar observations had already been made with other mechanical parts made of DELRIN in the FRECOPA experiment.

The use of unprotected DELRIN in precision mechanical assemblies can therefore pose problems in space applications.

MoS_2 lubricant

There was MoS_2, used in powder form, on the screw and on the nut. No quantitative measurement had been made before the flight. Comparison between ground and flight models showed a great decrease of lubricant on the areas exposed to the environment.
In the protected areas (nut threads and ball thrust bearing), however, the presence of MoS_2 was still observed.

This type of lubricant should therefore be used with a system of protection from the environment.

Thermal coating

The whole structure of the canisters was treated with black chromic anodizations to maintain thermal equilibrium and protect the metal surface.
All the exposed zones were subject to ageing with a change of colour (black becoming grey) and some areas were cracked.
In the places where the gears had acted as screens, their shadows were left on the underlying structure (as seen in fig. 3).
Fine measurements carried out in these zones to determine the alteration of the thermo-optical properties did not show significant variations.

The thermal coating showed signs of ageing; its use in long-term missions should be considered in relation to its exposure.

TIG welding

The structure carrying the boxes was welded using a TIG process (Tungsten Inert Gas).
Inspection of the welds showed one small corrosion spot which was attributed to insufficient rinsing after dye checking before flight.
We also observed a small crack attributed to ageing of the weld.

We concluded that these welded assemblies present good mechanical properties without alterations attributable to the space environment.

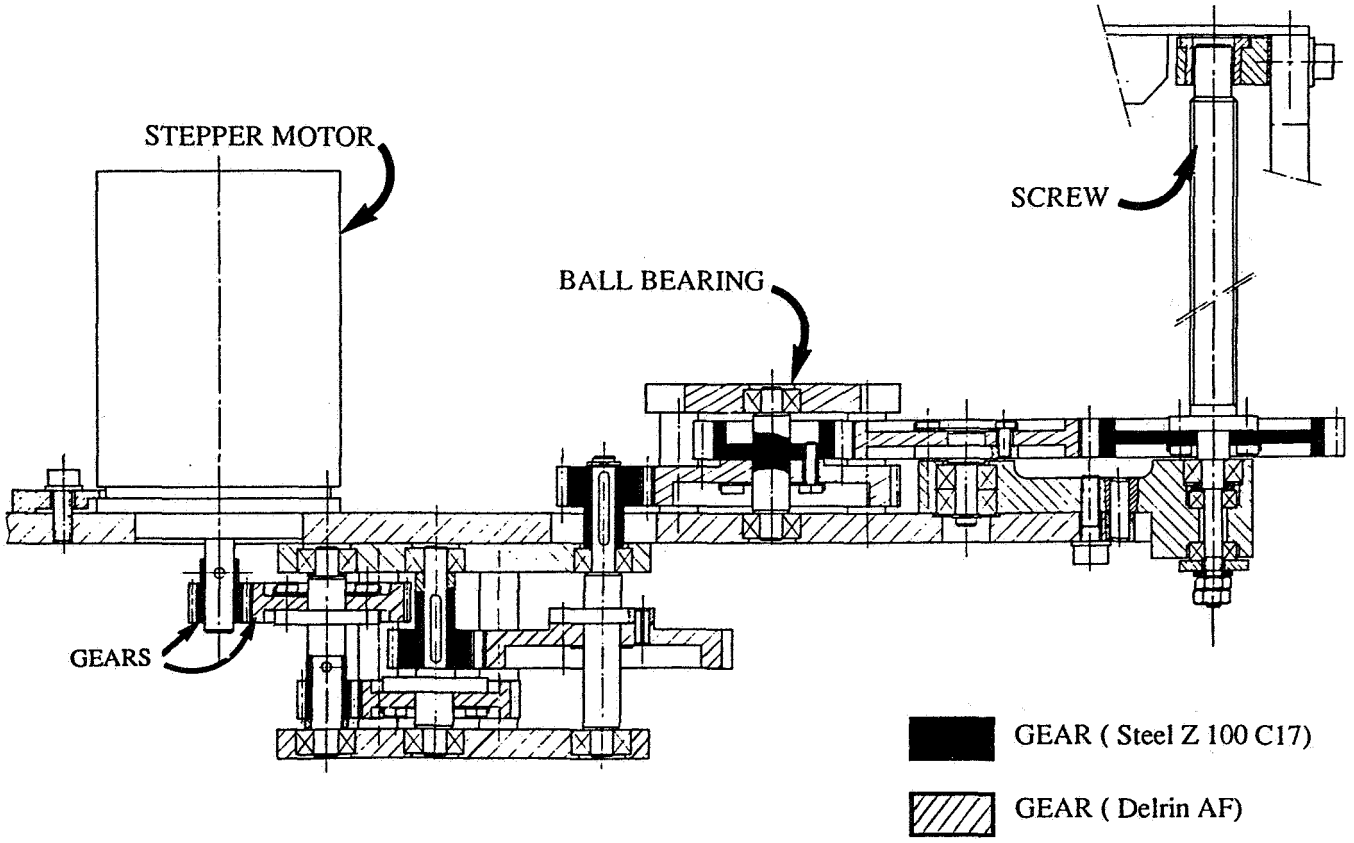

Figure 1. Kinematic reduction mechanism

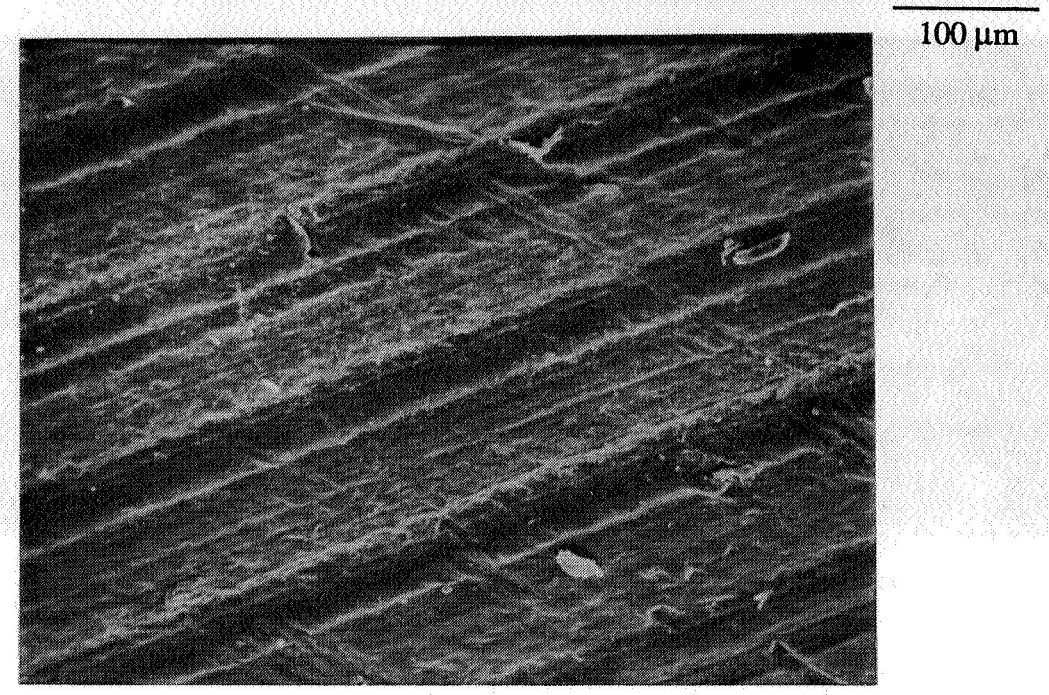

Reference sample

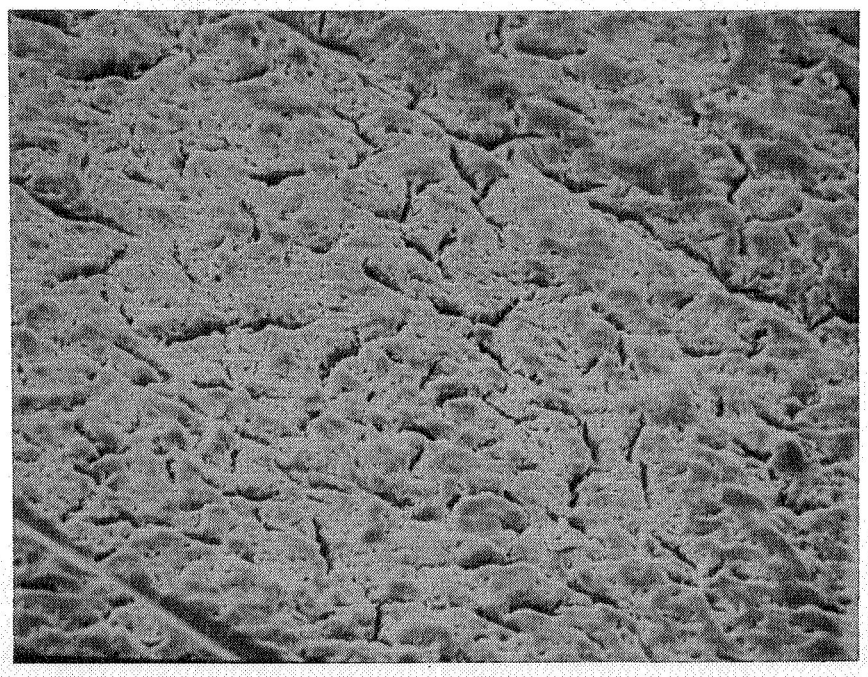

Flight sample

Figure 2. Delrin gears, SEM observations

ORIGINAL PAGE
BLACK AND WHITE PHOTOGRAPH

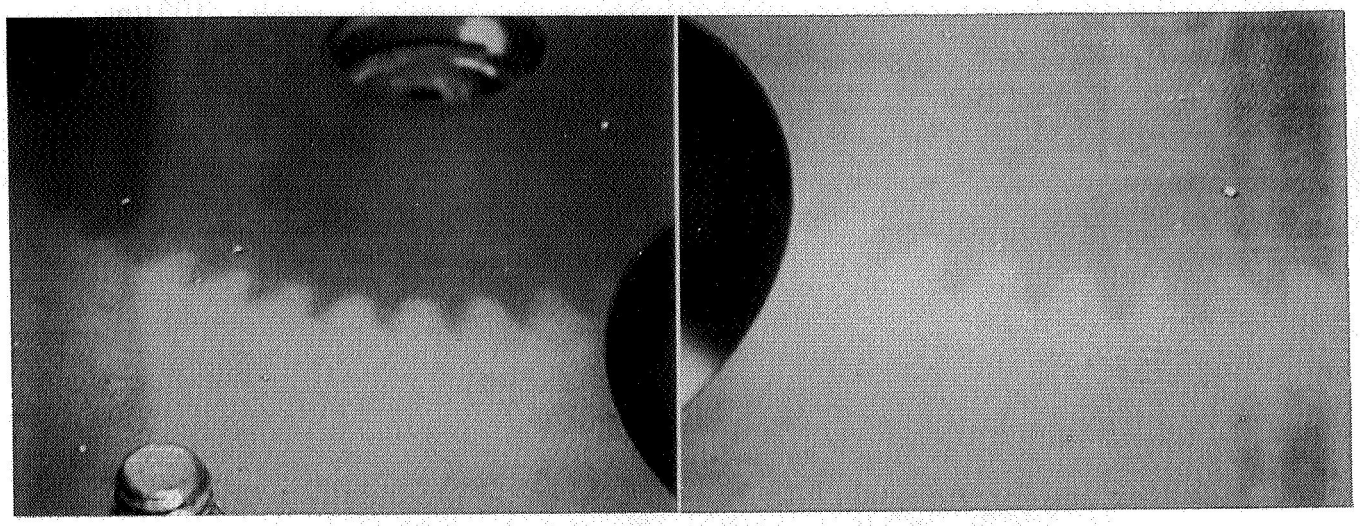

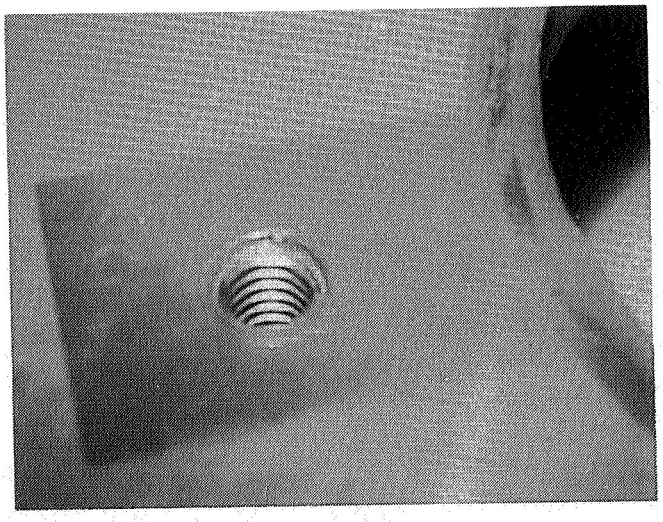

Figure 3. Gears and motor hold-down clip shadows on the main structure

FRECOPA SUPPORT STRUCTURE CONTAMINATION

We observed numerous shadows caused by contamination deposited on the FRECOPA support structure. They were noted inside the structure as well as on the back surface which was protected from the direct environment. To study this problem, we used three complementary techniques for surface analysis : SEM (Scanning Electron Microscopy), RBS and ESCA.
We also carried out thermo-optical measurements to study the influence of the layers of contaminants. Our aim was to gain a better understanding of the process, to determine the origin and the direction of the fluxes and, if possible, the materials responsible. Three zones were analyzed :

- the internal aluminum surface of the support where the shadow of one of the canisters was visible. This contamination was on just one of the sides and originated from outgassing of the organic materials present on the satellite, then condensing of the residues uniformly on all the cold parts during the night. At sunrise, under the effect of UV irradiation, the condensation is polymerized on the side that is lit up most rapidly. On the other, which warms up more slowly, it has the time to evaporate. As the canister acts as a screen, its shadow remains projected on the surface. The sample was taken from the exposed/contaminated zone. As reference, we sampled a zone protected from the direct environment.

- on the back surface, we took samples on the four thermal blankets protecting the inside of FRECOPA. They were made from PTFE-treated glass fabric with a layer of aluminized Mylar painted black on the surface analyzed. For this material, the reference was blankets which had remained in storage on the ground. Contamination was observed in the form of unequally distributed iridescence. Samples were taken from these areas.
On the structure, other samples analyzed concerned surfaces exposed to varying contaminant fluxes. Other zones (shadows of bolts and electric wires, as seen in fig. 4.) with difficult access presented the same signs of contamination.

- our third task was to analyse the multiple shadows around the rivets on the outer surface of the support (as seen in fig 5.). The reference zone was out of the shadows, the contaminated zone was inside the shadow or shadows (see figure below).

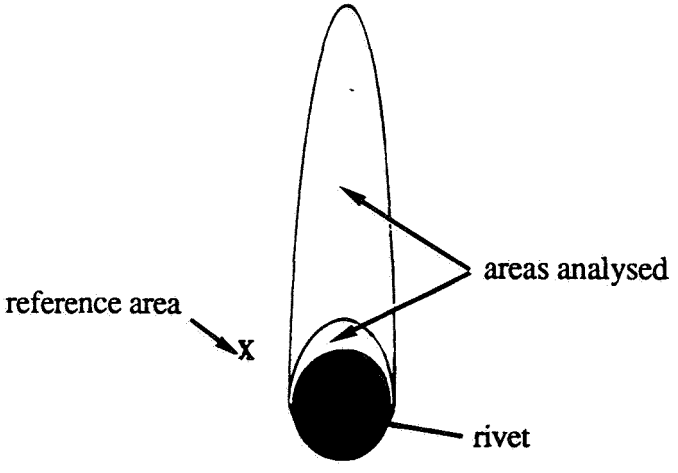

The various surfaces concerned are indicated in the figure 6.

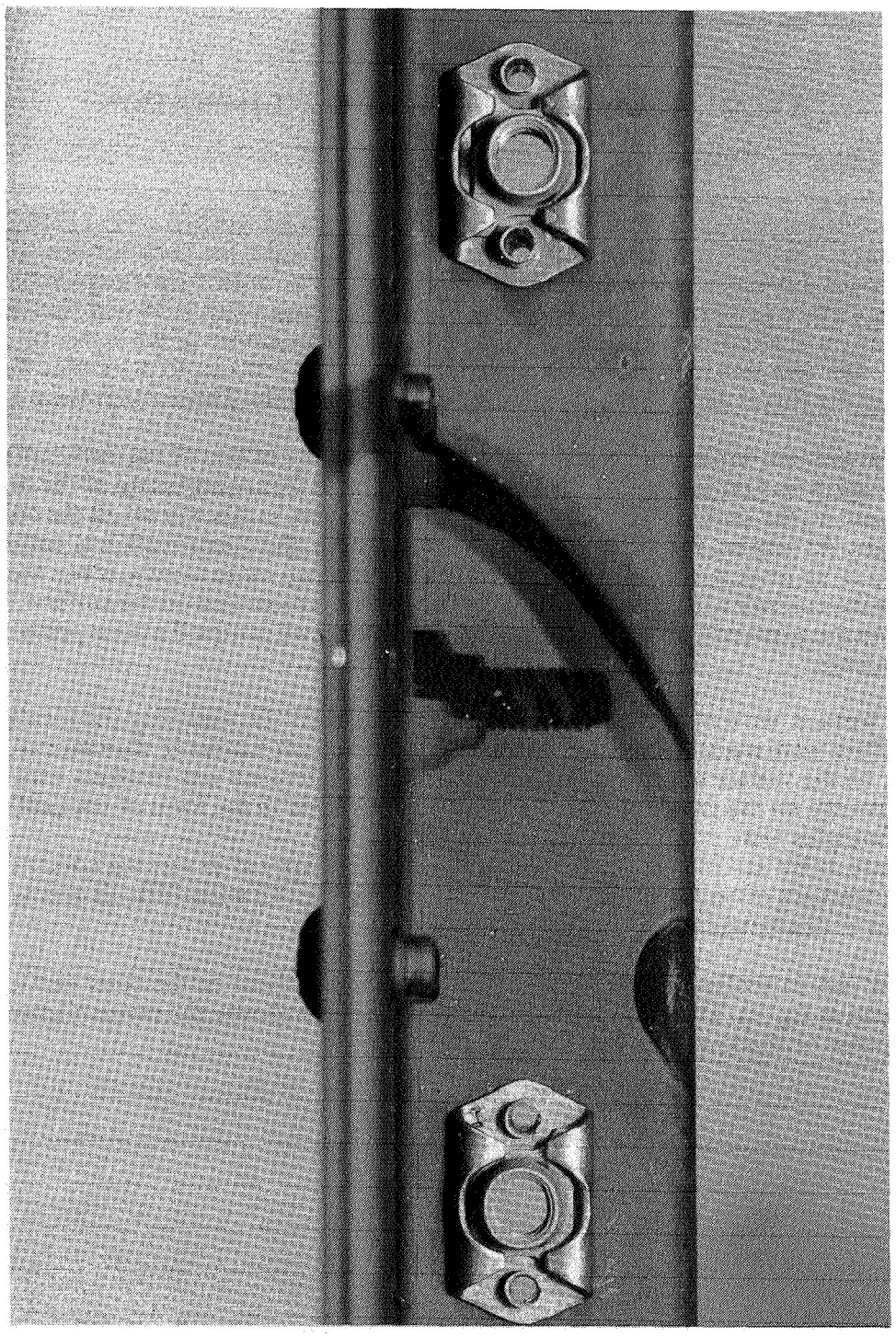

Figure 4. Bolt and wire shadows
on the back face of the tray

ORIGINAL PAGE
BLACK AND WHITE PHOTOGRAPH

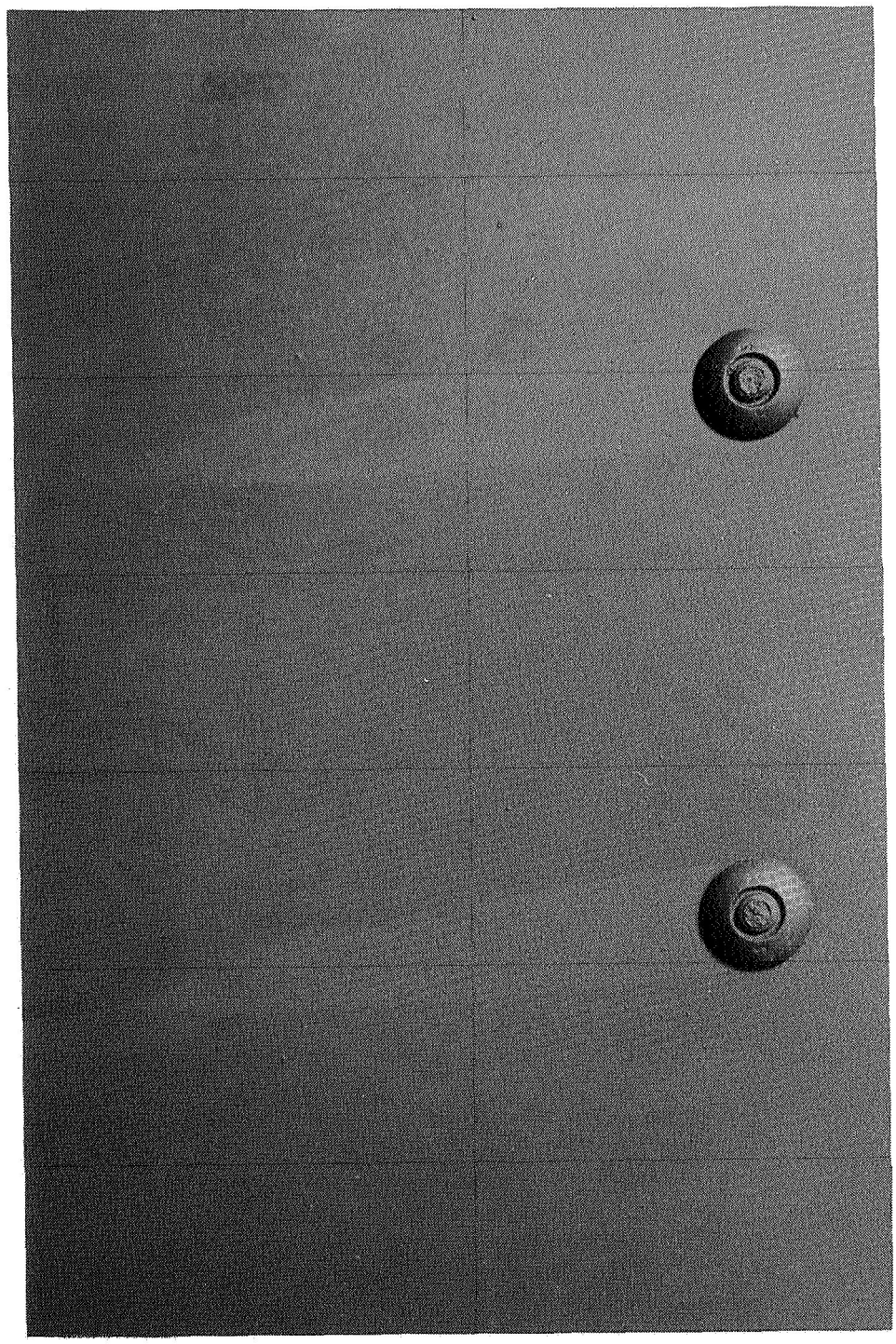

Figure 5. Rivets shadows on the lateral sides of the tray

ORIGINAL PAGE
BLACK AND WHITE PHOTOGRAPH

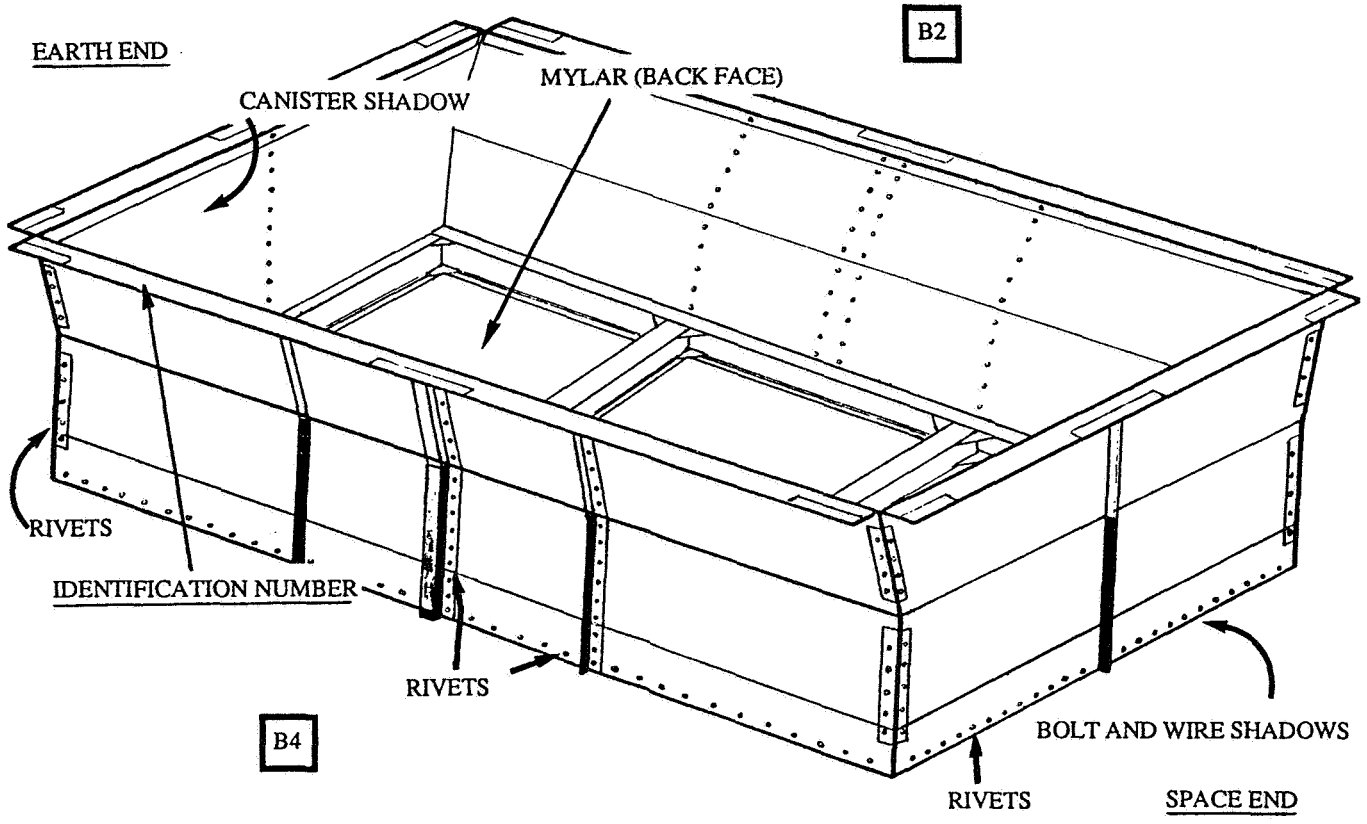

Figure 6. Areas analysed on the tray

The contaminations results are summarized in the table in figure 7. The following conclusions can be drawn from the table :

- very slight changes in thermo-optical properties. The only notable change is a 9 % increase in the solar absorptance value of aluminum.

- SEM gave very few results, probably owing to too great a thickness being analyzed.

- RBS gave some interesting informations :
  . the Mylar was contaminated with a layer of SiO_2 and metallic elements (Ag, In)
  . No change for yellowed aluminum.
  . Presence of SiO_2 and heavy elements (Cu, Ag, In) on the light part of the right-angled bracket.
  . Rivets: contamination with a layer of SiO_2 around the shadows (20 Å) and on the large dark area (30 Å) but no SiO_2 was detected on the white zone.

- ESCA gave certain additional informations :
  . On the Mylar, there were two types of contamination : SiO_2 and CO or CO_2.
  . For the yellowed aluminum : layer of SiO_2 with Ag underneath.
  . Bracket: the whole bracket must have been contaminated by SiO_2.

Note should be made of the direction of contaminant flux visible around the rivets.

Multiple shadows indicate fluxes from several directions (as seen in fig 8.). The direction is from the inside of the LDEF towards space. We measured the variation of the rivet shadow angle on three of the surfaces of the support; on the fourth, this was impracticable (as seen in fig 9. for Earth and space end). The variations seem to indicate one or two sources of flux. A scale drawing (as seen in fig 10. for the space end) indicates the origin of the fluxes to be the inter-plate gaps (as seen in fig 11.) which must have let through atomic oxygen and UV radiation, which were able to react with the materials (silicone paint) present inside the satellite and/or draw in contaminants.
The processes of material degradation and the chemical reactions are probably at the origin of the differences of thickness measured for the contaminants (SiO_2).

These results demonstrate that the problem of contamination can be more important than expected and that numerous contaminants can be found even inside the satellite, which would be very prejudicial for optics and for sensitive mechanisms.

CONCLUSIONS

In spite of the satisfactory operation of the FRECOPA experiment, our post-flight appraisals showed ageing of the organic materials, essentially under the action of UV radiation in our case. We noted erosion, discoloration and increased fragility calling into question the use of these materials unprotected. Moreover, their outgassing causes heavy contamination.

The findings also pose the problem of outgassing tests on the ground which seem, for the moment, to be insufficient to model the complex synergistics of the parameters of a space environment.

The behavior of metals appears to be satisfactory once problems of lubrication and micro-welding have been taken into account.The welded assemblies were totally satisfactory.

	SITUATION	α / ε	X	R.B.S.	E.S.C.A.
Mylar (Ref)	Back Face	0.98 / 0.92	C,O,Si	C,O,Si,Ca	C (49%) O (23%) Si (28%)
Mylar (Flight)	Back Face	0.98 / 0.92	C,O,Si Na,Mg,Al S,P	C,O,Si,Ca P,Ge,Ag,In SiO_2	C 22%,O 50% Si 28%,S,N ---> SiO_2
Al (Ref)	Inside Tray	0.47 / 0.186	C,O,Na,Mg Al,Si,S,Cl,Cr Fe,Cu	Al,O,S,Ca,V Cr,Fe Al_2O_3	C,O,S,Al,Na Si after scouring
Al (yellow)	Inside Tray	0.51 / 0.178	C,O,Na,Mg Al,Si,S,Cl,Cr Fe,Cu	Al,O,S,Ca,V Cr,Fe Al_2O_3	C,O,S,Al,Na Si ---> SiO_2
right angle bracket (light)	Lower part of the tray	/ / /	/ / /	C,N,O,Si,Fe S,Ca,Cu,Ag,In SiO_2	C,N,O Si,S
right angle bracket (dark)	Lower part of the tray	/ / /	/ / /	C,N,O,Si,Fe S,Ca	C,N,O Si,S
Rivets	Sides	/ / /	/ / /	C,N,O,Si,Fe S,Ca,Cu,Ag,In SiO_2 except light zone	/ / /

Figure 7. Surface analysis results

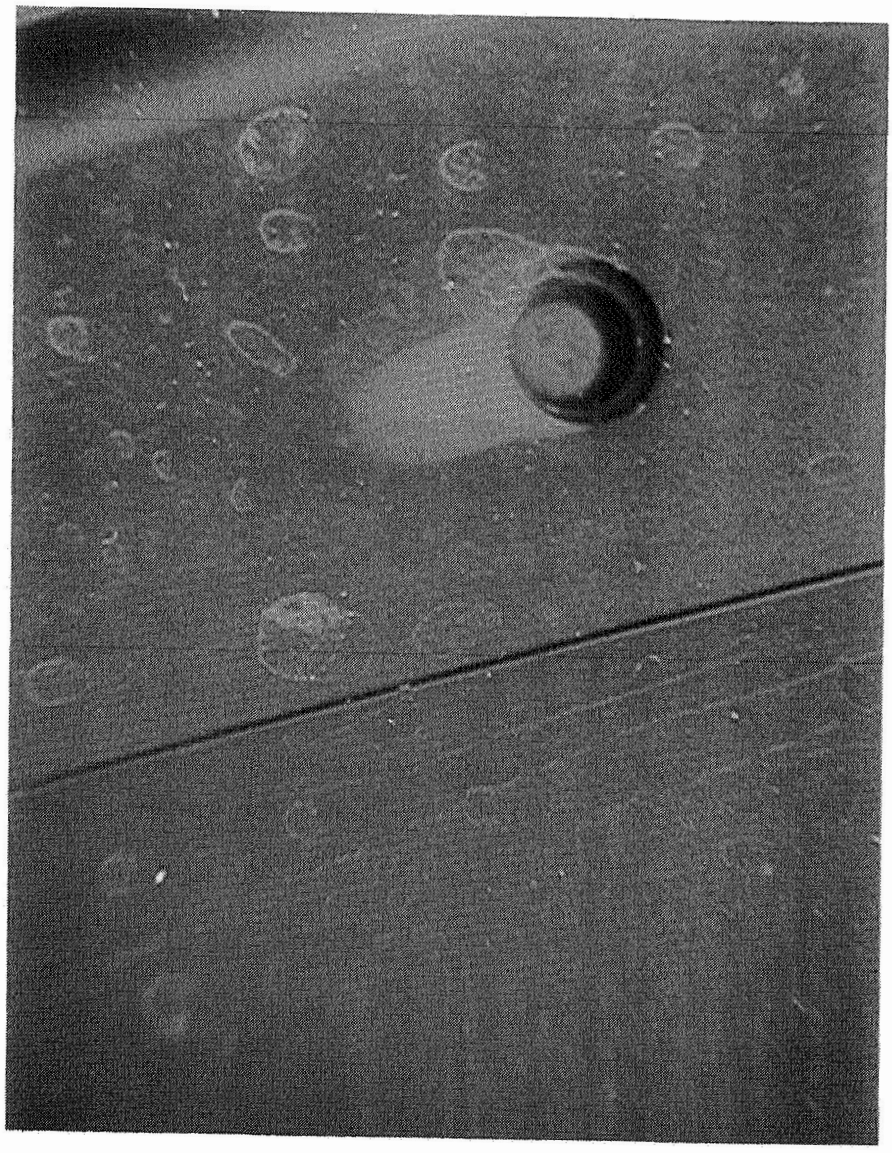

Figure 8. Fluxes directions

ORIGINAL PAGE
BLACK AND WHITE PHOTOGRAPH

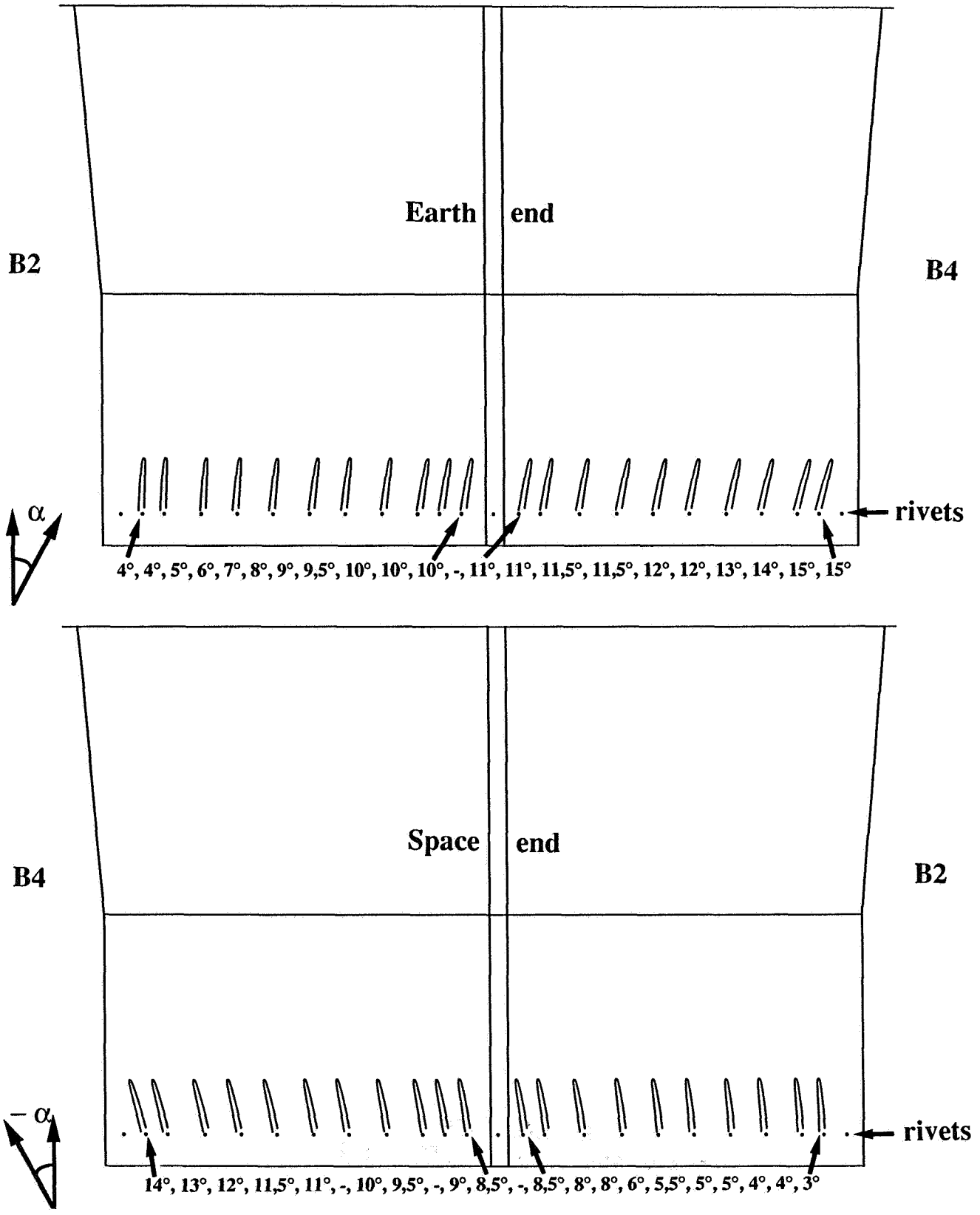

Figure 9. Angle measurements on rivets shadows

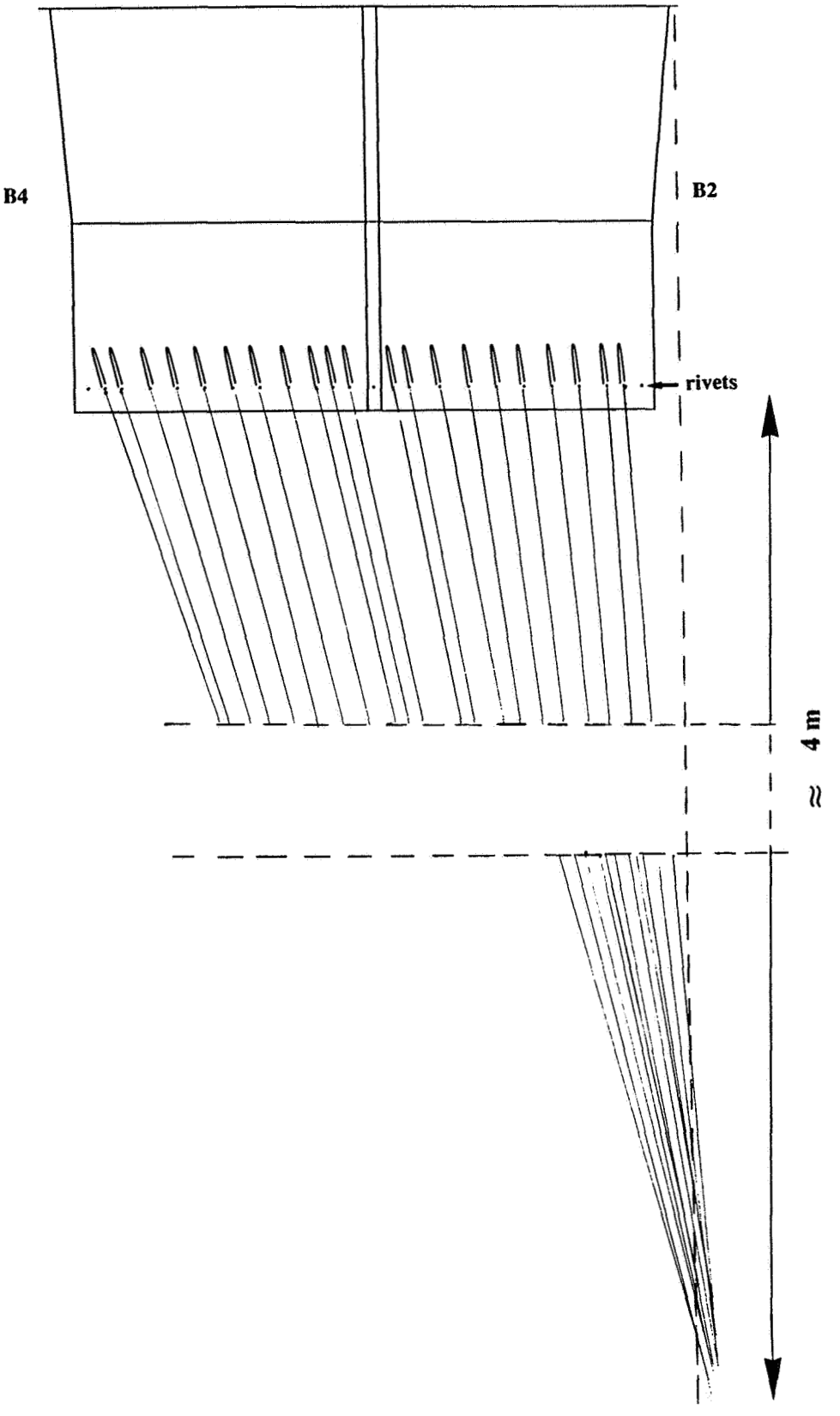

Figure 10. Origin of contamination flux (space end)

Figure 11. Gaps inter-trays on LDEF (NASA photo)

ORIGINAL PAGE
BLACK AND WHITE PHOTOGRAPH

Bibliography

1. Ch. DURIN *"Expertises du système FRECOPA"*
Doc CNES 92

2. E.CONDE *"FRECOPA, Expertise des mécanisme des boitiers au retour du LDEF"*
Doc CNES aout 91

3. A. SIRVEN, F. ESTAGER *"Expertises du plateau FRECOPA"*
Rapport de stage juin 92

N93-29689

DEGRADATION OF ELECTRO-OPTIC COMPONENTS ABOARD LDEF

561724
P16

M. D. BLUE
Georgia Tech Research Institute
Georgia Institute of Technology
Atlanta, Georgia 30332
Phone: 404/894-3646, Fax: 404/894-5073

SUMMARY

Remeasurement of the properties of a set of electro-optic components exposed to the low-earth environment aboard LDEF indicates that most components survived quite well. Typical components showed some effects related to the space environment unless well protected. The effects were often small but significant. Results for semiconductor infrared detectors, lasers, and LED's, as well as filters, mirrors, and black paints are described. Semiconductor detectors and emitters were scarred but reproduced their original characteristics. Spectral characteristics of multi-layer dielectric filters and mirrors were found to be altered and degraded. Increased absorption in black paints indicates an increase in absorption sites, giving rise to enhanced performance as coatings for baffles and sunscreens.

INTRODUCTION

The LDEF Active Optical Systems Component Experiment consisted of over 100 electro-optic components both mounted on an LDEF tray and stored as controls. The tray location was near the space end and toward the rear of the satellite. A preliminary report was presented at the 1991 First LDEF Post-Retrieval Symposium[1]. During the past year we have continued measurement and analysis of component properties. Design of the mounting hardware, along with the associated thermal and structural considerations, was discussed in the previous report[1]. Here, we present additional data and discuss our conclusions regarding the observed property changes for the components. Component measurements are still in process, and modifications to our conclusions are possible.

The objective of these measurements is to establish guidelines for the selection and use of such components in space-based electro-optic systems.

PRECEDING PAGE BLANK NOT FILMED

INFRARED DETECTORS

No changes were found in the properties of six large-area silicon photovoltaic detectors (800 mm^2) after retrieval. Typical results for measurements of junction capacitance, junction leakage current, and noise spectral density are presented in Figures 1-3 respectively. Capacitance, Fig. 1, was unchanged for all devices. Junction current in Fig. 2 represents current for a diode struck by a micrometeorite leaving a visible scar. A photograph of the impact site was presented previously.[1] Fig. 3 shows that the current noise for the device was well below specifications after recovery. Responsivity and noise show no change for any of our silicon detectors. These devices were mounted so as to expose the active surface to the space environment in order to maximize possible degradation effects.

Remeasurement of properties of other infrared detectors is in process. The task is made more difficult because of the extended time period between original and present measurements. In some cases it has been difficult to reproduce the original measurement conditions because of changes in equipment. At this time, the only infrared detectors in this set of components which indicate apparent degradation are part of a group of pyroelectric detectors.

Properties of a group of 31 pyroelectric infrared detectors (including 10 stored as controls) were reported by Dr. James Robertson, NASA Langely Research Center.[2] Detectors fabricated from several pyroelectric materials were included in the group. Triglycine sulphate material did not perform well. All detectors but one made from this material failed including the controls. Triglycine sulfate is an exception to the overall good performance of all detector materials measured to date.

LASERS AND RELATED COMPONENTS

While the gas lasers in our component set did not survive the extended period in orbit, GaAlAs semiconductor lasers were not changed by their exposure to the space environment. Remeasurement of Nd:YAG laser rods awaited refurbishment of the original laser cavity which had deteriorated. With new pump lamps and a replated cavity, the rods performed even better than the original measurements. The results are presented in Table 1.

Three Nd:YAG rods were included in the components set. Two were mounted in the tray beneath an aluminum cover (simulating the minimum protection expected in a typical installation) while the third was stored as a control. Characterization of the rods assumes a linear relation between input pump energy and output laser-pulse energy with an intercept on

the pump-energy axis. The measurements then provided the slope and intercept characterizing this relationship between input and output energies for the rods in specific positions in the three-rod laser cavity. The required cavity improvements made the cavity more efficient, and the remeasured coefficients indicated better performance than the original measurements.

Table 1. Nd:YAG Rod Properties

	Control	Rod #1	Rod #2
Prelaunch			
Slope Efficiency, (mJ/J)	24.6	22.6	23.6
Intercept, (J)	7.6	7.1	7.0
Postrecovery			
Slope Efficiency, (mJ/J)	36.2	35.0	35.2
Intercept, (J)	3.8	3.1	3.1

The space-exposed rods and the control had the same relative change in measured characteristics. The relationship among the rods remains the same as in the original measurements. Even the 1/4-λ coating on the ends of each rod survived in good condition. We conclude that the changes in parameters were due only to the changes in the cavity, and that space exposure did not change the rod properties.

Other laser related components in this group were an ADP (ammonium-dihydrogen phosphate) electro-optic modulator and a laser flash lamp. No changes were found in the properties of these components post-recovery. The spectral output of the flashlamp reproduced the original measurements. For the modulator, the transmission, roll-off frequency, and half-wave voltage were unchanged. Laser-cavity mirrors are discussed in a separate section.

Light emitting diodes (Monsanto GaAsP LED's) also remained unchanged whether stored in our laboratory or mounted on the LDEF tray. Figure 4 shows light output for a space-exposed diode and a control diode. The original characteristics for both diodes are well reproduced. The stored diode has slightly greater quantum efficiency, while the plastic dome of the space-exposed diode carries the indentations of small micrometeorites.

OPTICAL FILTERS

Our set of nine optical filters included three different filter types. These types were narrow-band filters, wide-band filters, and neutral-density filters. One example of each filter type was placed under an aluminum cover to protect it from direct space exposure. The remaining filters were directly exposed to the space environment.

The narrow-band filters, composed of quarter-wave thick stacks of dielectric materials, showed evidence of reduced transmittance, shift of the center wavelength, and bandpass broadening, although the covered filter showed only a reduction in transmittance with no shift of center wavelength or bandpass. Wide-band filters (composed of 11 pairs of ZnS/ThF_4) also had reduced transmittance and showed evidence of deterioration of the interference coatings as a result of the space exposure. The covered filter experienced a similar but smaller amount of degradation than the exposed filter.

Neutral density filters did not use quarter-wave dielectric stacks. These filters are composed of a single layer of Inconel metal which provides approximately uniform attenuation across the visible spectrum. The sample exposed to the space environment had slightly increased transmission. The covered sample was unchanged.

Explanations of the unexpected results must consider the differences between the exposed and covered filters, the modest amount of ionizing radiation (less than 300 krads), the negligible oxygen flux (less than one oxygen atom per 100 surface atoms), and the absence of any visible deterioration after retrieval.

Consideration of the results for the filters, mirrors (following section), and detector windows leads to the following speculations regarding the physical phenomena that are believed to be the major causes of the observed changes in this set of optical filters. Details concerning the degradation of the filters can be found in an earlier paper.[3]

Narrow-Band Filters (Three Effects)

Drop in Transmittance

Degradation and aging of the cement or varnish used to attach the cover glass by UV and other radiation increases opacity and reduces throughput.

Band-Pass Shift

Years of temperature cycles (>32000) increase packing density and reduce average filter-layer thickness which causes a band-pass shift toward the blue (depends upon materials).

Band-Width Increase

Temperature driven interdiffusion between the interference layers reduces interlayer reflectivity and increases filter bandwidth (depends upon materials).

Wide-Band Filters (Two Effects)

Disruption of Design Tolerance

As with the narrow-band filters, interdiffusion disrupts the design balance and reduces the effectiveness of the design causing degraded cutoff slope and deeper and wider ripples in the transmission spectra.

Drop In Transmittance

The reduced interlayer reflectivity not only degraded the design, but also caused reduced transmittance. Thus, even the hot mirror under cover suffered reduced transmittance. In addition, the exposed filter may have experienced erosion as contamination at the exposed surface caused additional transmittance loss.

Neutral-Density Filters (One Effect)

Increase In Transmittance

The slight increase in transmittance for the exposed filter is likely due to erosion plus a small amount of pre-launch and pre-recovery oxidation. The covered filter may have a slight (less than 0.1%) increase in transmittance due also to oxidation.

LASER MIRRORS

A set of 25 laser mirrors were provided by AFWL (now Phillips Lab.) for the component set. The mirrors were quarter-wave dielectric stacks over copper- or silver-plated quartz or metal substrates. All mirrors were optimized for high reflectivity at 2.8 μm or 3.8 μm. Post-retrieval examination of the mirrors revealed no evidence of peeling, flaking, or loss of adhesion. Scratches and lap marks were evident along with residual particles of lapping compound at the end of some of the tracks. No unusual features such as dendrite formation or impact craters were noted during surface examination. A more extensive search should reveal some craters since they were seen on other trailing-edge components.

During a general refurbishment and updating of the component set in 1983, six laser mirrors were found to be developing pin holes, or flaking and peeling. These mirrors were replaced. Many of the deteriorating mirrors were constructed using ZnS/ThF_4 layer pairs.

Most mirrors show a five to twenty-five percent drop in reflectance assuming that the original reflectance was close to 100 percent. As with the optical filters, small changes in properties of these multi-layer films can result in significant changes in reflectivity and loss of performance. The source of the changes may be interdiffusion at the interface between the layers, erosion or contamination at the surface, and damage in the layers from the particulate radiation falling on the surface.

Figure 5 shows the normal spectral reflectance of the best mirror in the set plotted against reciprocal wavelength (wavenumbers). Original records indicate that this mirror was

composed of (Ge/ZnS) layers on a copper-plated metal substrate, and was designed for high reflectance at 3.8 μm (3571 cm^{-1}). The edges of these mirrors were covered by the attachment hardware and always had a different reflectance characteristic. As judged by the results of this set of filters, the conventional ZnS/ThF_4 or $ZnSe/ThF_4$ dielectric pairs are not as suitable as some of the other material combinations included in this group of mirrors. The use of Si/SiO pairs gave better stability, and Ge/ZnS was the best material combination.

BLACK PAINTS

Figure 6 shows the normal reflectivity at extreme infrared wavelengths for Chemglaze Z306. These results are typical for all six black paint samples in our component set. After recovery, all black paint samples showed decreased reflectance in this spectral region. The solid lines are calculated using the expressions developed by Smith[4] and using the parameters found by Smith for Z306 for the prelaunch case. Postrecovery calculations used the same parameters except that the imaginary part of the refractive index was increased from 0.06 to 0.22. The implication is that exposure increased the number of absorption sites and made the paints blacker. Energy loss caused by increased scattering was negligible. The fit could be improved by allowing the real and imaginary indices to vary with wavelength, but we have no firm physical basis for such modifications at this time. Details of the reflectance spectra analysis can be found in an earlier paper.[5]

CONCLUSIONS

The findings of other investigators as well as our own suggest that material characteristics play a major role in determining degradation of optical components in space. Dielectric stack coatings are sensitive indicators of change in dimensions or physical parameters. Rigid materials such as ceramics, glasses, and covalently-bonded semiconductors such as silicon, withstand space exposure well.

Weakly-bonded materials such as some of the halides and plastics, as well as multi-layer dielectric structures in mirrors and filters are at risk. Protection for devices using such materials should be provided if possible.

Radiation levels are modest for most optical devices, although not all. Radiation protection can easily be provided in most cases. Contamination of optical surfaces can be significant as shown by the results for the LDEF. Again, some type of surface protection is

necessary in order to permit the contaminants to condense elsewhere and become fixed in place before exposing sensitive optical surfaces to the environment.

REFERENCES

1. Blue, M.D.: "LDEF Active Optical Components Experiment." 69 Months in Space--First LDEF Post-Retrieval Symposium, NASA CP-3134, Part 3 January 1992.

2. Robertson, J.B.: "Pyroelectric Detectors On LDEF." 69 Months in Space--First LDEF Post-Retrieval Symposium, NASA CP-3134, Part 3 January 1992.

3. Blue, M.D. and Roberts, D.W.: "Effects of Space Exposure on Optical Filters." Applied Opt., vol. 31, no. 25, pp. 5299-5304, September 1992.

4. Smith, S.M.: "Specular Reflectance of Optical-Black Coatings in the Far-Infrared." Applied Opt., vol.23, pp. 2311-2326, 1984.

5. Blue, M.D. and Perkowitz, S.: "Space Exposure Effects on Optical-Baffle Coatings at Far-Infrared Wavelengths," Applied Opt., vol. 31, pp. 4305-4309, July 1992.

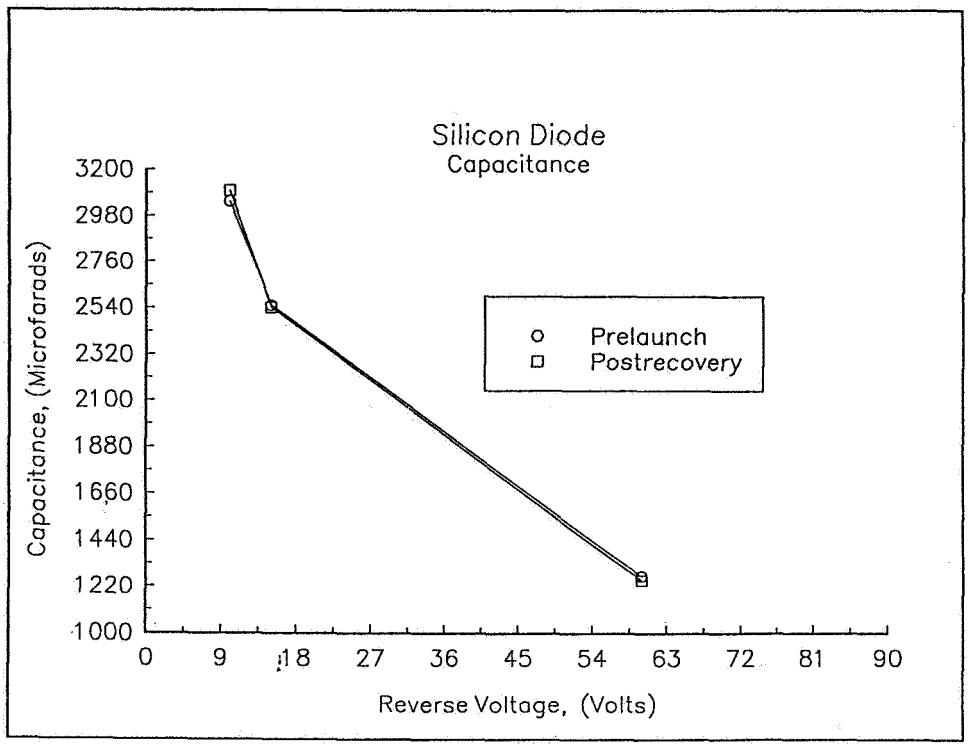

FIGURE 1. Junction capacitance versus reverse voltage for a silicon photodiode exposed to the space environment. There was no change in junction capacitance in any silicon device over the twelve years between measurements.

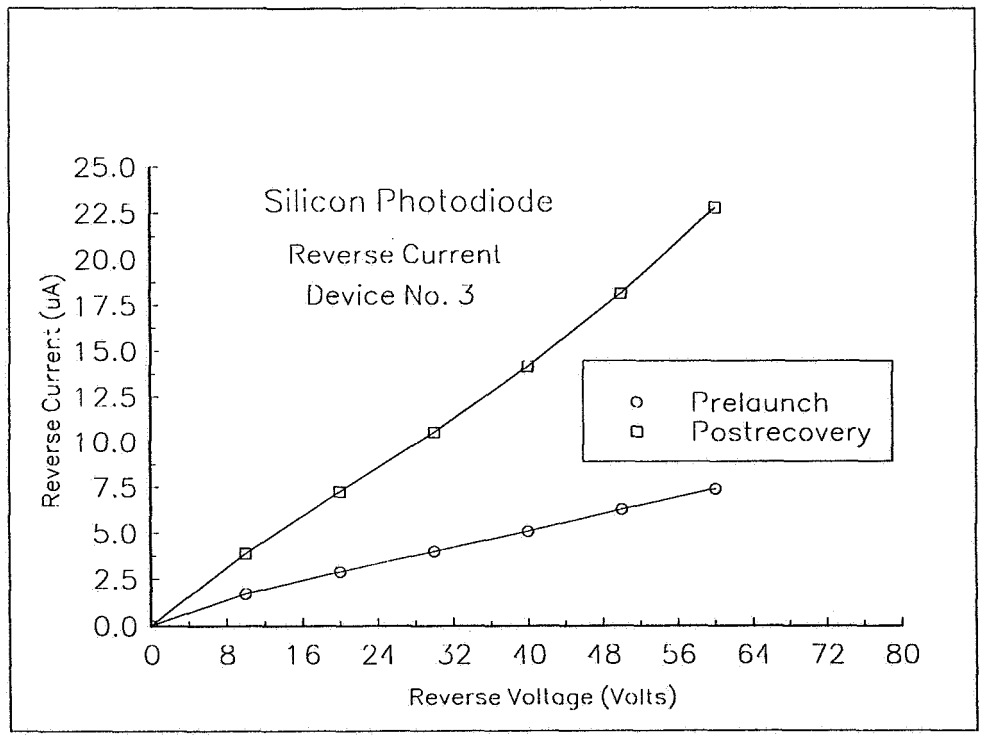

FIGURE 2. Junction current versus reverse voltage for a silicon photodiode exposed to the space environment. This diode had a scar from a micrometeorite impact. No change in diode leakage current occurred.

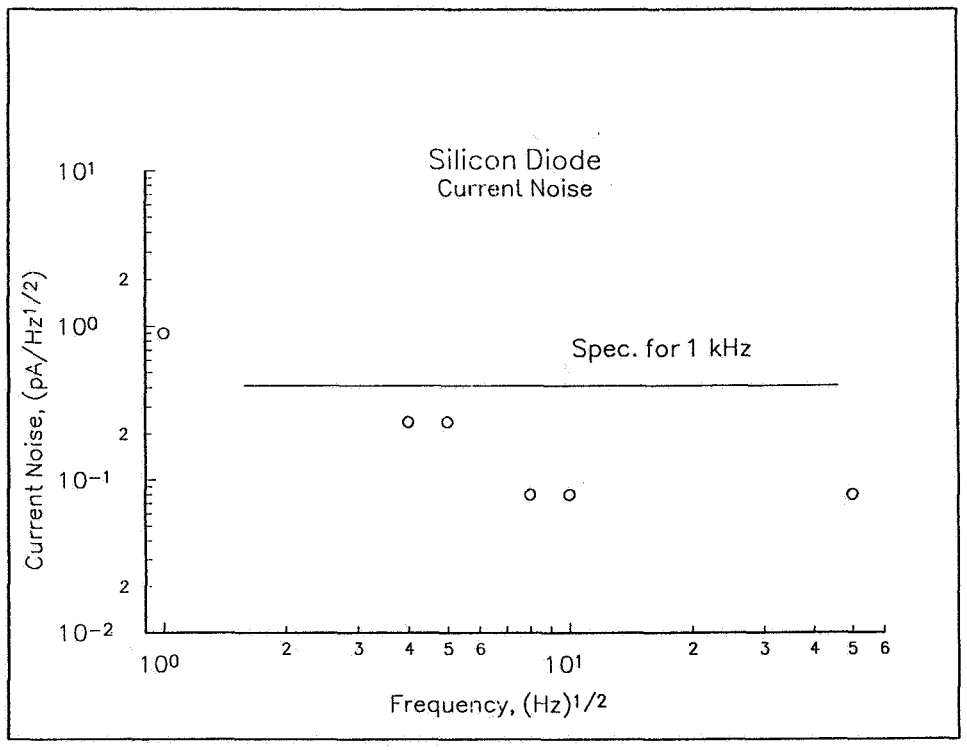

FIGURE 3. Current noise spectral density for a silicon photodiode diode. The current noise remains well within the manufacturers specification. At low frequencies, 1/f noise appears at a low level.

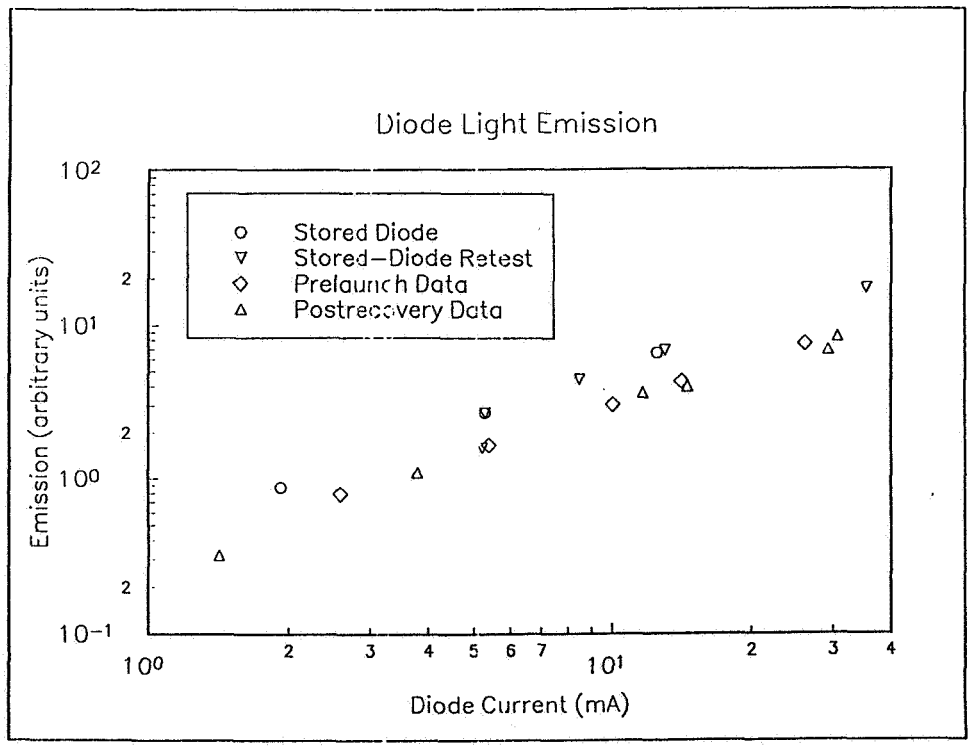

FIGURE 4. Diode emission versus current for a pair of GaAsP light-emitting diodes. Heating and hysteresis effects are characteristic of these devices. Nonetheless, the original characteristics are well reproduced.

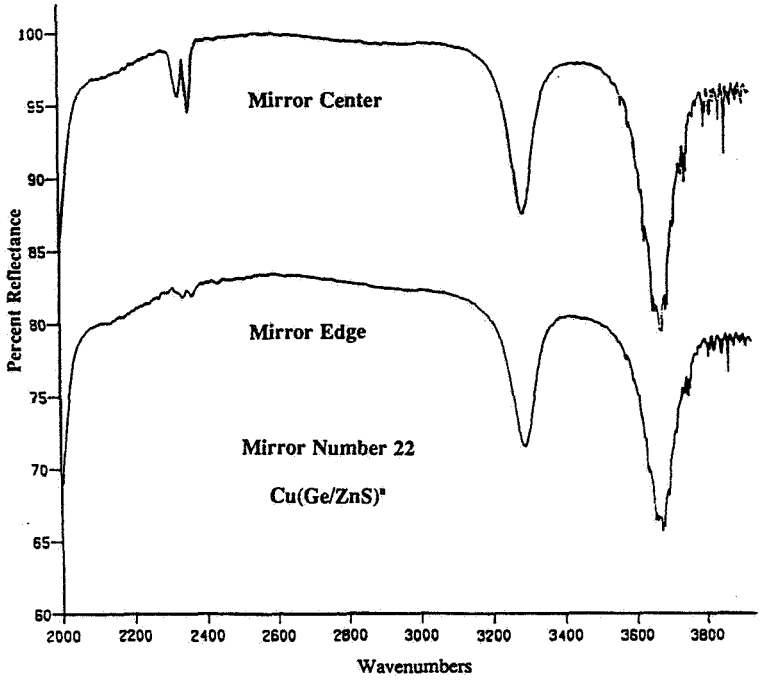

FIGURE 5. Spectral reflectance of a multilayer-dielectric mirror optimized for high reflectivity at 3.8 μm (3571 wavenumbers) after recovery. Attachment hardware covered the edges of the mirrors, often providing different relectance spectra from the mirror center.

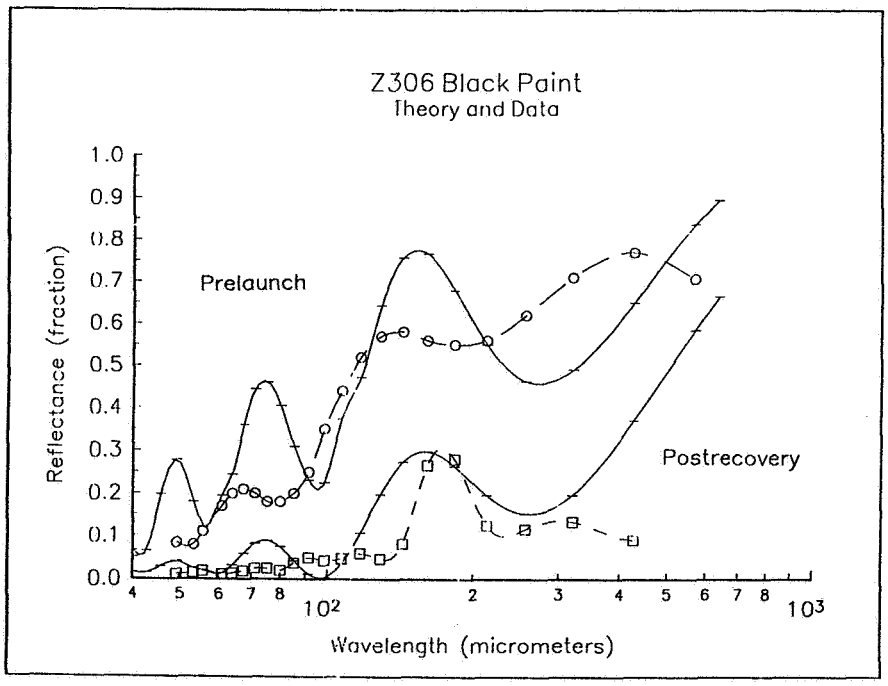

FIGURE 6. Spectral reflectance at normal incidence for Z306 black paint at extreme infrared wavelengths. Circles represent measured data. The two calculated curves represent the theory of Smith[4] using two different values for the imaginary component of the index of refraction. The change in properties is caused by a change in absorption, not by a change in scattering.

N93-29690

LDEF SPACE PLASMA-HIGH VOLTAGE DRAINAGE EXPERIMENT POST-FLIGHT RESULTS

501725
P3-12

J.Y. Yaung, B.K. Blakkolb, W.C. Wong, L.E. Ryan,
H.J. Schurig and W.W.L. Taylor

TRW, Space & Technology Group
One Space Park
Redondo Beach, CA 90278

INTRODUCTION

The Space Plasma-High Voltage Drainage Experiment (SP-HVDE) was comprised of two identical experimental trays. With one tray located on the leading (ram facing, B10) edge and the other located on the trailing (wake facing, D4) edge of the LDEF, it was possible to directly compare the effects of ram and wake spacecraft environments on charged dielectric materials. Six arrays of Kapton dielectric samples of 2 mil, 3 mil, and 5 mil thicknesses maintained at +/- 300 +/- 500, and +/- 1000 voltage bias formed the experimental matrix of each tray. In addition, each tray carried two solar cell strings, one biased at +300 volts and the other at -300 volts, to study current leakage from High Voltage Solar Arrays (HVSA).

The SP-HVDE provides the first direct, long-term, in-flight measurements of average leakage current through dielectric materials under electric stress. The experiment also yields information on the long term stability of the bulk dielectric properties of such materials. Data and findings of the SP-HVDE are an extension of those from shorter term flight experiments such as the PIX-I (Plasma Interaction Experiment) and PIX-II [1,2,3] and are therefore valuable in the design and evaluation of long-lived space systems with high voltage systems exposed to the low earth orbital environment.

This paper is a summary the SP-HVDE post flight analysis final report delivered to the LDEF Project Office under contract to the National Aeronautics and Space Administration.

MISSION PROFILE

The LDEF was placed in a 482 km, near circular, orbit of 28.4 degree inclination on April 7, 1984 by the Space Shuttle Challenger. The LDEF was to have been retrieved from space after a two-year mission, but due to a catastrophic Shuttle launch incident and subsequent two-year hiatus from Shuttle launches, the LDEF was not retrieved until January 12, 1990 by the Columbia orbiter at an altitude of 340 km. The SP-HVDE gathered data over the first 233 days of the LDEF mission.*

Even though the objective of the SP-HVDE was not to characterize the space environment, knowledge about that environment is helpful in understanding the experimental results, therefore a summary of the LDEF environment experienced by SP-HVDE is included in Table 1. The ram-facing tray of the SP-HVDE saw micro meteoroids and space debris (M/D) as well as energetic atomic oxygen. On the wake-facing side of the LDEF, the trailing-edge tray saw a substantially lower flux of atomic oxygen and space debris. Both trays incurred essentially the same natural radiation dose.

---

* Harry Dursch, LDEF Systems Special Investigation Group, private communication, 1991.

Table 1. SP-HVDE Space Environmental Exposure Summary

	Leading Edge (D-10)†	Trailing Edge (B-4)†
Atomic Oxygen	$7.88 \times 10^{21}/cm^2$	$1.15 \times 10^{5}/cm^2$
UV	10698 Eqv. sun hrs.	10458 Eqv. sun hrs.
M/D	187 Impact sites (1.3×10^{-5}) (Frational Area Coverage)	23 Impact sites (2.0×10^{-6}) (Frational Area Coverage)

† Tray location designation

SP-HVDE CONFIGURATION

A schematic of the SP-HVDE is shown in Figure 1. Separate coulombmeters were employed to obtain time integrals for the leakage current and bias voltages for each set of samples. These devices can record currents flowing in either direction by either deplating or plating the electrodes. The Plessey coulombmeters used in the experiment had been plated to 10,000 mA-seconds by the manufacturer. The duty cycle of the storage capacitor was 0.5%, with the power processing unit, consisting of DC-DC power converters controlled by a switching circuit, satisfying the duty cycle requirement.

Each tray contained six sets of four dielectric samples, with each set maintained at a different bias voltage (i.e., ±300, ±500 or ±1000 volts). The sets were comprised of various combinations of Kapton/VDA film in one of three thicknesses (i.e., 2 mils, 3 mils, and 5 mils) bonded to the fiberglass/epoxy substrate with a 60 wt% silver loaded epoxy. Thus, the long-term average leakage current and resistivity were determined by using a matrix of dielectric samples of different thicknesses and biases comprising 22 dielectric samples per tray. The adhesive and the VDA (Vapor Deposited Aluminum) served as conducting layers of the dielectric stack for collecting leakage current. The layered construction of the dielectric stacks is shown in Figure 2. Both trays also contained two solar cell modules, one maintained at +300 and the other at -300 volts bias. Each cell module consisted of three solar cells in a closed loop circuit with a load resistor.

POST-FLIGHT RESULTS

The striking contrast in the post-flight condition of the leading and trailing edge trays is evident in Figures 3 and 4. The trailing edge tray appears essentially the same as it did when the LDEF was deployed, but the leading edge tray shows the result of exposure to an atomic oxygen fluence of $7.88 \times 10^{21}/cm^2$. Of course the complete erosion of the Kapton material radically changes the dielectric properties of the experiment, but over the intended functional period of the experiment, approximately 1.5 mils of Kapton were eroded by the action of energetic atomic oxygen. Leakage current data, taken during the 233 day design life of the SP-HVDE, are presented below.

Leakage Current Measurements

Average leakage currents versus sample thickness and bias voltage for both trays are shown in Table 2. The average leakage current was obtained by measuring the current required to deplate the coulombmeters back to the pre-flight condition of 10,000 mA-seconds. The deplating process serves to integrate leakage current over time and yields an average over the operational life of the experiment. During the course of post-flight measurement, 6 of the 152 coulombmeters exhibited anomalous behavior, *i.e.*, 3 showed "open circuit" such that the readout equipment could not deplate the coulombmeter and 3 coulombmeters showed "short circuit" such that deplating during readout did not terminate at the pre-flight endpoint.

Table 2. Average Leakage Current (micro amperes)

Trailing-edge Thickness (mil)	Bias Voltage(V) +300	+500	+1000	-300	-500	-1000
5	N/D	0.53	0.11	N/D	0.17	0.196
3	0.196	0.43	1.9	0.194	N/D	0.184
2	0.36	0.16	N/D	0.27	0.2	N/D
Leading-edge Thickness (mil)	**Bias Voltage(V) +300**	**+500**	**+1000**	**-300**	**-500**	**-1000**
5	N/D	1.3	0.61	N/D	0.496	0.48
3	0.598	1.0	1.2	0.497	0.38	0.487
2	0.58	-0.65	N/D	N/D	N/D	N/D

N/D=No Data

Ground simulations predicted leakage current to increase with positive bias voltage and decrease with greater dielectric sample thickness. Figure 5 shows the leakage current data for positively biased samples on the leading and trailing edge trays. The data show that only the 3 mil samples followed the predicted trend and that the 5 mil samples showed an unexpected decrease in leakage current over the 500 to 1000 +volt range. The limited data obtained for the 2 mil samples also seems to follow the atypical trend, although the 2 mil sample did demonstrate an expectedly larger leakage current compared to the thicker samples at the 300 +volt bias.

Leakage current data shown in Figure 6, for negatively biased samples, are distinctly different compared to those for positively biased samples. For the negatively biased condition, the leakage currents obtained are lower than those measured for the positive bias condition by a factor of three. Also of significance is the smaller change in leakage current across the voltage range. It is speculated that for the negatively biased surfaces even the lowest voltage (i.e., -300 volts) is beyond the threshold at which interaction with the space plasma results in localized but intense electrodischarge events. The occurrence of such discharges is consistent with the lower post-flight average leakage currents measured and also consistent with work performed by Thiemann, et al. (ref. 4) which reported greater numbers of discharges for negatively biased surfaces during ground simulations. The reason for the dip in the leakage current at -500 volts for the 3 mil sample on the leading edge tray is unclear at this time, but it should be noted that a similar phenomenon was seen in the data from the PIX-I experiment (see ref. 1).

Dielectric Property Measurements

The leakage current time integrals and bias voltages permit the calculation of an average resistivity across the dielectric sample stack. Tables 3 and 4 show the average voltages and resistivities derived from post-flight measurements.

Table 3. Average Voltage (V)

Bias Voltage (V)	+300	+500	-300
Trailing-edge Tray	123.4	N/D	57.1
Leading-edge Tray	16.2	N/D	326.2

N/D=No Data

Table 4. Derived Resistivity (ohm-cm)

Trailing-edge Tray Thickness (mil)	Bias Voltage(V) +300	-300
5	N/D	N/D
3	2.3×10^{13}	1.1×10^{13}
2	2.0×10^{13}	1.2×10^{13}
Average:	2.2×10^{13} ohm-cm	1.2×10^{13} ohm-cm

Leading-edge Tray Thickness (mil)	Bias Voltage(V) +300	-300
5	6.8×10^{11}	N/D
3	1.4×10^{12}	6.2×10^{13}
2	5.5×10^{12}	6.6×10^{13}
Average:	3.8×10^{12} ohm-cm	6.4×10^{13} ohm-cm

Unflown reference Kapton: $\rho = 3 \times 10^{15}$ ohm-cm at +300 V bias.

Solar Cell Module Characterization

We were very pleased to be able to locate the original set of control samples for the SP-HVDE solar cell modules after some ten years since the experiment was first conceived. These control samples gave us the opportunity to compare not only the relative performance of leading and trailing edge flight specimens but also to compare the flight data to a baseline reference. Having found the control cells, there was however some question as to exactly what type of cells they were and the type of coverglass used. Based on the age and configuration of the cells it is reasonably certain that the cells are of a low efficiency, 10 ohm-cm, single crystal silicon type with fused silica coverglass and conventional bar interconnects.

One of the cells on a leading edge module experienced an impact by a micro meteoroid or debris particle which, from the data shown in Tables 5 and 6, resulted in a significant reduction in performance. Scanning electron micrographs of the impact site are presented in Figure 7. The particle penetrated the coverglass and the silicone coverglass adhesive and produced a raised and melted spall zone on the silicon solar cell. The damage to the cell extends well beyond the immediate impact site with radial cracks in the coverglass extending 0.25 inches from the impact center. Elemental analysis of the impact site did not reveal any material that could be conclusively identified as extraterrestial or as anthropogenic debris.

Environmental Interaction

The metal interconnect strips between the cells of each module were exposed to the ambient space plasma, providing a path for current leakage. The area ratio of interconnect to coverglass is 2.8%. As with the other charged surfaces of the experiment, average current integrals were obtained through coulombmeters. The average current integrals for each cell flight module are presented in Table 6.

Table 5. Electrical Characteristics of
LDEF SP-HVDE Solar Cell Modules

Cell Module Number/Type	V_{oc}(V)	I_{sc}(A)	V_{mp}(V)	I_{mp}(A)	P_{mp}(W)	Comment
# 1, Trailing	1.63	0.285	1.36	0.271	0.369	
# 2, Trailing	1.63	0.286	1.36	0.272	0.370	
# 3, Leading	1.63	0.290	1.36	0.272	0.369	
# 4, Leading	1.64	0.223	1.51	0.222	0.336	Particle Impact
# 5, Control	1.64	0.287	1.37	0.275	0.377	
# 6, Control	1.64	0.287	1.37	0.273	0.374	

Table 6. Derived Current Integrals & Average Currents

Trailing-edge Tray:

Bias Voltage:+300 V		Bias Voltage: -300 V	
Current Integral (mA-second)	I_{av} (micro ampere)	Current Integral (mA-second)	I_{av} (micro ampere)
-469.74	-2.3×10^{-2}	1509.85	7.5×10^{-2}

Leading-edge Tray:

Bias Voltage:+300 V		Bias Voltage: -300 V	
Current Integral (mA-second)	I_{av} (micro ampere)	Current Integral (mA-second)	I_{av} (micro ampere)
5411.92	2.7×10^{-1}	355.30	1.8×10^{-2} (one cell damaged by M/D impact)

CONCLUSIONS

The concept of the High Voltage Solar Array (HVSA) was created around 1973. The goal of this power-efficient concept was to allow power conversion directly from the modular solar array to high voltage systems. In the early 1980s, the solar array community envisioned that SDIO would require many large solar power systems employing HVSA technology. Instead, the interest in the HVSA concept has materialized in the form of the proposed Space Station Freedom. The Space Plasma-High Voltage Drainage Experiment has extended the existing data base on spacecraft charging and current leakage phenomena first studied by the PIX-I and PIX-II experiments. The SP-HVDE also makes a substantive contribution to the overall LDEF solar cell data package which has confirmed the robustness of design practices and materials selection. The information obtained from the retrieved the LDEF has made an incalculable contribution to the database of space environmental effects on materials and spacecraft aging.

REFERENCES

1. N.T. Grier and N.J. Stevens, "Plasma Interaction Experiment (PIX) Flight Results", Spacecraft Charging Technology -1978, NASA CP-2071/AFGL-TR-79-0082, 1979, pp. 295-314.(AD-A084-626/1)

2. N.T. Grier, "Plasma Interaction Experiment II(PIX-II): Laboratory and Flight Results", in Spacecraft Environmental Interactions Technology - 1983, NASA CP-2359/AFGL-TR-85-0018, 1985, pp. 333-348.

3. N.J. Stevens, "Summary of PIX-2 Flight Results Over the First Orbit", AIAA-86-360, AIAA 24th Aerospace Sciences Meeting, Jan. 6-9, 1986, Reno, Nevada.

4. I. Thiemann and K. Bogus, "Anomalous Current Collection and Arcing of Solar-Cell Modules in a Simulated High-Density Low-Earth-Orbit Plasma", ESA J., 10, 43, (1986).

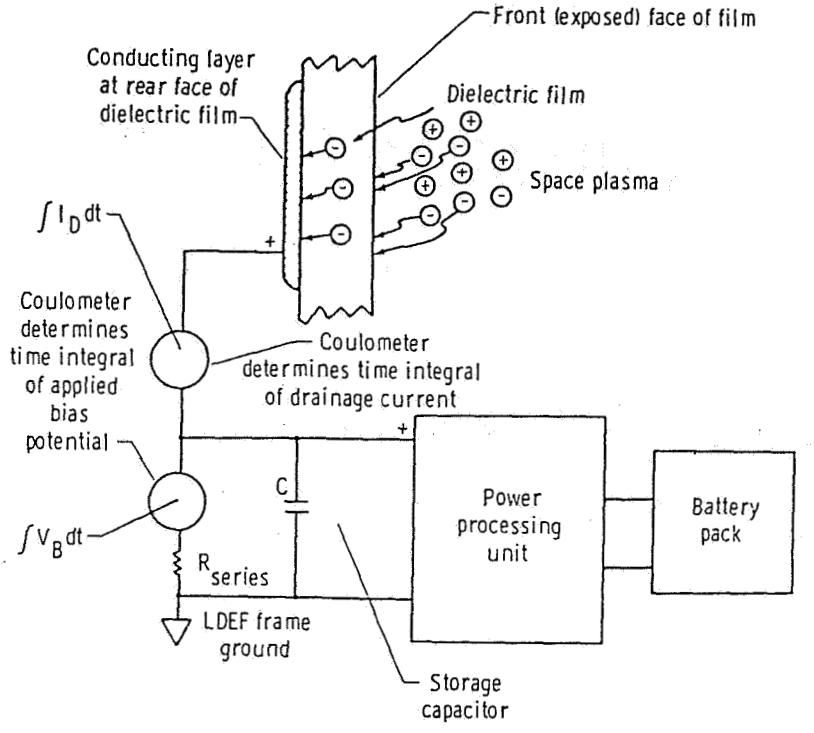

Figure 1. Schematic of SP-HVDE

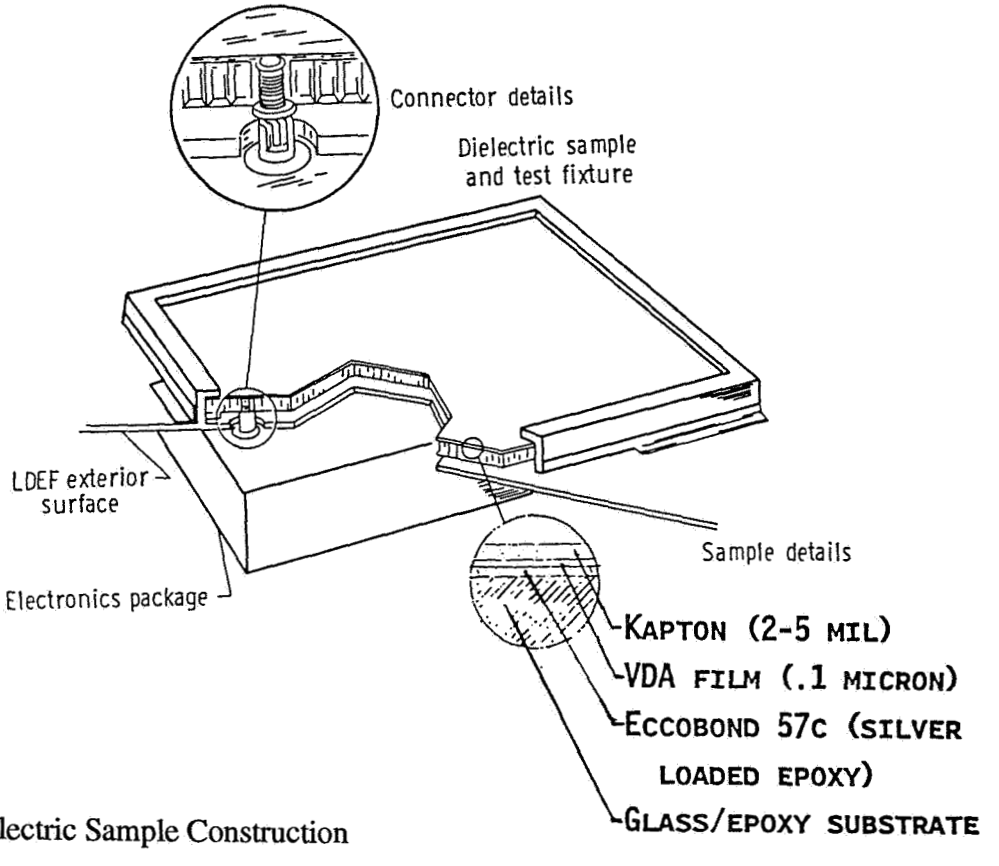

Figure 2. Dielectric Sample Construction

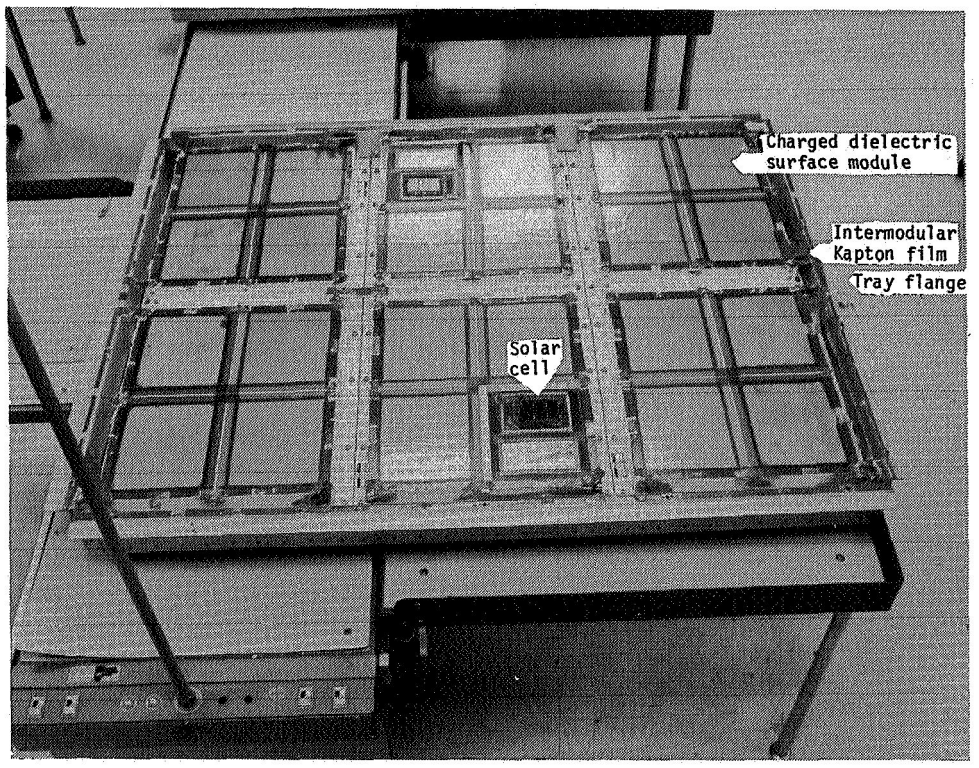

Figure 3. Leading Edge SP-HVDE Tray (Post Flight)

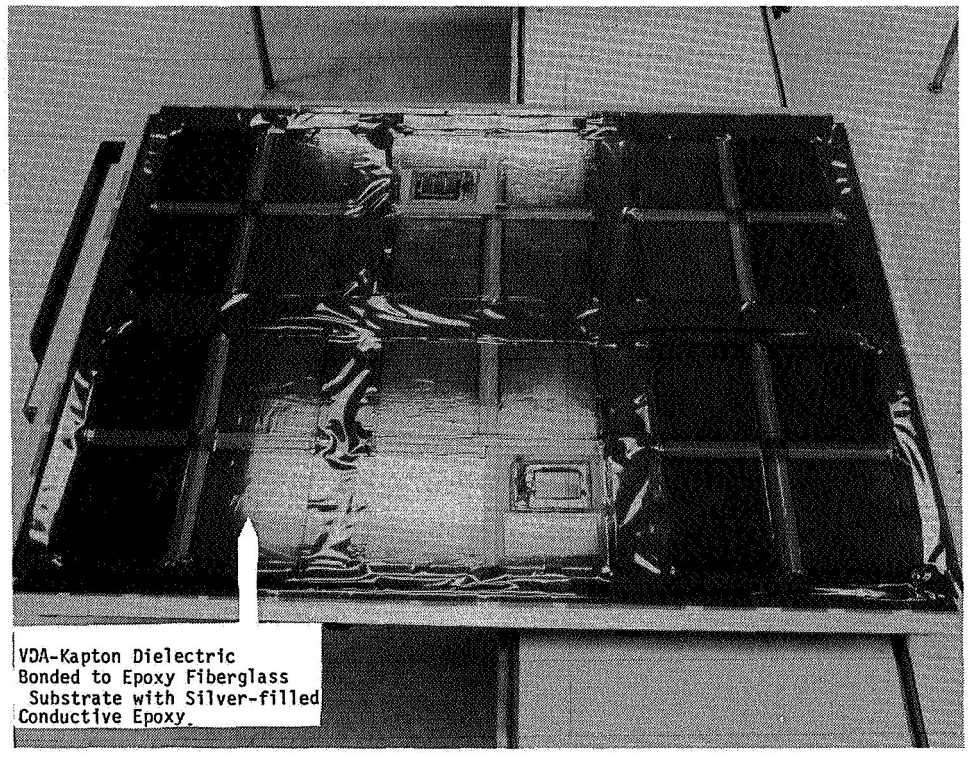

Figure 4. Trailing Edge SP-HVDE Tray (Post Flight)

ORIGINAL PAGE
BLACK AND WHITE PHOTOGRAPH

Ram-Facing Tray

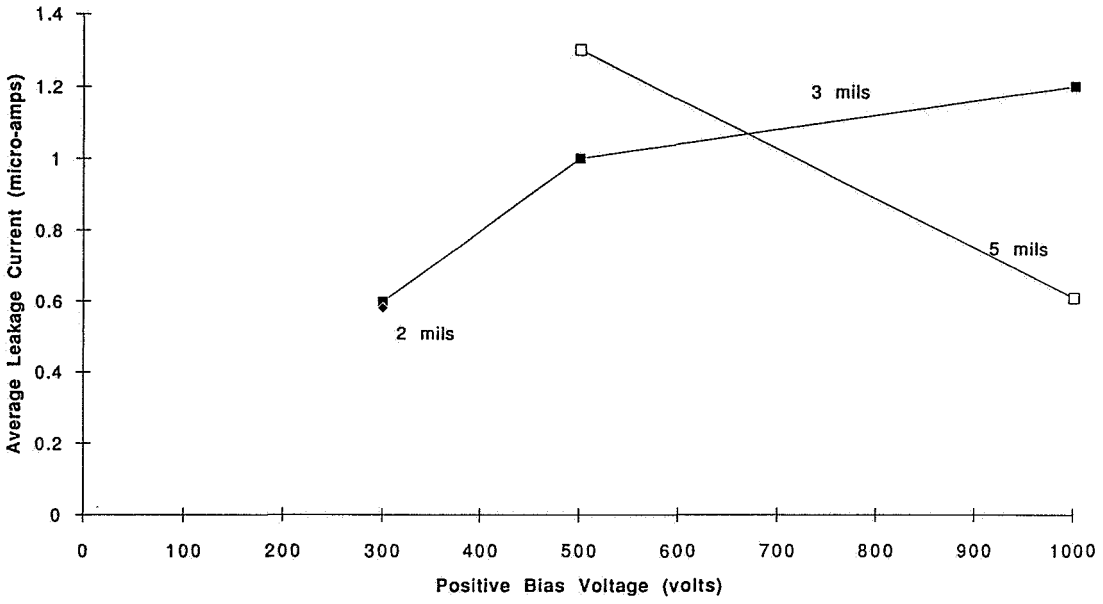

Wake-Facing Tray

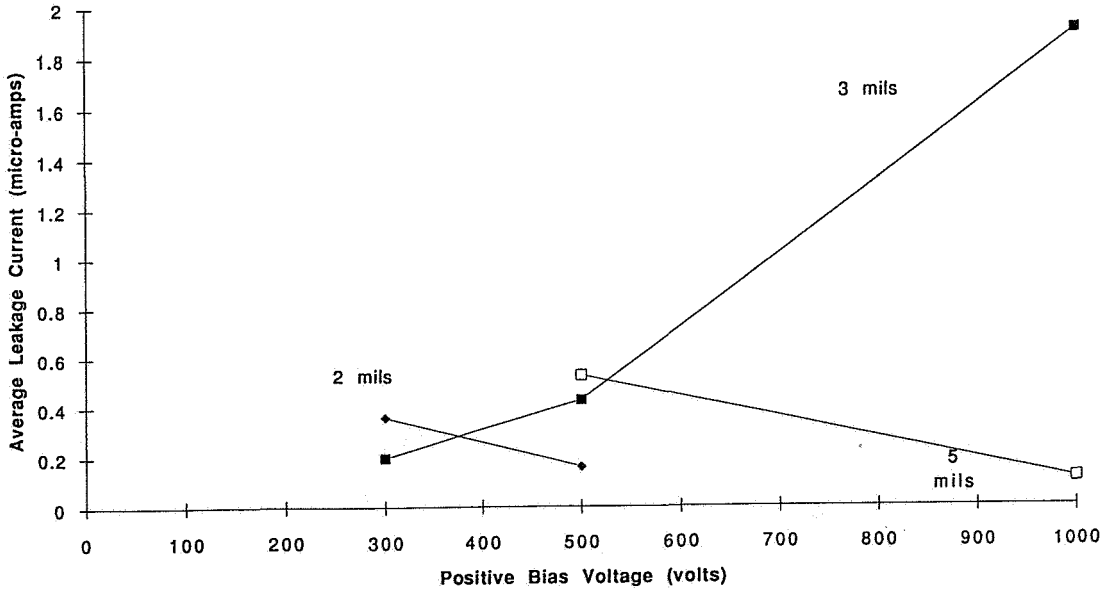

Figure 5. Average Leakage Current Data for Positive Bias Voltage Samples

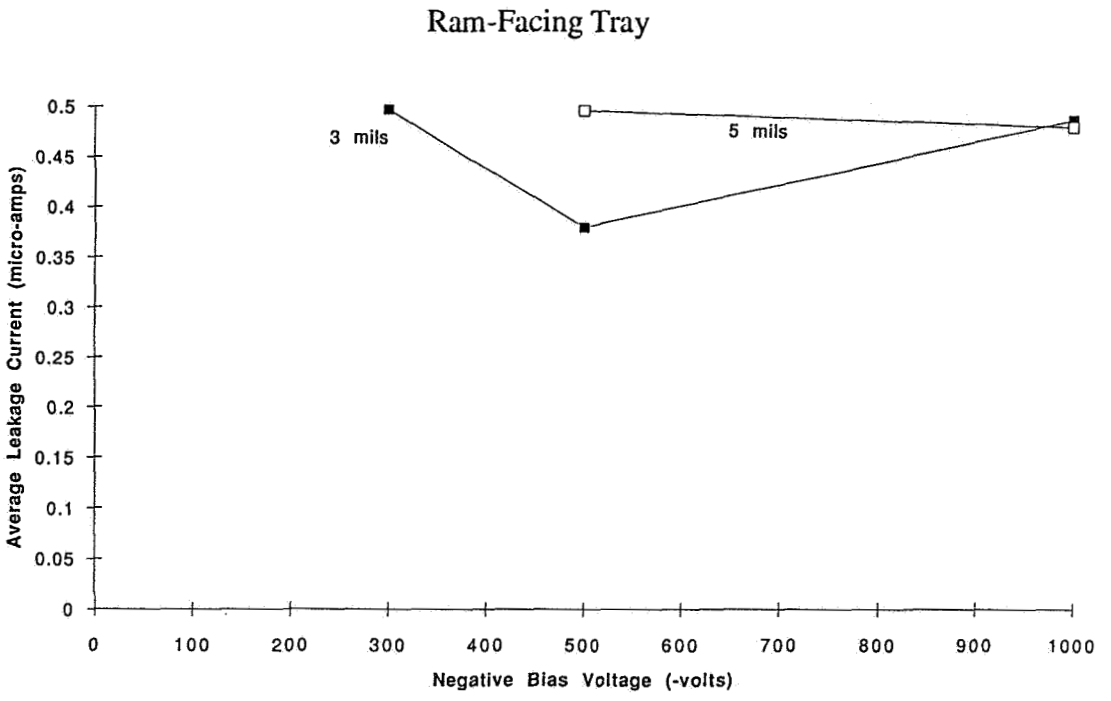

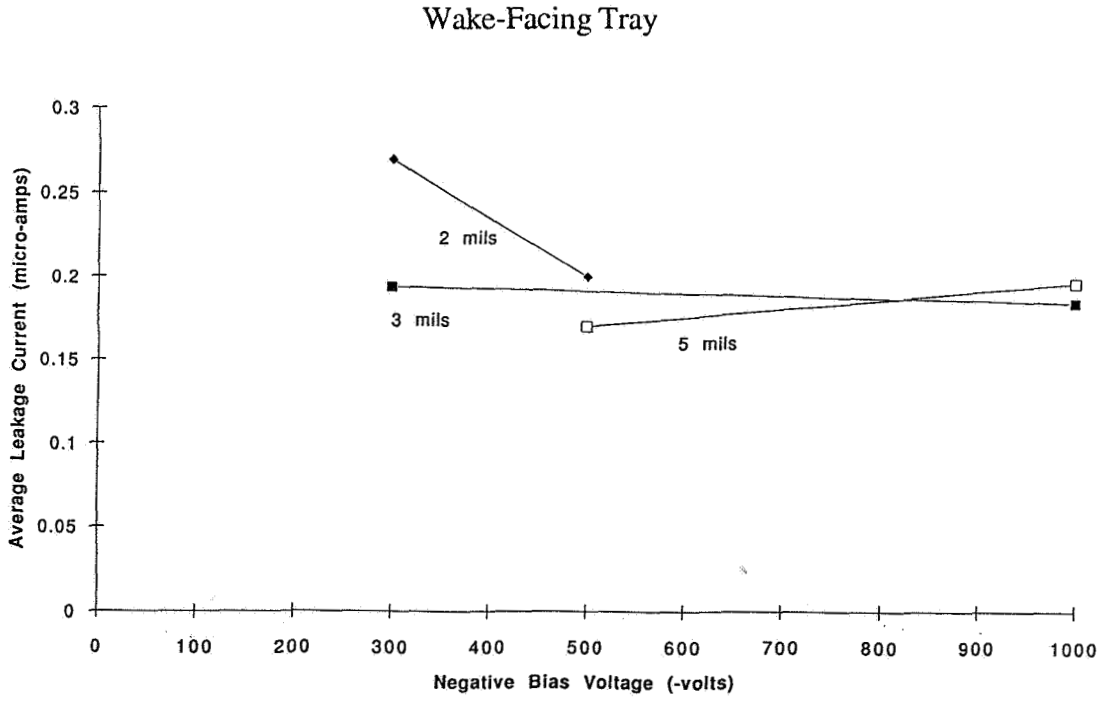

Figure 6. Average Leakage Current Data for Negative Bias Voltage Samples

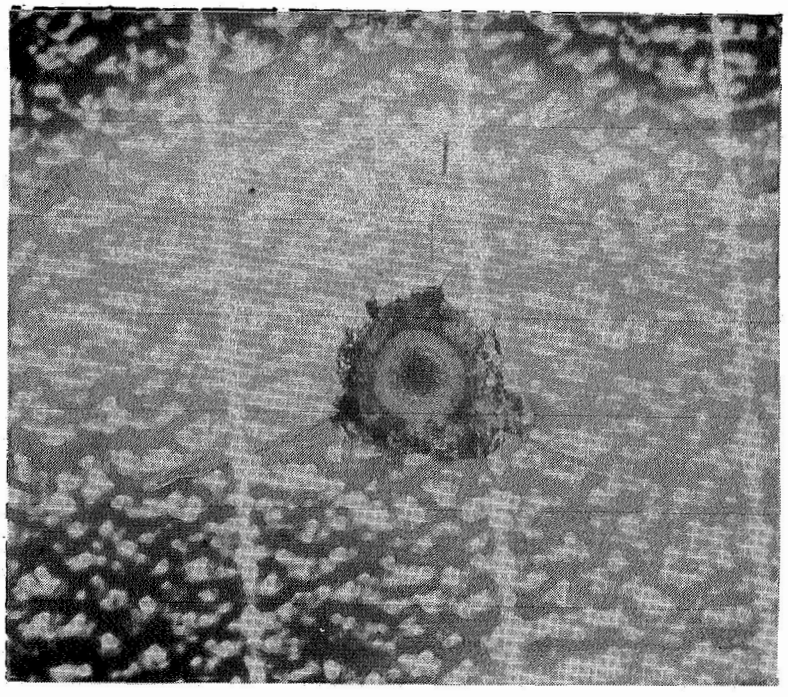

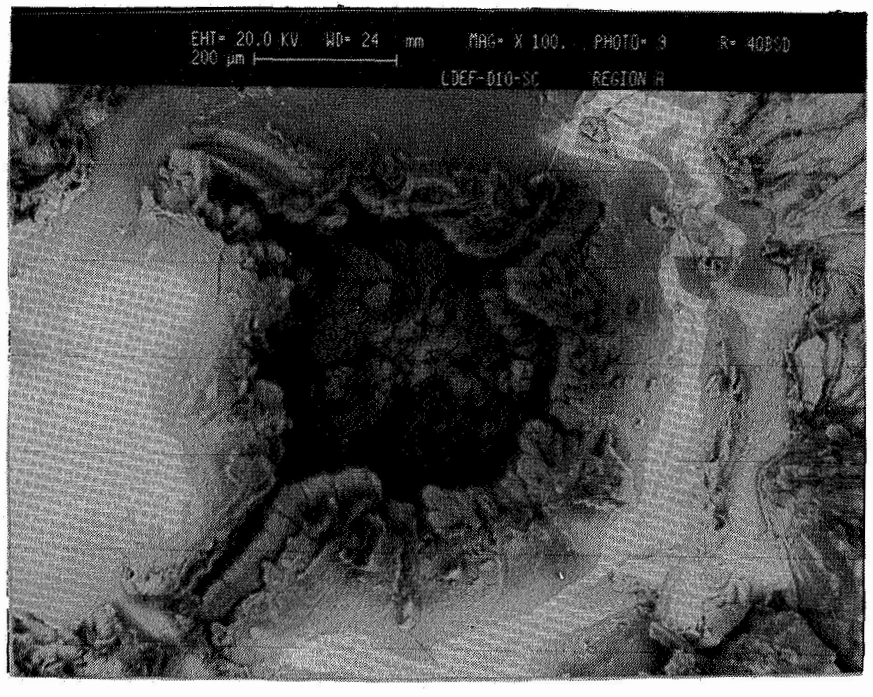

Figure 7. Impact Site on Photovoltaic Cell Stack

ORIGINAL PAGE
BLACK AND WHITE PHOTOGRAPH

N93-29691

501729

IN ORBIT DEGRADATION OF EUV OPTICAL COMPONENTS IN THE WAVELENGTH RANGE 10-40 nm AO 138-3

J.P. Delaboudinière, Ch. Carabétian, J.F. Hochedez

INSTITUT D'ASTROPHYSIQUE SPATIALE
Campus de l'Université Paris Sud - Bât. 121.
91 405 ORSAY CEDEX

ABSTRACT

A complement of EUV optical components, including mirrors and thin film filters, has been flown as part of LDEF AO 138-3. The most original amongst these components were multilayered interference reflectors for the 10-40 nm wavelength range. Very moderate degradation has been observed for those components which were exposed to the sun. The degradation is compatible with the deposition of a few nanometers of absorbing material on the surface of the samples.

I] INTRODUCTION

In preparation for the SOHO mission planned by NASA / ESA for launch in 1995, we placed test samples of optical components to be used by the Extreme Ultraviolet Imaging Telescope (EIT) on board LDEF [1]. These components include thin film filters used for visible light rejection, and a new type of optical reflectors developed for the EUV since 1975 [2 3]. These reflectors consist of a periodic stack of multilayered thin films, deposited on glass substrates. They operate by building up reflectivity from constructive interference of individual beams reflected at the interface between successive highly and weakly absorbing materials. The layer thicknesses are a fraction of the wavelength of the light beam to be reflected so that the period of the structure is $\lambda/2$ (λ being the operating wavelength). We placed samples of such mirrors in the LDEF in order to evaluate the effect of thermal cycling, and surface contamination in low Earth orbit.

II] EXPERIMENTAL PROCEDURE

The samples were produced by electron beam vacuum deposition at Institut d'Optique (IOTA). Their reflectivity was measured at the synchrotron radiation source ACO of LURE (Université d'Orsay). Two lots of samples were placed in one of the FRECOPA containers for launch on board LDEF. This container was vacuum tight and filled with dry nitrogen at 10 mbar pressure several months before launch on the Space Shuttle. The pressure within the container was monitored until very close to the launch date, so that by extrapolation it was certain that the samples had been exposed only to dry nitrogen before deployment. The container was opened several days after the LDEF had separated from the Shuttle. After seven months in orbit the container was again closed under high vacuum conditions. Seven years later this container and the samples were returned to ground. After two months of spacecraft processing, it was found that the pressure in this container was still very low (of the order of 2.10^{-3} mbar) providing evidence that the samples had been very well protected during recovery and the long period in orbit. Meanwhile, many things had happened on the ground, including the closure of the ACO facility which had been used to measure the optical properties before launch. The flight samples were again stored for several years under high vacuum in their container which was evacuated by vacuum ion pumps. Spare components in a spare container have been kept on ground in the same high vacuum conditions. Using a new facility for the optical test in the 10-150 nm wavelengh range, which recently became

operational on the new SUPER-ACO synchrotron machine, it has been possible to reevaluate all these multilayered mirrors nearly 10 years after they were produced. The components which were exposed to the low Earth orbit space environment on board LDEF consisted of two identical lots, the first being exposed to the sun, while the second was kept in the shade and never received solar light. Direct impingement of atmospheric particles (atomic oxygen...) would only have been possible for the lot exposed to the sun. However the FRECOPA container was placed in the wake of the LDEF spacecraft so that bombardment by atomic oxygen was probably minimal in a situation more reminiscent of what is expected for the SOHO spacecraft, at the L1 Lagrangian point between the earth and the sun (1.5 million kilometers away from the earth).

III] RESULTS

We present data concerning the normal incidence reflectivity of the mirror samples in the wavelength range for which they were designed.

The measurements were obtained using a classical reflectometer in which rotation of the detector around the sample makes the measurement of the intensity of the incident and reflected light beam alternatively possible within the source stability time span. The wavelength of the incident light beam could be varied using a grazing incidence monochromator illuminated by the synchrotron radiation continuous spectrum from the positron storage ring. The spectral resolution of the monochromator is 0.2 nm, and a useful light beam can be produced in the 10-150 nm range.

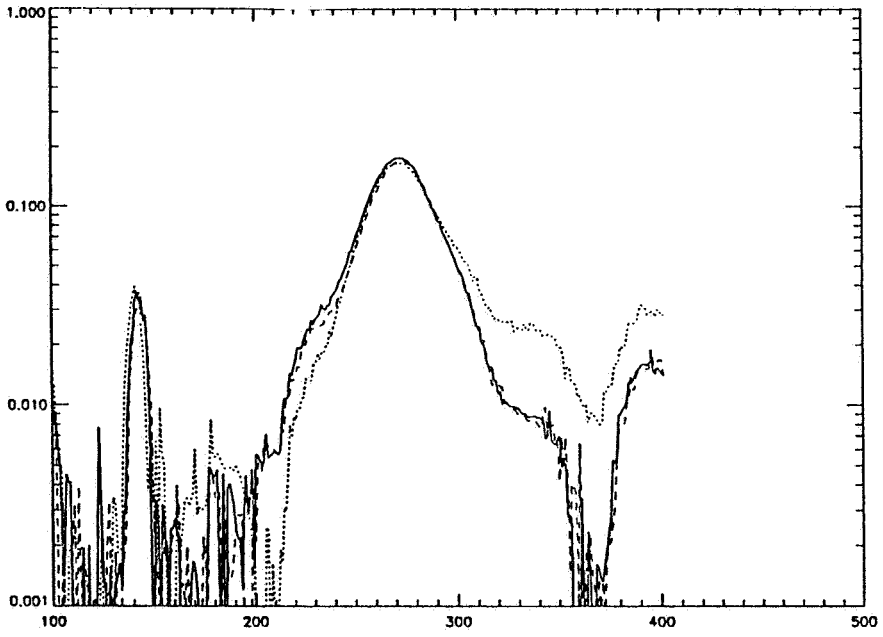

Fig.1 : Reflectivity Measurements of Si / WRe multilayers vs. Wavelength (Å). Detector is an Al/Al2O3 NIST photocathode. Plain line (a) is a 'reserve' sample, dashed line (b) is a 'shadow' sample, and dotted line (c) is an 'exposed to the sunlight' sample.

The reflectivity curves measured in the conditions close to normal incidence (10 degrees) are shown in figure 1 (a, b, c) for samples of Si / WRe multilayers manufactured simultaneously. Two Bragg peaks corresponding to the first and second order interference standing waves in the multilayered stack can be observed in the range 10-40 nm corresponding to the 15 nm period of the metallic structure. We notice that the peak reflectivities are consistent with those which were measured before flight (1), i.e. in the range

10-15%. We have more confidence in comparative data obtained with the same equipment at the same time rather than in comparison between measurements made 10 years apart with completely different equipment; thus interpretation should rather concentrate on the comparison between samples a ,b and c which were respectively kept on ground under vacuum (a), exposed to space in the shadow (b), and exposed to solar light and space environment for a considerable period of time (c), (several months if we consider that only one third of the time was spent during night on the orbit, and another fraction with inappropriate orientation of the LDEF). We notice that the positions of the reflection peaks have not changed, which shows that the geometrical periodicity of the structure has not changed under moderate but persistent thermal cycling. The efficiency of the mirrors has remained quite high at the nominal wavelength with a relative decrease of less than 10 % for the mirror exposed to sunlight. However, we find that the rejection of the light around 35 nm for this mirror has noticeably degraded which means that the most exposed mirror has become slightly less selective.

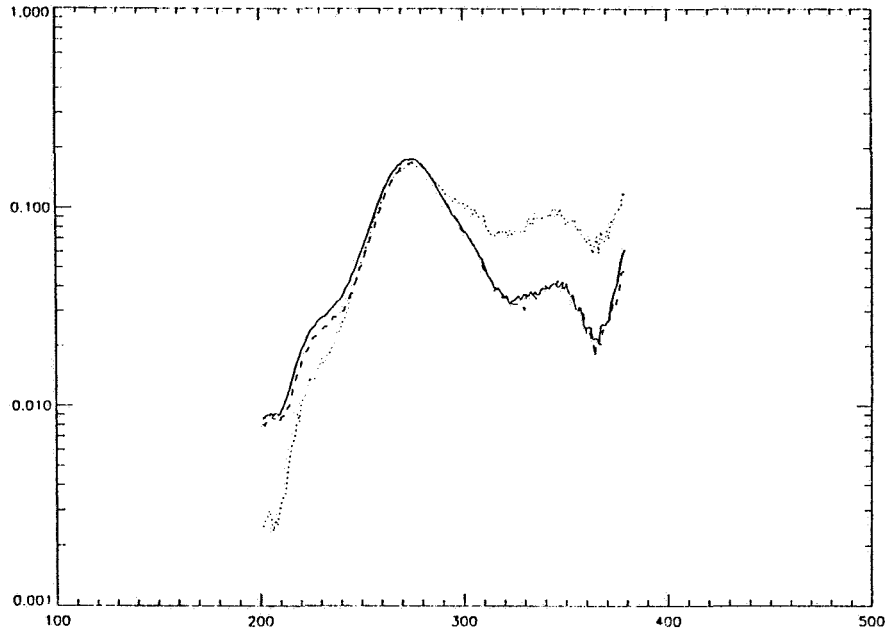

Fig.2 : Reflectivity Measurements of Si / WRe multilayers vs.Wavelength (Å). Detector is a channeltron. Plain line (a) is a 'reserve' sample, dashed line (b) is a 'shadow' sample, and dotted line (c) is an 'exposed to the sun light' sample.

Measuring this effect has been rather difficult however because of the low reflectivity involved. Our standard detector is an NBS windowless photodiode which exhibits a good linearity and dynamics, but whose reading is prone to inaccuracy at low flux level due to the drift of the electrometer in the range 10^{-14} amps. Better measurements above 20 nm were obtained using a channeltron detector behind an aluminum filter used to reduce the photon flux and suppress possible second order contributions from wavelengths shorter than 17 nm for measurements around 30 nm (see fig.2 a, b, c). The overall properties of the interference mirrors have been fairly well preserved, which is noticeable and encouraging for this wavelength range. The multilayered mirrors are in general much less sensitive to contamination than classical bulk material mirrors. This can be understood if one recalls that classical mirrors do not work well in the 10-40 nm range because the bulk absorbtion in the material occurs at a depth greater than the EUV wavelength: low contrast leads to low reflectivity. Deposition of a contaminant usually decreases the contrast at the transition between the vacuum and the mirror, and so the reflectivity diminishes still more. On the

contrary, in the case of a multilayered mirror, all layers participate in the reflectivity, and a degradation of the top layer has smaller consequences within the nominal band pass. On the other hand the occurence of a region of minimum reflectivity at wavelenths longer than the main reflectivity peak for the multilayers is due to destructive interferences between the front surface and the deeper layers. Destroying the front surface leads to a less effective rejection of the reflected light in this region.

IV] INTERPRETATION OF THE RESULTS

The mirrors consist in 6 periods of 5nm WRe, and 10 nm Si. We can compute the theoritical reflectivity of a mirror easily, but a fit to real data is rather complex given the large number of possible parameters . We discuss only crude models where two paramaters are deemed sufficient to describe qualitatively the main observations. Thus we introduce a roughness parameter of 1.2 nm rms to explain the slightly reduced reflectivity (compared to a perfect mirror) in the first order peak, and the observed ratio of the first to second order peaks (see fig. 3).

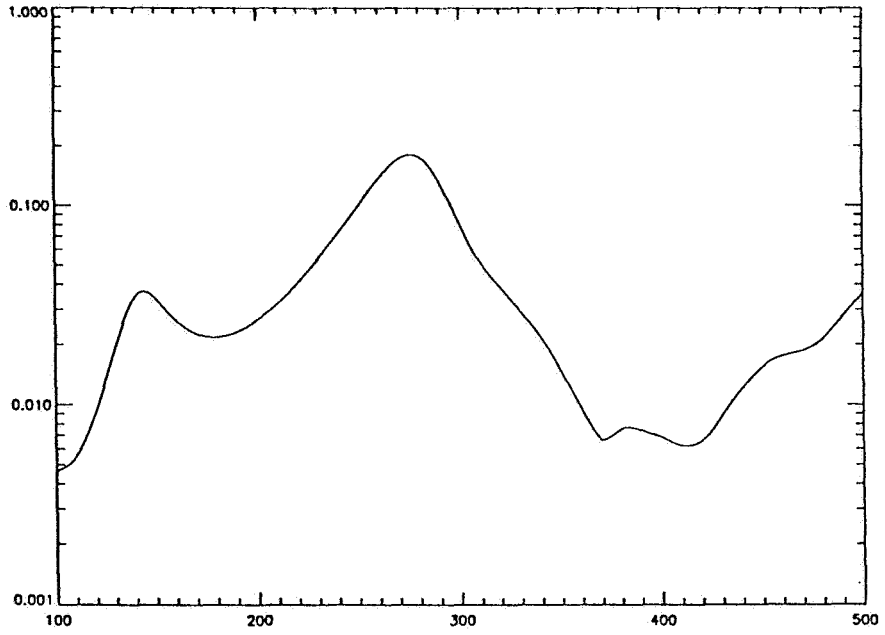

Fig.3 : Reflectivity Model for Si / Re multilayers vs.Wavelength (Å).

The sun-exposed mirror results can then be explained by a contamination layer on top of the initial structure. We tested two possible contaminants : namely pure carbon and silicon oxide,which could represent, with some likelihood, what may be deposited in flight via photochemical reactions involving hydrocarbons and silicon products. We find that no more than 3 nm of contaminating carbon are necessary to explain the observations (see fig.4)

Optical measurements alone cannot discriminate between every possible composition of the deposited contaminant (see fig.5 which compares the effect of carbon and silicon dioxide). It would be necessary to use sensitive surface microanalysis methods in order to measure in more detail the very thin layer, which we believe has been deposited.

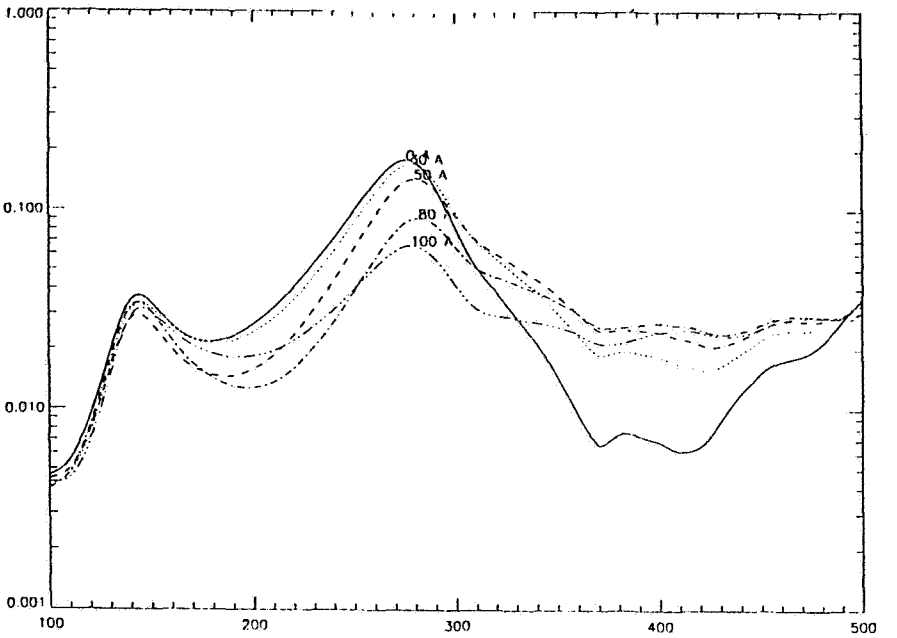

Fig.4 : Reflectivity Model for Si / Re multilayers vs.Wavelength (Å) ; Effect of different thicknesses of carbon as a contaminant (0, 30, 50, 80, and 100 Ångströms).

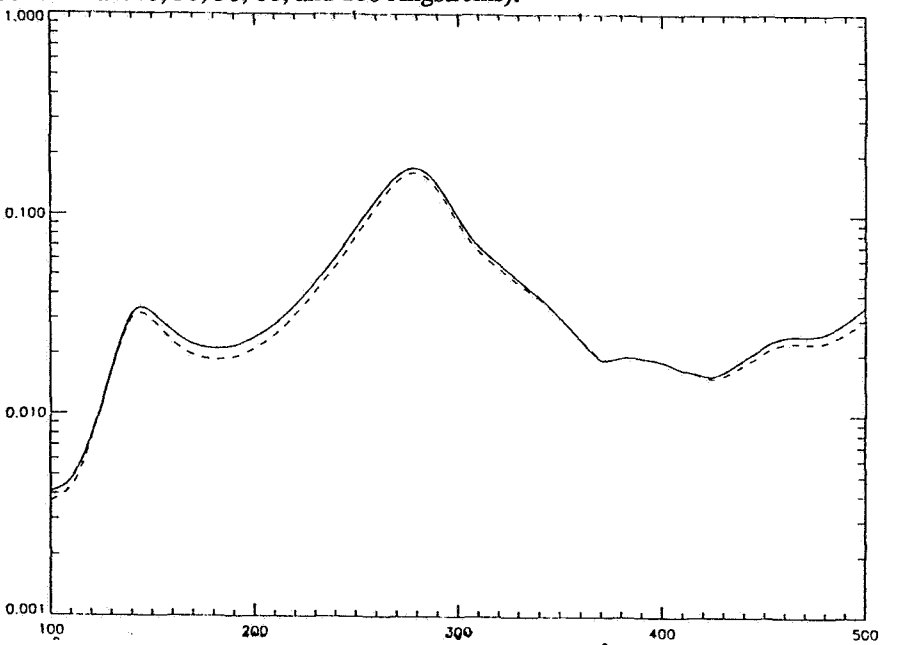

Fig.5 : Reflectivity Model for Si / Re multilayers vs. Wavelength (Å). Comparison of the effect of 30 Å of Carbon (plain line), or 30 Å of SiO2 (dashed line).

V] CONCLUSION

We have shown that multilayer coated mirrors for the EUV wavelength range are not too sensitive to contamination in orbit and can effectively be protected by careful handling. In the worst case observed, which involves solar illumination, only 3 nm of contaminant were probably present after seven month exposition in space. The effect of such a contamination on the optical properties of multilayers is acceptable. This low contamination level has been obtained using rather straightforward but stringent handling procedures which involve the control of the ambiant atmosphere by a vacuum tight vessel during storage and space launch.

VI] ACKNOWLEDGEMENTS

This work was supported by CNES as part of the French contribution to the FRECOPA experiment on board NASA's LDEF. The multilayered coatings were manufactured by J.P. CHAUVINEAU and L. VALIERGUE from Institut d'Optique(IOTA). The measurements were done using the Calibration Facility of IAS connected to the Super ACO storage ring from LURE (Université d'Orsay) .

---

[1] DELABOUDINIERE J.P., CHAUVINEAU J.P., MARIOGE J.P., (1985) SPIE Proc. 563, p.44

[2] SPILLER E., (1976) Applied Optics 16, 89

[3] VINOGRADOV A.V., ZELDOVICH B.Ya, (1977) Applied Optics 16, 89

N93-29692

501730
g5-19

DEGRADATION OF OPTICAL COMPONENTS IN A SPACE ENVIRONMENT

Linda L. DeHainaut
John R. Kenemuth
Cynthia E. Tidler
USAF Phillips Laboratory/LITC
Kirtland AFB, NM

David W. Seegmiller
W. J. Schafer Associates, Inc.
Albuquerque, NM

SUMMARY

Phillips Laboratory's LDEF optical experiment is designed to determine the adverse effects of the natural space environment on laser optical component and coating materials. The experiment consists of 10 sample sets, each containing six different material samples. The materials were chosen because of their common use in laser optical components. Sample characterization is divided into three phases. Phase I testing is limited to visual and optical performance evaluation. Phase II tests investigate the fundamental causes of the performance degradation quantified in Phase I. During Phase III, selected samples will be cleaned and some Phase I measurements repeated to determine if acceptable optical performance can be restored, and laser damage testing will be performed on a small number of samples. Performance deteriorations will be correlated to exposure duration, sample location on the LDEF, atomic oxygen levels, and other space environment conditions. Preliminary results obtained on the optical samples are discussed in this paper.

EXPERIMENT DESCRIPTION

The Phillips Laboratory (PL) experiment consists of 60 samples organized into 10 identical sets of 6 samples each. The samples are finished on both sides, so a total of 120 surfaces are available for characterization and analysis. Each set includes one sample each of: 1) uncoated fused silica, 2) magnesium fluoride coated fused silica, 3) uncoated molybdenum, 4) molybdenum coated with chromium, silver and thorium fluoride, 5) diamond turned copper, and 6) diamond turned nickel plated copper. Two sample sets were never flown (ground control samples), one set was flown on the trailing edge but was not exposed (flight control samples), and one set was flown on the leading edge and exposed for 70 months. The remaining six sets were exposed for 3, 6, and 9 months on both the leading and trailing edges. The Phillips Laboratory optical experiment is unique in that identical samples were exposed for various durations of time on both the leading and trailing edges of the LDEF.

All but one of the PL flown sample sets were located in Environmental Control Canisters (ECC). The canisters were not opened during the first 14 days in orbit when the immediate environment contained a heavy concentration of contamination introduced by the Shuttle [1]. Also, after 9 months, the canisters were closed, preventing sample exposure to the high fluxes of atomic oxygen encountered late in the mission. The canisters still possessed a partial vacuum when disassembly was performed in the clean room environment at Kennedy Space Center. The ECC samples should be relatively contamination free compared to the samples exposed on the leading edge for 70 months. It is anticipated that observed differences in optical performance degradation will be seen between those samples exposed for 3, 6, 9 and 70 months.

CHARACTERIZATION PROGRAM

Phillips Laboratory has developed a three phase characterization plan to determine sample optical performance degradation and correlate measured degradation with space exposure. Phase I is restricted to visual, microscopic and optical evaluation. Phase II tests are designed to gain an understanding of fundamental material changes affecting optical performance, and Phase III will include laser damage testing and optical component cleaning. Results from all phases will be correlated with sample exposure location and duration. It is anticipated that samples flown on the leading edge (LE) will have suffered more performance degradation than samples on the trailing edge (TE). It is also feasible that samples exposed to the space environment for longer periods of time will show more performance degradation than those exposed for shorter periods of time.

Phase I measurements are nondestructive and include, but are not limited to: 1) full surface photography, 2) high resolution microscopy and photography, 3) absorption, 4) transmission and reflectance, 5) ellipsometry, 6) scatter (BRDF), and 7) an impact site count. A detailed surface map will also be made of each surface. The surface mapping consists of a visual and microscopic examination which provides a qualitative measure of the types of damage sustained by each sample and is being used to locate and identify unusual damage sites.

Phase II analysis will determine surface morphology and chemistry, film depth profiles, atomic population density, erosion depth and mass loss. Techniques designed to investigate the fundamental reasons for performance degradation are in many cases intrusive and will not be undertaken until Phase I measurements are complete.

During Phase III, selected samples will be cleaned according to standard optical cleaning and/or innovative procedures. Selected Phase I tests will be repeated to determine if the sample's

performance can be restored to an acceptable level. A small number of samples will be laser damage tested.

PRELIMINARY CHARACTERIZATION RESULTS

Full Surface Photography. Full surface photography has proven to be a valuable tool for surface mapping and is a simple technique in which the sample is placed in a dark room, illuminated by a high intensity light at a high angle of incidence, and photographed. The photograph shows surface irregularities as points of scattered light. All full surface photographs were taken in a class 100 clean environment. Each sample surface (front and back) has been photographed twice, once with the sample fiducial mark at zero degrees to the direction of illumination and again at 90 degrees. The photographs reveal that surface contamination and damage vary greatly from sample to sample.

Figure 1 is a full surface photograph of a diamond turned, nickel plated copper, flight control sample. The sample surface was coated at the time of manufacture with a protective film that was not removed until just before the sample was photographed. The photograph shows a clean surface devoid of scatter sites. Figure 2 is a photograph of a magnesium fluoride coated fused silica ground control sample. There are several scatter sites on the surface showing that even the ground control samples, which were stored under good conditions, display some contamination. Figure 3 is a photograph of a molybdenum sample which was flown on the LDEF trailing edge and exposed for 3 months. There are significantly more scatter sites on this sample than the control sample, implying that the LDEF space environment significantly increased surface contamination and/or damage. The increase in contamination/damage becomes even more apparent in photographs of samples exposed for longer periods of time. A coated molybdenum sample exposed for 70 months is shown in Figure 4. The scattered light from this surface identifies a rather large ($\approx$ 1 cm diameter) damage site.

The scatter sites shown in the full surface photographs are being investigated with a Nomarski microscope, and photomicrographs are being made for unusual contamination areas and impact sites. Optical measurements are being made on the highly blemished surface areas as well as on the cleaner areas.

Microscopy. Initial microscopy on the PL optical samples was performed by The Aerospace Corporation at the time the samples were removed from the trays. Phillips Laboratory is performing a final microscopic evaluation on each sample. The full surface photographs which have been taken of each surface are assisting in locating some sites requiring careful examination in Phase I and Phase II characterization.

The damaged area of the coated Mo sample discussed above (Figure 4), upon high levels of magnification, appears as shown in Figure 5. It is obvious that the overall damage area is many times the diameter of the crater. The mechanism for the coating failure in the vicinity of the strike is probably thermal or shock related or possibly a synergistic combination of both. It is evident from the photograph that the damage is quite severe and of considerable spatial extent. This type of damage has a pronounced effect, from a systems standpoint, on scatter. It is anticipated that the damage site will also have a significant effect on absorption.

The extent of debris and micrometeoroid caused damage varies. Figure 6 shows a strike on MgF_2 coated fused silica (LE, 9 month exposure) where the damage is relatively constrained. In contrast to Figure 6, Figure 7 documents an impact on uncoated fused silica (LE, 70 month exposure) which produced localized chipping and fracture zones extending many particle diameters. Figure 8 is a dark field photograph of a 1 mm diameter area on a fused silica sample which was exposed on the LE for 70 months. Each bright spot is light being scattered off a damaged area. When the dark field is removed, typical chipping associated with impact sites can be seen in the damaged areas. This sample will be photographed under higher magnification to verify that these damaged areas are impact sites. Optics with damaged areas such as these are potentially high scatter and high absorption optics.

Scatter Measurements. BRDF measurements made on the optical samples are being made on a research grade scatterometer, High Resolution Scatter Mapping Instrument (HRSMI), operated in the PL Optical Components Branch. The HRSMI is capable of high resolution scatter measurements and surface scatter mapping. All scatter data reported in this paper was taken at 6328 Angstroms. It is anticipated that samples flown on the leading edge and/or exposed for longer periods of time may be more highly scattering than samples flown on the trailing edge and/or exposed for shorter periods of time.

A scatter map of a fused silica sample is shown in Figure 9. The sample surface was exposed on the LE for 70 months; therefore, we anticipated that this surface would be highly scattering. The scatter map shows scatter varying two orders of magnitude across the sample surface.

The effects of micrometeoroid damage are important for brittle materials. Investigators have found fracture lines extending 2 cm from impact sites [2]. Figure 10 is a scatter map of an impact site on the LE, 70 month, fused silica sample. Scatter intensity from the center of the crater is five orders of magnitude greater than the sample background. Fracture lines extending from the crater are high scatter sites on the surface and are indicated in the mapping by rows of peaks. The intensity of the peaks is between one and three orders

of magnitude greater than the surface background. This map demonstrates the severe scatter effects of impact damage on brittle materials.

A graph of scattered intensity versus detector angle for various uncoated fused silica samples is shown in Figure 11. Eleven measurements were taken across each sample, and the eleven data points for a given detector angle were averaged to give one data point on the graph. The line defined by "+" symbols is scatter measured from a clean superpolished substrate which is not part of the LDEF sample set. The other four graphs represent data from uncoated fused silica samples. The data shows the expected trend between TE and LE samples. The ground control sample and the TE, 3 month sample are the lowest scattering of the four samples, while the LE samples are the most highly scattering. The two LE data curves have the same shape implying that the contamination and/or contributing to scatter is the same on both surfaces. It is interesting to note that the measured scatter of both the 70 month and 9 month exposed samples is the same. Two possible explanations for this phenomena are: 1) whatever is causing the scatter reached a condition where scatter is no longer affected, or 2) contamination on the 70 month sample was removed by atomic oxygen, radiation, or some other type of scrubbing effect which lowered the scatter to a level comparable to the 9 month exposure sample.

A preliminary attempt to determine the presence and magnitude of scattering from surface contamination was made. Scatter from the unexposed side of the LE, 70 month, uncoated fused silica sample was measured; and the data, represented by squares in Figure 12, shows that the surface is highly scattering. The surface was then blown with an air brush in an attempt to remove contamination, and the scatter measurement was repeated. The data, represented by triangles in Figure 12, shows that the surface scatter was not reduced. An alcohol drag was then performed twice on one-half of the surface, and the scatter was remeasured. The data, represented by diamonds, shows that cleaning the surface reduced the scatter three orders of magnitude. This is a significant reduction in scatter, indicating that there is considerable contamination on the sample surface.

Preliminary scatter data has also been collected on selected MgF_2 coated fused silica samples (Figure 13). Again, we anticipated that the LE samples would be more highly scattering than TE samples. The data, however, shows the complete opposite trend - TE samples are more highly scattering than LE samples. The reverse trend may possibly be attributed to the sample's coating. It has been shown that coating an optic increases its surface scatter; therefore, if the coatings on the LE samples have been removed by the space environment then the LE samples will be less scattering than the TE samples. All ten samples in this sample set will be measured to verify the preliminary data, and tests will be performed to determine each coating's condition.

CONCLUSIONS

The Phillips Laboratory optical experiment is unique. Identical samples were flown on both the leading and trailing edge and were exposed for variable lengths of time. Therefore, the potential exists to correlate optical performance to exposure duration and position.

Preliminary investigations indicate that these samples have experienced severe contamination and damage levels. Initial scatter data has shown that there is a potential relationship between sample exposure position and duration and surface scatter. These observations indicate that optical systems which are critically impacted by high scatter levels or high local absorption may be adversely affected by space environments similar to that experienced by LDEF.

REFERENCES

1. LDEF - 69 Months in Space, First Post-Retrieval Symposium, Part I, June 2-8, LDEF Science Office, NASA Langley Research Center, 1991.

2. "Meteorite and Debris Impact Features Documented on the Long Duration Exposure Facility." Preliminary Report, NASA Publication #94 (Aug 1990).

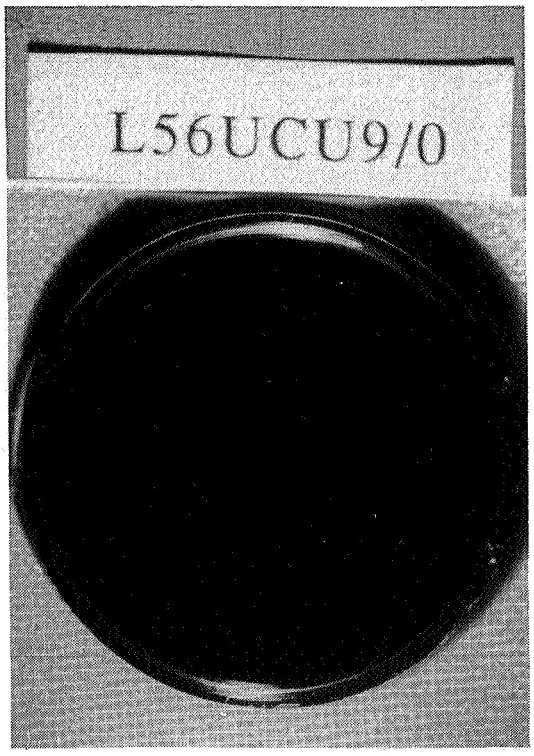

FIGURE 1: Full surface photograph of a clean optical surface. Sample is nickel plated copper.

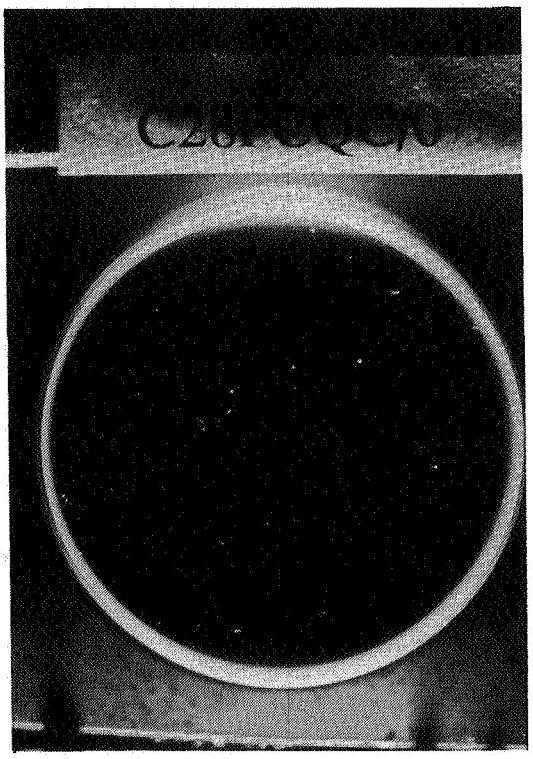

FIGURE 2: Full surface photograph of MgF_2 coated fused silica control sample.

ORIGINAL PAGE
BLACK AND WHITE PHOTOGRAPH

FIGURE 3: Full surface photograph showing many scatter sites on a molybdenum sample.

FIGURE 4: Full surface photograph showing a large damage site on a coated molybdenum sample.

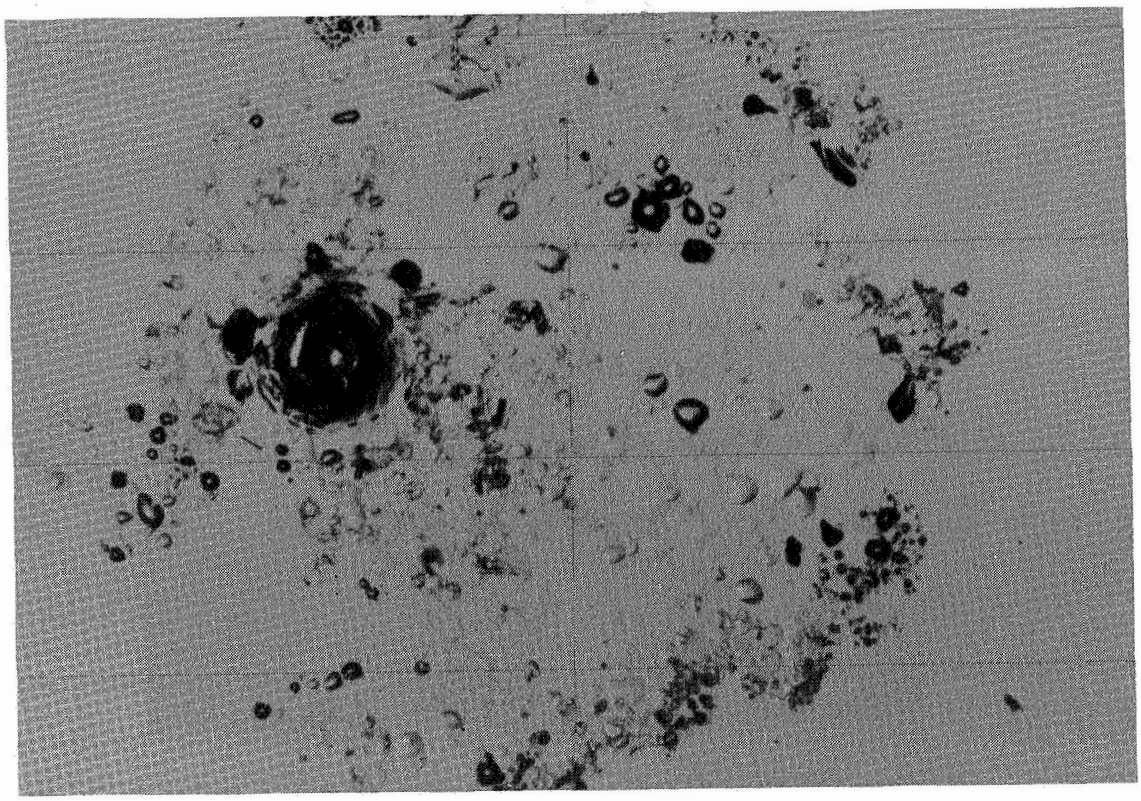

FIGURE 5: Micrometeoroid impact site surrounded by localized damage.*

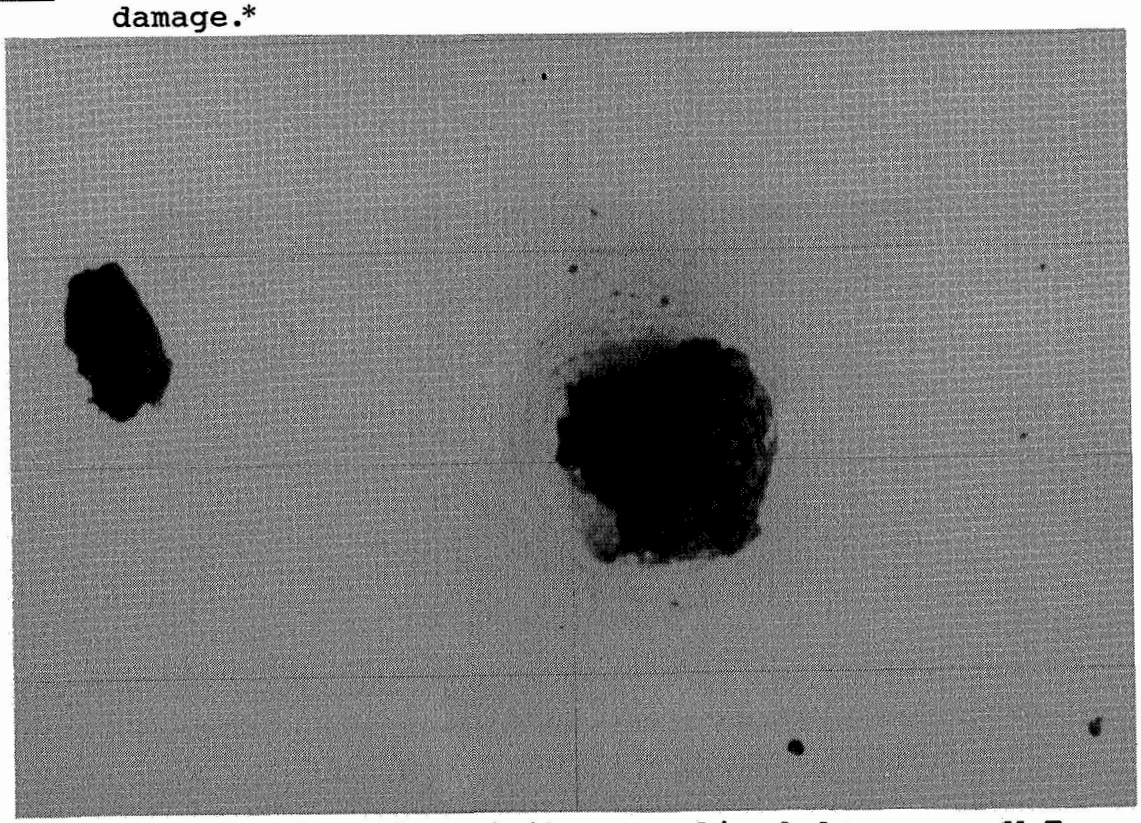

FIGURE 6: Impact site with limited localized damage on MgF_2 coated fused silica.*

*Photograph Courtesy of The Aerospace Corporation.

ORIGINAL PAGE
BLACK AND WHITE PHOTOGRAPH

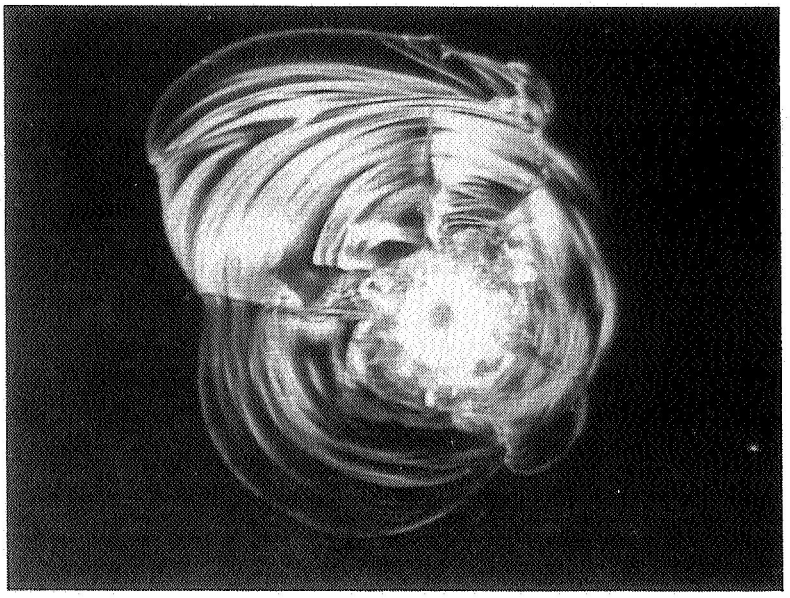

FIGURE 7: Micrometeoroid impact site surrounded by localized damage.*

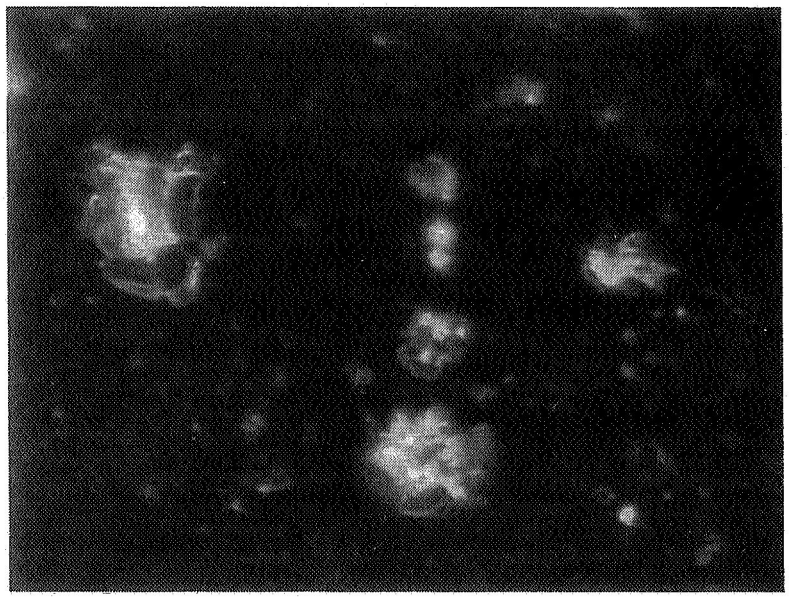

FIGURE 8: Dark field photograph showing fracture zones on a fused silica surface.

*Photograph Courtesy of The Aerospace Corporation.

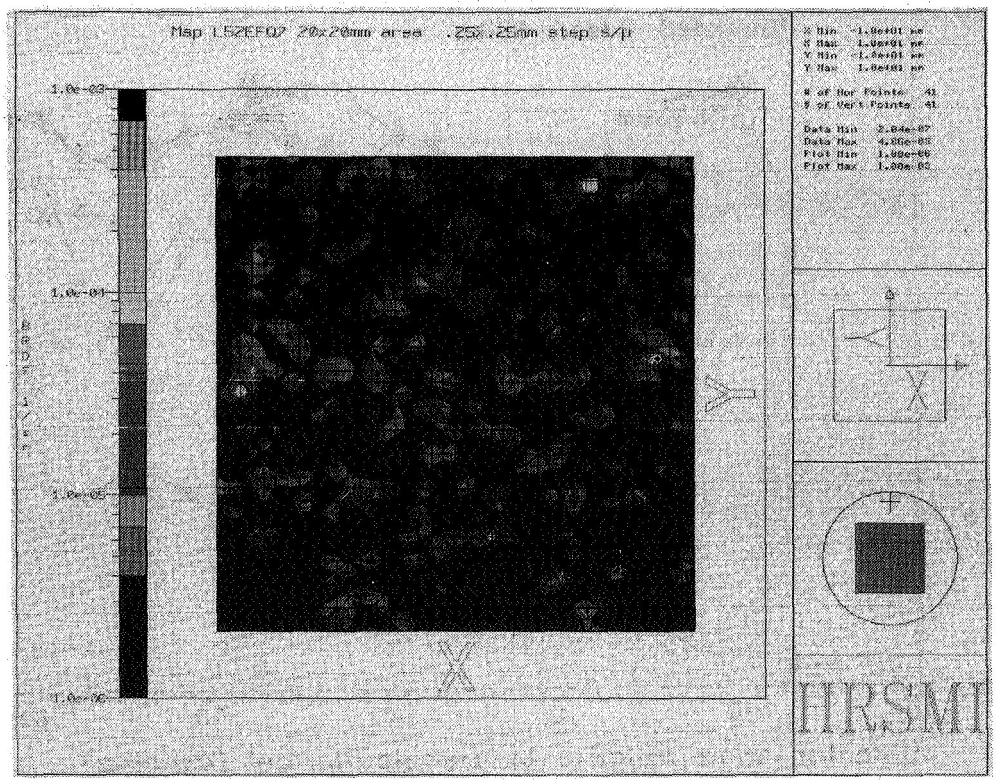

FIGURE 9: Scatter map of fused silica sample.
See color photograph on page 1563.

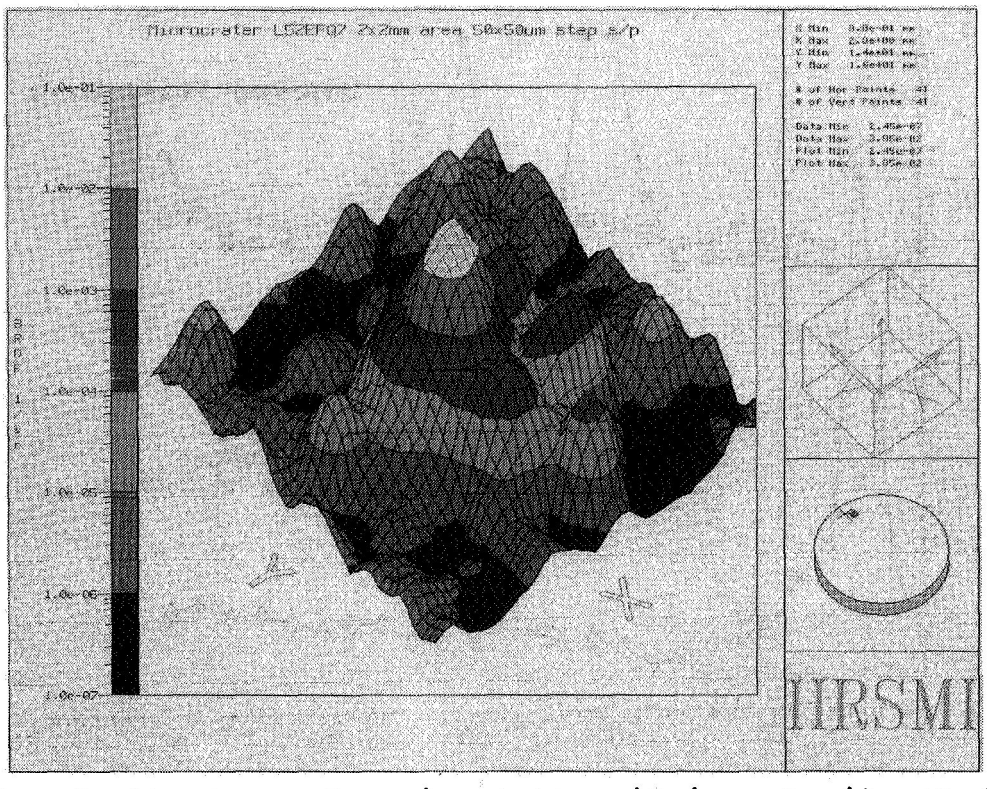

FIGURE 10: Scatter map of a micrometeoroid impact site on fused silica.
See color photograph on page 1564.

ORIGINAL PAGE
BLACK AND WHITE PHOTOGRAPH

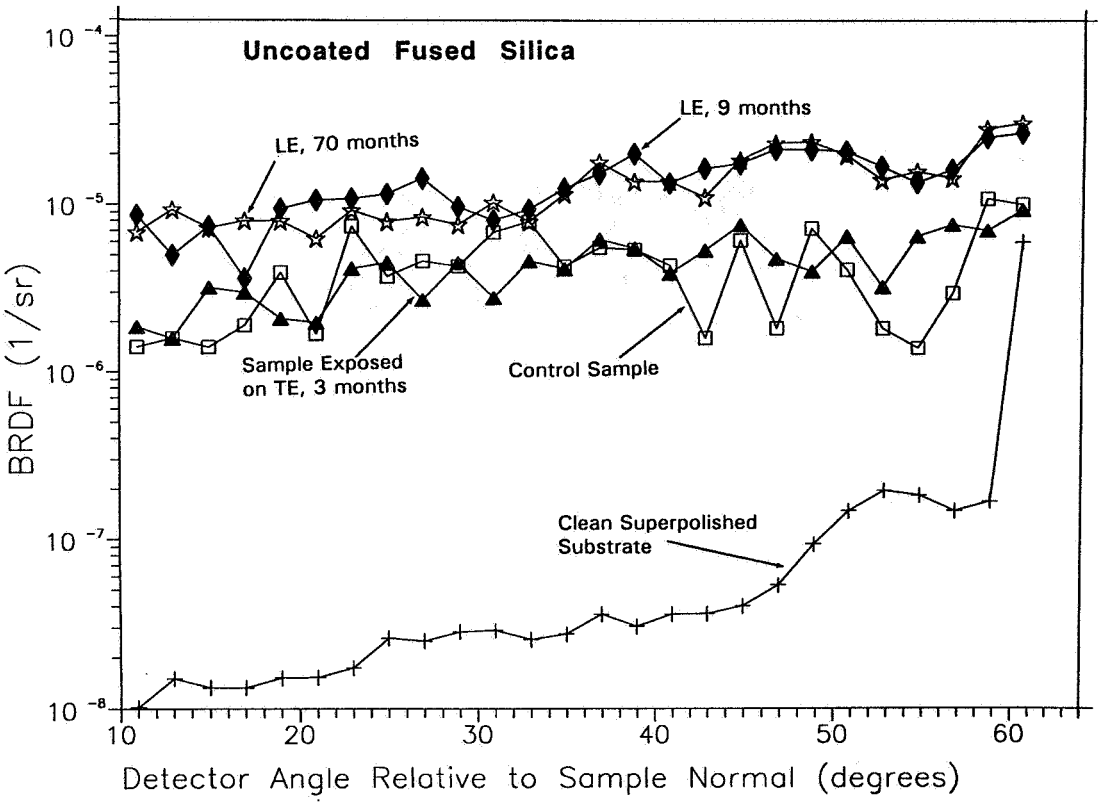

FIGURE 11: Graph of scattered intensity versus detector angle for four fused silica samples.

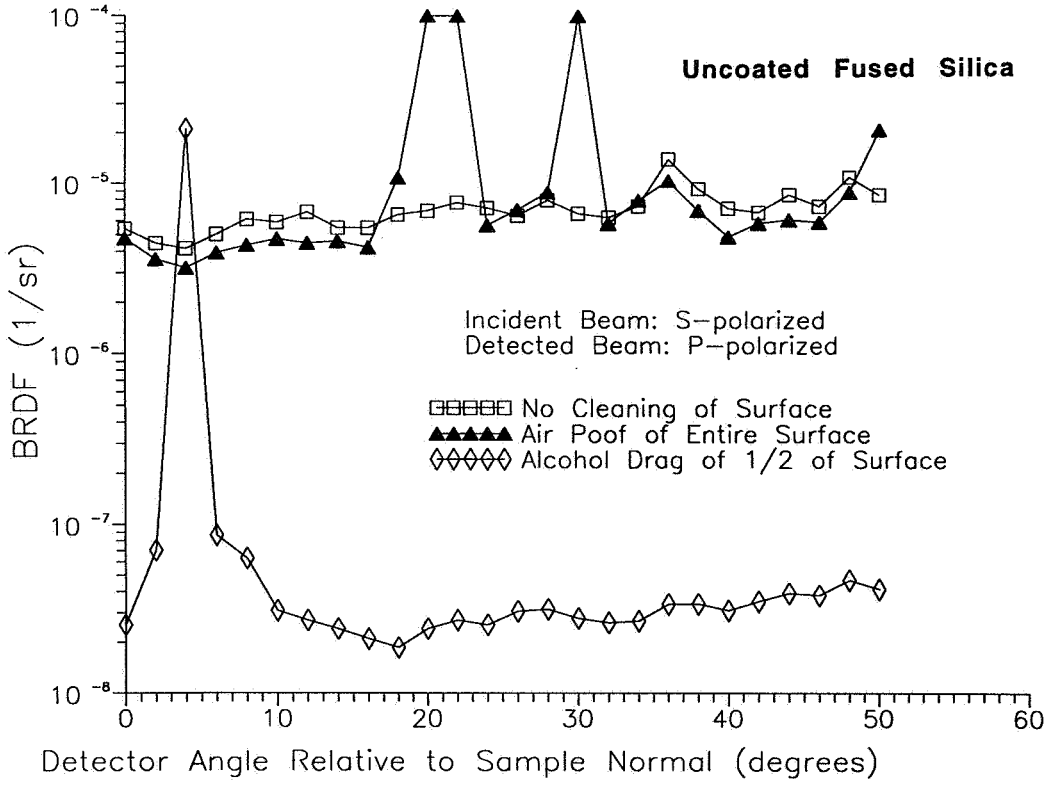

FIGURE 12: Scatter data showing effects of surface cleaning on fused silica sample.

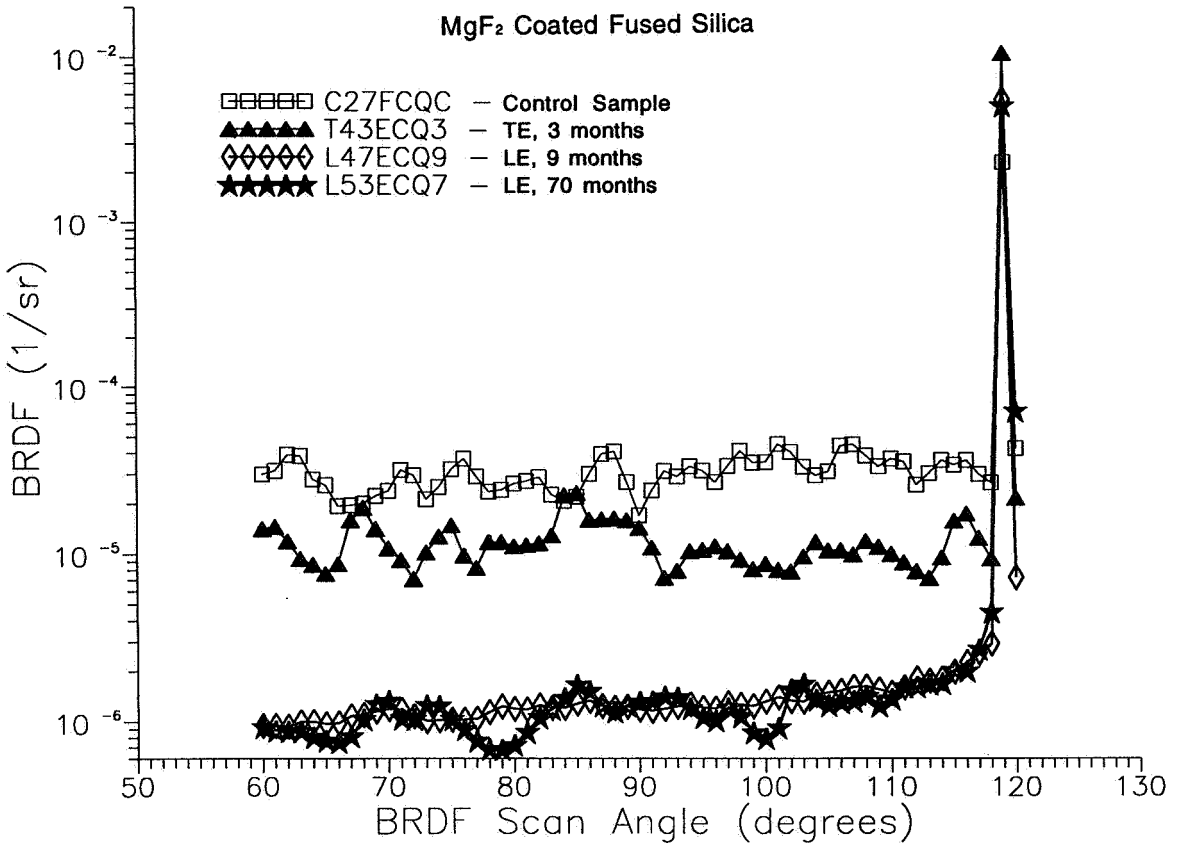

FIGURE 13: Graph of scattered intensity versus detector angle for four MgF_2 fused silica samples.

N93-29693

501733

STUDIES OF EFFECTS ON OPTICAL COMPONENTS AND SENSORS: LDEF EXPERIMENTS AO-147 (ERB COMPONENTS) AND S-0014 (APEX)

John R. Hickey
The Eppley Laboratory Inc.
P.O. Box 419, Newport, RI 02840
Phone: 401/847-1020, Fax: 401/847-1031

David J. Brinker
NASA Lewis Research Center
Cleveland, OH 44135
Phone 216/433-2236, FAX 216/433-6106

Philip Jenkins
Sverdrup Technology Inc., LeRC Group
Brook Park, OH 44142

SUMMARY

Some additional results of testing of optical filters and window materials and thermopile sensors of the two experiments are included here. The APEX interference filters exhibited much greater degradation in space than the ERB filters. The adhesion of the Indium washers to the APEX interference filters is reported.

INTRODUCTION

This paper is a continuation of a paper presented at the First LDEF Post-Retrieval Symposium (ref. 1). The Passive ERB experiment of the LDEF mission (AO147) was composed of sensors and components associated with the measurement of the Earth Radiation Budget from Nimbus satellites. The flight spare sensors from the Earth Radiation Budget (ERB) experiment which operated on the Nimbus 6 (ref. 2) and Nimbus 7 (ref. 3) satellites comprised the major part of experiment AO147. The Nimbus 7 instrument is still returning data as of this date (July 1992). The 10 solar sensors were mounted in LDEF tray B-8 along with 10 (non-ERB) interference filters supplied by Barr Associates (ref. 4). The 4 earth-flux sensors were mounted in LDEF tray G-12 on the earth facing end. A cavity radiometer, similar to channel 10C of Nimbus 7 was included as part of the Advanced Photovoltaic Experiment (APEX) which was mounted in LDEF tray E-9 (ref. 5). While PEERBEC was a passive experiment APEX was active. This presentation includes some results relative to the APEX experiment (S0014); notably information relative to the interference filters of the filter radiometer . Much of the background information regarding the 2 experiments is included in the

This work supported by NASA Langley Research Center under contract NAS1-15350 and NASA Lewis Research Center under contract NAS3-25958

references and other LDEF documentation. The association of the two is that the Eppley Laboratory was involved with the design and fabrication of both experiments in addition to the fact that the cavity radiometer related to the Nimbus experiment was mounted in the APEX to assure a position on the leading edge (RAM). The APEX was mainly a photovoltaic experiment. The solar cell results are discussed in the proceedings of the first symposium (ref. 5) and elsewhere in these proceedings (ref. 6). The cavity radiometer and the filter based spectral radiometer were intended as calibration reference instruments for the solar cell measurements.

In the following sections we present selected results from these experiments. A bibliography of recent references to the Nimbus ERB analysis and results is included.

SUMMARY OF RESULTS: EXPERIMENT AO 147

The Examination and testing of the returned ERB components generally confirmed the earlier contention that contamination of optical surfaces caused the degradation of most of the Nimbus 6 and 7 ERB data with time. The cleaning of these same surfaces (Nimbus) by atomic oxygen (AO) was also confirmed. Those channels which showed no recovery, notably ERB channel 7, were determined to have deposited layer materials which are not suitable for space use with high UV exposure. Also, the Suprasil W windows on the total irradiance channels showed some degradation in the UV transmittance region due to UV exposure. Interior optical elements appeared to be free of contamination. Interference filter transmittance changes were minor for channels 6 and 9, confirming another interpretation of the ERB results.

Earth-Flux channels on the earth facing surface (tray G-12) showed contamination deposits on the outer filter hemispheres. After cleaning, the transmittance was relatively unaffected except for transmittance loss in the UV region (ref. 7). The open channels, 11 and 12, were unaffected.

The thermopile sensors in all 14 channels appear to be unchanged by the space environment, even those of channels 3, 11 and 12 which had no protecting optical components to shield them from contamination, AO exposure and UV exposure.

The most important result of this effort was the retrieval, and subsequent testing of the cavity radiometer which was mounted in the APEX experiment. The post-retrieval intercomparisons and reflectance tests have had a major impact on the interpretation of the low percentage changes in the total solar irradiance. Previously these changes were questioned because of possible instrument degradation.

Contamination is determined to be the major factor in the reliability of a well designed ERB type experiment. When the solar maximum, with the increase in AO flux, occurs after the deposition of the contamination there is a possibility of total cleansing of some components and partial cleansing of others. The Nimbus 7 ERB has experienced this sequence twice since its launch in November 1978. The second factor is the decrease in UV transmittance of the broad band window materials which are necessary to separate the short wave flux from the total flux in ERB experiments. Our results combined with the APEX and other LDEF investigations indicate that Corning 7940 has less degradation than the Suprasil W. However, the Suprasil W was purchased in the 1970's, and was chosen for ERB applications based on the absence

of water (OH) absorption bands at the near infrared end of the spectrum, which was felt to be more appropriate for radiometric measurement purposes.

THE APEX (S 0014) FILTERS

There was some delay in removing and testing the filters of the APEX filter radiometer. This was because of the difficulty experienced in trying to remove the filters from their mounts. It was feared that the information on the transmittance would be lost if the filters were separated during the removal process. It was originally thought that the sticking was caused by a flow of the epoxy, which held the 2 filter substrates and spacer together. After carefully machining the outer surface of the mounting ring from one of the filter holders, it was found that the adhesion was caused by the Indium washers which were included for thermal transfer from the rear substrate to the holder. It was then decided to remove all 16 filters by machining as necessary. The following table is a summary of the condition of the filters after machining of the mounts (H blocks).

APEX PROJECT - FLIGHT FILTER CONDITION ON REMOVAL

Filter Number	Nominal Wavelength Angstoms	NOTES ON CONDITION after removal from H block	back substrate (glass type)
1	3250	together - like ERB filter with spacer	clear
2	3750	together - like ERB filter with spacer	clear
3	4250	together - like ERB filter with spacer filter broke during milling	clear
4	4750	separated - front filter speckled	clear
5	5250	separated - front filter speckled and has pin holes	yellow
6	5750	separated - front filter speckled and has pin holes	yellow
7	6250	separated - epoxy ring on front of rear substrate	orange
8	6750	together - probably the best looking filter	red
9	7250	separated - glass ring: scratch on front deposit and haze	red
10	7750	separated - epoxy or glass ring (broken)	red
11	8250	separated - epoxy or glass ring	dark red
12	8750	separated - hit on front - glass ring between	
13	9250	separated	dark red
14	9500	separated - bubbled front coating	dark red
15	11000	separated	dark red
16	12500	together - crystallized chips loose inside between substrates	dark red

An additional problem with the identification of the actual deposited layers and rear substrates was that the manufacturer could not locate the fabrication information and formulas because of the long time since manufacture and the death of the individual who specified the filters. The front substrates are believed to be Corning 7940. The

search for manufacturing information continues.

The post flight transmittance curves for the filters are given in figures 1 through 17. The first is a composite for the filters 1 through 13 on the same scale (60% transmittance full scale). The upper plots are all pre-flight transmittance and the lower are post-flight and after removal and/or separation as discussed above. It can be seen that all 13 filters suffered loss of transmittance. Some of the changes are drastic. It can also be seen that the wavelength band for each filter was retained to a high degree. There are no major band shifts apparent on this plot. Figures 2 through 17 are expanded transmittance plots for each filter showing the change from the original plots. Plots for the red end filters, 14, 15 and part of 16, are included in this group. Please note that the full scale ordinate value is not the same on all of the individual filter plots. Filter 14 appears to have experienced a band shift to the longwave.

It is apparent that the APEX filters experienced much greater changes than did the ERB filters (reported last year). Without the information on the layer materials, it is unlikely that the reason can be fully explained. From examination, it appears that the substrate materials were not a major contributor to the degradation. It is possible that a study of the first year flight data for the filter radiometer may help in identifying the onset of the experienced degradation.

REFERENCES

1. Hickey, J.R.: Passive Exposure of Earth Radiation Budget Experiment Components, LDEF Experiment AO-147: Post-Flight Examinations and Tests, First LDEF Post-Retrieval Symposium, NASA CP-3134, Part 3, pp 1493 - 1509, 1992
2. Nimbus 6 Users' Guide: (J.E. Sisala, ed.) NASA Goddard Space Flight Center, February 1975
3. Nimbus 7 Users' Guide: (C.R. Madrid, ed.) NASA Goddard Space Flight Center, August 1978
4. Mooney, T.A. and Smajkiewicz, A.: Transmittance Measurements of Ultra Violet and Visible Wavelength Interference Filters Flown Aboard LDEF. First LDEF Post-Retrieval Symposium, NASA CP-3134, Part 3, pp 1511 - 1522, 1992
5. Brinker, D.J., Hickey, J.R. and Scheiman, D.A., Advanced Photovoltaic Experiment, S0014: Preliminary Flight Results and Post-Flight Findings, First LDEF Post-Retrieval Symposium, NASA CP-3134, Part 3, pp 1395 - 1404, 1992
6. Brinker, D.J., and Hickey, J.R., The Effects of The Low Earth Orbit Environment on Space Solar Cells: Results of The Advanced Photovoltaic Experiment (S0014), Second LDEF Post-Retrieval Symposium, NASA CP-3194, 1993
7. Eppley Laboratory, Final Report on LDEF Experiment AO 147: Passive Exposure of Earth Radiation Budget Experiment Components, July 1992

BIBLIOGRAPHY

GENERAL REFERENCES

Clark, L.G., Kinard, W.H., Carter, D.J. and Jones, J.L. Jr. (eds), The Long Duration Exposure Facility (LDEF): Mission 1 Experiments, **NASA SP-473**, 1984

Predmore, R.E., Jacobowitz, H. and Hickey, J.R.: Exospheric Cleaning of the Earth Radiation Budget Solar Radiometer During Solar Maximum, Proceedings of the SPIE, 338, 1982, pp. 104-113

Working Report No. 162: International Pyrheliometer Comparisons IPC VII, 24 September to 12 October 1990, Results and Symposium, Swiss Meteorological Institute, March 1991

RECENT PUBLICATIONS AND PRESENTATIONS ON NIMBUS ERB RESULTS

Hickey,J.R., Kyle,H.L., Hoyt, D.V. and Ardanuy, P.E., "Nimbus-7 ERB Total Solar Irradiances for 158 Months", 1992 AGU ANNUAL MEETING PRESENTATION

Kyle,H.L. Ardanuy, P.E. and Hickey, J.R., "Long-Term Earth Radiation Budget Observations", 1992 AGU ANNUAL MEETING PRESENTATION

Kyle, H.L., D.V. Hoyt, and J.R. Hickey, 1992, "Comparison of the Measured Total Irradiance During Solar Maximum for Cycles 21 and 22", EGU meeting, Edinburgh, Scotland, April 1992

Hoyt, D.V., H.L. Kyle, J.R. Hickey and R.H. Maschhoff, 1992 "The Nimbus-7 Solar Total Irradiance: A New Algorithm for its Derivation", **J. Geophs. Res**,97, No.A1, 51-63

Hickey, J.R., R.G. Frieden and D.J. Brinker , 1991, "Report on an H-F Type Cavity Radiometer after Six Years in Space Aboard the LDEF Satellite", **METROLOGIA**, 28, 269-273, 1991

Hickey, J.R., B.M. Alton, H.L. Kyle and D.V. Hoyt, 1988, "Total Solar Irradiance Measurements by ERB/Nimbus-7, a Review of Nine Years", **Space Sci. Rev.**, 48, 321-342

Hickey, J.R., B.M. Alton, H.L. Kyle and E.R. Major, 1988 "Observation of Total Irradiance Variability from Nimbus Satellites", **Adv. Space Res.**, 8,(7)5-(7)10

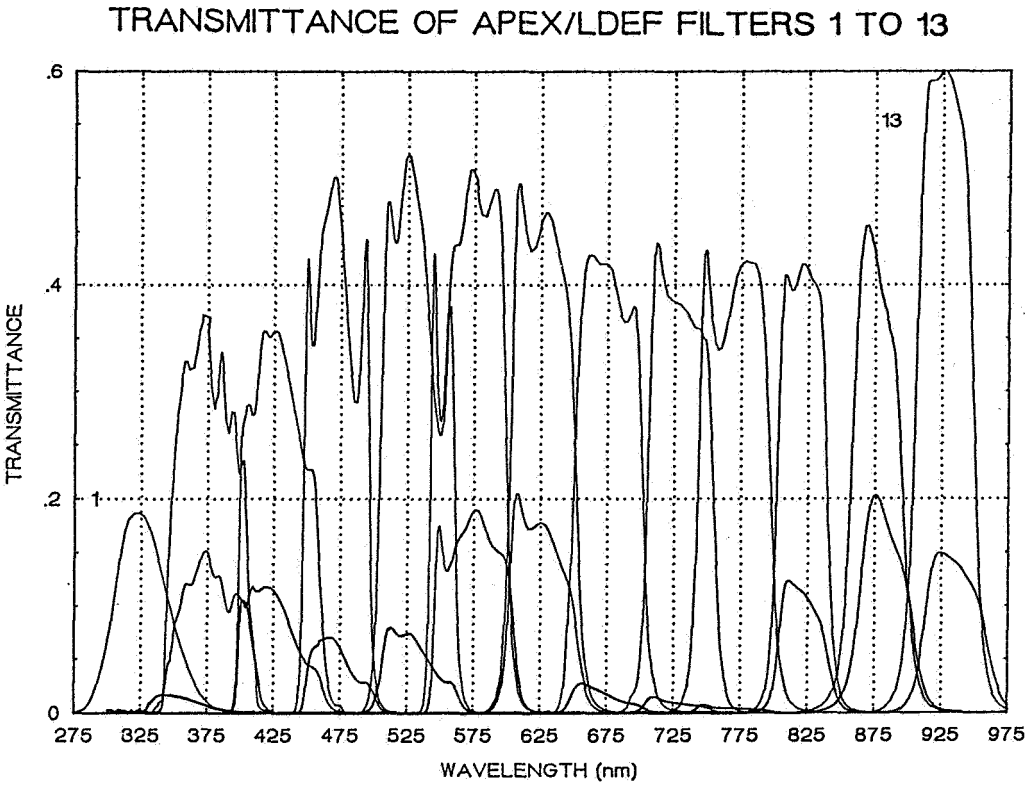

Figure 1

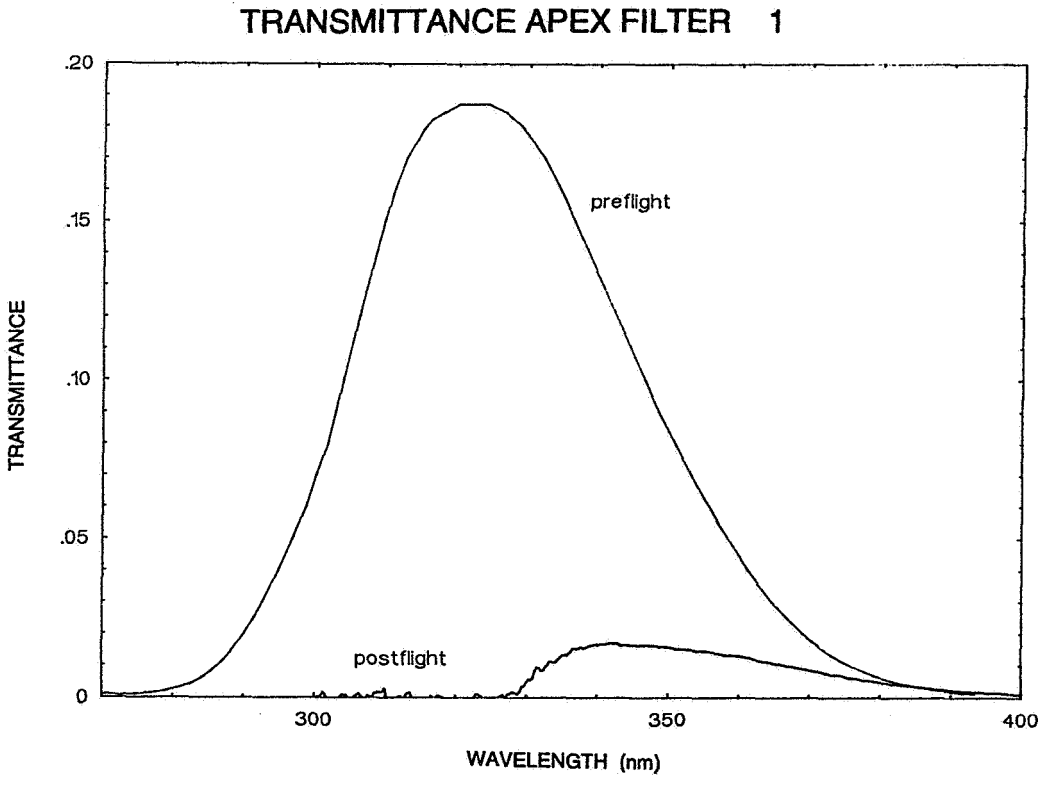

Figure 2

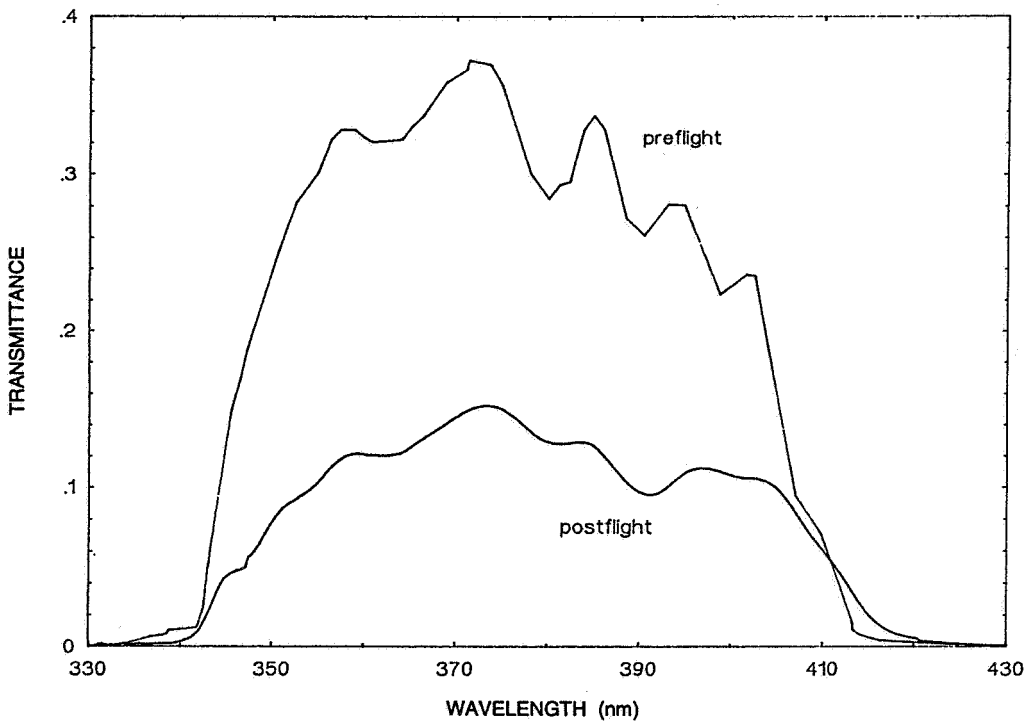

Figure 3

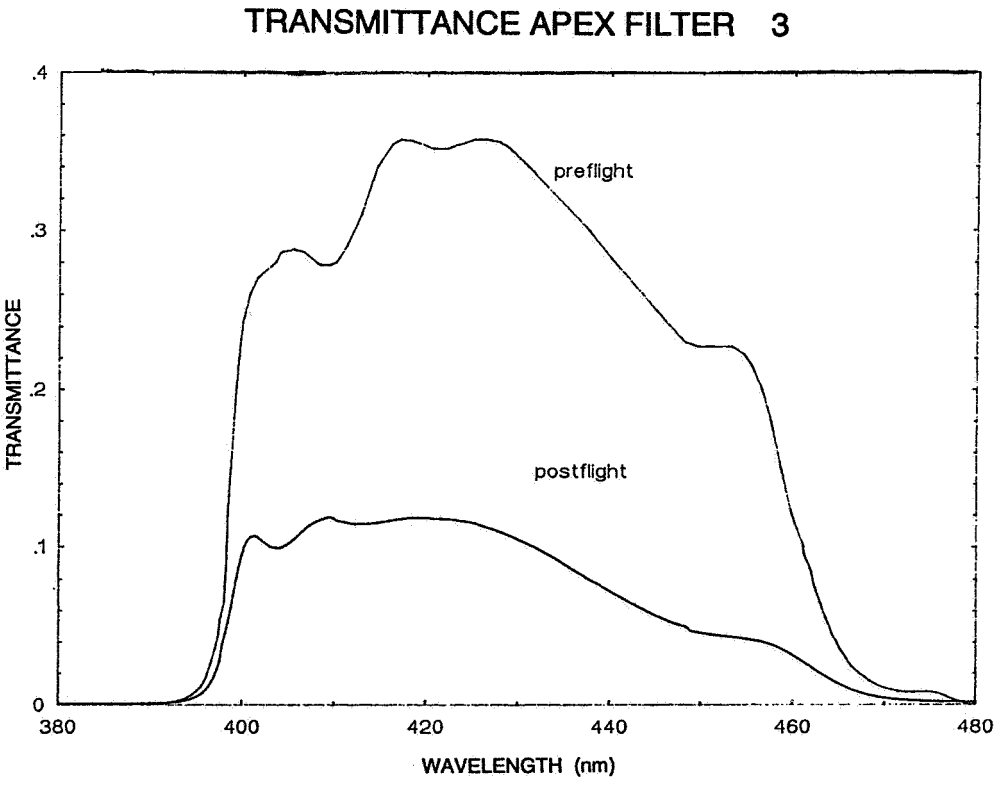

Figure 4

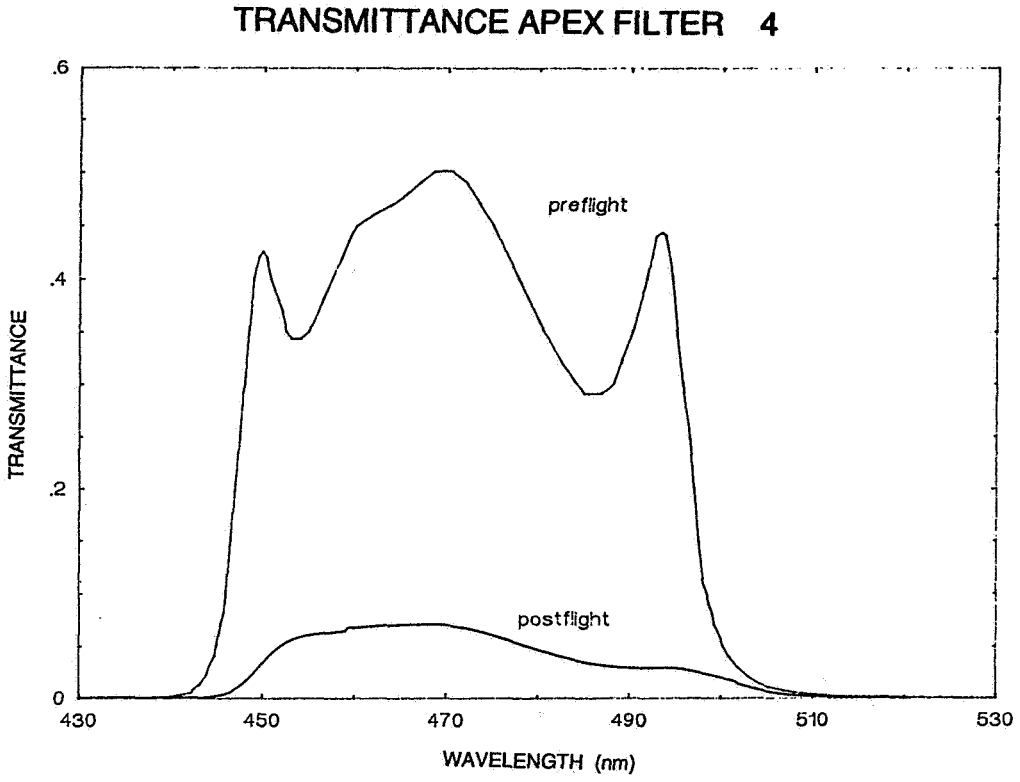

Figure 5

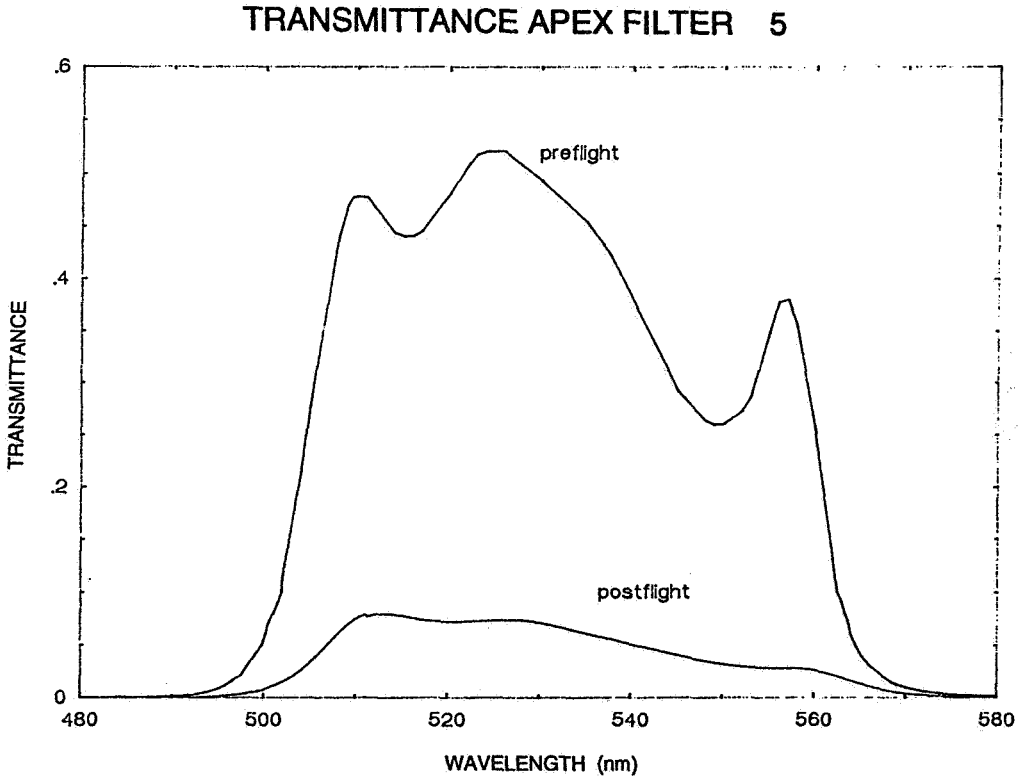

Figure 6

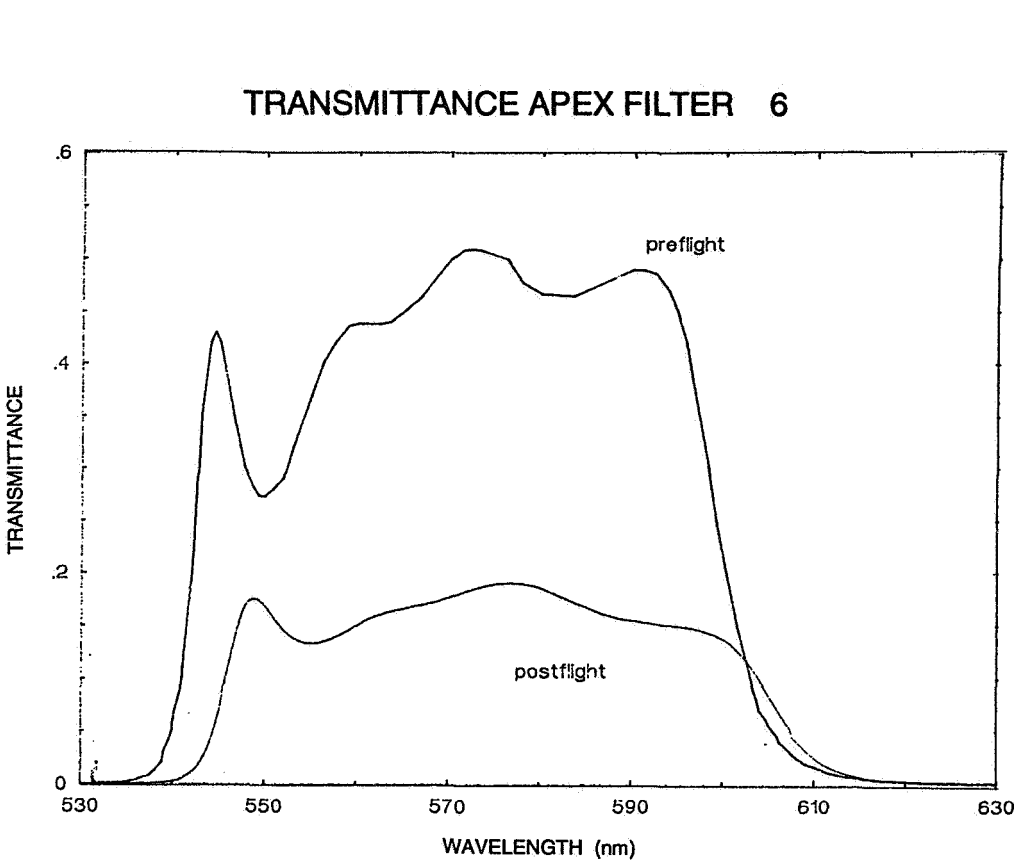

Figure 7

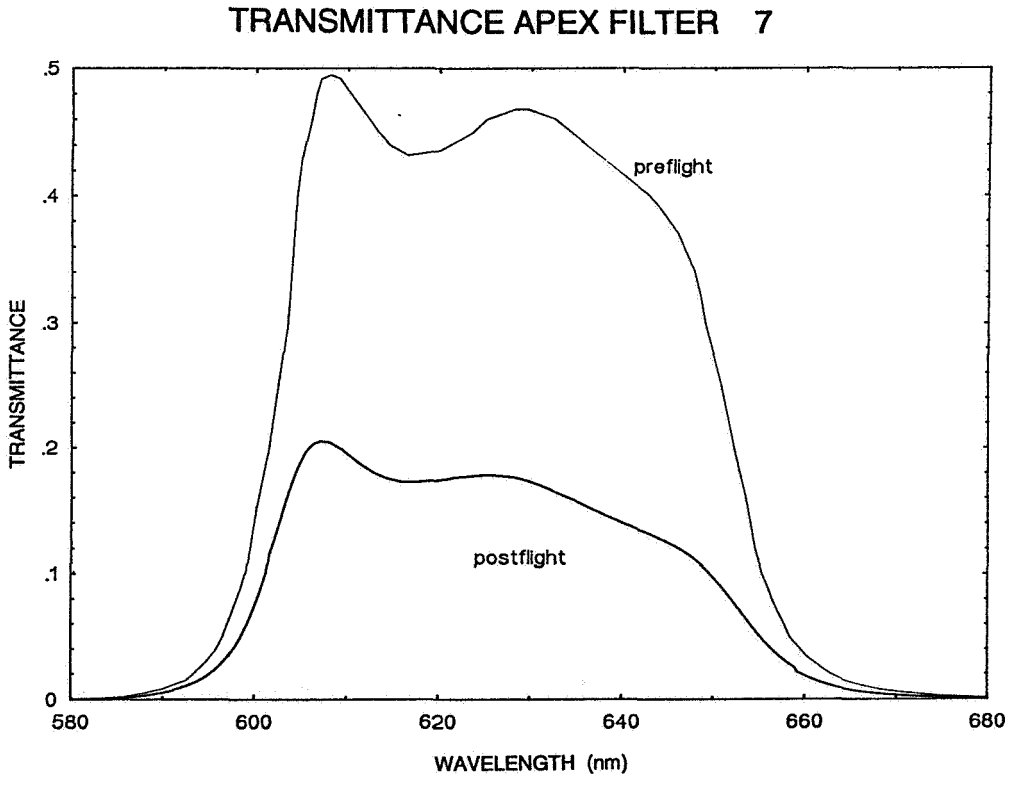

Figure 8

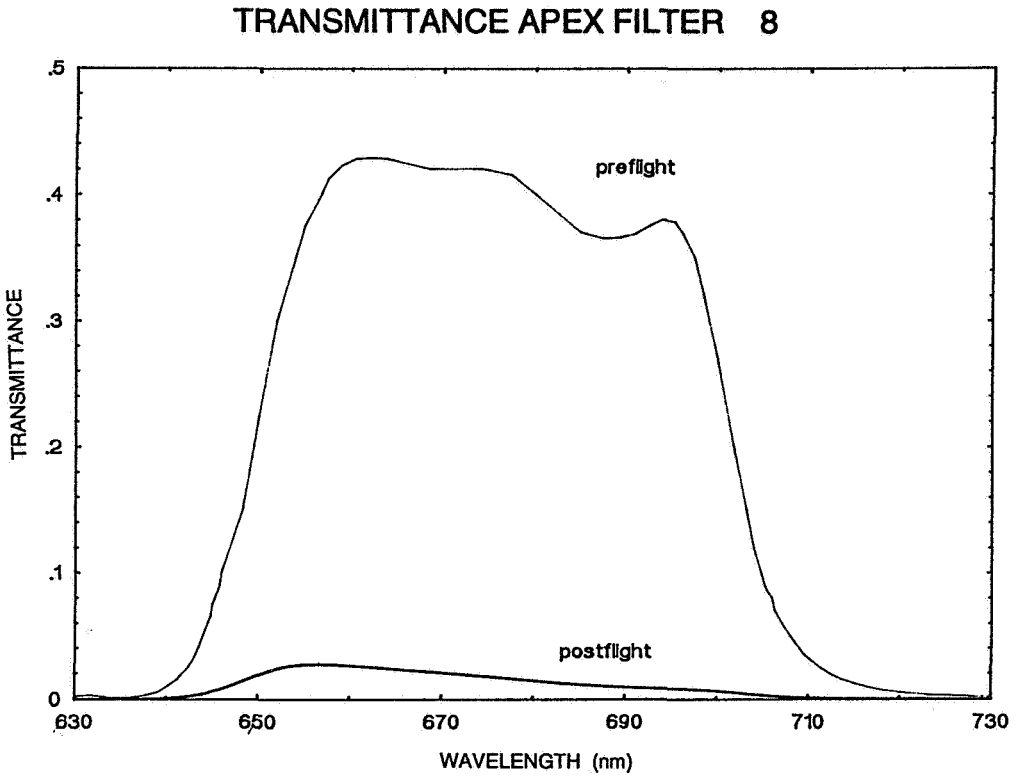

Figure 9

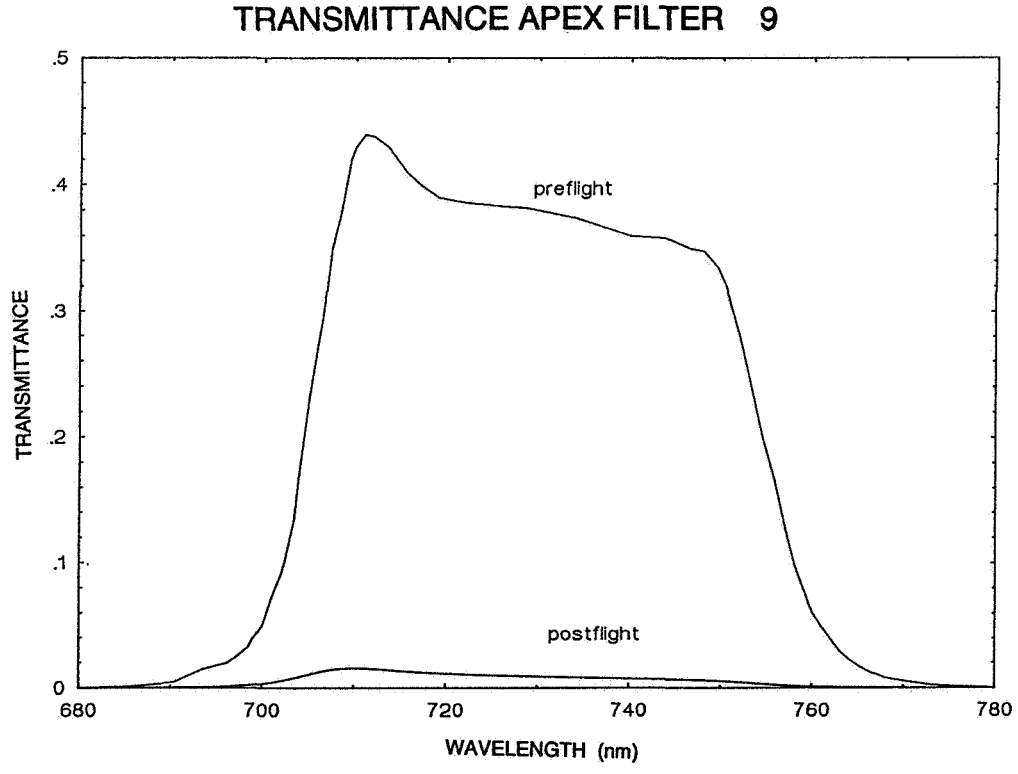

Figure 10

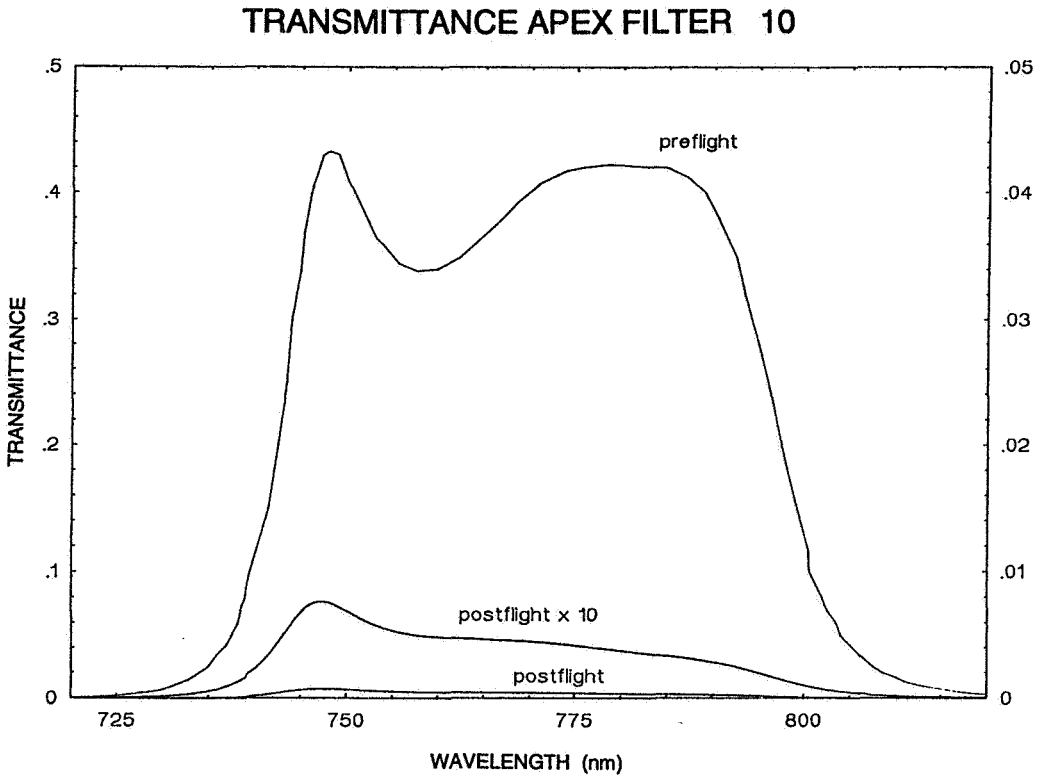

Figure 11

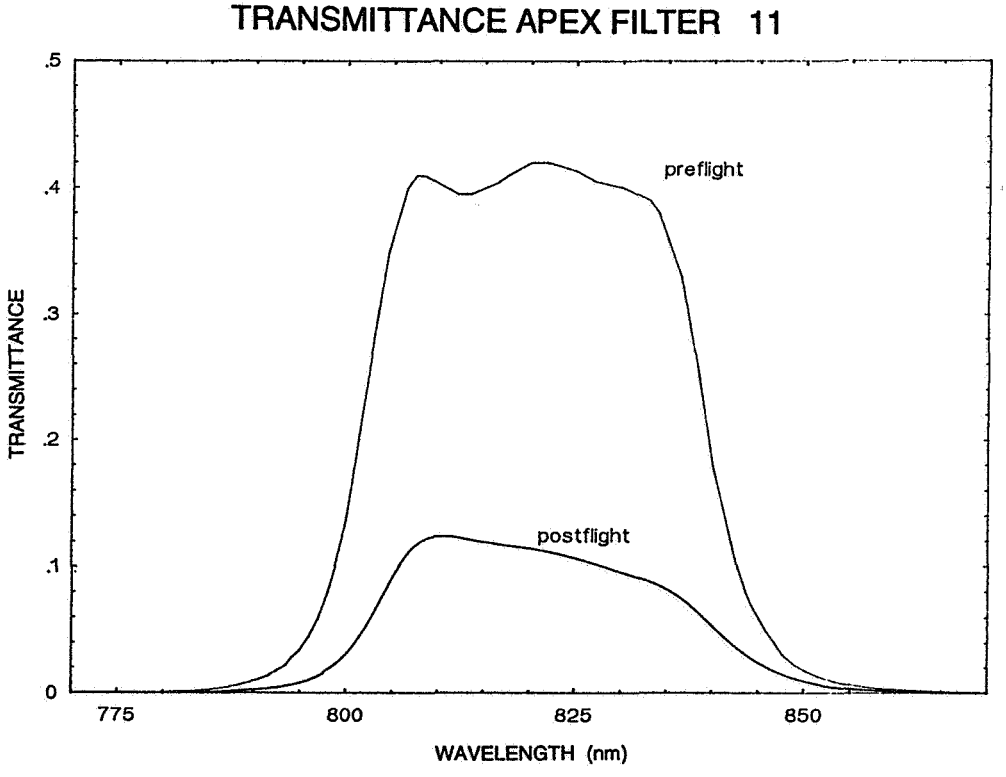

Figure 12

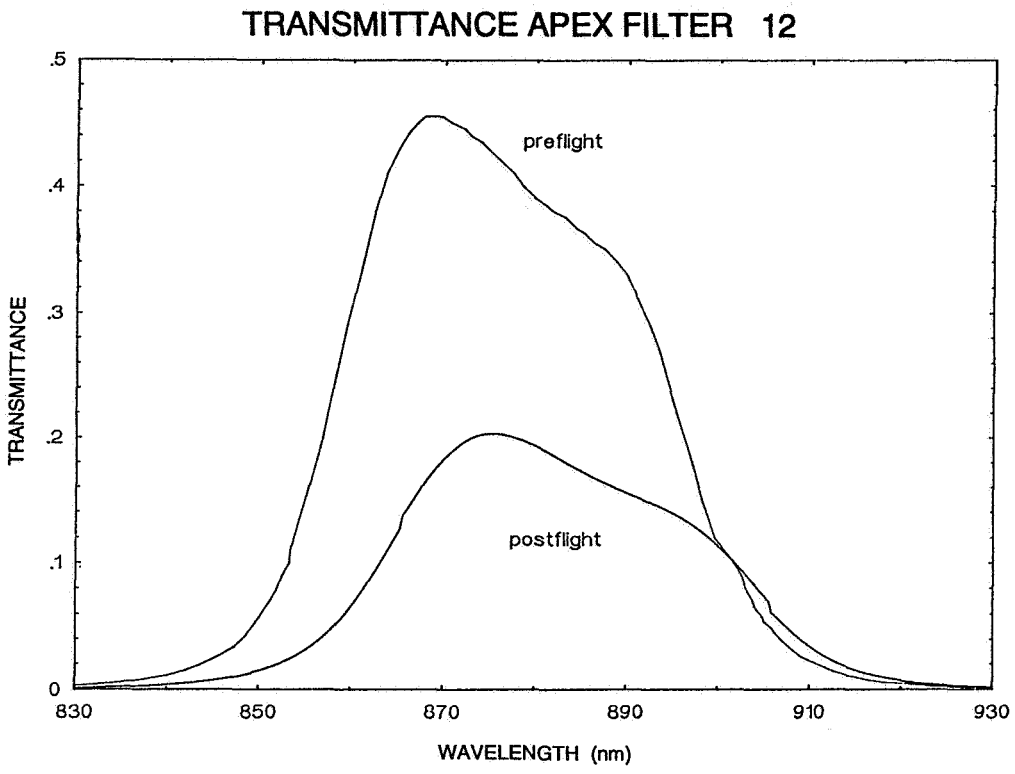

Figure 13

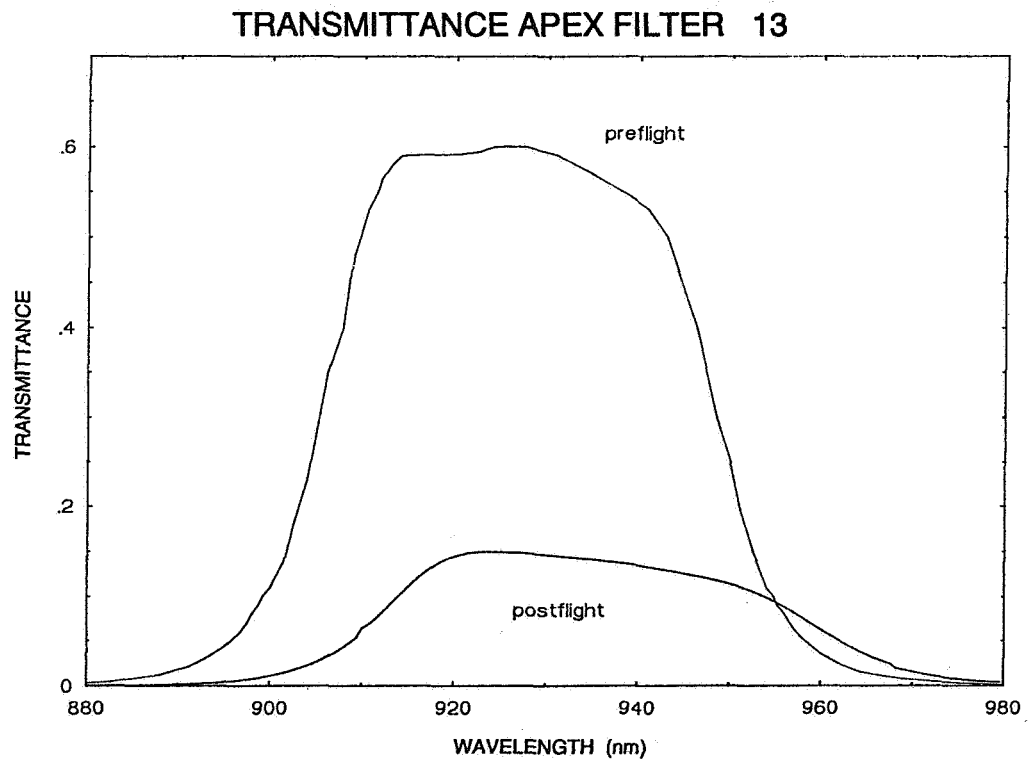

Figure 14

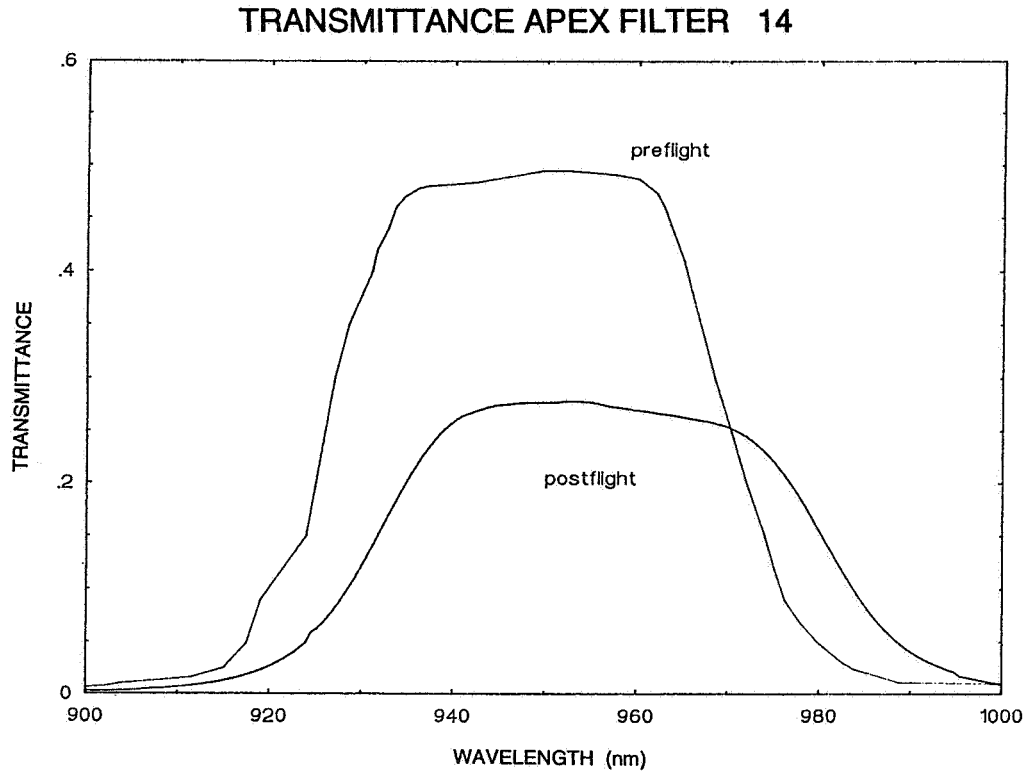

Figure 15

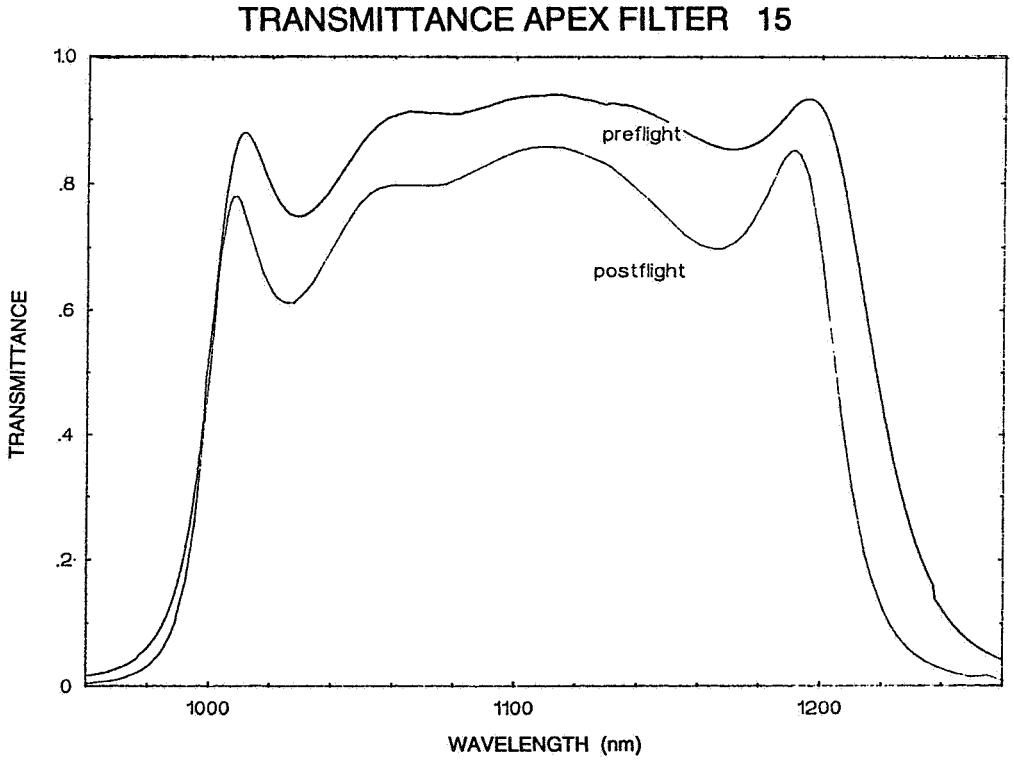

Figure 16

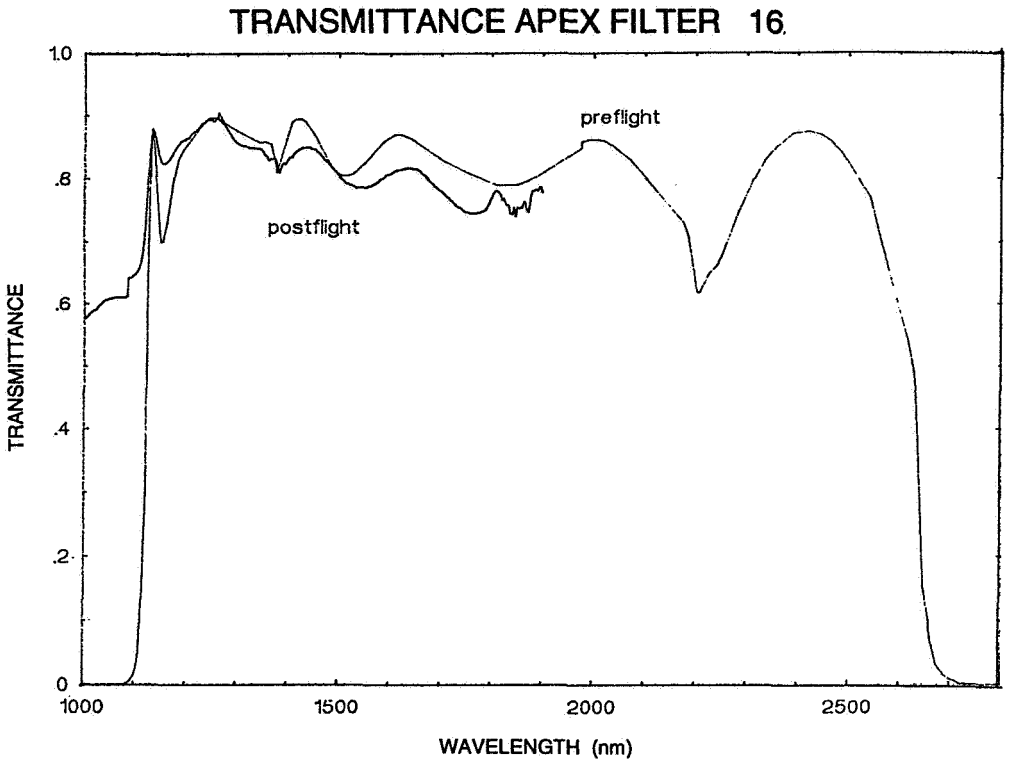
TRANSMITTANCE APEX FILTER 16
1.0
.8
.6
.4
.2
0
TRANSMITTANCE
preflight
postflight
1000
1500
2000
2500
WAVELENGTH (nm)

Figure 17

N93-29694

EFFECTS OF LONG TERM SPACE ENVIRONMENT EXPOSURE ON OPTICAL SUBSTRATES AND COATINGS (S0050-2)

501734
6s10

Keith Havey, Arthur Mustico, and John Vallimont
Eastman Kodak Company
Rochester N.Y.

Eastman Kodak Company included twelve substrate and coating samples on the LDEF structure. There were three Fused Silica and three Ultra Low Expansion (ULE™) uncoated glass samples, two ULE™ samples with a high reflectance silver coating, two Fused Silica samples with an antireflectance coating, and two Fused silica samples with a solar rejection coating. A set of duplicate control samples was also manufactured and stored in a controlled environment for comparison purposes.

Kodak's samples were included as a subset of the Georgia Institute of Technology tray, which was located on row 5-E, tray S0050-2. This placed the samples on the trailing edge of the structure, which protected them from the effects of atomic oxygen bombardment.

An evaluation of the flight samples for effects from the 5 year mission showed that a contaminant was deposited on the samples, a micrometeoroid impact occurred on one of the samples, and the radiation darkening which was expected for the glass did not occur. The results are listed below in more detail.

SAMPLE DESCRIPTION

Twelve samples were chosen for inclusion in the radiation experiment. The sample size was 1.250 inches in diameter and .040 inches thick, consistent with an ANSI break strength size. Both the faces and edges of the samples were polished. The substrate materials and coatings selected for the samples were chosen from those which have been specified on previous or current space flight optics.

The orientation of the coating samples in the LDEF simulated as closely as possible their actual mounting configurations when used on prime hardware. The high reflectance coating was on the outside of the sample facing the environment (the inside surface was also coated). The solar reflectance coating also faced the environment, but was on the inside face of the sample, and was protected by its fused silica substrate. The antireflectance coating was on both sides of the substrate.

All of the samples were measured for transmission, reflection, and stress prior to launch and after retrieval. Wash and tape tests were also performed on the samples to insure coating durability and adhesion. The set of control samples was also tested for comparison purposes.

The samples were delivered directly to NASA and assembled into the LDEF tray in a clean room environment to insure the cleanliness of the samples was maintained. A fine vacuuming of the samples was performed and close up pictures were taken just prior to sealing of the LDEF tray. The method of securing the samples in the tray is shown in Figure 1. A picture of the flight samples mounted in the LDEF tray is shown in Figure 2.

Twelve baseline samples identical to the space radiation samples were also simultaneously manufactured and tested. The purpose of these samples was to provide a direct comparison between exposed and non-exposed samples. The baseline samples were double sealed in nylon and anti-static polyethylene film and stored until retrieval of the flight samples.

POST FLIGHT EVALUATION

A thorough evaluation was performed on the LDEF samples for effects from the space environment. This included contaminant analysis, measurement of optical performance, induced stress, and BRDF. The control samples were also measured and the results compared to the flight data. Specific details of this evaluation follow.

MICROMETEOROID IMPACT

A micrometeoroid impact site was found on one of the samples. The impact crater measured .3 mm in diameter by .03 mm deep. Multiple fractures occurred in the glass at the impact site and are shown in Figure 3.

SAMPLE CLEANING

One sample of each type was cleaned after the initial optical performance measurements were made. The contaminate, a light brown in coloring, was removed fairly easily from all of the samples using normal cleaning methods and Isopropyl alcohol, with the exception of the Antireflection coated sample. On this sample, the contaminate could not be removed. It was not affected by either the alcohol, Toluene, Methyl Ethyl Ketone, Cyclohexene, 50/50 Nitric-Sulfuric acid, or heated Tri-Chlorobenzene. Only after exposure to an Oxygen plasma did some reduction in coloring occur. Three hours exposure to an Oxygen plasma reduced the brown discoloration, and increased the spectral transmission through the sample, as can be seen in Figure 4. The sample will be given additional exposure to the Oxygen plasma and its transmission will be measured after each exposure.

RADIATION DARKENING

Some radiation darkening could be expected of the Ultra Low Expansion (ULE™) glass which is not a radiation tolerant glass. No darkening of either the ULE™ or the Fused Silica glass was evident. There was no change in the transmission values of the pre-flight and after cleaning measurements, as shown in Figures 5 & 6.

OPTICAL PERFORMANCE

The flight samples were measured for optical performance from 350 to 1200 nm. Figures 4 thru 10 document the performance pre-flight, after flight, and after cleaning. As the figures show, all of the substrates and coatings experienced a significant performance reduction after flight, but after cleaning (except for the Antireflection coated sample which we couldn't clean), their performance returned to the pre-flight measured values. Of interest is the fact that the density of the contaminant deposited on the samples varied between coatings and substrate material. As an example, the transmission of the uncoated Fused Silica sample was reduced from 94% to 68% at 350 nm, while that of the uncoated ULE sample was reduced from 94% to 45%.

BRDF MEASUREMENT

A high reflectance silver coated flight sample (with contaminant) and a control sample were measured for Bidirectional Reflection Distribution Function. An increase in scattered light was measured on the flight sample versus that of the control sample, as shown in Figure 11.

STRESS MEASUREMENT

The samples were measured photoelastically for stress before and after flight using birefringence polarimetry. The control samples were also measured for comparison purposes. Table 1 lists the measured substrate stress values, the results of which are summarized as follows:

1) On the uncoated glass and high reflectance silver coated samples, the contaminant, on the average, induced a compressive stress of 42 psi. After cleaning, the stress levels closely matched those of the pre-flight measurements.

2) On the fused silica anti-reflectance coated sample, the contaminant did not induce any measurable stress.

3) A stress change could not be measured on the solar rejection coated samples due to the high level of stress in the coating, and the variation in stress between samples. A reduction in the stress levels in this coating was measured on both the flight and control samples.

4) No significant stress change was measured between the flight samples after cleaning and the control samples.

CONTAMINANT ANALYSIS

The contaminant on the samples was analyzed using X-ray Photoelectron Spectroscopy (XPS), which showed it to be a thin layer of polymer which contained silicon. The contaminant on the Antireflection coated sample and uncoated ULE™ sample appeared to be slightly different than that deposited on the other samples. On these two samples the energy peaks from the silicon, as listed in table 2, were representative of the binding energy of silicone rubber.

On the other samples, the energy peaks were higher, and more representative of the binding energy of SiO2. However, neither the relative atomic percentages or the relative sizes of the silicon and oxygen peaks from the XPS conclusively prove that the contaminant is a residue from the mounting rubber gasket.

Depth sputtering through the Antireflection coating, as can be seen in Figure 12, clearly shows the SiO2/TiO2 layers for both the control and flight samples. However the flight sample has a layer at the surface approximately 30 Angstroms thick, rich in carbon and silicon. The carbon content rises as the contamination layer is sputtered away and disappears at the contamination - antireflection layer interface. The total time required to sputter to the bottom of the SiO2/TiO2 layers was almost identical for both the flight and control samples. Since the hardness of the coating on both samples was similar, the sputtering rates would have been equivalent, making the total coating thicknesses the same. This indicates that either the top surface of the flight coating has been removed and replaced with the silicon/carbon layer, or the silicon/carbon has fused into the SiO2 layer.

SUMMARY

The 5+ year exposure of the samples to the space environment resulted in a contaminant being deposited on the samples which reduced optical performance, induced stress, and varied in composition between the samples depending on the coating. One sample received a micrometeoroid impact. After cleaning the contaminant from the samples, all of the coatings and substrates, with exception of the anti-reflection coated samples, returned to their original pre-flight performance.

LDEF SAMPLE STRESS DATA				
	STRESS PSI			
SAMPLE DESCRIPTION	PRE-FLIGHT	POST-FLIGHT	AFTER CLEANING	CONTROL SAMPLE
FUSED SILICA UNCOATED	9.26 T (6)	35.3 C (1)	2.27 T (1)	10.7 T (3)
ULE™ UNCOATED	9.51 T (6)	38.5 C (1)	8.0 T (1)	17.1 T (3)
ULE™ H. R. COATED (both sides)	14.5 T (6)	33.1 C (1)	9.0 T (1)	15.4 T (3)
FUSED SILICA A. R. COATED	15.6 T (6)	16.4 T (2)	-------	20.1 T (3)
FUSED SILICA S. R. COATED	676 C (6)	553 C (1)	569 C (1)	557 C (3)
FUSED SILICA S. R. COATED (uncoated side)	210 T (6)	185 T (1)	160 T (1)	150 T (3)
	( ) NUMBER OF SAMPLES MEASURED "T" INDICATES TENSION "C" INDICATES COMPRESSION			

Table 1. Stress measurements in LDEF samples

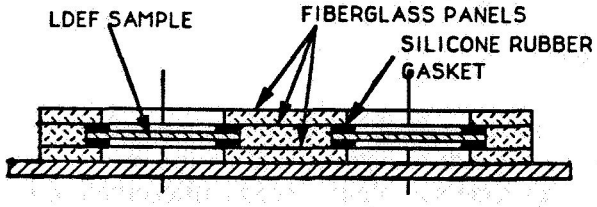

Figure 1. Sample mounting

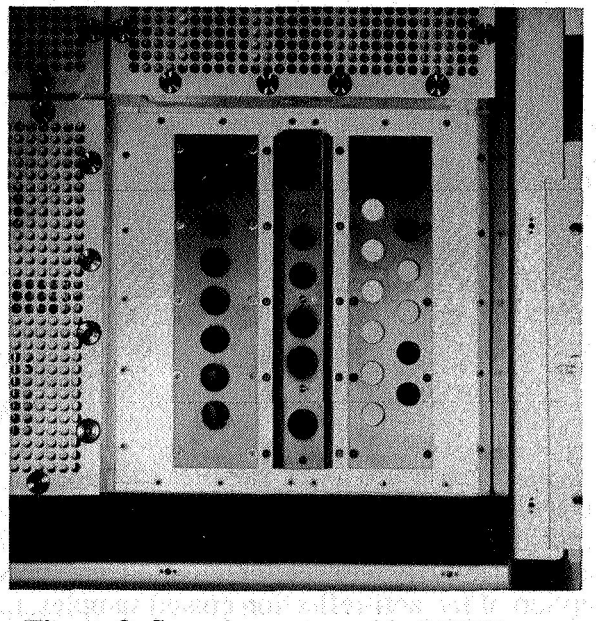

Figure 2. Samples mounted in LDEF tray (12 samples on right)

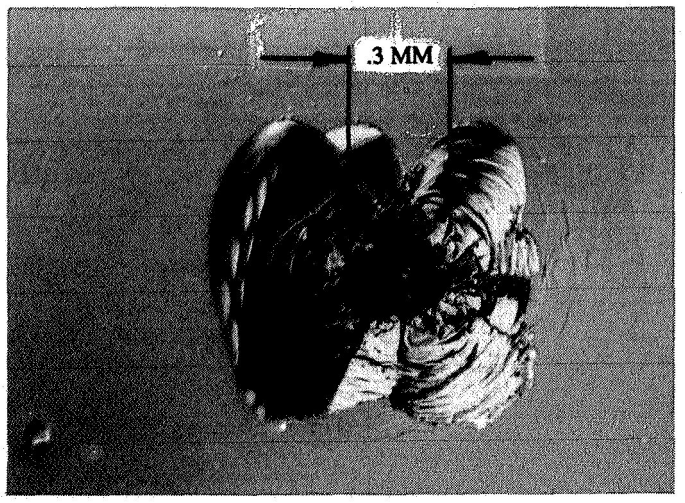

Figure 3. Micrometeoroid impact crater

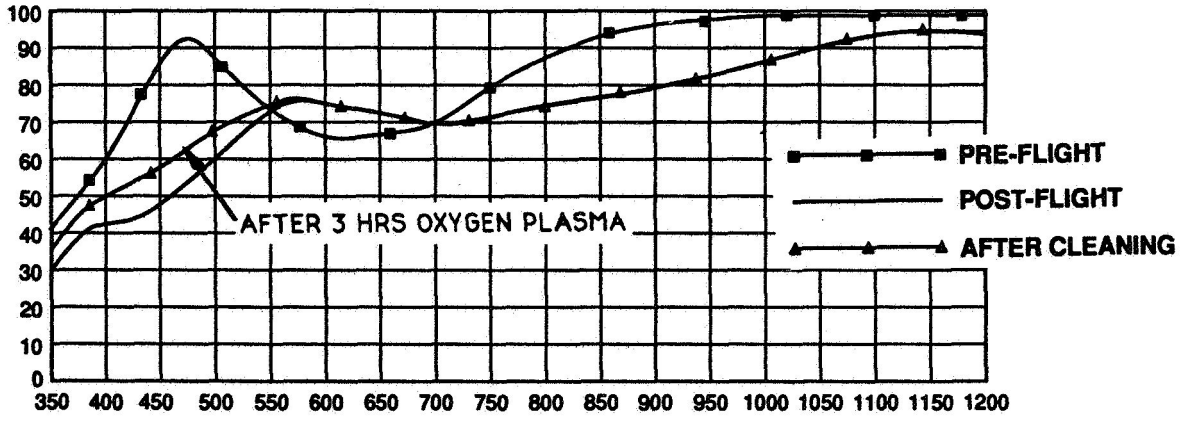

Figure 4. Spectral transmission of fused silica anti-reflection coated at 1.06λ

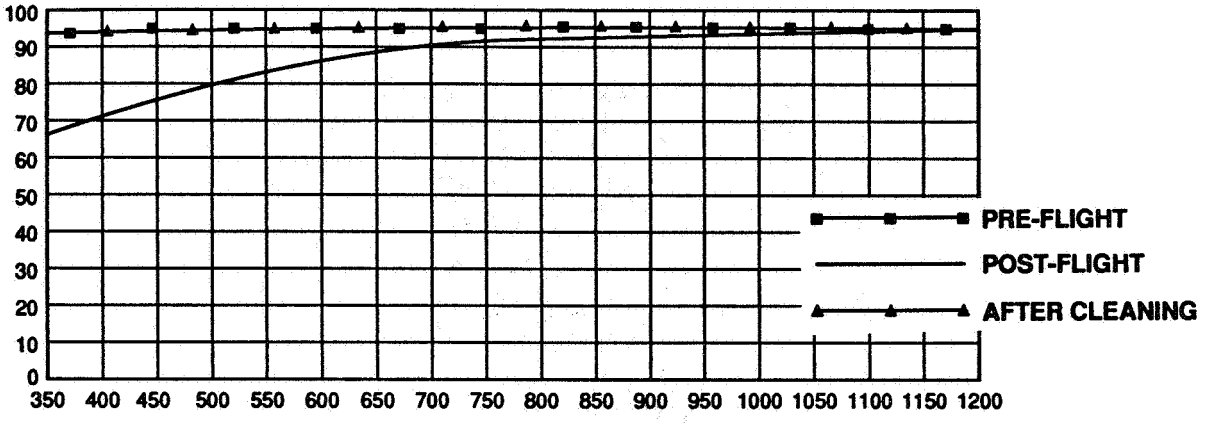

Figure 5. Spectral transmission of uncoated fused silica

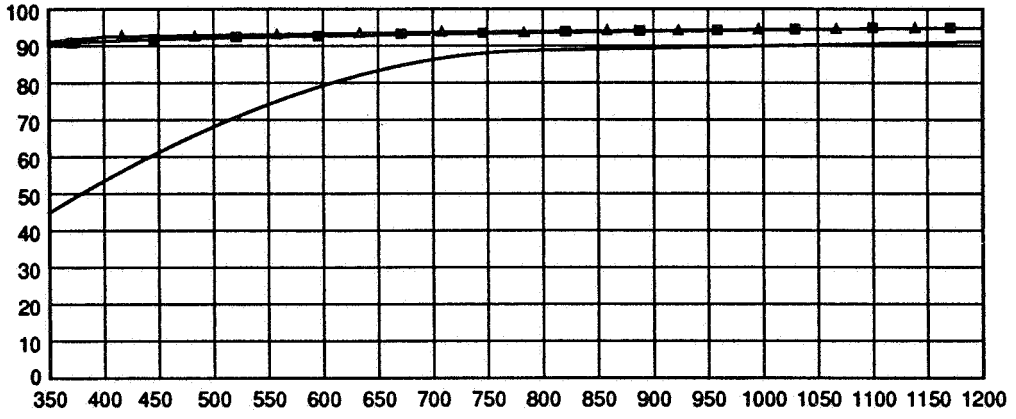

Figure 6. Spectral transmission of uncoated ULE™ sample

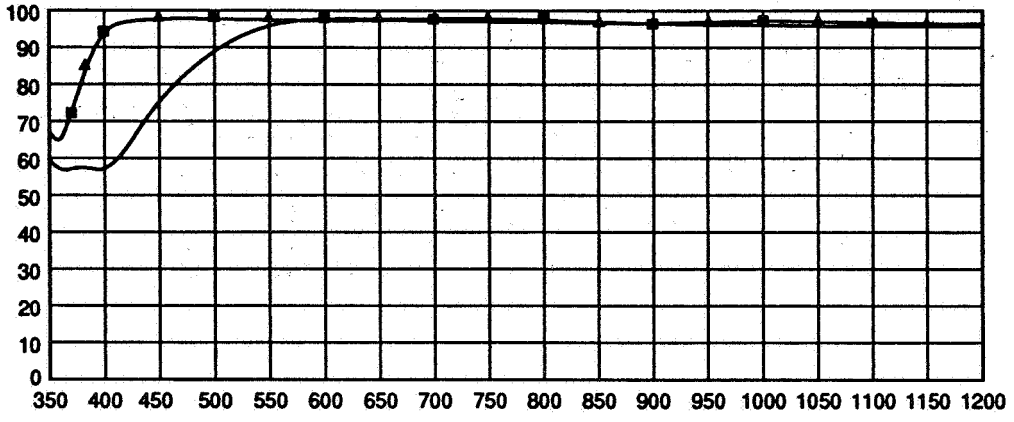

Figure 7. Spectral reflection of ULE™ H.R. silver coated outboard

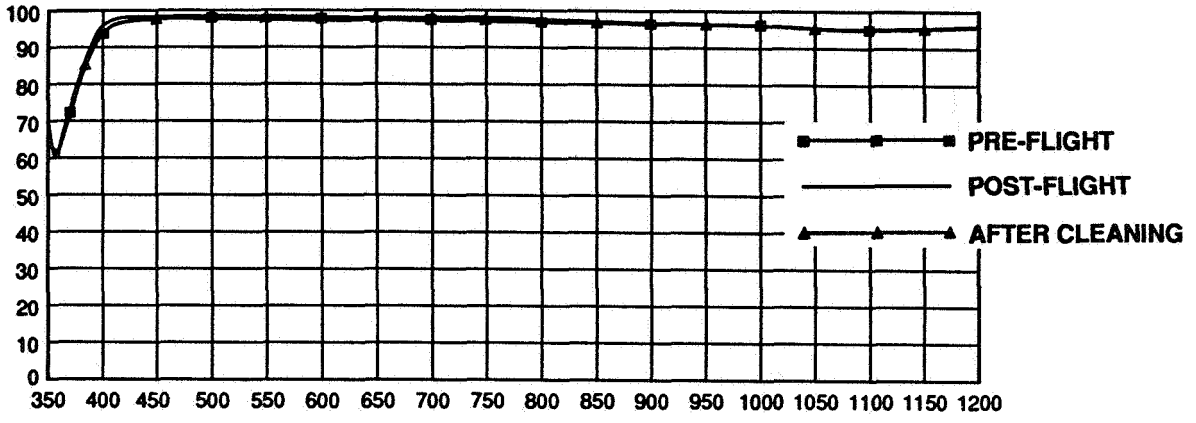

Figure 8. Spectral reflection of ULE™ H.R. silver coated inboard

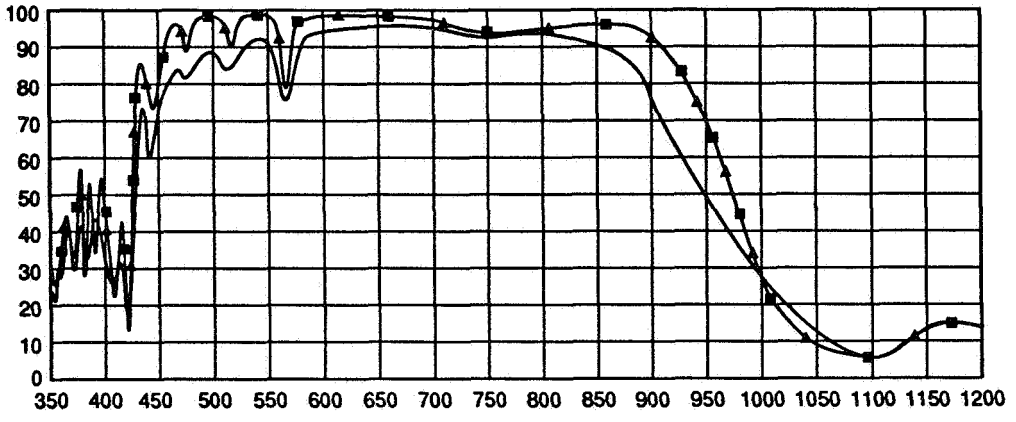

Figure 9. Spectral reflection of fused silica solar rejection coated

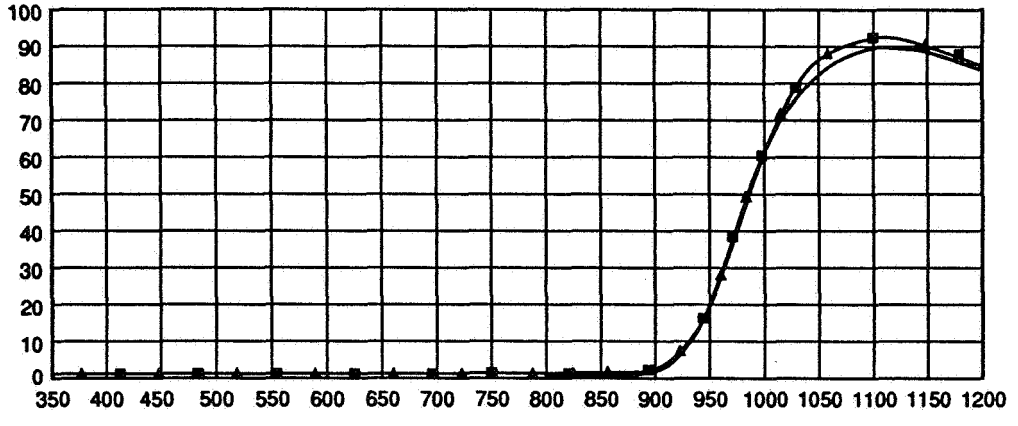

Figure 10. Spectral transmission of fused silica solar rejection coated

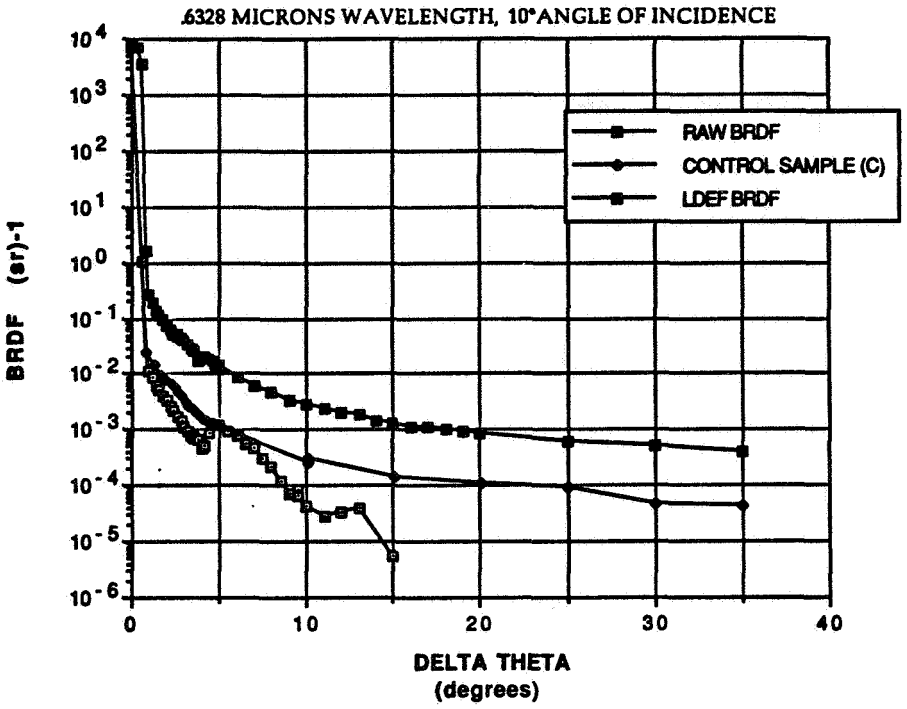

Figure 11. BRDF measurement of LDEF flight and control sample high reflectance silver coated

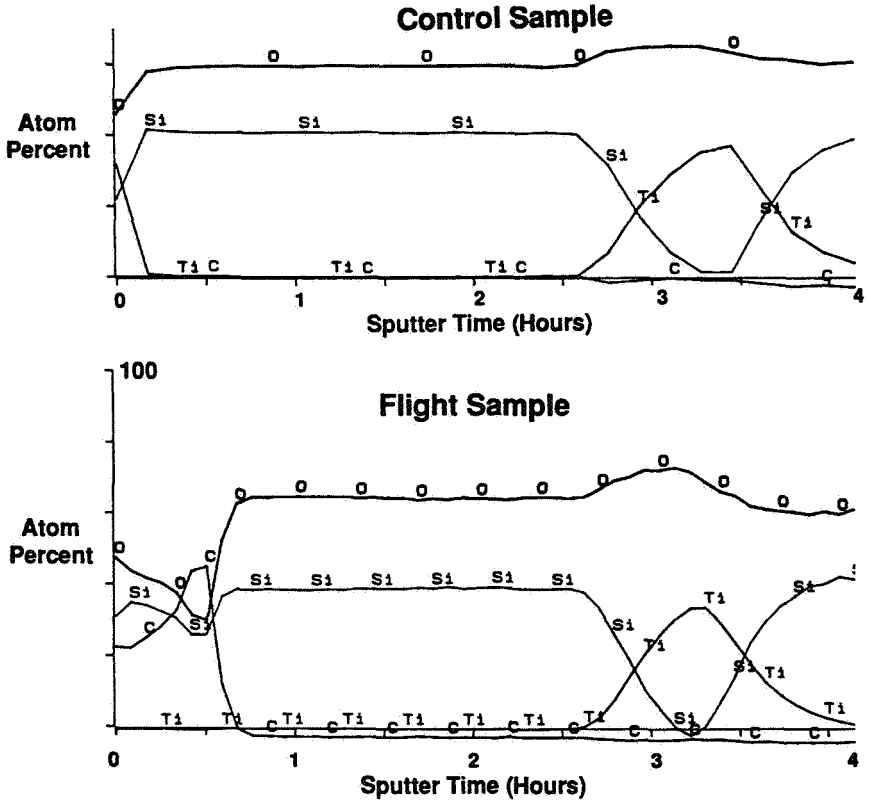

Figure 12. XPS profiles antireflection coated fused silica

LDEF Witness Samples Atomic Percents, Ratios and Peak Positions Carbon, Oxygen and Silicon						
		O		Si		
	C	Position (eV)	Area (%)	Position (eV)	Area (%)	O/Si Ratio
Fused Silica Uncoated Control Sample	25.5	532.2	45.2	103.0	24.2	1.87
Fused Silica Uncoated Flight Sample	32.2	532.7	41.7	103.2	25.0	1.67
Ultra Low Expansion Uncoated Control	25.0	532.1	45.8	102.9	24.1	1.90
Ultra Low Expansion Uncoated Flight	53.0	532.2	24.1	102.4	22.6	1.07
High Reflectance ULE™ Control Sample	62.5	531.7	30.6	na	na	na
High Reflectance ULE™ Flight Sample	31.7	532.7	43.1	103.1	23.5	1.83
Anti Reflectance Fused Silica Control	28.9	532.7	45.6	103.1	23.5	1.94
Anti Reflectance Fused Silica Flight Sample	30.8	532.2	41.6	102.2	26.1	1.59
Mounting Gasket Silicone Rubber	47.0	532.3	23.4	102.3	27.4	0.85

Silicone 101.5 - 102 eV Binding Energy

SiO2 103 - 103.5 eV Binding Energy

Table 2. XPS analysis data

N93-29695

501737

81

LDEF SPACE OPTICS HANDBOOK

Robert J. Champetier
Science Applications International Corporation
Santa Monica, CA 90401

Dale R. Atkinson
POD Associates, Inc.
Albuquerque, NM 87106

William T. Kemp
Phillips Laboratory, PL/VTET
Albuquerque, NM 87117

SUMMARY

There is a need to present design guidelines derived from the LDEF space optics experiments to hardware designers. In response to this need a small study program has just been started by SAIC and POD Associates for the Phillips Laboratory. The objective is to prepare a top-level review of available results on the behavior of certain optical components in the LDEF space experiments. The optics interest centers on optical surfaces and coatings, and fabrication processes for laser windows and mirrors. The program has two main parts: the first phase, to be completed by the end of 1992, consists of identifying and acquiring data from the appropriate investigators. The second phase, ending in December 1993, comprises report preparation as well as selected, prioritized, additional characterization of certain samples, coordinated with the principal investigators and the Phillips Laboratory. This program is getting under way at the time of the Symposium and does not warrant more than the present summary at this time.

N93-29696

501739
B1

RULED AND HOLOGRAPHIC EXPERIMENT
(A0 138-5)

Francis BONNEMASON
Instruments S.A/Jobin Yvon - Longjumeau FRANCE
Fax n°33.1.69.09.07.21

ABSTRACT

The A0 138-5 experiment has been designed, via the FRECOPA (FRench COoperative PAyload) experiment with the aim to study the optical behavior of different diffraction gratings submitted to space vacuum long exposure and solar irradiation.

Samples were ruled and holographic gratings, masters or replica, and some additional control mirrors with various coatings.

The experiment was located on the B3, trailing edge of the LDEF and has been protected against Atomic Oxygen flux. The experienced thermal cycling has been evaluated from -23°C to 66°C during the flight, 34,000 orbits.

The samples (two batches of four pieces) were located on a dedicated plate, by a pair of equivalent gratings or mirrors; optical faces were located on the external side. The plate was inside a canister, which had been opened in space for ten months. When the satellite returned to Kennedy Space Center, the remaining vacuum in the canister was still correct.

The analysis has been focused on the triple point characterization including light efficiency, wavefront flatness quality and stray light level.

Tests were conducted on control mirrors and gratings (ruled and holographic master or replica) loaded but not exposed to cosmic dust or direct solar irradiations. They did not show any significant variations.

Solar exposure had damaged the coating (aluminum and platinum) reflectivity in the Ultra-Violet region; the degradation is higher with the gratings, in terms of efficiency. However, wavefront flatness quality and stray light level tests revealed no additional changes.

N93-29697

HOLOGRAPHIC DATA STORAGE CRYSTALS FOR THE LDEF*

501740
B5-10

W. Russell Callen
School of Electrical Engineering
Georgia Institute of Technology
Atlanta, Georgia 30332-0250
Phone: 404/894-2912, FAX: 404/853-9171

Thomas K. Gaylord
School of Electrical Engineering
Georgia Institute of Technology
Atlanta, Georgia 30332-0250
Phone: 404/894-2931, FAX: 404/853-9171

SUMMARY

Crystals of lithium niobate were passively exposed to the space environment of LDEF. Three of the four crystals contained volume holograms. Although the crystals suffered the surface damage characteristic of that suffered by other components on the Georgia Tech tray, the crystals remained suitable for the formation of volume holograms.

INTRODUCTION

Lithium niobate is a significant electro-optic material, with potential applications in ultra high capacity data storage and processing systems. Lithium niobate is the material of choice for many integrated optical devices and holographic mass memory systems. The objective of the experiment is to test the spaceworthiness of electro-optic crystals for use in ultrahigh capacity space data storage and retrieval systems.

VOLUME HOLOGRAPHIC STORAGE

Volume holographic storage offers a unique capability for ultrahigh capacity data storage and processing systems. In addition to the potential storage of up to 10" bits in a single crystal, holographic storage is insensitive to point damage of the medium. Holographic storage is particularly suitable for the processing of data in page-oriented form and can be used either in a read-write-erase mode or in an archival

*This work was performed under NASA Contract No. NAS1-15370.

storage mode. By using electro-optic beam deflectors, mechanical motion can be eliminated. The principal advantages of volume holographic storage are listed in Table 1.

To record the volume holograms in the lithium niobate, two plane waves, produced by the same laser, are interfered within the crystal, as shown in Fig. 1. The interference maxima and minima produce a corresponding refractive index variation in the photorefractive crystal, which produces the volume hologram. By passing one of these beams, the "object" beam through a data page mask prior to incidence on the crystal, digital data in page oriented format may be stored as a volume hologram. The data page may be displayed by subsequent illumination with the reference beam alone. This writing and reading process is shown in Fig. 2. By rotation of the crystal with respect to the laser beam, multiple pages of data can be stored. Figure 3 illustrates the data storage in a page-oriented optical phase holographic memory.

OPTICAL SYSTEM

Much of our effort centered on developing a precise system for writing and evaluating the holograms. Systems were developed for hologram formation with both helium-neon (λ = 632.8 nm) and argon (λ = 514.5 nm) lasers. The apparatus for the holography study with helium-neon lasers is shown in Fig. 4. This apparatus achieves page rotation by rotating the reference beam angle with respect to a stationary object beam and stationary recording crystals. The reference beam angle is controlled by a stepper motor that drives a rotating mirror. The angular rotation resulting from a single step is 19.6 mirroradians. [1]

LDEF EXPERIMENT

For the LDEF experiment, holograms were recorded in 10 mm x 10 mm x 2 mm samples of iron-doped lithium niobate, with the optic axis lying in the plane of the surface. The crystals were specified to be iron doped to .005 mole percent iron in the melt. The samples were flown as part of the overall Georgia Tech experiment, LDEF experiment S0050, "Investigation of the Effects of Long-Duration Exposure on Active Optical Components," with principal investigator M.D. Blue. Our experiment consisted of the materials shown in Table 2.

The diffraction efficiency (diffracted power divided by incident power) as a function of read beam angle for a typical plane wave hologram is shown in Fig. 5. This diffraction efficiency could be used to monitor the degradation of the hologram with time.

RESULTS

To date, no holograms have been observed remaining in any of the samples because of the long exposure time involved. Although the crystals were recovered intact, they

suffered the same surface damage characteristic of that of other optical components on the Georgia Tech tray. A very significant result is that the crystals still retained their photosensitivity. A recently recorded hologram from one of the LDEF crystals is shown in Fig. 6.

ACKNOWLEDGMENTS

The authors express their appreciation to NASA for sponsoring this research, and to Mr. Mark Lehi Jones for the photographs shown in Fig. 6.

REFERENCE

1. J.E. Weaver, "Angular Addressing Properties of Volume Fourier Transform Holograms in Iron-doped Lithium Niobate," Ph.D. Thesis, Georgia Institute of Technology, 1979.

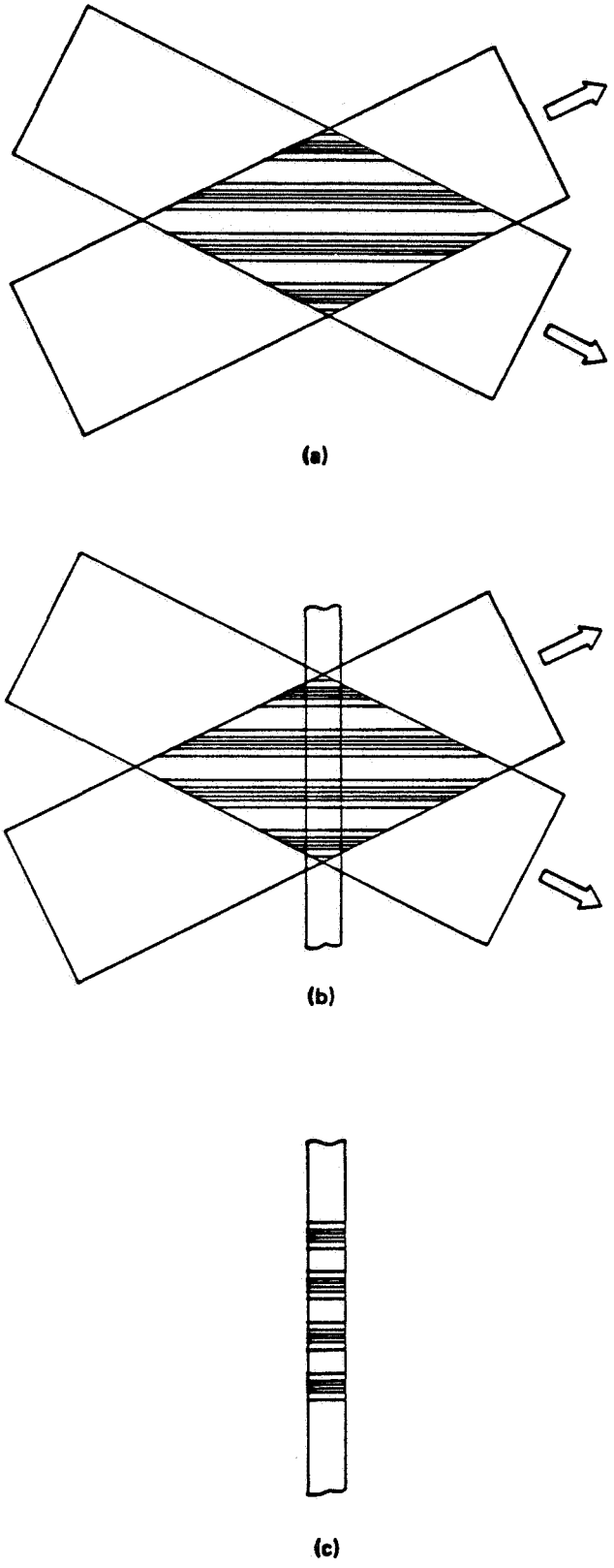

Figure 1. Volume hologram recording (a) interfering beams (b) crystal recording (c) recorded holograms.

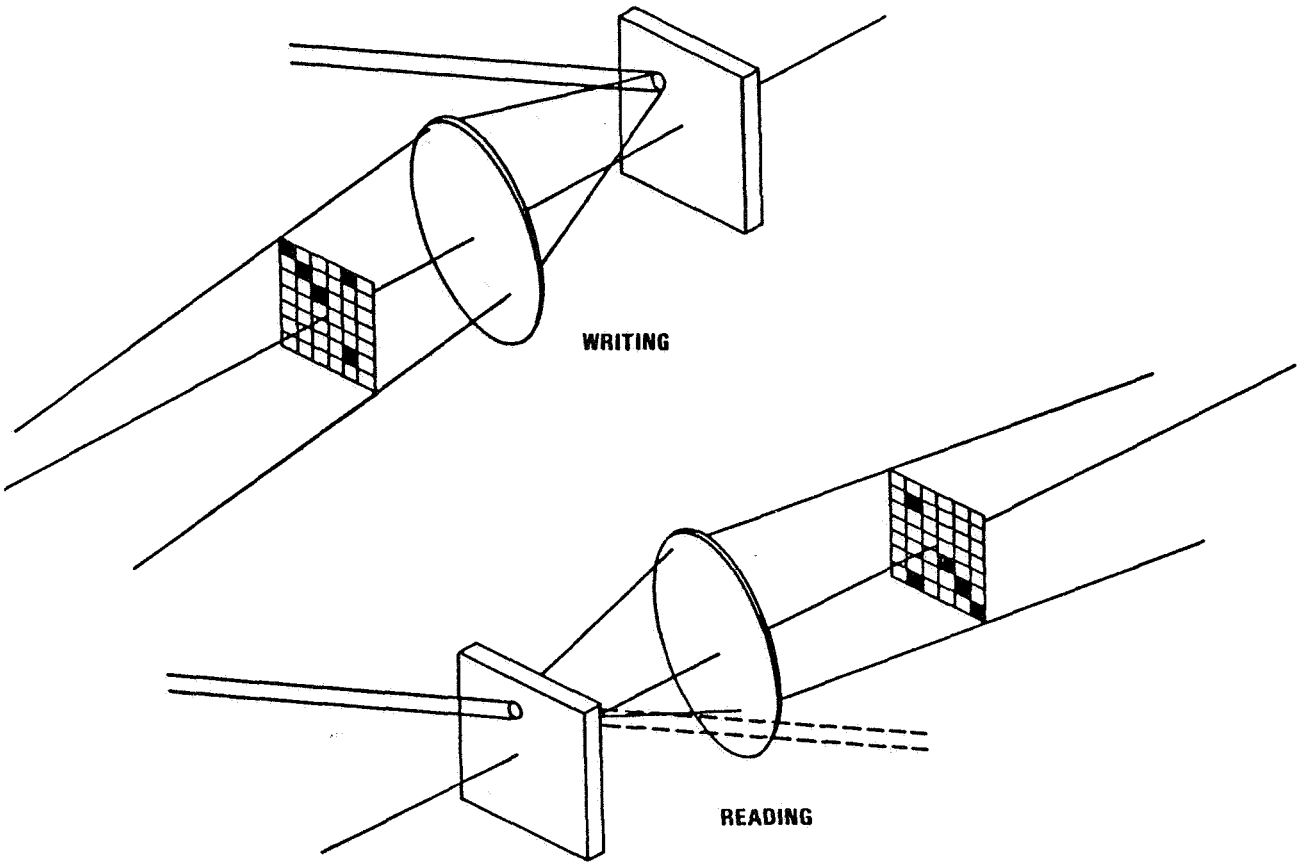

Figure 2. Writing and reading a data page hologram.

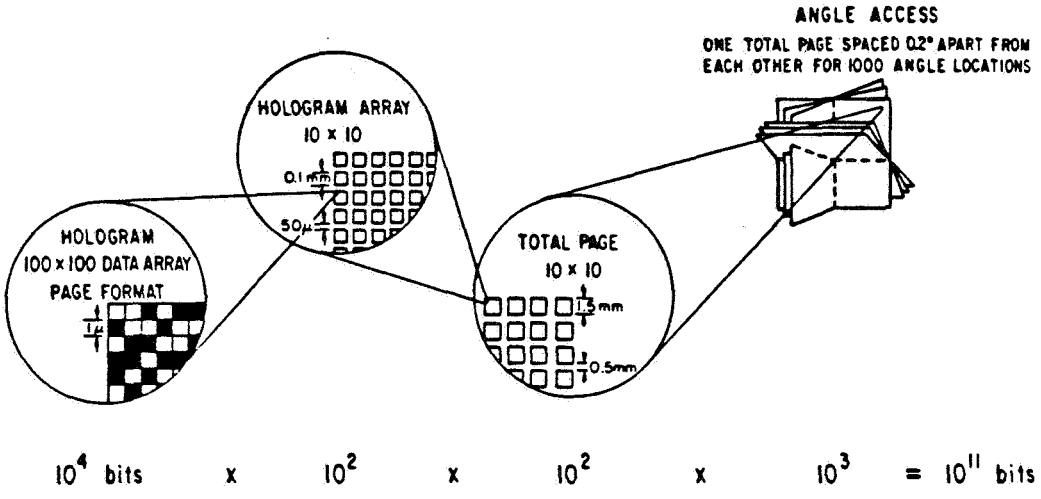

Figure 3. Data storage in a page-oriented optical holographic memory.

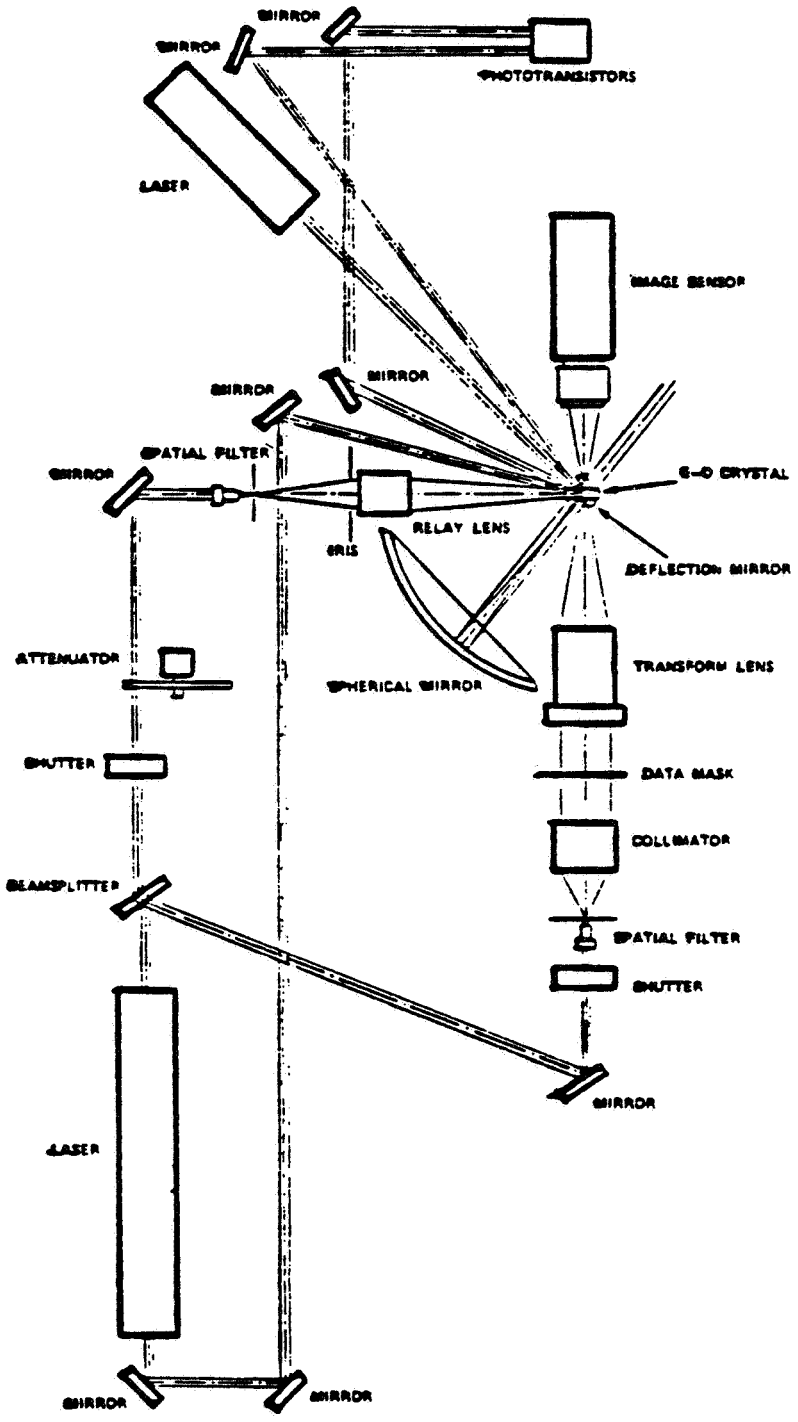

Optical System Diagram

Figure 4. Hologram recording and reading apparatus (helium-neon laser) (reference 1).

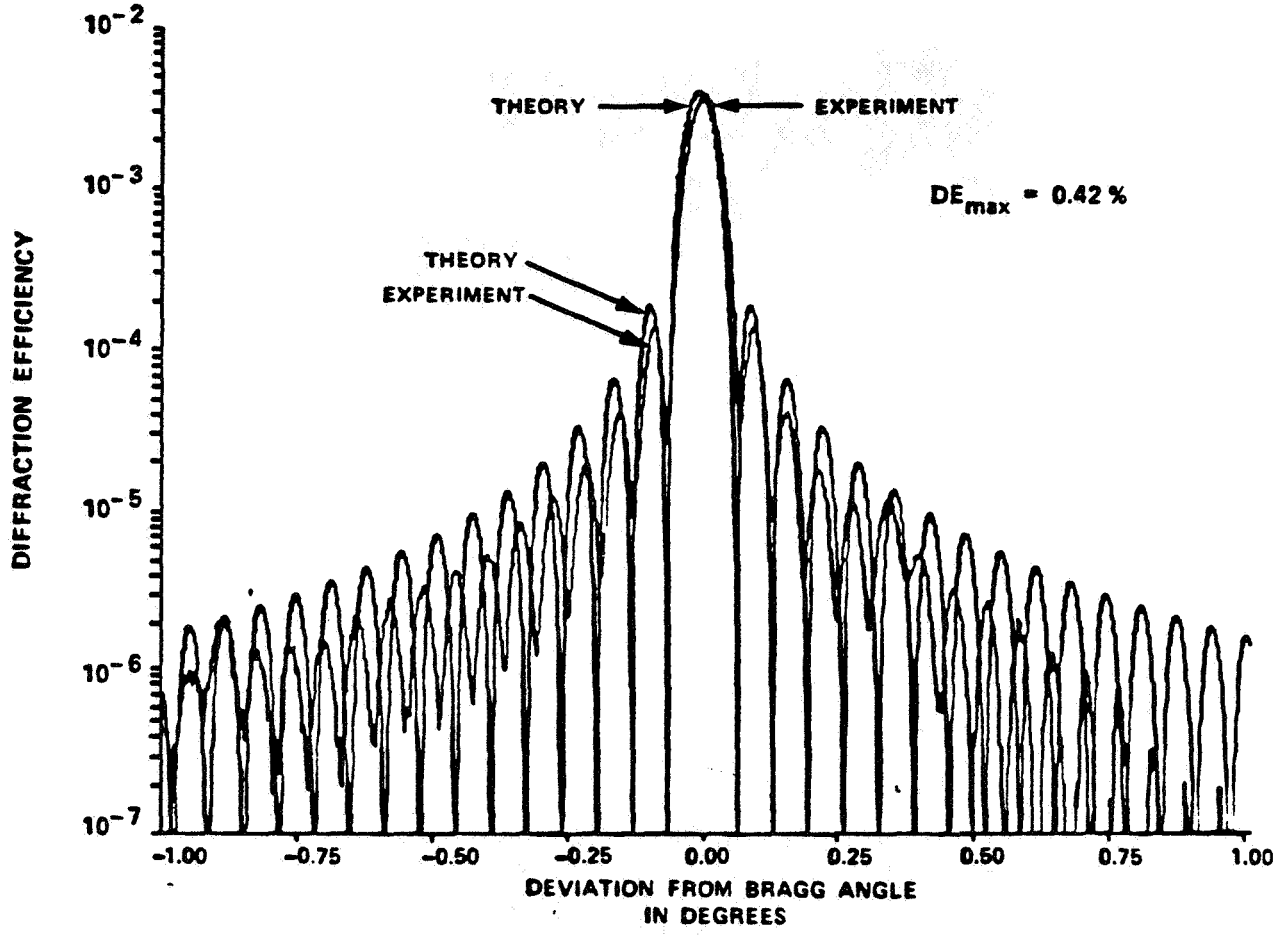

Figure 5. Diffraction efficiency versus angle (reference 1).

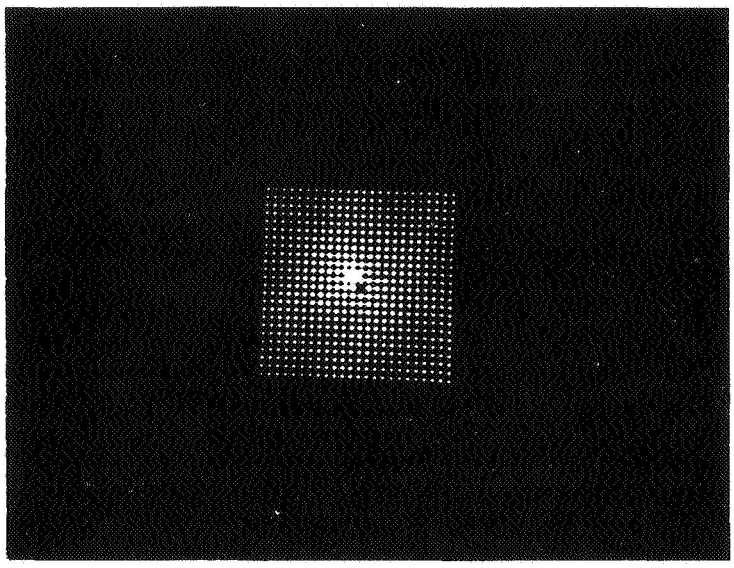

(a)

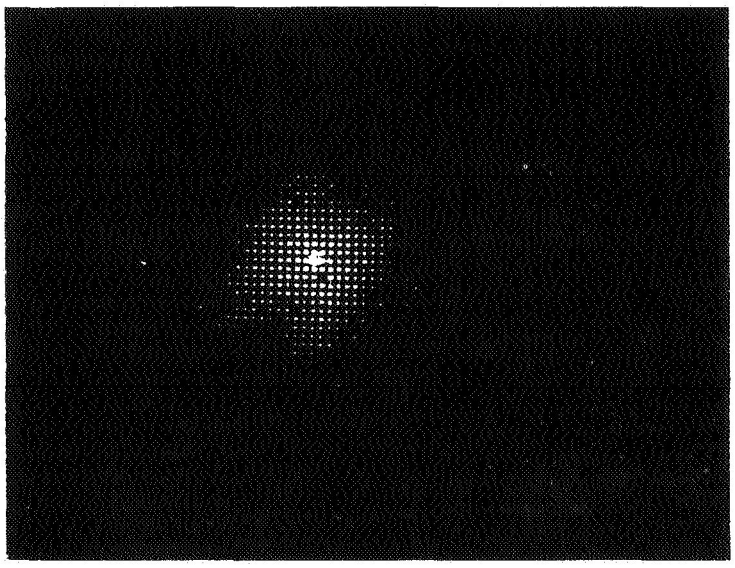

(b)

Figure 6. Hologram produced with LDEF crystal (a) object beam data page (b) hologram of object beam.

ORIGINAL PAGE
BLACK AND WHITE PHOTOGRAPH

Table 1. Characteristics of volume holographic storage.

VOLUME HOLOGRAPHIC STORAGE

HIGH INFORMATION CAPACITY

REDUNDANT

READ-WRITE-ERASE OR ARCHIVAL

NON MECHANICAL (ELECTRONIC & OPTICAL)

INHERENT TWO-DIMENSIONAL STORAGE

PROCESSING CAPABILITY

Table 2. LDEF samples.

Five Samples Flown

1. Lithium Niobate, heat treated for maximum sensitivity, blank
2. Lithium Niobate, plane wave hologram, helium-neon laser
3. Lithium Niobate, plane wave hologram, argon laser
4. Lithium Niobate, spoke pattern hologram, argon laser
5. Glass control sample

Two Control Crystals

1. Lithium Niobate, plane wave hologram, helium neon laser
2. Lithium Niobate, plane wave hologram, argon laser

N93-29698
501742
f-12

CHARACTERIZATION OF A SPACE ORBITED INCOHERENT FIBER OPTIC BUNDLE

Stephen A. DeWalt, Edward W. Taylor

AFSC Phillips Laboratory
Directorate of Space and Missiles Technology
Kirtland AFB, NM 87117-6008
Telephone: (505) 846-4741; FAX: (505) 846-2290

ABSTRACT

The purpose of this paper is to report the results of a study performed to determine the effects of adverse space environments on a bundle of over 1800 optical fibers orbited for 69 months. Experimental results are presented on an incoherent fiber optic bundle oriented in low Earth orbit aboard the Long Duration Exposure Facility (LDEF) satellite as part of the Space Environment Effects Experiment (M0006). Measurements were performed to determine if space induced radiation effects changed the fiber bundle characteristics. Data demonstrating the success of light transmitting fibers to withstand the adverse space environment are presented.

INTRODUCTION

The M0006 experiment was implemented and managed by the Air Force Technical Applications Center (AFTAC) located at Patrick AFB, FL. One subset of the experiment consisted of an incoherent fiber optic bundle some 62 cm in length. The bundle contained approximately 1800 individual optical fibers. The M0006 and bundle location were 40° distant from the trailing edge of the LDEF. The M0006 experiment was contained within one of five experiment exposure control canisters (EECC) and remained open roughly between the period of April 21, 1984 through March 15, 1985, exposing the fiber optic bundle and other components to the space environment.

At the request of AFTAC, the Phillips Laboratory performed an investigation to determine the effects of the space environment on the fiber optic bundle in conjunction with an ongoing analysis of LDEF Exp # M0004 (Ref 1). In the next sections, the manner by which the measurements were performed and the resulting data are discussed. These measurements included investigation of the attenuation of optical signal transmission, numerical aperture and fiber spectral responses over a wide wavelength range. The measurements were performed in a sequenced manner or hierarchy in order to determine if the optical fibers experienced any space radiation induced attenuation. Thus as shown in Table 1, attenuation measurements were first performed at long wavelengths to determine the fiber attenuation without activating the photobleaching of any space radiation induced attenuation.

Thermal Parameters

Orbital temperature data for the LDEF satellite was recorded by the Thermal Measurement System (THERM) experiment P0003 (Ref 2). Post orbit thermal modeling of many positions or nodes on LDEF were matched to THERM data. Thermal modeling of representative external and internal nodes aboard the LDEF structure determined that the M0006 EECC and optical fiber bundle were exposed to wide external transient orbital temperatures. These temperatures ranged from 42.6 °C at +52° ß to -32.1°C at -52° ß while the EECC was opened. Here, ß is the angle between the plane of the orbit of the LDEF satellite and the sun illumination vector. Temperatures of 34.6° C at +52° ß and 18.1° C at -52° ß were experienced while the EECC was closed.

The M0006 characterization studies were performed over a room temperature range (T_R) of 21°C ≤ T_R ≤ 25° C.

Measurement Techniques

Shown in Figure 1 is the substitution measurement method used to determine optical signal attenuation. The substitution method consists of injecting a known reference power level into the incoherent fiber optic bundle (IFOB) of unknown attenuation and maximizing the throughput to the detector (Ref 3). The alignment position (see Figure 1) is then keyed to allow removal of the orbited IFOB during other tests, and to allow the measurements to be repeated for accuracy. By measuring the optical power out of the IFOB and comparing to the known reference power level through the Sample fiber optic bundle (see Figure 1a) an attenuation value is obtained for the orbited IFOB. The attenuation for the IFOB can then be correlated to its total length to yield an attenuation value per unit length.

Attenuation and Spectral Measurements

The attenuation (a) measurements were performed as shown in Table 1 and carefully avoided inducing annealing of any orbital induced radiation color centers (Ref 4). The experiment configuration is shown in Figure 1. The attenuation measurements were first performed at _ = 1.30 μm (a_1). This first measurement was performed to establish a baseline to which succeeding attenuation measurements could be compared. By determining the IFOB attenuation at a wavelength far removed from known photobleaching wavelengths, a measure of non-space radiation induced attenuation can be made. The measurement is next repeated at a significantly lower wavelength (_ = 0.86 μm). This lower wavelength is nearer to an annealing wavelength and the attenuation is again noted (a_2) (Refs 5, 6). Finally the measurement was repeated at _ = 1.30 μm, and all three attenuation values were then compared as shown in Table 1. The above procedure should therefore result in a *decreased* a for the repeated _= 1.30 μm measurement if any laboratory induced photobleaching of space induced radiation damage occurred at 0.86 μm.

As can be seen in Table 1, a *decrease* of $a_3 - a_1$ = -0.20 dB/m was measured at 1.30 μm, following the 0.86 μm measurement, which could indicate that space radiation induced attenuation occurred. However, this measured a is not thought to be significant since the accuracy of the substitution measurement method as shown in Figure 1 was determined to be ± 8.1 % or ± 0.42 dB/m (limitations of the detector system and reflections induced by the interface of the sample fiber optic bundle and IFOB) at _ = 1.30 μm.

Next, a measurement of increased optical power (≤ 5 μW) at the lower 0.86 μm wavelength was performed and again was followed by a measurement at 1.30 μm of an optical power of less than 1 μW. This procedure should result in a *decreased* a for both repeated wavelengths if any laboratory photobleaching of space induced attenuation occurred. In this instance a *decrease* of $a_4 - a_2$ = -0.35 dB/m was measured at 0.86 μm and an *increase* was seen in a_5 at 1.30 μm. Thus, it was clear that no systematic photobleaching was occurring since one would expect the attenuation a_5 to mimic the a_3 measurement or *decrease* from the a_3 value. Again, the measured attenuation difference ($a_4 - a_2$) at 0.86 μm is not thought to be significant since the accuracy of the substitution method was determined to be ± 0.46 dB/m at 0.86 μm or ± 8.1 % of the a_2 measurement. Furthermore, the radiation dose received by the space orbited bundle was 210.2 rads (LiF) as measured by thermoluminescent dosimeters (TLDs) on board the experiment which is a very low dose and was not expected to induce radiation damage in the IFOB. These TLDs were shielded by aluminum which provided an effective mass thickness of 0.43 g/cm^2 while the EECC was opened and 10 g/cm^2 while EECC was closed (ref. 7,8).

Following measurement sequence #5 in Table 1, further attempts to determine space radiation induced attenuation were accomplished by measuring the IFOB's spectral irradiance response over a wide wavelength range (i.e. 0.40 μm ≤ _ ≤ 0.70 μm). This intense and low wavelength scan would be expected to photobleach any shallow color centers sites, thus resulting in *lower* a values at _ = 1.30 μm and _ = 0.86 μm then were previously measured.

The scan was performed using a 100 W mercury arc lamp with a 0.5 % current ripple peak to peak (0.17 % RMS) and a monochromator-data acquisition system with a system reliability of ± 3 percent in spectral irradiance (refer to Figure 2). A spectral irradiance reference point was established at 0.65 μm of 3.43 μW cm^{-2} nm^{-1} ± 0.1 μW cm^{-2} nm^{-1} to assure continuity for other spectrophotometry scans.

Partial scans were performed ranging from 0.40 μm through 0.70 μm, and from 0.70 μm through 1.10 μm. In between these two spectrophotometer scans and after the second spectrophotometer scan of 0.70 μm through 1.10 μm, a comparison of results to detect photobleaching was again performed on the fiber bundles at 1.30 μm and 0.86 μm at an optical power of less than 1 μW.

As may be observed in Table 1, attenuation measurements were performed following the first spectral scan (measurement sequences #6 and #7). It is apparent in the measurement sequences #6 and #7 that both attenuation measurements $a_6 - a_1 = -0.27$ dB/m at 1.30 μm and $a_7 - a_2 = -0.25$ dB/m at 0.86 μm were *lower.* However, one may attribute both decreases in attenuation to their respective inherent measurement uncertainties of ± 0.42 dB/m at _ = 1.30 μm and ± 0.46 dB/m at _ = 0.86 μm, and hence are not perceived to be significant. Again, the attenuation differences measured were not significant for the orbited fibers, indicating that no permanent degradation resulted due to the space exposure. Nor did the spectral scans of the control and orbited fibers show any significant deviation in absorption bands or transmission differences throughout the spectral range of 0.60 μm through 1.00 μm as may be viewed in Figure 3. One can again conclude photobleaching was not a factor in any of our measurements and is readily apparent in the final attenuation measurement sequences #8 and #9 of Table 1 (i.e. $a_8 - a_1 = -0.17$ dB/m at 1.30 μm and $a_9 - a_2 = -0.28$ dB/m at 0.86 μm) which are well within the measurement accuracies.

Numerical Aperture

To further correlate the orbited and control IFOBs, a measurement of numerical aperture (NA) was performed under far field conditions.

The far field measurement was made by using a Fourier transforming and relay lens system (Ref 9). The acceptance angles were determined to be 62.8° ± 2.5° for the control bundle resulting in a numerical aperture of 0.52 ± 0.02. The orbited bundle measurements resulted in an acceptance angle of 64.7° ± 2.5° and a numerical aperture of 0.54 ± 0.02.

Since previous records of the composition of the IFOB were incomplete, these measurements and comparisons were crucial. Through a collaborative effort with the manufacturer, several possible optical glass fiber types were identified. The exact optical glass fiber type was identified by comparing the experimentally determined far field numerical aperture to a list of possible types supplied by the manufacture.

Digitized Mapping of End Surfaces of the IFOBs

The cabled optical fiber bundle was protected during its orbital space exposure except for the very ends of the 61.7 cm fiber lengths. These flattened ends appeared to have been cleaved and polished before they were placed in the M0006 experimental tray. While no analysis could provide information on the historical preparation of the optical fiber end conditions prior to launch, a qualitative examination of the condition of the optical fiber ends was accomplished. A comparison of both the control and orbited fiber bundle ends revealed only slight variations. The control bundle showed, on one end, that roughly 20% of the individual fibers had been chipped. This damage may have been caused during the storage of the control bundle. In contrast, the space orbited bundle showed very pristine polished optical fibers, devoid of any visible damage.

Digitized mapping of both end surfaces of each fiber bundle was accomplished by using the infrared microscope-camera arrangement of Figure 4. An individual fiber count was possible by radially sectioning the mapped bundle surface into sixteen 22.5° sections (refer to Figure 5). Some 1,862 ± 16 fiber waveguides were measured within the control bundle and 1,838 ± 16 fiber waveguides were measured within the space orbited bundle. It is estimated that an error of 1 fiber waveguide per 22.5° section was inherent in the measurement, and hence a total error of ± 16 fiber waveguides was measured for both control and space orbited bundles.

The individual optical fibers were measured to have a core diameter of 60 μm ± 5 μm. The cladding thickness surrounding the core was measured to be 75 μm ± 5 μm.

Mapping was necessary to positively identify that the control bundle provided was of the same manufactured lot as that of the orbited bundle. This positive identification also allowed traceability of the

control sample to the material composition of the optical fibers. Using this identification process, correlations of the control and orbited fiber samples could be made with similar samples of fiber provided by the manufacturer of the fiber bundles.

Final Spectrophotometry Measurements

During the hierarchy of attenuation measurements a total of two scans were performed on the control and space orbited bundles (refer to Table 1). These scans revealed no significant deviations of spectral irradiance levels over the range of 0.60 μm to 1.00 μm in either the control or the flight bundle scans. Following the digitized mapping and far field measurements a final spectrophotometry scan was performed. This final scan repeated the previous results and again supported our conclusion that the space orbited fiber optic bundle did not experience any permanent radiation induced attenuation over the wavelength range of 0.60 μm to 1.00 μm (refer to Table 1 and Figure 6).

Attenuation Measurements by the Cutback Technique

While the attenuation measurements performed in Table 1 were made by substitution techniques which are non-destructive and could be repeated many times, this is not the case involved when using the cutback technique for measuring attenuation. Generally, the cutback technique is associated with single fibers, but in the following measurements the technique was applied to a fiber bundle. A final cutback attenuation measurement was executed on both bundles after all previous measurements had been completed. This test was done in order to further verify the control and orbited bundle attenuations previously measured in the substitution method. By cutting back the specimens some three times to result in varying fiber lengths, different signal attenuations are measured through smaller increments of fiber.

However, as expected, the attenuation measurements for the cutback method were lower than those obtained by the substitution method. The reason for this is that only random mating of the sample and orbited fibers (see Figure 1b) within the bundles is accomplished with the latter technique. The sample and orbited fibers of approximately 1,800 fibers in one bundle with 1,838 ± 16 fibers in the second bundle is very lossy. In contrast, the cutback technique as applied here involves the complete illumination and constant injection of light at one end of the bundle while at the opposite end the measurements and cuts on the bundle are administered. A large difference (i.e. at _ = 0.86 μm substitution attenuation averaged minus cutback attenuation resulted in 2.6 dB/m) may be attributed to both the random coupling and the control and space orbited bundle's special fiber end preparation. The control and orbited fibers were equipped with an off-axis or canted polished surface. This canted surface was polished off on both ends of each bundle after the substitution attenuation measurements and before the cutback attenuation measurements were performed. The fiber ends were polished for ease of completion of the cutback attenuation measurements.

Due to the known accuracy of the cutback method (accuracies can be made to less than ± 0.01 dB) for determining intrinsic fiber transmission losses, the cutback attenuation data was accepted as the most accurate (Ref 10,11). For the control bundle at the wavelength 0.86 μm the attenuation was measured to be a_C (Control Bundle) = 2.77 dB/m ± 0.14 dB/m, and the orbited bundle was measured to be a_O = 2.85 dB/m ± 0.14 dB/m. Table 2 compares the results of the space orbited and control fiber bundle ameasurements using these two methods and lists other observed and measured parameters. Thus, the intrinsic attenuation between the control and space orbited fiber bundles was $a_O - a_C$ = 0.08 dB, or well within the measurement accuracy of ± 0.14 dB/m.

CONCLUSION

This study successfully identified and characterized a fiber optic bundle composed of 1,838 ± 16 individual fibers orbited aboard the LDEF satellite. Quantification of the fiber bundle parameters included numerical aperture, intrinsic attenuation, and fiber count. A determination of the fiber bundle's physical condition was also accomplished. A strict hierarchy of measurement procedures was invoked to determine the existence of any space radiation induced attenuation. Due to the extremely short length of the optical waveguides involved, measurement accuracies were limited to a = ± 0.14 dB/m. No photobleaching of suspected permanent space induced radiation damage was observed for 0.60 μm ≤ _ ≤ 1.0 μm and _ = 1.30 μm. The analysis of this optical fiber bundle is unique since the data benchmarks the only known incoherent optical fiber bundle orbited for 69 months in low Earth orbit.

REFERENCES

[1] Taylor E. W., et. al: Preliminary Analyses of WL Experiment #701, Space Environment Effects On Operating Fiber Optic Systems, *LDEF - 69 Months in Space - First Post Retrieval Symposium*, Report No. NASA CP-3134.

[2] Berrios W. M.; Sampair T. R.: Long Duration Exposure Facility Post-Flight Thermal Analysis; Calculated Flight Temperature Data Package - Preliminary, Vol. 2, pp. E-21, *NASA/LaRC MS 434*, Hampton VA 23665-5225.

[3] Fiber Optic Test Procedure - 171 (FOTP-171), "Attenuation by Substitution Measurement for Short Length Multimode Graded Index and Single Mode Optical Fiber Cable Assembles," EIA/TIA - 455-53A-90, *Electronic Industries Association* (EIA), 2001 Pennsylvania Avenue, Washington D.C. 20006, (202) 457-4900.

[4] Robert, N.; Scwartz, G.; Blair, R.; Tangunan, G. L.: Radiation Damage of Germanium-Doped Silica Glasses: Spectral Simplification by Photo and Thermal Bleaching, Spectral Identification and Microwave Characteristics, *Jour. App. Phys*, Vol. 59, No 9, 15 April 1986, pp. 30-36.

[5] Schulman, J. H.; Compton, W. D.: Experimental Methods in Color Center Research, *Color Centers in Solids*, MacMillan Company, 1962, pp.32-49.

[6] Allard, F. C.: Optical Fibers, Fiber Optic Test Methods, *Fiber Optics Handbook for Engineers and Scientists*, McGraw-Hill, 1990, pp. 1.25-1.32, 4.42-4.52.

[7] Chang, J.; Kantorcik, T.; Stauber, M.: Results of M0006 Dosimeter Readings, Presented to LDEF Ionizing Radiation SIG Meeting, NASA/MSFC, Orlando FL, 25 Jan 91.

[8] Chang, J.; Giongano, D.; Kantorcik, T.; Stauber, M.; Snead, L.: Thermoluminescent Dosimetry for LDEF Experiment M0006, (To be published in LDEF Proceedings.)

[9] Fiber Optic Test Procedure - 47 (FOTP-47), "Output Farfield Radiation Pattern Measurements", EIA/TIA - 455 - 47A, *Electronic Industries Association (EIA)*, 2001 Pennsylvania Avenue, Washington D.C. 20006, (202) 457-4900.

[10] Fiber Optic Test Procedure - 78 (FOTP-78), "Spectral Attenuation Cutback Measurement for Optical Fibers", EIA/TIA 455-78A-90, *Electronic Industries Association (EIA)*, 2001 Pennsylvania Avenue, Washington D.C. 20006, (202) 457-4900.

[11] Allard, F. C.: Fiber Optic Test Methods, pp. 4.8-4.9, 4.12, 4.14.

LIST OF FIGURES AND TABLES

Table 1
Hierarchy of Attenuation Measurements

Measurement Sequence	Measurement Performed	Wavelength (μm)	Optical Power (μW)	Control Bundle (dB/m)	Space Orbited Bundle (dB/m)
1	Attenuation	1.3	< 1	α_1 = 5.14	4.92
2	"	0.86	< 1	α_2 = 5.97	5.63
3	"	1.3	< 1	α_3 = 5.20	4.72
4	"	0.86	≤ 5	α_4 = 5.42	5.28
5	"	1.3	< 1	α_5 = 5.35	4.96
Spectrophotmetry Scan I		0.4 ≤ λ ≤ 0.7	----------	----------	----------
(Spectral Irradiance (SI) W/cm^{-2}- nm^{-1})			----------	----------	----------
3.3e-6 ≤ SI ≤ 5.4e-5			----------	----------	----------
6	Attenuation	1.3	< 1	α_6 = 5.27	4.65
7	"	0.86	< 1	α_7 = 5.80	5.38
Spectrophotmetry Scan I I		0.7 ≤ λ ≤ 1.1	----------	----------	----------
4.0e-6 ≤ SI ≤ 1.6e-5			----------	----------	----------
8	Attenuation	1.3	< 1	α_8 = 5.41	4.75
9	"	0.86	< 1	α_9 = 5.66	5.35

Table 1 - The measurements are sequentially listed as they were performed. The Substitution measurement technique was used on all attenuation measurements. It is evident from the data that no photobleaching was observed in the Space Orbited fibers. The variance in attenuation at 1.30 μm for both Control and Space Orbited Bundles is ± 0.01 dB/m and ± 0.02 dB/m, respectively. At 0.86 μm the variance is ± 0.05 dB/m for the Control Bundle and ± 0.02 dB/m for the Space Orbited Bundle.

Table 2
Fiber Optic Bundle Parameters

CABLE	CONTROL BUNDLE	SPACE ORBITED BUNDLE
Material	PVC	PVC
Color	Black	Black
Length	63.5 cm	61.7 cm
Diameter	3.2 mm	3.2 mm
Fiber Quantity	1862 ± 16	1838 ± 16
Condition - March 1990 [1]	Excellent	Excellent
FIBERS		
Core Material	Flint Glass (Predominately Silica and Lead)	
Clad Material	Alkaline Resistant Glass (Soda, Lime and Silicate)	
Core Diameter	60 um ± 5 um	
Clad Diameter	75 um ± 5 um	
Operational Wavelength [2]	Visible and Infrared	
ATTENTION VALUES		
Cutback Method	2.77 dB/m ± 0.14 dB/m	2.85 dB/m ± 0.14 dB/m
Manufacturer	1.20 dB/m ± 0.10 dB/m	1.20 dB/m ± 0.10 dB/m

FOOTNOTES
1) Bundles are in four pieces as a result of Cutback Method measurements.
2) Tested at 400 nm through 1100 nm and, 1300 nm.

Table 2 - Known and observed incoherent fiber optic bundle characterizations.

Figure 1a

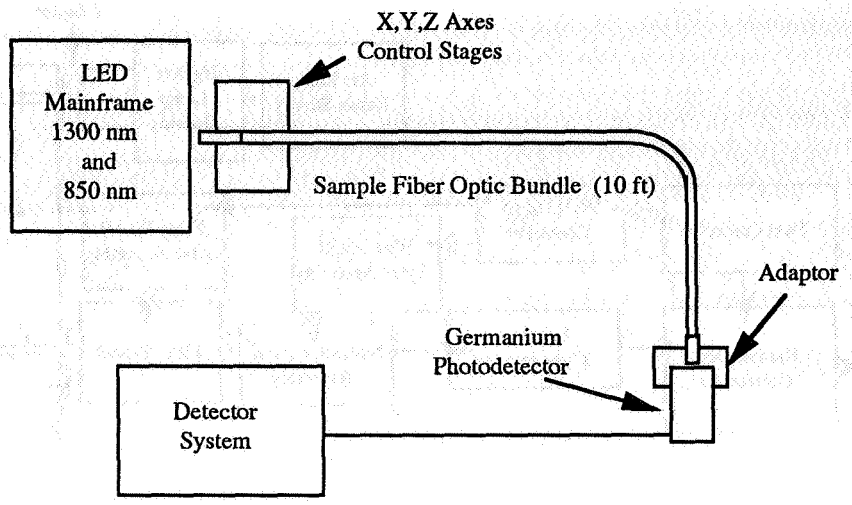

Figure 1b

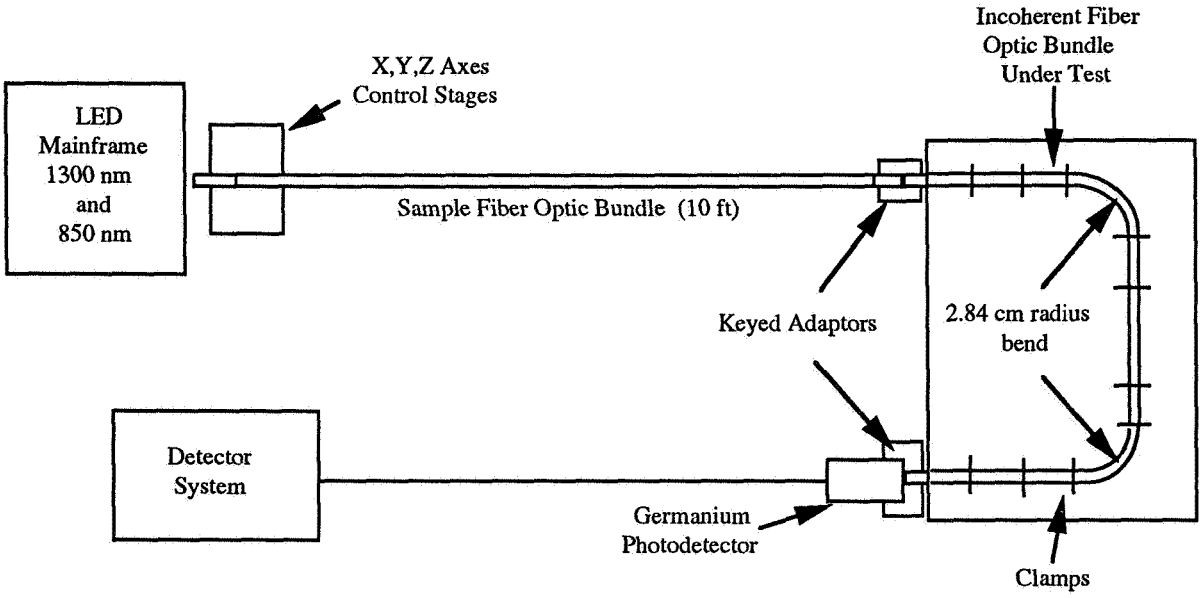

Figure 1 - Measurement of attenuation by the substitution method is shown above. In Figure 1a, a reference power measurement is established by uniformly injecting light into the Sample fiber optic bundle and detecting the power at the Photodetector. In Figure 1b a second attenuation measure is performed and in theory, the added attenuation is attributed to the Incoherent Fiber Optic Bundle Under Test. The Keyed Adaptors in Figure 1b are to insure consistency of measurement technique.

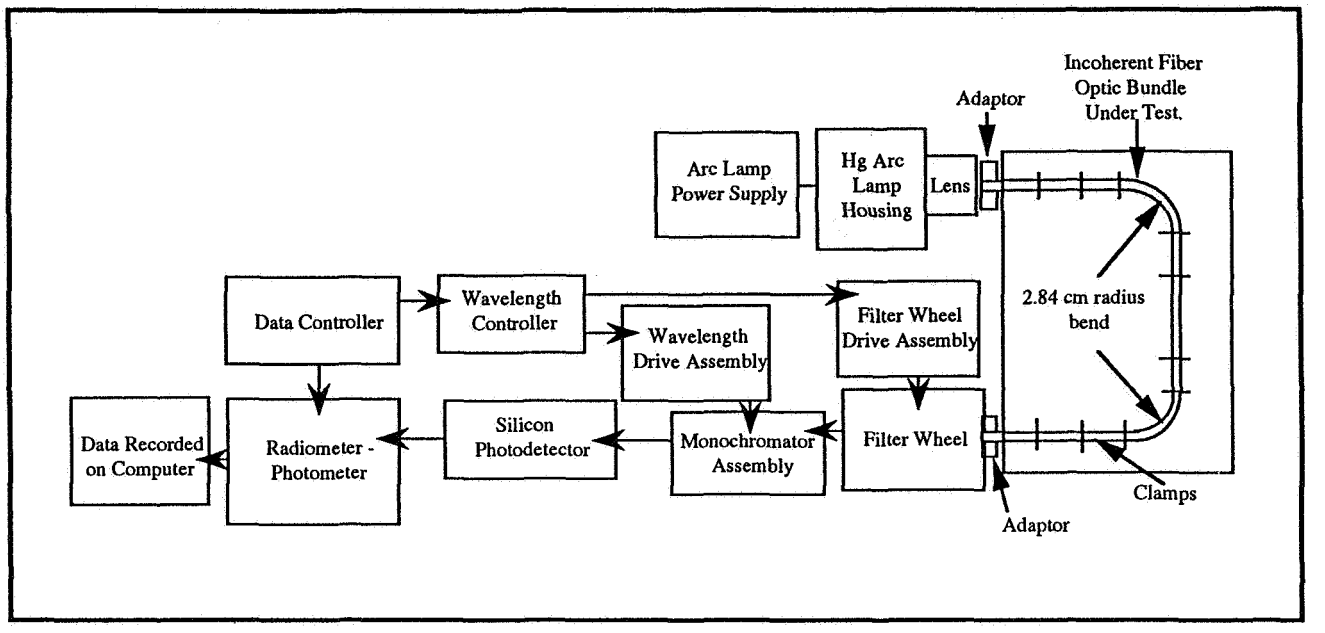

Figure 2. Spectrophotometry equipment to detect α and photobleaching is shown. A total of three spectrophotometry scans were performed on both the control and space orbited bundles. The Data Controller initiated the scans. Arrows connecting equipment represent logic flow.

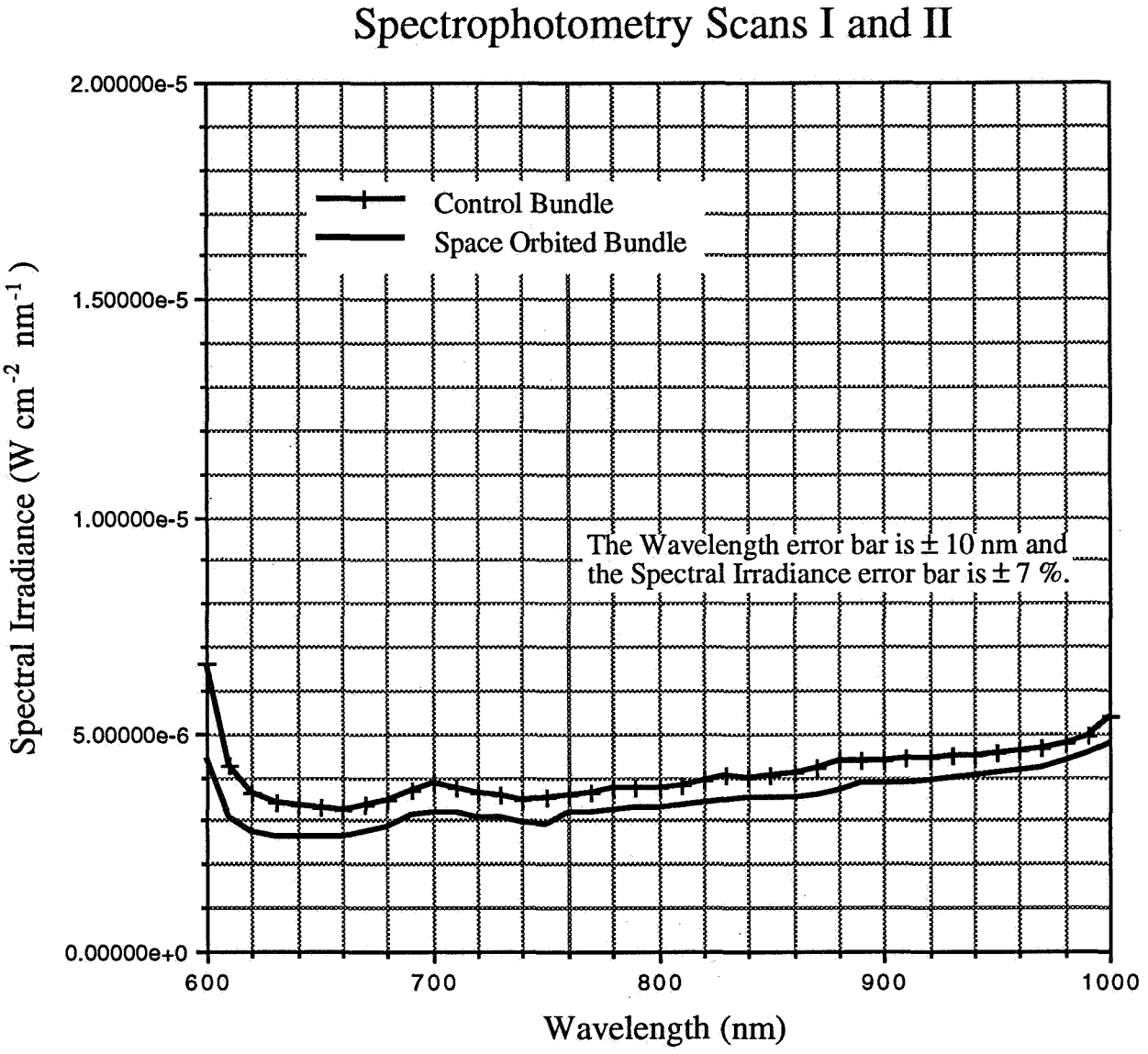

Figure 3 - The Spectrophotometery Scans I and II have been combined to reveal no significant signal transmission differences in the Control to Space Orbited fiber optic bundle comparision.

Note: Due to fluctuations in the spectrophotometry system no conclusions could be drawn over the ranges 400nm to 600nm and 1000nm to 1100nm. This fluctuation was caused by a non-synchronization of monochromator's settling times and data acquisition system's data transfer timing.

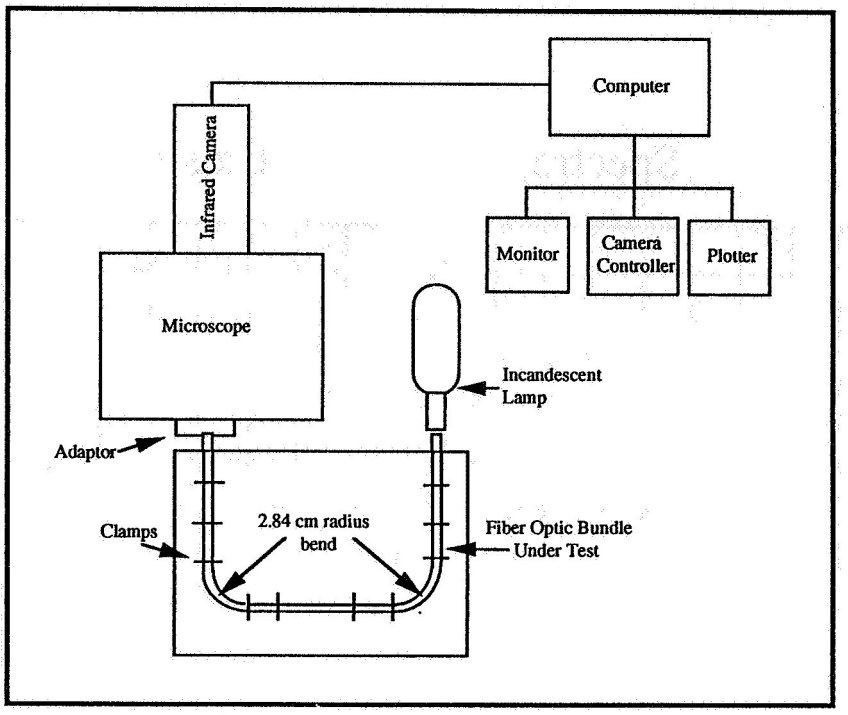

Figure 4 - An individual fiber indentification was performed on both bundles with the configuration shown. The Incandescent Lamp was positioned to uniformly illuminate the Fiber Optic Bundle Under Test.

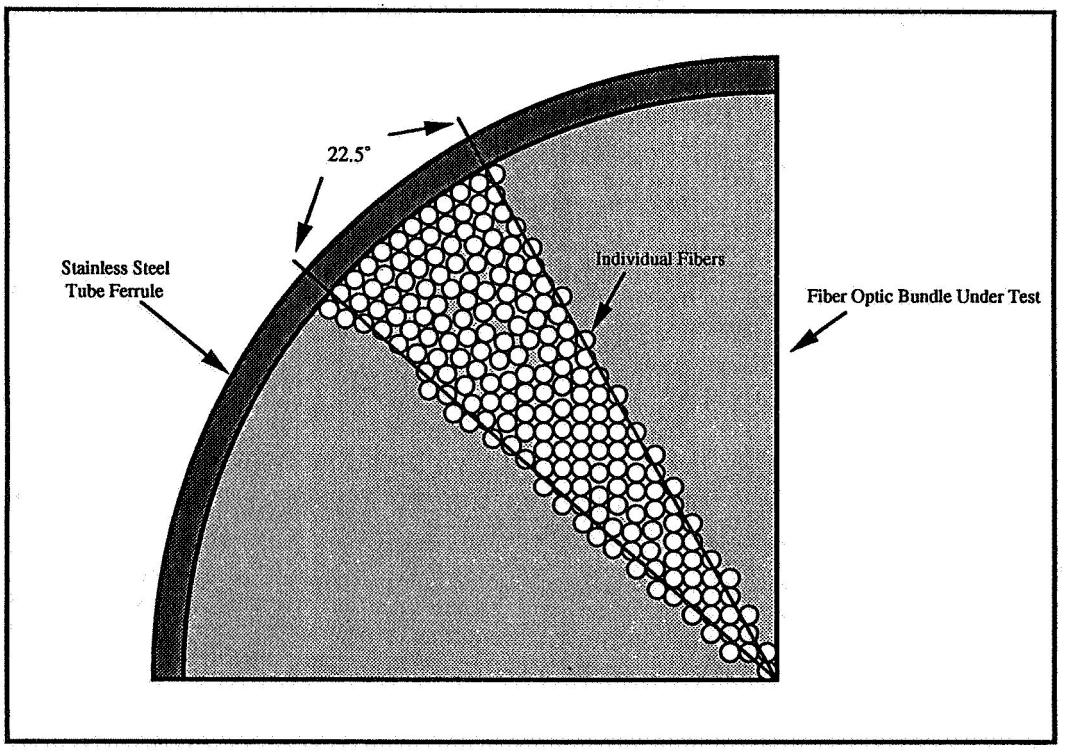

Figure 5 - An end quarter section view of the fiber optic bundle is shown. A total fiber count was obtained by sectioning the Fiber Optic Bundle Under Test into a 22.5° section as shown. Only the portion of the Individual Fibers which laid in the 22.5° section was counted. The number of Individual Fibers was then extrapolated to estimate the number of fibers in the Space Orbited and Contol bundles.

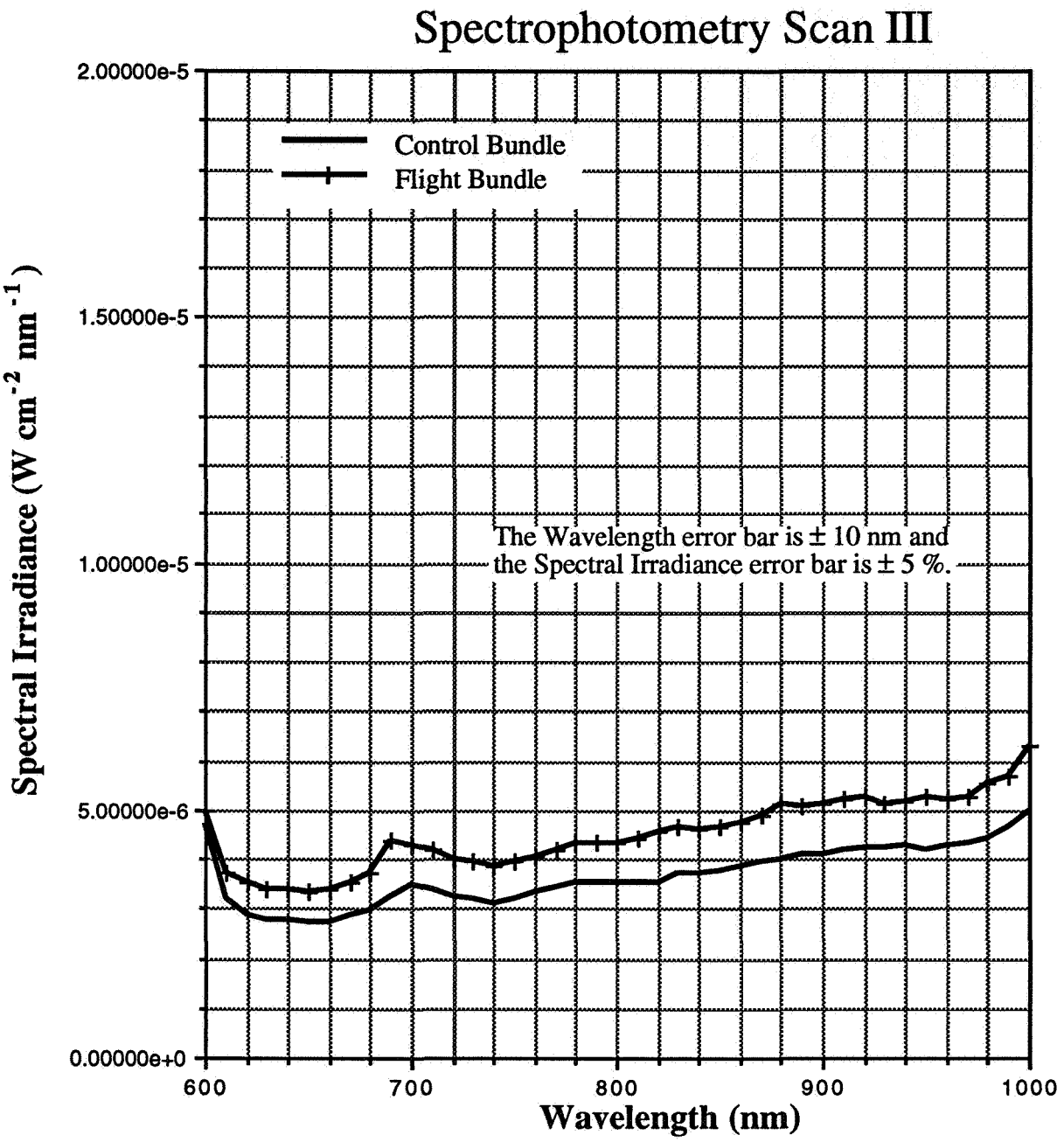

Figure 6 - The final spectrophotometry scan reveals little deviation between the Control and Space Orbited Bundles within the 600 nm to 1000 nm region.

Note: Due to fluctuations in the spectrophotometry systems no conclusions could be drawn over the ranges 400 nm to 600 nm and 1000 nm to 1100 nm. This fluctuation was caused by a non-synchronization of the monochromator's settling times and data acquisition system's data transfer timing.

N93-29699

501746
B-5/4

ANALYSES OF SPACE ENVIRONMENT EFFECTS ON ACTIVE FIBER OPTIC LINKS ORBITED ABOARD THE LDEF

E. W. Taylor, T. W. Monarski, J. N. Berry, A. D. Sanchez
R. J. Padden, and S. P. Chapman

AFSC Phillips Laboratory
Directorate of Space and Missiles Technology
Kirtland AFB, NM 87117-6008
Telephone: (505) 846-4741; FAX: (505) 846-2290

ABSTRACT

This analysis correlates the results of the "Preliminary Analysis of WL Experiment #701, Space Environment Effects on Operating Fiber Optic Systems," [Ref 1] with space simulated post retrieval terrestrial studies performed on the M0004 experiment. Temperature cycling measurements were performed on the active optical data links for the purpose of assessing link signal to noise ratio and bit error rate performance some 69 months following the experiment deployment in low Earth orbit. The early results indicate a high correlation between pre-orbit, orbit, and post-orbit functionality of the first known and longest space demonstration of operating fiber optic systems.

INTRODUCTION

The Air Force Systems Command (AFSC) Phillips Laboratory (PL) Experiment #701 (formerly Weapons Laboratory Experiment #701), also referred to as Experiment M0004, "Space Environment Effects on Fiber Optic Systems," [Refs 1,2,3] was deployed aboard the Long Duration Exposure Facility (LDEF) into space orbit by the shuttle ***Challenger*** on 6 April 1984. The experiment was positioned in tray location F8, 30° from the direction of the LDEF velocity vector, placing it close to the leading edge of the satellite. The LDEF was retrieved on 12 January 1990 by the shuttle ***Columbia*** after a nearly six year exposure to the adverse space environment elements of radiation, debris, micrometeorites, temperature cycling, and atomic oxygen scavenging.

The objective of the experiment was to measure the effects of the space environment on cabled fiber optics for correlation to previous extensive radiation effects studies performed nearly a decade ago [Ref 4-10]. End results on the effects of space debris and micrometeorite impacts as well as contamination experienced by the experiment space exposed surfaces have also been documented [Ref 11]. The intent of this paper is to report on the observed responses of three of four operational fiber optic links responding to orbital temperature cycling (the fourth link was not operational due to a micrometeorite or debris impact experienced after the first year in orbit). As a result, the loss of optical signal waveguiding resultant from temperature induced refractive index changes has been observed to various degrees in the three

links. Radiation induced effects are reported elsewhere [Refs 1-3, 12, 13, 14]. Analysis on the losses in the individual components of each link is underway and will be reported in a later paper. However, the intent of this paper is to identify and bound the influence of the orbital temperature changes on the performance of links 1-3.

ANALYSES

Shown in Figure 1 is the experimental arrangement used to measure the operational performance of the optical fiber links during the first year of orbit. For the first six months in space, data was collected every six days, with the first measurement accomplished on the sixth day of orbit. During the last six months of orbit, data collection occurred every fourth day, totaling 76 measurements performed over the first year. Data collection and measurement, both in orbit and terrestrially, of several link parameters including signal to noise ratio (SNR), number of errors, types of errors, and temperature induced attenuation was accomplished using digital processing methods [Refs 1, 2, 3, 9].

In Figure 1, the experiment controller actuates a pseudo-random pulse generator and an error detector circuit which are switched successively between the four optical fiber links. A stream of 130,944 bits then passes through the link under measurement, and the processed signal is compared to the output of the pseudo-random generator. Any mismatch is considered an error as identified by Gilbert Statistics (Type I, II, and III) [Refs 6-7]. If the number of errors counted is less than 128 Type I errors, the counters are cleared, the threshold level of the detector comparator circuit is then incremented by +1.25 mV, and another bit stream is sent through the link. When 128 or more independent (Type I) errors were detected, the experiment terminated the run, stored the data for use in the SNR determinations, and proceeded to exercise the next link in the measurement sequence.

The optical sources used to power the optical fibers in the experiment were light emitting diodes, three of which operated at a wavelength of 830 nm, while the fourth optical source operated at a wavelength of 1300 nm. Three of the optical fibers were plastic coated silica (PCS) step index fibers, while the fourth fiber operating at λ = 1300 nm was a semi-graded glass-glass fiber. Silica PIN photodiodes were used in the detection scheme. Analog temperature sensors (thermistors) were placed at different locations within the tray volume, and were read by an incrementing procedure using the digital to analog converter of Fig. 1, similar to the manner by which the threshold voltages were measured for each fiber link. The temperature resolution was determined to be within ± 0.1°C at room temperature (20°C) degrading to ± 2°C at the extremes of -80°C and +150°C. It was over this range that the optical detector output was evaluated by the experiment comparator circuitry to determine the changes in the link threshold voltages. These changes representing the overall link performance over a one year period are shown in Fig. 2.

As shown in Figure 2, the orbital performance of the four optical fiber links was directly related to the temperature conditions internal and external to the tray. (While minimal radiation induced effects were also present, and the magnitude of the dose received was

measured, the results not included in this analysis are reported elsewhere [Refs 1-3].) The cyclic variation of the measured temperatures within the tray are attributed to the incident solar heat flux impinging the tray surface and conducting/radiating to the inner tray volume. Illustrated in Fig 3 is a comparison of an internal tray sidewall temperature measured by one of the experiment thermistors and the NASA THERM-Longeron 6 temperature [Ref 15]. The THERM data provided by NASA was also collected actively during spaceflight. Considering the two measurements were made several longerons apart, and are not the same time interval for $t > 125$ days, the measurements are in close agreement. The disagreement in orbital temperature data for $t < 125$ days is currently under investigation.

The large deviations in the optical signal levels observable in Figs 2a and 2b are believed due to the temperature induced loss of waveguiding in the fibers as previously reported [Ref's 6-8]. The difference between the cladding region index (n_{cl}) and the core index (n_c) is given as $\Delta n = n_c - n_{cl}$. Due to the non-equivalent temperature induced index changes experienced by these regions, the fiber waveguiding efficiency decreases as n_c and n_{cl} change at different rates. Here, n_{cl} decreases rapidly at low temperatures. A re-polymerization phase process may occur in the cladding during low temperature cycling, leading to an optical transmission hysteresis phenomenon [Ref 6]. Of course, any radiation induced color center losses also add to the decrease in signal transmission, and the likelihood of temperature annealing of these defects is decreased significantly at low end temperatures [Ref 6-8]. Mechanical stress or bending effects can also cause the large deviations. Macro and microbending effects as a function of temperature can cause signal losses at lower temperatures. Also, fiber movement within the cabling due to thermal expansion and contraction can result in causing misalignments within the optical connectors which in turn can degrade the optical signal throughput.

Comparison of pre- and post-orbit absorption/emissivity (α/ϵ) measurements on the space-exposed panels of M0004 was conducted. There are two different paint colors on the exposed part of the tray: white and gray. The fiber plates were colored gray, and the rest of the exposed area was white. Pre-orbit measurements of α/ϵ were taken at four different places on the experiment, as shown in Fig 4. The α/ϵ measurements for those points are as follows: A = .55/.89, B = .70/.89, C = .70/.89, and D = .30/.85. It follows that A-C have similar values of α since they were all gray. Also, since point D is on a white panel, it should have a lower α than the adjacent gray panels. Following the experiment retrieval, α/ϵ measurements were taken again at Kennedy Space Center (KSC). However, measurements were not taken for points A-C so as not to disturb the exposed fiber cables. Thus a comparison can only be made at point D. Its post-orbit α/ϵ value was .32/.908. Thus, while there were changes in both the absorption and emissivity, the overall ratio only changed from 0.35 to 0.36. Since this α/ϵ measurement consisted of a different color than that of the other three, it is not assured that α/ϵ did not change at the other points. However, it appears that the exposed areas of the tray, and thus the fiber links which were in contact with those areas, experienced consistent temperature cycling throughout the duration of the spaceflight, and this point of view is assumed in the following analysis.

The experimental setup for the pre-orbit temperature measurements is shown in Fig 5. Sensors 2 and 3, which were attached to the back of the fiber plates, were averaged to get the temperature readings seen in Figure 6. Links 2 and 3 were fitted with ITT UNILUX/FOS connectors, while link 1 has Amphenol 906-110-5016 connectors. These were the connectors used during flight. The light source for all three links was a pigtailed RCA LED operating at $\lambda = 820$. The detector used was a UDT power meter. The data acquisition scheme was as follows for all links: start at room temperature; raise the oven temperature to 60°C; lower the temperature to -40°C; raise the temperature back to room temperature. Data was taken in a continuous manner. For convenience of comparison, the data was converted to illustrate optical signal attenuation in dB, where increased attenuation is shown in the negative y-direction.

During post-orbit testing, the fiber plate temperature measurements were made in a slightly different fashion. The major difference here was that data was collected by operating the experiment at different temperatures to obtain individual fiber link SNR values. These SNRs were converted into optical power, and then into attenuation. This approach was used to prevent fully de-integrating the fibers from the experiment, since follow-on investigations will be performed on the experiment. Another difference was the manner in which the temperature cycling was performed. For link 1, the starting point for the temperature measurements was room temperature; next, the temperature was lowered to -40°C; finally, the temperature was raised to 60°C. For links 2 and 3, the starting point was 60°C, with decreasing temperature points to -40°C. The different approaches were made based on pre-flight testing hysteresis information. The comparison between pre and post-orbit fiber link responses to temperature cycling can be viewed in Fig 6.

For link 1, there are some notable differences between the pre- and post-orbit data. First, the post orbit data showed an increase in performance at higher temperatures. But more importantly, at the lower temperatures, there was increased attenuation in the performance of the post-orbit data with respect to the temperature. Also, the slope of attenuation was greater than the pre-orbit data. While incrementally increasing the link temperature during post-orbit analysis, the link did not regain performance at the same point at which it was lost displaying hysteresis. It took another 10°C in temperature increase for this link to "turn on."

For link 2, the pre- and post-orbit data were somewhat similar. The major difference here was that the post-orbit data displayed near step function characteristics at 0°C (performance went from normal operating levels to an off state for a change of 10°C) while the pre-orbit data showed a gradual degradation in performance (performance went from normal operating levels to an off state in 60°C). Another difference was that the pre-orbit data showed a greater attenuation than the post-orbit data. But this is most likely a result of the data acquisition process of the experiment electronics. Specifically, when the SNR is determined for a given link, the initial threshold level is not set to zero signal output. Thus, it is not necessarily possible to obtain the minimum power level being detected by the receivers.

For link 3, the pre- and post-orbit data are very similar. Most notable is the close agreement between the pre- and post-orbit data, and the high performance of the link across

the entire temperature range. Also, there is a slight increase in performance at low temperatures for both the pre- and post-flight data.

Since the fiber used in links 2 and 3 are very similar in composition, but the performances of these links were rather different, an interesting conclusion can be drawn. The only difference between the two is that the cabling for link 2 is a loose tube configuration, while the cabling for link 3 was a tight conformal wrap. Thus it appears that the cabling of fiber optic links plays a major role in controlling temperature effects.

Another type of temperature cycling calibration was performed during the post orbit analysis. This calibration involved cooling the entire experiment tray, as experienced in space, rather than cooling the isolated fiber plate, as previously discussed in this paper. The purpose for doing this was two-fold. First, it was an attempt to correlate the entire tray temperature response with the orbital data. Second, it was an attempt to determine if temperature changes of the electronics (which only happened during the whole tray testing) had any effect on the performance of the links. The results of the fiber plate and entire tray testing were very similar, and thus the electronics were ruled out as being a cause of any of the temperature effects seen in performance in the orbit data. This is not unexpected, since the use of thermal blankets between the space exposed cover plates and the inner volume provided thermal insulation between the space exposed optical fibers and the experiment electronics, optical sources, and optical receivers. Our next analysis will use external sources and detectors to measure the effects of temperature cycling on the cabled optical fibers, thus removing any uncertainty introduced by the experiment A-D circuitry.

In conclusion, we have reported the first known data measuring the performance of step and graded-index optical fibers operating in a prolonged space environment under widely varying temperature conditions. It was observed that no permanent damage was experienced by either the glass or PCS optical fiber links due to the orbital temperature cycling experienced by the space exposed fibers. Also, it was shown that the cabling configuration plays a significant role in the control of temperature effects. While directly subjected to the harsh space environment, the cabled fibers and their optoelectronic components were recorded to operate, but were highly degraded at the low temperature extreme. Finally, it must be noted that the fibers which were subjected to the space environment are those of a much earlier generation technology. Considering the advances which have been made since the experiment was launched, newer generation fiber optics systems should be a reliable resource for use in space.

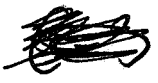

REFERENCES

[1] Taylor, E. W.; Berry, J. N.; Sanchez, A. D.; Padden, R. J.; and Chapman, S. P.: Preliminary Analysis of WL Experiment #701, Space Environment Effects on Operating Fiber Optic Systems. NASA Conference Publication 3134 *LDEF - 69 Months in Space - First Post Retrieval Symposium Part 3.* June 2-8, 1991.

[2] Taylor, E. W.; Berry, J. N.; Sanchez, A. D.; Padden, R. J.; and Chapman, S. P.: First Operational Space Fiber Optic Links Orbited Aboard the Long Duration Exposure Facility - Lessons Learned. *Proc. DoD Fiber Optics '92.* March 24-27, 1992. McLean, VA. pp. 25-28.

[3] Taylor, E. W.: Performance of the First Operable Fiber Optic Systems in Prolonged Space Orbit. *Proc. International Society for Optical Engineering.* Vol. 1691, Small Satellite Technologies and Applications. April 20-24, 1992.

[4] Taylor, E. W.: Fiber Optics Space Effects. *Proc. of Fiber Optics and Communication,* Sep. 1978, pp. 245-247.

[5] Taylor, E. W.: Some Recent Fiber Optics Research, Development and Applications Conducted by The Air Force. *Proc. Fiber Optics in the Nuclear Environment.* Vol 1: Applications. DNA 5308P-1, pp. 209-221, (May 1980).

[6] Taylor, E. W.; Emmes, J. M.; Barnes, C. E.; and Wiczer, F.: Behavior of Irradiated Plastic Clad Silica Fibers at Low Temperatures. *Photon 80 Conf. Proc.* Compte-Rendu, Paris, FR, pp. 110-117 (October 1980).

[7] Taylor, E. W.; Emmes, J. M.; Ayres, W. R.; Wiltse, J. D.; and Merritt, J. K.: Response of Irradiated Optical Waveguides at Low Temperatures. *Society of Photo-Optical Instrumentation Engineers,* Vol. 296, pp. 40-50 (August 1982).

[8] Taylor, E. W.; Myatt, L. J.; and Wiltse, J. D.: Low Temperature Gamma Irradiation of Polymer Coated Optical Waveguides. Presented at Photon 83, Paris, FR *Society of Photo Optical Instrumentation Engineers,* Vol. 404, pp. 55-59 (May 1983).

[9] Johnston, A. R.; Bergman, L. A.; and Taylor, E. W.: Fiber Optic Experiment For The Shuttle Long Duration Exposure Facility. *Society of Photo-Optical Instrumentation Engineers,* Vol. 296, pp. 40-50 (August 1982).

[10] Taylor, E. W.: Space Effects on Fiber Optics Systems. NASA SP-473, *The Long Duration Exposure Facility, Mission 1 Experiments,* edited by L. G. Clark et al., Washington, DC pp. 182-184 (1984).

[11] McKnight, D. S.; Dueber, R. E.; and Taylor, E. W.: Space Debris and Micrometeorite Events Experienced by WL Exp #701 In Prolonged Low-Earth Orbit. *J. Geophys. Res, Space Physics,* Vol. 96, No. A6, pp. 9829-9833, June 1, 1991.

[12] Taylor, E. W.: An Experiment for Studying Monolithic Integrated Optics Performance in the Space Environment. *SPIE Cambridge Symposium on Optical and Electro-optical Engineering, Integrated Optical Circuit Engineering II,* Vol. 548, pp. 46-50, September 1985.

[13] Benton, E. V.; and Heinrich, W.: Ionizing Radiation Exposure of LDEF. *USF-TR-77,* August 1990.

[14] Armstrong, T. W.; and Colborn, B. L.: Scoping Estimates of the LDEF Satellite Induced Radioactivity. *SAIC-90/1462,* September 1990.

[15] Bourassa, R. J.; and Gillis, J. R.: Solar Exposure of LDEF Experiment Trays. *NASA Contract Report 189554,* February 1992.

LIST OF INCLUDED FIGURES

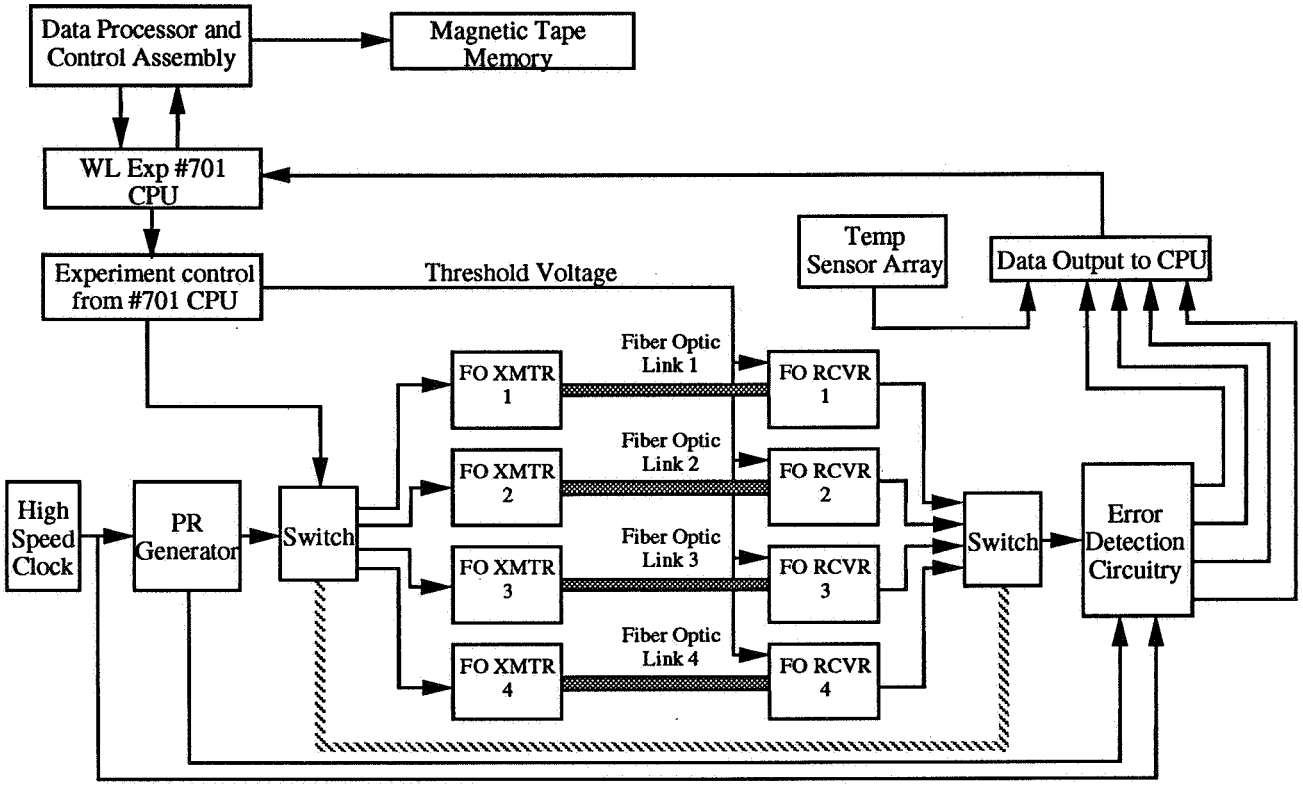

Figure 1. Configuration of experiment hardware. This hardware was used to measure the performance of the four active digital fiber optic links contained in PL Experiment #701 (M0004). The experiment measured the temperature at various locations within the tray volume and the performance of the fiber optic links by measuring the Signal-to-Noise Ratio and Bit-Error Rate of each link.

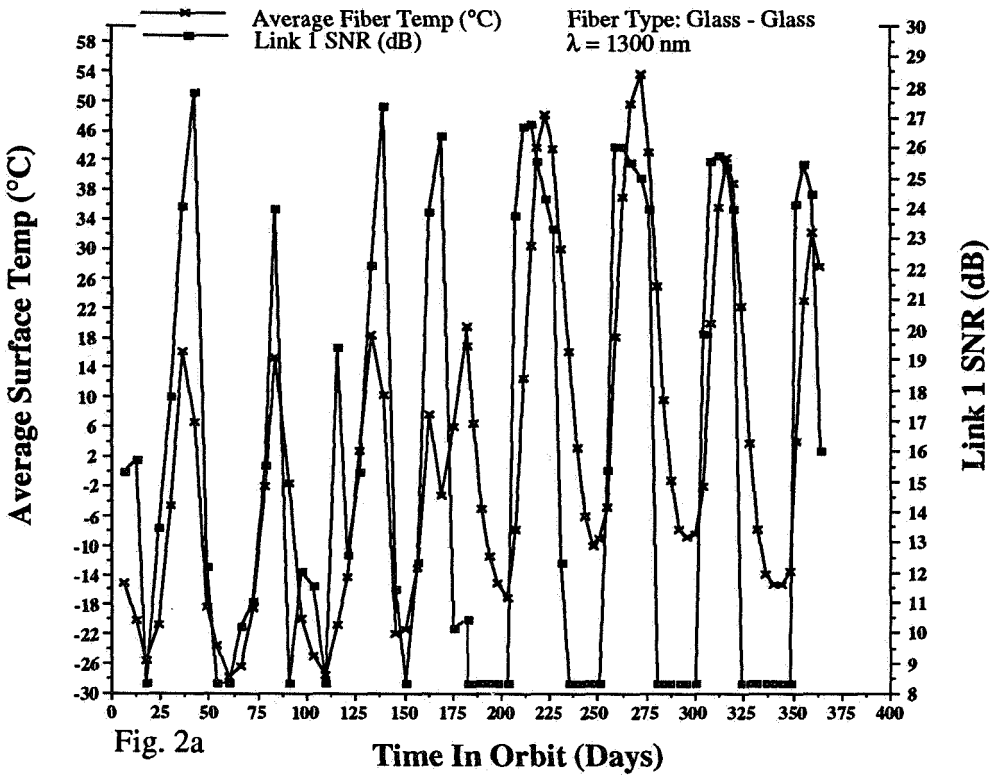

Fig. 2a

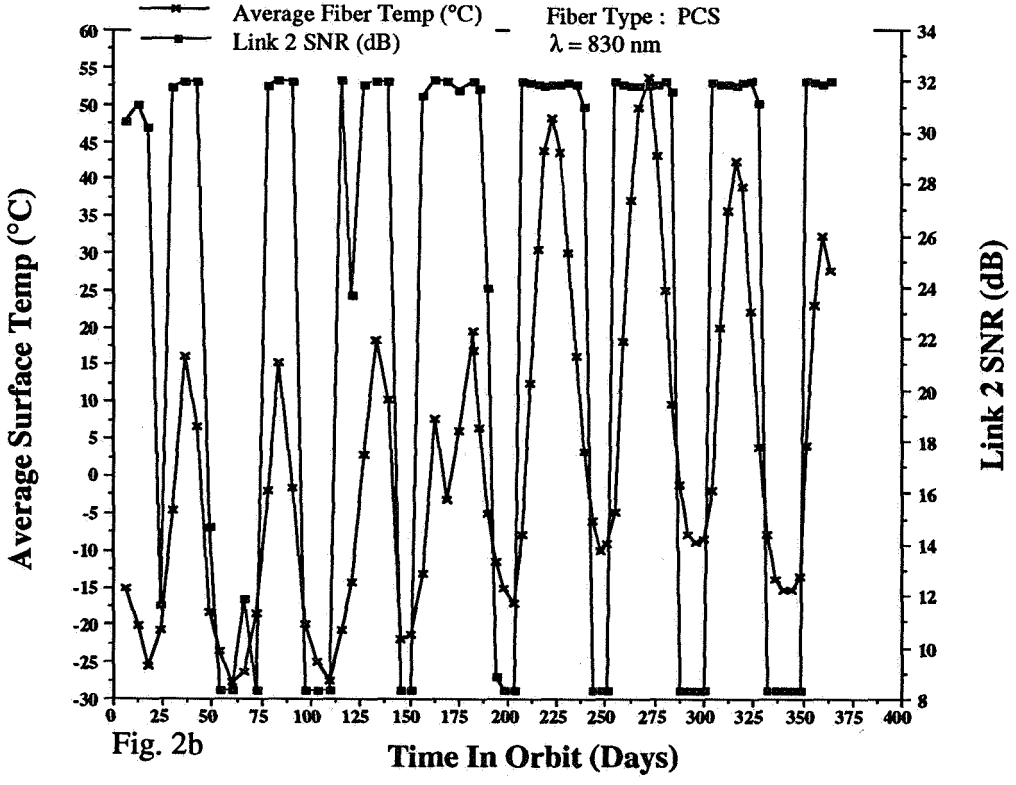

Fig. 2b

Figures 2a - 2b. Orbital performance data on PL Exp # 701 (M0004) Space Environment Effects on Fiber Optic Systems

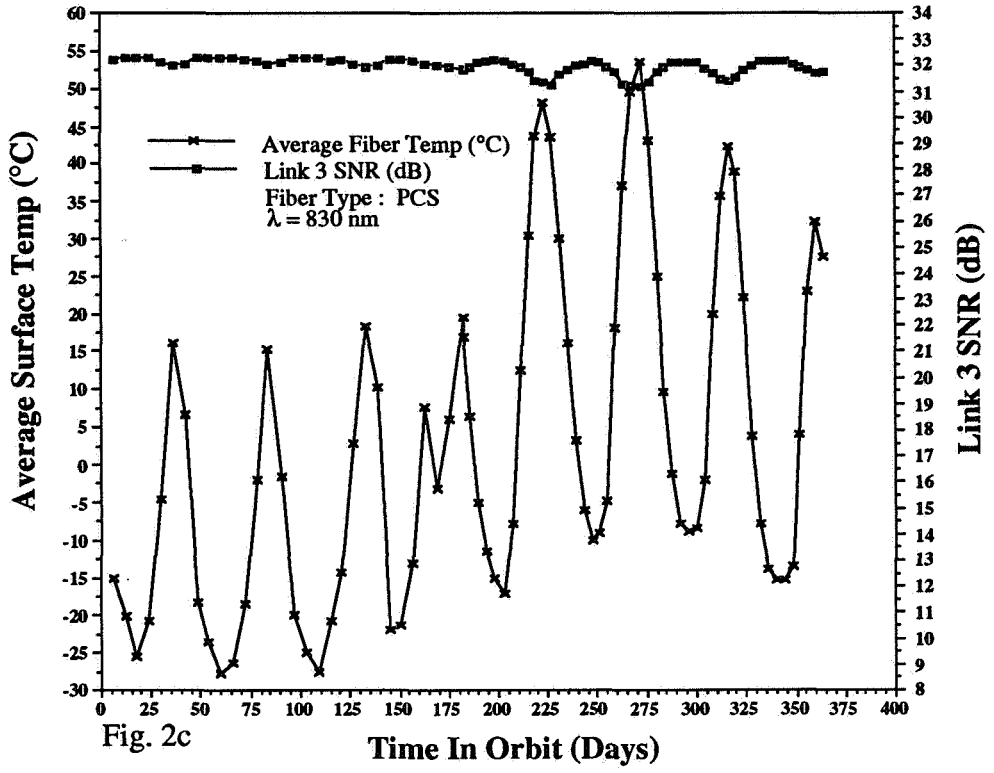

Fig. 2c

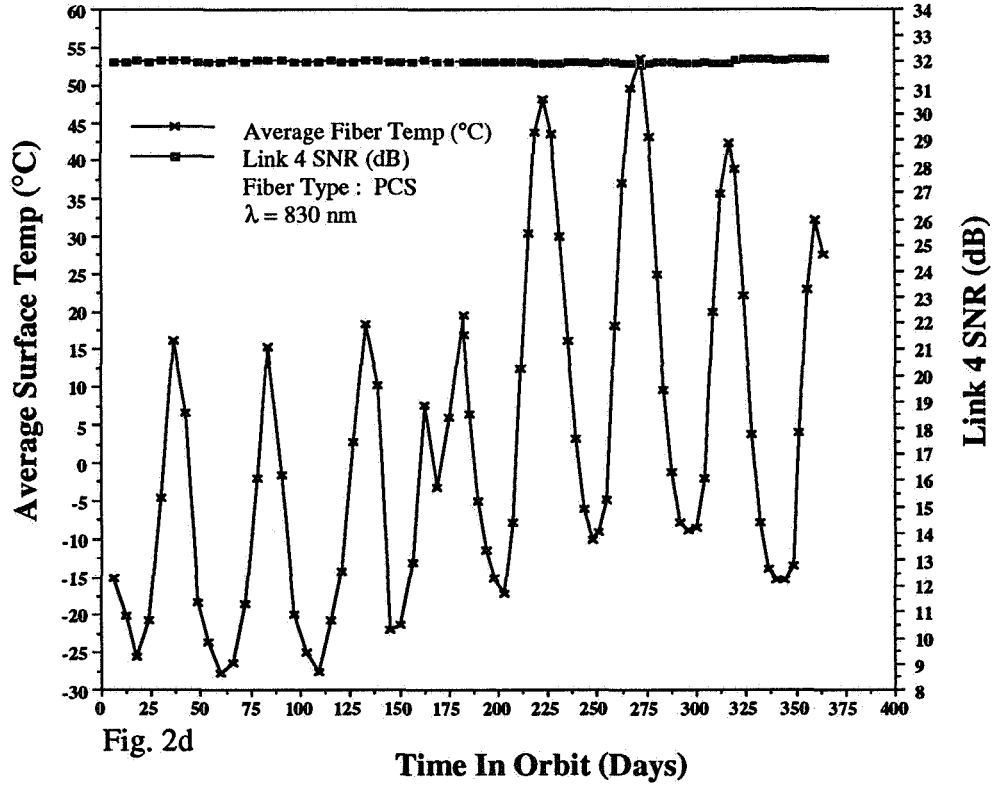

Fig. 2d

Figures 2c - 2d. Orbital performance data on PL Exp # 701 (M0004) Space Environment Effects on Fiber Optic Systems

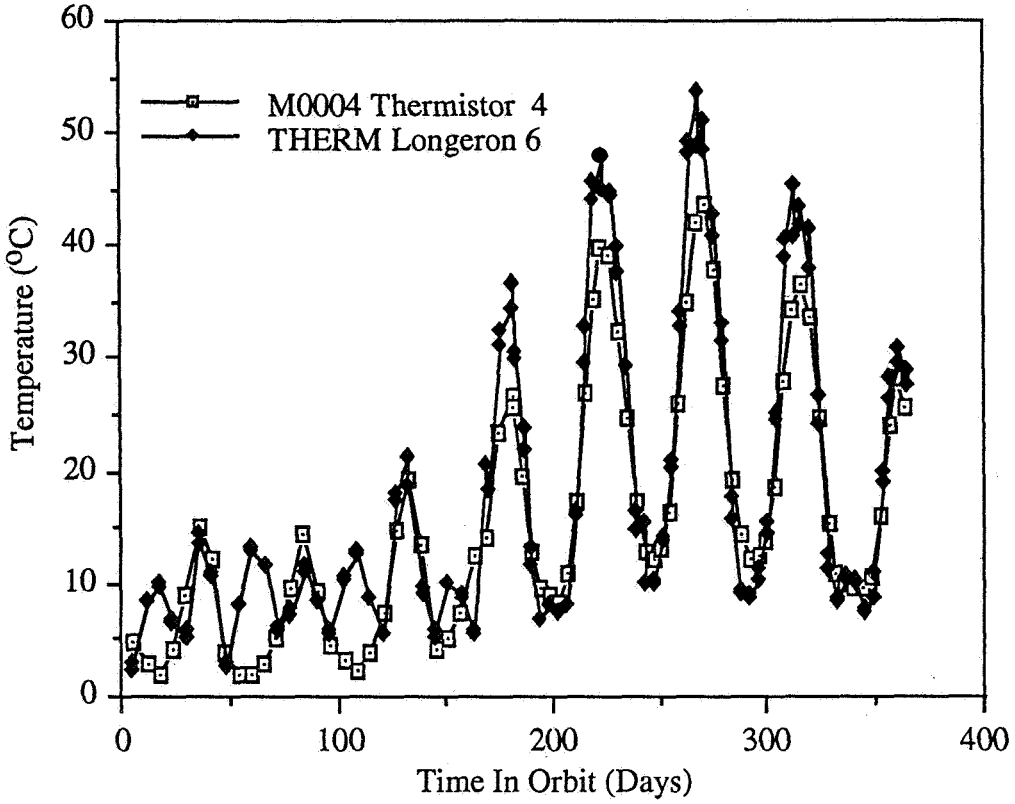

Figure 3. Comparison of M0004 Thermistor 4 and LDEF THERM Longeron 6 data. This comparison shows the good correlation between the two sets of orbit data.

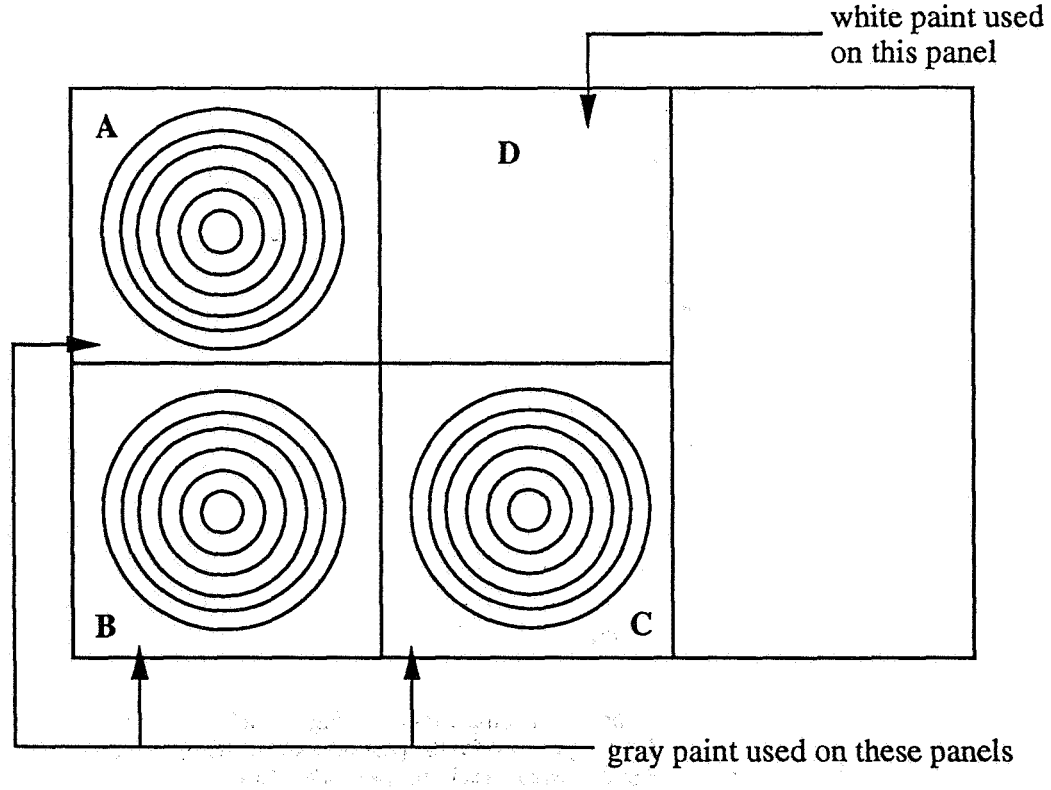

Figure 4. Location of pre and post-orbit α/ε measurements

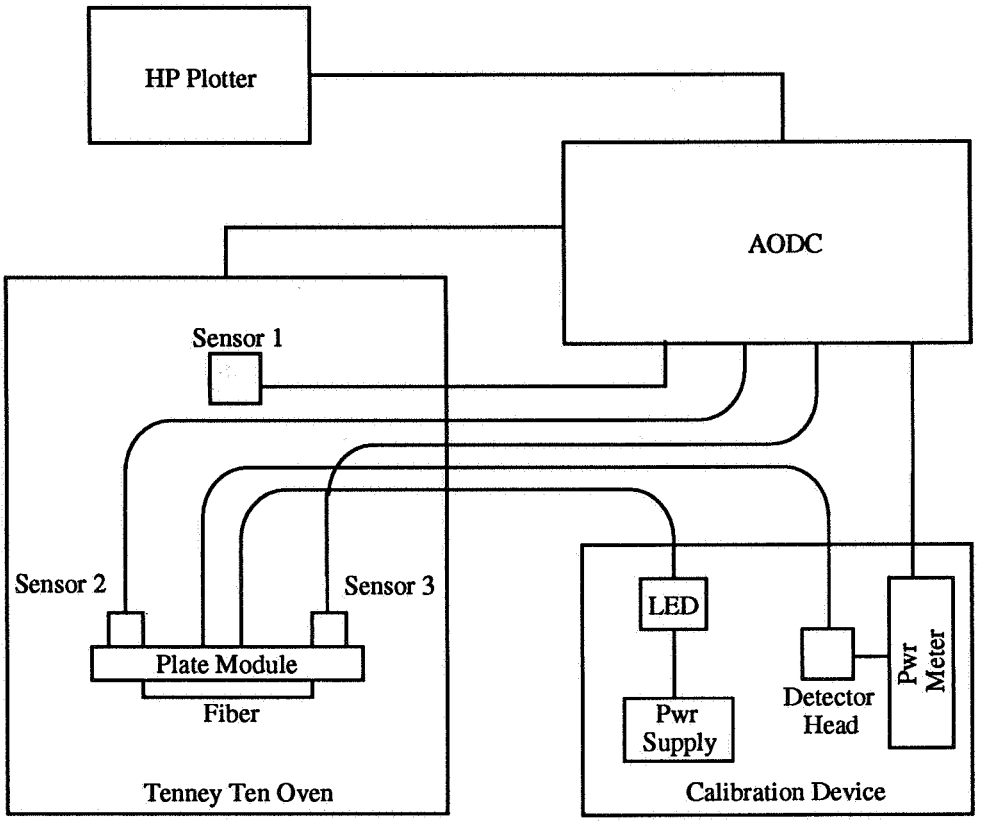

Figure 5. Experimental set up for terrestial temperature cycling and transmission measurements

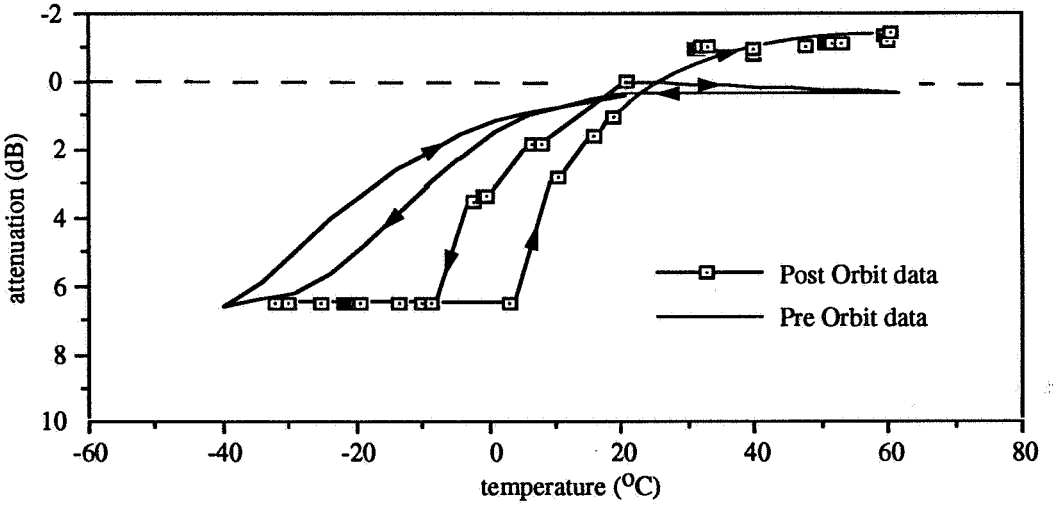

Figure 6a. Comparison of pre and post orbit temperature cycling on link #1. Here, signal attenuation occurs at a higher temperature for the post orbit data. Also, it can be observed that there is a greater degree of hysteresis in the post orbit data.

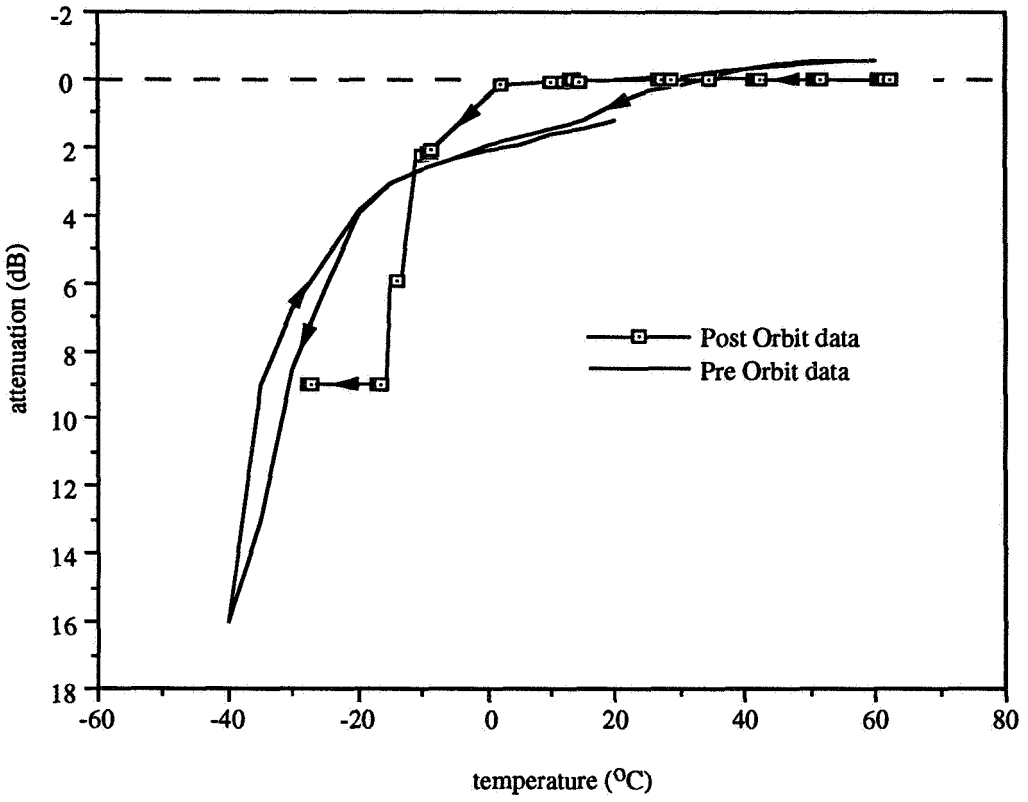

Figure 6b. Comparison of pre and post orbit temperature cycling on link #2. Although there is some correlation between pre and post orbit data, some subtle differences do exist. The "bottoming-out" of the attenuation for the post orbit data is most likely a result of the data acquisition process of the experiment electronics, and not a result of temperature cycling.

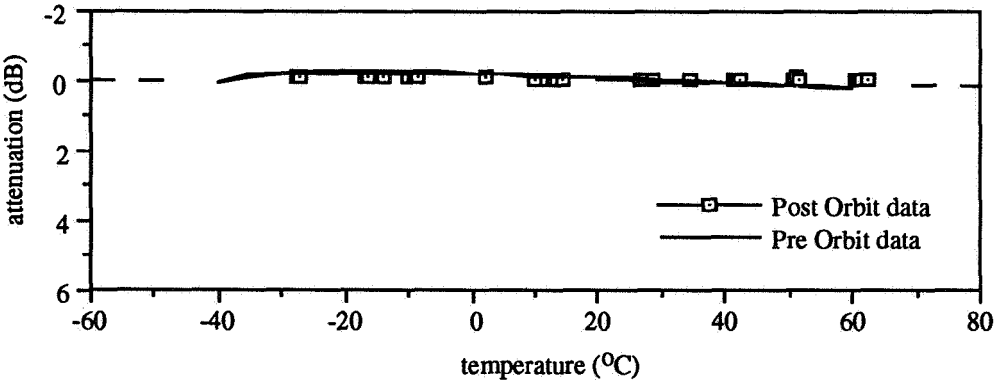

Figure 6c. Comparison of pre and post orbit temperature cycling on link #3. Here, the pre and post orbit correlation is excellent, and there is high link performance across the entire temperature range.

501755 N93-29700

RADIATION AND TEMPERATURE EFFECTS ON LDEF FIBER OPTIC SAMPLES

A. R. Johnston 818/354–4054
R. Hartmayer 818/354–1925
L. A. Bergman 818/354–4689

Jet Propulsion Laboratory
California Institute of Technology
Pasadena, California 91109, Fax: 818/393–4820

SUMMARY

This paper will concentrate on results obtained from the JPL Fiber Optics LDEF Experiment since the June 1991 Experimenters' Workshop. Radiation darkening of laboratory control samples and the subsequent annealing was measured in the laboratory for the control samples. The long–time residual loss was compared to the LDEF flight samples and found to be in agreement. The results of laboratory temperature tests on the flight samples, extending over a period of about nine years, including the pre-flight and post–flight analysis periods, are described. The temperature response of the different cable samples varies widely, and appears in two samples to be affected by polymer aging. Conclusions to date are summarized.

1. INTRODUCTION

This paper presents results from the JPL fiber optic LDEF experiment obtained since the last LDEF symposium in June 1991. These results relate, first, to laboratory measurements of radiation–induced loss in control samples and the recovery of this loss with time. The test data was compared to the already measured loss increment in the LDEF flight samples, with the purpose of determining whether the short–term lab tests could be used to correctly estimate the loss accumulated in a much longer orbital mission. Secondly, additional temperature testing of both the flight samples and controls has indicated the possibility of long–term changes in temperature–induced loss due to the orbital exposure, as well as large differences in the magnitude of this effect between different types of fiber optic cables.

Post–flight fiber optic loss measurements, spectral loss measurements, temperature effects, and micrometeoroid impact experience were described in a paper presented at the first LDEF Post Retrieval Symposium (ref. 1). This paper supplements the earlier one, and extends some of the information found there.

The LDEF carried a number of fiber optic experiments (ref. 2). The length of the orbital exposure, over 5 1/2 years, and the fact that experimenters were able to recover samples and examine them in the laboratory are unique. In our experiment, the duration of the exposure to ionizing radiation, although admittedly at a low level, provides a considerably longer time base than any prior laboratory experiments (For example, see refs. 3, 4.) for examining the effects of annealing on radiation damage. In addition, no attempt has been made in other laboratory work to simulate realistically the combination of environments, including radiation, temperature, and vacuum found in an orbital spacecraft, and it would be very difficult to do so.

PRECEDING PAGE BLANK NOT FILMED

In the next section, our short–term radiation and annealing measurements are described, as well as the simple model used to extrapolate data taken over a 2 day period to much longer times. The following section, Section 3, contains a summary of temperature cycling measurements and briefly describes the change in temperature response observed on one flight sample. The following section describes an analysis of contamination found on one connector termination, and finally, the conclusions to date from our post–flight data analysis are presented.

2. LONG TERM RADIATION DAMAGE

Description of Fiber Cable Samples

Our LDEF flight experiment contained four fiber optic cable samples arranged in planar coils on the outer surface of the experiment tray, thus exposing them to space over one hemisphere. The samples were terminated in connectors which were held by brackets underneath the supporting plate. The external samples experienced approximately 1 krad total mission dose, calculated from dose vs shielding depth curves given by Benton and Heinrich (ref. 5). This dose is at the fiber; the dose incident on the cable jacket was at least one order of magnitude larger. Although the dose rate was not uniform over one orbit, on average it accumulated at an approximately constant rate during the 5.7 year mission. The external samples by design experienced quite a large temperature swing during each orbit, roughly 50° to 60° C each cycle, and from about –60° to +80° C extremes over the entire mission.

In addition, six internal samples, each in the form of a multiturn coil, were mounted to the bottom surface of the tray with cable ties. They were terminated in connectors also mounted in brackets. Shielding by the aluminum cover plates reduced the dose to these samples to approximately 200–300 rads. The temperature environment of the internal samples was benign, remaining near room temperature. None of the samples were cold, so annealing of the radiation damage was not arrested. No photobleaching was expected, and none was observed.

Similar terminated control samples were prepared from the same cable lot that was used for each flight sample. The control samples were stored in a laboratory environment for the duration of the mission and were used for comparison measurements of the flight sample loss after recovery and before the current radiation tests were begun. These loss measurements were already summarized in our earlier LDEF Symposium paper (ref. 1) and were presumed to be caused by the exposure to radiation during the flight, an issue that will be mentioned again later in this paper.

Laboratory Radiation Damage Measurements

Each control sample was exposed to a Co^{60} gamma–ray source for approximately 260 seconds to produce a dose of 2.0 krads. In order to observe the recovery of the initial radiation – induced loss as a function of time, the tests followed procedures for transient radiation testing of optical fibers that are described in the literature (ref. 6). However, the duration of the radiation exposure from the Co^{60} source was much longer than in the recommended test procedure, a minor difference because our interest was in the long–term residual loss increment.

The sample coil was aligned with its axis projecting through the source so the entire circumference of the coil was at the same distance from the source. The dose was measured at points adjacent to and within the coil to determine the average dose seen by the sample.

The loss was measured for each control sample as a function of time, the data beginning before the exposure and extending for approximately 2.5 days after exposure. Changes were recorded with respect to the pre–exposure transmission. The time scale was measured from the mid–point of the approximately 4 minute radiation exposure period.

The results for control sample P–1 are shown in Figure 1. The measurement accuracy in terms of db/km was limited by the stability of the recording system, which is estimated to be about .01 to .02 db, because the sample length was quite short. The disturbance at about 1.5 x 10^5 sec was a result of temperature changes in the radiation vault caused by personnel entering to conduct other unrelated tests that particular weekend.

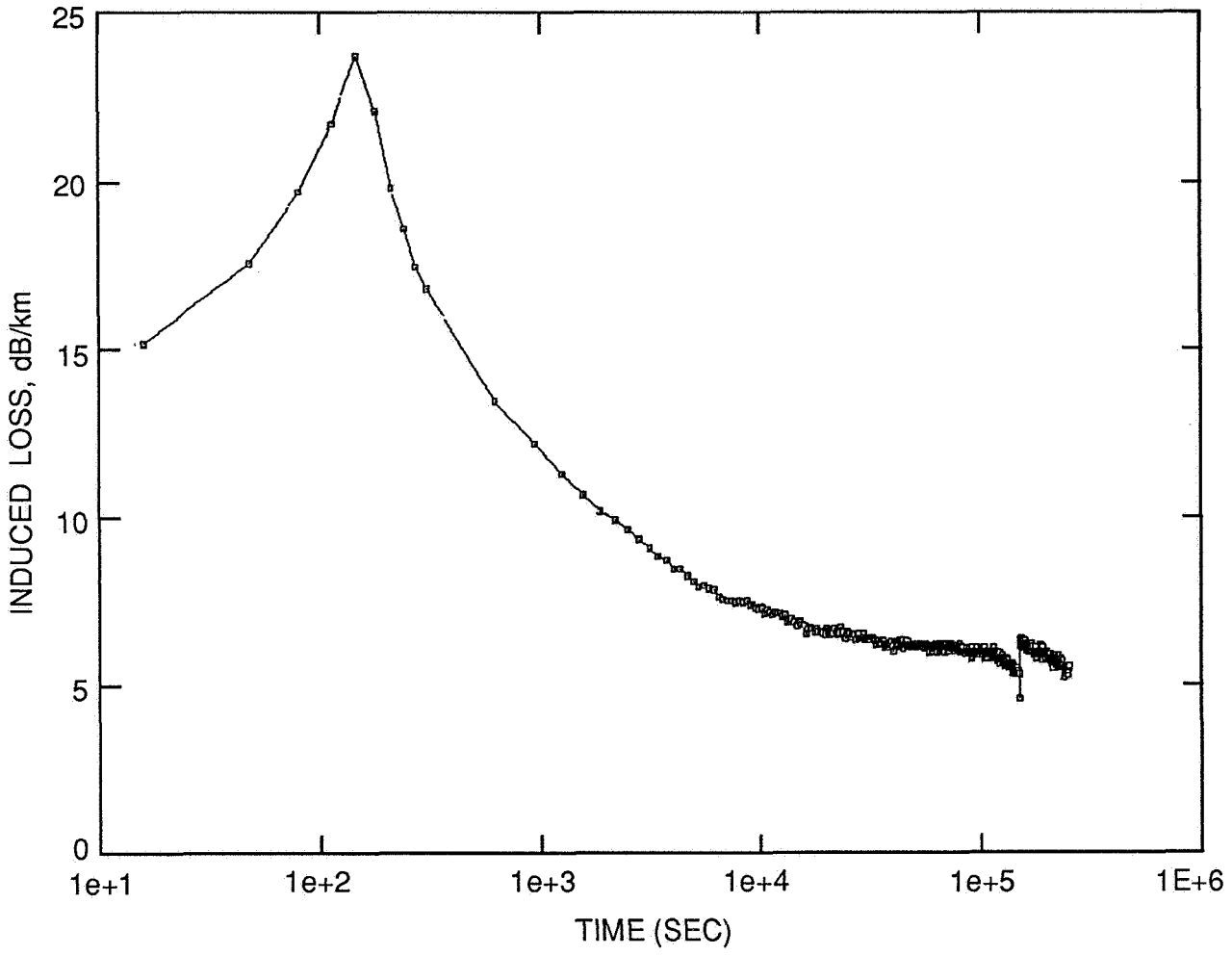

Figure 1. Transient radiation–induced loss control sample P–1. The total dose was 2.0 krad.

Sample P–1 was a 100/140 um core/clad diameter fiber with a partially graded germanium doped core and a pure fused silica cladding. There was a small amount of phosphorus added along the axis of the core to improve manufacturability. The P–1 fiber was very similar to a Corning type 1508.

Results for the same test for control sample C–1 are shown in Figure 2. Sample C–1 was a 50/125 um core/cladding diameter graded index fiber with a germanium doped fused silica core. The core was doped throughout with phosphorus, which strongly inhibits annealing of the initial damage and results in a much higher residual loss. The data points beyond about 2 x 10^5 sec were obtained by a direct measurement of attenuation, described in our earlier paper (ref. 2) after removing the sample from the

radiation exposure setup. No adjustment was made to fit these measurements to the in–situ data. We do not have an explanation for the observed increase in loss during the first 3–4 hrs; other samples also exhibited this characteristic. However our estimate of the long–term residual loss was not significantly affected by the initial rise.

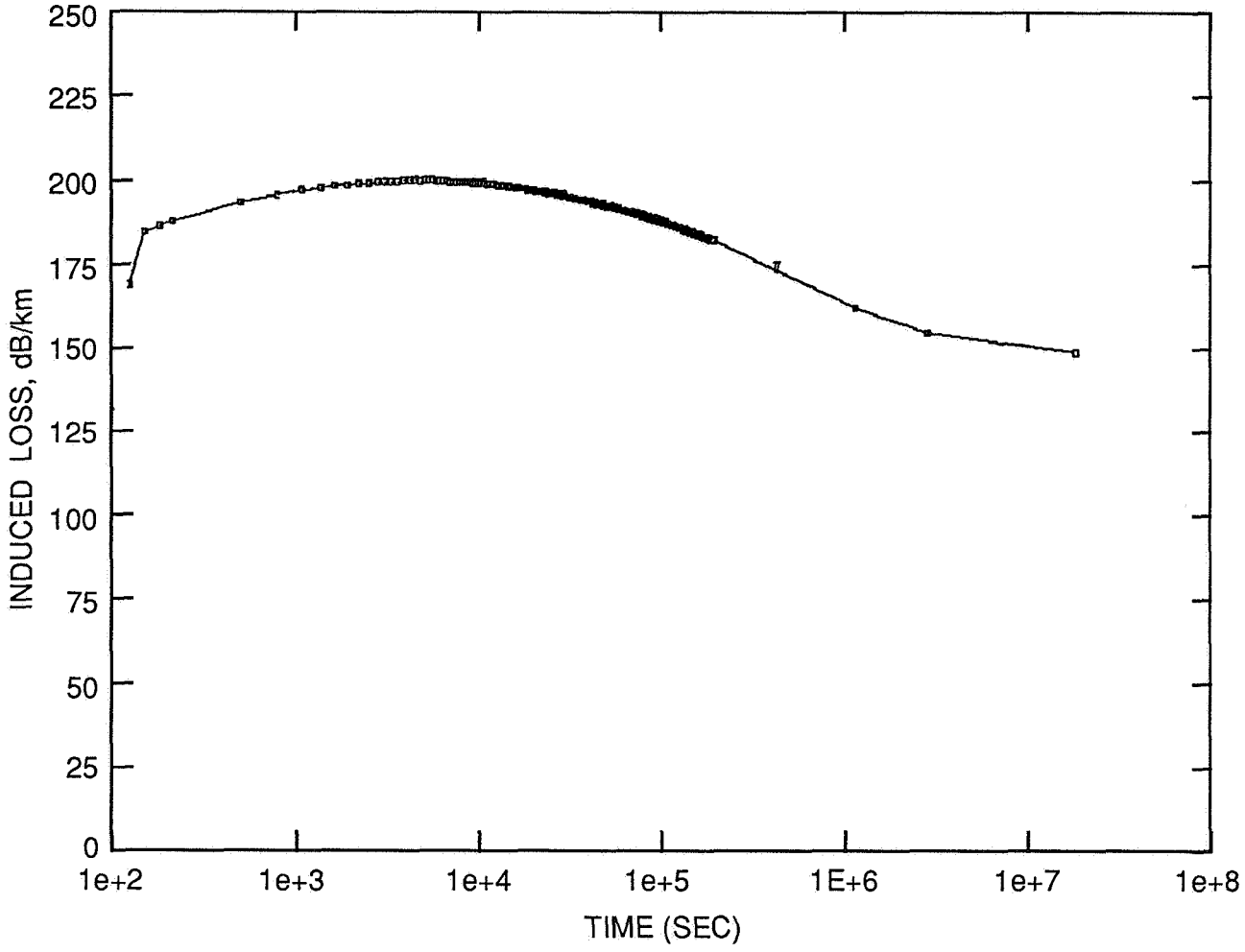

Figure 2. Transient radiation–induced loss for control sample C–1. The total dose was 2.0 krad.

Extrapolation to Long Time

Friebele (ref. 7) suggests, on very general grounds related to chemical reaction kinetics, that the recovery of radiation–induced loss can be described by the expression:

$$A(t) = (A_o - A_f)\left[1 + \frac{t}{\tau}\left(2^{(n-1)} - 1\right)\right]^{-\frac{1}{n-1}} + A_f$$

where A(t) is the time–dependent radiation–induced loss following a short radiation exposure, A_o and A_f are the initial and final loss increments, and τ is a time constant. The index n is an adjustable parameter representing the order of the reaction kinetics. It is typically 2 for pure fused silica and can be as large as 5 or 10 for doped cores.

The expression above was used to estimate the long–time limit of the induced loss from the data shown in Figures 1 and 2, as well as from similar data for the other three externally mounted samples. The results are summarized in Table 1. In the table, the specific induced loss from flight data is calculated from our observed loss increment for the flight samples, converted into db/km–krad. The specific induced loss from our lab data are the results from the laboratory exposures just described. The single value from the literature was given by Friebele (ref. 8) for Corning type 1809.

Table 1. Comparison of Flight and Laboratory Radiation Damage

	P–1	P–2	P–3	P–4	C–1
Fiber type	100–140μm graded	100–140μm step	200μ PCS step	50–125μm graded	50–125μm graded
Material	Ge doped core	– – –	silica core	silica–borosilicate	Ge–doped core
LDEF flight dose estimate	1.0 krad	0.9	1.3	1.0	0.2
Specific induced loss from flight data	<4 db/km krad	70 ± 5	110 ± 5	95 ± 5	50 ± 10
Specific induced loss from our lab data	3 ± 1 db/km–krad	27 ± 5	72 ± 10	75 ± 7	64 ± 2
Specific induced loss estimated from published data (1)	1.7 db/km krad	– – –	– – –	– – –	– – –

(1) E.J. Friebele (ref.3)

The agreement is quite satisfactory. In the case of sample P–1, the resolution is limited by the sample length and the relatively small loss increment. Within the estimated measurement accuracy, the data agree, except for sample P–2. There is some indication that the loss increase of the other flight samples is somewhat larger than predicted by the short–term radiation tests, but the difference is not significant.

However, sample P–2 showed considerably more loss increase for the flight sample than for the lab test. It should be noted that flight sample P–2 is the one discussed in the following section because it exhibited an increase in temperature–induced loss between pre–flight and post–flight tests. There may have been changes in the properties of the buffering or cabling polymers as a result of the space exposure which caused an increase in room–temperature loss, as well as an increase in the loss increment occurring as a result of temperature change.

3. LONG–TERM CHANGE IN TEMPERATURE EFFECTS

In this section we present the results of a series of temperature tests for one of the flight samples. These tests were distributed over a long period of time, extending from pre–flight, in 1983, to 1991. Similar results are also given for a sample that showed good performance for comparison.

Description of the Temperature Tests

Typically, fiber cables suffer increased loss as their temperature decreases. The cause is the large difference in thermal expansivity between the fused silica optical fiber and the polymers used in the buffer layers and in the cable structure, which causes microbending. The magnitude of the temperature–induced loss varies over a wide range, depending on cable design.

Our LDEF experiment was passive, with no measurements being taken during the flight. However, the temperature induced loss was measured for the flight samples before launch and a number of times (at least twice) after recovery. The control samples were also tested during the post–flight period for comparison.

Figure 3 shows the result of the most recent temperature cycling test for flight sample P–1. The temperature was cycled between +70° C and – 55° C three times. Each cycle was 230 minutes in length, with the temperature holding 20 minutes at each extreme and changing at a fixed rate between. The complete test took about 12 hours.

This sample had the best temperature performance of the ten LDEF samples. The fiber was coated with a UV cured acrylate buffer consisting of two layers, the inner layer with a low (Young's) modulus, and the outer with a higher modulus (ref. 9) The two layers had an outer diameter of 0.5 mm, and were contained in a hytrel tube with 0.5 mm inside diameter and 1.0 outside diameter. The entire structure was a tight fill, not loose tube, construction **(footnote 1)**.

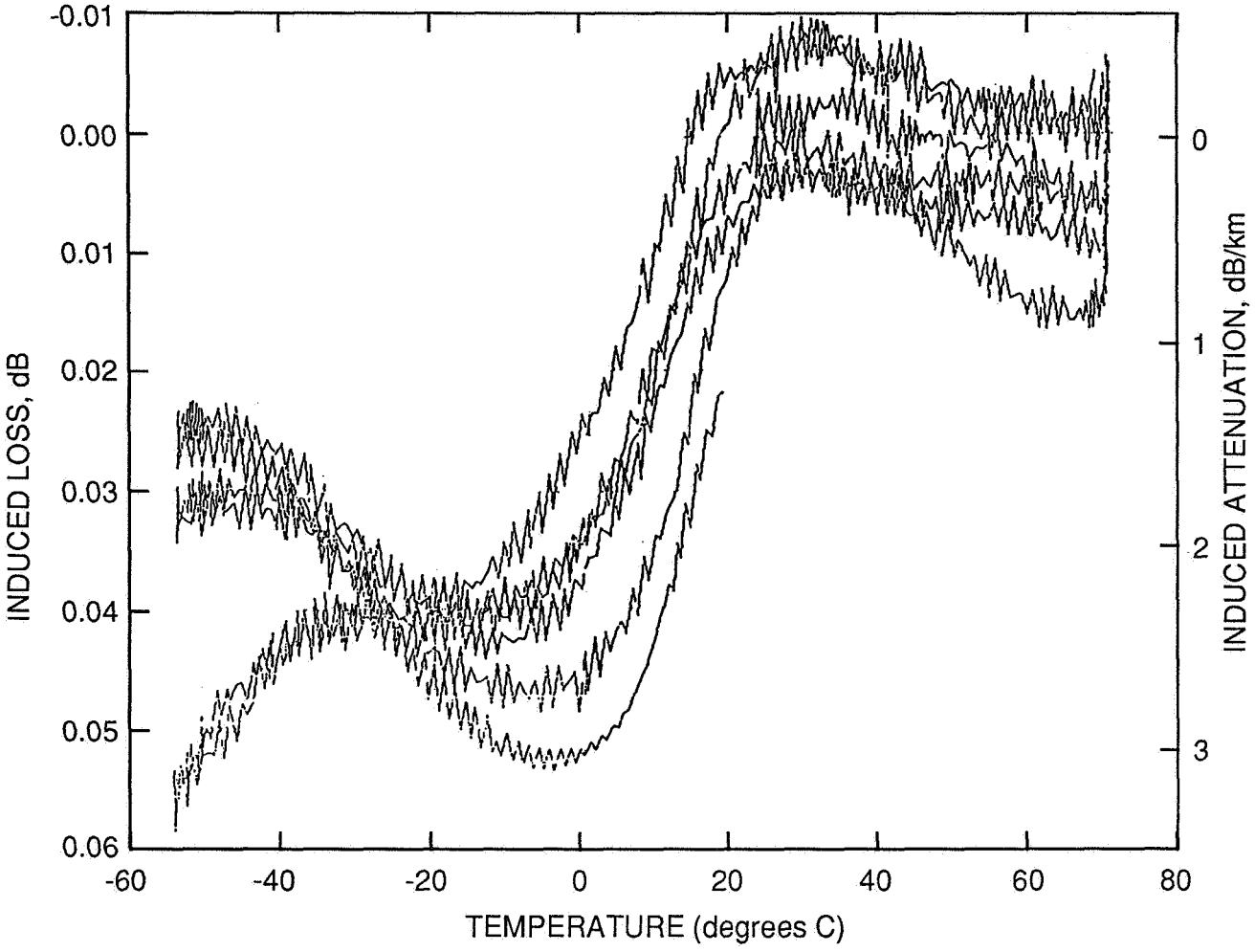

Figure 3. Temperature–induced loss for a temperature cycling test of flight sample P–1.

The total change in loss due to temperature change was 0.045 db for the sample, or 1.7 db/km over the –55° C to + 70° C temperature range. The instrumental stability was about 0.01 db or 0.4 db/km. However, we feel that the data reaching – 0.055 db near one low temperature extreme was caused by other activity nearby which changed the ambient laboratory temperature and should be disregarded. This performance was notably better than the average temperature induced loss of all the samples, which was about 1.5 db, or 30 db/km and also significantly better than the next–best performer, at 0.5 db, or 11 db/km.

The results shown in Figure 3 were obtained after the flight exposure and after a number of cycling tests in the laboratory, the total time of observation covering nearly nine years. There is no indication of growth in the temperature–induced loss increment for this sample.

Results for Sample P–2

Figures 4 thru 7 show the temperature–induced loss for sample P–2. Figure 4 shows the result of a pre–flight test, made in March 1983. Figure 5 is data obtained after the flight, in February 1991, for the control sample. Figure 6 shows a post–flight single cycle test made in early 1991 of the flight sample and Figure 7 shows data from a multi–cycle test made in September 1991.

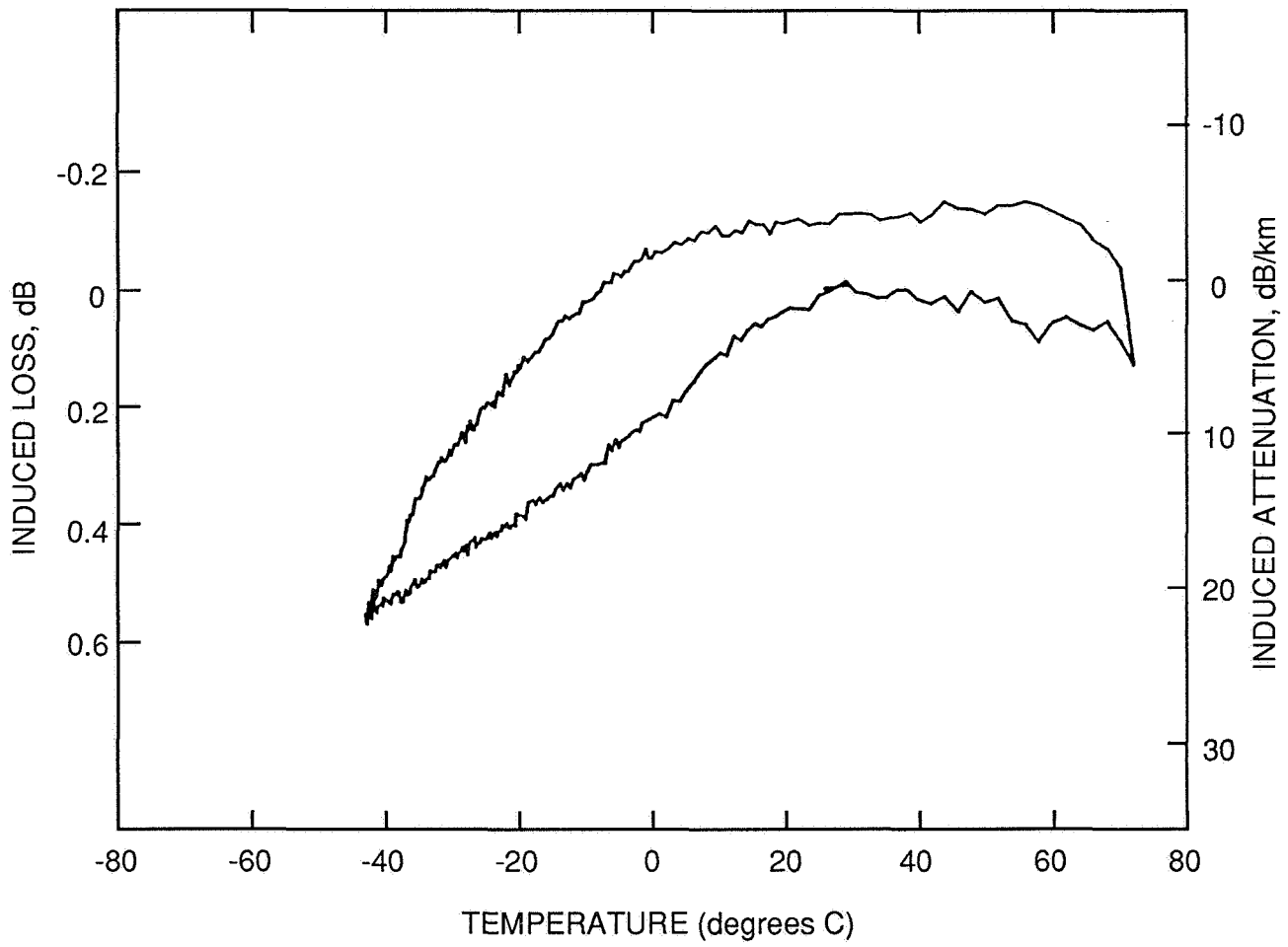

Figure 4. Temperature–induced loss for flight sample P–2 measured before the flight, in March 1983.

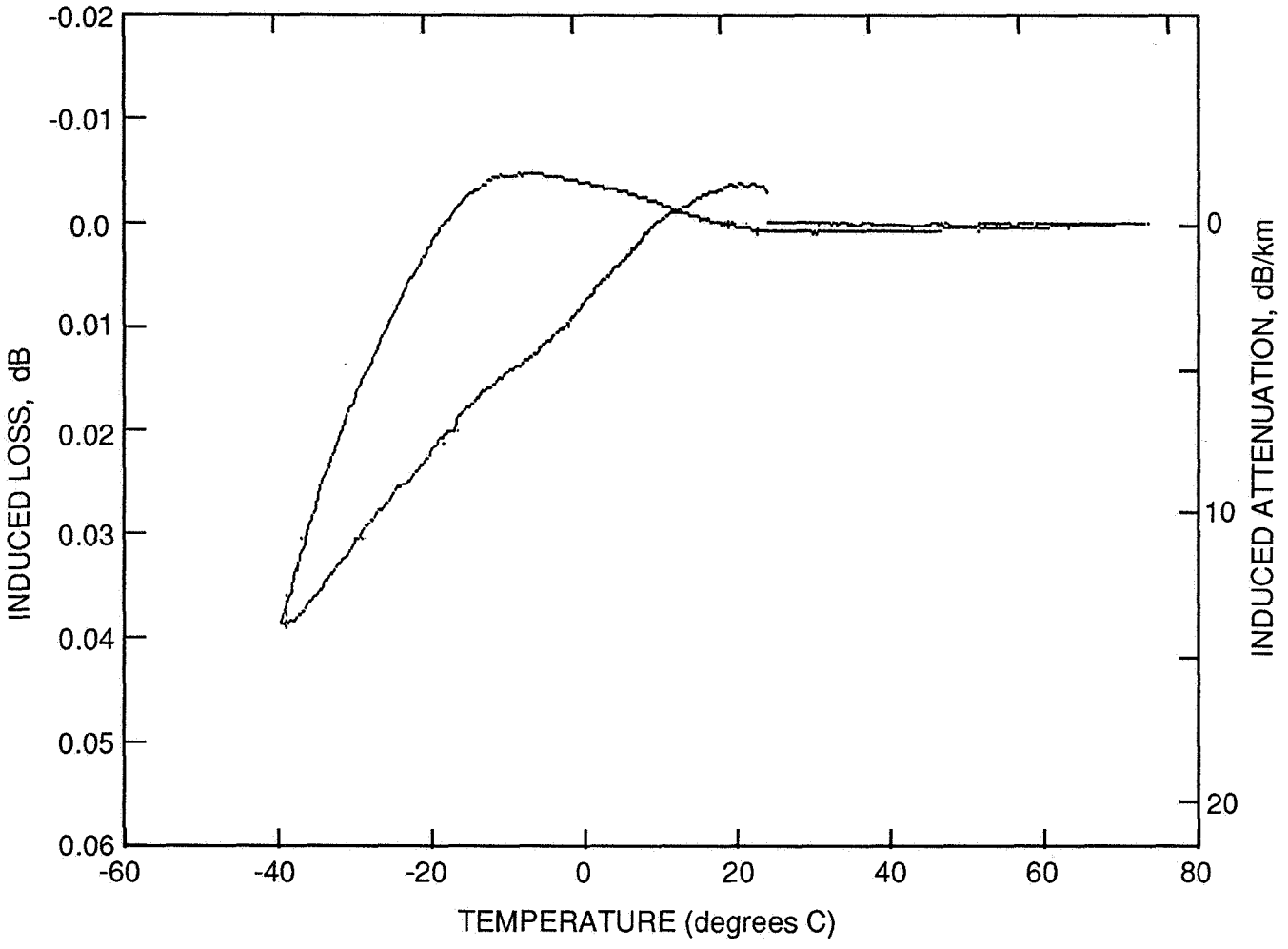

Figure 5. Temperature–induced loss for control sample P–2, measured post–flight, in February 1991.

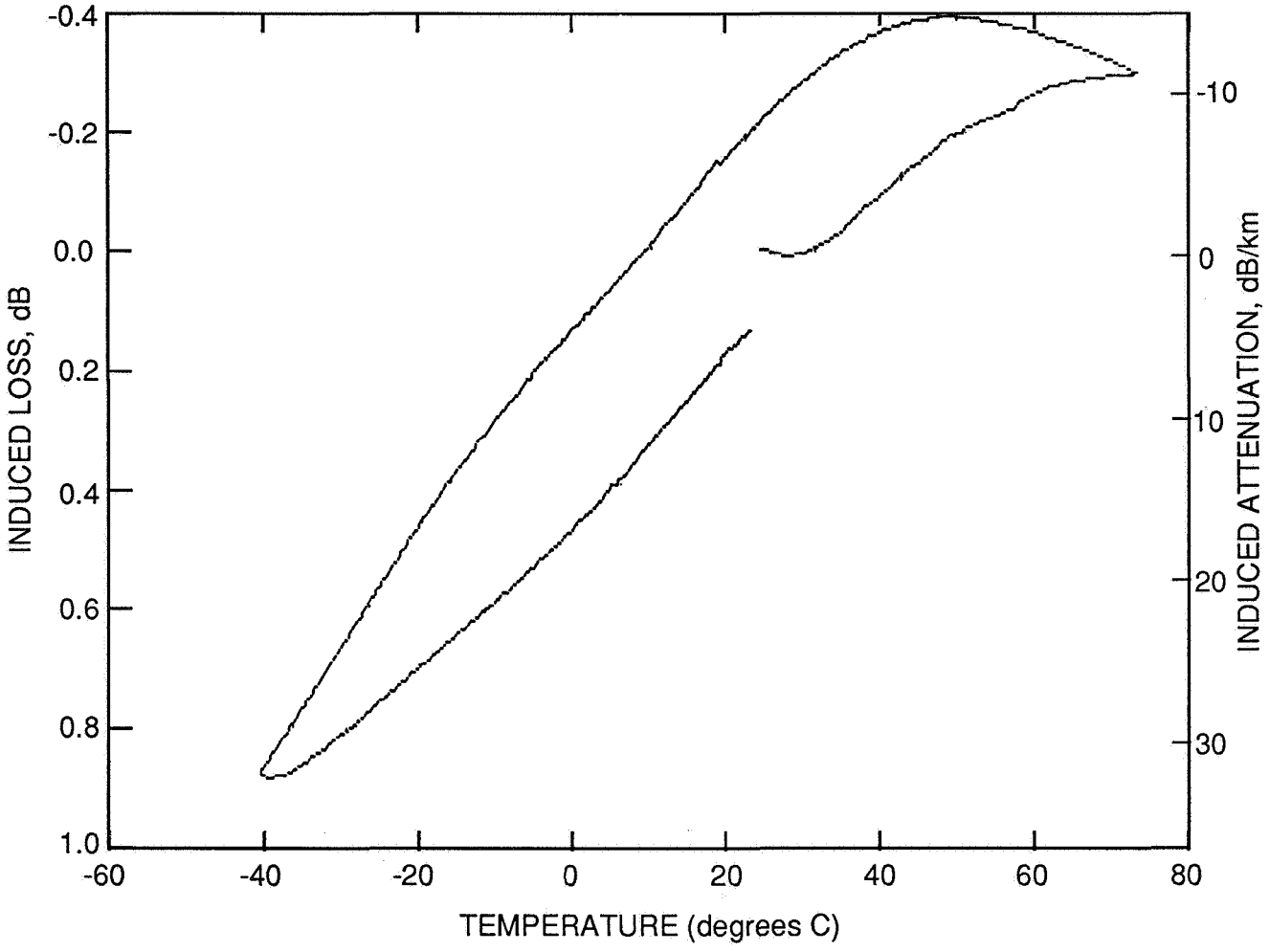

Figure 6. Temperature–induced loss for flight sample P–2, measured post–flight, in April 1991.

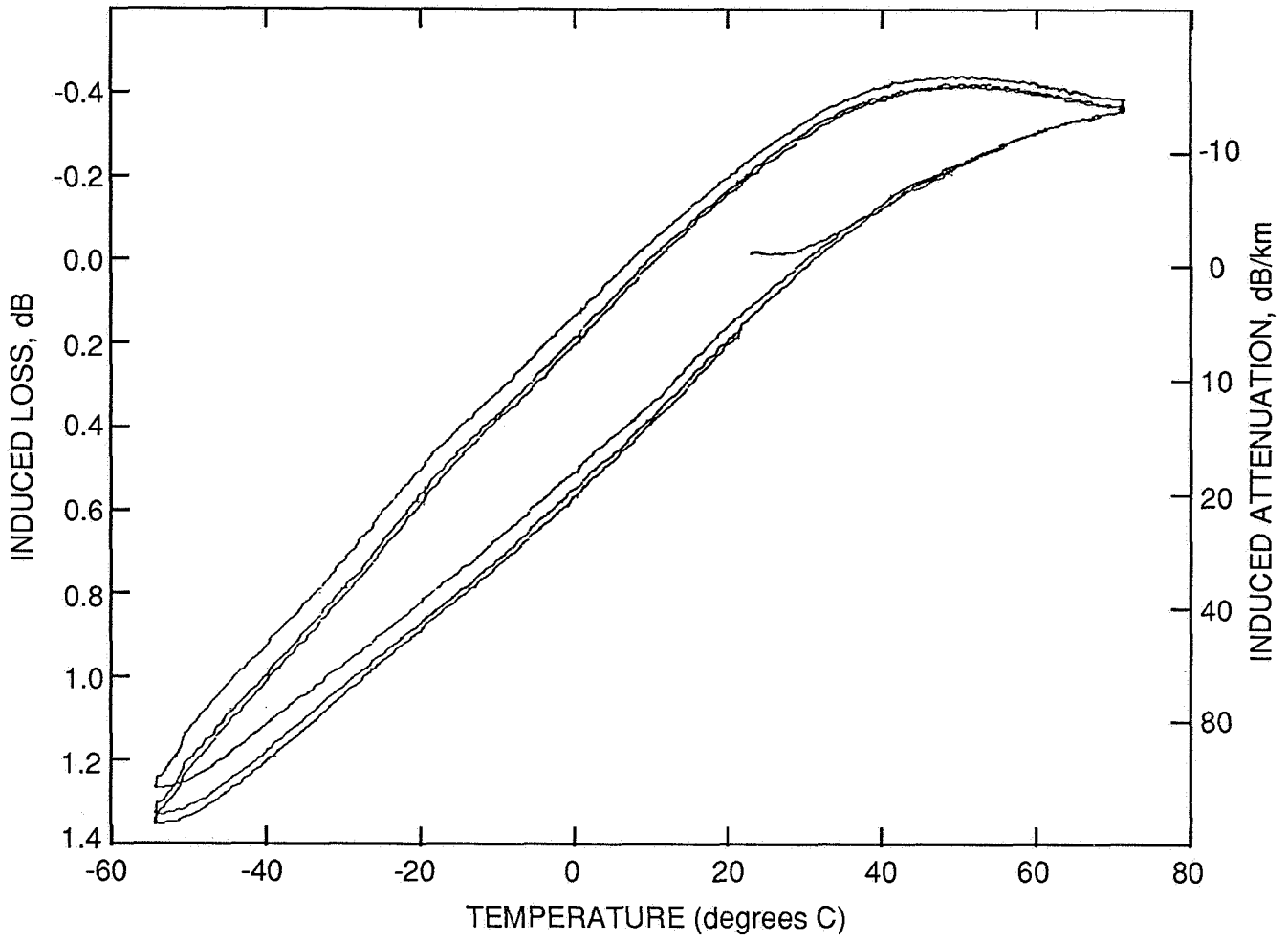

Figure 7. Temperature–induced loss for flight sample P–2, measured in September 1991.

The instrumental stability was improved significantly between the first and last tests. The pre–flight setup did not include stabilization of the LED power and was sensitive to room temperature. The stability was no better than 0.2 db. The latest instrumentation incorporated temperature stabilization of the electronics and compensation for changes in LED power and was stable to 0.01 db, possibly better if not disturbed.

We have assumed that the observed losses are distributed uniformly over the sample length, and that they can be described in terms of a loss per unit length (db/km). No measurements have been made during the temperature tests to verify this assumption, but no indication of non–uniform attenuation was found in our earlier OTDR tests. We feel that this assumption is a reasonable one.

The loss increment for the pre–flight test and the control sample are in agreement, and we feel the control sample data showing a change in loss of 23 db/km is the more reliable. The first post–flight test of the flight sample indicated a loss increment of 51 db/km and the subsequent multicycle test resulted in 1.65 db, or 63 db/km. Thus, there is a small, but probably not significant, increase between the two post–flight measurements of the flight sample, but a clear difference between the behavior of the control and flight sample. One other sample (C–6) showed similar behavior, but there was no clear difference between pre–flight and post–flight measurements for the other eight samples. The two samples showing the growth in temperature response were very poor performers under low temperature pre–flight. At this time, we are not able to explain these somewhat anomalous results in terms of the cabling configuration.

4.. ANALYSIS OF CONNECTOR CONTAMINATION

In the June 1991 LDEF Symposium, we reported that four of the twenty connector terminations had observable contamination on the polished end surface of the connector ferrule, although none of the foreign material appeared on the core area of any of the fibers. Since that time, we have subjected termination C–1b (from sample C–1), shown in Figure 8, to a more detailed analysis.

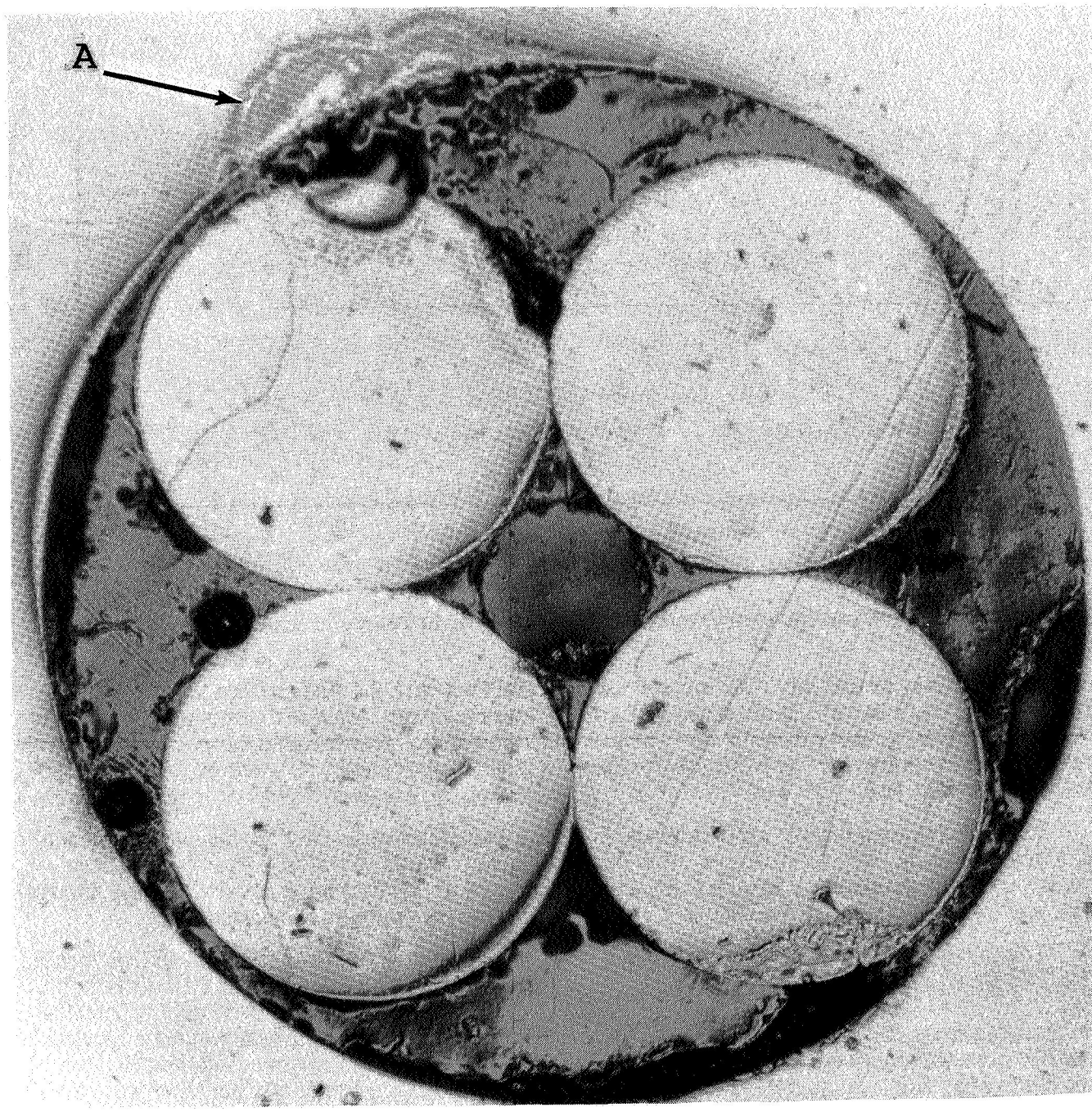

Figure 8. A photograph of termination C–1b showing deposit (A) which was determined to be epoxy material.

ORIGINAL PAGE
BLACK AND WHITE PHOTOGRAPH

The visible contaminant near the outer edge of the locating pins in the ferrule was examined spectroscopically in the IR (footnote 2). A fourier transform IR spectrometer adapted with a microscope was used to observe the light reflected from a very small selected area of substrate. The focal spot could be made as small as several microns in diameter to examine a small particle of material on the substrate (the polished ferrule surface).

In the photograph, Figure 8, the particle marked "A" was found to be epoxy and aliphatic amine epoxy curing agent. The conclusion is that for this connector, the epoxy material used in the termination was not properly mixed or cured. It may be desirable to devise techniques for quality assurance in this area for future flight hardware.

The particles seen on termination C–3a, not shown, were found to be foreign particles, not derived from materials in the fiber cable or connector. Thus, at this point, two (of the 20) terminations show deposits which are felt to be derived from materials used in cables and connectors, one from an unsuitable jacket material and one from the epoxy used to make up the connector termination.

The other conclusions stated in the earlier paper remain valid:

- There was no measurable attenuation due to connector contamination.
- Mated connectors would have had lower probability of contamination.

5. CONCLUSIONS

Radiation damage to optical fibers is well known, and there has been a great deal of work on the subject, extending over many years. There has been significant progress toward developing rad hard fibers since the 1982 time frame when these fibers were made. Our best fiber, sample P–1, with a specific radiation–induced loss of about 2–3 db/km–krad, would have been adequate for many applications. However, fibers have recently been developed with orders of magnitude less responsive to low–dose rate long term radiation, particularly at 1.3 μm. Several fibers have been reported with less than 10^{-2} db/km–krad, the lowest reported value being 10^{-4} db/km–krad for a long–term low dose rate exposure (ref. 8).

However, the basis for extrapolating laboratory data on annealing, most of which extend only to 1 day (10^5 sec) and some to $\sim$ 100 days is less firm, and the model is quite empirical in nature. Confirmation is needed that no annealing process is present with a long time constant, which may be overlooked when investigating the dominant short–term recovery. Our LDEF data, although not as accurate as we would like because of our short samples, lends support to the model used for extrapolation, at least out to 6 years. The hardest fibers appear to be those with pure fused silica cores, which have a short time constant for annealing. Fortuitously, their rapid recovery facilitates measurement of the annealing curve with a short–term test.

Much less effort has been dedicated to understanding temperature induced loss in detail, and it is quite possible that there is no single mechanism to understand. Although we found that one sample performed well, even after the order of 3 x 10^4 temperature cycles in orbit, most of our samples exhibited more than 10 db/km excess loss over the –55° to +70° C range, and would not be suitable for a long exposed run. Some were much worse. More work and more testing at low temperature would be productive. The progressive change in temperature behavior seen in sample P–2 is a separate, but probably overlapping issue. Both effects are felt to be a function of buffering and cabling, both in materials and in configuration.

Our general conclusions to date are the following, with the conclusions from our earlier paper restated and included:

- All our LDEF samples were functional and, with a few exceptions, would have performed well in a properly designed spacecraft system.

- The observed radiation darkening for the LDEF samples was consistent with an extrapolation from a 2–day laboratory recovery test.
- Connectors performed well, but quality control of epoxy cements is needed.
- Low temperature extremes should be avoided.

Long runs, of the order of 1 km or more, or exposed cable runs will require a thorough understanding of:

- Radiation–induced loss and its subsequent recovery.
- Temperature effects on cables.
- Outgassing and aging effects from polymers in cables and connectors.
- Risk of damage from micrometeoroid impacts.

The importance of these issues depends strongly on the application, both in terms of the environment seen by the fiber optic components and of the system configuration (i.e. link length). In a small system, tens of meters in extent, there is little cause for concern because adequate design margins are available. However, if the system is long enough to be loss–limited, or if the radiation environment is severe enough, then the first two issues, radiation damage and temperature extremes, may be quite important. Polymer aging and micrometeoroids are second order issues. Protection of exposed cable from micrometeoroid impacts is desirable, but note that the LDEF experience does not prove that fiber cables are more susceptible to damage than copper wires of comparable size.

There is another issue arising if extreme low temperature operation of the fiber cable is a possibility. Annealing of radiation–induced loss is thermally driven, and does not occur at low temperature (e.g. –70° C). As a result, the long–term low dose rate attenuation coefficient could increase by 1–2 orders of magnitude if the fiber stays cold (ref .7). Intentional photobleaching may alleviate this problem, but design to avoid sustained temperatures much below room temperature is a preferable approach, if possible.

To summarize, the LDEF experience has indicated that fiber optics can function well in a spacecraft system, and the most important design issues are radiation and low temperature.

ACKNOWLEDGEMENTS

The authors would like to acknowledge the contributions of project team member Shannon Jackson, who carried out the tests described in this paper. We thank Dave Shaw and Mike Wiedeman of JPL for their invaluable help in performing the radiation exposures. We also thank Joan Brandt for preparing the manuscript for publication.

The research described in this paper was carried out at the Jet Propulsion Laboratory, California Institute of Technology, and was sponsored by the National Aeronautics and Space Administration. Reference herein to any specific commercial product, process, or service by trade name, trademark, manufacturer, or otherwise, does not constitute or imply its endorsement by the United States Government, NASA, or the Jet Propulsion Laboratory, California Institute of Technology.

REFERENCES

[1] Johnston, A.R.; Bergman, L.A.; and Hartmayer, R.: LDEF Fiber Optic Exposure Experiment No. S–0109. Part 3. *Proceedings, First LDEF Post–Retrieval Symposium, Kissimmee, Florida.* NASA Conference Publication 3134, June 1991, page 1283.

[2] Johnston, A.R.; and Taylor, E.W.: *A Survey of the LDEF Fiber Optic Experiments.* JPL Report No. D–10069, 1992.

[3] Friebele, Joseph E.; Atkins, Charles G.; and Gingerich, Michael E.; Effect of Low Dose Rate Irradiation on Doped Silica Core Optical Fibers. *Applied Optics,* vol. 23, 1984, p. 4202.

[4] Friebele, E.J.; Long, K.J.; Askins, C.G.,;Gingerich, M.E.; Marrone, M.J.; and Griscom, D.L.: Overview of Radiation Effects in Fiber Optics. *SPIE Proceedings,* vol 541, 1985, p. 70.

[5] Benton, E.V;. and Heinrich, W.: *Ionizing Radiation Exposure of LDEF.* University of San Francisco Report, USF–TR–77, August 1990.

[6] Friebele, E.J.; Lyons, P.B.; Blackburn, J.C.; Henschel, H.; Johan, A.; Krinsky, J.A.; Robinson, A.; Schneider, W.; Smith, D;, Taylor, E.W.; Turquet de Beauregard, G.; West, R.H.; and Zagarino, P.: Interlaboratory comparison of radiation–induced attenuation in optical fibers. Part III: Transient exposures. *J. Lightwave Tech,* vol. 8, 1990, pp. 977–989.

[7] Friebele, E.J.; Askins, C.G.; Shaw, C.M.; Gingerich, M.E.; Harrington, C.C.; Griscom, D.L.; Tsai, T.E.; Paek, U–C.; and Schmidt, N.H.: Correlation of Single–mode fiber radiation response and fabrication parameters. *Appl. Optics*, vol. 30, 1991, p. 1944.

[8] Campbell, A.B., et. al. ; NRL Memorandum Report, 1992, p. 6982.

[9] Quan, F.; Lynn, M.; and Berkey, G.; A practical fiber coating system. *Proceedings FOC '80, 3rd International Fiber Optics and Communications Exposition.* Information Gatekeepers, Inc., 1980.

FOOTNOTES

1. Sample P–1 was packaged in a Siecor type 144 cable.
2. Anderson, Mark: JPL internal memo, May 18, 1992.

N93-29701

501757
B524

LONG DURATION EXPOSURE FACILITY (LDEF) LOW TEMPERATURE HEAT PIPE EXPERIMENT PACKAGE (HEPP) FLIGHT RESULTS

Roy McIntosh
NASA Goddard Space Flight Center
Greenbelt, Maryland 20770
Phone: 301/286-8618, Fax: 301/286-6237

Craig McCreight
NASA Ames Research Center
Moffett Field, CA 94035-1000
Phone: 415/604-6549, Fax: 415/604-6997

Patrick J. Brennan
OAO Corporation
Greenbelt, Maryland 20770
Phone: 301/345-0750, Fax: 301/286-6237

SUMMARY

The Low Temperature Heat Pipe Flight Experiment (HEPP) is a fairly complicated thermal control experiment that was designed to evaluate the performance of two different low temperature ethane heat pipes and a low-temperature (182°K) phase change material. A total of 390 days of continuous operation with an axially grooved aluminum fixed conductance heat pipe and an axially grooved stainless steel heat pipe diode was demonstrated before the data acquisition system's batteries lost power. Each heat pipe had approximately 1 watt applied throughout this period. The HEPP was not able to cool below 188.6°K during the mission. As a result, the preprogrammed transport test sequence which initiates when the PCM temperature drops below 180°K was never exercised, and transport tests with both pipes and the diode reverse mode test could not be run in flight. Also, because the melt temperature of the n-heptane PCM is 182°K, its freeze/thaw behavior could not be tested.

Post-flight thermal vacuum tests and thermal analyses have indicated that there was an apparent error in the original thermal analyses that led to this unfortunate result. Post-flight tests have demonstrated that the performance of both heat pipes and the PCM has not changed since being fabricated more than 14 years ago. This paper presents a summary of HEPP's flight data and post-flight test results.

PRECEDING PAGE BLANK NOT FILMED

INTRODUCTION

A schematic of the HEPP is presented in Figure 1. This system contains an axially grooved aluminum constant conductance heat pipe (CCHP) and a stainless steel axially grooved liquid trap diode heat pipe (DHP). Both heat pipes use ethane as the working fluid for operation in the range of 150 to 250°K. The condenser of each heat pipe is thermally coupled to a radiant cooler system. A phase change material (PCM) canister is integrated with the radiator to provide temperature stability at its 182°K melting point. The PCM is n-heptane and it is used to provide a 27 watt-hr latent heat capacity for constant temperature operation during transport tests. Data acquisition and data recording were provided by an Experiment Power Data System (EPDS) which was integrated with the HEPP in Tray F12.

Power to the HEPP's electronics module was provided by a Direct Energy Transfer (DET) Power System which included a 12-ampere-hour, 28 VDC Nickel Cadmium battery, four solar array panels and power system electronics. The DET was installed into Tray H1 and connected by power cables to the HEPP in Tray F12. Analysis of the flight data shows that the power system provided nominal operation without any anomalies over the 390 days of recorded data. Nominal DET operation was also demonstrated prior to deintegration from LDEF at KSC. A detailed discussion of this system is presented in Reference 1.

In addition, five sets consisting of a total of 65 thermal control coating samples were attached to trays F12, H1 and F9 for evaluation with the HEPP. Flight results for these samples are presented in Reference 2.

The LDEF and its extended mission provided a unique opportunity for the long term evaluation not only of the ethane heat pipes but also of the various space flight subsystems that were needed to support the HEPP. This paper summarizes results obtained for the heat pipes, the PCM, the HEPP's electronics module and instrumentation, and the EPDS.

EXPERIMENT DESCRIPTION

A schematic of the total HEPP Experiment System is presented in Figure 2. The structural support of the HEPP is provided by a welded stainless steel tubular assembly. A primary radiator and specular shield surfaces, fabricated from aluminum and coated with silver teflon and vapor deposited aluminum respectively, are fastened to this frame. The cooler's radiator/shield configuration is designed to minimize parasitic heat inputs from the sun, earth and spacecraft while maximizing radiation to space. Thermal isolators are employed at all structural mounting locations and multi-layer insulation (MLI) blankets cover the experiment components and all inboard surfaces.

The HEPP assembly also includes an electronics module for signal conditioning and power sequencing, kapton foil heaters and platinum resistance temperature sensors (PRTs). The HEPP and its EPDS were flown in Tray F12. The HEPP EPDS also recorded

Figure 1. Low Temperature Heat Pipe Experiment Package (HEPP)

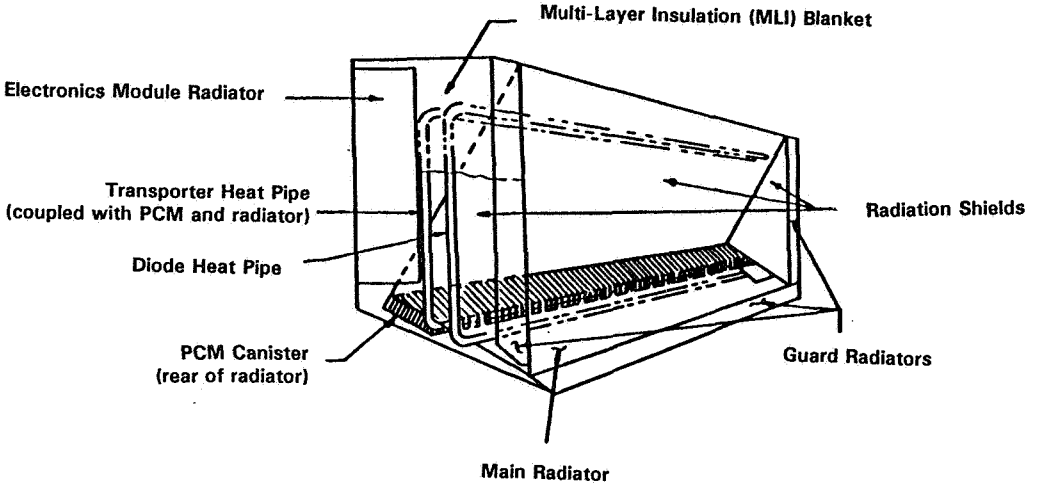

Figure 2. HEPP System Description

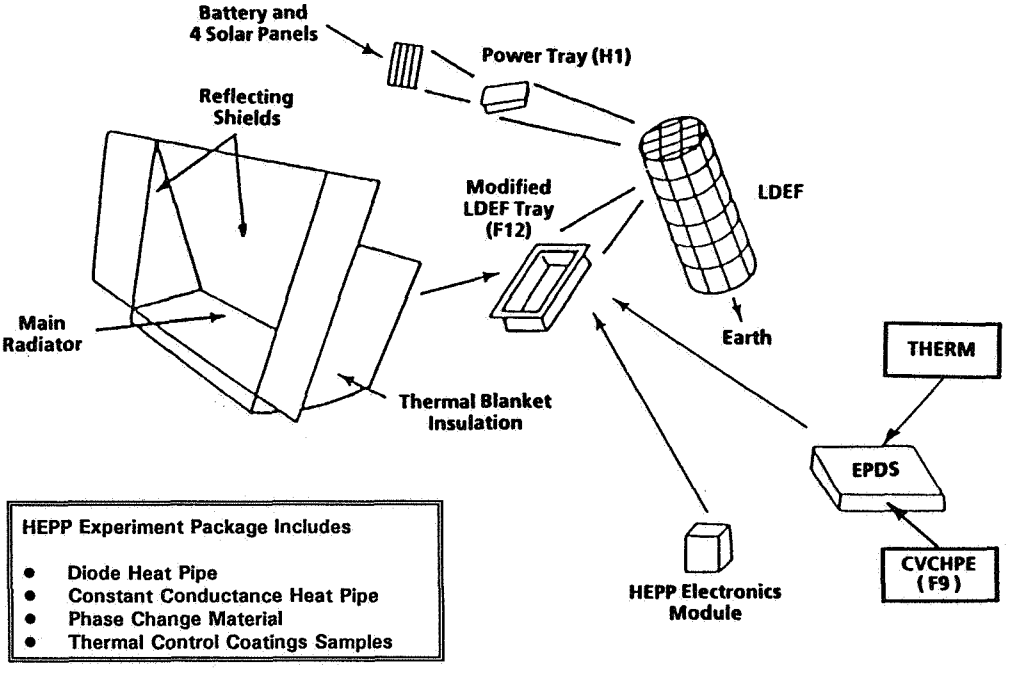

temperature data from six thermocouples and two thermistors from the THERM (P0003)[3] and 6 thermistors from the CVCHPE (A0076)[4] experiments. Figure 3 provides an electrical block diagram for the HEPP and its interfaces with THERM and CVCHPE. HEPP subsystems and components are summarized in Table 1.

COMPONENT DESCRIPTION

Constant Conductance Heat Pipe (CCHP)

The CCHP is an axially grooved design which was extruded from 6063 aluminum alloy. The grooved tubing was originally developed for the ATS-F heat pipe program and has well defined performance characteristics.[5] This heat pipe was selected to demonstrate the application of low cost, high reliability axially grooved heat pipe technology in the low temperature and cryogenic ranges. The CCHP is charged with ethane and will operate in the 120° to 270°K range. It has a predicted "0-g" heat transport capability of 33-watt-meters at 180°K. A design summary of the CCHP is presented in Table 2.

Thermal Diode Heat Pipe

The thermal diode heat pipe which was furnished by the NASA-Ames Research Center employs a liquid trap to accomplish shutdown in the reverse mode. It consists of cold forged axially grooved stainless steel tubing charged with ethane. The stainless steel provides a high strength, low thermal conductance envelope which minimizes axial conduction effects during reverse mode shutdown. A reservoir is attached to the evaporator end of the pipe and it contains a stainless steel wire mesh core which acts as a liquid trap during shutdown. A design summary of the diode heat pipe is presented in Table 3.

PCM Canister

The phase change material (PCM) canister is located on the underside of the experiment's main radiator and is thermally coupled to both heat pipes and the radiator. The heat dissipation capability of the radiator at the nominal test temperature (182°K) is substantially less than the heat loads associated with the maximum heat transport limits of either pipe. The PCM canister was included to provide a constant temperature heat sink during transport tests by absorbing up to 27 W-hr of latent energy through its melting process.

The n-heptane PCM material is contained within a Tungsten Inert Gas (TIG) welded aluminum rectangular box which is filled with a partially expanded aluminum honeycomb core. The high conductance of the honeycomb in combination with its large contact area with the PCM results in a high thermal diffusivity which provides good response with

Figure 3. HEPP Electrical Block Diagram

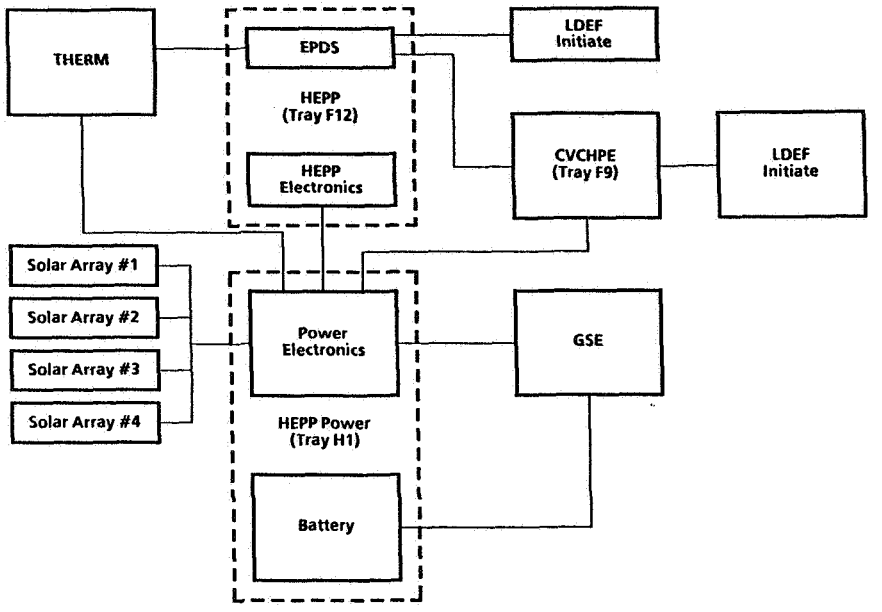

Table 1. HEPP Subsystems and Component Summary

THERMAL

1. Ethane/Aluminum Axially Grooved Heat Pipe.
2. Ethane/Stainless Steel Axially Grooved/Liquid Trap Diode Heat Pipe.
3. n-Heptane/Aluminum Phase Change Material Canister.
4. Low Temperature Radiator/Shield System Including Silver Teflon and VDA Optical Surfaces.
5. Platinum Transducers (28 PRTs) and Nichrome Ribbon and Kapton Foil Resistance Heaters.
6. MLI Blankets, Velcro Fasteners, Phenolic Snaps and Fasteners.
7. Bonding Compound for PRTs and Tape for Blankets, G-10 Fiberglass and Thermal Isolators.
8. 65 Thermal Control Samples.

ELECTRICAL

1. Electronics Module Including Signal Conditioning and Power Sequencing Command Logic.
2. EPDS Including Lithium Battery, Data Acquisition, Power Conditioning and Magnetic Tape Recorder.
3. HEPP DET System Power Supply
   - Nickel Cadmium Battery
   - Solar Array (4 Panels)
   - Power Conversion & Conditioning Electronics
4. Current and Voltage Sensors, Connectors and Harnesses.

MECHANICAL

1. HEPP Stainless Steel Tubular Structure.
2. DET Honeycomb Baseplate and Bond Materials.
2. LDEF Trays (F12 & H1)

Table 2. Constant Conductance Heat Pipe (CCHP) Design Summary

Wick Configuration	ATS Extruded Axial Groove (27 Grooves)	
Material	Ethane	
Working Fluid	6063 Extruded Aluminum	
Operating Temperature Range	120° - 270°K	
Geometry	in.	cm
O.D.	5/8	1.59
Lengths		
Overall	50.8	129.0
Evaporator	6.0	15.2
Adiabatic	26.8	68.1
Condenser	18.0	45.7
Effective	38.8	98.6
Internal Pressure @ 27°C	630 psia	
Burst Safety Factor @ 27°C	7.1	
Transport Capacity (0-g)	33 W-m @ 180°K	
Conductance	5.0 W/°C	

Table 3. Liquid Trap Diode Heat Pipe Design Summary

Wick Configuration		
Heat Pipe	Axially Grooved (20 Grooves)	
Liquid Trap Reservoir	30 Mesh Cylindral Slab, 100 Mesh Bridges, Circumferentially Grooved Wall	
Material	Stainless Steel	
Working Fluid	Ethane - 9.0g	
Operating Temperature Range	120° - 270°K	
Geometry	in.	cm
Heat Pipe O.D.	413	413
Heat Pipe Lengths		
Overall	46.85	46.85
Evaporator	4.0	4.0
Adiabatic	24.45	24.45
Condenser	18.40	18.40
Effective	35.65	35.65
Reservoir O.D.	1.00	2.54
Reservoir Length	4.00	10.16
Internal Pressure @ 70°C	815 psia	
Burst Safety Factor @ 70°C	9.5	
Transport Capacity (0-g)	16.4 W-m @ 180°K	

Table 4. PCM Canister Design Summary

Canister - Construction	TIG Welded 6061-T6 Aluminum Assembly
Core	3/16-in. Cell by 0.002-in. Thick 5052 Aluminum Honeycomb
Adhesive	Hysol Ea 934
PCM	753-g of n-heptane
Heat Storage Capacity	27 W-hr
Minimum Thermal Conductance	8 W/°C
Total Weight	2.73 Kg (6.02 lb)

minimum temperature drops across the canister. The PCM design is summarized in Table 4 and Reference 6.

Radiant Cooler System

The main radiator uses silver teflon (α/ϵ = 0.12/0.76) as its optical coating. This radiator is oriented parallel to the earth's limiting ray to eliminate direct albedo inputs. For the LDEF's average orbital altitude (225 nautical miles) the radiator was tilted 71° with respect to the earth's normal.

The main radiator is partially surrounded by shields that were fabricated from aluminum sheet and coated with vapor deposited aluminum (VDA) which has optical properties of α/ϵ = 0.13/0.04. These specular shields increase the radiator's net heat rejection by reducing direct inputs from the sun and spacecraft and by minimizing reflected albedo as well as reflected and direct infrared inputs. Auxiliary guard radiators, which are integral flanges extending from the shields, are coated with silver teflon to reject heat conducted from the shields and effectively reduce shield temperatures. This further reduces infrared inputs to the main radiator.

Structure

The support structure for the HEPP is a welded assembly of 0.5-inch diameter stainless steel tubing which is attached to a 0.69-inch thick aluminum baseplate in four (4) places by fiberglass isolators. This frame supports the radiator and shields, the heat pipes, and PCM canister. Thermal isolators are used at all attachment locations to minimize conductive parasitics.

Insulation

Multi-layer insulation (MLI) blankets cover all inboard surfaces of the HEPP and where possible completely envelop the heat pipes and PCM canister. The blankets consist of 14 layers of 1/3 mil double aluminized Kapton separated by Dacron cloth. One milsingle-sided aluminized Kapton is used for the external layers of the blankets with the Kapton side out. Velcro was used to attach the blankets to the various surfaces.

Instrumentation

The HEPP was instrumented with 28 platinum resistance (500 ohm) thermometers (PRTs) to measure temperatures throughout the experiment. Three of these measured battery temperatures in Tray H1. Nichrome ribbon heaters or Minco Kapton foil heaters were installed to provide electrical heat loads to the evaporators of each heat pipe, and to the main radiator to raise its temperature for diode reverse mode tests. The heaters were attached to

the surfaces using Kapton tape. Voltages and currents were also measured to provide battery performance data and to determine applied heater power throughout the mission.

Power and Electronics

Power for the experiment is provided from two separate sources. A standard LDEF Experiment Power and Data System (EPDS) uses lithium batteries to power the data acquisition and recording portions of the experiment. Power for the experiment heaters, signal conditioning, command sequencing and execution of the experiment logic is provided to the HEPP electronics module by the DET which is mounted in a separate tray on the space viewing end of the LDEF.

EXPERIMENT OBJECTIVES

Primary objectives for the HEPP in their order of precedence can be summarized as follows:

1. Record temperature data for the HEPP, CVCHPE and THERM experiments.
2. Demonstrate long-term low temperature heat pipe operation (180-250°K).
3. Evaluate low-temperature heat pipe start-up from near super-critical conditions.
4. Determine heat pipe transport limits and thermal conductances.
5. Evaluate diode heat pipe reverse mode shutdown and restart.
6. Evaluate the low temperature PCM canister's performance including energy storage capacity, freeze/thaw characteristics, subcooling effects and thermal conductance.
7. Evaluate the thermal performance of a heat pipe/radiant cooler system.

Secondary objectives included:

8. An evaluation of the effect of the Flight Environment on 65 thermal control samples, MLI blankets and solar cells.
9. An evaluation of long-term nickel-cadmium battery performance.
10. An evaluation of the long term effect of the flight environment on electronics, instrumentation, and thermal and mechanical interfaces and subsystems.

Achievement of the first three objectives represents the minimum success criterion for the HEPP.

FLIGHT RESULTS

Operation of the HEPP commenced upon deployment of the LDEF when the HEPP radiator system began to cool down. Also, upon deployment of the LDEF, its initiate is activated and simultaneously power from the DET is transferred to the HEPP electronics module which was preprogrammed to apply 1.2 watts and 1.0 watt to the evaporator heaters of the diode, and CCHP, respectively. This is the HEPP's long term forward mode and also its default mode. During this mode, data is collected every 112 minutes. This mode of operation was exercised immediately to insure that minimum success was achieved. Unfortunately, with the 2.2 watts applied the PCM never cooled below 192°K and the programmed sequence for transport tests and diode reverse mode shutdown and restart could not be executed. These tests were to be performed after the PCM had frozen and its temperature dropped below 180°K. This temperature was selected consistent with the PCM's 182°K melt temperature so that the PCM would freeze and then it's heat of fusion would provide a constant temperature heat sink for the heat pipe transport tests.

Post flight thermal analyses and thermal vacuum tests confirmed that there was an apparent error in the original thermal model that resulted in overestimating the HEPP radiator's cooling capacity. Time and resource constraints prohibited conducting TV tests with the HEPP after its radiator and shields had been modified for flight aboard the LDEF. This test might have uncovered the problem and the flight program sequence adjusted to accomplish all objectives.

Fortunately, minimum success was achieved and good complete data for the first 390 days was obtained for the HEPP and THERM. Temperature data for the CVCHPE was also obtained for its first 45 days of operation until its thermistor circuit battery lost power. In addition to accomplishing the first three objectives, the thermal performance of the heat pipe radiant cooler system was evaluated and correlated with an updated thermal model. Also, all secondary objectives were accomplished with extensive data obtained. Preliminary results for the DET and thermal control samples are published in References 1 and 2.

Heat Pipe Flight Data

Figures 4 and 5 show the transient cycling of the evaporator and condenser sections of the CCHP and the DHP, respectively. The temperature cycling is due to changes in the external environment that affect the net cooling capacity and correspondingly the temperature of the HEPP radiator. The temperature drops across each heat pipe are shown in Figure 6. These results show that both heat pipes are nearly isothermal with continuous operation over the range of 192°K to 260°K throughout the 390 days of recorded data. In flight, the diode evaporator's temperature drop is less than 1°C whereas ground tests show more than a 15°C temperature drop at the diode's evaporator when it is "dried-out" at an adverse tilt. A 10°C drop was observed in the CCHP when it was "dried-not" with 1.0 watt applied versus the average 0.6°C drop recorded in flight.

Figure 4A. CCHP Evaporator - Location A

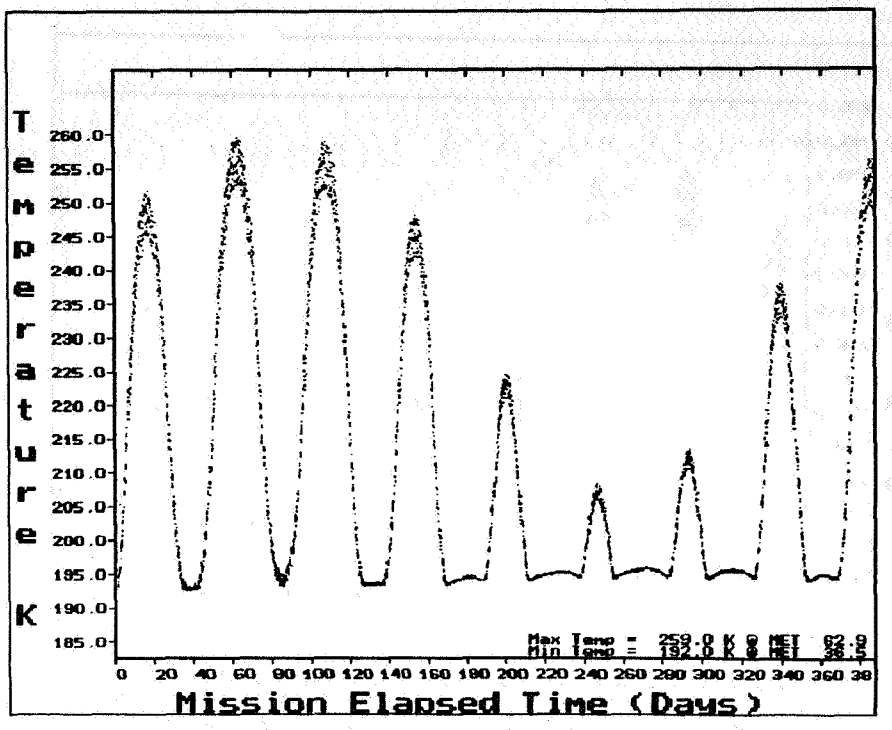

Figure 4B. CCHP Condenser - Location C

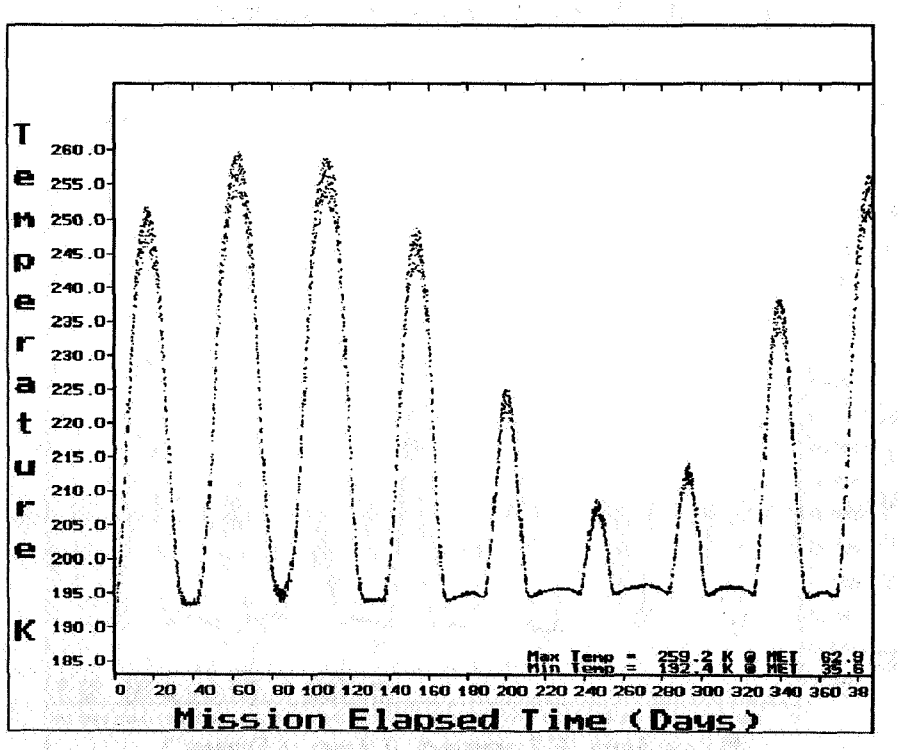

Figure 5A. Diode Evaporator - Location A

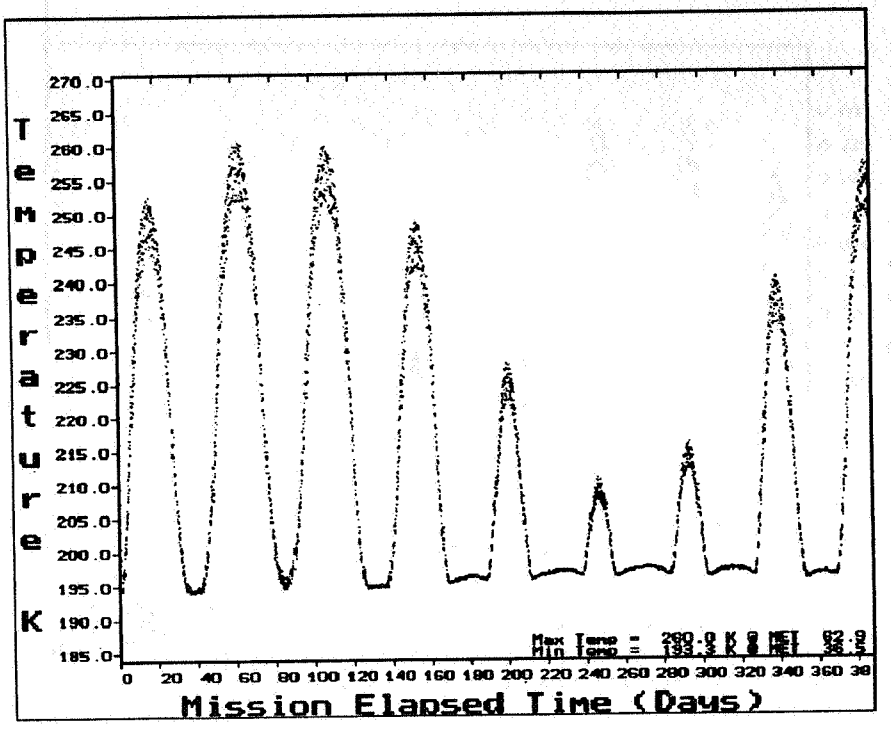

Figure 5B. Diode Condenser - Location C

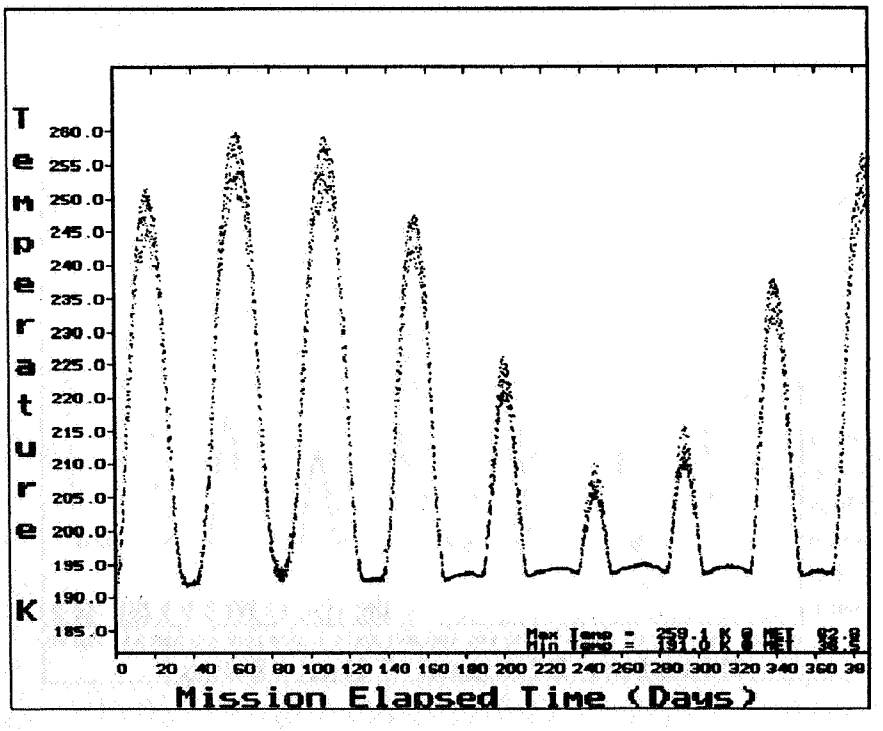

Figure 6A. CCHP Temperature Drops vs Mission Time at Maximum and Minimum Beta Angles

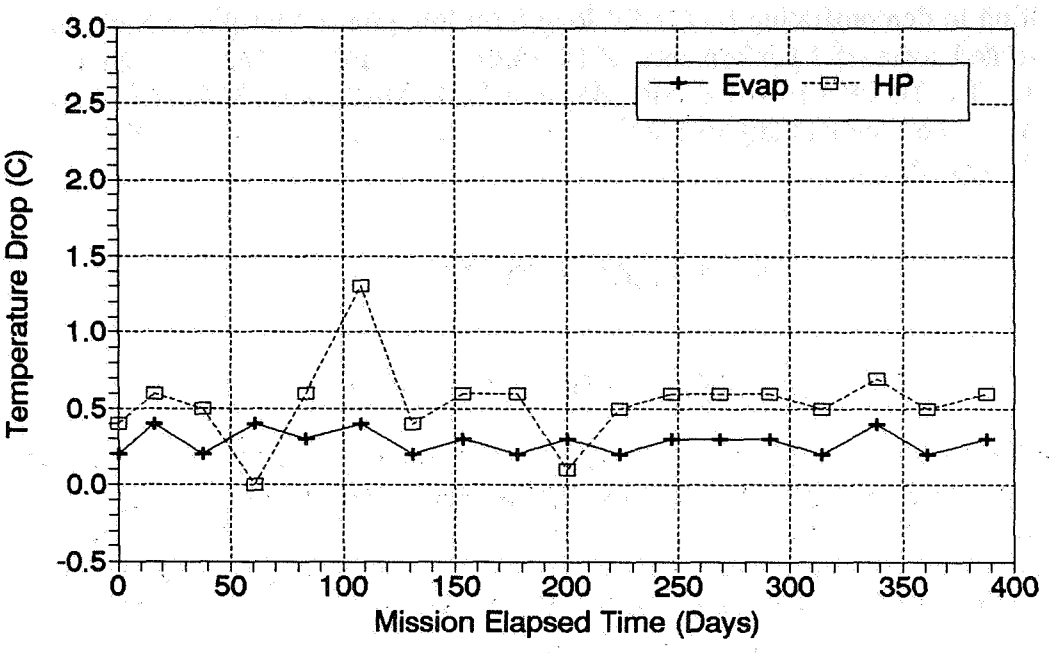

Figure 6B. Diode HP Temp. Drops vs Mission Time at Maximum and Minimum Beta Angles

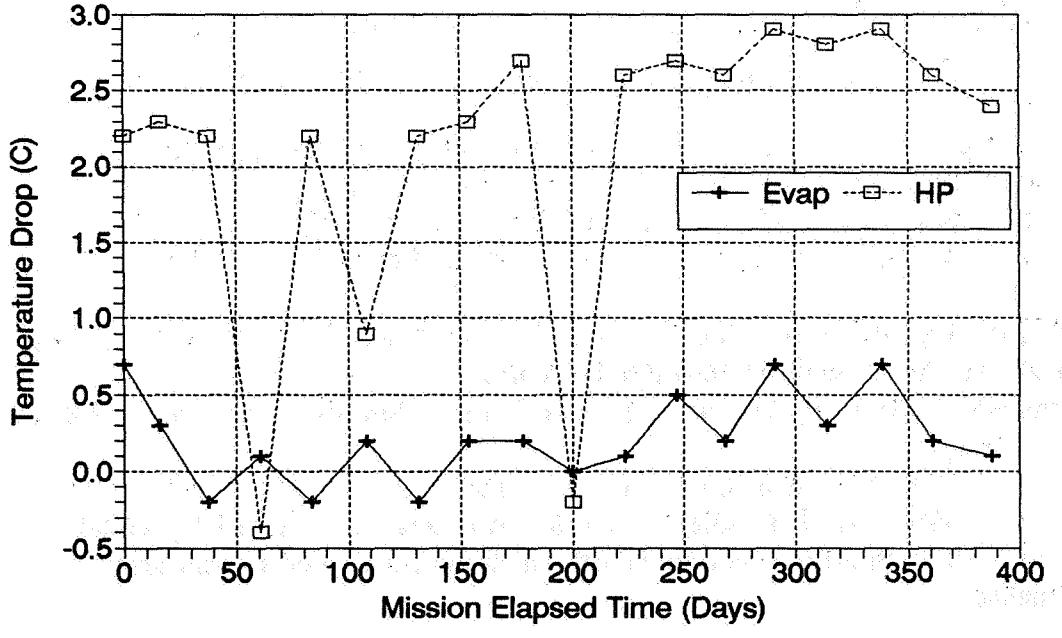

Radiator and PCM temperatures are shown in Figure 7. These temperatures are essentially the same since the PCM is attached directly to the HEPP radiator as are the condenser sections of each heat pipe. The temperature cycling corresponds directly to the orbital variations in the solar heat flux that occur throughout the mission.

In addition to demonstrating successful long term low power heat pipe operation, the HEPP demonstrated successful performance of the electronics module, and associated instrumentation. The HEPP's EPDS and its Magnetic Tape Memory (MTM) and lithium batteries also performed without any difficulty. The HEPP's DET battery and solar arrays also performed as designed.

POST FLIGHT RESULTS

HEPP/CVCHPE/THERM/LDEF Integrated Test Results

A functional test was conducted with the HEPP (Trays F12 and H1), the CVCHPE (Tray F9), and the THERM integrated with the LDEF prior to Deintegration at KSC. Before conducting this test, the lithium batteries in each experiment were disconnected and GSE NiCad cells were connected with GSE harnesses. The HEPP NiCad flight battery which is contained in Tray H1 was discharged and recharged two days earlier. The Integrated Test is basically a functional check of the various electrical subsystems for each experiment.

The following is a summary of the results obtained from analysis of the HEPP NiCad battery data and the Integrated Test data.

1. All electronics systems including the EPDS, HEPP's Electronics Module, and the DET's electronics functioned properly.
2. All HEPP power profiles were executed indicating that the experiment heaters were in working condition and that the preprogrammed test sequence could have been executed.
3. All telemetry was within calibration for the ambient temperature operation.
4. The flight battery was essentially at 0 voltage across each of the 18 cells. It recharged rapidly (within 30 hours) and uniformly across each cell. The third electrode "came on" within approximately 12 hours after each cell had reached 1.4 volts.
5. The HEPP relay latched on when the third electrode reached a pressure of 250 psi which was consistent with its pre-flight behavior.
6. The temperature data for the heat pipes indicated that they still contained an ethane fluid inventory.
7. Each of the solar arrays was illuminated individually with a high intensity halogen lamp at the conclusion of the Integrated Test. An increase in the battery voltage was observed when each array was illuminated which indicated good overall array performance.

Figure 7A. Main Radiator - Location C

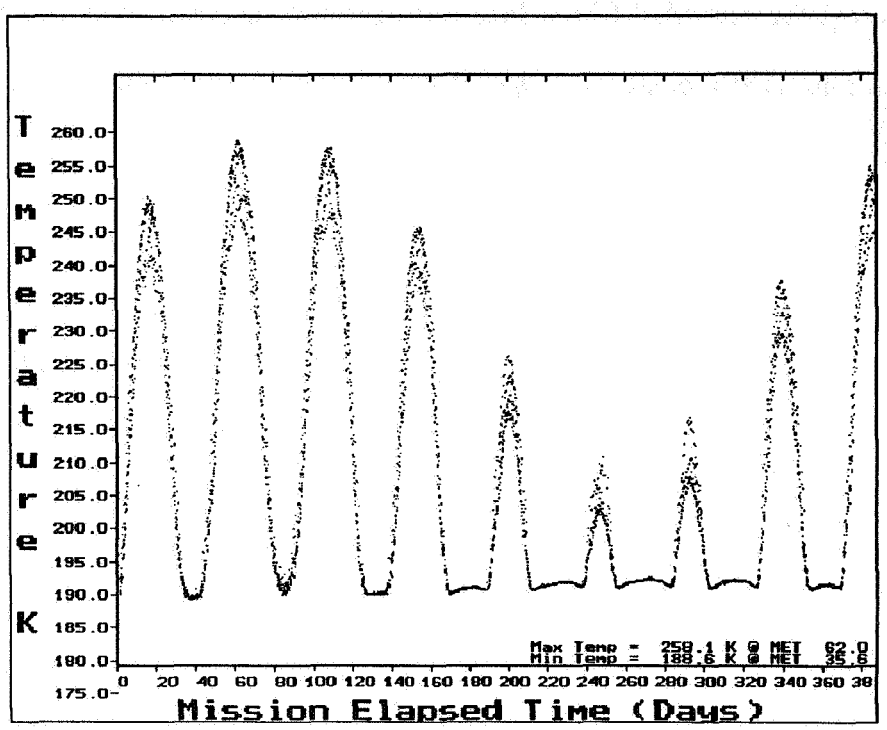

Figure 7B. PCM - Location C

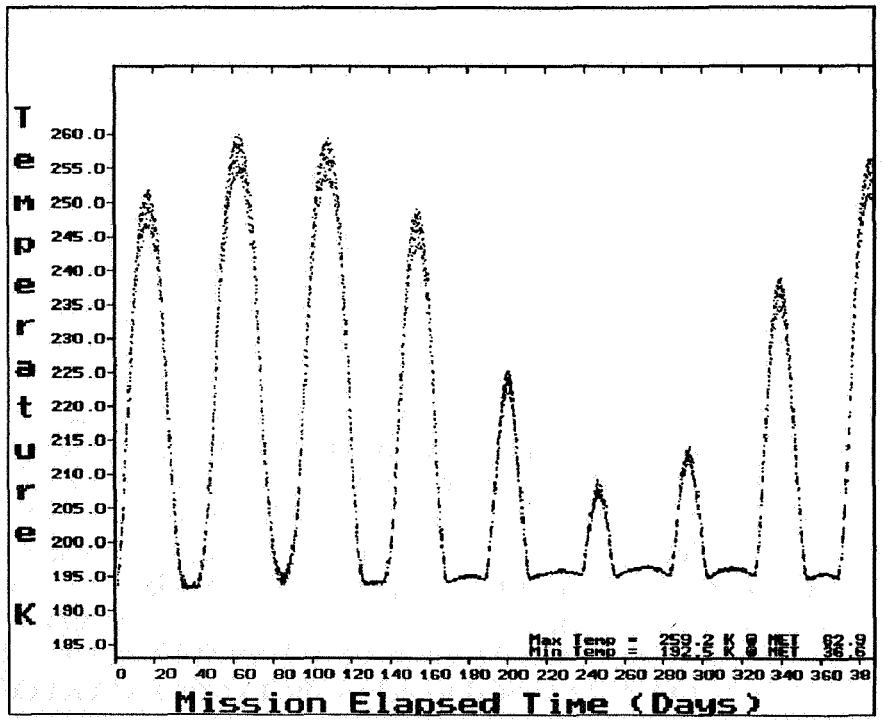

8. Data recording through the EPDS was demonstrated with an alternate flight recorder. The flight MTM had been removed approximately one month earlier to transcribe the flight data. This component was determined to be in good operating condition and the recorded flight data was complete and had good quality.

In summary, all HEPP electrical systems were functioning properly after retrieval. Visual observations and the Integrated Test data indicated that the mechanical and thermal integrity of the HEPP were also intact.

Thermal Vacuum Tests

The HEPP was removed from its LDEF tray and installed into a test fixture that was fabricated to conduct thermal vacuum (TV) tests. This fixture included a liquid nitrogen cold plate to simulate the HEPP's radiation in deep space. Electrical heaters were attached to permit simulation of external solar, infrared and albedo inputs. A Ground Test Set was used to replace the EPDS and operate the HEPP electronics module. Tests were conducted in the large chamber in the Optical Coating Laboratory at Goddard Space Flight Center. Once the fixture was installed into the chamber its tilt was adjusted so that the two heat pipes which are coplanar were at an adverse tilt with the evaporator leg located above the condenser leg. The TV tests were conducted to accomplish the following objectives:

1. Simulate flight conditions and obtain transient cooldown temperature data for comparison with the flight data and correlation with thermal models.
2. Measure the heat transport capability of each heat pipe at two adverse elevations for comparison with pre-flight data.
3. Observe the freeze/thaw characteristics of the PCM canister and compare with pre-flight data.

A comparison of flight and TV test data is given in Figure 8 for the HEPP's radiator which is less than 1°K cooler than the PCM temperature. This data is for the "Long Term Forward Mode" of operation. This corresponds to the Flight Mode with 1.2 watts applied to the DHP and 1.0 watts applied to the CCHP. Flight data is for the first 36 hours of HEPP operation after LDEF deployment. These temperatures were the coldest that the HEPP ever achieved. The transient cooldown and steady state temperatures are essentially identical with the lowest temperature being 192.5 °K both in flight and in the TV test. Since the updated thermal model had correlated flight data, the close match of the TV test and flight data tends to imply that the updated model is correct.

The difference between the updated simplified model and the original thermal model appeared to be that the radiative parasitics from the LDEF's interior were not properly coupled to the HEPP's radiator and shields in the original model. This resulted in these parasitics having an insignificant effect on the HEPP radiator's predicted net cooling capacity. The net effect is that a higher heat rejection rate at a given radiator temperature and faster cooldown were predicted with the original thermal model. This condition was simulated in the TV tests by cooling the chamber walls with liquid nitrogen to eliminate parasitic input from the chamber. When the Long Term Forward Mode was repeated, the result was that the radiator and PCM cooled to below the freezing temperature of the

Figure 8. Comparison of Flight Data to TV Data for Radiator Cooldown- Long Term Forward Mode

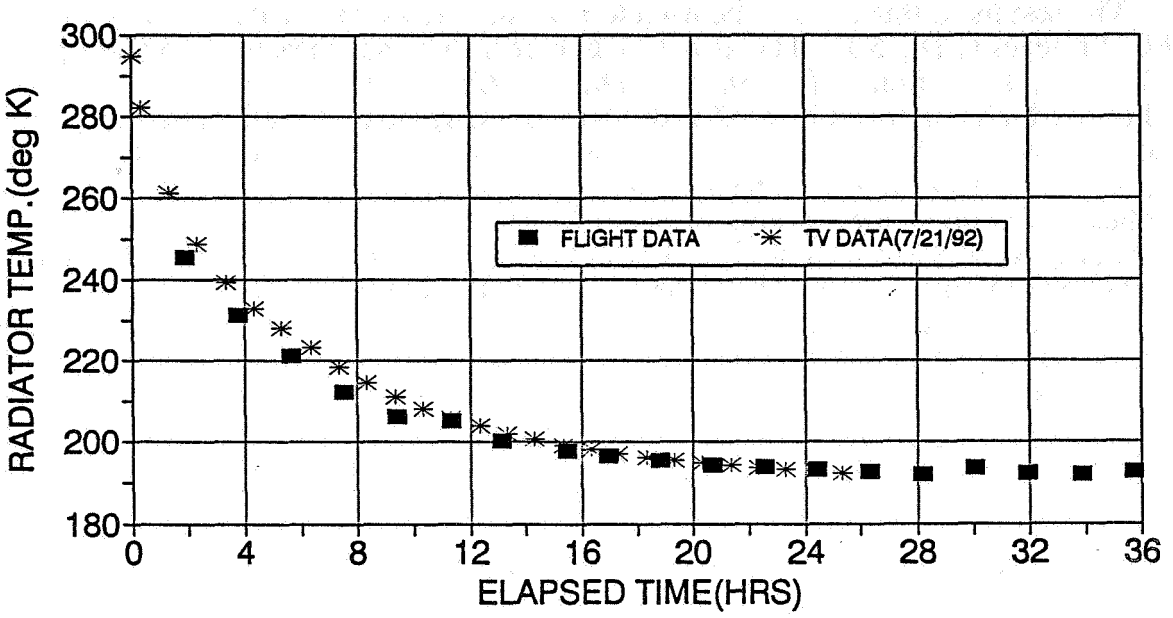

Figure 9. Long Term Forward Mode Cooldown with Cold Plate and Chamber Shroud LN Cooled

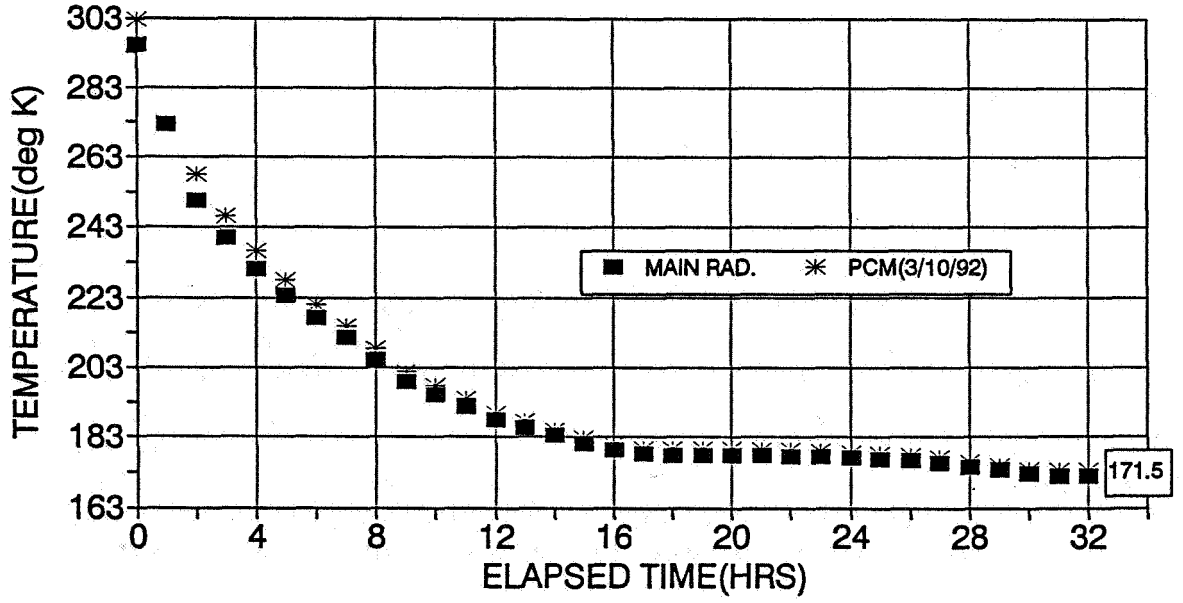

PCM as shown in Figure 9. These results are exactly as predicted with the original thermal model and tend to substantiate where the error occurred. Cooldown to 171.5°K was achieved after 32 hours prior to discontinuing the test.

The results of this test can be used to evaluate the PCM behavior. They show that the PCM freezes at 181.5°K. This is only 1°K higher than was measured 15 years prior and is well within the accuracy of the instrumentation. Also, freezing occurred for a total of 11.5 hours which corresponds to 57 watt-hours of energy based on the radiator's net heat rejection capacity at 181°K. The heat pipes were transporting 2.2 watts into the radiator at this time or 25.3 watt-hours of energy. The 31.7 watt-hours difference corresponds to the latent heat given up by the freezing of the PCM. This is approximately 20% higher than the energy predicted based on the 753 grams of n-heptane that are in the PCM canister but is well within the accuracy of the thermal estimate. The 31.7 watt-hours also corresponds exactly to thermal vacuum test results obtained in 1977. When the transport tests were conducted, the PCM melted at 181.5°K which again corresponds to its original melting temperature. In summary, the post flight thermal vacuum test results shown in Figure 9 demonstrate that the n-heptane canister is behaving almost exactly as it had 15 years ago. Also, there has been no apparent loss of n-heptane due to leakage over this period.

The results of the post flight heat pipe transport tests are shown in Figure 10 and Table 5. Again, the Long Term Forward Mode is exercised in ground tests for a one to one comparison with the flight data. Figure 10 compares the temperature drops across each heat pipe as a function of time from the start of cooldown. Also shown in Figure 10 are the temperature responses of each evaporator. Flight data again is for the first cooldown cycle so that heat pipe priming can be evaluated. The temperature drop and evaporator data show that the CCHP is primed and can carry the 1 watt heat load on the ground and in flight. The negative temperature drop in flight is instrumentation error which is less than 0.5°K.

The data for the diode heat pipe shows that it was fully primed by the time the first flight data point was recorded and the DHP had cooled to approximately 250°K. In the TV test however, which was conducted at an adverse tilt of 4.0 mm, the DHP was not fully primed until it had cooled to 220°K. Similar results were obtained in component tests with the DHP in 1978. A maximum evaporator temperature gradient of 42°K had occurred due to the 1.2 watt heat load prior to the DHP's priming. This same temperature drop would have occurred in flight if the DHP were not operating properly. Once primed, the ground and flight temperature drops are virtually identical at 1.1°K.

Table 5 summarizes the results of post flight transport tests that were conducted with each heat pipe at adverse tilts of approximately 2.4 and 4.0 mm. These tests were conducted by cooling the system and freezing all of the PCM and then using the pre-programmed test sequence with the electronics module and the flight heaters. This allows the transport tests to be conducted at a constant temperature of approximately 182°K. The CCHP held 25.2 watts and "Dried Out" at 29.5 at the 2.4 mm tilt. The theoretical maximum transport is 24 watts at this tilt and the 182°K test temperature. Component tests in 1977 verified the theoretical prediction. The slightly higher performance that is now being exhibited is probably due to the inability to accurately establish the tilt in systems tests.

Figure 10a. Comparison of CCHP Temperature Drop Between Flight & TV Test Data (4 mm Tilt)

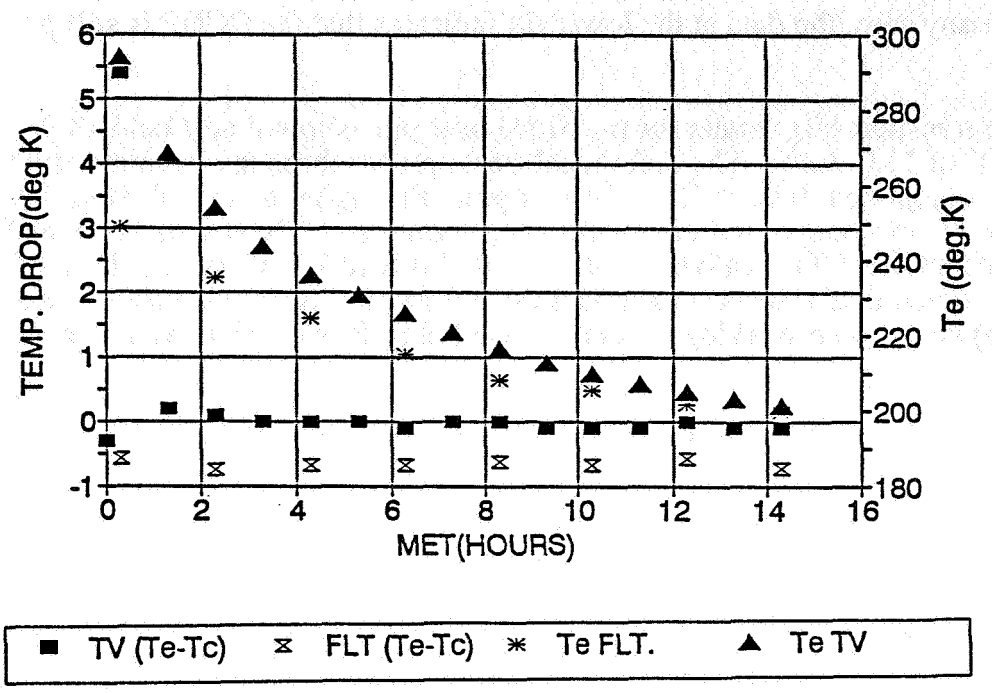

Figure 10b. Comparison of DHP Temperature Drop Between Flight & TV Data (4 mm Tilt)

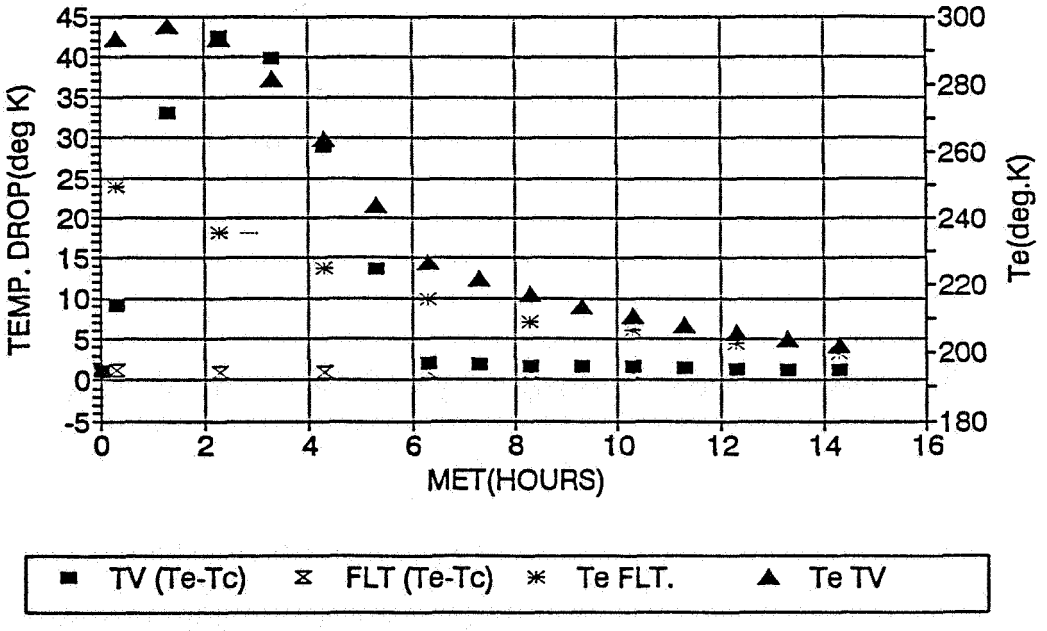

The lowest power in the pre-programmed sequence is 21.4 watts and this caused immediate "Dry Out" of the CCHP at the higher tilt. The theoretical transport is 17 watts at this tilt. In any case, the data at the lower tilt indicates that the CCHP is still performing properly.

The transport test results for the diode heat pipe show that it held 14.9 watts and "Dried-Out" at 16.6 watts. The theoretical transport for these test conditions which was verified by component tests is 12.5 watts. Again, the higher test result is probably due to the inability to accurately measure the tilt in systems tests. The results from the DHP transport test at the 4.0 mm adverse tilt show that it held 7.3 watts and "Dried-Out" at 8.5 watts. The theoretical transport for this tilt is 8.0 watts. Again, we can say that the diode heat pipe appears to be working properly since being fabricated 14 years ago.

Table 5. Summary - Post Flight Transport Test Data

	6/10/92 PRE ELEV @ 2.2 MM POST ELEV @ 2.8 MM		7/10/92 PRE ELEV @4.0 MM POST ELEV @ 4.0 MM	
	POWER (W)	DTe(deg K)	POWER (W)	DTe(deg K)
CONSTANT CONDUCTANCE HEAT PIPE * DENOTES DRY OUT	0.0 25.2 29.5 2.0 2.0	0.0 6.6 30.0* 32.0 1.2	21.4	DRY OUT
DIODE HEAT PIPE * DENOTES DRY OUT	0.0 8.5 11.0 14.9 16.6 0.7	0.0 4.7 6.7 5.8 9.0* 3.2	0.0 7.3 8.5 0.8	0.0 4.2 8.0* 3.5

REFERENCES

1. Tiller, S.E. and Sullivan, D.: Long Duration Exposure Facility Low-Temperature Heat Pipe Experiment Package Power System Results. Proceedings of the First LDEF Post-Retrieval Symposium, NASA CP-3134, 1992, Part 3, pp. 1441-1454.

2. Kauder, L.: Preliminary Results for LDEF/HEPP Thermal Control Samples. Proceedings of the First LDEF Post-Retrieval Symposium, NASA CP-3134, 1992, Part 2, pp. 797-800.

3. Berrios, W.M.: Use of the Long Duration Exposure Facility's Thermal Measurement System for the Verification of Thermal Models. Proceedings of the First LDEF Post-Retrieval Symposium, NASA CP-3134, 1992, Part 1, pp. 69-84.

4. Grote, M.G.: Results from the LDEF/A0076 Cascaded Variable Conductance Heat Pipe Experiment. Proceedings of the First LDEF Post-Retrieval Symposium, NASA CP-3134, 1992, Part 3, pp. 1455-1466.

5. Kroliczek, E.J. and Brennan, P.J., "Axial Grooved Heat Pipes - Cryogenic Through Ambient," ASME Paper No. 73-ENAs-48, 1973.

6. Brennan, P.J., Suelau, H.J. and McIntosh, R., "Development of a Low Temperature Phase Change Material Package," AIAA Paper No. 77-762, June 1977.

SPACE ENVIRONMENTAL EFFECTS

BIOLOGY

PRECEDING PAGE BLANK NOT FILMED

ORIGINAL PAGE
BLACK AND WHITE PHOTOGRAPH

L-90-9944

501760
N93-29702 B-14

FINAL RESULTS OF SPACE EXPOSED EXPERIMENT DEVELOPED FOR STUDENTS

Doris K. Grigsby
NASA/AESP
Oklahoma State University
Stillwater, Oklahoma 74078-0422
Phone: 405/744-7015, Fax: 405/744-7785

SUMMARY

"The SEEDS experiment gave students ownership in their future of space study. They felt important; they felt their information was of value." This comment from an elementary teacher, is representative of responses from many of the nearly 8,000 educators who submitted students' data for the SEEDS (Space Exposed Experiment Developed for Students) final report. SEEDS was a cooperative endeavor of NASA Headquarters, the NASA Langley Research Center, and the George W. Park Seed Company. Approximately 132,000 SEEDS kits containing Rutger's tomato seeds that had flown on LDEF, as well as similar seeds that had been stored in a climate-controlled warehouse for the same time period, were sent to schools in every state and 30 foreign countries. Student researchers from kindergarten through university compared germination and growth characteristics of the space-exposed and Earth-based seeds and returned data to NASA for analysis. Important scientific information was gained as students reported very little difference between the two seed groups.

INTRODUCTION

NASA, sharing a national concern for the declining numbers of young people opting for careers in science and engineering, has developed a number of programs to stimulate student interest in an effort to increase enrollment in upper-level pre-college science and mathematics courses. Realizing attitudes toward science and mathematics are formed prior to secondary education and knowing students learn best when they are active participants, the SEEDS project was conceived with the following objectives:

1. To involve a very large number of students in a national project designed to generate interest in science and related disciplines.

2. To offer students from elementary through university level an opportunity to participate in first-hand experiences with materials flown in space.

3. To provide the opportunity for sharing results among all participants.

BACKGROUND

Several brainstorming sessions resulted in the decision to fly 12.5 million Rutger's tomato seeds on the LDEF (Long Duration Exposure Facility). The seeds were packed into five aluminum canisters which were sealed at 101kPa (14.7 psi) pressure/atmospheric gases and 20 percent relative humidity. Four layers of seeds (A, B, C, D) were placed in each canister, with each layer confined by Dacron bags. Layer A was near the exterior of the satellite. A passive maximum temperature thermometer was placed in each canister and thermoluminescent passive dosimeters were placed between the layers of seeds. The

PRECEDING PAGE BLANK NOT FILMED

canisters were fastened inside a tray which was loaded onto the LDEF. An equal number of seeds was placed in Park Seed Company's controlled environment of 21°C, 101kPa pressure, and 20 percent relative humidity.

The LDEF was launched April 984, aboard Space Shuttle Challenger, Mission 41-C, and deployed one day after launch for what was expected to be a one-year mission. Retrieved in January 1990, by the crew of Columbia during Mission STS-32, the SEEDS tray was the first experiment removed from the LDEF. The Park Seed Company assembled and distributed the SEEDS kits. Grades 5-9 kits contained an instruction manual, an activity book, a data collection booklet, a press release, a letter from the U. S. Department of Agriculture regarding the safeness of experimenting with the seeds, and two packets of fifty seeds; one packet of space-exposed seeds from throughout the four layers from a single canister and one packet of Earth-based seeds. The high school kit contained the written materials and three packets of seeds; one packet of 50 Earth-based seeds, one packet of 25 seeds from layers A and B and another packet of 25 seeds from layers C and D from the same canister. The college kit was similar, but contained five packets of seeds; 50 Earth-based seeds and four packets of 25 seeds from each layer within a canister.

Distribution of over 132,000 SEEDS kits to 64,000 teachers representing 40,000 classrooms and 3.3 million kindergarten through university students was a good indication that objectives 1 and 2 would be achieved. The kit originally intended for grades 5-9 was frequently requested and distributed to grades kindergarten through four. Seventy-seven percent of all data returned came from grades K-9; twenty percent was from high schools, with the remaining three percent from higher education. Most participants used an integrated approach, emphasizing the interdependence of the various disciplines students study each year. A comment from an elementary teacher perhaps best sums up the impact upon the total school curricula. "This project jibed well with our science curriculum and as part of math lessons, it generated many useful graphs. Since we do a great deal of writing, the students also wrote wonderful stories--from factual journals to imaginative fiction about the aliens in the seeds! I enjoyed the SEEDS project because it was *REAL* -- not the teachers and not NASA knew the results! That is so unlike the rest of our mundane science experiments where we *contrive* projects to prove what we *already* know. Your contribution makes both teaching and learning more exciting and relevant." Objective 3 was achieved as the summary report, *SEEDS: A Celebration of Science*, was sent to each data respondent. Schools returning data also received a Certificate of Participation. Figures 1-12 illustrate the phases of the SEEDS Experiment.

RESULTS AND DISCUSSION

The primary value of the SEEDS project was students' involvement in the scientific process as they observed, measured, classified, experimented, interpreted, communicated, developed models and practiced safety. The figures at the end of this paper focus on students' development of the science process skills. While many reports indicated Earth-based seeds germinated more quickly than space-exposed seeds, overall data analysis suggests space-exposed seeds did germinate at a slightly faster rate. This difference was more evident as data among the three levels were compared and correlations made between germination time and germination media. Those students using moistened paper towels were able to observe radicle emergence at an earlier stage than those covering seeds with soil. Variations in reported observations increased as growth proceeded. Reports ranged from differences in plant size, shape, color, odor, leaf position, and stem thickness to resistance to pests. Many students reported Earth-based plants being eaten by deer, birds, rabbits, gerbils, moose, ferrets, ants, and cockroaches while the space-exposed counterparts were untouched or only slightly nibbled. Individual reports of space-exposed plant variations included stunted plants, plants that added a leaf instead of the usual flower at the end of the flower frond, and fruit produced from a flower with a variegated calyx bearing seeds producing albino plants, while fruit from a green calyxed flower from the same plant bore seeds producing green plants.

Young student researchers, influenced by many hours of science-fiction treatment through print, audio and video media were eager in their search for mutations. Some were disappointed because the

Rutger's California Supreme tomato is relatively genetically stable. Radiation data indicated layer A within each canister received approximately 725 rads, while layer D received 350 rads. Students asked lots of questions when their data supported variation in both the Earth-based seeds and the space-exposed seeds. Their questioning increased when the media published articles warning of the possibility of poisonous fruit from the space-exposed seeds. This pursuit generated a greater understanding of genetics and radiation, two topics typically stimulating a number of misconceptions. The development of critical-thinking skills was enhanced. SEEDS allowed for concrete experiences with abstract concepts and provided many opportunities for open-ended discussions and experimentation.

There was much evidence of the use of problem-solving skills reported from all grade levels. Many schools had to acquire the materials and equipment necessary to successfully participate in the SEEDS project. Many recycled materials were used as germination and growth containers. Sophisticated problem solving included the assembly of a robotic watering system by an elementary class and the development of hydroponic growth systems by several secondary classes.

Creativity was abundant whether classes chose to complete the NASA-suggested experiment or to design their own experiments to compare various characteristics of the space-exposed and Earth-based seeds. In almost all participating schools, creativity was manifested in the selection of sites for growing a very large number of tomato plants. On-site school gardens ranged from greenhouses to outdoor classrooms, newly tilled gardens to trenches, and various-sized containers to simply planting in bags of potting soil. Off-site gardens ranged from large fields to containers on patios or in windows of high-rise apartments.

Community involvement was an important aspect and pleasant outcome of the SEEDS project. Many materials and hours of labor were donated by local businesses, organizations and families; gardening expertise was provided by horticulturists, experienced gardeners, and often by grandparents and other older citizens. High school biology and agriculture classes worked with elementary classes. Partnerships were formed that will endure far beyond the completion of SEEDS.

Tables 1--4 at the end of this paper represent the data of many novice as well as a few seasoned researchers. Interpretation must include an understanding of and appreciation for the fact that most of the data was returned by novices. One teacher summarized it well by stating, "Measurements were truly student done--with misunderstandings and errors no doubt abundant."

Growth data, analyzed at the end of 56 days, indicated the initially faster growth in the space-exposed group began leveling out after four weeks. Correlations made between growth data and the growing environment indicated that plants grown indoors with limited sunlight or under artificial lights were weak-stemmed and spindly. Students were sometimes hampered in experimental efforts because of requirements that lights and heating be turned off when school was not in session. Data collection was often incomplete due to problems encountered when plants were undertended, overtended, measured, transplanted and transported. One secondary teacher noted, "The radiation above the atmosphere over a period of six years is negligible when compared to the dangers of a small classroom where 100 students come and go and check and water plants."

Secondary and college students devised experiments beyond those suggested by NASA. Bacterial studies of seed coats of space-exposed and Earth-based seeds revealed several species of Bacillus as well as a lactose fermenting bacteria. Unidentified fungi species were found on tested seeds. No differences were found in pH between fruits produced from space-exposed and Earth-based seeds. Space-exposed plants performed normally in tests of phototropism, geotropism, tissue culturing, and seed weight. Chromatography tests indicated space-exposed plants had greater levels of chlorophylls and carotenes than Earth-based plants. Tests found that light absorbence was greater in extracts made from space-exposed plant tissues. Results from laser-induced fluorescent spectroscopy led one team of researchers to conclude that space-exposed seeds exhibited premature chlorophyll development. They suggested this might partially explain the rapid initial growth of the space seedlings.

A secondary teacher reported, "We learned through the process that science is not easy. Many experiments were done to try to increase our chances of finding something new. If nature has it that nothing new is obtained, we do not consider it a failure. We consider ourselves one step closer in our search for information."

Student researchers concluded that space may be a safe place for long-term storage of seeds from many of Earth's endangered plants, as well as seeds from plants upon which the world population depends for food. In space, the seeds would be secure from unpredictable environmental factors on Earth.

Almost one-half of the participants returning data booklets indicated they would continue the SEEDS project with studies of second and subsequent generations. A need still exists in this nation for students at all levels to become involved in relevant, meaningful science activities. A parent wrote, "Our children were eager NASA scientists, fascinated with the concept of 'space' tomatoes, and were rewarded not only by their satisfaction coming from the completion of an independent scientific search, but also by the realization of working on a national project with *unknown* results. They felt part of something *really* important, and had an introduction to scientific methodology as well. Thank you for this unique and wonderful opportunity! You have provided the children with a special and well-designed experience which they'll always remember."

LDEF-USERS CHALLENGE

Scientists and engineers participating in LDEF research have an opportunity to become active in science education. An elementary teacher wrote, "The students felt important participating in what we felt would help make future decisions in space." Capitalize on this sense of contribution. Help relate the value of their research to the Space Station, Mission to Mars, Return to the Moon and other NASA projects. Volunteer to meet with classes and science and engineering clubs to discuss career opportunities and the necessary academic preparation. Serve as tutors, mentors and role models. Encourage female and minority students to enter science-related careers. Regardless of grade level, inform students about what they can do today to prepare themselves for a successful future. Give students examples in their everyday lives of applications and outcomes of a particular area of science or engineering. Offer to assist teachers with curriculum planning. Volunteer for eight hours a month to work with a local school. Give students an opportunity to associate science with a real person!

ACKNOWLEDGMENTS

The author gratefully acknowledges those educators who facilitated SEEDS, enabling their students to experience the joy of scientific investigation. Special thanks are directed to Bill Kinard's team at the NASA Langley Research Center, Jim Alston and the Park Seed Company, the Education Division at NASA Headquarters and the NASA Aerospace Education Services Program team at Oklahoma State University for their support of the SEEDS project.

REFERENCES

1. Melton, Bob: *SEEDS: A Celebration of Science*, NASA EP-281, 1991.

Table 1. Summary Data: All Grade Levels

Space-exposed, Across All Canisters and Layers

	Number reporting	Mean	Std. Dev.	Min.	Max.
Germination rate: percent of seeds germinated 14 days after planting	7931	66.3	23.3	1.0	100.0
Average number of days required for germination within 14 days after planting	7288	8.4	2.6	1.0	14.0
Number of plants measured	4420	18.1	12.5	1.0	88.0
Average height (cm) at 56 days	4679	21.2	9.7	8.0	38.0
Average width (cm) at 56 days	4208	12.0	4.4	4.0	16.0
Flowering rate: percent of plants producing flowers	2118	73.4	34.4	1.0	100.0
Average number of days to first flower within 56 days	538	46.7	8.2	28.0	56.0
Percent of plants producing fruit	1849	74.6	34.2	1.0	100.0
Average number of days from planting until first fruit formed on plant	1621	94.3	25.5	35.0	150.0

Earth-based

	Number reporting	Mean	Std. Dev.	Min.	Max.
Germination rate: percent of seeds germinated 14 days after planting	7854	64.6	23.5	1.0	100.0
Average number of days required for germination within 14 days after planting	7281	8.5	2.7	1.0	14.0
Number of plants measured	4414	18.6	13.3	1.0	99.0
Average height (cm) at 56 days	4600	20.9	9.7	8.0	38.0
Average width (cm) at 56 days	4160	11.9	4.4	4.0	16.0
Flowering rate: percent of plants producing flowers	2106	72.3	34.9	1.0	100.0
Average number of days to first flower within 56 days	524	46.9	8.5	28.0	56.0
Percent of plants producing fruit	1773	76.1	33.0	1.0	100.0
Average number of days from planting until first fruit formed on plant	1570	94.4	25.8	35.0	150.0

Table 2. Summary Data: Grades K-9

Space-exposed, Across All Canisters and Layers

	Number reporting	Mean	Std. Dev.	Min.	Max.
Germination rate: percent of seeds germinated 14 days after planting	6157	65.8	23.9	1.0	100.0
Average number of days required for germination within 14 days after planting	5717	8.4	2.6	1.0	14.0
Number of plants measured	3459	19.1	12.9	1.0	83.0
Average height (cm) at 56 days	3684	20.9	9.7	8.0	38.0
Average width (cm) at 56 days	3273	11.9	4.4	4.0	16.0
Flowering rate: percent of plants producing flowers	1726	72.5	34.9	1.0	100.0
Average number of days to first flower within 56 days	396	46.6	8.5	28.0	56.0
Percent of plants producing fruit	1472	72.8	35.3	1.0	100.0
Average number of days from planting until first fruit formed on plant	1295	95.2	25.5	35.0	150.0

Earth-based

	Number reporting	Mean	Std. Dev.	Min.	Max.
Germination rate: percent of seeds germinated 14 days after planting	6104	64.0	23.9	1.0	100.0
Average number of days required for germination within 14 days after planting	5731	8.6	2.7	1.0	14.0
Number of plants measured	3478	18.5	12.8	1.0	90.0
Average height (cm) at 56 days	3615	20.6	9.6	8.0	38.0
Average width (cm) at 56 days	3251	11.8	4.4	4.0	16.0
Flowering rate: percent of plants producing flowers	1736	70.9	35.7	1.0	100.0
Average number of days to first flower within 56 days	385	46.7	8.7	28.0	56.0
Percent of plants producing fruit	1416	74.2	34.1	1.0	100.0
Average number of days from planting until first fruit formed on plant	1268	95.0	25.8	35.0	150.0

Table 3. Summary Data: Grades 10-12

Space-exposed, Across All Canisters and Layers

	Number reporting	Mean	Std. Dev.	Min.	Max.
Germination rate: percent of seeds germinated 14 days after planting	1494	67.4	20.7	1.0	100.0
Average number of days required for germination within 14 days after planting	1335	8.1	2.6	1.0	14.0
Number of plants measured	816	14.9	10.7	1.0	88.0
Average height (cm) at 56 days	843	21.6	9.6	8.0	38.0
Average width (cm) at 56 days	798	12.3	4.3	4.0	16.0
Flowering rate: percent of plants producing flowers	342	79.3	30.5	1.0	100.0
Average number of days to first flower within 56 days	126	47.3	7.3	29.0	56.0
Percent of plants producing fruit	298	81.1	28.8	1.0	100.0
Average number of days from planting until first fruit formed on plant	260	91.5	25.1	36.0	150.0

Earth-based

	Number reporting	Mean	Std. Dev.	Min.	Max.
Germination rate: percent of seeds germinated 14 days after planting	1481	66.1	22.4	1.0	100.0
Average number of days required for germination within 14 days after planting	1328	8.3	2.7	1.0	14.0
Number of plants measured	795	19.2	14.8	1.0	99.0
Average height (cm) at 56 days	837	21.5	9.7	8.0	38.0
Average width (cm) at 56 days	777	12.5	4.3	4.0	16.0
Flowering rate: percent of plants producing flowers	328	80.2	30.1	1.0	100.0
Average number of days to first flower within 56 days	125	47.6	7.9	28.0	56.0
Percent of plants producing fruit	287	82.6	27.6	1.0	100.0
Average number of days from planting until first fruit formed on plant	244	92.2	26.2	35.0	150.0

Table 4. Summary Data: College

Space-exposed, Across All Canisters and Layers

	Number reporting	Mean	Std. Dev.	Min.	Max.
Germination rate: percent of seeds germinated 14 days after planting	280	71.1	19.8	2.0	100.0
Average number of days required for germination within 14 days after planting	236	8.1	2.4	2.3	14.0
Number of plants measured	145	12.1	8.6	1.0	70.8
Average height (cm)	152	25.0	9.7	8.0	38.0
Average width (cm)	137	14.1	3.2	4.0	16.0
Flowering rate: percent of plants producing flowers	50	63.7	36.2	1.0	100.0
Average number of days to first flower	16	46.9	8.2	30.0	56.0
Percent of plants producing fruit	79	82.6	27.6	5.3	100.0
Average number of days from planting until first fruit formed on plant	66	89.9	24.6	38.5	150.0

Earth-based

	Number reporting	Mean	Std. Dev.	Min.	Max.
Germination rate: percent of seeds germinated 14 days after planting	269	69.8	21.5	4.0	100.0
Average number of days required for germination within 14 days after planting	222	8.1	2.5	2.0	14.0
Number of plants measured	141	18.1	16.8	1.0	96.0
Average height (cm)	148	25.0	9.9	8.0	38.0
Average width (cm)	132	14.1	3.3	4.0	16.0
Flowering rate: percent of plants producing flowers	42	69.5	34.1	2.0	100.0
Average number of days to first flower	14	47.2	6.9	34.0	56.0
Percent of plants producing fruit	70	87.2	23.9	10.0	100.0
Average number of days from planting until first fruit formed on plant	58	89.6	22.6	40.0	137.0

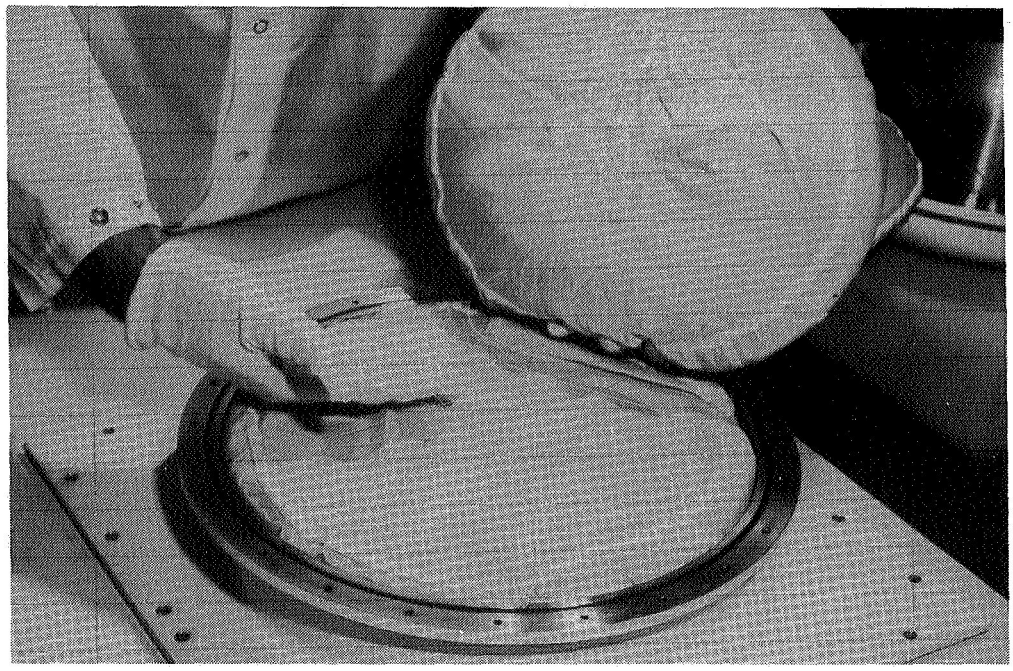

Figure 1. Layering seeds into canister.

Figure 2. Securing canisters into tray.

ORIGINAL PAGE
BLACK AND WHITE PHOTOGRAPH

Figure 3. Announcing SEEDS project to community.

Figure 4. Transplanting seedlings.

ORIGINAL PAGE
BLACK AND WHITE PHOTOGRAPH

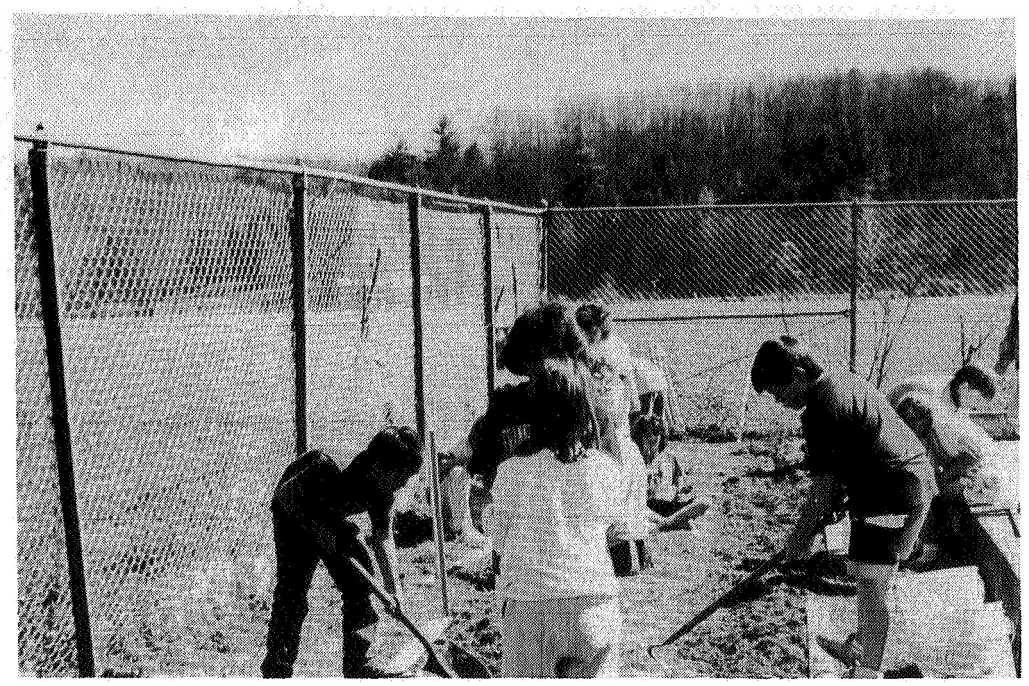

Figure 5. Transforming playground into tomato garden.

Figure 6. Observing and measuring.

ORIGINAL PAGE
BLACK AND WHITE PHOTOGRAPH

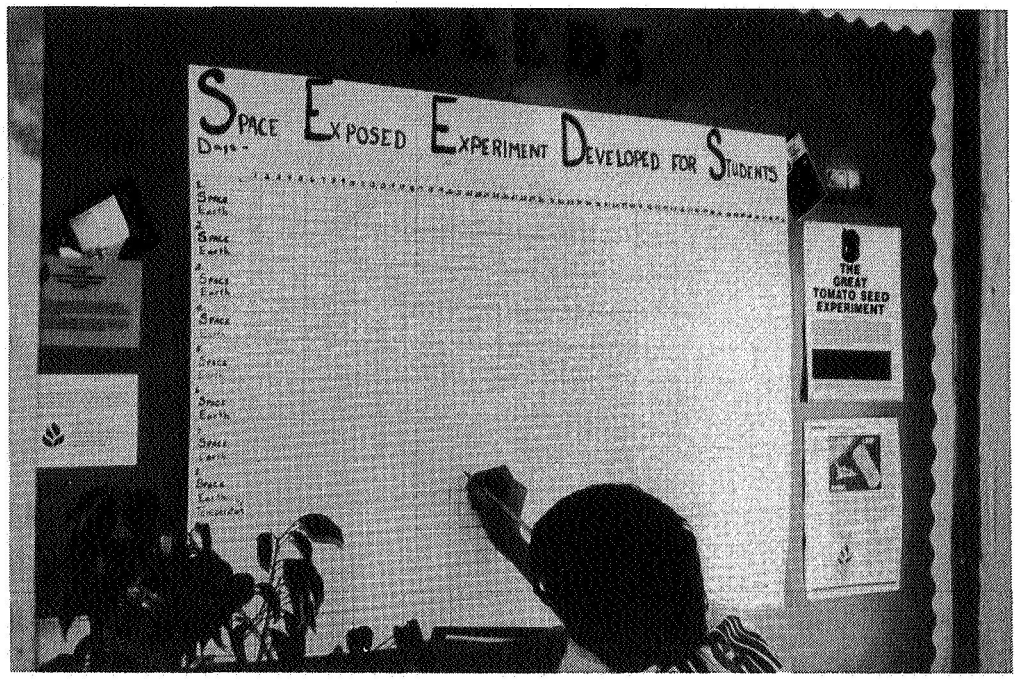

Figure 7. Recording data.

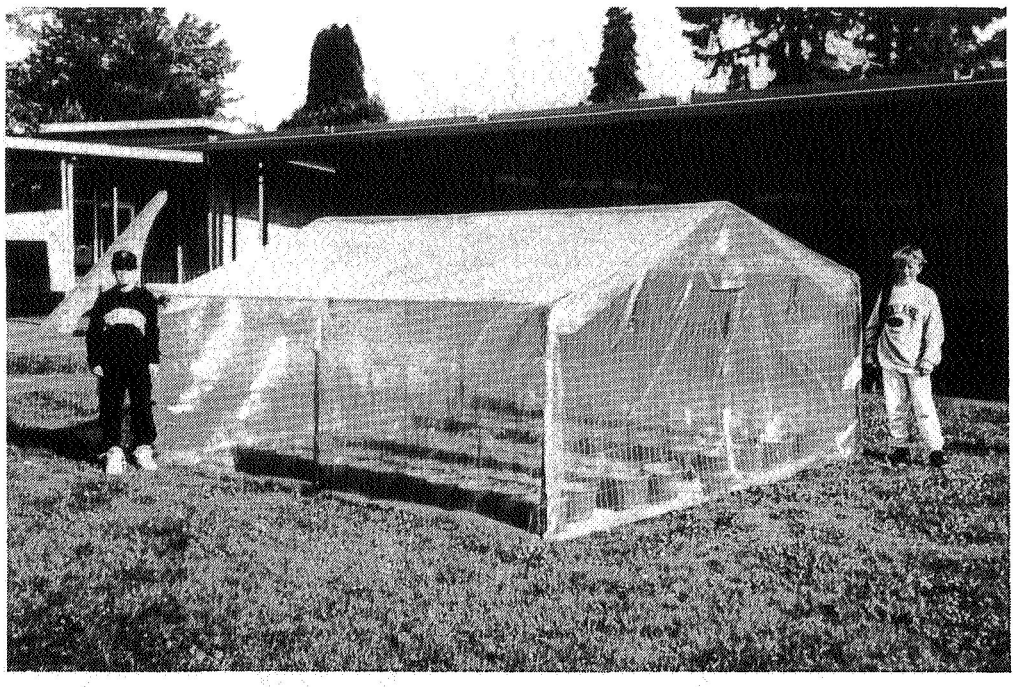

Figure 8. Developing short-term solution for problem.

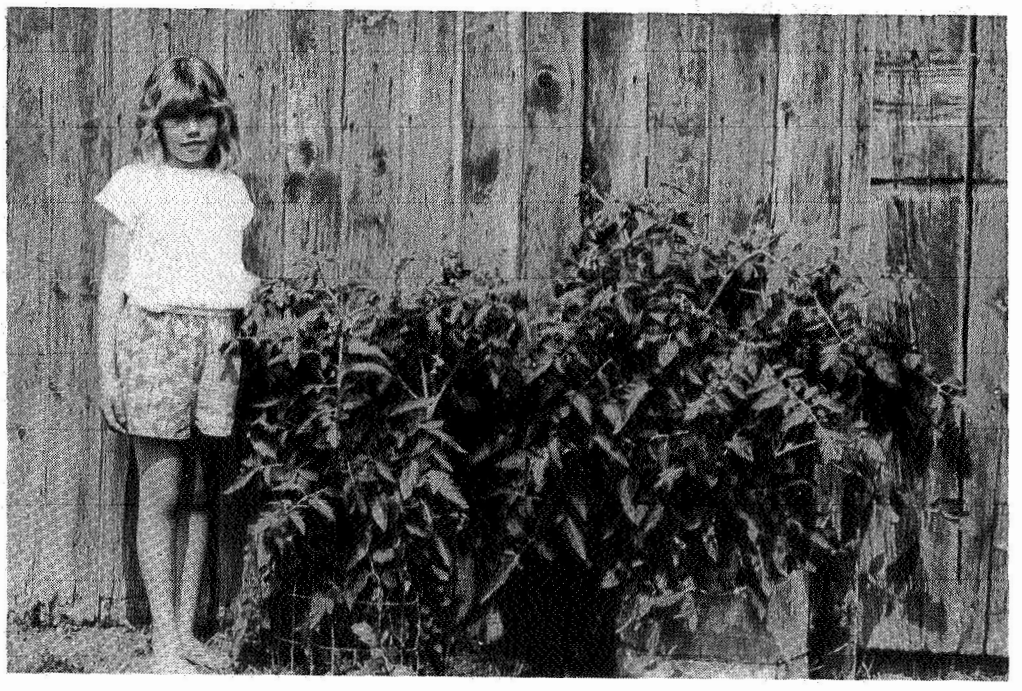

Figure 9. "Adopted" plants taken home.

Figure 10. Removing seeds for second generation studies.

ORIGINAL PAGE
BLACK AND WHITE PHOTOGRAPH

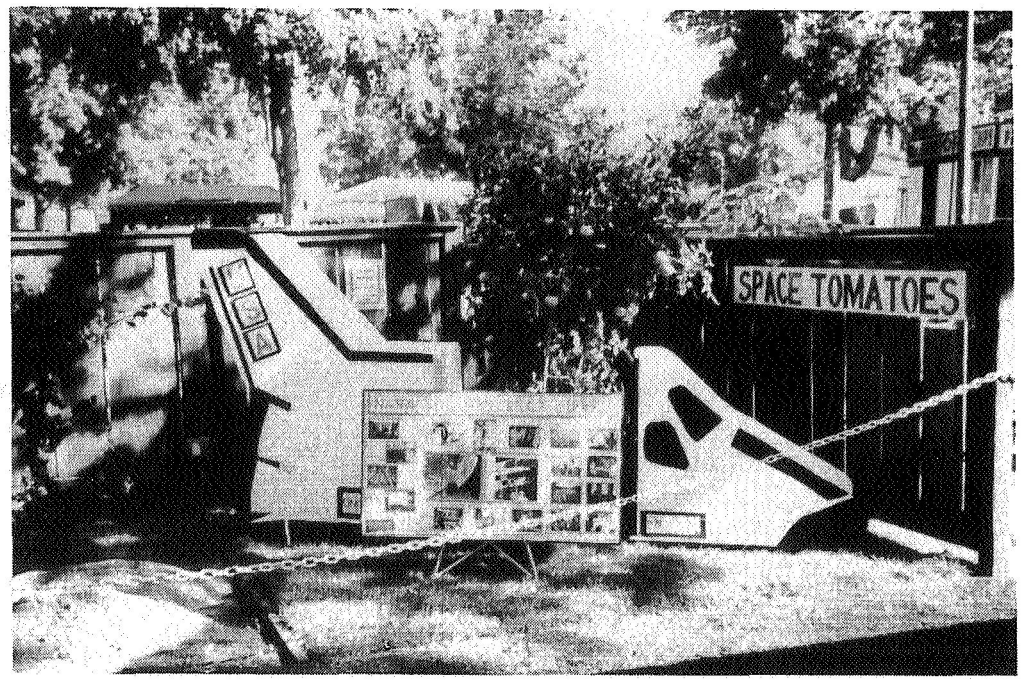

Figure 11. Displaying pride in involvement.

Figure 12. Model building.

N93-29703
501762
pg 6

CONTINUED RESULTS OF THE SEEDS IN SPACE EXPERIMENT

Jim A. Alston
Park Seed Company
Greenwood, SC 29648-0031
Phone: 803/941-4445, Fax: 803/941-4239

SUMMARY

Two million seeds of 120 different varieties representing 106 species, 97 genera and 55 plant families were flown aboard the Long Duration Exposure Facility (LDEF). The seed were housed on the Space Exposed Experiment Developed for Students (SEEDS) tray in the sealed canister number 6 and in two small vented canisters. The tray was in the F-2 position. The seed were germinated and the germination rates and the development of the resulting plants were compared to the performance of the control seed that stayed in Park Seed's seed storage facility.

The initial results were presented in a paper at the First LDEF Post-Retrieval Symposium. There was a better survival rate of the seed in the sealed canister in space than in the storage facility at Park Seed. At least some of the seed in each of the vented canisters survived the exposure to vacuum for almost six years. The number of observed apparent mutations was very low. In the initial testing, the small seeded crops were not grown to maturity to check for mutations and obtain second generation seed. These small seeded crops have now been grown for evaluation and second generation seed collected.

INTRODUCTION

The purpose of the experiment was to evaluate the effects of prolonged space exposure on the survivability of a diverse group of seed stored in space under sealed and vented conditions and to determine possible resulting mutations and changes in mutation rates. Both flower and vegetable seed were represented in the experiment. Seed have been flown in space a number of times, but not in these quantities and not with maximum exposure for the duration that LDEF was in space.

MATERIALS AND METHODS

The basic materials and methods were discussed in a previous

paper (ref. 1). Fourteen of the smaller seeded items (table I) that had flown in space were sown in the spring of 1992. Since germination rates had already been established, this aspect of testing was not redone at this sowing. The plants were grown to maturity for the purpose of evaluating the populations for mutations and to collect second generation seed. Second generation plants of two items, Zea mays and Allium cepa, were grown for observation.

RESULTS AND DISCUSSION

With three exceptions which will be noted, all the plants grew normally and produced seed. The space seed of the Petunia x hybrida produced more robust plants that the control seed. This is probably a result of the aging process of the control seed. One plant of the Sedum supurium was dwarfed but otherwise like the other plants. One Lobelia Erinus plant had a chlorophyll deficiency.

The abnormalities observed in the Sedum and the Lobelia were likely the result of mutations since the phenotypes have not been observed in any populations that we have grown.

It is our conclusion that the mutation rate of the seed that flew in our experiment is very low, occurring less than one in a thousand.

REFERENCES

1. Alston, Jim A.: Seeds In Space Experiment. First LDEF Post-Retrieval Symposium, NASA CP-3134, 1992.

TABLE I LIST OF SEED

Lobelia Erinus
Sinningia speciosa
Begonia x semperflorens
Sedum supurium
Lobularia maritima
Cyperus alternifolius
Achimenes hybrids
Saintpaula ionantha
Portulaca grandiflora
Calceolaria crenatiflora
Petunia x hybrida
Salpiglossis sinuata
Lagerstroemia indica
Antirrhium majas

THE FUTURE

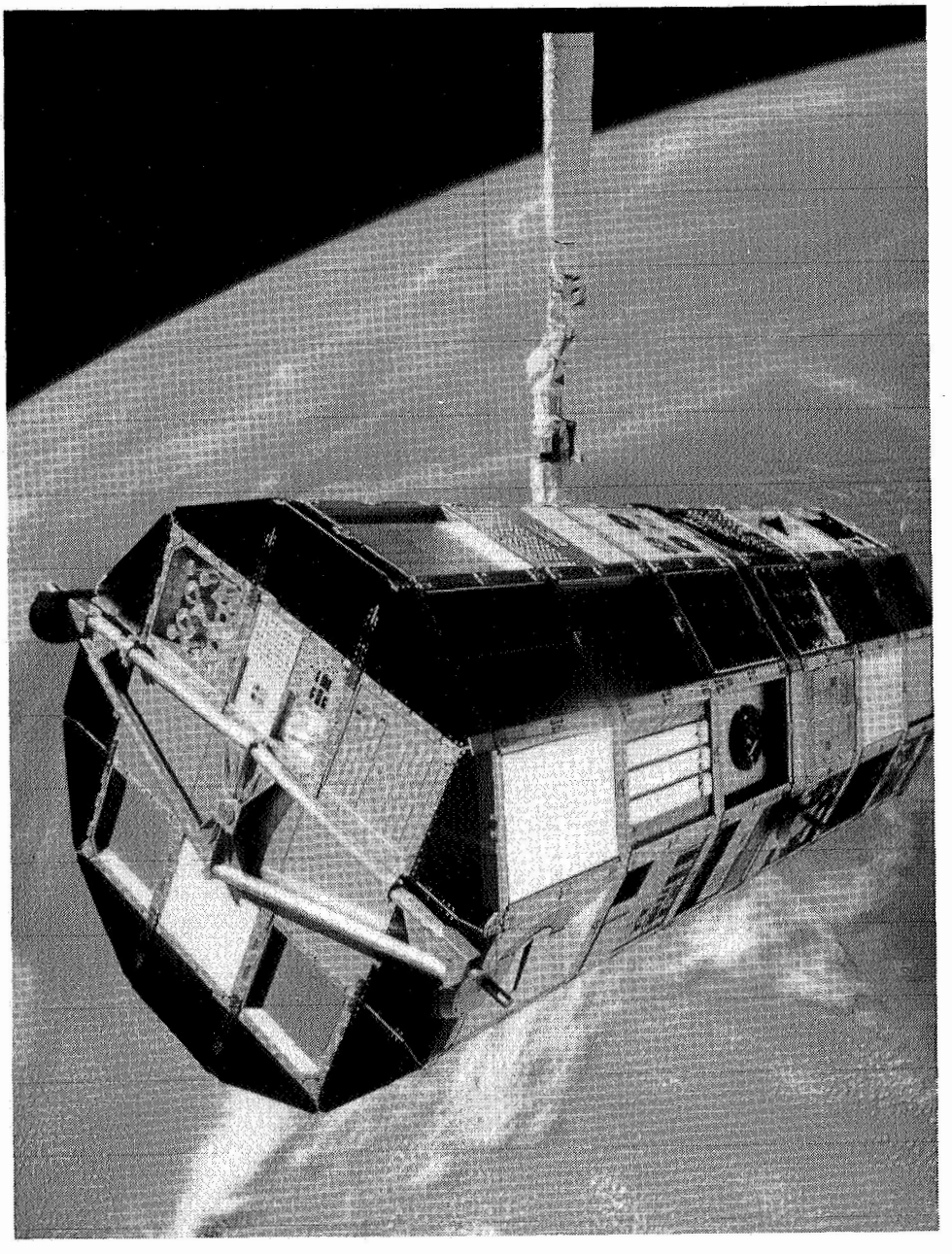

L-84-4323

ORIGINAL PAGE
BLACK AND WHITE PHOTOGRAPH

PRECEDING PAGE BLANK NOT FILMED

N93-29704

LDEF ARCHIVAL SYSTEM PLAN

501764
B-12

Brenda K. Wilson
W. J. Schafer Associates, Inc.
NASA Langley Research Center
9 N. Wright Street, M/S 404
Hampton, VA 23681-0001
Phone: 804/864-8458 Fax: 804/864-8094

INTRODUCTION

The Long Duration Exposure Facility (LDEF) has provided the first significant opportunity to extensively study the space environment and its effects upon spacecraft systems and materials. The long-term value of the data obtained from LDEF, which is applicable to a wide range of areas including space environment definition, space environmental effects and spacecraft design, will depend upon the system developed to archive and retrieve the data. Therefore, in addition to the large effort undertaken to analyze LDEF data, a substantial effort is also necessary in order to retain and disseminate LDEF resources for future research and design. W. J. Schafer Associates, Inc., has a task subcontract to develop the LDEF archival system.

The LDEF resources include data, hardware, photographic records and publications which cover the 20-year history of LDEF from concept design through data analysis. Chronologically, pre-launch resources include documentation of facility and experiment development, testing, integration and operation. Post-retrieval resources are the observations, testing, analysis and publications since the January 1990 retrieval of LDEF. A third set of resources is the experiment and facility hardware and specimens, including more than 10,000 test specimens flown on LDEF and subsequently divided and distributed among investigators at numerous laboratories. Many valuable science and technology investigations have been undertaken with LDEF experiments and hardware, and many more investigations are being identified in areas not yet explored.

LDEF data applications encompass primarily low-Earth orbit spacecraft and structures. The nearly six-year space exposure of LDEF has provided data to evaluate materials, systems and living specimens exposed to radiation, meteoroids, debris and other constituents of the low-Earth environment. Structural, mechanical, electrical, optical and thermal systems were studied, and materials with applications in all aspects of space systems were exposed to the space environment.

The objectives of the LDEF archival system are to maintain the existing LDEF hardware, data, analysis, publications and photographs as a long term resource, and to provide a quick and simple mechanism by which LDEF resources can be identified, located and applied.

BACKGROUND

Other systems exist within NASA and in the broader areas of space and planetary sciences which have goals similar to those of the LDEF archives. In particular, the goals of these systems are to preserve and disseminate data in order to further space and planetary understanding. An evaluation of these systems is useful in developing the LDEF archival system, and in addition, cooperative efforts can benefit both existing and new data archival systems. In this section, some of these data systems are discussed.

NASA's National Space Science Data Center (NSSDC) was established 26 years ago as an active repository for space and Earth science data obtained through space and ground observations. The NSSDC is the primary archive for many NASA missions and it provides data to the broad research communities beyond the principal investigators in the fields of atmospheric, terrestrial and ocean sciences, astronomy, planetary sciences, astrophysics, and ionospheric, magnetospheric and solar-terrestrial physics.[1] The NSSDC is part of the Space Science Data Operations Office of the Space Sciences Directorate at the NASA Goddard Space Flight Center (GSFC).

In 1978, the NSSDC developed a centralized data base system for its holdings, and eventually it developed a Master Directory for computerized searching and identification. In recent years, however, the quantity and complexity of space and Earth science data has grown such that the NSSDC has moved toward a more decentralized organization consisting of independent archives at different locations, although still accessed through one master directory.

The NSSDC maintains both on-line and off-line data resources. The data center includes approximately 4,000 data sets from over 1,000 space flight experiments which flew on several hundred spacecraft.[1,2] Also included are rocket data, ground data and models. The NSSDC handles primarily reduced science data records and not engineering data. The data systems and centers accessible through the NSSDC include the Pilot Land Data System, the Crustal Dynamics Data Information System, the near Earth solar wind magnetic field and plasma data set, the Astronomical Data Center, the Planetary Data System and the Astrophysics Data System. The NSSDC is accessible electronically or through personal communication; the NSSDC manages the Space Physics Analysis Network (SPAN).

Another NASA system, EnviroNET, contains space environment tabular data, graphs, text and models which can be accessed in a user-friendly fashion. As described in another paper in this conference publication, EnviroNET is an on-line data base of technical information on space environmentally-induced interactions.[3] A pointer or node for EnviroNET is in the Master Directory of the NSSDC.

Another of NASA's programs which is concerned with large volumes of data is the Earth Observing System (EOS). The EOS program will include a number of archive centers, some of which will be closely related to the Global Change Data Center at the Goddard Space Flight Center. As the EOS program develops, it will necessitate significant attention toward science data handling and archival for efficient use.

NASA's lunar sample, Antarctic meteorite and cosmic dust collections are curated at the Johnson Space Center (JSC), and analysis results and detailed inventories are maintained there. Each collection has an associated detailed data base in order to locate and distribute information, and they are accessible via SPAN or INTERNET. These curatorial systems facilitate the acquisition, analysis and documentation of test specimens.

What does not appear within NASA's existing data systems is a comprehensive system to address the space environment and its effects upon spacecraft and their operation. NASA maintained a focused space environmental effects program only during the first decade of the Agency's history. This was the Environmental Factors Branch of the Space Vehicles Division of the Office of Advanced Research and Technology. Products of this program include many of the design criteria documents and the bases for natural meteoroid models used today. Due to budget restrictions and shorter-term priorities, the Environmental Factors Branch no longer existed beyond 1970. Over the past 20 years, NASA has given attention to the subject of the space environment and its effects through different programs, which has led to the current situation of separate efforts to study parts of the space environment without a cohesive strategy for the long term. Recently, however,

NASA Headquarters has shown growing interest in a coordinated space environmental effects program.

DEVELOPMENT APPROACH

The LDEF archives are being established with the view that they should evolve into a cohesive space environments and space environmental effects data system. Archives of related data from future space flight experiments, laboratory experiments, spacecraft development testing and analytical studies should be added to the LDEF archives to form the space environments and space environmental effects data system, a simple view of which is shown in Figure 1.

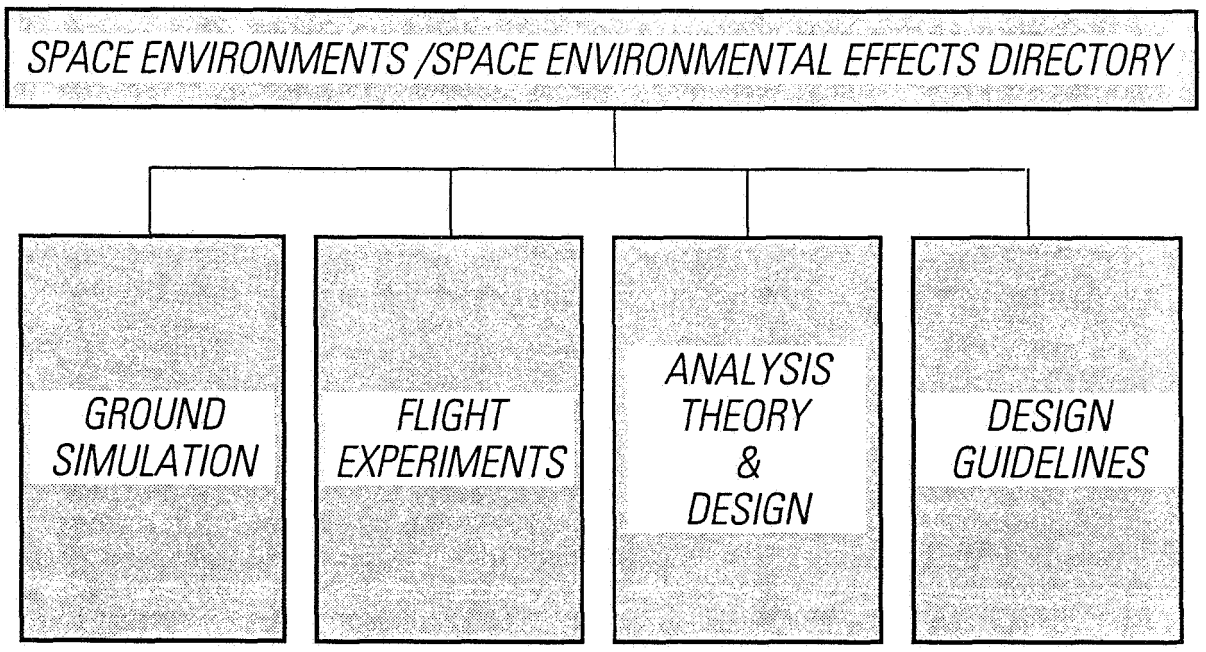

Figure 1. Space environments and space environmental effects data system.

The LDEF archives are meant to encompass the many aspects of the LDEF program which have occurred over the past 20 years. A chronological representation of these activities is shown in Figure 2. The design and fabrication of the LDEF structure occurred at Langley Research Center (LaRC) between 1974 and the launch of LDEF in 1984. During this same period, experiments were developed and fabricated at investigators' laboratories after their selection to fly on LDEF. Operations were coordinated between Langley Research Center, and Kennedy and Johnson Space Centers. By 1984, all facility and experiment elements of LDEF had been integrated and the facility was placed in orbit.

Following the retrieval of LDEF from orbit in 1990, the individual elements were again dispersed back to the principal investigators' laboratories, as well as to other laboratories that conducted special investigations. The facility structure was maintained at the Cape Canaveral Air Force Station (CCAFS) by Kennedy Space Center (KSC) personnel, and some facility elements were the subjects of special investigations at other laboratories. In July 1992, the facility structure was returned via barge to Langley Research Center.

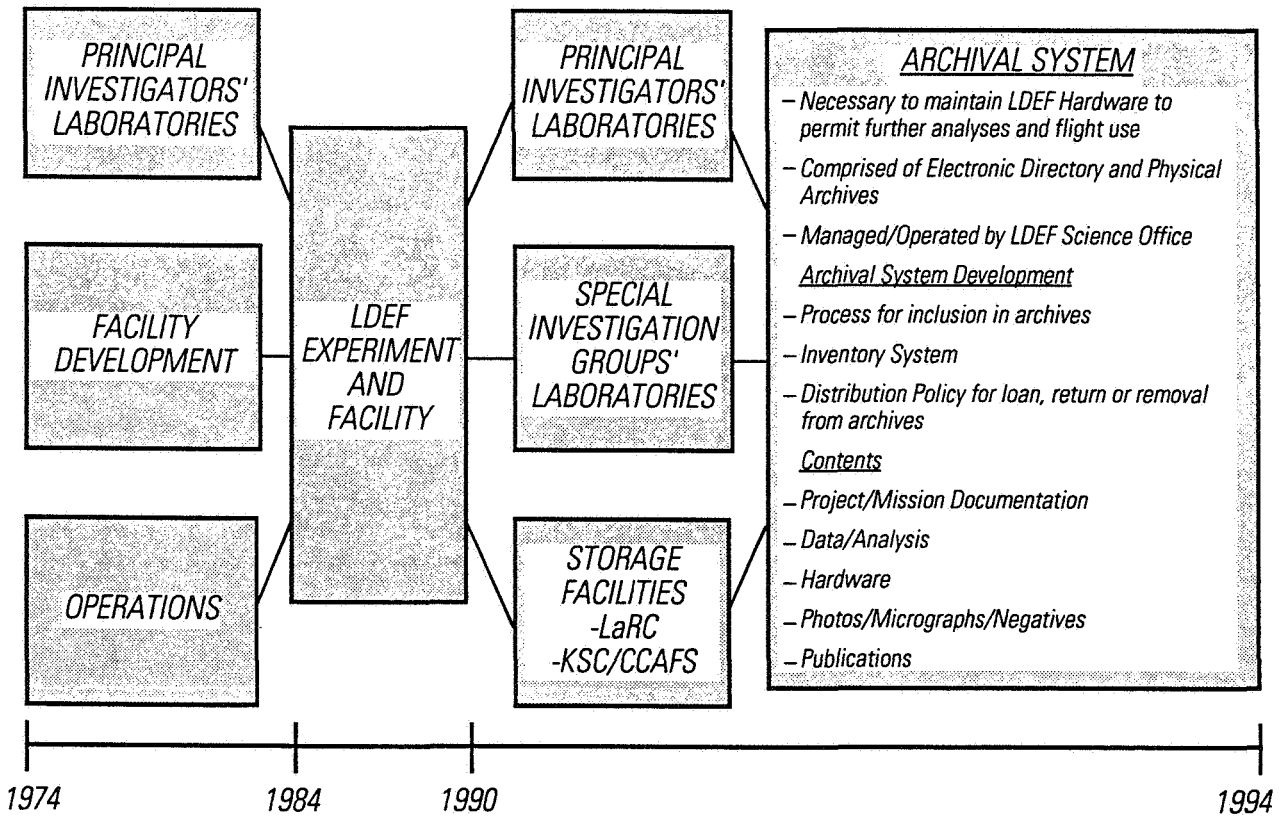

Figure 2. LDEF chronological development.

The first step in developing the LDEF data bases and archives has been the development of a number of data bases for the analysis and cataloging of LDEF data by individual organizations. Some of these individual data bases were created initially for internal purposes while others were designed for distribution to interested researchers. They have been created on different media including electronic disks, magnetic tapes, optical disks, photographs and paper journals. The principal goal of the LDEF archival effort is to develop a centrally-accessible archive system that contains these individual data bases, the large quantity of data that has not been placed in any data base, and the hardware, photographs and publications. Every effort will be made to not duplicate or homogenize what is in existence, but instead to develop a comprehensive system, link the existing parts together, provide access to these parts and identify missing portions. The LDEF archival system relies upon a directory for organization and access.

ARCHIVAL SYSTEM DESCRIPTION

The archival system contains the following elements, as shown in Figure 3:

I. LDEF ARCHIVE DIRECTORY
II. PROJECT / MISSION DOCUMENTATION ARCHIVE
III. DATA / ANALYSIS ARCHIVE
IV. HARDWARE ARCHIVE
V. PHOTOGRAPHS ARCHIVE
VI. PUBLICATIONS ARCHIVE

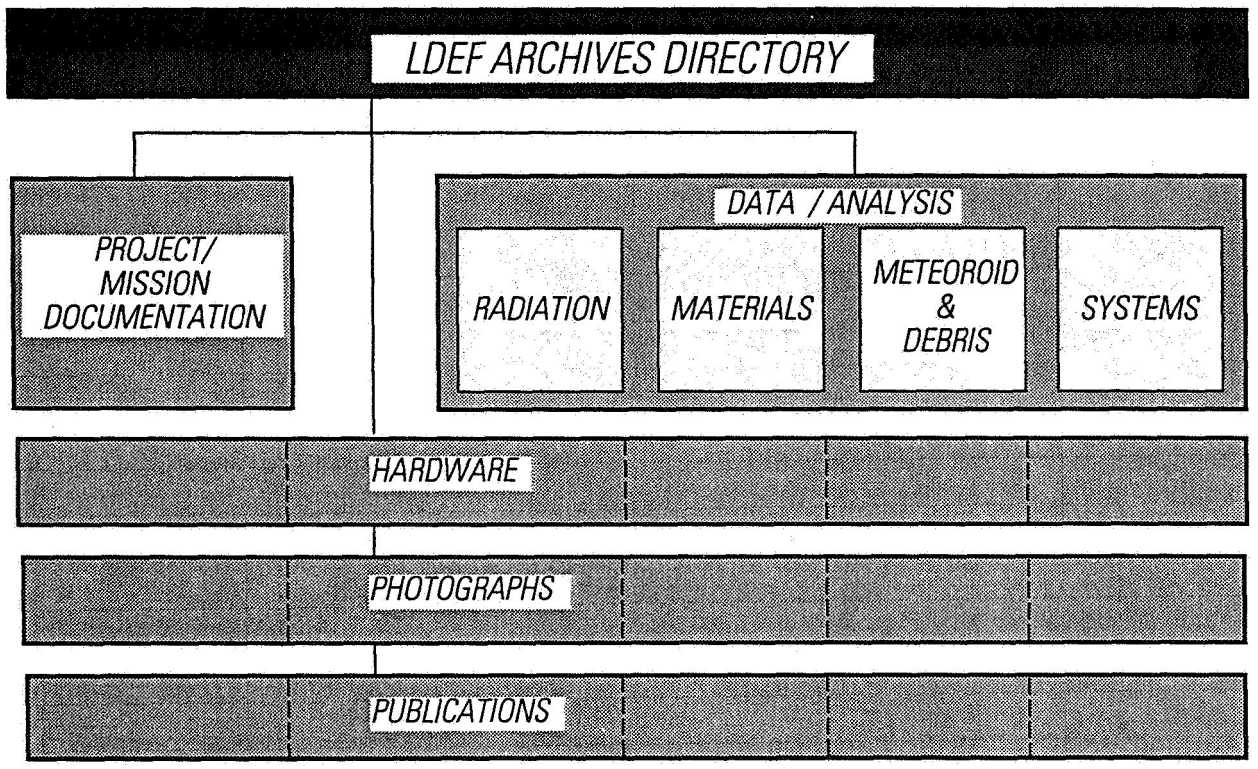

Figure 3. LDEF archival system.

The LDEF archives are categorized into five distinct archives. The project / mission documentation archive is organized chronologically. The data / analysis archive is categorical. The hardware and photographic archives are organized by location on the surface of LDEF and by experiment number. The publications will be kept alphabetically according to author. Two key identifiers, LDEF experiment number and bay / row location, will be associated with all items archived wherever applicable. These are the most commonly used references for LDEF information.

The materials to be placed in the archives are currently located throughout the LDEF community while research is being conducted. The project / mission documentation is primarily at Langley Research Center. The data / analysis archive contains many dispersed segments, and it is the most widely distributed body of information due to the participation of the large number of researchers. The hardware and test specimens are likewise widely held. A large collection of NASA photographs are being catalogued at Langley Research Center, while sizeable collections are maintained at other NASA centers and with principal investigators. A library of publications at Langley Research Center is being established, and a large collection of LDEF-related publications has been indexed. The remainder of this section describes the five archives within the LDEF archive system.

I. LDEF ARCHIVE DIRECTORY

This is an electronic directory intended to do a combination of the following: 1) identify if LDEF information is available on the subject of interest; 2) provide requested information directly; 3) identify additional databases, LDEF or other, that should be searched; 4) identify reports or data records; 5) identify related photographs; and, 6) refer to individual points of contact. It will contain the following elements:

A. Project / Mission Documentation Directory
B. Data / Analysis Directory
C. Hardware Directory
D. Photographs Directory
E. Publications Directory

The extent to which the directory either provides information directly or refers the user to other contacts or data bases for information will depend upon issues such as the current means of access for the data and the availability of other data bases. The driving factor behind the archive design is simplicity of data access.

The following are a few examples of what the directory is expected to do. The directory should identify the systems and materials which flew as parts of LDEF experiments, their locations, quantities and space environment exposures. It will also identify the purpose for the system or material, and whether it was part of the structure or part of an experiment. It is planned to summarize related research and results to date. For specific data, the directory is anticipated to refer the user to other existing data bases in the areas of interest. For instance, a user may be directed to the LDEF Materials Data Base on the Materials and Processes Technical Information System (MAPTIS) at the Marshall Space Flight Center for materials data, or to the LDEF Meteroid and Debris Data Base at the Johnson Space Center for specific information on crater locations, diameters, origins or chemistry.

II. PROJECT / MISSION DOCUMENTATION ARCHIVE

This chronological archive contains documentation generated over a period that has lasted 20 years to date. It includes drawings, technical plans, management plans, safety analysis records including flammability and hazard analysis, stress corrosion, electromagnetic interaction, and structural failures testing for static deflection and dynamic vibrational modes. This archive includes documentation on the Announcement of Opportunity process to acquire experiments and the memoranda between NASA and other organizations inside and outside of the U.S. It also will include the data recorded during flight operations involving Johnson and Kennedy Space Centers. It has the following elements:

A. General
B. Concept Development and Design Philosophy
C. Facility Design and Development
D. Acquisition and Project Tasks in Experiment Development
E. Experiment Development Organization Tasks
F. Experiment / LDEF Integration Engineering
G. LDEF / Space Transportation System (STS) Integration Engineering
H. Integration Operations
I. Launch
J. Sixty-Nine Months in Orbit
K. Retrieval
L. Post-Retrieval Deintegration Operations

III. DATA / ANALYSIS ARCHIVE

The data/analysis archive, the largest of the archives, is structured parallel to the four LDEF special investigation groups since data are currently being collected and maintained separately by these groups. This archive is intended to be the long-term location for the diverse data and models in the areas of ionizing radiation, meteoroid and debris, systems and materials currently kept by principal

investigators and special investigation groups. Each specific LDEF data set or model will be either contained or referenced in this archive.

In addition to the categorization of information according to special investigation group area, a subcategorization is that of space environment data and models, and space environmental effects data and models. The radiation and meteoroid and debris data reflect the environment as well as environmental effects, while the systems and materials data are focused upon environmental effects primarily.

Figure 4 is an simple illustration of the categorization of the data and analysis archive.

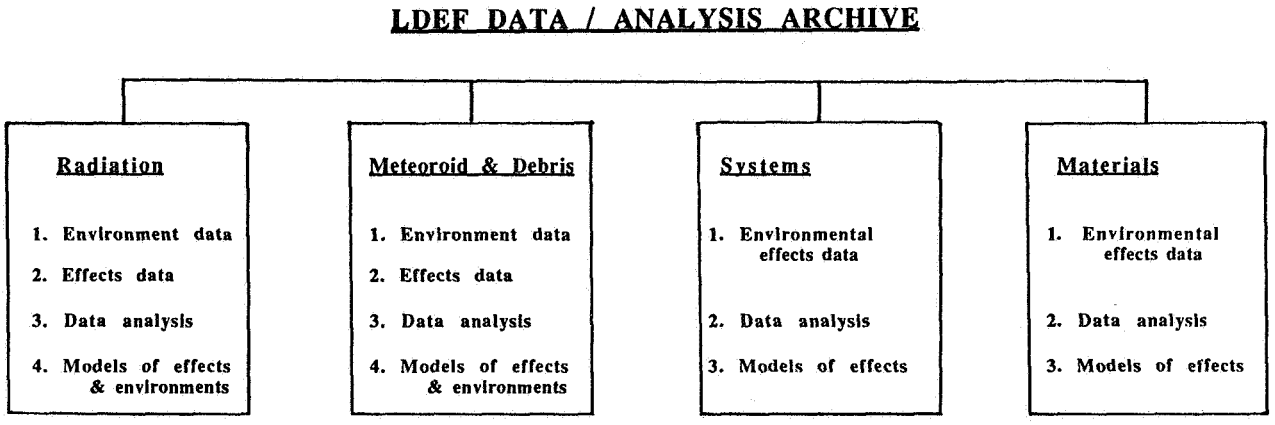

Figure 4. Data / analysis archive structure.

IV. HARDWARE ARCHIVE

A detailed and complete hardware archive has two primary benefits: it provides traceability of hardware pieces, and, it enables further research to be performed with the hardware. All experiment and facility hardware are organized according to bay / row coordinates mapped on the surface of LDEF, and additionally by location within tray. Experiment hardware and samples will also carry the associated experiment number. Subdivision of tray elements will employ the parent / daughter concept similar to some other NASA archival systems. For example, an assigned number of A02E01 would indicate bay A, row 2, experiment hardware item 01. A later specimen may have the number A02E04,1, to indicate that this is experiment hardware item 04, and that it came from a subdivision of hardware item 01. Drawings and experiment development documentation will be referenced, and the processing histories from deintegration through current location are being included.

An initial post-retrieval inventory of LDEF experiment and facility hardware has been developed by W. J. Schafer Associates based on information and documentation collected to date. Several inventory entries are shown in Figure 5. The approach used in the development of this hardware inventory system considered an individual experiment as one entity until its elements were divided and distributed, at which point the individual elements were tracked. Figure 5 details the shipment of a coating specimen mounting plate used in LDEF experiment S0010, Exposure of Spacecraft Coatings, by NASA Langley Research Center. In the nomenclature of this data base, 'Distribution 01,' the last common post-retrieval location for LDEF experiment and facility hardware was the Spacecraft Assembly and Encapsulation Facility II (SAEF-II) building at the NASA Kennedy

Space Center. Between February and May 1990, after the inspection, radiation and photographic surveys of LDEF in SAEF-II, the LDEF experiment trays and facility hardware were deintegrated and distributed. The S0010 coating specimen mounting plate was shipped via an air-ride van to Wayne Slemp, the experiment principal investigator, March 21, 1990. This is recorded as 'Distribution 02'. On April 7, 1990, this item was transferred to Don Humes, also at LaRC, for meteoroid and debris study. The item remains at this 'Distribution 03' location, LaRC building 1200, room 131. This data base system, created with the 4th Dimension program version 2.0 (© 1989 ACIUS, Inc.), is being used in constructing an all-inclusive inventory of LDEF hardware.

Experiment Number :	S0010
Hardware Item :	Coating specimen mounting plate
Item Division :	None

Distribution 0 2 From NASA Kennedy Space Center

Location :

NASA Langley Research Center

Contact:

Mr. Wayne S. Slemp
NASA Langley Research Center
36 Marvin Road
Mail Stop 183
Hampton VA 23665-5225 USA
Telephone : 804-864-1334
Telefax : 804-864-3800

Investigator : PI
Date : 3/21/90

Documentation / Comments
Air-ride van/climate controlled 70-72 degrees F.

Distribution 0 3 From NASA Langley Research Center

Location :

NASA Langley Research Center

Contact:

Mr. Donald H. Humes
NASA Langley Research Center
18 Ames Road
Mail Stop 493
Hampton VA 23665-5225 USA
Telephone : 804-864-1484
Telefax : 804-864-3800

Investigator : M&D
Date : 4/7/90

Documentation / Comments
Building 1200, Room 131. This is current location.

Figure 5. LDEF hardware archive entry.

V. PHOTOGRAPHS ARCHIVE

More than 20,000 individual photographs of LDEF, LDEF experiments, samples and research efforts are currently in the collections of LaRC, KSC, JSC, MSFC and principal investigators. These are being assembled by the LDEF Science Office in a central location and catalogued according to mission chronology, location on LDEF, and subject of interest. Individual photographic surveys were taken during the STS-32 retrieval flight, Edwards Air Force Base operations, and Kennedy Space Center operations including those at the Demating, Orbital Processing, Operations and Checkout Facilities and the Spacecraft Assembly and Encapsulation Facility II. The SAEF-II photographic records are extensive and cover the initial visual inspection period, deintegration of experiments, facility and systems, and the operations to place LDEF in storage. During deintegration, each experiment tray was the subject of a detailed photographic survey.

The LDEF archives will contain each photograph, a negative, a description of the photograph and documentation. The electronic directory will contain the photographic index, and it is intended to enable searches based on a broad set of interests, for instance, M&D craters, silver teflon, a specific polymer, or a crystal growth system. Figure 6 is an example of the photographic records currently being assembled by Lockheed Engineering and Science Corporation under contract to Langley Research Center.

from the **LDEF RETRIEVAL FLIGHT PHOTO SURVEY**

TRAY #	JSC negative # LaRC negative # Experiment # (s) and title abbreviation(s) Photograph details
TRAY B2	S32-78-16 L90-10,427 S0001: SPACE DEBRIS IMPACT Green/pink cast due to preflight anodization - appears in preflight condition
TRAY C2	S32-89-029 L90-10,498 AO015: BIOSTACK AO187: CHEMICAL & ISOTOPIC MEASUREMENTS OF MICROMETEOROIDS M0006: SPACE ENVIRONMENT EFFECTS Biostack canisters have light brown discoloration; AO187 thin foils ruptured and curled
TRAY D2	S32-89-031 L90-10,495 AO189: QUARTZ CRYSTAL OSCILLATORS AO172: SOLAR RADIATION ON GLASSES S0001: SPACE DEBRIS IMPACT Mounting plates for AO189 & AO172 have dark brown discoloration; S0001 appears in preflight condition - row 3 scuff plate appears discolored (darker) than preflight
TRAY E2	S32-89-018 L90-10,496 AO178: ULTRAHEAVY COSMIC RAY NUCLEI Silvered teflon thermal cover appears specular - cover taut and tiedown points evident
TRAY F2	S32-89-023 L90-10,497 P0004-1: SEEDS IN SPACE P0004-2: SPACE EXPOSED EXPERIMENT DEVELOPED FOR STUDENTS Silvered teflon thermal cover possibly shows evidence of diffuse area

Figure 6. Photographic archive records.

VI. PUBLICATIONS ARCHIVE

The LDEF archives will contain a copy of all LDEF-related publications available. These include publications from professional journals, NASA publications, other government publications, books and other sources. A publications library is growing through the identification and indexing of publications as they become available. The directory will catalog all publications according to author, experiment number and bay / row location, and searches will be possible based on areas of interest.

IMPLEMENTATION OF PLAN

The archival system is currently in the development stage. Project documentation archives are being organized. Data / analysis archives remain in the early development stage, although the special investigation groups have developed to varied extents their own archives of data and analysis. The directory for the retrieved hardware has been established and will continue to be expanded as hardware is circulated and subdivided. Retrieval and deintegration photograph archives have been established, and the contents are being indexed. The publications archive is also being assembled. A number of focused data bases and systems have been prepared through special investigation groups and principal investigators, and these will be either indexed or folded into the LDEF archives. The interaction and relation to existing data systems and data centers are being studied.

A number of these existing data bases were discussed at the LDEF Second Post-Retrieval Symposium, 2-7 June, 1992, and the written papers associated with these presentations are included in this Conference Publication. These presentations were on the materials data base activities, meteoroid and debris data bases, and principal investigator data bases. A session was held on materials data base activities, with presentations by the staff of the Materials and Processes Technical Information System (MAPTIS) on the LDEF Materials Data Base,[4] and by Boeing Aerospace and Defense Group researchers on a set of independent data bases on topics including optical experiments and thermal control materials developed for use on MacIntosh and IBM-compatible computers.[5] The Meteoroid and Debris special investigation group presented details of their data base, which includes five separate data tables with detailed crater data, allocation histories and other information, and it is accessible electronically via several networks.[6] The Aerospace Corporation has developed a data base of observations of LDEF experiment M0003, and this contains an extensive set of photographs and recorded observations made during the post-retrieval period.[7] Related topics discussed at the symposium included the development of handbooks on space environments and effects upon specific systems.

Individual principal investigators and special investigation groups have access to the hardware and samples in their possession until they no longer have use for them, at which time they should be returned to the LDEF Science Office. Acquisition of archived hardware elements will be handled through a review process to evaluate requests, to ensure that the maximum benefits are obtained from hardware and that the hardware are not consumed before all research opportunities are exhausted. For elements other than hardware, the LDEF archival system will meet any reasonable request for archived materials. The archive directory will be the main point of entry or contact for those seeking information on space environmental effects and LDEF.

For the archives to be utilized to the fullest extent, the space research community beyond the LDEF researchers should be made aware of the archives, their contents and applications and their accessibility. The LDEF Science Office plans to publicize its holdings to this broader community.

CONCLUDING REMARKS

The data obtained from LDEF analyses are a valuable resource, this value will be lost if not maintained for future access. Similarly, the hardware must be retained for future study and reference as part of the validation of the data obtained. Advancement of research depends upon the ease of accessibility of archived resources. Scientific conclusions are only of value if the facts upon which they are based can be traced and explained.

The LDEF archives are planned as an active and accessible library, and not a remote storage facility. The LDEF archives should be available to all who could use them. Efforts will be made to provide access to LDEF resources for educational and museum purposes when the investigators' science and technology research has been completed. As with all space flight hardware, the Smithsonian Institution has the right of first refusal if NASA decides to relinquish its possession.

The LDEF archival system is intended to form the basis of a comprehensive space environment and space environmental effects archive, and it is expected to be used by space environment and environmental effects researchers and spacecraft designers. Data from existing and future space flight experiments will be more effectively utilized with such an archival system in existence. This involves more than simple storage; it involves maintaining an active library with sufficient materials and resources.

REFERENCES

1. *A Guide To The National Space Science Data Center.* NSSDC 90-07, June 1990.

2. Blasso, Leonard, and Carol Kanga, eds., *NSSDC News.* National Space Science Data Center, Fall/Winter 1991.

3. Lauriente, Michael, EnviroNET: On-Line Information for LDEF. *LDEF - 69 Months in Space: Second Post-Retrieval Symposium*, NASA CP-3194, 1993.

4. Davis, John and John Strickland, Materials and Processes Technical Information System MAPTIS) LDEF Materials Data Base. *LDEF - 69 Months in Space: Second Post-Retrieval Symposium*, NASA CP-3194, 1993.

5. Bohnhoff-Hlavacek, Gail, Data Bases for LDEF Results. *LDEF - 69 Months in Space: Second Post-Retrieval Symposium*, NASA CP-3194, 1993.

6. Meteoroid and Debris Special Investigation Group Panel Discussion, Second LDEF Post-Retrieval Symposium, San Diego, CA, 2-7 June, 1992.

7. Gyetvay, S. R., H. K. A. Kan, J. M. Coggi and M. J. Meshishnek, Long Duration Exposure Facility Experiment M0003 Deintegration Data Base. *LDEF - 69 Months in Space: Second Post-Retrieval Symposium*, NASA CP-3194, 1993.

N93-29705

501767

RETRIEVABLE PAYLOAD CARRIER --NEXT GENERATION LONG DURATION EXPOSURE FACILITY: UPDATE '92--

A.T. Perry, J.A. Cagle, S.C. Newman
American Space Technology, Inc. (AmSpace)
2800 28th Street, Suite 155
Santa Monica, CA 90405-2934
Phone: 310/450-7515, Fax: 310/450-7304

ABSTRACT

Access to space and cost have been two major inhibitors of low Earth orbit research. The Retrievable Payload Carrier (RPC) Program is a commercial space program which strives to overcome these two barriers to space experimentation. The RPC Program's fleet of spacecraft, ground communications station, payload processing facility, and experienced integration and operations team will provide a convenient "one-stop shop" for investigators seeking to use the unique vantage point and environment of low Earth orbit for research. The RPC is a regularly launched and retrieved, free-flying spacecraft providing resources adequate to meet modest payload/experiment requirements, and presenting ample surface area, volume, mass, and growth capacity for investigator usage. Enhanced capabilities of ground communications, solar-array-supplied electrical power, central computing, and on-board data storage pick up on the path where NASA's Long Duration Exposure Facility (LDEF) blazed the original technology trail. Mission lengths of 6-18 months, or longer, are envisioned. The year 1992 has been designated as the "International Space Year" and coincides with the 500th anniversary of Christopher Columbus's voyage to the New World. This is a fitting year in which to launch the full scale development of our unique ship of discovery whose intent is to facilitate retrieving technological rewards from another new world: space. Presented here is an update on progress made on the RPC Program's development since the November 1991 LDEF Materials Workshop.

INTRODUCTION

The RPC spacecraft which AmSpace has been developing for the past 4 years is designed for compatibility with a number of active and passive payload classes: materials exposure, space environment characterization, microgravity processing, life sciences, and remote sensing. Serving as a space-based technology test bed, the RPC also enables in situ technology demonstration and Space Station Freedom precursor experimentation. In situ technology demonstration provides for simultaneous exposure to multiple space environments in a manner which cannot be duplicated on the ground. Precursor experimentation permits a phased approach to the maturing of science data and hardware in preparation for more extensive and expensive station-based experimentation, thus reducing long term risk for the investigator.

Progress on the RPC Program has been made on several fronts since the November 1991 LDEF Materials Workshop held at NASA's Langley Research Center, including NASA, experimenters, and the concept itself. The intent here is primarily to provide a program update and not repetition of previously presented material [1]. Included in the following discussion is a brief review of the program components and current status.

PRECEDING PAGE BLANK NOT FILMED

Carrier Element

The baseline RPC spacecraft is designed for shuttle launch and retrieval on a regular basis. The RPC is a gravity-gradient stabilized free-flyer. The RPC maintains the same 13.5 foot diameter cross-section as LDEF, a twelve-sided regular polygon, and uses the same low cost aluminum I-beam construction (Figure 1). However, in contrast with LDEF's 30 foot length, the baseline RPC is only 40 inches long which increases opportunities for manifesting in the shuttle cargo bay for launch and retrieval, helps lower the early launch costs, and reduces orbital life-limiting atmospheric drag effects at lower altitudes. On the first mission, the design provides for 600 W of 28 Vdc electrical power, 9.8 kbps downlink data rate, 10 gigabits data storage, and central computing capability, with even greater capabilities planned for future missions. The empty weight is 2,443 pounds with a maximum payload capacity of 5,600 pounds, for a total maximum weight of 8,043 pounds. Use of the full shuttle cargo bay cross-section increases the volumetric efficiency which reduces the launch cost.

The RPC flies edge-on into the velocity vector (ram direction). The # 6 position is always nadir pointing (toward the Earth's center) and the # 12 position is always deep space pointing. Stabilization booms 33 feet in length with 100 pound payload tip masses project out of the # 9 and # 12 peripheral positions on the RPC. Magnetic torquers provide for additional stability.

A number of experiments can be accommodated on the RPC in stacked or unstacked configurations. In Figure 1, several duplicate experiments are distributed around the RPC in locations which may be of interest for taking simultaneous data: ram direction, trailing edge, deep space pointing (zenith), and earth pointing (nadir). Gravity gradient booms, with powered and controlled pallets at the tips, provide reduced spacecraft-induced environments for those payloads.

Although two duplicate experiments are shown in the # 3 peripheral pallet, 1-4 duplicate or different experiments can be mounted in a pallet equal in size to an LDEF end tray (Figure 2). Multiple experiment capacity in a single pallet may permit larger active and passive sample sizes.

The approach calls for a fleet of at least two of these low cost spacecraft to be alternately launched. As the market grows over time, opportunities will exist for families of dedicated missions.

The overall functional block diagram is included to indicate various services and resources available to payloads, including relatively precise Global Positioning System (GPS) 3-dimensional location information (Figure 3). This may be of use for correlation with, for example, atomic oxygen erosion rates on samples as a function of altitudes which typically range from 150-225 nmi. New, low cost, solid state gyroscopes will provide 3-axis attitude information accurate to 0.1 degree. This position and attitude data can be continuously stored and dumped to the ground on a daily basis along with active sample data.

Carrier Sizing Rationale

With the objective of reducing overall costs, a deliberate attempt to minimize the RPC length has been made because commercially launched shuttle payloads, such as the RPC, must pay NASA on the basis of a launch pricing formula as a function of length or weight. The formula is:

Launch cost = standard transportation costs + optional service costs, where:

Standard transportation costs = (greater of length cost factor or weight cost factor) X (full cargo bay price / cargo bay utilization factor)

RPC length cost factor = RPC length/cargo bay length = 40 in / (60 ft x 12 in/ft) = 0.056

RPC weight cost factor = RPC weight / maximum shuttle payload to orbit performance = 8,043 lbm (assuming a fully loaded RPC) / 65,000 lbm (originally advertised shuttle capability) = 0.124

Cargo bay utilization factor = 0.75 (NASA imposes this additional cost factor to account for average inefficiencies in using the full shuttle payload weight-to-orbit capability; that is, on most missions, the full length of the cargo bay is filled with payloads that cumulatively use only about 75 percent of the full weight-to-orbit capability)

Optional service charges cover those services which are "non-standard" in nature, such as deployment, retrieval, associated training, non-standard altitude, and many others, and are priced according to published NASA rates.

For transportation costs, RPC customer cumulative payload weights in excess of 1,168 pounds drive the cost to the weight cost factor. Early in the RPC life cycle, when still building the market and capital is limited, length is the driver, thus it is important to keep the length as short as possible while still meeting experimenter requirements. However, as the market increases, there is the opportunity to increase the RPC length to meet evolving experimenter requirements, and yet, not suffer an undue launch cost penalty. Because of the simple, bolted construction, the RPC's length can be increased relatively easily.

By using the full cross-section of the shuttle cargo bay and a dense-packaging philosophy, the RPC's volumetric efficiency far exceeds most other carriers. That is, more payload mass is carried in less volume, resulting in approximately a 70 percent payload-to-total-spacecraft mass fraction. This is an important consideration when using a limited national resource such as the shuttle.

In originating the RPC, holding down the development and operational expense is paramount to keeping customer charges affordable. Private sector commercial development and operations costs of a program of this nature have been shown to be 25-50 percent of a government developed program cost estimate and is another important decision factor in today's austere economic climate. Aside from lower costs to the taxpayer, the RPC Program provides for technology transfer to private industry and for creation of a new industry infrastructure element, the cornerstone of the U.S. Government's 1991 Commercial Space Policy Guidelines.

Ground Station/Mission Operations Center Element

The ground station, Mission Operations Center (MOC), is an off-the-shelf, low cost Master Ground Station (MGS) for the command and control of multiple low Earth orbiting satellites, experiments, and remote ground terminals. It provides mission planning, satellite command and control, digital store-forward communications, and spacecraft and experiment telemetry readout. The MGS operates at UHF (with VHF and S-band as options). The MGS consists of an operator console, a transceiver unit and antenna group, and can be operated remotely.

Ground-based data acquisition by an experimenter would occur by modem access to the AmSpace secure, off-line hard drive on which downlinked data is stored after each pass over the ground

station to be located in Florida, or possibly by direct downlink. Control of payloads is accommodated by the experimenter providing time-tagged command stacks to the ground station via modem which are verified for non-interference with spacecraft operations and then uplinked and executed or stored for later on-board execution.

Payload Processing Facility Element

The AmSpace Payload Processing Facility and the Mission Operations Center will be located near Kennedy Space Center, Florida, either at an industrial park near Titusville, Florida or the Cape Canaveral area. AmSpace intends to provide a first-rate building with the needed space for experiment checkout, RPC integration, operations, administration and expansion to meet projected demands for the next 15 to 20 years. AmSpace is currently investigating whether construction of a new facility, buying an existing building, or leasing a facility is the most cost effective approach.

Although other locations were considered, such as Los Angeles, Houston, and Huntsville, Alabama, selection of the Florida Space Coast included the following considerations:

- Proximity to the launch site
- Transportation cost and route access to the launch site
- Land, construction, and facility leasing cost
- Room and cost for expansion
- Material costs and availability
- Proximity to related businesses
- Labor pool availability, skills, and costs
- Local ordinances, licensing, and permit requirements
- Community and state positive attitudes towards space industry

The Payload Processing Facility includes offices, conference rooms, and the Mission Operations Center located at the front of the facility. Sufficient offices are provided to accommodate the AmSpace staff and provide limited office or experiment build-up space for RPC experimenters. The Mission Operations Center is located in the center of the building's office space to provide a degree of security. The two high bays, located in the rear of the facility, have 20-25 foot ceilings to permit lifting and loading or removing an RPC to or from a transportation container. Typical high bays have higher ceilings (30 feet or more), but AmSpace intends to perform limited lifting using floor-based lifters. The lower high bay ceilings will reduce the expense of maintaining environmental control of the high bay volume. Also, using floor-based lifters will preclude the expense of installing and maintaining overhead cranes. A clean room is provided primarily for customer use during experiment build-up and post-flight examination.

Initially, only one high bay will be outfitted. As the second RPC comes on-line, the second high bay will be activated. Access to the high bays are through walk-in airlocks, or the main airlock which is used for moving major equipment items. Sufficient high bay floor area is provided for moving the RPCs around. Simultaneous work on floor-accessible and upper portions of the RPC is facilitated by a work platform. A rotator hub rotates to provide access to other RPC locations. Various tools, electronic test equipment, racks, jacks, hoists, power outlet panels, gas distribution and air pallets are located within the high bays. A machine shop located outside the high bay will meet simple manufacturing needs.

Electric power to the MOC, selected offices, high bays and the clean room will be 120/240 volts AC power protected by an Uninterruptable Power Supply (UPS). Using a UPS will provide protection to delicate experiments and test equipment in the event of unannounced power outages

or fluctuations. Electric power to most offices, and the machine shop, will not be UPS protected. The electrical system in the high bays, offices, and clean room will not be hazard proofed.

Inert gases, such as nitrogen, clean air, and helium, will be distributed to selected offices, high bays and the clean room using K-bottles. The equipment and system to vent inert gases to the outside atmosphere will also be provided. The use of other inert gases, such as argon, will require special arrangements and as with the above gases, will be vented outside the facility. Volatile gases, such as oxygen and hydrogen, will not be available at the processing facility.

All required safety and fire protection equipment will be provided in the facility. This includes eye washes, electrical safety equipment (shorting sticks, rubber electrician gloves, etc.) and emergency lighting. In addition, containers for the disposal of hazardous waste will be provided. Sufficient fire extinguishers will be available in the offices and work areas and a sprinkler system will be installed in the administrative work areas. A Halon Discharge System will be installed in the MOC, high bays and clean room.

CUSTOMER ACCOMMODATIONS

Experiment Build-up and RPC Integration

The Payload Processing Facility will provide sufficient space to allow experimenters to build-up and test their experiments before being integrated with the RPC. Customers will be assigned an area or office space to build-up their experiments, perform pre-installation checks and test their experiments. The facility will provide basic test equipment, tools, stabilized power, handling devices, and some administrative support, e.g. tables, chairs, telephones, desk, etc. Special test equipment, tools, computers or diagnostic equipment must be provided by the customer. The area assigned for experiment build-up and check-out can be secured. If special environmental controls are required, customers will be scheduled to use the facility clean room. Support requirements such as housing, transportation, and meals are the responsibility of the customer.

RPC Integration and Post-flight De-integration Scheduling

Detailed scheduling for all RPC integration and de-integration activities is planned. A 72 hour, 11 day schedule, similar to the Kennedy Space Center Integrated Control Schedule, will be published each work day. Integration/de-integration activities, facility maintenance, scheduled power outages, and any other planned activity which affects productive integration/de-integration time will be included in the 72 hour, 11 day schedule. RPC customers and the AmSpace staff will coordinate the preparation of all schedules. Also, long range schedules, up to five years, will be developed for long term planning purposes. AmSpace intends to develop facility use schedules which provide customers sufficient integration time and ensure cost-effective use of the processing facility.

AMSPACE SRM&QA PROGRAM

AmSpace plans to develop and implement a dynamic and comprehensive Safety, Reliability, Maintainability and Quality Assurance Program (SRM&QA). The AmSpace SRM&QA program will complement and in some cases exceed NASA SRM&QA requirements. All Occupational

Safety and Health Act (OSHA) Standards are to be rigorously applied at the AmSpace Payload Processing Facility. State of Florida safety regulations, occupational health criteria and environmental requirements will be strictly enforced by a staff of experienced SRM&QA professionals. However, the distinguishing characteristic of the AmSpace SRM&QA program is its customer orientation.

The AmSpace SRM&QA philosophy is to assist and advise customers and to provide a safe working environment for the integration and post-flight de-integration of their experiments. AmSpace's assistance should aid in lowering ground processing and launch costs, and facilitate experiment integration. With regard to a safe working environment, a first-rate facility with all required safety equipment will be provided. Furthermore, AmSpace intends to train and, if necessary, certify customer engineers and technicians on the operation of any system, equipment or devices they use in the build-up and integration of their experiment.

AmSpace is fully committed to the safe and successful integration, launch, mission operations, and de-integration of the RPC. SRM&QA criteria and standards cannot be compromised.

Customer Safety Implications

Before any payload is processed at the launch site and flies on the shuttle, stringent SRM&QA criteria must be met. The RPC must have formal NASA certification for launch site processing and flight. The RPC and customer payloads' construction, wiring, materials, and interfaces with the launch vehicle and other payloads must comply with exacting engineering standards. AmSpace, serving as a Payload Organization (PO), is responsible to ensure that the RPC and its payload complement complies with all applicable design, manufacturing and operations specifications. AmSpace must demonstrate to NASA, through engineering analyses and reviews, that the RPC and payloads comply with applicable engineering criteria and no hazards will be introduced, either during ground processing or flight, which endangers life, other payloads, or the shuttle.

The process of obtaining NASA certification, which allows a payload to be processed at the launch site and to eventually fly on the shuttle, is usually a lengthy process. Depending on the complexity of the payload, the certification process can take up to three to five years for the most complex experiments. Typical experiments may take six to eighteen months. A myriad of documents and engineering analyses must be submitted by AmSpace for NASA review and evaluation. In addition, AmSpace must make formal presentations to a NASA Ground Processing Safety Review Panel and a Flight Safety Review Panel at various stages of the experiments' or RPC's development to ensure compliance with NASA SRM&QA requirements.

The PO obtains NASA certification to proceed with launch site ground processing and fly a payload by participating in NASA's Payload Phased Safety Reviews. Phased reviews take place for both ground processing and flight and generally are conducted independently of each other. For both ground and flight, there are four Phased Safety Reviews, Phase 0 through Phase III. These reviews correlate with the milestones that occur during a typical program life-cycle: concept review (Phase 0); 30% design review (Phase I); 60% design review (Phase II); and 90% design review (Phase III). Normally, the Ground Phased Safety Reviews and the Flight Phased Safety Reviews occur at the same time in the life-cycle development of the payload.

The phased reviews are scheduled by the PO, with NASA concurrence. A Phased Safety Data Package for each Flight and Ground Phased Safety Review is submitted to the applicable NASA Center Safety Office no later than 45 days before the agreed upon meeting date. Ordinarily, Flight Phased Safety Reviews are held at Johnson Space Center, Texas, while Ground Phased Safety Reviews are held at Kennedy Space Center, Florida. The safety data packages, for both flight and

ground processing, contain an explanation of the payload's mission, description of the payload and vital background data. Most importantly, the safety data packages contain Hazard Reports (HRs). For every hazard that the PO expects will occur or is introduced by the payload, during either ground processing or flight, an individual HR is prepared. Since the phased safety review process is an iterative process, the Phase 0 HR usually identifies the hazard and minimal information is provided regarding control or abatement of the hazard. During the subsequent submission of the HR, in the Phase I through III data packages, detailed explanation is provided on how the hazard is either eliminated or is controlled by design improvements, procedures or warning devices. The PO must submit supporting engineering data and drawings with each HR to support engineering assessment. Upon submission of the phased safety data packages, selected NASA engineers, at the launch site for ground processing packages and JSC for flight packages, perform an exacting engineering review of each HR. This NASA review is to ensure the PO has sufficiently and accurately identified, considered, and assessed all possible hazards.

The Phased Safety Reviews, for each phase level, are scheduled presentations during which the PO provides a briefing on the payload and discusses in detail each HR. Any questions and issues are resolved during the presentation. If there are any concerns that require additional research, action items with suspense dates are assigned. If there are no problems, individual HRs are signed by both the PO and the Chairman of the Phased Safety Review Panel to indicate the HR has been approved for the applicable phase review.

To facilitate this phased safety review process, lower processing costs, and lessen the burden on prospective experimenters of the preparation of SRM&QA documentation, AmSpace intends to serve as a focal-point and prepare all required phased safety data packages. AmSpace plans to begin an early dialogue with potential experimenters so they will be aware, in the conceptual phase of their experiment, of the NASA SRM&QA requirements for ground processing and flight. This early dialogue not only serves to make AmSpace's job of preparing the phased safety data packages easier, but it will hopefully aid experimenters in the design, development, and manufacturing of their experiments.

With the experimenter's decision to fly on the RPC, AmSpace intends to provide a tutorial and detailed written instructions on the steps and procedures necessary to obtain NASA safety certification to process and launch the experiment on the RPC. Depending on the complexity of the experiment, this initial briefing can be accomplished either at the experimenter's offices, or at the AmSpace Payload Processing Facility. For less complicated experiments, the initial SRM&QA briefing can be conducted by teleconference. The purpose of this introductory tutorial is to acquaint prospective experimenters with the documentation required by NASA. Furthermore, it acquaints experimenters with the list of regulations, directives, codes, standards, and specifications which must be met in the design, development, construction, transportation, ground processing and eventual flight of an experiment. Also, AmSpace's early contact with potential customers fosters cooperation and contributes to a team approach in the integration of the RPC.

AmSpace will necessarily rely on the basic engineering data and information provided by prospective experimenters in order to prepare engineering assessments and the ground and flight safety data packages. The AmSpace SRM&QA staff expects to have continuing discussions with experimenters. Questions regarding design and construction of an experiment will be encouraged. AmSpace's policy will be to expedite answers to questions from our customers. Furthermore, the AmSpace SRM&QA and engineering staff intends to make informed suggestions to prospective customers regarding the experiment design and construction, which should facilitate NASA approval to process and fly on the RPC.

Another related service, which the AmSpace SRM&QA Office intends to provide, is to act as an intermediary between customers and appropriate NASA offices. Since the members of the AmSpace SRM&QA staff will possess previous experience working with numerous NASA offices

and managers at both KSC and JSC, AmSpace will represent RPC experimenters at technical interchange meetings, scheduling meetings, safety reviews, and support requirements meetings, reducing the experimenters travel expenses. The AmSpace Payload Processing Facility will be near KSC so interfacing with NASA managers at the launch site is expected to be on a day-to-day and face-to-face basis.

In summary, AmSpace intends to establish a customer-oriented SRM&QA program. The company will serve as a focal point in the preparation of Phased Safety Data Packages, as well as other required SRM&QA documents. The intention is to provide an SRM&QA expertise to customers and assist experimenters in the preparation of safety, quality assurance, reliability and maintainability data. In addition, AmSpace intends to provide customers with a safe processing facility for the build-up, testing, integration, and de-integration of their experiments.

TEAM ELEMENT

Of the four RPC Program elements, the team is the most important because it is the one which implements the remaining elements. The following discussion outlines the innovative approach to be taken in ensuring that the best possible services are provided to customers. The AmSpace strategic human resources (HR) plan integrates business-level strategy and career management. AmSpace has adopted a "team member" approach as opposed to the traditional "employee" approach to staffing. Technical quality management techniques are employed. A mentor-protege relationship has been formalized to reduce the learning curve and preclude haphazard time-consuming trial and error methods of accomplishing tasks. Training and development are provided on-site and off-site (possibly at KSC). The "defender" and "prospector" approaches are combined, where a defender is focused on efficiency/doing things right/problem solving, and a prospector is concerned with effectiveness/doing the right things/problem finding.

Finally, a direct link between company success and paycheck size will be emphasized. The HR plan has "hooks" and "scars" into customer requirements and results in the greatest possible satisfaction of customer needs.

CURRENT STATUS

Contact with NASA on this program was initiated in 1988. A draft Joint Endeavor Agreement (JEA) was completed by NASA and AmSpace in February 1992 in anticipation of approval of the RPC Program business plan. In March 1992, an extensive RPC Program business plan was submitted by AmSpace to NASA and is still under review. The business plan must be approved before the JEA can be circulated through NASA for approval. JEA terms and conditions are currently proprietary pending finalization and NASA approval, but are generally similar to earlier JEAs. Customer flights under this JEA are particularly favorable in an economic sense. The JEA is a tool NASA has at its disposal to assist industry in demonstrating a new space capability with commercial promise. As of the completion of this paper in November 1992, major reorganizations of NASA offices interacting with AmSpace are continuing, inauguration of a new president is imminent, and the RPC Program is still awaiting approval. Government, industry, university, and international customers continue to express strong interest in flying payloads on the RPC via numerous letters of interest. Materials exposure, environment characterization, life sciences, and technology demonstration experiments dominate current customer interest. Investors await NASA decisions and customer commitments. The RPC spacecraft is anticipated to be available for launch as early as 24 months after capitalization.

REFERENCE

1. "Retrievable Payload Carrier (RPC)-Next Generation Long Duration Exposure Facility," Arthur T. Perry, NASA CP-3134, First LDEF Post-flight Symposium, Orlando, FL, June 4, 1991.

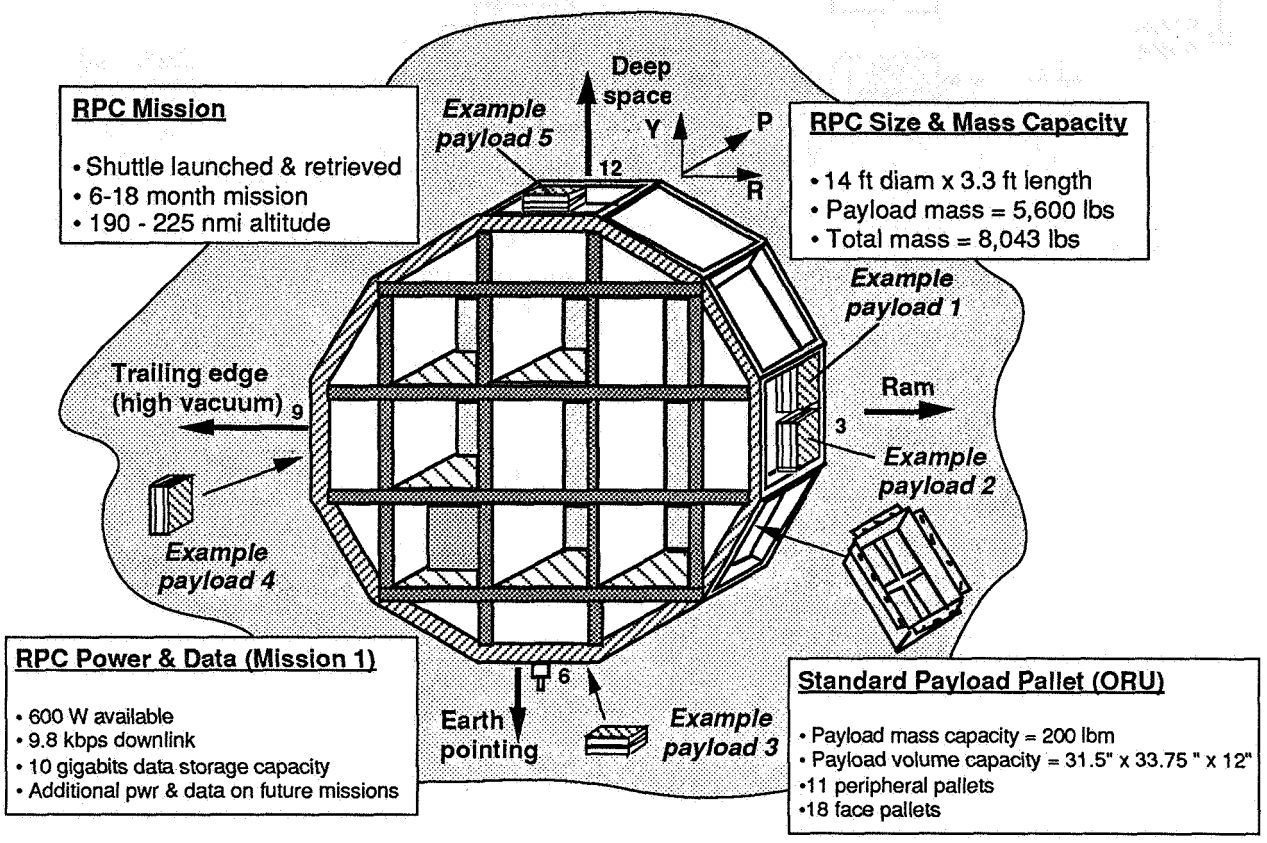

Figure 1. RPC Configuration and Duplicate Experiment Location Options

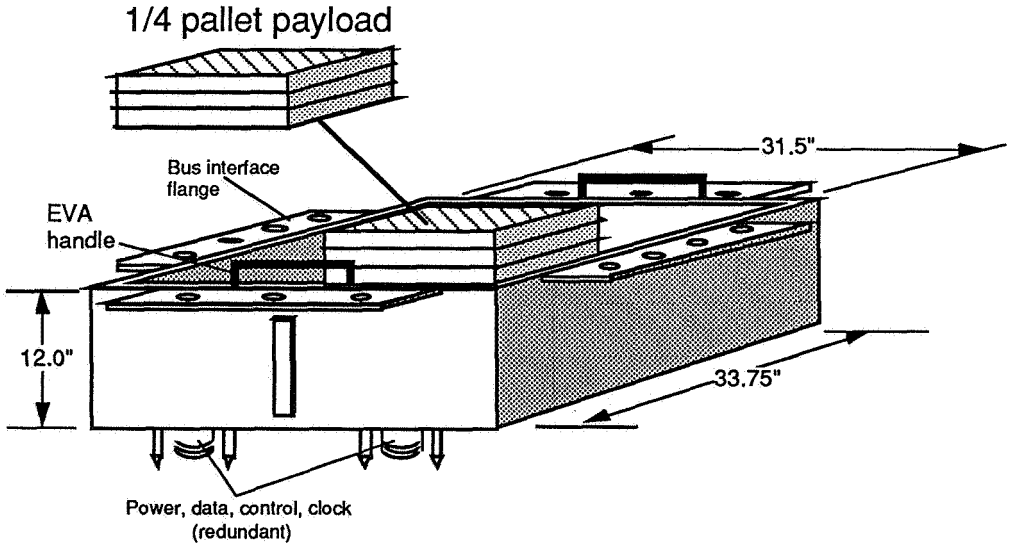

Figure 2. RPC Standard Payload Pallet (Orbital Replacement Unit-ORU)

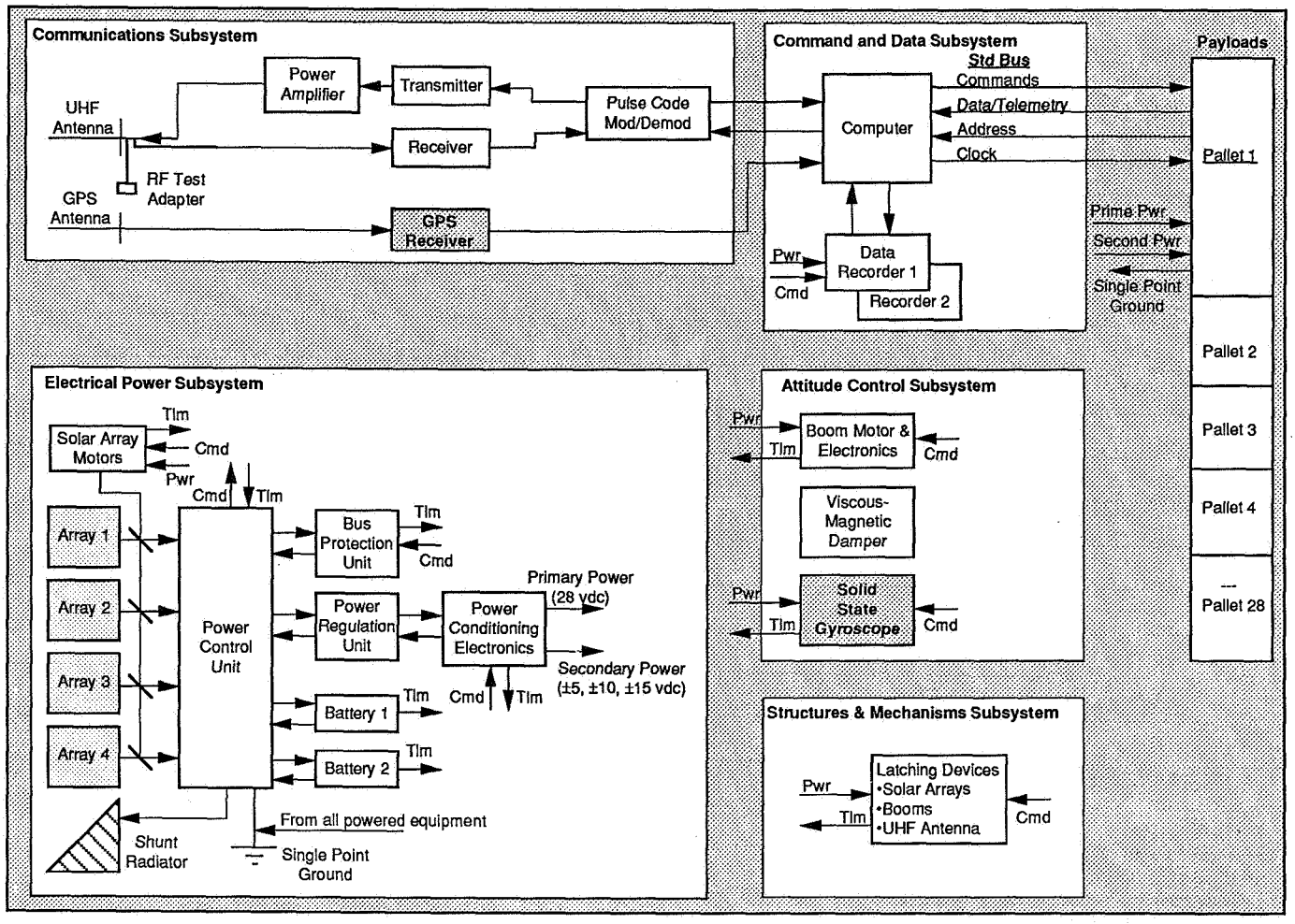

Figure 3. RPC Functional Block Diagram

N93-29706

501762
pg 14

NEXT GENERATION OPTICAL INSTRUMENTS AND SPACE EXPERIMENT BASED ON THE LDEF THERMAL CONTROL SURFACES EXPERIMENT (S0069)

Donald R. Wilkes
AZ Technology, Inc.
3322 Memorial Parkway SW, Suite 93
Huntsville, Alabama 35801
Phone: 205/880-7481, Fax: 205/880-7483

SUMMARY

The Thermal Control Surfaces Experiment (TCSE) was a successful experiment to study the effects of the space environment on thermal control surfaces using in-space optical properties measurements combined with post-flight analyses. The TCSE reflectometer performed well on the LDEF mission demonstrating that a portable compact integrating sphere spectroreflectometer can be built that is rugged and space rated. Since the retrieval of the TCSE package from space, several other instruments have evolved from its pioneering technologies. These are the Optical Properties Monitor (OPM), the Laboratory Portable SpectroReflectometer (LPSR), and the Space Portable SpectroReflectometer (SPSR). These instruments and experiment packages are the subject of this paper.

OPTICAL PROPERTIES MONITOR

Optical materials (including thermal control surfaces) continue to play increasingly important roles on operational spacecraft and in scientific instruments. The stability of materials used in the space environment continues to be a limiting technology for space missions. This technology is important to all users of space -- NASA, Department of Defense (DoD), Industry, and Universities. The Optical Properties Monitor (OPM) offers a comprehensive space research program for studying the effects of the space environment -- both natural and induced -- on optical, thermal, space power and other materials. The OPM will provide an in-space materials testbed for the optics and thermophysics communities. This common in-space testing facility will become an important part of many materials and space hardware development.

The OPM is being developed under the NASA Office of Aeronautics and Space Technology (OAST) In-Space Technology Experiment Program (INSTEP). The OPM program is currently in Phase B with the PDR scheduled for August, 1992. The Phase A effort selected the optical instruments and environmental monitors to study a wide variety of materials problems in space. It is currently planned for the OPM to fly aboard a reflight of the ESA's EURECA free flier in 1997. EURECA provides an early opportunity for extended space exposure and retrieval of the OPM and its test samples.

Experiment Objectives

The primary objective of the OPM Experiment is to study the natural and induced effects of the space environment on optical, thermal control, and other materials. Specific objectives are:

A. *To determine the effects of the space environment on materials* - the effects of the space environment on materials are not well understood. This experiment will provide detailed in-situ optical measurements of these effects to enhance the understanding of the damage mechanisms caused by the synergistic constituents of the space environment. This understanding will enhance the efforts to develop space stable materials.

B. *To provide flight testing of critical spacecraft and optical materials* - The constituents of the space environment--and certainly the combined environment--cannot be simulated exactly. For this reason, the only sure test of materials--particularly newly developed materials--is to test the material in space, eliminating the uncertainties of simulation testing. The materials to be tested include, but are not limited to those shown in Figure 1.

Thermal Control Surfaces
- sprayable coatings
- conversion coatings (anodize, alodine, etc.)
- Optical Solar Reflectors (OSR)
- second surface Teflon mirrors

Solar power materials
- flexible substrates
- protective coatings
- interconnects
- coverglasses
- solar dynamic mirrors

Optical materials and coatings
- mirrors
- windows
- gratings
- filters
- lenses

Figure 1. Candidate OPM test materials.

C. *To validate ground test facilities and techniques* - The current generation of laboratory space simulation facilities is extremely complex and well-designed. However, because of the inability to simulate the space environment exactly, these facilities provide only relative performance of test materials in these limited conditions. Past flight measurements show significant disagreement between flight and laboratory data. An important objective of this experiment is to provide a "calibration" for ground test facilities and techniques with in-space measurements of the same properties measured in ground tests.

D. *To develop a multifunction, reusable flight instrument for optical studies* - There is a need to test many different materials in space and under different conditions of environment, orientation, temperature, duration, etc. More than one space experiment will be required to satisfy the many requirements. The OPM flight instrument will be designed to be reflown with minimum refurbishment and will allow easy reprogramming to meet varied mission requirements.

Experiment Description

The Optical Properties Monitor (OPM) is a reusable multifunction in-flight laboratory for in-situ optical studies of materials. Selected materials will be exposed to the space environment and the effects of this exposure measured with on-board optical instruments.

The OPM instruments will measure total hemispherical reflectance, Total Integrated Scatter (TIS) and Vacuum UltraViolet (VUV) reflectance/transmittance. Selected constituents of OPM mission environment are monitored including irradiance, atomic oxygen fluence and molecular contamination. Flight versions of laboratory instruments will be used to perform in-space measurements. A summary of the OPM measurements is shown in Figure 2.

The OPM is a fully integrated package as shown in Figure 3 with the three optical measuring instruments positioned around the periphery of a circular sample carousel. The two contamination monitors (TQCM) and the Atomic Oxygen (AO) monitor are mounted on either side of the exposed portion of the carousel and have the same view of space as the exposed test samples. The Data Acquisition and Control System (DACS) is located inside the OPM enclosure and beneath the carousel.

The test samples are arranged on a circular carousel in four rows. The outside three rows of samples are called "active" samples because they are measured by the OPM optical instruments. The samples on the inner row are designated as "passive" because these samples are not measured in space, but are evaluated in pre- and post-flight testing. The outside row of samples is measured by the VUV spectrometer. The VUV samples must be on the outside to allow for the detector calibration. The second row of samples is measured by the integrating sphere reflectometer. These samples are mounted on calorimeter sample holders for the determination of solar absorptance and total emittance. The third row of samples is measured by the TIS instrument. The integrating sphere, the TIS Coblentz sphere, and one of the two VUV detectors are positioned above the carousel and measure the test samples as the carousel rotates each sample into position.

Spectral Total Hemispherical Reflectance

1. Spectral range - 250 to 2500 nm
2. Accuracy - ± 3%
3. Repeatability - ± 1%
4. Spectral resolution - 5% of wavelength or better

Total Integrated Scatter

1. Wavelengths
   a. 532 nm
   b. 1064 nm
2. Scatter collection angle - 2.5 to 80 degrees from specular
3. Accuracy - ± 10%
4. Repeatability - ± 2%
5. Surface rms measurement range - 5-500 Å

VUV Transmittance/Reflectance

1. Wavelengths
   a. 121.6 nm
   b. 160.6 nm
   c. 170 nm
   d. 180 nm
   e. 200 nm
   f. 250 nm
2. Accuracy - ± 5%
3. Repeatability - ± 5%

Calorimetric Measurements

1. Total emittance: Accuracy - ± 5%
2. Solar absorptance: Accuracy - ± 5%

Environmental Monitors

1. Molecular contamination
   a. Temperature-controlled Quartz Crystal Microbalance (TQCM)
   b. Specially selected witness samples for post flight analysis
2. Atomic oxygen monitor: multiple carbon film sensors
   a. Sensitivity - 1 x 10^{16} atoms/cm^2
   b. Fluence range - 1 x 10^{18} to 5 x 10^{20} atoms/cm^2
   c. Fluence range is adjustable by varying carbon film thickness
3. Irradiance monitors
   a. Direct solar
   b. Earth albedo
   c. Earth IR emittance
   d. Measurement accuracy - 5%

Figure 2. OPM measurement summary.

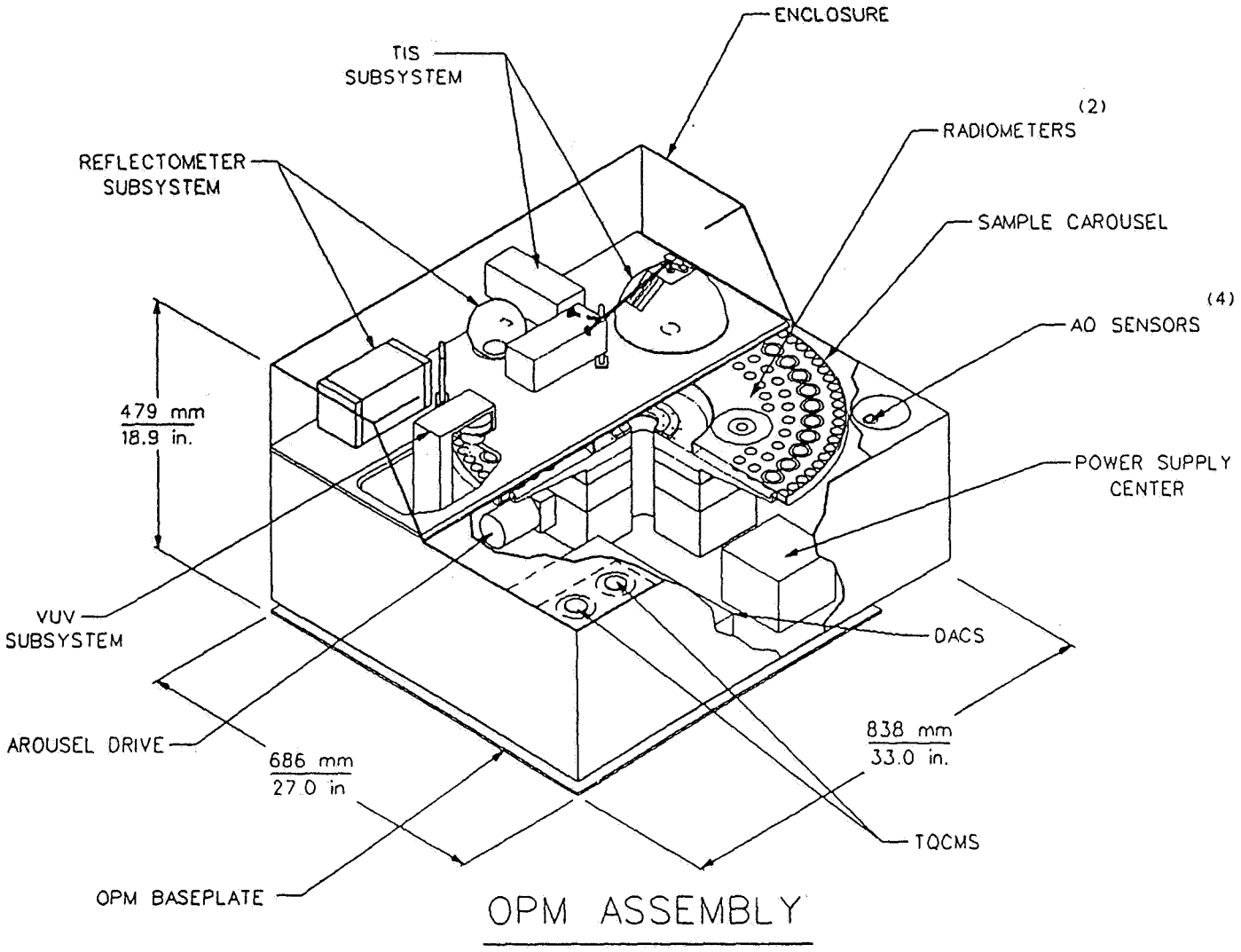

Figure 3. OPM instrument assembly.

C-4

Only half of the carousel and the test samples are exposed at one time. The samples that will be exposed during the operational orbit are not exposed during ground processing, launch, orbital transfer maneuvers (OTM), and deorbit operations. A second set of samples is exposed during these periods and will be measured before and after OTM to the operational orbit and again before and after OTM to the parking orbit for retrieval by the Shuttle.

LABORATORY PORTABLE SPECTROREFLECTOMETER (LPSR)

The Laboratory Portable SpectroReflectometer (LPSR) is a unique integrating sphere instrument for easily and quickly measuring total hemispherical reflectance of almost any surface over the solar region of the spectrum (250-2500nm). The instrument incorporates innovative optical, mechanical, and electronic designs to provide state-of-the-art performance in a compact and portable configuration. The LPSR has been designed for use both in the field for measuring the extended surfaces of operational or developmental hardware and for use in the laboratory on test specimens of varying sizes. The LPSR provides highly precise and accurate data on all types of surfaces without the errors present in some less sophisticated designs.

The LPSR user interface provides one button operation for standard measurement scans or selectable options for special measurements. A manual operation mode is also provided. The menu-driven data display leads the user through the setup and operation of the LPSR including the display of the measurement data. Automatic integration of the reflectance data is performed to calculate and display solar absorptance. Internal non-volatile storage of up to 40 full measurement scans is provided for field measurements.

Interface and database software is provided for a host PC compatible computer for retrieving, archiving, and data display of LPSR data. Remote operation is also provided by the host software with full control of all LPSR functions. The LPSR/PC host connection is made through a standard PC serial interface.

LPSR-200 Specifications

The AZ Technology LPSR model 200 is a commercially available instrument to perform total hemispherical spectral reflectance measurements on almost any shape, size or type surface. The measurement is of the "absolute" type, provided by the integrating sphere measurement technique.

The basic measurement performance specifications are:

- Reflectance repeatability: ± 1%
- Wavelength range: 250 to 2500 nm in 100 steps
- Wavelength repeatability: ± 1%

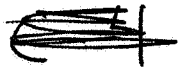

- Spectral resolution: 5% of wavelength or better
- Scan Time: ≤ 120 seconds
- Sample size: 0.5 in. or larger
- Size/weight
  - Measurement head: 8 3/8" x 10 1/8" x 12 3/8"; 15 pounds
  - Power supply/carry case: 16" x 20" x 14"; 25 pounds

The LPSR optical design shown in Figure 4 is similar to laboratory system and to the TCSE reflectometer. Figures 5 and 6 are photographs of the LPSR. The repeatability of the LPSR is shown in Figure 7. Figures 8 to 10 demonstrate the measurement comparison of the LPSR and the computer controlled Beckman DK-2A/Gier Dunkle 8 inch integrating sphere reflectometer at the Marshall Space Flight Center.

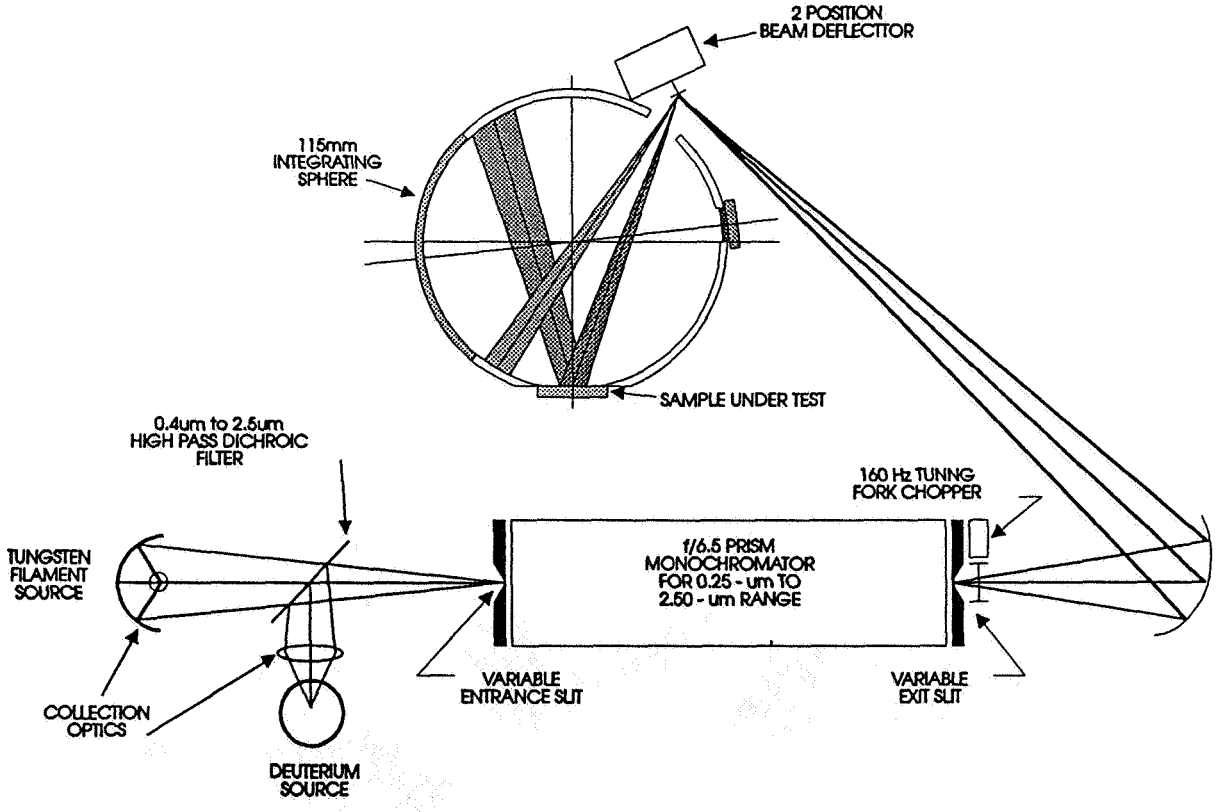

Figure 4. Optical schematic.

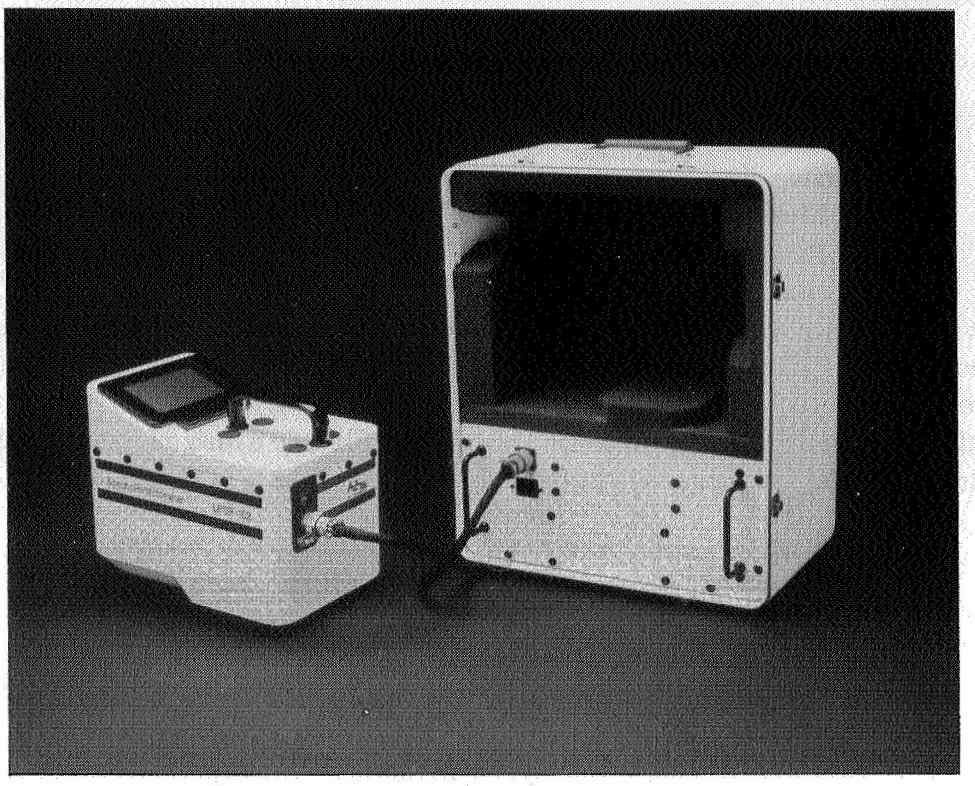

Figure 5. LPSR measurement head and carrying case.

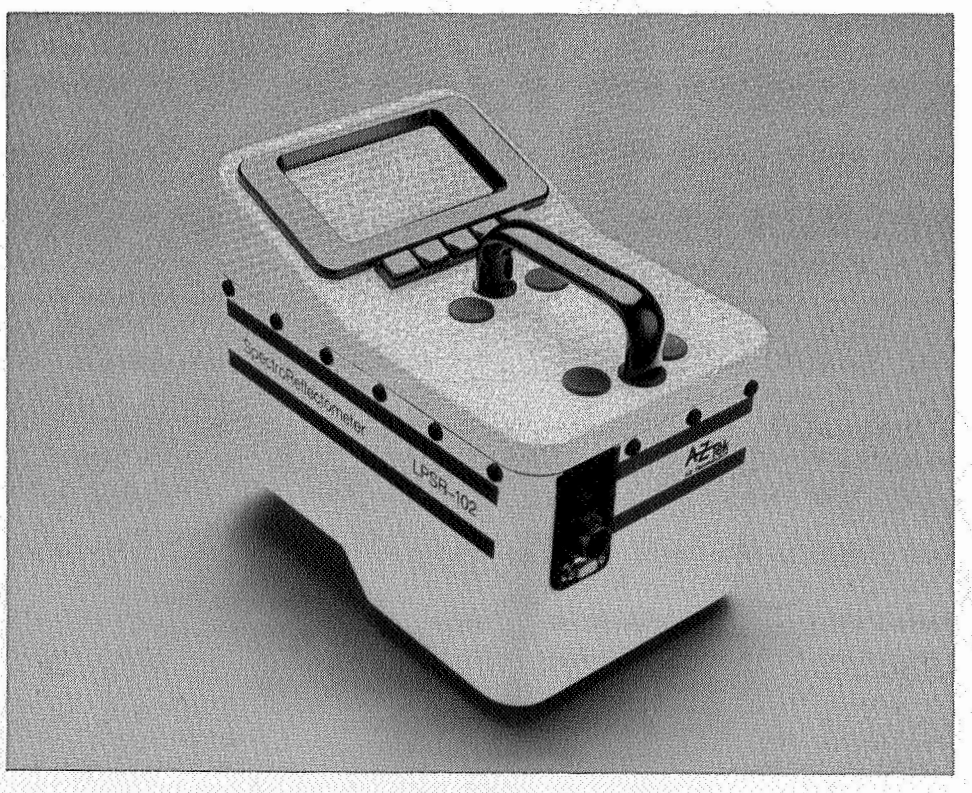

Figure 6. LPSR measurement head.

ORIGINAL PAGE
BLACK AND WHITE PHOTOGRAPH

LPSR repeatability is demonstrated by this plot of three separate measurements of S13G/LO white paint.

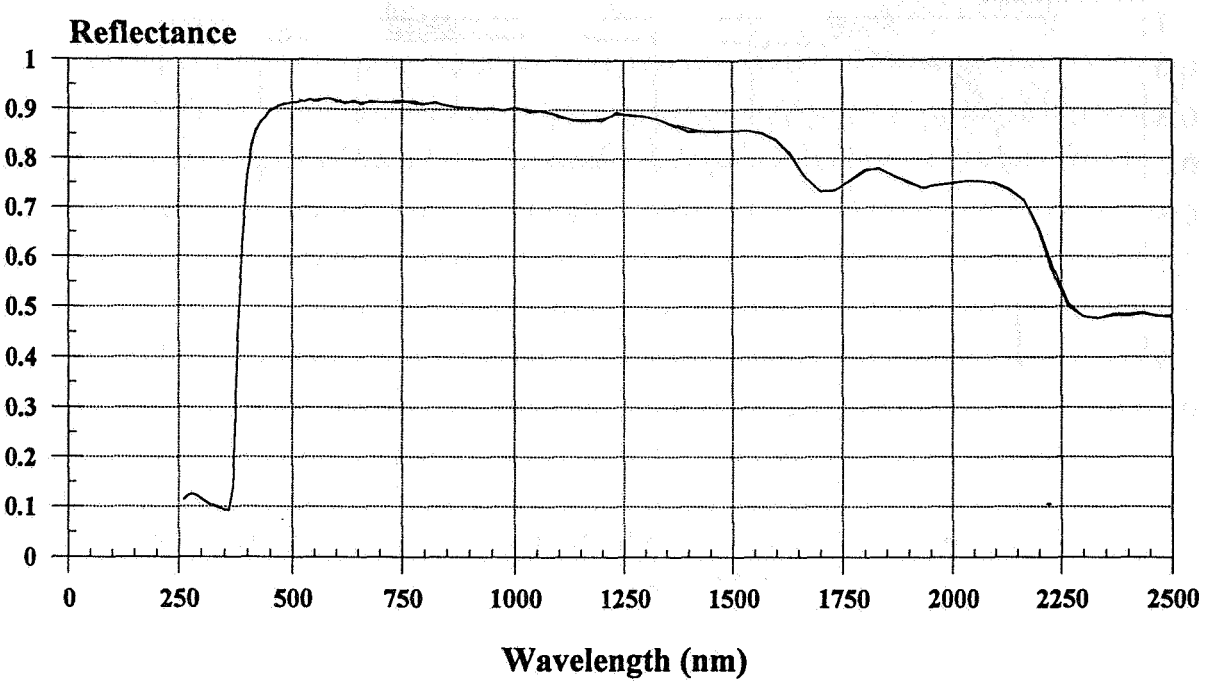

Figure 7. LPSR repeatability.

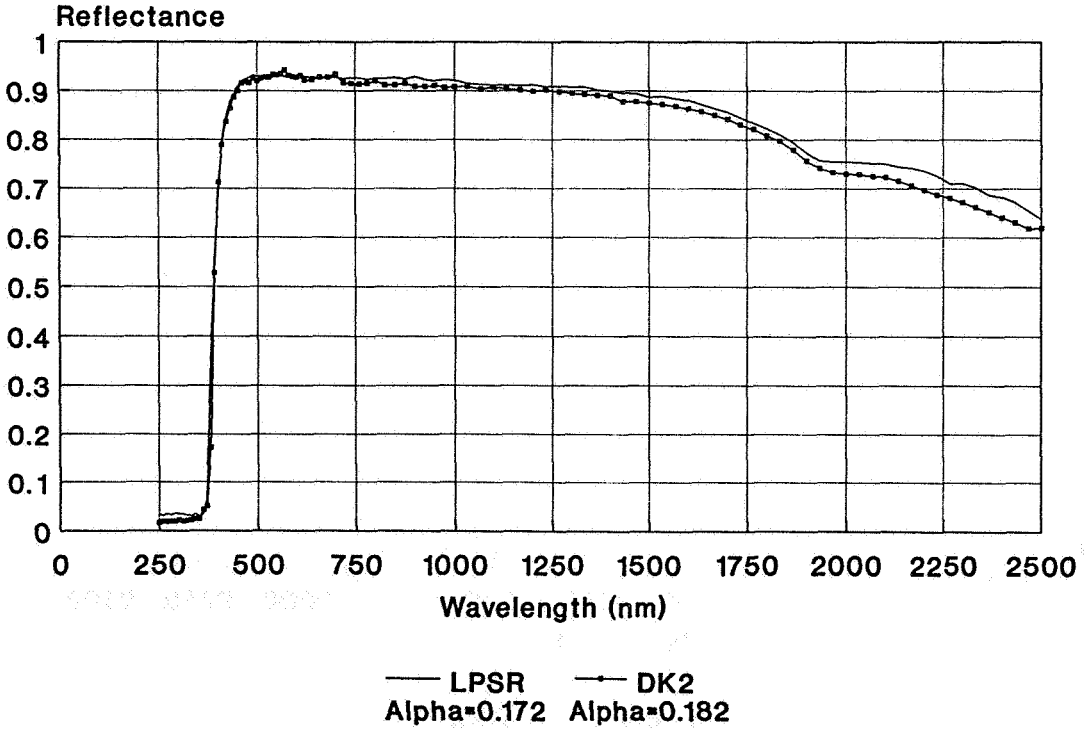

Figure 8. LPSR/DK2 reflectance data comparison - Z93 white paint.

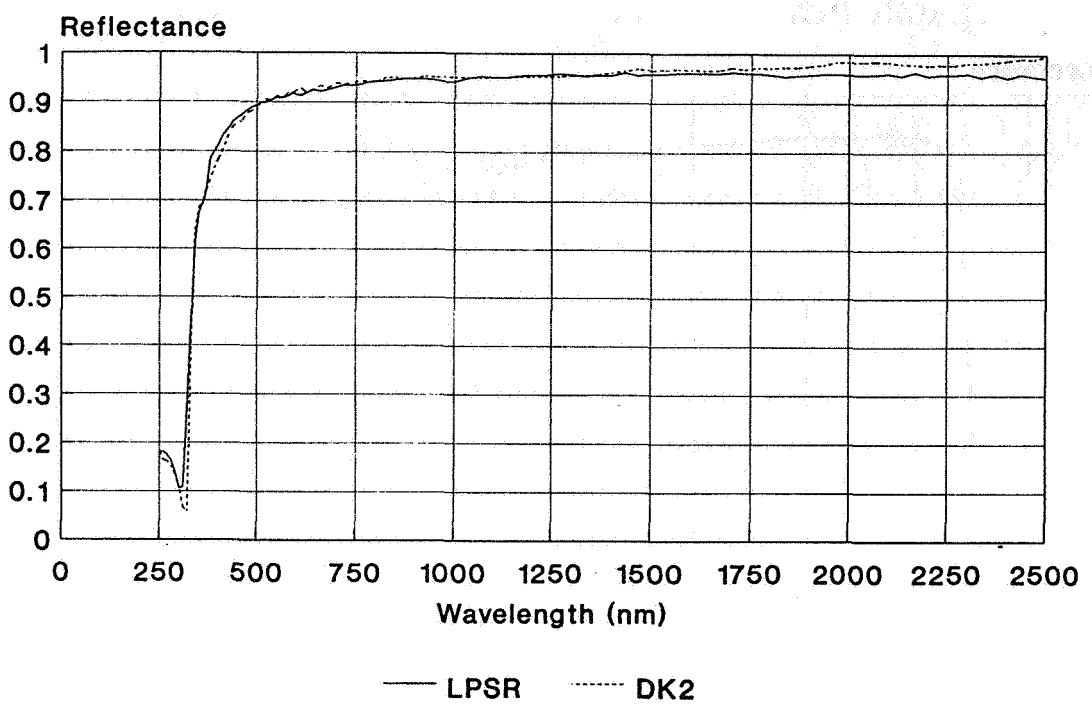

Figure 9. LPSR/DK2 reflectance data comparison - silver teflon.

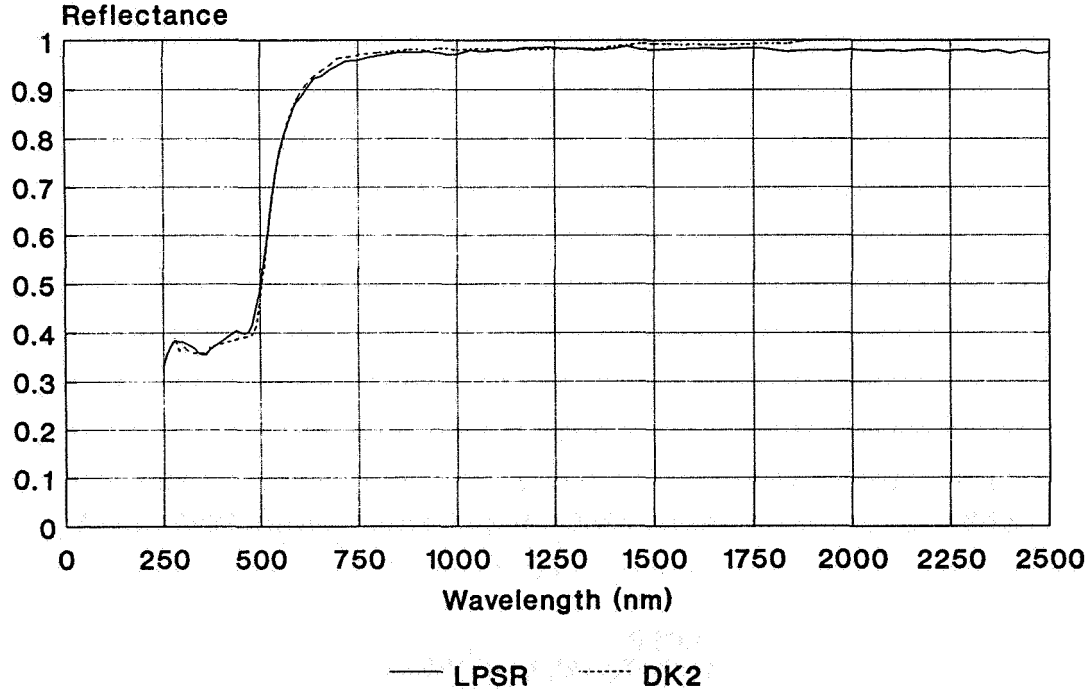

Figure 10. LPSR/DK2 reflectance data comparison - gold mirror.

SPACE PORTABLE SPECTROREFLECTOMETER (SPSR)

The condition of external surfaces is critically important to the success of long duration missions. These surfaces are susceptible to degradation by the natural and spacecraft induced environments. Therefore, there is a need to measure the properties of spacecraft surfaces to verify surface conditions and determine when and if maintenance, repair or replacement are required.

To address this need the Space Portable SpectroReflectometer (SPSR) is being designed to measure the total hemispherical reflectance of practically any external surface on a spacecraft while it is in orbit. The SPSR will become a standard utility instrument for routine long term space operations. Two configurations of SPSR are being developed including a hand-held unit much like the laboratory instrument (LPSR), and a remotely operated instrument which is operated using the Remote Manipulator System (RMS) aboard the Space Shuttle or Space Station Freedom. The SPSR concepts are illustrated in Figures 11 and 12.

The SPSR is being developed under the Small Business Innovative Research (SBIR) program and is currently in Phase II. The SPSR electro-optical subsystem is based on the TCSE reflectometer and incorporates the same improvements and performance as the LPSR. In this phase, the program will verify: (1) measurement performance on typical spacecraft surfaces with variations in size, shape, and material, (2) operational capability under simulated mission conditions, and (3) viability of the SPSR design for in-space operation. Prototypes of both configurations of the SPSR will be built and tested.

The handheld and remotely operated versions of the SPSR incorporate the same electro-optical system as the LPSR. The handheld design provides a larger handle and switches to accommodate the EVA suit glove. Also included are target illumination lamps and contact sensors to aid an astronaut in positioning the SPSR on a surface for measurement.

The remotely operated version (shown in Figure 13) also incorporates the target illumination lamps and contact sensors. In addition, other positioning aids include a laser range finder and a video camera.

The current SPSR effort will be completed in mid 1993. A flight opportunity is needed to flight test the SPSR as a utility instrument for space operations. Potential applications include Space Station Freedom, the maintenance mission for the Hubble Space Telescope, other space system maintenance missions, routine space vehicle commissioning, and the Space Exploration Initiative.

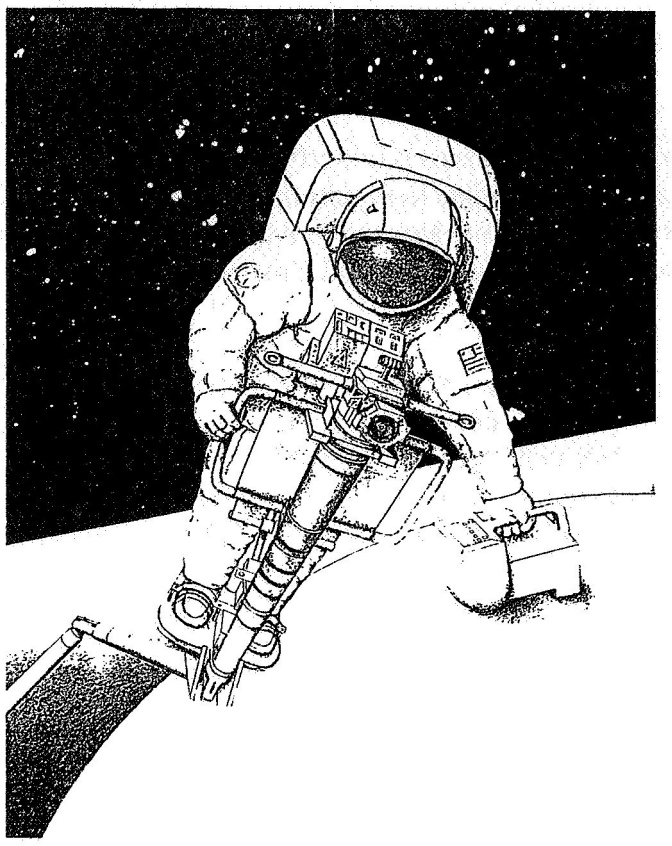

Figure 11. Concept for the handheld SPSR.

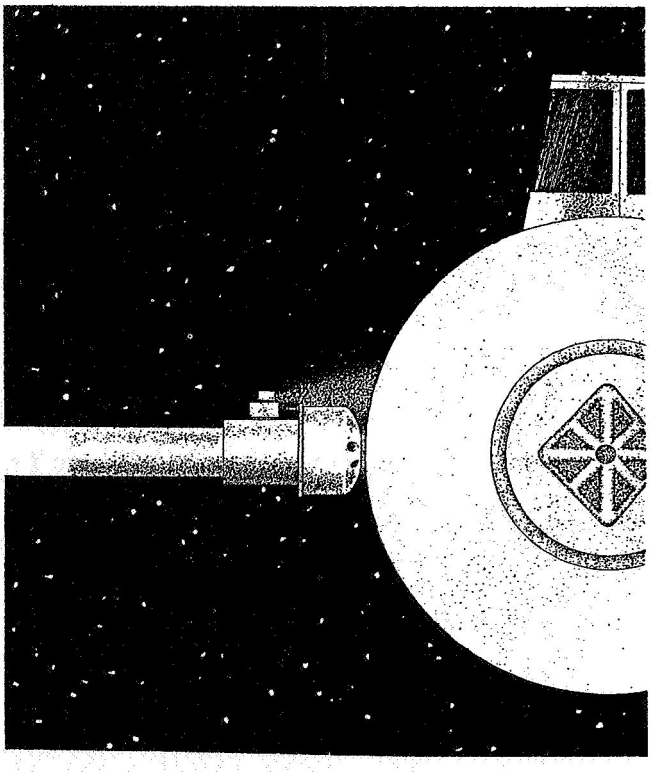

Figure 12. Concept for the remotely operated SPSR.

ORIGINAL PAGE
BLACK AND WHITE PHOTOGRAPH

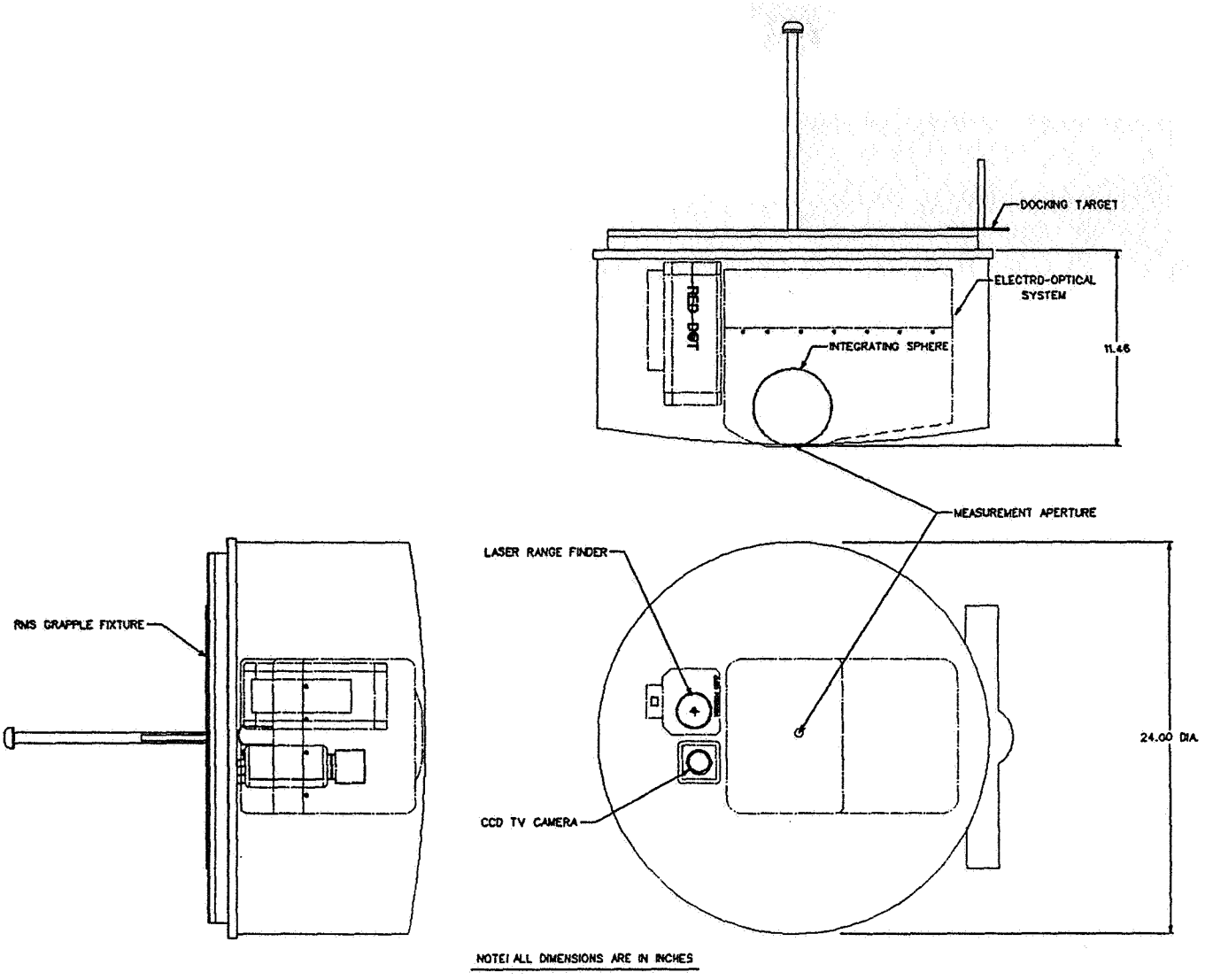

Figure 13. Remotely operated SPSR configuration.

N93-29707

AN LDEF II DUST INSTRUMENT FOR DISCRIMINATION BETWEEN ORBITAL DEBRIS AND NATURAL PARTICLES IN NEAR-EARTH SPACE

50/70
6s16

A.J. Tuzzolino, J.A. Simpson, R.B. McKibben
Laboratory for Astrophysics and Space Research
The University of Chicago
Chicago, IL 60637, U.S.A.

H.D. Voss
Lockheed Space Sciences Laboratory
3251 Hanover Street
Palo Alto, CA 94304, U.S.A.

H. Gursky
Space Science Division
Naval Research Laboratory
Washington, DC 20375, U.S.A.

ABSTRACT

We discuss the characteristics of a space dust instrument which would be ideally suited to carry out near-Earth dust measurements on a possible LONG DURATION EXPOSURE FACILITY reflight mission (LDEF II). As a model for the trajectory portion of the instrument we propose for LDEF II, we summarize the characteristics of a SPAce DUSt instrument (SPADUS) currently under development for flight on the USA ARGOS mission to measure the flux, mass, velocity and trajectory of near-Earth dust. Since natural (cosmic) dust and man-made dust particles (orbital debris) have different velocity and trajectory distributions, they are distinguished by means of the SPADUS velocity/trajectory information. The SPADUS measurements will cover the dust mass range ~ 5×10^{-12} g (2 μm diameter) to ~ 1×10^{-5} g (200 μm diameter), with an expected mean error in particle trajectory of ~ 7° (isotropic flux). Arrays of capture cell devices positioned behind the trajectory instrumentation would provide for Earth-based chemical and isotopic analysis of captured dust. The SPADUS measurement principles, characteristics, its role in the ARGOS mission, and its application to an LDEF II mission are summarized.

INTRODUCTION

In near-Earth space, it is well known that both orbital debris and natural particles contribute to the particulate environment (refs. 1-6). For some time, it has been recognized that the orbital debris component represents a serious and growing hazard to future space operations, both from the point of view of catastrophic collision, as well as erosive damage to critical surfaces (sensors, optics) resulting from long-term exposure to the smaller orbital debris particles (refs. 2,4). For cosmic dust particles, it has been shown that the only means of determining their sources (comets, asteroids, interstellar) is by *in-situ* velocity/trajectory measurements (ref. 1). Similarly, for near-Earth dust particles, velocity/trajectory measurements would provide the ability to discriminate between debris and natural particles (ref. 7). However, because of the limited exposure of velocity/trajectory sensors to near-Earth space up to the present time, the spatial distribution, mass spectrum, trajectory, and time variations of the small particle component (< 1 cm diameter) of orbital debris have not been well determined (refs. 2,4).

PRECEDING PAGE BLANK NOT FILMED

The first LONG DURATION EXPOSURE FACILITY (LDEF I) (refs. 5,6) has demonstrated the value of the LDEF concept for an overall survey of the near-Earth space radiation environment. In particular, the 5.8 year space exposure of LDEF I has yielded a wealth of impact feature data from near-Earth particulates (orbital debris and cosmic dust) having a wide range of dimensions and impact velocity (refs. 5,6).

Although LDEF I did not carry a dust instrument which could have provided direct measurements of particle mass, velocity, and trajectory, the Interplanetary Dust Experiment (IDE) aboard LDEF I demonstrated that debris particles appear to dominate the particulate environment at LDEF I altitude and that a large fraction of the debris particles are encountered as transient particle clouds (ref. 8). However, at the present time, quantitative classification of LDEF impact particle types and their sources is just beginning to emerge (ref. 9). The present-day lack of quantitative measurements of the flux, velocity/trajectory, and time characteristics of small debris particles continues to hamper development of reliable evolutionary modeling for orbital debris (ref. 4), and the need for these data remains as an important goal in this field.

A second LDEF mission (LDEF II) carrying the dust instrument we describe here would directly address this need, as well as provide important information on a) the orbital characteristics and possible sources of near-Earth cosmic dust and b) the flux and mass distribution of meteor-stream particles which may be encountered by LDEF II.

PROPOSED LDEF II DUST INSTRUMENT

The main design objective of the particle velocity/trajectory instrumentation which has been under development by the University of Chicago group has been the capability to measure individual particle trajectories with sufficient accuracy to permit identification of their parent bodies. This, combined with chemical and isotopic analysis of the captured material in a capture cell device (and/or returned sensors), permits a direct study of the physical, chemical and isotopic composition of matter from a known parent body.

This objective and ongoing developments have led to the basic concept behind the dust instrumentation we propose for an LDEF II mission, which is illustrated schematically in Figure 1. The main components are: a) a dust trajectory system, consisting of two identical planar arrays (D1 and D2) of polyvinylidene fluoride (PVDF) dust sensors, and b) a capture cell system, consisting of an array of capture cell devices placed behind the D2 array.

The trajectory system would provide measurements of impacting particle flux, mass, velocity (by time-of-flight) and trajectory. The capture cell system would provide for capture of particle residues following penetration of the trajectory system by the impactor. Subsequent Earth-based analyses would yield chemical and isotopic composition of the residues. Thus, the combined trajectory-capture cell instrumentation provides the capability to measure the orbital elements of individual particles prior to capture. Although unambiguous identification of a specific source body will probably not be possible for most of the impacts, identification of generic classes (i.e., comet, asteroid, interstellar, orbital debris) will be possible, with the corresponding particle chemical and isotopic composition determined by analysis of the captured residue. In what follows, we describe some of the characteristics of these two systems.

LDEF II Dust Trajectory System

As a model for the dust trajectory system for LDEF II, we describe the characteristics of a SPAce DUSt (SPADUS) instrument currently under development for launch on the Advanced Research and

Global Observation Satellite (ARGOS) in 1995. This instrument will be jointly developed by groups at The University of Chicago (dust sensors and linear electronics), the Lockheed Space Sciences Laboratory (digital electronics), and the Space Sciences Division of the Naval Research Laboratory (mechanical design and construction). SPADUS will be integrated and flown by the DOD Space Test Program, with funding for The University of Chicago portion of SPADUS development provided by the Office of Naval Research and NASA. A schematic of the SPADUS instrument is shown in Figure 2.

SPADUS Sensors

Each of the two sensor arrays (D1 and D2 in Figure 2) contains 16 PVDF copolymer dust sensors. The theory, characteristics, and development of the PVDF and PVDF copolymer dust sensors developed at The University of Chicago have been discussed in detail in earlier reports (refs. 10-12). Briefly, a PVDF (or PVDF copolymer) sensor, shown schematically in Figure 3a, consists of a thin film of permanently polarized material. A hypervelocity dust particle impacting the sensor produces rapid irreversible local depolarization in the sensor volume destroyed (penetration hole), which results in a large and fast (ns range) current pulse at the input to the electronics. The output pulse amplitude, in general, depends on impacting particle mass and velocity (refs. 10-12) and is sharp in time, as illustrated in Figure 3b. We note that this fast output pulse permits a high counting rate capability for the sensor (up to 10^4 impacts s^{-1} with no corrections, and up to 10^5 impacts s^{-1} with known corrections).

The highly successful performance of the University of Chicago PVDF-based instruments (Dust Counter and Mass Analyzer - DUCMA) (ref. 11) throughout the VEGA 1/2 missions to comet Halley proved the high space reliability of PVDF sensors and their value for space dust studies (refs. 13,14). Continuing studies of PVDF sensors and electronics led to a) instrumentation for particle velocity determination using thin sensors in a time-of-flight arrangement (ref. 15), which is the basic concept behind the SPADUS trajectory system, and b) development of the PVDF copolymer dust sensor (ref. 12), which is expected to have advantages over pure PVDF sensors, and which will be used for the SPADUS trajectory sensors. In Table 1, we summarize the characteristics of PVDF sensors.

SPADUS Particle Velocity Determination

Particle velocity may be determined by a time-of-flight (TOF) arrangement (ref. 15), as illustrated in Figure 4, and the particle velocity determining characteristics of two PVDF copolymer sensors in this TOF arrangement are illustrated in Figures 5 and 6. Our calibrations (ref. 12) show that for impactors having diameter $D_p > 10$ μm and impact velocity $< \sim 10$ km/s, SPADUS will determine impact velocity by TOF with an accuracy ~ 1-4%. For impact velocities > 10 km/s, particle vaporization, ablation, and fragmentation become important, and velocity information may be lost for a significant fraction of all impactors having $D_p < \sim 40$ μm. For $D_p > \sim 40$ μm, we anticipate that > 50% of all impactors will provide TOF data with an expected error in velocity measurement of ~ 20-30%, this larger error resulting from the relatively large impactor velocity loss upon D1 penetration (ref. 12).

SPADUS Particle Trajectory Determination

With regard to particle trajectory measurement, it had been suggested that a ~ 1° trajectory error might be required in order to distinguish particles of cometary origin from particles of asteroidal origin (ref. 1). However, it is not clear that this degree of trajectory accuracy is warranted, since it has been shown that particles from these two sources have different distributions of trajectories (ref. 7). Consequently, although the University of Chicago group has developed two-dimensional position-sensing PVDF sensors (x,y sensors) which yield particle impact coordinates with typical errors of ~ 1-3 mm for x and y (trajectory error of ~ 1° for two x,y sensors separated by ~ 20 cm) (refs. 15,16), our SPADUS design has

been chosen to provide a trajectory accuracy of the order of 5° by using arrays of non-position-sensing PVDF sensors.

This is illustrated in Figure 7, which shows the computed distribution of error angle θ, which is the angle between the computed trajectory (i.e., the detector centers) and any allowed trajectory involving the D1 and D2 detectors (ref. 15). The data plotted show that approximately one-half of all computed trajectories will be in error by less than ~ 7°, which should permit discrimination between classes of trajectory (i.e., comets *vs* asteroids).

SPADUS Data

For each SPADUS dust impact, 65 Kbits of data are generated which include a) impact time on D1 (1 s accuracy), b) TOF between D1 and D2 (0.25 μs resolution), c) D1, D2 wave forms (2000 points, 0.25 μs per point, 8-bit pulse-height-analysis (PHA) per point) for each of four records, d) identification of the D1 and D2 sensors impacted, and e) PHA over 32 mass intervals, for each of the 32 dust sensors. These data, when analyzed in terms of the different velocity/trajectory distributions for cosmic and debris dust particles (mean of ~ 20 km/s for cosmic dust, and ~ 13 km/s for orbital debris), are expected to permit discrimination between these two particle classes for a substantial fraction of all analyzed events. Further, the time-velocity-trajectory capabilities of SPADUS will permit identification of possible transient debris clouds, as well as meteor stream encounters.

SPADUS Electronics

A simplified block diagram of the SPADUS electronics is shown in Figure 8. The primary electronics for each dust sensor consists of an amplifier chain, a discriminator, a 16-channel PHA, and a timing register. Amplified and shaped D1 signals which exceed the discriminator threshold start the PHA, TOF, and transfer the current clock count to the timing register. From the D1 to D2 TOF and electronic identification of the D1,D2 sensors impacted, particle velocity and trajectory are determined. Summed signals from the 16 sensors of each sensor plane are generated and analyzed by 8-bit flash analog-to-digital converters running at 4 MHz (2000 time points) and an additional 16-channel PHA is recorded. Particle mass is determined from the amplitude of the signal measured by the PHAs and the particle velocity (refs. 10-12).

Recording of the D1,D2 wave shapes not only provides redundant TOF data and redundant high resolution PHA measurements, but also permits identification of possible multiple fragments impacting D2, as well as possible spurious sensor signals resulting from acoustic backgrounds (refs. 10,11). Instrument commanding provides for deletion of any of the sensors from the electronic chains and various threshold and gain changes. Dual computers provide redundancy, collect, format, and store all dust data (16 Mbits storage), operate the in-flight calibration system, and perform all spacecraft interface functions. Custom rad-hard gate arrays, containing both analog and digital sections, are used throughout the electronics. The main characteristics of the SPADUS instrument are summarized in Table 2.

LDEF II Capture Cell System

The capture cell system we would propose for LDEF II would consist of stacked thin foils and/or aerogels (ref. 17). The results which have already been obtained for combined PVDF trajectory-capture cell systems (stacked foils) have established that, for ~ 75% of the impactors with velocities < ~ 8 km/s, thin PVDF trajectory systems satisfy the requirements of a) velocity/trajectory determination, b) of identification of the location of particle fragments in capture cells, and c) of sufficient fragment mass following

penetration of the trajectory sensors for successful capture and subsequent chemical and isotopic analysis (refs. 12,17).

SPADUS ROLE IN THE ARGOS MISSION AND APPLICATIONS TO LDEF II

The ARGOS objective is to demonstrate advanced attitude and position determination, electric propulsion, and conduct upper atmosphere imaging and environment studies, with SPADUS providing measurements of the particulate environment. Figure 9 summarizes the characteristics of the spacecraft, mission, and experiments. SPADUS dust data to be obtained on the ARGOS mission (833 km altitude) during the time frame ~ 1995-1998 would be ideally complemented by corresponding data which could be obtained by a SPADUS-type instrument (with capture cells) carried by an LDEF II spacecraft at lower altitude over the same time interval. These combined data would provide important information regarding the altitude/inclination dependence of near-Earth orbital debris fluxes, as well as provide an important data base to aid in reliable evolutionary modeling for orbital debris.

Of special interest for both ARGOS and an LDEF II would be an energetic nucleon (electrons, ions, neutrals) telescope, which could be mounted within the SPADUS digital electronics box, for continuous monitoring of the ARGOS and LDEF II nucleon environments, and the addition of this telescope (Lockheed group) is currently planned for SPADUS.

The prime purpose of the energetic nucleon telescope is to obtain nucleon flux data which would a) be of diagnostic value in resolving possible ambiguities in the low event-rate SPADUS dust data, and b) provide information of importance to the other experiments aboard ARGOS and LDEF II, since it is well known that x-ray, UV, and optical systems can be upset by solar proton events, as well as trapped radiation-belt particles. Its secondary purpose is to obtain an *in-situ* map of the radiation-belt nucleon environment and obtain new science on the angular and energy distributions of precipitating electrons and ions. Although final design of the telescope is not yet complete, it will consist of an ion/neutral telescope (ref. 18) and an electron telescope located within the SPADUS digital electronics box.

SPADUS REQUIREMENTS

Mounting and Orientation

To maximize the impact rate, SPADUS requires that the normal to the trajectory sensors be pointed along the spacecraft velocity vector (~ 1° accuracy), as illustrated in Figure 2.

The SPADUS electronics will contain an instrument clock (activated by SPADUS Power On and continuously running with 1 s resolution). For each impact, the SPADUS clock records the impact time (1 s accuracy), and particle velocity/trajectory data with respect to the SPADUS trajectory system axes is stored in SPADUS memory. To determine the particle orbital parameters from these data, SPADUS requires a) a spacecraft time signal (1 s accuracy) to correlate a SPADUS particle impact time with a unique spacecraft time, and b) access to a continuous record (~ 1 s resolution) of spacecraft position, velocity and attitude.

Electrical Connections

Electrical connections are required between the SPADUS instrument and the spacecraft for operating power, commands, and telemetry. Unregulated 28 V dc voltage from the spacecraft would be acceptable.

with all voltage conversion and regulation being carried out within the SPADUS electronics. Estimated SPADUS power required is 6.5 W continuous.

Telemetry and Commands

SPADUS requires active spacecraft data transmission to ground stations at an average bit rate of ~ 4 bits/s. Upon Power On, SPADUS operates in NORMAL MODE and continuously accumulates dust particle data. Occasionally (~ once per month), SPADUS is put into CALIBRATE MODE (either by ground command or automatically) which provides an electronic calibration of the instrument. Additional commands (threshold changes, etc.) might be used occasionally, but only under special circumstances (CONTINGENCY).

CONCLUSIONS

We have described the characteristics of a combined trajectory-capture cell dust instrument for a possible LDEF II which would provide quantitative measurements of particle flux, mass, velocity and trajectory, as well as permit capture of particle residue for Earth-based chemical and isotopic residue analysis. The velocity/trajectory capability of the instrument would distinguish orbital debris from natural dust and provide important information on the orbital characteristics and possible sources of the natural component.

Data from this instrument on LDEF II, when combined with corresponding data from an identical instrument (without capture cells) to be carried on the ARGOS near-Earth satellite, would provide important *in-situ* information regarding the altitude/inclination dependence of near-Earth orbital debris fluxes, as well as provide a new data base to aid in modeling of orbital debris generation and evolution.

ACKNOWLEDGEMENTS

The authors thank M. Perkins, E. LaRue, F. DiDonna, L. DiDonna, F. Sopron and T. Economou at The University of Chicago, R.A. Baraze, T.R. Fisher, J.R. Kilner, J. Mobilia and R.R. Vondrak at the Lockheed Space Sciences Laboratory, and M. Lovellette, G. Fritz and D. Woods at the Naval Research Laboratory for their important contributions to SPADUS design and development. The University of Chicago group is grateful to R.G. Joiner for his continuing sponsorship of SPADUS, and for his efforts in obtaining partial support for SPADUS development. Finally, we thank the DOD Space Test Program for providing the SPADUS flight on ARGOS, the Aerospace Corp. and Rockwell International staff who have made integration of SPADUS into ARGOS possible, and W.H. Kinard for providing important information related to planning activities for a possible LDEF II mission. The University of Chicago effort for SPADUS is supported in part by ONR Grant N00014-91-J-1716 and NASA Grant NAGW-3078. The Lockheed effort is supported in part by the Lockheed Independent Research Program, and the Naval Research Laboratory effort is supported by the Office of Naval Research.

REFERENCES

1. Trajectory Determinations and Collection of Micrometeoroids on the Space Station, ed. F. Hörz, LPI Tech. Rep. 86-05, Lunar and Planetary Institute, Houston (1986).

2. U.S. Congress, Office of Technology Assessment, Orbiting Debris: A Space Environmental Problem - Background Paper, OTA-BP-ISC-72, Washington, DC: U.S. Government Printing Office (September 1990).

3. Proceedings of the Workshop on Hypervelocity Impacts in Space, University of Kent at Canterbury, in press (1992).

4. Proceedings of the Symposium on "Preservation of Near-Earth Space for Future Generations", University of Chicago, to be published (1992).

5. LDEF - 69 Months in Space: First Post-Retrieval Symposium, NASA Conference Publication 3134 (June 1991).

6. Second LDEF Post-Retrieval Symposium Abstracts Volume, NASA Conference Publication 10097 (June 1992).

7. A.A. Jackson and H.A. Zook, "Orbital Evolution of Dust Particles from Comets and Asteroids", Icarus, 97, 70 (1992).

8. J.D. Mulholland, J.P. Oliver, S.F. Singer, J.L. Weinberg, W.J. Cooke, N.L. Montague, P.C. Kassel, J.J. Wortman, W.H. Kinard and C.G. Simon, "LDEF Interplanetary Dust Experiment: A High Time-Resolution Snapshot of the Near-Earth Particulate Environment", in: Proceedings of the Workshop on Hypervelocity Impacts in Space, University of Kent at Canterbury, in press (1992).

9. F. Hörz and R. Bernhard, "Compositional Analysis and Classification of Projectile Residues in LDEF Impact Craters", NASA Technical Memorandum 104750 (June 1992).

10. J.A. Simpson and A.J. Tuzzolino, "Polarized Polymer Films as Electronic Pulse Detectors of Cosmic Dust Particles", Nucl. Inst. & Meth., A236, 187 (1985).

11. M.A. Perkins, J.A. Simpson and A.J. Tuzzolino, "A Cometary and Interplanetary Dust Experiment on the VEGA Spacecraft Missions to Halley's Comet", Nucl. Instr. & Meth., A239, 310 (1985).

12. A.J. Tuzzolino, "PVDF Copolymer Dust Detectors: Particle Response and Penetration Characteristics", Nucl. Instr. & Meth., A316, 223 (1992).

13. J.A. Simpson, R.Z. Sagdeev, A.J. Tuzzolino, M.A. Perkins, L.V. Ksanfomality, D. Rabinowitz, G.A. Lentz, V.V. Afonin, J. Ero, E. Keppler, J. Kosorokov, E. Petrova, L.S. Zabo and G. Umlauft, "Dust Counter and Mass Analyzer (DUCMA) Measurements of Comet Halley's Coma from VEGA Spacecraft", Nature, 321, 278 (1986).

14. J.A. Simpson, D. Rabinowitz, A.J. Tuzzolino, L.V. Ksanfomality and R.Z. Sagdeev, "The Dust Coma of Comet P/Halley: Measurements on the VEGA-1 and VEGA-2 Spacecraft", Astron. and Astrophys., 187, 742 (1987).

15. J.A. Simpson and A.J. Tuzzolino, "Cosmic Dust Investigations II. An Instrument for Measurement of Particle Trajectory, Velocity, and Mass", Nucl. Instr. & Meth., A279, 625 (1989).

16. A.J. Tuzzolino, "Two-Dimensional Position Sensing PVDF Dust Detectors for Measurement of Dust Particle Trajectory, Velocity and Mass", Nucl. Instr. & Meth., A301, 558 (1991).

17. C.G. Simon, "Hypervelocity Impact Testing of Micrometeorite Capture Cells in Conjunction with a PVDF Thin-Film Velocity/Trajectory Sensor and a Simple Plasma Velocity Detector", submitted for publication in Int. J. Impact Eng. (1991).

18. H.D. Voss, J. Mobilia, H.L. Collin and W.L. Imhof, "Satellite Observations and Instrumentation for Imaging Energetic Neutral Atoms", Society for Photo-optical Instrumentation Engineering (SPIE), 1744, 79 (1992).

Table 1. Characteristics of Polyvinylidene Fluoride (PVDF) Dust Detectors

- Require no operating bias voltage.
- Long term stability during storage. Operate indefinitely -50°C to +100°C with no degradation in dust response.
- Recent development of PVDF copolymer sensors expected to extend stability range to -60°C to +115°C.
- Highly radiation resistant. No measurable change in response up to $\approx 10^7$ rad.
- Response to dust impacts unaffected by high background fluxes of charged particles.
- Fast detector response (few ns) enables accurate counting for high dust fluxes (intense transient dust streams, planetary rings).
- Proven space performance on VEGA-1/2 missions to comet Halley.

Table 2. Characteristics of the SPADUS Instrument*

DUST PARTICLES

Single sensor:	36 cm^2, 6 μm thick PVDF copolymer.
Particle mass (10 km/s):	$5x10^{-12}$ g (D_p = 2 μm) to $1x10^{-5}$ g (D_p = 200 μm).
Particle velocity:	1 to 10 km/s with 1 to 4% error. Greater error for velocity > 10 km/s.
Particle trajectory:	mean angular error of 7° for isotropic dust flux.
Sensitive area of D1 array (16 sensors):	0.058 m^2.
Geometry factor for isotropic dust flux:	a) D1 array -- 0.18 m^2 sr. b) D1,D2 arrays -- 0.04 m^2 sr.
Field of view (full cone):	a) 180° for flux. b) 120° for trajectory.
Low resolution Pulse-Height-Analysis:	32 channels for each of 32 dust sensors.
High resolution Pulse-Height-Analysis:	2000 time points, 8-bits/point, each of 4 channels.
Expected impact rate:	a) ~ 2/day to 20/day (flux). b) ~ 0.2/day to 2/day (trajectory).

PHYSICAL

a) Estimated total power: 6.5 W. Estimated total weight: 18 pounds.
b) thermal: operating temperature range -40°C to +50°C for dust sensors and electronics.
c) mounting: dust sensor normals along spacecraft velocity vector.
d) data readout: readout at an average bit rate of ~ 4 bits/s.
e) commands: CALIBRATE and CONTINGENCY commands occasionally.
f) attitude: spacecraft attitude (~ 1° accuracy) and velocity (~ 1% accuracy) required.

* The addition of an energetic nucleon telescope to SPADUS would provide measurements of electrons (20 keV to 2.5 MeV) and ions (20 keV to 20 MeV) and would add ~ 3 pounds and ~ 3.5 Watts to the SPADUS weight and power values listed above.

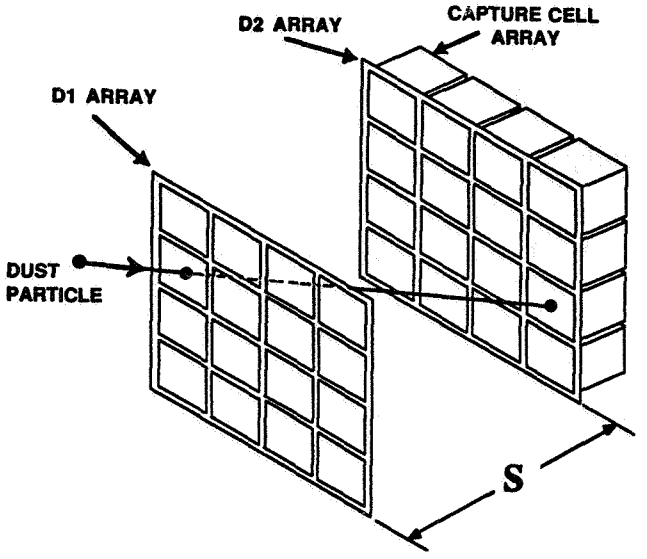

Figure 1. Schematic illustration of the dust instrumentation proposed for LDEF II, consisting of a trajectory system (D1 and D2 PVDF sensor arrays with separation *S*), and a capture cell system (an array of capture cell devices positioned behind the D2 sensors).

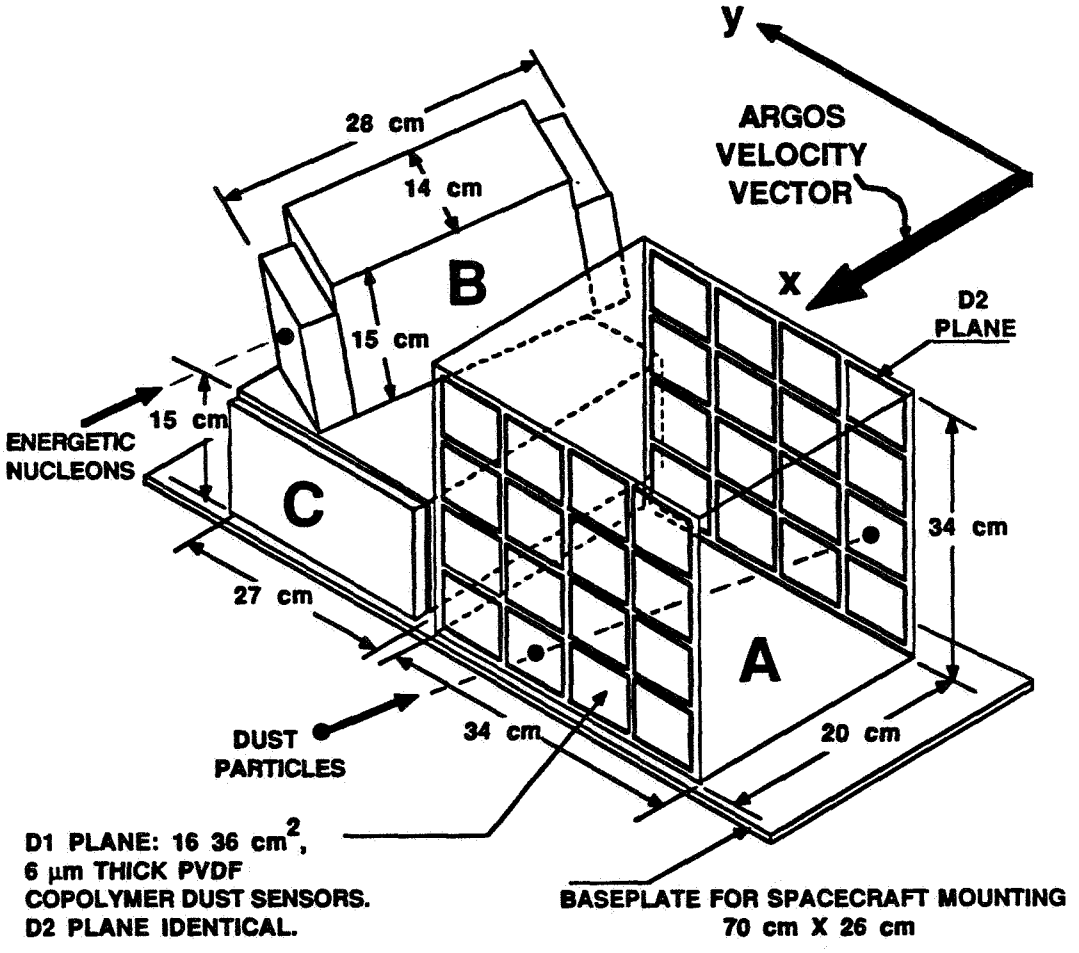

Figure 2. Schematic of the SPADUS instrument showing the dust trajectory system (A), the digital electronics box containing an energetic nucleon telescope (B), and the linear electronics box (C).

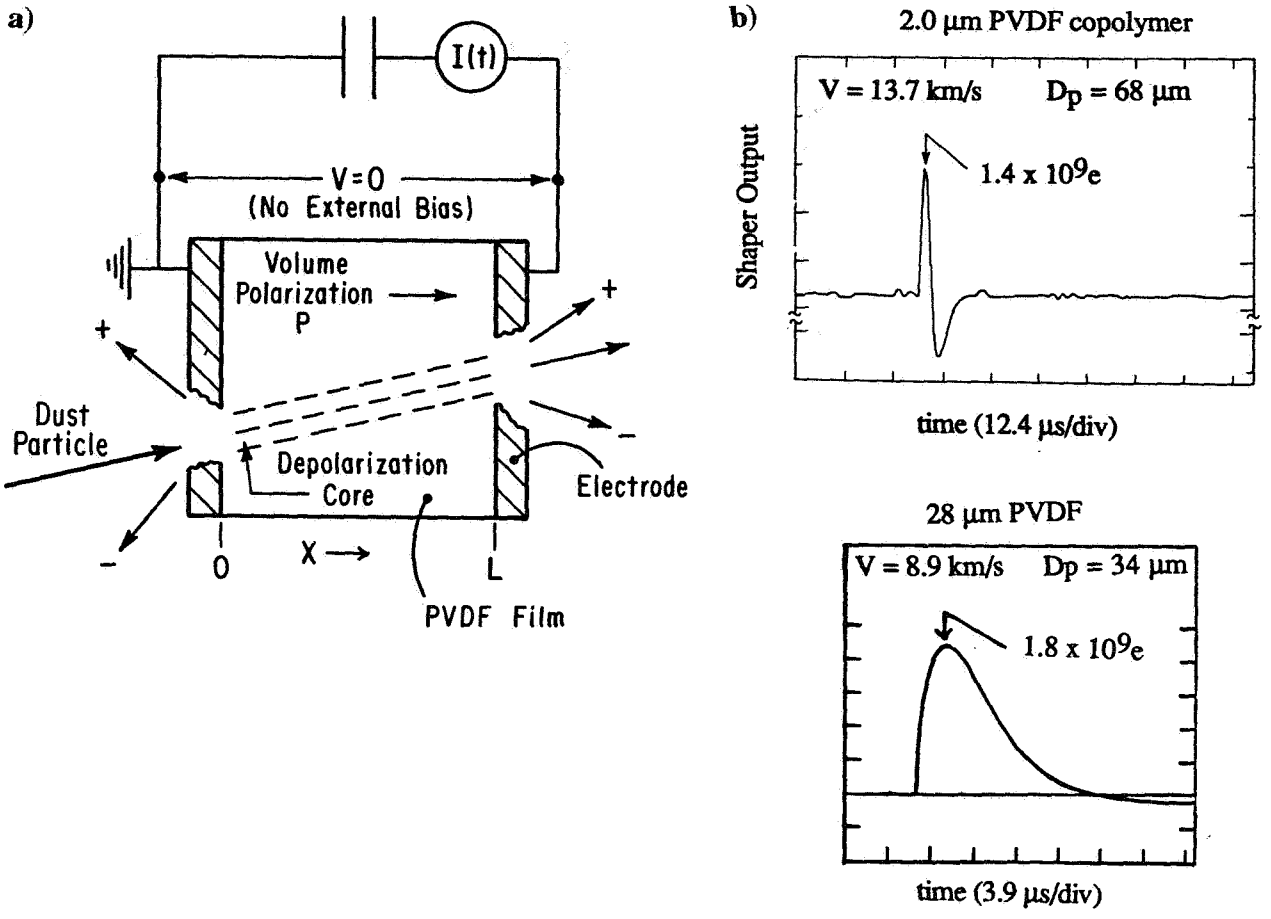

Figure 3. **a)** Schematic drawing of a polarized polyvinylidene fluoride (PVDF) dust sensor. The sensor film, of thickness L, has a built-in volume polarization P, as shown. **b)** Examples of output pulses from PVDF sensors resulting from glass impactors having impact velocity V and diameter D_p. The signal amplitudes in units of number of electron charges are indicated.

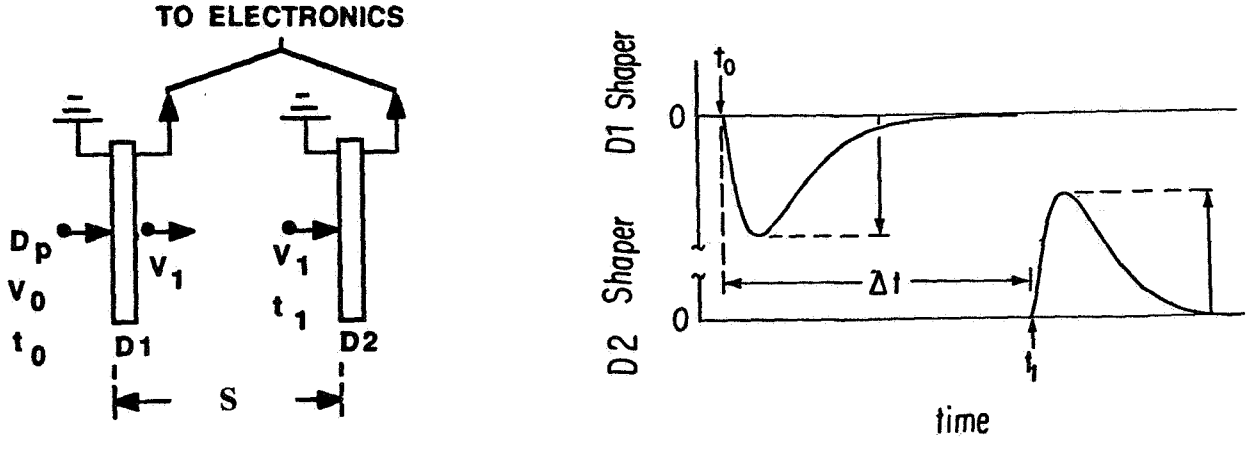

Figure 4. Illustration of particle impact velocity determination by time-of-flight. An impactor with velocity V_0 and diameter D_p impacts a thin PVDF D1 sensor at time t_0, emerges from D1 with reduced velocity V_1 and impacts D2 at a later time t_1, with $\Delta t = t_1 - t_0$. With S known and Δt measured, $V_1 = S/\Delta t$. From the amplitude of the D1 output pulse and V_1, both V_0 and D_p are determined from calibration data.

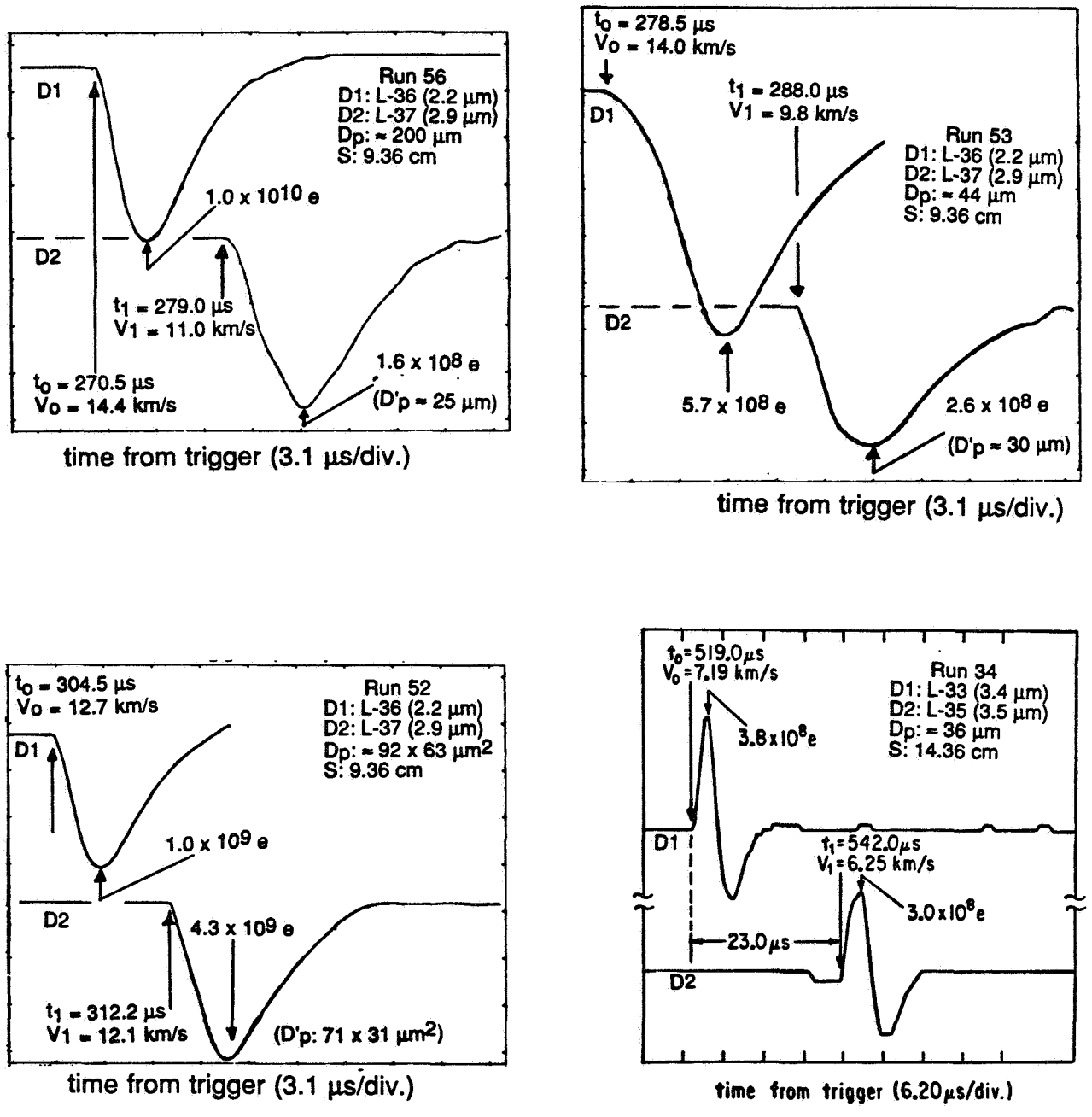

Figure 5. Examples of TOF data obtained during dust calibrations carried out at the Munich (Germany) dust accelerator facility. Indicated are the D1,D2 sensor thicknesses, impactor diameter D_p, and D1,D2 separation S.

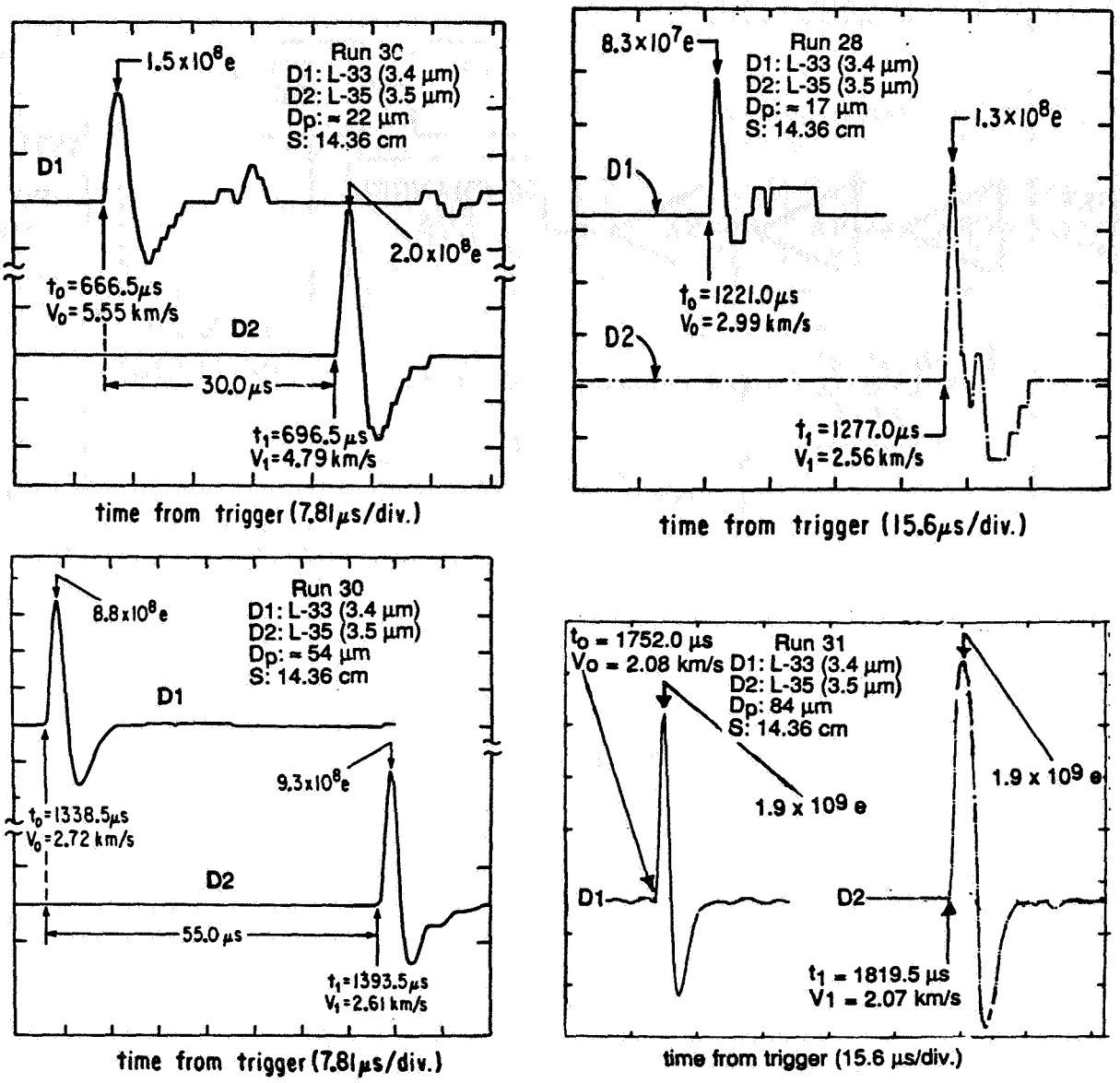

Figure 6. Examples of TOF data obtained during dust calibrations carried out at the Munich (Germany) dust accelerator facility. Indicated are the D1,D2 sensor thicknesses, impactor diameter D_p, and D1,D2 separation S.

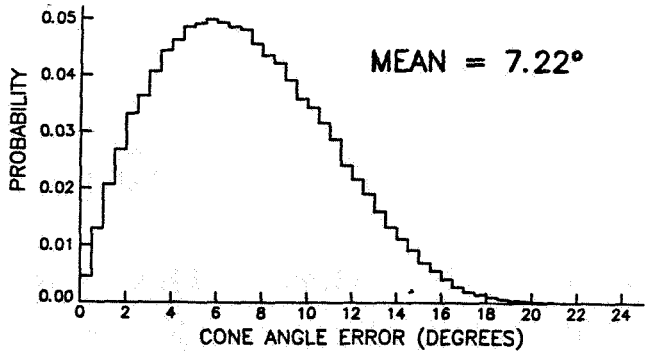

Figure 7. Distribution of error angle θ for an isotropic dust flux obtained from a Monte Carlo run for the SPADUS trajectory system shown in Figure 2.

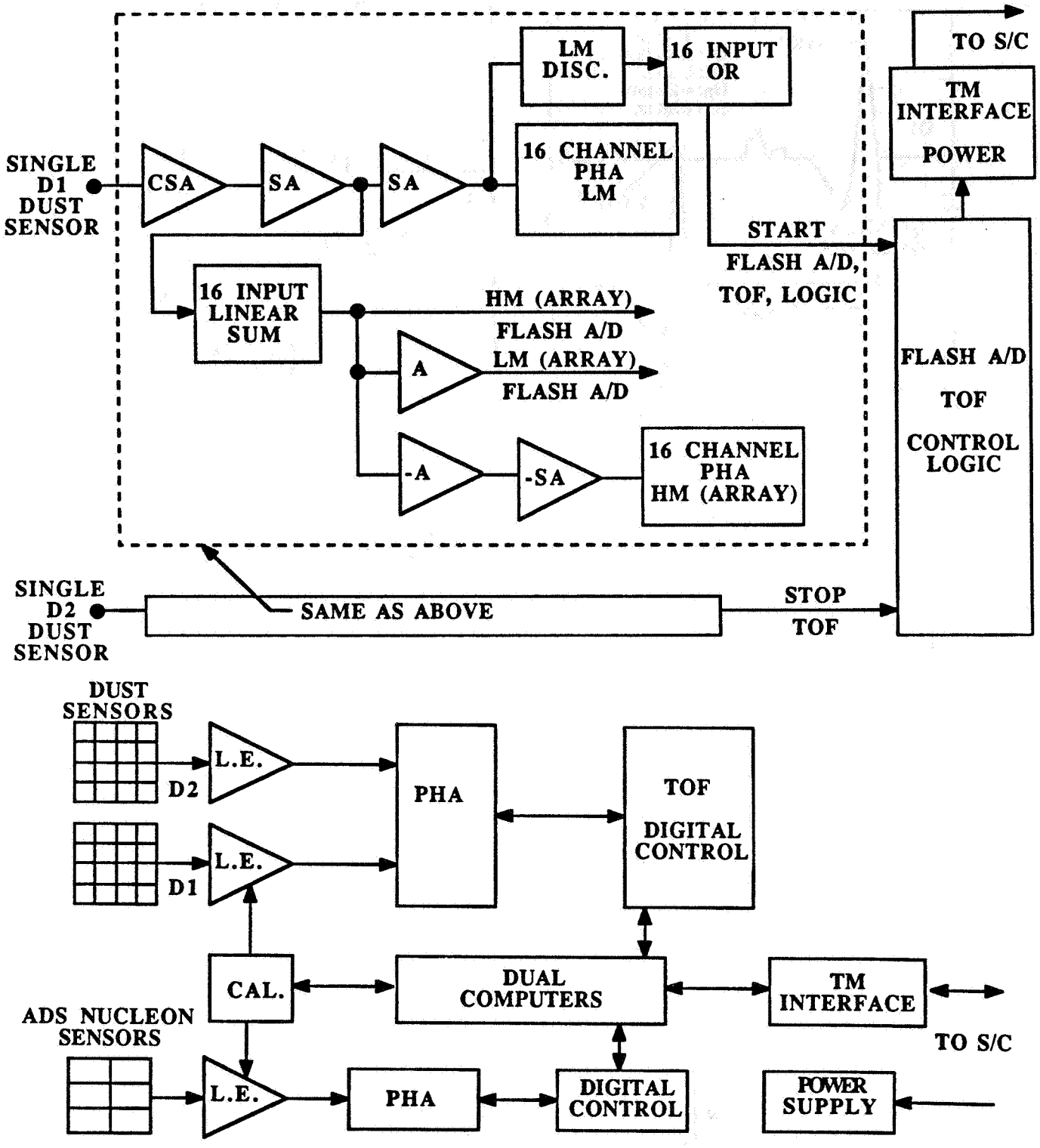

NOTE: TOF - Time-Of-Flight; TM - Telemetry; PHA - Pulse Height Analysis; ADS - Ancillary Diagnostic Sensor; L.E. - Linear Electronics; CAL. - Calibrate; LM - Low Mass; HM - High Mass; A/D - Analog to Digital; SA - Shaping Amplifier

Figure 8. Simplified schematic of SPADUS electronics.

ARGOS

(ADVANCED RESEARCH AND GLOBAL OBSERVATION SATELLITE)

Integrated Space Vehicle

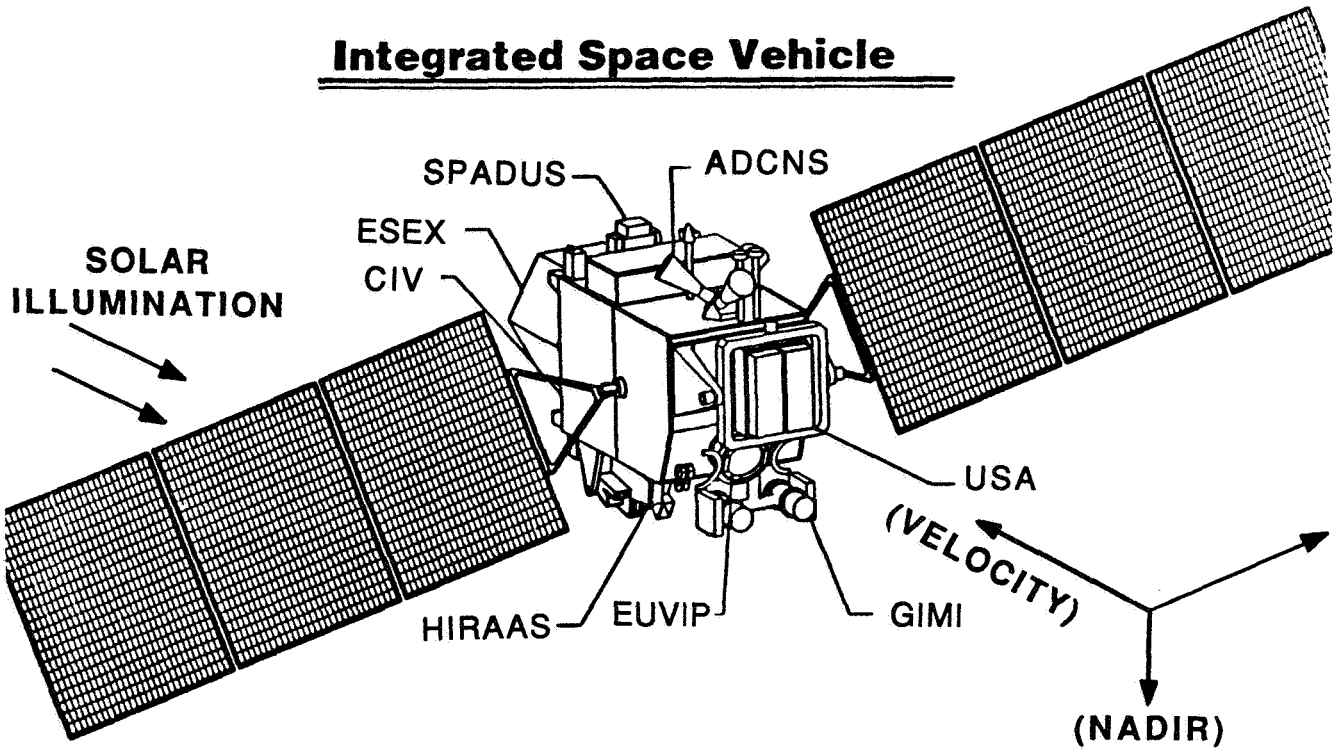

ARGOS EXPERIMENTS

1.	EUVIP	ARMY	UV Imager
2.	HIRAAS	NRL	UV Spectroradiometer
3.	USA	NRL	Unconv. Stellar (X-Ray)
4.	GIMI	NRL	UV Camera
5.	CIV	Phillips	Critical Ionization Velocity
6.	ESEX	Phillips	Arcjet Propulsion Engine
7.	ADCNS	DARPA	Attitude Determination Control & Navigation System
8.	SPADUS	ONR	Space Dust Experiment

ARGOS MISSION CHARACTERISTICS

a) ORBIT: Circular near polar (98.7^{o}), 833 km altitude (sun synchronous).
b) MISSION DURATION: 3 years.
c) STABILIZATION: 3 - axis stabilized
d) LAUNCH VEHICLE: Delta II
e) EXPERIMENTS: Total of 8
f) FLIGHT INSTRUMENT DELIVERY: September 1994.
g) LAUNCH: September 1995.

Figure 9. Integrated ARGOS space vehicle, mission characteristics, and experiments.

N93-29708

FUTURE RADIATION MEASUREMENTS IN LOW EARTH ORBIT

50177
B-516

James H. Adams, Jr.
E. O. Hulburt Center for Space Research
Code 7654, Naval Research Laboratory
Washington, DC 20375-5000
Phone: 202/767-2747, Fax: 202/767-6473

SUMMARY

The first LDEF mission has demonstrated the value of the LDEF concept for deep surveys of the space radiation environment. This paper discusses the kinds of measurements that could be done on a second LDEF mission. Ideas are discussed for experiments which: a) capitalize on the discoveries from LDEF I; b) take advantage of LDEF's unique capabilities and c) extend the investigations begun on LDEF I. These ideas have been gleaned from investigators on LDEF I and others interested in the space radiation environment. They include new approaches to the investigation of ^{7}Be that was discovered on LDEF I, concepts to obtain further information on the ionic charge state of cosmic rays and other energetic particles in space and other ideas to extend the investigations begun on LDEF I.

INTRODUCTION

LDEF I carried several space radiation experiments and additional experiments were done with parts of the satellite that were not originally intended as experimental material. This first mission demonstrated the utility of LDEF for certain kinds of investigations of the space radiation environment.

The first LDEF mission produced the discovery of large amounts of cosmogenic ^{7}Be in the exoatmosphere at 310 km altitude[1]. LDEF I also produced further evidence for heavy ions trapped in the earth's magnetic field[2] which may be due to trapped anomalous cosmic rays[3] or some new source of trapped heavy ions. The mission also demonstrated that three axis stabilized satellites are non-uniformly irradiated by trapped protons due to the guiding center asymmetry in low earth orbit[4]. This mission furthered the investigation of the ionic charge state of cosmic rays and is helping to demonstrate the richness of this new information channel on ionizing particle radiation[5].

The world's largest cosmic ray experiment was onboard LDEF I. This experiment returned information of the elemental composition of the heaviest and rarest cosmic ray nuclei[6]. The LDEF satellite also carried experiments to measure the radiation doses and LET spectra on LDEF[7,8,9,10]. Samples taken from LDEF were used to investigate the quantities of radionuclides produced in LDEF materials and their distribution within the spacecraft[11,12,13,14].

COSMOGENIC NUCLEI IN LOW EARTH ORBIT

The most surprising discovery to date on LDEF was the ^{7}Be that was found imbedded on the windward surfaces of LDEF[1]. This discovery was not made by a planned LDEF experiment but as a

PRECEDING PAGE BLANK NOT FILMED

result of a test conceived prior to retrieval. It was found that the implanted ^{7}Be ions implied an atmospheric abundance of ^{7}Be that far exceeded the production in the ambient atmosphere at the orbital altitude of LDEF. Petty[15] has proposed an explanation for this ^{7}Be. He proposes that the ^{7}Be is produced much lower in the atmosphere. Above the turbopause, at about 100 km, the constituents of the atmosphere are collisionally decoupled and gravitational fractionation occurs. Petty proposes that above the turbopause, the ^{7}Be is in the form of ^{7}Be atoms which become increasingly abundant at higher altitudes due to gravitational fractionation. He calculates the density of ^{7}Be at the orbit of LDEF to be about 1/4 of the observed lower limit on the abundance, but this calculation is quite uncertain because it depends on latitude, the altitude of the turbopause, and the upper atmospheric temperature.

A second LDEF mission could follow up on this discovery and test the dependences in Petty's theory as well as more detailed atmospheric models. Also other cosmogenic nuclei from the atmosphere below LDEF could be searched for using carefully planned experiments. Figure 1 shows three concepts for experiments that have been suggested by G. W. Phillips*and the author. These experiments, to be located on the windward side of LDEF, will extend the investigation of ^{7}Be. In figure 1a, an experiment to investigate the time variations in the ^{7}Be is depicted. The idea is to collect ^{7}Be ions on a moving strip of aluminum foil that is exposed through an aperture. The movement of the foil must be started approximately 100 days prior to recovery of LDEF. This will require the second LDEF mission to have a command receiver. The foil will be moved at a rate that gives a time resolution of about 1 day. If the temperature of the upper atmosphere varies or solar flares occur during the last 100 days of the mission, the dependence of the ^{7}Be on can be examined. To find the latitude dependence of the ^{7}Be, the experiment depicted in figure 1b is suggested. Here the ^{7}Be is recorded on an aluminum disk which rotates with the orbital period. This disk should be set in motion during the last 100 days of the mission. Only a small sector of the disk is exposed thorough the triangular opening in the shield, so the latitude dependence of the ^{7}Be is determined with a resolution of 1/10 of the orbit.

Another factor that can affect the transport of ^{7}Be up to LDEF's orbit is its charge state. It is quite possible that solar UV photons have ionized the ^{7}Be atoms to $^{7}Be^{+1}$ ions. Figure 1c. depicts a concept for an instrument to distinguish the ^{7}Be ions from ^{7}Be atoms. The three sections of the instrument allow the effects of no electric field to be compared with that of two electric field levels. The neutral ^{7}Be atoms will implant to the same areal density in the three sections of the experiment, while $^{7}Be^{+1}$ implantation will be prevented in the two sections that are covered by retarding potential grids. In the first section, the retarding potential of 2.5V potential is only sufficient to prevent implantation of $^{7}Be^{+1}$ but will permit the implantation of ^{7}Be if it is in the form of $^{7}BeO^{+1}$ ions. In the second section, the 8V retarding potential is sufficient to prevent both $^{7}Be^{+1}$ and $^{7}BeO^{+1}$ ions from implanting.

In addition to ^{7}Be, other cosmogenic ions may also be enhanced at LDEF's orbit. J. C. Gregory * and G. W. Phillips* have suggested that experiments on the second LDEF mission should also look for evidence of ^{10}Be, ^{14}C, and ^{3}H. Unlike ^{7}Be, these other ions have long half-lives. The plan is to chemically remove them from witness plates flown on LDEF and identify them by accelerator mass spectrometry.

ENERGETIC HEAVY IONS BELOW THE GEOMAGNETIC CUTOFF

A second discovery on LDEF I is the presence of energetic heavy ions below the geomagnetic cutoff[16,2]. The origin of these ions has not yet been established. One possibility is that some of these observations are due to trapped anomalous cosmic rays[3], but it is unlikely that the Fe group ions observed on LDEF[16] are from the anomalous cosmic ray component. We know that the ionization states of anomalous cosmic rays[17] and solar cosmic rays[18] provide unique information about these components of the space radiation environment. It now seems possible that ionization states will provide a new channel of information on other components of cosmic rays. Below, two experiments are suggested for the second LDEF mission that could extend these investigations.

*Private communication. See footnote list at end of paper.

LDEF I carried the Heavy Ions In Space (HIIS) experiment which discovered stopping Fe group ions in low inclination - low earth orbit[16]. A second HIIS experiment, HIIS II is proposed for the second LDEF mission. This experiment would also comprise two trays on the space facing end of the vehicle. HIIS II would differ from the version flown on the first LDEF mission. It would have a thinner window in the top of each module and would make more use of the CR-39 plastic track detector. All the track detectors would be sealed in an atmosphere of dry air with a much larger ballast volume of air than in the first mission to improve the detector performance (see figure 2). This experiment would once again be entirely passive.

The second experiment to measure stopping heavy ions was suggested by Rudolf Beaujean*. This would be similar to the experiment flown on SPACELAB I[19,20]. It would consist of a fixed detector stack and a rotating one (see figure 3). The rotating stack would rotate in both directions with its position always adjusted to coincide with the local geomagnetic cutoff. This experiment would require power and telemetry. The down-link telemetry would carry housekeeping data on the instrument and its operation. The up-link would be used to update the onboard data base that controls the rotation of the stack to correct for changes in the orbital period as the orbit decays. A 57° orbit is prefered for this experiment and a 9-12 month flight.

ULTRAHEAVY COSMIC RAYS

Figure 4 compares the integral number of galactic cosmic ray iron ions collected above any threshold energy for several past, present, and proposed ultraheavy cosmic ray experiments. The Skylab[21], HEAO[22], and Ariel[23] experiments are completed. The UHCRE[6] and the HIIS[5] are in analysis and the TREK experiment[24] is presently being exposed onboard the MIR Space Station. The HNC experiment[25] was accepted for the reflight of the original LDEF spacecraft. The HNC experiment was well into development when the LDEF re-flight was cancelled following the Challenger accident. Subsequently HNC was accepted to fly on the Spacestation, but due to reductions in the size and capabilities of the Spacestation, this flight has been indefinitely delayed.

Since the HIIS and UHCRE experiments were prepared for the first LDEF mission, a new high resolution phosphate glass detector has been developed[26]. Accelerator tests indicate that this new detector should be capable of individual elemental resolution throughout the periodic table. Its use will make possible detailed measurements of the elemental composition of ultraheavy cosmic rays. These measurements can be used to investigate the origin and evolution of matter in our galaxy and search for evidence of new forms of matter such as superheavy elements and magnetic monopoles. HNC can also be used to test theories of the propagation of cosmic rays in the Galaxy. The scientific objectives of HNC have been repeatedly given high priority by NASA advisory panels (see, for example, NASA's Space Physics Strategy Implementation Study for 1995 - 2010[27]).

Because ultraheavy cosmic rays are rare, an HNC detector on LDEF II should be as large as possible, utilizing all the trays on the sides and space end of LDEF. The size of the data sample can be further increased by a mission of 6 years or more in a 57 degree inclination orbit. Figure 5 shows an LDEF tray filled with a mosaic of stacks of phosphate glass detectors. The detectors are held between silicon separators which allow for differential expansion and protection from shock and vibration. Each tray will be filled to its maximum weight limit with these glass detectors and the tray will be covered with a thermal blanket. There is no need for sealing the detectors in an atmosphere of air as in the case with plastic detectors.

HNC is a simple passive experiment requiring no power or telemetry. It makes minimum demands on the spacecraft. The experiment will rely on passive thermal controls to minimize the temperature excursions of the experiment during flight. Since thermal blankets have proven effective micrometeoroid collectors, HNC would be compatible with a micrometeoroid experiment that used the retrieved thermal blankets for their data source.

COMPOSITION AND ENERGY SPECTRA OF COSMIC RAYS ABOVE 3 TeV/amu

It is thought that the bulk of cosmic rays are accelerated by shock waves from supernovae of various ages. It is recognized, however that these shocks have a limited strength and may be unable to accelerate cosmic rays much above 10 TeV/amu[28]. Indeed, indirect ground-based observations have produced persistent reports of anomalies in the intensity and composition versus total kinetic energy in the energy range of 100 to 10,000 TeV. Above an energy in the range of 10 to 100 TeV/amu, a different mechanism may be responsible for cosmic ray acceleration. Superbubble shocks powered by multiple supernovae[29,30] and a shock associated with the termination of the Galactic wind[30] are among the suggestions for the acceleration mechanism at these high energy cosmic rays.

To investigate the transition region from supernova shock acceleration to the mechanism at higher energies, Y. Takahashi* has proposed to measure the elemental composition and energy spectra of cosmic ray nuclei heavier than Na in the energy range from 3 to 100 TeV/amu. This will be done with a passive calorimeter consisting of plastic track detectors, nuclear emulsions, X-ray films, and lead absorbers. This approach has a long heritage. It has been used successfully for years by the JACEE collaboration to make similar measurements on balloon flights. LDEF will allow a large increase in both exposure time and payload mass allowing the measurements to be carried to higher energies.

Figure 6 shows an LDEF tray containing the calorimeter. The calorimeter can be designed to weigh as little as 180 lbs per tray, but would benefit from more mass per tray. A minimum of 6 trays are needed for a one year mission in any orbit. The calorimeters are completely passive and require no power, telemetry or onboard data recording. The trays of this experiment can be located on the sides or space-facing end of LDEF. Because of their mass, they could be used to establish the desired mass distribution for LDEF II. This experiment is also compatible with space debris sub-experiments utilizing the thermal covers and perhaps solar arrays if the experiment can be kept cool under the solar arrays.

DOSIMETRIC AND SPECTROSCOPIC MEASUREMENTS OF RADIATION

The space radiation environment is known to pose a radiation hazard to men in space. The radiation dose-equivalent comes from many sources. The external radiation environment of the manned spacecraft consists of trapped protons and electrons, cosmic rays and occasionally solar energetic particles. In passing through the walls of the spacecraft these radiations are attenuated and modified by nuclear interactions. Inside the spacecraft the penetrating external components and their fragments are present but their intensity is non-uniform and anisotropic due to the non-uniform shielding provided by the spacecraft. In addition to particles originating outside the spacecraft there are additional radiations that result from the nuclear reactions caused by the external components. These radiations consist of neutrons, protons and heavier fragments of the atoms of the nuclei from which the spacecraft is constructed.

With the dose-equivalent to the crew coming from so many non-uniform and anisotropic components, predicting the exposure in a given mission is a complex problem. To investigate this problem for the planned Spacestation, LDEF I was instrumented with several kinds of radiation detectors. Considerable progress has been made in understanding the relative importance of the various components and the non-uniformities caused by the mass distribution in a spacecraft from the measurement made on LDEF I[9,10,31-38]. These results have shown that detailed spacecraft modeling

calculations can generally reproduce the complex pattern of doses and anisotropies observed on LDEF, but more detailed investigations are needed.

Figure 7 shows the proposed locations of four types of advanced passive and active dosimeters on the second LDEF mission that have been suggested by E.V. Benton*. The first of these, the Trackoscope, provides a 4π survey of the anisotropy in protons, galactic cosmic rays and secondary charged particles coming from the spacecraft material. To investigate the real-time distribution of radiation doses around the orbit, an active tissue equivalent proportional counter (TPEC) has been proposed. This unit measures the LET spectrum in real-time and can be used to investigate how this spectrum varies with orbital location. To investigate the importance of secondary neutrons from the spacecraft material and its dependence of shielding, Bonner Spheres will be flown in four locations around the LDEF. Finally, shielded stacks of various passive detectors are proposed to investigate the effects of shielding on the incident radiation from the space environment. These detectors will measure LET spectra, particle fluences, dose and dose-equivalent under various amounts of shielding.

The total weight of the proposed detector packages for this experiment is about 40 Kg, distributed as shown in figure 7. Each location takes only a small fraction of a tray. The active instruments will be battery powered and will record their data onboard. No power or telemetry will be required. A 28° inclination orbit at 450 km is preferred because it's the same as the Spacestation and a mission duration of three years is preferred.

CONCLUSION

A sampling of space radiation experiments have been discussed which show the breadth and richness of the investigations that could be conducted on a second LDEF mission. The experimental concepts discussed here are by no means complete. Many additional concepts have already been proposed and, no doubt, others would emerge if NASA makes the decision to offer flight opportunities on additional LDEF missions. The range of experiments that can be conducted on the LDEF carrier and the number of individual investigations that can be accommodated on each flight make LDEF a cost-effective way to meet the needs of several science and engineering disciplines for access to space.

REFERENCES

1. Fishman, G.J., et al.: Observation of ^{7}Be on the surface of LDEF spacecraft. *Nature*, vol. 349, 1991, pp. 678-680.
2. Beaujean, R., Jonathal, D., and Enge, W.: Heavy Ion Measurements on LDEF. *First LDEF Post-Retrieval Symposium*, NASA CP-3134, 1991, pp. 393-398.
3. Grigorov, N.L., Kondratyeva, M.A., Panasyuk, M.I., Tretyakova, Ch.A., Adams, Jr., J.H., Blake, J.B., Schulz, M., Mewaldt, R.A., and Tylka, A.J.: Evidence for Trapped Anomalous Cosmic Ray Oxygen Ions in the Inner Magnetosphere. *Geophys. Res. Letters*, vol. 18, 1991, pp. 1959-1962.
4. Gregory, J.C., Fishman, G.J., Harmon, B.A., and Parnell, T.A.: The Interactions of Atmospheric Cosmogenic Radionuclides with Spacecraft Surfaces. *First LDEF Post-Retrieval Symposium*, NASA CP-3134, 1991, pp. 237-248.
5. Adams, Jr., James H., Beahm, Lorraine P., and Tylka, Allan J.: Progress Report On The Heavy Ions in Space (HIIS) Experiment. *Second LDEF Post-Retrieval Symposium*, NASA CP-3194, 1993.
6. Thompson, A., O'Sullivan, D., Bosch, J., Keegan, R., Wenzel, K.-P., Jansen, F., and Domingo, C.: Progress Report on The Ultra Heavy Cosmic Ray Experiment. *Second LDEF Post-Retrieval Symposium*, NASA CP-3194, 1993.
7. Blake, J.B., and Imamoto, S.S.: Measurements fo The Radiation Dose to LDEF By Means of The Passive Dosimetry. *Second LDEF Post-Retrieval Symposium*, NASA CP-3194, 1993.

8. Bourrieau, J.: LDEF: Dosimetric Measurement Results (AO 138-7 Experiment). *Second LDEF Post-Retrieval Symposium*, NASA CP-3194, 1993.
9. Frank, A.L., Benton, E.V., Armstrong, T.W., and Colborn, B.L.: Absorbed Dose Measurements and Predictions On LDEF. *Second LDEF Post-Retrieval Symposium*, NASA CP-3194, 1993.
10. Oda, K., Henke, R.P., Frank, A.L., Benton, E.R., Frigo, L.A., Parnell, T.A., Watts, Jr., J.W., and Derrickson, J.H.: Charge, Energy And LET Spectra Measurements of Charged Particles In P0006 Experiment of LDEF. *Second LDEF Post-Retrieval Symposium*, NASA CP-3194, 1993.
11. Reeves, James H., Arthur, Richard J., and Brodzinski, Ronald L.: Sensitivity of LDEF Foil Analyses using Ultra-Low Background Germanium Vs. Large NaI(Tl) Multidimensional Spectrometers. *Second LDEF Post-Retrieval Symposium*, NASA CP-3194, 1993.
12. Reedy, Robert C., and Moss, Calvin E.: Radioactivities Induced In Some LDEF Samples. *Second LDEF Post-Retrieval Symposium*, NASA CP-3194, 1993.
13. Smith, Alan R., and Hurley, Donna L.: A Photon Phreak Digs The LDEF Happening. *Second LDEF Post-Retrieval Symposium*, NASA CP-3194, 1993.
14. Harmon. B.A., Fishman, G.J., Parnell, T.A., and Laird, C.E.: Induced Activation Study of LDEF. *Second LDEF Post-Retrieval Symposium*, NASA CP-3194, 1993.
15. Petty, G.W.: Equilibrium Profiles of Atomic ^{7}Be and ^{10}Be in the Atmosphere Above 100 KM. *Geophys. Res. Letters*, vol. 18, 1991, pp. 1687-1690.
16. Adams, J.H., Jr., Beahm, L.P., and Tylka, A.J.: Observations from LDEF of Heavy Ions Below the Geomagnetic Cutoff. *Proc. of the 22nd International Cosmic Ray Conf.*, vol. 1, 1991, pp. 619-622.
17. Adams, Jr., J.H., Garcia-Munoz, M., Grigorov, N.L., Klecker, B., Kondratyeva, M.A., Mason. G.M., McGuire, R.E., Mewaldt, R.A., Panasyuk, M.I., Tretyakova, Ch.A., Tylka, A.J., and Zhuravlev, D.A.: The Charge State of The Anomalous Component of Cosmic Rays. *Ap. J. (Letters)*, vol. 375, 1991, pp. L45-L48.
18. Luhn, A. et al.: Ionic Charge States of N, Ne, Mg, Si, and S in Solar Energetic Particle Events. *Adv. in Space Res.*, vol. 4, 1984, pp. 161-164.
19. Oschlies, K.; Beaujean, R.; and Enge, W.: On the Charge State of Anomalous Oxygen. *Astrophys. J.*, vol. 345, 1989, pp. 776-81.
20. Beaujean, R., Shmidt, M., Enge, W., Siegmon, G., Krause, J., and Fischer, E.: Isotopic Stack: Measurement of Heavy Cosmic Rays, *Science*, vol. 225, 1984, 193-195.
21. Shirk, E.K., and Price, P.B.: Charge and Energy Spectra of Cosmic Rays with Z≥60: the Skylab Experiment. *Ap.J.* vol. 220, 1978, pp. 719-733.
22. Binns, W.R., Garrard, T.L., Gibner, P.S., Israel, M.H., Kertzman, M.P., Klarmann, J., Newport, B.J., Stone, E.C., and Waddington, C.J.: Abundances of Ultraheavy Elements in the Cosmic Radiation: Results from HEAO 3. *Ap.J.*, vol. 346, 1989, pp. 997-1009.
23. Fowler, P.H., Walker, R.N.F., Masheder, M.R.W., Moses, R.T., Worley, A., Gay, A.M.: Ariel 6 Measurements of the Fluxes of Ultraheavy Cosmic Rays. *Ap.J.*, vol. 314, 1987, pp. 739-746.
24. Afanasyev et al.: TREK: A Cosmic Ray Experiment on the Soviet Space Station MIR. *Proc. of the 22nd International Cosmic Ray Conf.*, vol. 1, 1991, pp. 623-626.
25. Price, P.B., Tarle, G., Salamon, M.H., and Barwick, S.W.: Flight Proposal for Space Station Attached Payload Heavy Nucleus Collector (HNC). NASA Proposal DRDA 89-1063, 1989.
26. Wang, Shicheng, Barwick, S.W., Ifft, D., Price, P.B., and Westphal, A.J.: Phosphate Glass Detectors with High Sensitivity to Nuclear Particles. *Nucl. Instr. and Meth.*, vol. B35, 1988, pp. 43-49.
27. Space Physics Subcommittee of the Space Science and Applications Advisory Committee: *Space Physics Strategy-Implementation Study*. NASA Hdqrs, Second Edition, April, 1991.
28. Lagage, P.C. and Cesarsky, C.J.: The Maximum Energy of Cosmic Rays Accelerated by Supernova Shocks. *Astron. Astrophys.*, vol. 125, 1983, pp. 249-257.
29. Jokipii, J.R. and Morfill, G.E.: A Model for the Origin of High Energy Cosmic Rays. *Proc. of the 19th Intl. Cosmic Ray Conf.*, vol. 2, 1985, pp. 132-5.

30. Streitmatter, R.E., Balasubrahmanyan, V.K., and Ormes, J.F.: Local Superbubble Model of Cosmic Ray Propagation. *18th Intl. Cosmic Ray Conf.*, vol. 2, 1983, pp. 183-190.
31. Benton, E.V., Frank, A.L., Benton, E.R., Csige, I., Parnell, T.A., and Watts, J.W., Jr.: Radiation Exposure of LDEF: Initial Results. *First LDEF Post-Retrieval Symposium*, NASA CP-3134, 1991, pp. 325-337.
32. Csige, I., Benton, E.V., Frank, A.L., Frigo, L.A., Benton, E.R., Parnell, T.A., and Watts, J.W., Jr.: Charged Particle LET-Spectra Measurements Onboard LDEF. *First LDEF Post-Retrieval Symposium*, NASA CP-3134, 1991, pp. 339-346.
33. Armstrong, T.W., Colburn, B.L., and Watts, J.W., Jr.: Ionizing Radiation Calculations and Comparisons with LDEF Data. *First LDEF Post-Retrieval Symposium*, NASA CP-3134, 1991, pp. 347-359.
34. Colburn, B.L. and Armstrong, T.W.: LDEF Geometry/Mass Model for Radiation Analysis. *First LDEF Post-Retrieval Symposium*, NASA CP-3134, 1991, pp. 361-5.
35. Csige, I., Benton, E.V., and Soundararajan, S.: Light-Heavy Ion Measurements In CR-39 Located On The Earth Side of LDEF. *Second LDEF Post-Retrieval Symposium*, NASA CP-3194, 1993.
36. Csige, I., Benton, E.V., Frigo, L.A., Parnell, T.A., and Watts, J.W., Jr.: Three Dimensional Shielding Effects On Charged Particle Fluences Measured In The P0006 Experiment of LDEF. *Second LDEF Post-Retrieval Symposium*, NASA CP-3194, 1993.
37. Colburn, B.L. and Armstrong, T.W.: Development and Application of A 3-D Geometry/Mass Model For LDEF Satellite Ionizing Radiation Assessments. *Second LDEF Post-Retrieval Symposium*, NASA CP-3194, 1993.
38. Armstrong, T.W., and Colburn, B.L.: Radiation Model Predictions and Validation Using LDEF Data. *Second LDEF Post-Retrieval Symposium*, NASA CP-3194, 1993.

FOOTNOTES

1. Phillips, G.W.: Private Communication, 1992.
2. Gregory, J.C.: Private Communication, 1992.
3. Beaujean, R.: Private Communication, 1992.
4. Benton, E.V.: Private Communication, 1992.
5. Takahashi, Y.: Private Communication, 1992.

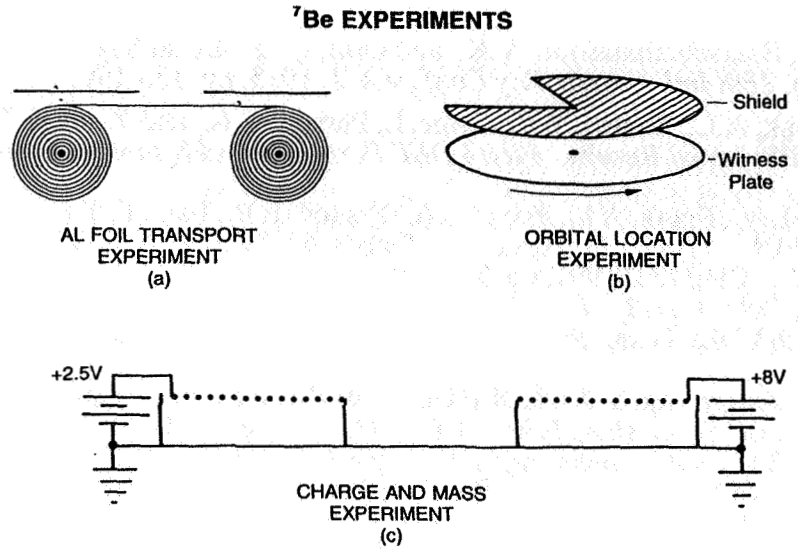

Figure 1: Concepts for further investigations of ^{7}Be in low earth orbit. (a) A device to measure the orbit-averaged ^{7}Be atmospheric density versus time. (b) A device to measure the density of ^{7}Be around the orbit of LDEF II. (c) A device to measure the charge and mass of an ion of ^{7}Be. If the ^{7}Be is charged, it can be repelled from the witness plate by an electric field. $^7Be^{+1}$ can be repelled by a 2.5V potential. Should the ^{7}Be be in a chemical form such as $^7BeO^+$ it can be repelled with an 8V potential.

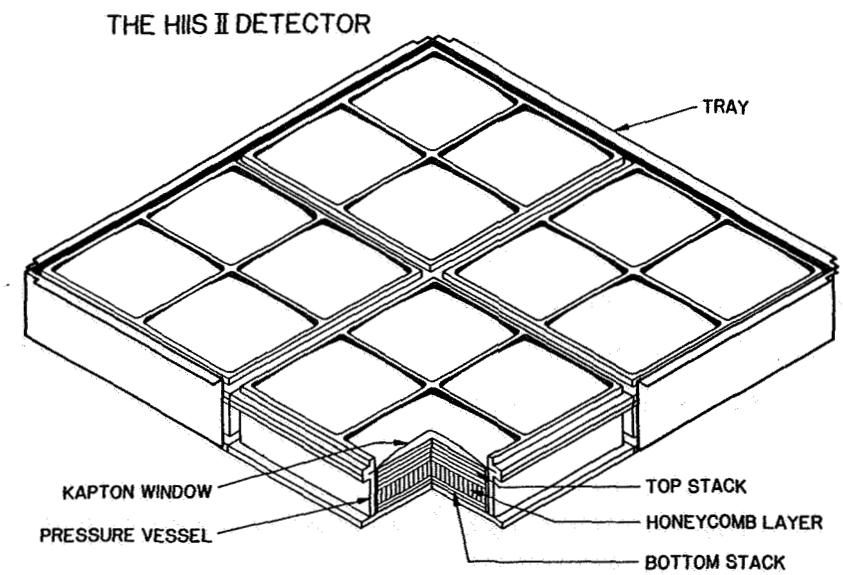

Figure 2: The HIIS II concept. Each tray will contain four track detector modules. Each module will contain two stacks of plastic track detectors. The upper stack will record the particles below the geomagnetic cutoff and will be under a 125 μm kapton window in the lid. The lower stack will be below a lead degrader at the bottom of each module and will record galactic cosmic ray iron group ions that come to rest after passing though the lead. Between the two stacks will be a ventilated honeycomb layer to contain ballast air for the module.

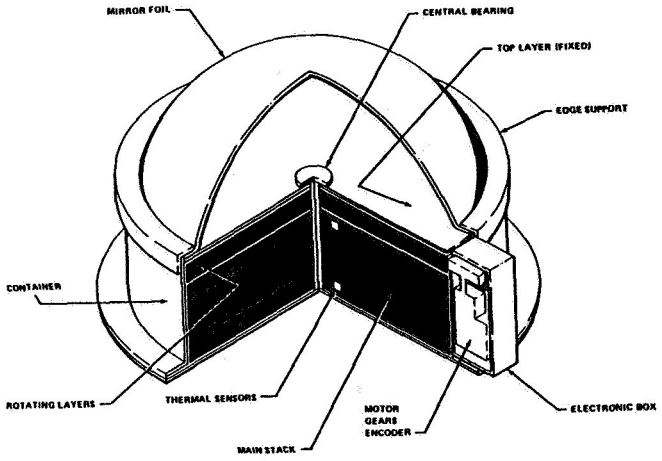

Figure 3: A concept for a rotating detector which records cosmic ray tracks at different geomagnetic cutoffs. The geomagnetic cutoffs at which the cosmic rays were recorded are determined by matching the tracks in the fixed and rotating detector stacks (courtesy of R. Beaujean, Kiel University).

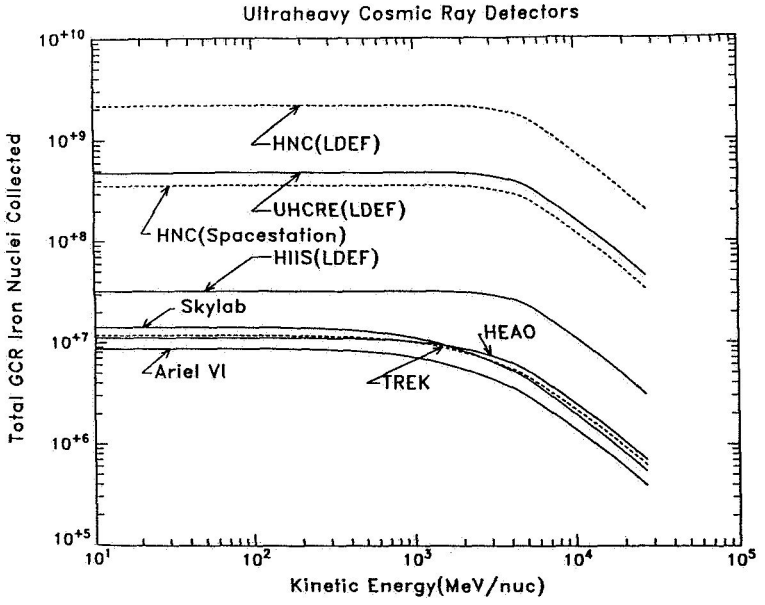

Figure 4: Present and proposed ultraheavy cosmic ray experiments are compared according to the number of cosmic ray Fe nuclei collected above any threshold energy. The Skylab, HEAO, and Ariel VI experiments are complete. The UHCRE and HIIS experiments are in analysis and the TREK experiment is currently collecting data on the MIR spacestation. The HNC experiment has been proposed as the logical next step in the investigation of ultraheavy cosmic rays. First HNC was selected for the re-flight of LDEF, but cancelled following the Challenger accident. It was also selected for Spacestation, but then indefinitely delayed due to the downsizing of Spacestation.

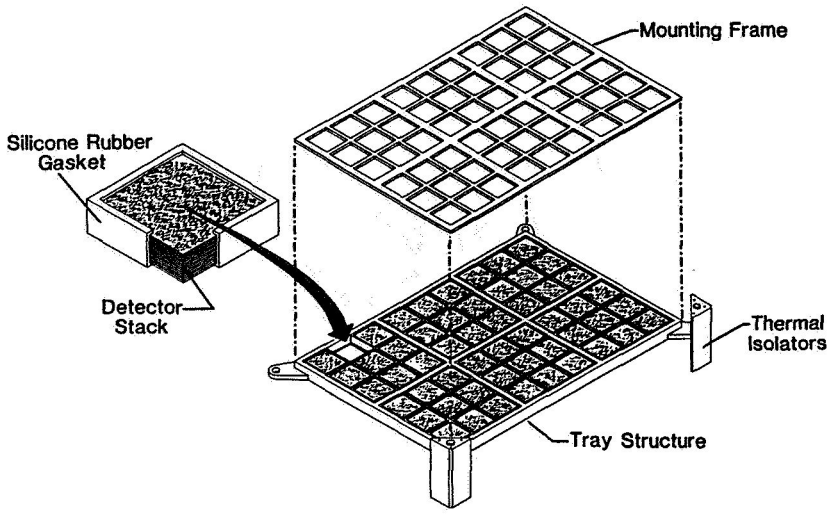

Figure 5: The HNC Detector and Tray Assembly Concept (courtesy of W. Kinard, LDEF Project Office, NASA LaRC).

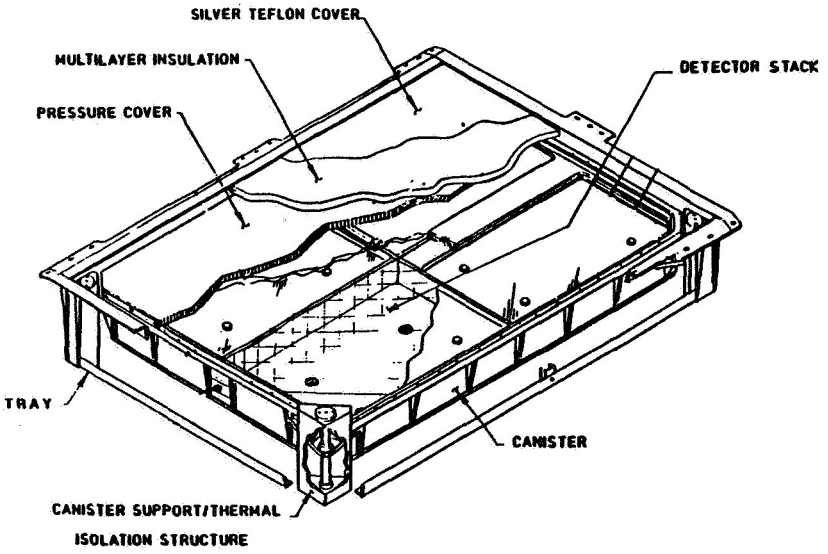

Figure 6: Concept of loading a detector stack unit of the High Energy Composition and Spectra Experiment into an LDEF tray (courtesy of Y. Takahashi, UAH).

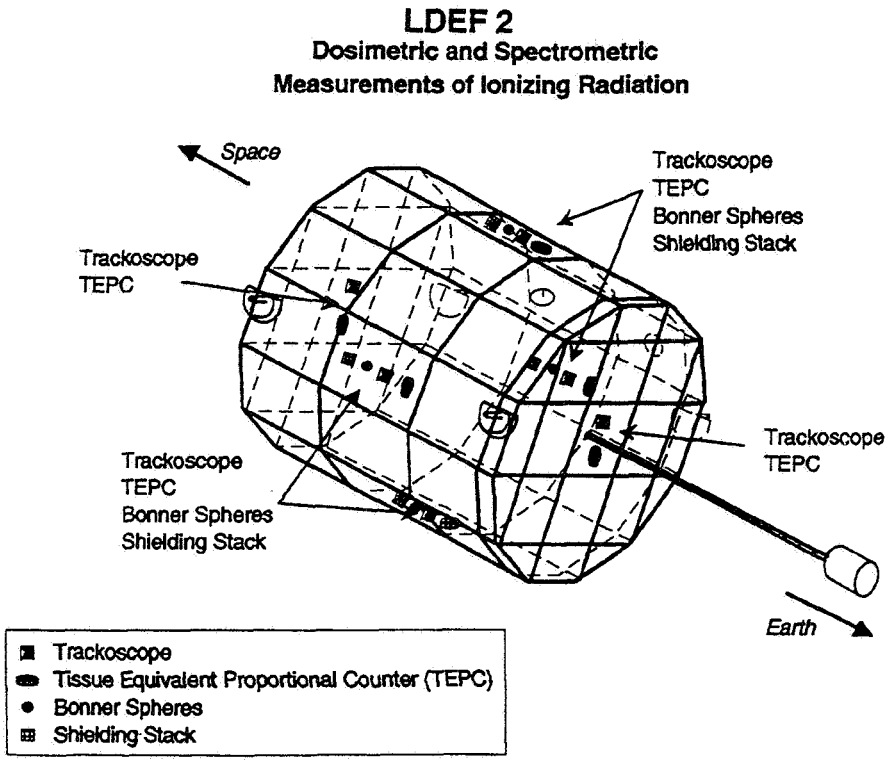

Figure 7: This figure shows the proposed locations of four types of advanced passive dosimeters that could make dosimetric and spectroscopic measurements of ionizing radiation on LDEF II (courtesy of E.V. Benton, U of SF).

COLOR PHOTOGRAPHS

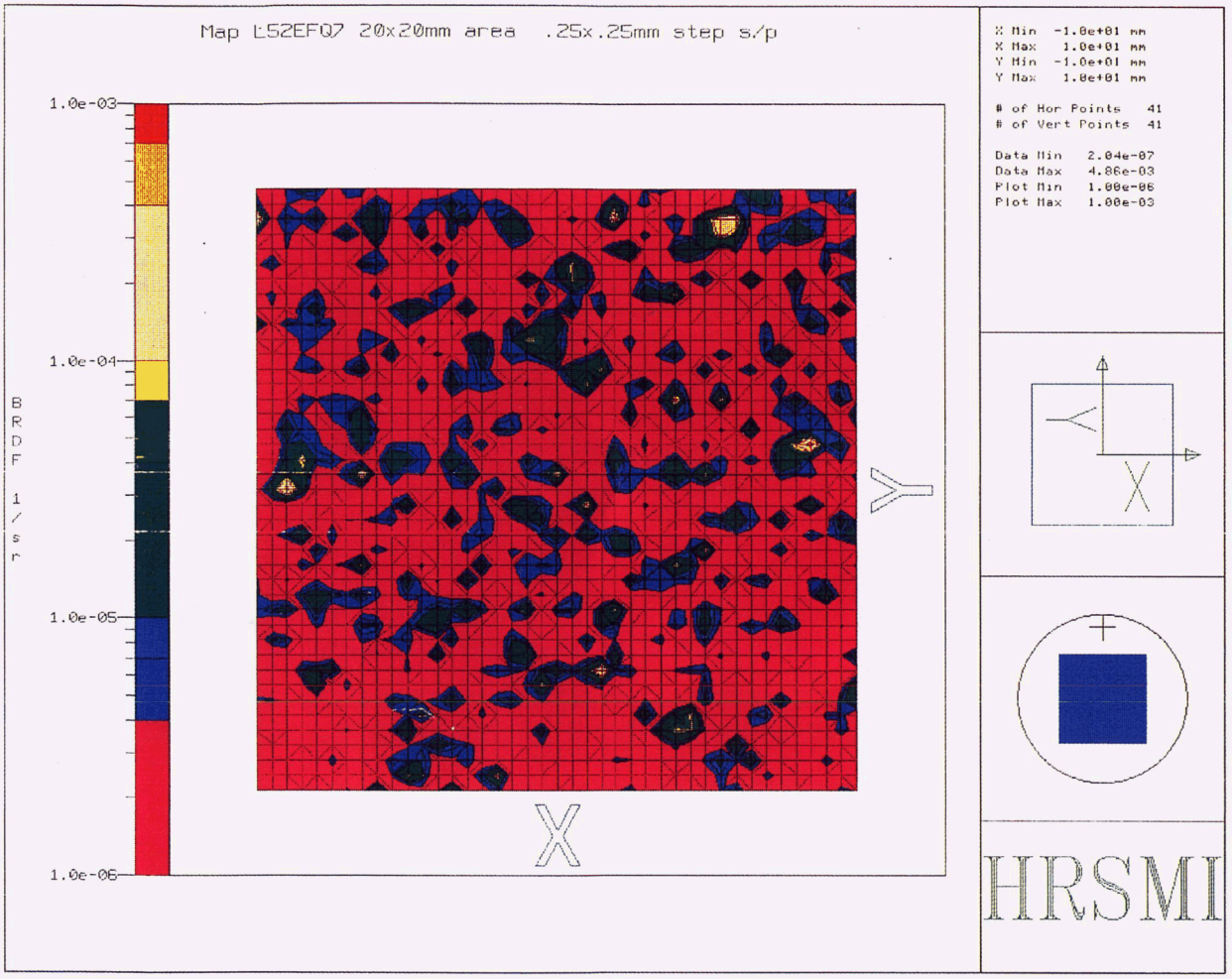

ORIGINAL PAGE
COLOR PHOTOGRAPH

Figure 9: Scatter map of fused silica sample.
(Color enlargement of black and white photograph on page 1371.)

PRECEDING PAGE BLANK NOT FILMED

ORIGINAL PAGE
COLOR PHOTOGRAPH

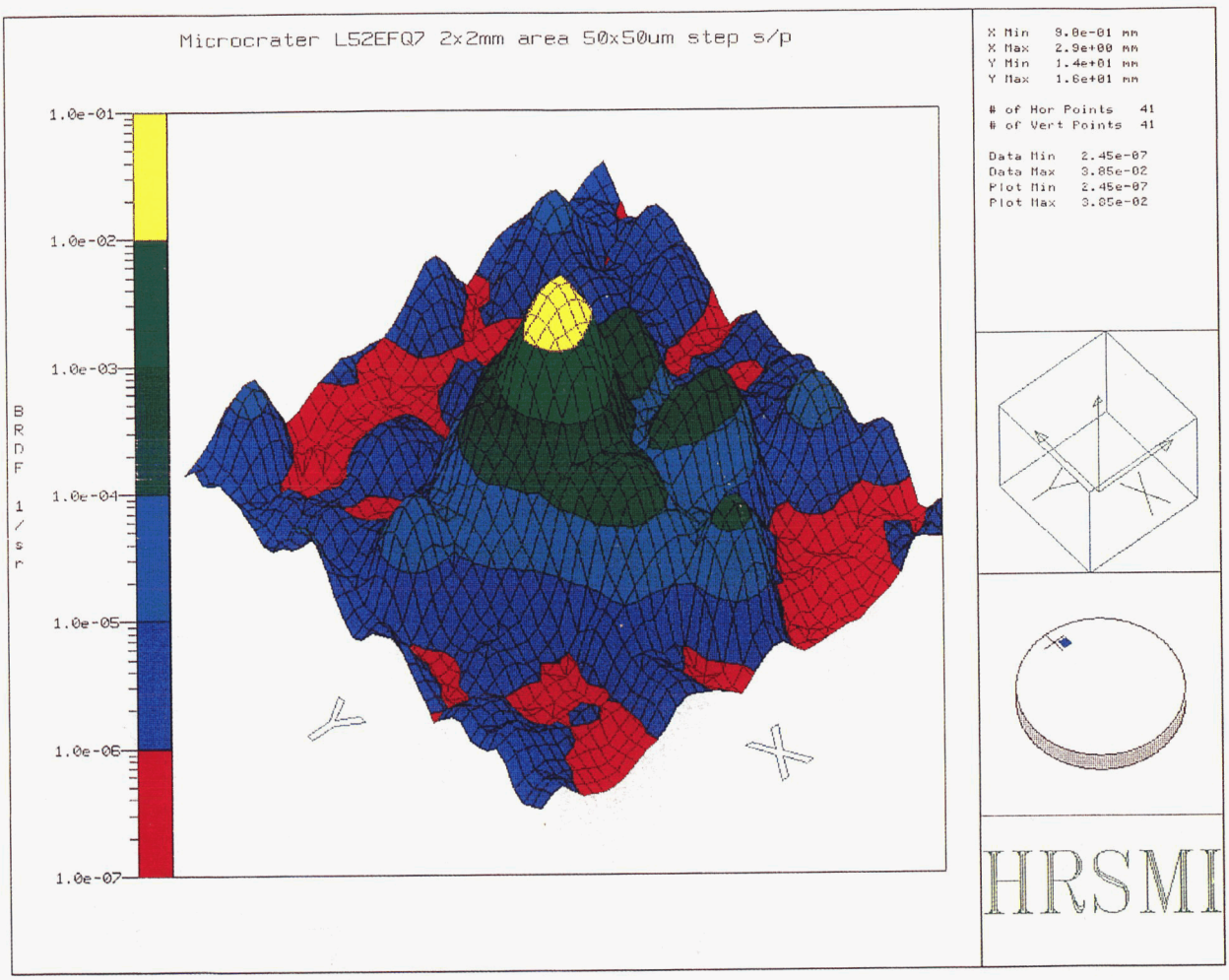

Figure 10: Scatter map of a micrometeoroid impact site on fused silica.
(Color enlargement of black and white photograph on page 1371.)

AUTHOR INDEX

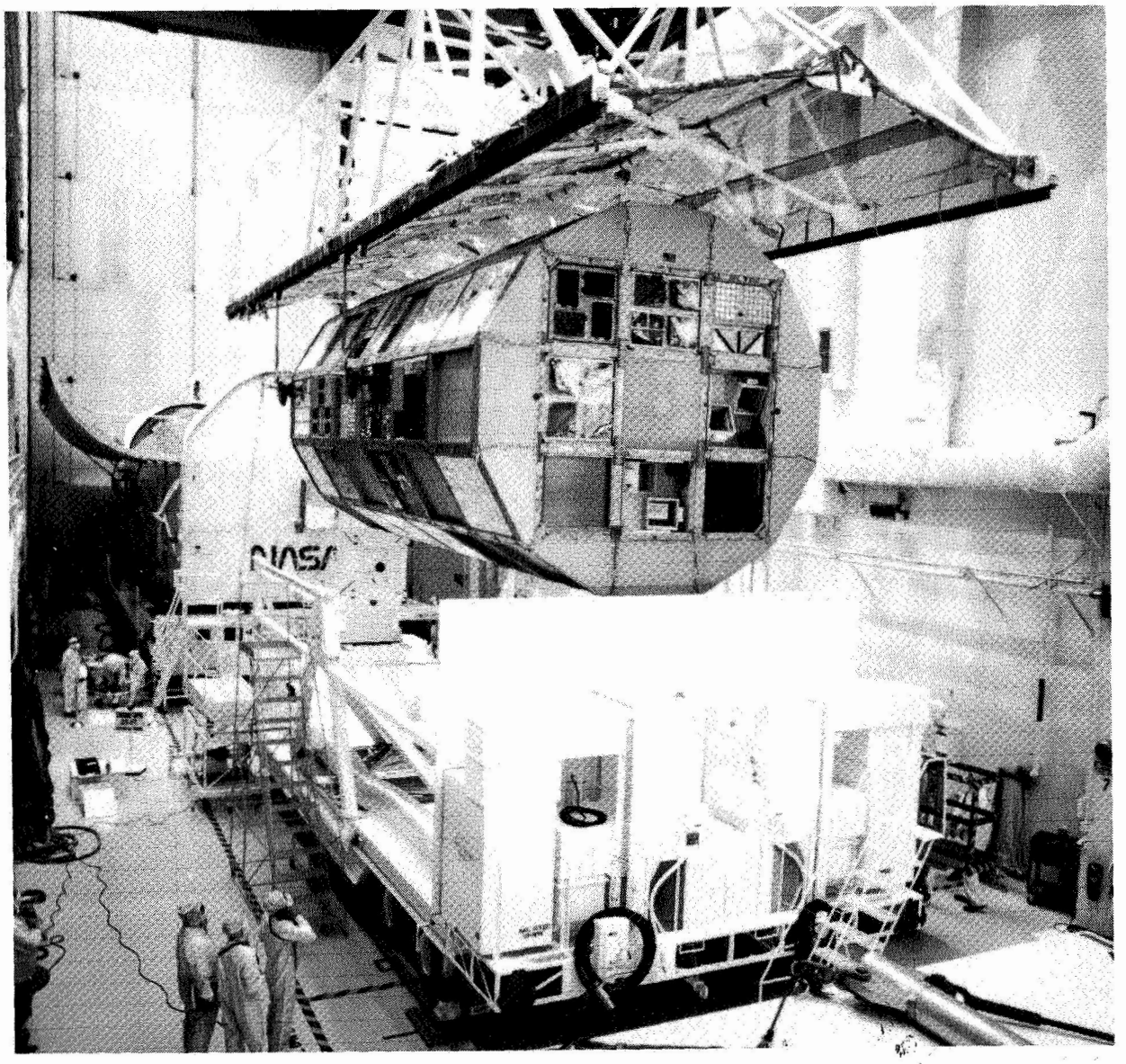

ORIGINAL PAGE
BLACK AND WHITE PHOTOGRAPH

L-90-11207

Author Index

Index Guide

Part 1, pages 1–274; Part 2, pages 275–738

Part 3, pages 739–1254; Part 4, pages 1255–1570

PRECEDING PAGE BLANK NOT FILMED

REPORT DOCUMENTATION PAGE

Form Approved
OMB No. 0704-0188

Public reporting burden for this collection of information is estimated to average 1 hour per response, including the time for reviewing instructions, searching existing data sources, gathering and maintaining the data needed, and completing and reviewing the collection of information. Send comments regarding this burden estimate or any other aspect of this collection of information, including suggestions for reducing this burden, to Washington Headquarters Services, Directorate for Information Operations and Reports, 1215 Jefferson Davis Highway, Suite 1204, Arlington, VA 22202-4302, and to the Office of Management and Budget, Paperwork Reduction Project (0704-0188), Washington, DC 20503.

1. AGENCY USE ONLY *(Leave blank)*	2. REPORT DATE	3. REPORT TYPE AND DATES COVERED
	April 1993	Conference Publication

4. TITLE AND SUBTITLE
69 Months In Space—Second LDEF Post-Retrieval Symposium

5. FUNDING NUMBERS
506-48-91-11

6. AUTHOR(S)
Arlene S. Levine, Editor

7. PERFORMING ORGANIZATION NAME(S) AND ADDRESS(ES)
NASA Langley Research Center
Hampton, VA 23681-0001

8. PERFORMING ORGANIZATION REPORT NUMBER
L-17196

9. SPONSORING/MONITORING AGENCY NAME(S) AND ADDRESS(ES)
National Aeronautics and Space Administration
Washington, DC 20546-0001

10. SPONSORING/MONITORING AGENCY REPORT NUMBER
NASA CP-3194, Part 4

11. SUPPLEMENTARY NOTES

12a. DISTRIBUTION/AVAILABILITY STATEMENT
Unclassified–Unlimited

Subject Category 99

12b. DISTRIBUTION CODE

13. ABSTRACT *(Maximum 200 words)*

This document is a compilation of papers presented at the Second Long Duration Exposure Facility (LDEF) Post-Retrieval Symposium. The papers represent the data analysis of the 57 experiments flown on the LDEF. The experiments include materials, coatings, thermal systems, power and propulsion, science (cosmic ray, interstellar gas, heavy ions, micrometeoroid, etc.), electronics, optics, and life science.

14. SUBJECT TERMS
Space experiment

15. NUMBER OF PAGES
330

16. PRICE CODE
A15

17. SECURITY CLASSIFICATION OF REPORT	18. SECURITY CLASSIFICATION OF THIS PAGE	19. SECURITY CLASSIFICATION OF ABSTRACT	20. LIMITATION OF ABSTRACT
Unclassified	Unclassified	Unclassified	

NSN 7540-01-280-5500

Standard Form 298(Rev. 2-89)
Prescribed by ANSI Std. Z39-18
298-102

NASA-Langley, 1993